FROTH WASHING IN MECHANICAL FLOTATION CELLS

Muammer Kaya

McGill University

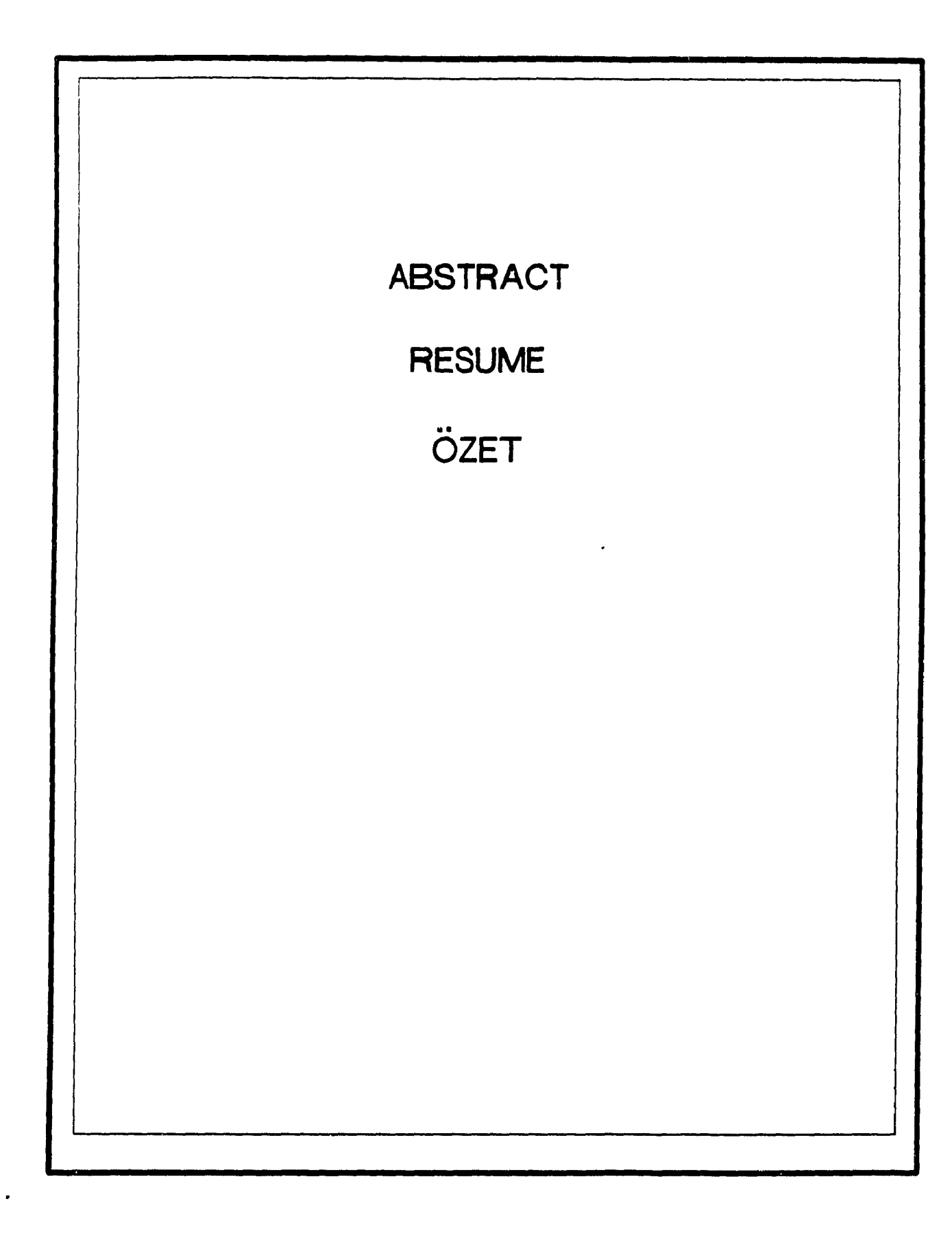
Department of Mining and Metallurgical Engineering

Montreal, Quebec, Canada

March 1989

A thesis submitted to the Faculty of Graduate Studies and Research in partial fulfillment of the requirements for the degree of Doctor Philosophy





1

ABSTRACT

This basic research project was aimed at assessing the potential of wash water for mechanical flotation machines. Test work at laboratory scale first examined the nature of entrainment, froth structures with and without wash water; and the location, geometry, and flowrate of wash water addition. The relationship between slurry, total water recovery and gangue recovery was characterized. Confirmatory work at pilot plant was completed.

The effect of wash water on metallurgical performance was tested with various streams from the Falconbridge Strathcona mill at laboratory and pilot and full plant scale, and with the secondary cleaner stage at the Eastmaque Kirkland Lake mill.

Results show that mechanical entrainment is the major means of gangue transport up to the slurry-froth interface. Transport into the froth is mostly hydraulic, although entrapment becomes dominant at low water recoveries. Free gangue recovery was closely related to slurry water recovery at all three scales. Wash water at an optimum superficial rate of 0.03 to 0.07 cm/s reduced entrainment by anywhere from 30 to 70%, typical values being around 50%.

Wash water can be further assisted by mechanical and ultrasonic vibration of the froth, difficult to achieve at plant scale, or with warm wash water, which becomes attractive if a waste heat source is available. A further rejection of 10 to 20% then becomes possible.

Distributor geometry was aimed at washing the entire froth surface at laboratory and pilot scale. It was observed that the recovery of hydrophobic minerals generally increased because the froth was stabilized. At plant scale, two perforated pipes close to the concentrate weir yielded the most reject. Froth stabilization was lost, and recoveries decreased.

RÉSUMÉ

Ce projet visait à évaluer le potentiel de l'eau de lavage en flottation mécanique. Nous avons d'abord étudié en laboratoire (6.5L) la nature des phénomènes d'entrainement, les structures d'écume avec et sans eau de lavage, et l'effet de l'emplacement et de la géométrie du mécanisme d'addition et du débit d'eau de lavage. Nous avons caractérisé le lien entre la récuperation d'eau de pulpe et d'eau totale d'une part, et la récupération de gangue d'autre part. Nous avons confirmé la validité des résultats obtenus à l'échelle pilote (65L).

Nous avons déterminé l'effet de l'eau de lavage sur la séparation par flottation de divers flux de l'usine Strathcona de Falconbridge à l'échelle laboratoir (6.5L), pilote (65L) et usine (2800 L), et du stage de deuxième nettoyage à l'usine de Kirkland Lake d'Eastmaque (2800L).

L'entrainement de gangue jusqu' à l'interface pulpe-écume est surtout mécanique. Dans l'écume la composante hydraulique domine, quoique à basses récupérations d'eau le coincement entre particules hydrophobes soit important. La récupération de gangue libérée peut être étroitement reliée à la récupération d'eau de la pulpe aux trois échelles étudiées. L'eau de lavage dont le taux d'addition superficial optimal varie de 0.03 à 0.07 cm/s, et réduit l'entraînement de 30 à 70%, dépendant du système.

Aux échelles laboratoire et pilote, laver toute la surface de l'écume la stabilise et augmente la récupération des minéraux hydrophobes. En usine, nous n'avons lavé que la partie frontale de l'écume, ce qui diminue cette récupération.

On peut augmenter l'effet du lavage en soumettant l'écume à des vibrations mécaniques ou ultrasoniques, ce qui est difficile à réaliser en usine, ou avec de l'eau de lavage chaude (20-40°C), une alternative attrayante si une source de chaleur dépendue est disponible. Le rejet de gangue libérée augmente alors de 10 à 20%.

Bu temel araştırma projesinin amaçı mekanik flotasyon makinalarında yıkama suyu kullanılabilirliginin araştırmasıdır. Gang kazanılmasının sebepleri, yıkama suyu ilavesiyle ve ilave edilmeden köpuk yapıları, yıkama suyu ilavesinin yeri, miktarı ve dagıtıcı yapısı laboratuvar ölçeginde incelendi Gang kazanılmasıyla pülp ve toplam su kazanılması arasındaki ilişki karakterize edildi. Pilot-fabrika ölçeginde sonuçları destekleyici testler yapıldı

Yıkama suyunun metallurjik sonuçlar üzerindeki etkileri Falconbridge Strathcona konsantratörünün degişik devrelerinden sağlanan numunelerle laboratuvar ve pilot-fabrika ölçeginde test edildi. Fabrika testleri Falconbridge'in Strathcona ve Eastmaque'ın Kirkland Lake konsantratörlerinde yapıldı.

Sonuçlar, gang parçacıklarının pülp-köpük arayüzeyine başlıça mekanik olarak taşındığını gösterdi. Köpükteki gang taşınması önçelikle hava kabarçıkları etrafindaki ince su filmiyle olmasına ragmen düşük su kazanılma oranlarında gang parçacıkları hava kabarcıkları arasına sıkışıp (köprülenip) taşınmaktadır. Serbest gang parçacıkları pülp suyu kazanılmasıyla her üç ölçekte ilişkilidir. En iyi yüzeysel yıkama hızı (0.03-0.07 cm/s), gang kazanılmasını %30 ile %70 arasında azaltmaktadır, ortalama uzaklastırma %50 cıvarındadır.

Mekanik ve ultrasonik köpük sarsıntısı, fabrikaya uygulaması zor, veya ılık yıkama suyu, eger kullanılmayan ilave ısı kaynagı varsa, %10 ile %20 lik ilave bir gang uzaklaştırması saglamaktadır.

Laboratuvar ve pilot-fabrika ölçeginde, su dagiticisinin geometrik yapısı tüm köpük yüzeyini yıkamak için ayarlandı. Böylece degerli parçacıkların kazanılma oranının köpügün stabil olmasıyla artıgı görülmüştür. Fabrika ölçeginde, konsantre taşma olugu tarafına konulan boydan boya delikli iki paralel boru en fazla gang uzaklaştırmasına sebep olmuştur. Köpük stabilitesi köybölmüş ve degerli mineral kazanılma oranı azalmıştır.

ACKNOWLEDGEMENTS	

ACKNOWLEDGEMENTS

First, I would like to thank my parents for their continuous support and encouragment throughout my post-graduate study abroad. Second, special thanks to my supervisor Prof. A.R. Laplante for his supervision, interest, criticism, and friendship for a long time.

I am sincerely grateful to the Scientific and Technical Research Council of Turkey (TBTAK) for providing me a NATO science fellowship for the initial three years of my study. Financial support of the Natural Sciences and Engineering Research Council of Canada (NSERC), Falconbridge Ltd. (Sudbury, Ontario), and Eastmaque Gold Mines Ltd. (Kirkland Lake, Ontario) is gratefully acknowleged.

The author also wishes to thank industrial participants for technical support and access to their plants for plant trials. Thanks to the staff, technicians, and my colleagues in the department.

TABLE OF CONTENTS

Abstact Resume Ozet Acknowledgements Table of Contents Claims for Originality General Introduction	Page(s) i-ii iii-iv v-vi vii viii-xiii xiv-xv 1-4
CHAPTER 1 SECONDARY CONCENTRATION OF MINERALS IN THE FROTH PHASE AND PREVIOUS PLANT APPLICATIONS	
Introduction	6
1.1 Theoretical Background 1.1.1 Hydrodynamic Regions in a Subaerated Flotation Machine 1.1.2 Gangue Recovery Mechanisms 1.2 Solutions to the Entrainment Problem 1.2.1 Flow Modifiers 1.2.2 Froth Vibration 1.2.3 Wash Water Addition 1.3 Previous Wash Water Applications in Plant Scale 1.3.1 Wash Water Distribution 1.3.2 Ore Applications 1.3.3 Coal Applications 1.4 Temperature Effect in Flotation 1.4.1 Objectives of Pulp Heating 1.4.2 Industrial Applications of Hot Flotation 1.5 Summary CHAPTER 2 A STUDY OF THE SLURRY PHASE OF MECHANICAL FLOTATION CELLS IN A TWO PHASE SYSTEM	7-8 9-12 12-13 13-15 15-18 18-20 20 20-22 22-27 27-29 30 30-31 31-34 34-35
Introduction	37-39
2.1 Theoretical Considerations 2.1.1 Gas-liquid Interfacial Area 2.1.2 Gas Holdup 2.1.3 Bubble Size 2.1.4 Gas Mixing Regimes in Agitated Vessels 2.2 Experimental 2.2.1 Set-up	39-41 41-47 47-50 50-52 52-58
2.2.2 Overall Gas Holdup Measurements in the Recovery Zone Using Level Rise and Overflow Techniques	60-61

151-152

	2.2.3 Point Gas Holdup in the Recovery Zone using	
	Conductivity Measurements	61-65
	2.2.4 Local Gas Holdup in the Recovery Zone Using Pressure Measurements	65-66
2.3	Results and Discussion	03-00
	2.3.1 Overall Gas Holdup in the Recovery Zone	66-75
	2.3.2 Local Gas Holdup in the Recovery Zone 2.3.3 Point Gas Holdup in the Recovery Zone	75-81
	Bubble Size	81-84 84-86
2.5	Impeller Dispersion Efficiency	86-90
2.6	Summary	90-91
	CUARTER	
	CHAPTER 3 A STUDY OF THE FROTH PHASE HYDRODYNAMICS IN MECHANICAL FLOTA	TION
	MACHINES WITH A TWO PHASE SYSTEM	TION
	IN THE PRESENCE OF WASH WATER	
Inti	roduction	93
2 1	Hydraulia Madal (Untar Dalana) in a Platetta and	
J. 1	Hydraulic Model (Water Balance) in a Flotation Cell 3.1.1 Water Entrainment From the Pulp to the Froth	93-97 97-100
	3.1.2 Water Drainage from the Froth to the Slurry	100-101
	3.1.3 Water into the Concentrate	101-103
	Cas Balance in a Flotation Cell	103-105
3.3	Momentum Conservation at the Interface and in the Froth Phase	105-109
	Bubble Surface Loss Froth Structure	109
	Experimental	109-117
	3.6.1 Set-up	117-119
	3.6.2 Conductivity Measurements to Determine Gas Holdup in	
	the Froth Phase 3.6.3 Electrode Assemblies	119-121
	3.6.4 Test Program	121 121-125
	3.6.5 Determination of the Amount of Water in the Concentrate	125-127
3.7	Results and Discussion	
	3.7.1 Froth Expansion 3.7.2 Water Balance and Point Gas Holdup Profile in the Froth	127-132
	Phase	132-143
	3.7.3 Prediction of Superficial Concentrate Rate	143-149
	3.7.4 Local Gas Holdup in the Froth Phase	149-151

3.8 Summary

CHAPTER 4 MIXING CHARACTERISTICS OF THE LABORATORY FLOTATION CELL

Introduction	154
4.1 Experimental	154-155
4.1.1 Measurement Techniques	155-159
4.2 Results and Discussion	
4.2.1 Liquid and Solid Residence Time in the Slurry Phase 4.2.2 Comparison of Solid and Liquid Residence Times in the	159-164 ne
Slurry Phase	164
4.2.3 Presence of Perfect Mixing	164
4.2.4 Gas and Liquid Residence Times in the Froth Phase	165-169
4.2.5 Feed Water Split	169-172
4.3 Summary	172-174

CHAPTER 5 DETERMINATION OF GANGUE PROFILES IN SLURRY AND FROTH PHASES

Int	roduction	176
5. 1	Theoretical Concepts of Mass Transfer and Particle Rejection	
	in Flotation Cells	176
	5.1.1 Mass Transfer Across the Slurry-Froth Interface	176-181
	5.1.2 Mass Transfer in the Froth Phase	181-187
	5.1.3 Particle Rejection Mechanisms in the Froth Phase	187-189
5.2	Experimental Procedure	189
	5.2.1 Set-up and Material	190
	5.2.2 Determination of Gangue Profile in the Slurry Phase	190-196
	5.2.3 Froth Sampling Techniques and Gangue Holdup Profiles	196-197
	5.2.3.1 Test Work	197
	5.2.3.2 Calculation Procedure	197-199
	5.2.4 Hydraulic Particle Rejection in the Froth Phase	199
5.3	Results and Discussion	
	5.3.1 Gangue Concentration Profiles in the Slurry Phase	199-204
	5.3.2 Solid, Liquid and Gas Contents of the Froth Phase	204-206
	5.3.3 Hydrophilic Particle Rejection in the Froth Phase	206-211
5.4	Summary	212

CHAPTER 6 DETERMINATION OF THE EFFECT OF WASH WATER ADDITION AND FROTH VIBRATION ON GANGUE ENTRAINENT AT LABORATORY SCALE

6.2 Experimental 6.2.1 Set-up	214-217 218 218-221 221-234
6.3 Results and Discussion	
6.3.1 Effect of Cell Dimensions on Entrainment	234
6.3.2 Visual Evidence of Cleaning Action in the Froth Phase 5.3.3 Effect of Wash Water Superficial Rate and Froth	234-237
	237
6.3.4 Effect of Feed Size	237-240
6.3.5 Effect of Water and Gangue Recovery	240-243
6.3.6 Effect of Impeller Speed	243-244
6.3.7 Effect of Wash Water Distributor Geometry	244
6.3.8 Effect of Wash water Distributor Location	245-250
6.3.9 Effect of Froth Vibration on Gangue Entrainment	250-255
	255-257
6.3.11 Effects of Wash Water Temperature and Depressant	
· · · · · · · · · · · · · · · · · · ·	257-261
6.3.12 Comparison Between Mechanical Cell and Flotation Column	261-263
6.3.13 Testing the Proposed Entrainment Model	263-269
	269-270

CHAPTER 7

EVALUATION OF WASH WATER ADDITION IN A PILOT-PLANT SCALE FLOTATION CELL USING TRACER TECHNIQUES IN A TWO PHASE SYSTEM

Introduction	272
7.1 Theoretical Background	272-274
7.2 Experimental	
7.2.1 Set-up	274-280
7.2.2 Methodology	280-289
7.3 Results and Discussion	
7.3.1 Electrode Calibration	289
7.3.2 Effect of Wash Water Flowrate and Temperature on	
Conductivity	289-294
7.3.3 Evaluation of Wash Water Distributor For Homogeneo	ous
Addition	294-299
7.3.4 Comparison of Wash Water Distributors	299-300
7.3.5 Wash Water Split	301-306
7.3.6 Effect of Wash Water on Slurry Water Rejection Usi	ing
the VEA	306-309

7.3.7 Effect of Wash Water and Air Flowrates on Feed Water Rejection 7.3.8 Estimation of Water Recovery in the Pilot-Plant Cell 7.4 Conclusions	309-311 311-314 314
CHAPTER 8	
LABORATORY AND PILOT-PLANT SCALE FLOTATION TESTS WITH THE STRATHCONA Cu-Ni ORE TO ASSESS THE POTENTIAL OF WASH WATER ADDITION IN MECHANICAL FLOTATION CELLS	
Introduction	317
8.1 Defining the Problem 8.1.1 Geology of the Ore Body 8.1.2 Falconbridge's Nickel Operations in Sudbury 8.1.3 Strathcona Mill 8.2 Experimental 8.2.1 Set-up 8.2.2 Samples 8.2.3 Test Procedures 8.2.3.1 Laboratory Scale Tests 8.2.3.2 Pilot-Plant Scale Tests 8.3 Results and Discussion 8.3.1 Laboratory Scale Tests 8.3.2 Pilot-Plant Scale Tests 8.4.3 Summary 8.4.1 Laboratory Scale Tests 8.4.2 Pilot-Plant Scale Tests	317 318 318-319 319-322 322-323 323-326 326-329 329-331 331-342 342-350 350-351
CHAPTER 9 PLANT SCALE WASH WATER AMENABILITY TESTS AT THE STRATHCONA MILL OF FALCONBRIDGE	
Introduction	352
9.1 Previous Investigations on the Non-Magnetic Circuit 9.2 Wash Water Distributor Design Considerations 9.3 Experimental Procedure 9.3.1 Test Program 9.3.2 Installation of the Wash Water Distributor Network 9.3.3 Wash Water Flowrate Calibration 9.3.4 Sampling Procedure 9.3.5 Sample Preparation 9.3.6 Calculation Procedure	352-355 355-360 360 361 361-363 363-368 368-370

9.4 Results and Discussion 9.4.1 Washing the Entire Froth Surface with Four Perforated Pipes in Each Cell 9.4.2 Washing the Front Part of the Froth Surface with Two Perforated Pipes in Each Cell 9.4.3 Effect of Wash Water on "Solid 9.4.4 Effect of Wash Water on the Grade Profile in the Froth Phase 9.5 Conclusions	370-374 374-386 386 386-390 390-391
CHAPTER 10 PLANT SCALE WASH WATER TESTS	
AT EASTMAQUE COLD MINES LTD.	
10.1 Background About Eastmaque	393-394
10.2 Experimental 10.2.1 Distributor Set-up 10.2.2 Test Work Program 10.2.3 Sample Preparation 10.2.4 Data Processing 10.3 Results and Discussion 10.3.1 Effect of Wash Water on Overall Flotation Circuit Performance 10.3.2 Effect of Wash Water on Bank Performance 10.3.3 Temperature Effect 10.3.4 Tracer Test Results 10.3.5 Economic Impact of the Wash Water on Flotation Performance 10.4 Summary	394-399 399 399-404 404-407 407-408 408-412 412-413
CHAPTER 11 GENERAL CONCLUSIONS	
11.1 General Summary 11.2 Scale-up 11.3 Limitation of Wash Water 11.4 Practical Implications of Wash Water for Plant Applications 11.5 Suggestions for the Future Work	414-418 418-419 419-420 420-421 422
Bibliography	423-429
Appendix	430

PEACE AT HOME, PEACE IN THE WORLD -ATATURK-

CLAIMS FOR ORIGINALITY

Although wash water sprinkling into the mechanical cells is being used in Soviet plants for coal and ores, it had been neglected in the western world. There was no fundamental study to explain why and how wash water can improve metallurgical performance and what are the best operating conditions. The purpose of this research thesis was to find the best addition type, location and flowrate from bench to plant scale.

The following claims for originality and contributions to the scientific and technical knowledge are made:

- 1. Froth cleaning by wash water in mechanical flotation cells was quantitatively determined at laboratory, pilot-plant, and plant scales,
- 2. Froth washing technology was fully developed and brought to the stage of plant implementation,
- 3. The use of wash water warmer than pulp was shown to reduce significantly both wash water requirement and gangue entrainment,
- 4. Vibrating the froth phase in a flotation cell by mechanical and ultrasonic means to further reduce gangue entrainment had never been tested before, and was shown to achieve moderate success,
- 5. Gangue recovery mechanisms in flotation were identified and their contribution was quantified in a laboratory system,
- 6. Conductivity measurements were used to determine gas holdup in the slurry and froth phases and to dynamically monitor froth washing efficiency.

- 7. Washing the entire froth surface was shown to stabilize the froth at laboratory and pilot plant scale and often increase the recovery of hydrophobic species at a shorter residence time in the slurry. At plant scale, washing was limited to the area adjacent to the concentrate weir to minimize water requirements. As a result, hydrophobic recovery decreased,
- 8. A classification coefficient originally used to describe the effect of particle size on entrainment was adopted to be used as a simplified predictor of entrainment at various scales. The effect of scale and wash water on the coefficient was determined, and
- 9. A simple model to predict froth height based on momentum conservation was developed. The model was shown to predict well the effect of gas rate and wash water on froth height. This model can be used to predict water recovery using the established weir discharge equation.

NOMENCLATURE

- A: interfacial area, 1/m
- ε: fractional holdup
- d: diameter, m
- P: aerated power consumption, W
- P.: unaerated power consumption, W
- V_{lp} : liquid volume in the pulp phase, m^3
- V_{\downarrow} : terminal bubble rise velocity, m/s
- J: superficial gas rate, m/s
- σ: serface tension, N/m
- ρ : density, Kg/m³
- N: impeller speed, rps
- D: impeller diameter, m
- N_{Re} : impeller Reynolds number
- N_p: power number
- Q: air flowrate, m3/s
- g: gravity accelleration
- $N_{\rm c}$: minimum impeller speed for air dispersion, rps
- μ: viscosity, Nsec/m²
- L: cell lenght, m
- P/P: power dissipation per unit volume, W/m³
 - K: constant in Eq. 2.17 (varies btw 1.3 and 1.6)
 - τ: residence time, sec
 - CF: frother concentration
 - K: constant in Eq. 2.20
 - η: impeller dispersion efficiency
 - T: cell diameter, m
 - $\epsilon_{\rm p}$: fractional gas holdup in the pulp phase
 - Δh: level difference, m
 - R: resistivity
 - q: specific resistivity
 - L/A: cell constant
 - C: conductivity
 - K: specific conductivity in Eq. 2.26
 - C: conductivity with aeration

```
C: conductivity without aeration
    A: electrode area, m<sup>2</sup>
   \rho_{\rm n}: pulp density, kg/m<sup>3</sup>
do/dc: change in surface tension
    C: concentration
  EMZ: efficient mixing zone
   J: superficial feed rate, m/s
   J.: superficial tails rate, m/s
   J: superficial concentrate rate, m/s
   J: superficial wash water rate, m/s
   J<sub>d</sub>: superficial drainage rate, m/s
   J.: superficial liquid rate, m/s
  J : superficial gas rate associated with liquid transfer, m/s
    δ: water film thickness around bubbles, m
    C: adjustable constant in Eq. 3.4
     S: cell cross-sectional area, m<sup>2</sup>
    k: velocity coefficient
     r: radius of Plateau borders, m
     H: the distance btw cell lip level and froth surface, m
     T: the distance btw cell lip level and interface, m
    FT: froth thickness (T+H), m
    Q: concentrate flowrate, m3/s
     w: cell width, m
    K: discharge coefficient
   Q_{ac}: volumetric froth flowrate to the concentrate, m^3/s
     a: froth removal efficiency
     P: momentum, Kg.m/sec
     m: mass, Kg
     v: velocity, m/s
   v<sub>13</sub>: joint bubble velocity, m/s
    N: number of bubbles
   V_{\rm bp}^{}: bubble rise velocity in the pulp phase, m/s
     n: number of bubbles
    \mathbf{H}: distributor height from the froth surface, \mathbf{m}
     Z: distance from the interface, m
```

J.-J: entrainment factor J_-J: drainage factor au_{1} : liquid residence time in the pulp phase, sec V: pulp volume, m³ Q: tails flowrate, m³/s τ_{nf} : bubble residence time in the froth phase, sec V: froth volume, m A: amount of tracer reporting to the concentrate, kg A: amount of tracer reporting to the tails, kg FT : maximum froth thickness, m k: entrainment rate constant, 1/sec x: mass of gangue in the pulp phase, kg t: time, sec N: total number of particles in the cell V: cell volume, m³ P: probability of entrainment α: distribution coefficient in Eq. 5.5 U: interstitial particle settling rate E: upward mass flowraate, kg/sec R: downward mass flowrate, kg/sec C: pulp gangue concentration at the interface, kg/m3 k_i: drop-back rate constant, 1/sec H: distance from the interface. m C: mass flowrate in the concentrate, kg/sec J: superficial bias rate, m/s ρ_{susp} : suspension density, kg/m³ G: gangue concentration $\epsilon_{_}$: fractional solid holdup $\tau_{\rm hf}$: bubble residence time in the froth phase, sec Z: classification coefficent Z: modified classification coefficent Q: impeller pumping capacity, m³/sec b: impeller blade thickness, m J: superficial fluid pumping rate, m/s H: cell height in Eq. 5.34

F: feed flowrate

Q_{sc}: slurry flowrate going to the concentrate, m³/s

x: total weight of water in the cell, kg

R: gangue recoevry

R: water recovery

Q : wash water flowrate directly going to the concentrate, m3/s

F : wash water flowrate, m3/s

β: fraction of water in concentrate from the slurry

R: total gangue recovery

d₈₀: 80% passing size

R: gangue recovery

HEA: horizontal electrode assembly

VEA: vertical electrode assembly

PPD: perforated pipe distributor

SN: spray nozzle

 Q_{ws} : wash water flowrate going to the slurry, m^3/s

R : slurry water recovery

BR: bias ratio

Q_b: bias flowrate, m³/s

Gn: gangue

Po: pyhrrotite

Pe: pentlandite

Ch: chalcopyrite

Au: gold

PRC: primary rougher concentrate

CNC: combined nickel concentrate

U/F: underflow

O/F: overflow

FT: final tails

SRC: secondary rougher concentrate

CRT: copper rougher tails

MFC: magnetic flotation concentrate

NMFC: non-magnetic flotation concentrate

 v_c : collision velocity, m/s

S: distance, m

R_b: bank recovery

c,f,t: concentrate, feed, and tails assays

C,F,T: concentrate, feed, and tails mass flowrates

 T_p : pulp temperature, C

 T_{ww} : wash water temperature, C

 T_f : feed temperature, C

Subscripts

sm: Sauter mean g: gas rl: recirculation

b: bubble bp: bubble in pulp fl: flooding

1: liquid lp: liquid in pulp www: wash water

f: feed t: tails g: gangue

GENERAL INTRODUCTION

This project was initiated three years ago based on the findings and observations of author's master thesis. Since laboratory and pilot flotation performance differ from actual plant flotation performance due to differences in scale, hydrodynamics, kinetics, and froth characteristics (e.g. stability, loading etc.), plant work was inevitable for scale-up. The project, therefore, was undertaken in three stages:

- 1. small scale laboratory tests (6.5 L) at McGill University,
- 2. pilot-plant scale tests (65 L) at McGill University, and
- 3. plant-scale tests (2800 L) at the Strathcona mill of Falconbridge Ltd. in Sudbury and Eastmaque Gold Mines Ltd. in Kirkland Lake.

This project, which is the first extensive fundamental study related to froth washing in mechanical cells, pays particular attention to the critical role of the froth phase and its effect on circuit performance along with pulp behaviour.

Chapter 1 introduces the theoretical background of gangue recovery mechanisms in flotation and covers a brief literature survey of secondary concentration in the froth phase with previous plant applications in the U.S.S.R.. This chapter also introduces alternative solutions to the entrainment problem in mechanical flotation cells.

In chapter 2, the main objective is to present some fundamental aspects of the flotation process in a two-phase system. Gas holdup and bubble size in the slurry phase, where the entrainment problem originates, are the main variables investigated.

Chapter 3 partly describes the froth zone properties by means of point and local gas holdup measurements and reviews froth hydrodynamic fundamentals.

The effect of operating variables on the mean residence time of gas, liquid, and solid in the slurry and froth phases with wash water was investigated in chapter 4. Variables affecting gangue entrainment, such as feed water recovery, are quantified.

In chapter 5, gangue profiles in the slurry and froth phases were determined at different operating conditions. An attempt was made to estimate gangue content in the froth phase.

A classification coefficient was correlated with bubble rise velocity and particle settling velocity in the froth phase.

In chapter 6, the applicability of froth washing and vibration in a laboratory cell to lessen gangue entrainment was studied. The main objectives were to explore how, how much, and where wash water should be added in mechanical cells. The effect of

main operating variables on gangue and water recoveries was quantified.

Tracer and conductivity techniques were used to evaluate the effect of wash water using the pilot cell in Chapter 7. Tracers were added into the wash water to determine wash water split, into the cell to determine slurry water rejection, and into the feed tank to determine feed water suppression.

In chapter 8, the results of laboratory and pilot-plant scale flotation tests with the Strathcona Cu-Ni ore to assess the potential of wash water in mechanical flotation cells are presented.

Chapter 9 presents the plant bank trial results at the Strathcona mill. Grade-recovery and recovery-recovery curves were generated and compared with and without wash water. For some tests, froth profile and size-by-size metallurgical performance were determined.

Chapter 10 gives the results of the full flotation plant scale tests at the Eastmaque mill to determine the amenability of wash water for the the 2nd cleaner bank. The size-by-size metallurgical performance and economic impact of wash water on the plant were determined.

CHAPTER 1 SECONDARY CONCENTRATION OF MINERALS IN THE FROTH PHASE AND PREVIOUS PLANT APPLICATIONS

Introduction

This chapter introduces the basic theoretical background of gangue recovery mechanisms in flotation and covers a brief review of secondary concentration of minerals in the froth phase, with previous plant applications.

Floatable and non-floatable particles follow a different sequence for transport from the pulp to the froth phase. For floatable particles, the principal recovery mechanism is true floatation (i.e. bubble attachment and levitation). Non-floatable particles are recovered by entrainment.

Gangue entrainment in mechanical flotation cells can significantly reduce separation performance, especially for fine feeds. It should be noted that although entrainment can in some respects be studied separately from true flotation, the converse is not true, because the recovery of mineral in conventional flotation cells, batch or plant, is always a combination of true flotation and entrainment; separation of the individual contributions is possible to a limited extent.

Entrainment is a problem in flotation because it is non-selective. There is no discrimination between hydrophobic and hydrophilic particles, both of which may be present in the inter-bubble water. True flotation, of course, is selective because only hydrophobic particles adhere to bubbles.

1.1 Theoretical Background

1.1.1 Hydrodynamic Regions in a Subaerated Flotation Machine

The subaerated flotation machine with externally-supplied air, as shown in Figure 1.1, has four distinct hydrodynamic regions, which are the key for flotation of particles. These corresponds to four essential features for all flotation machine designs: mixing, transport, separation, and froth removal.

Mixing region is located at the bottom of the cell, which essentially eliminates solids build-up in this zone. During the flotation of particles from a slurry, it is necessary to have a hydraulic transport region for conveyance of the mineral-laden bubbles from the mixing region to the separation region. Once the mineral-laden bubbles enter the separation region hydrophobic particles continue to rise toward the surface while gangue particles exit this region to reenter the hydraulic transport region. The mineral-laden bubbles enter the froth removal region, which is used for separating entraped gangue particles from the froth and removing of this mineralized froth from the flotation machine.

All four hydrodynamic regions differ significantly in turbulence, ranging from a highly turbulent flow condition in the mixing region to a smooth laminar flow condition in the froth removal region; the major transition from turbulent flow conditions to laminar flow conditions takes place between the transport and separation regions.

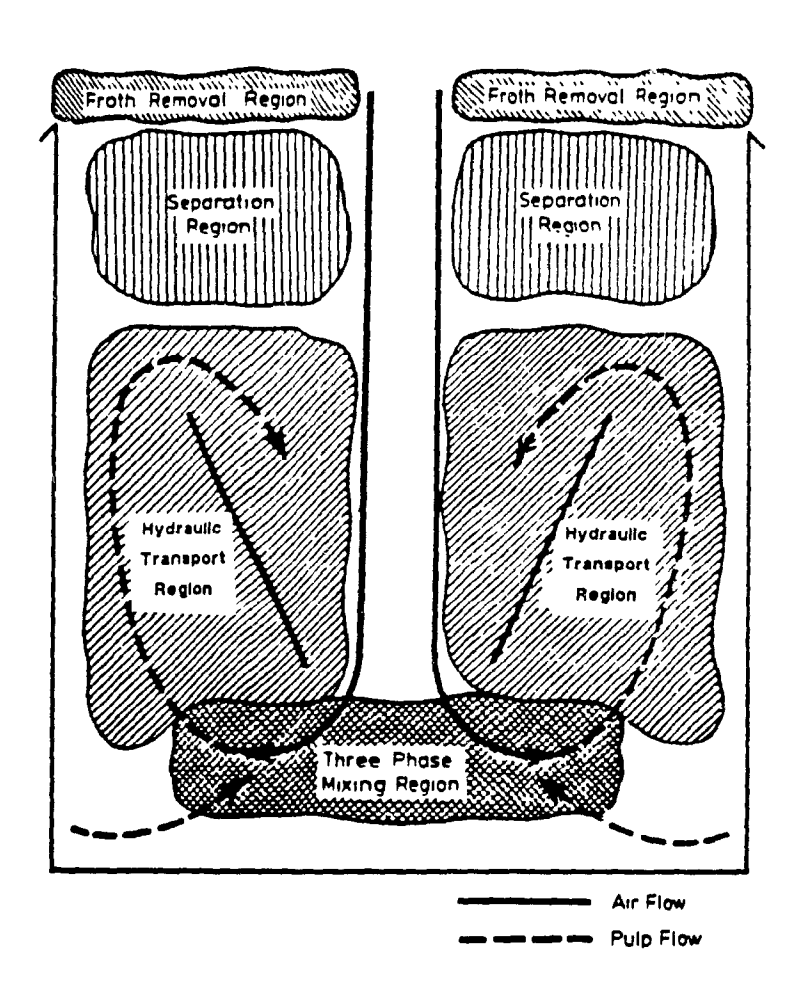


Figure 1.1: Hydrodynamic regions in a subaerated flotation cell.

(From Plouf, 1979)

1.1.2 Gangue Recovery Mechanisms

Gangue recovery mechanisms in flotation are different in the slurry and froth phases. In the froth phase, gangue particles can be recovered by either entrapment or hydraulic entrainment. There are two different gangue recovery mechanisms in the slurry phase (Figure 1.2) slime coating and entrainment. Entrainment can also be subdivided into two classes: hydraulic and mechanical. Some investigators use hydraulic entrainment while others use mechanical entrainment for the combination of these mechanisms. In this study, the distinction and contribution of these mechanisms will be clarified.

Some of the hydrophilic particles are represent by entrapment in which non-floatable particles are thought to be held in the froth by bridging across floatable particles held by adjoining bubbles. Entrapment mainly occurs in the quiescent froth phase or near the interface rather than the turbulent slurry phase. Entrainment and slime coating are generally followed by entrapment.

Each bubble leaving the slurry phase carries a sheath (envelope) of water, which contains fine gangue particles, into the froth (i.e. hydraulic entrainment or carry over with inter-bubble water). Some of the inter-bubble water and the larger particles enter the base of the froth column and then drain back into the pulp; the remainder is carried upwards and is ultimately recovered in the concentrate. The wetter the froth the greater the proportion of the particles in the concentrate that will be recovered by entrainment rather than by true flotation.

GANGUE RECOVERY MECANISMS

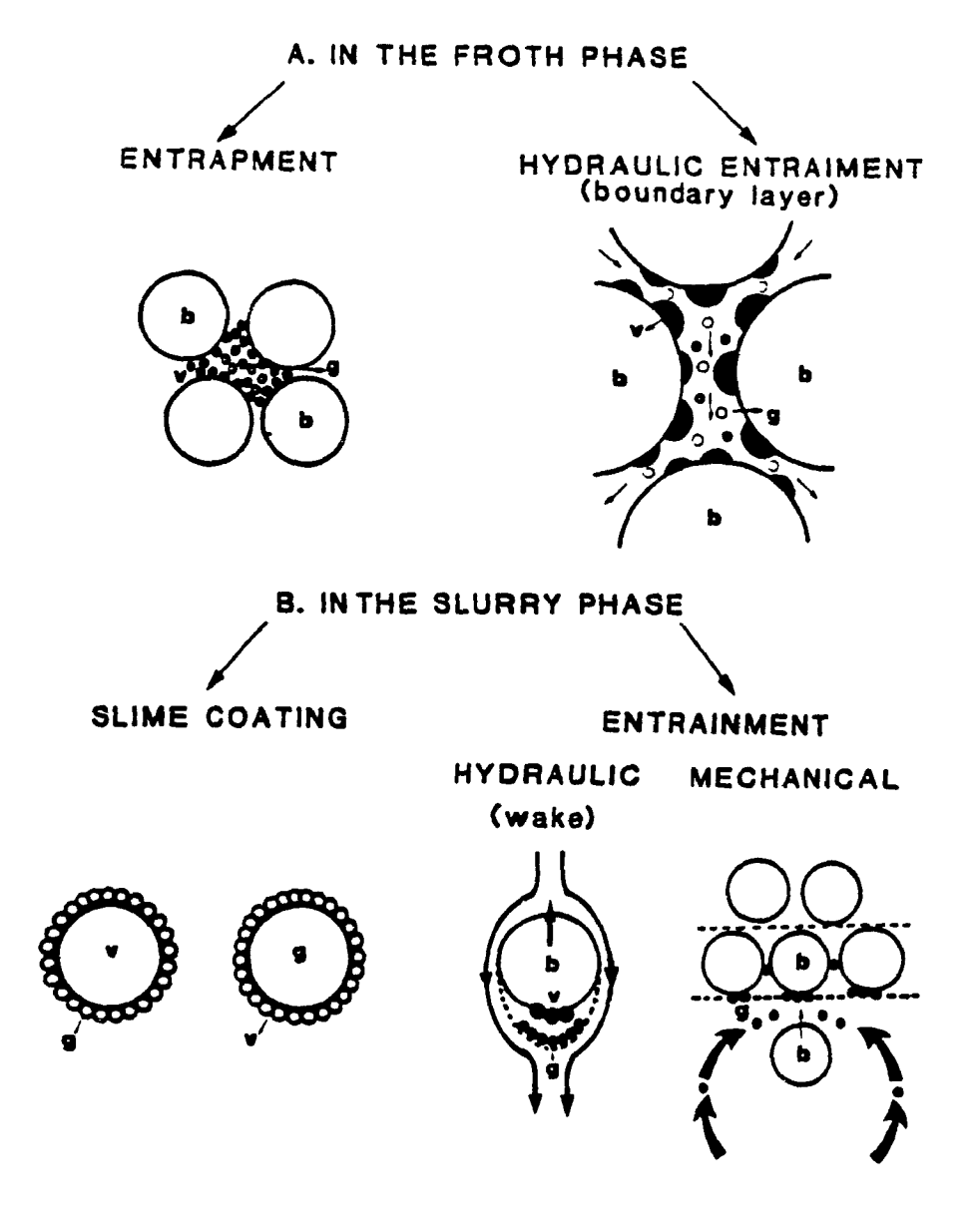


Figure 1.2: Gangue recovery mechanisms in flotation.

(b: bubble, g: gas, and v: valuable particle)

Gangue particles mainly reach the interface by either hydraulic or mechanical entrainment. Hydraulic entrainment occurs when particles are carried in the wakes of rising bubbles. Bubbles and their wakes rise up and reach the base of the froth phase. The bubbles continue to rise, becoming enlarged by coalescence, till they reach the top of the froth and are scraped off carrying their load of attached particles or overflow the concentrate weir Recovery of hydrophilic fines within boundary layers and wakes by hydraulic entrainment is related to water recovery in the concentrate.

Mechanical entrainment is caused by impeller motion, which gives rise to turbulence and brings some fine hydrophilic particles to the slurry-froth interface; some of it will report to the concentrate via entrapment or hydraulic entrainment. Bulk displacement of particles by internal flow patterns can be determined in the absence of aeration.

Slime coating is another likely source of gangue transfer to the froth phase. Slimes, which inhibit bubble attachment and adsorption of frother and/or collector, often deleteriously affect recovery and reagent consumption. In slime coating, there is an electrical attraction between gangue and valuable particles; it is most severe when slimes are uncharged or oppositely charged to the mineral being floated. Increasing the concentration of slimes increases the slime coating density (Sun, 1943). In general, some form of desliming can be carried out prior to flotation, but this results in an inevitable loss of values.

Slime coating is detrimental to concentrate grade if the fine particles are valuable mineral and coarse particles are gangue minerals. When the fine particles consist of gangue minerals that coat the coarse particles of the valuable mineral, these particles prevent the attachment of air bubbles and the recovery of valuable mineral may be decreased significantly. Fine particle or slime coating is not always undesirable in flotation, as it is the basis of carrier flotation process. Slimes may also stabilize the froth. Fine particles may coat coarse particles of the same mineral, and may thus float, like in scheelite and phosphate flotation (Koh and Warren, 1979).

1.2 Solutions to the Entrainment Problem

The removal of undesirable particles from the froth is called "secondary concentration" to distinguish it from the primary concentration processes occurring in the pulp. Secondary concentration is desirable because it will reduce the extent of further cleaning operations.

There are two major limitations for fine particle flotation in mechanical flotation cells:

- a. the recovery of gangue particles by entrainment in the water reporting to the concentrate.
- b. the finite capacity of the froth phase to carry valuable particles entering in the froth (i.e. carrying capacity problem).

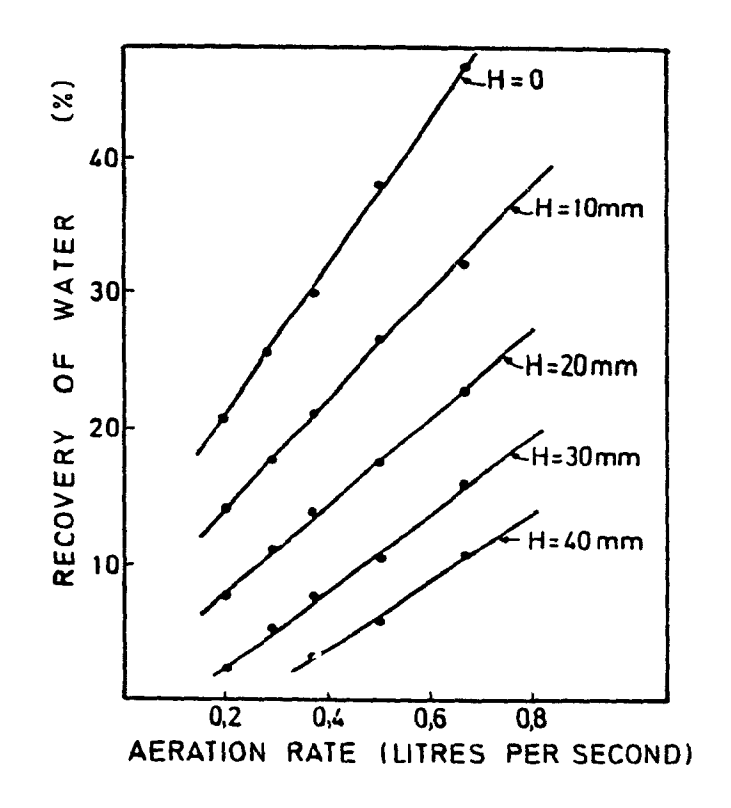
These limitations lower the concentrate grade and valuable particle recovery. There are some common solutions used currently in the industry to alleviate the entrainment problem (see Figure 1.3):

- a. use of deeper froth thicknesses and/or lower aeration rates (i.e. increasing residence time in the froth phase) to reduce water recovery to the concentrate (North American practice),
- b. dilution of the pulp phase by adding water into the concentrate launders or conditioning tanks (Australian practice).

The drawbacks of these common solutions are the decreased recovery for the former case, due to decreased water recovery to the concentrate and addition of tremendous amounts of water to achieve the necessary dilution in the latter case. In both cases, sequential stage flotation is needed to achieve the desired grade specifications. Alternative approaches to alleviate the above limitations in mechanical flotation cells are the use of flow modifiers, froth vibration, and froth washing to increase the secondary concentration in the froth phase.

1.2.1 Flow Modifiers

Moys (1984) showed that bubbles entering the froth phase near the concentrate weir have a very short residence time in the froth. Entrained liquid and particles are thus afforded little opportunity to drain back to the slurry and it is reasonable to suspect that most entrained gangue that reports in the concentrate originates from this area of the froth. He suggested to insert a baffle (flow modifier) in the froth phase close to the concentrate



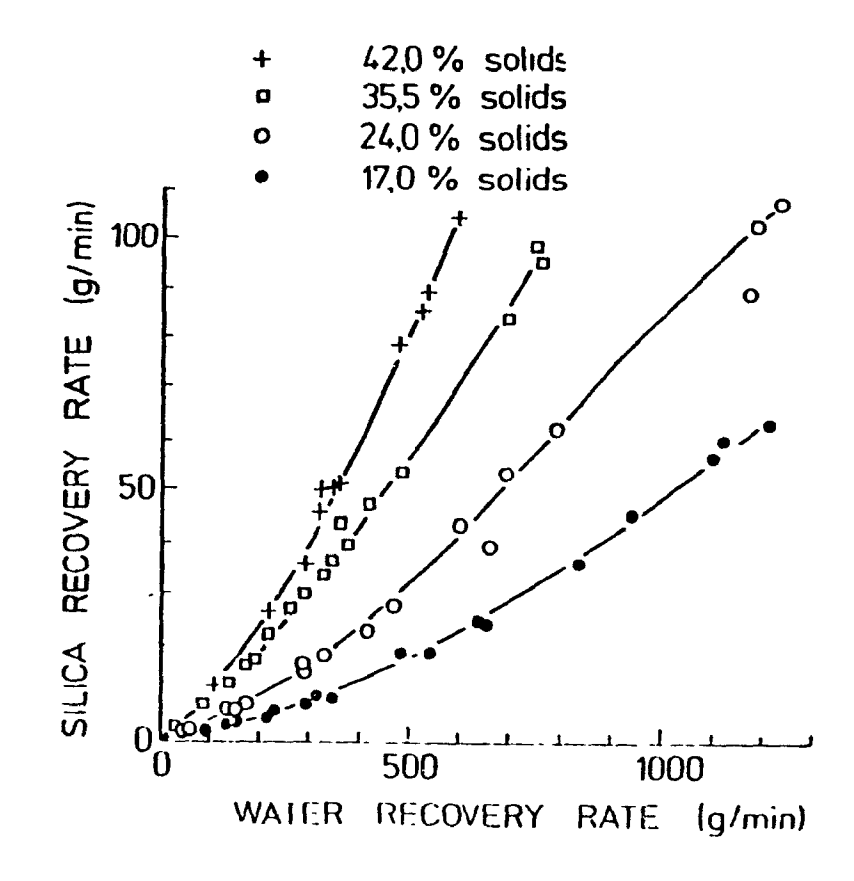


Figure 1.3: Effect of aeration rate, froth thickness, and percent solid on gangue entrainment.

(from Engelbrecht and Woodburn, 1975 and Lynch et al., 1974).

(H: Froth thickness)

weir. This flow modifier would ensure that bubbles entering the froth close to the concentrate weir are diverted from the concentrate weir and are retained in the froth for a longer time. Therefore, residence time in the froth is locally increased to enhance secondary concentration in the froth phase.

1.2.2 Froth Vibration

Mechanical or ultrasonic vibration was used for reasons other than entrainment reduction in mineral processing by American and Russian investigators as early as 1951 (Table 1.1). A search of the literature soon revealed that the concept of influencing flotation by the superimposition of an acoustic field was by no means novel, but unfortunately the conclusions drawn from much of the published work are of limited value because of lack of recognition of many of the factors controlling flotation. Furthermore, many of the experiments to investigate the effects of ultrasounds in fact only examine their effect on conditioning prior to flotation.

Numerous investigations have shown that intense ultrasonic vibrations can effectively change the state of a material causing dispersion, coagulation, and emulsification, changing the rate of dissolution, and crystallization, bringing about some chemical conversions, and accelerating considerably multi-phase processes. In recent years, ultrasonics have become of increasingly important in different industries.

The flotation process mainly depends on the state of the mineral surface. The introduction of ultrasonic energy into a flotation system can speed up flotation of some minerals. Table 1.1 shows a literature survey on the applications of ultrasounds in flotation. In most cases, ultrasounds are used for pretreatment of pulp or water outside the flotation cell. All investigations were carried out in small laboratory cells.

Froth vibration generated mechanically and ultrasonically will be tested as an auxiliary operation for reducing entrainment and enhancing secondary concentration of minerals in the froth phase in this study.

Stoev (1967) investigated the influence of ultrasonic vibrations on the secondary concentration of coal and barite minerals in froth. His results, obtained at the Warren Spring laboratory, showed that sonic vibrations intensified the secondary concentration process. The vibrations, at a frequency from 50 to 100 c/sec and an amplitude from 0.1 to 2 mm, were applied to the froth in the flotation cell and also after its removal into a separate vessel. A large intensification of the secondary concentration process with ultrasonic treatment was claimed (i.e. concentration process with ultrasonic treatment is better than that after 45 min without such treatment). A practical disadvantage is the introduction of undesirable noise into the working environment.

Table 1.1: Applications of ultrasounds in flotation.

Objective	Reference	Application
defrothing tough froths	Sun (1951)	Coal flotation
desliming and upgrading ores	Sun & Mitchell (1956)	tungsten and tin
pulp sonification pretreatment	Asai and Sasaki (1958)	to increase coal recovery
emulsification of sparingly soluble reagents	Revnitzev & Dmitriev (1963)	for selectivity
effect of ultrasounds on bubble dispersion	Stoev & Kuzev (1966)	fine coal flotation
secondary concentration	Stoev (1967)	coal and barite
water sonification to increase recovery	Agranat et al. (1973)	zircon, rutile, Beilmenite, jarosite spodumene, quartz chalcopyrite, moly and limonite flotation
pulp sonification pretreatment	Zubkov & Belov (1982)	rare metal ore flotation
pulp sonification pretreatment	Raghavan & Hsu (1982)	molybdenum ore flotation
oulp sonification oretreatment	Dyatalov (1983)	to increase coal recovery
fine particle flotation in an acoustic field	Nicol et al. (1986)	methylated silica flotation with a Hallimond tube
oretreatment to speed-up flotation cinetics	Slaczka (1987)	barite, fluorite and quartz flotation

Nicol et al. (1986) showed that the superimposition of an acoustic field on fine particle flotation process was helpful in improving recovery in the low size range (principally less than 20 μ m). Using a modified Hallimond tube with an ultrasonic probe (horn) attached, they showed that there was a 25% to 50% increase in fine particle recovery due to presence of acoustic fields at 0.40 W/mm² and 1.18 W/mm², respectively.

Slaczka (1987) found that ultrasonic pretreatment of minerals causes an increase in the flotation rate of barite and a decrease in the flotation rate of fluorite using an ultrasonic field of 22kHz and intensity of 0.5 W/cm². He selectively separated barite from a barite-fluorite-quartz ore.

Malinovskii (1970) used a screen 1 and 2 cm from the froth surface (in a 12 litre Mekhanobr cell) to investigate how firmly hydrophobic particles attached on the liquid-air boundary. The screen, with openings of 2 or 5 mm, was mechanically vibrated at 900 and 1200 vibrations per minute (vpm) with an amplitude from 5 to 10 mm. He showed that the presence of a screen had no detrimental effect on hydrophobic particle recovery (i.e. copper-pyrite, copper-zinc, and lead-zinc ores).

1.2.3 Wash Water Addition (Froth Spraying)

The froth acts as a separating medium (filter) to segregate and remove the valuable mineral particles from the gangue particles of the ore. Selective rejection of gangue in the froth phase can be fostered by careful and uniform water spraying of

the entire froth surface. Froth sprinkling washes loosely held gangue particles from the froth and compensates for water lost in the upper layers, thus increasing froth stability. Many gangue particles are not attached to bubbles in the froth and can be selectively removed from the froth by water draining from the air bubbles.

The thickness of the aqueous films between air bubbles in the froth, the rate, and amount of water draining between the bubbles play an important role in the process of secondary concentration. The greater the thickness of this layer and the larger the amount of water draining from the froth, the more effective is secondary concentration. An improvement in the concentrate grade obtained with spraying is largely due to washing away of gangue particles, which are entrained into the froth or weakly attached.

Water spraying reduces the coalescence of bubbles in the froth and for optimum addition of water increases the stability of the froth. Without spraying, the film of water between bubbles in the upper portion of the froth is sufficiently thin for particles to maintain contact with two or three bubbles. With spraying, the films thicken in all regions of the froth column, and the number of larger particles held in the froth is increased. Also. some fine particles adhere to bubbles more firmly. Spraying of the froth therefore generally increases concentrate grade recovery while decreasing reagent and consumption and even decreasing the number of cleaning stages required in the flotation (Klassen and Mokrousov, 1963).

The effectiveness of froth washing may be improved by using mechanical means to ensure intimate mixing of the water and froth flows: this is examplified by the Leeds column. The Wemco/Leeds column has an impeller below the froth barrier and demonstrates that the advantages of highly efficient froth washing with reflux water can be applied to the mechanical cells (Degner and Sabey, 1988).

1.3 Previous Wash Water Applications at Plant Scale

A literature survey showed that wash water spray into the mechanical flotation cells has been widely used for coal and ore in the USSR for more than 25 years (Klassen and Mokrousov, 1963). Unfortunately, the use of wash water in mechanical flotation cells in the Western world is neglected. There are at least three wash water applications in Chile, Zaire and Canada.

Russian investigations carried out in many flotation plants with coals and ores have shown that a separation of particles of different sizes and different hydrations takes place in the froth phase. In most flotation froths, the content of the valuable mineral and % solid increase and particle size becomes finer toward the top of the froth zone.

1.3.1 Wash Water Distribution

There are two kinds of reported wash water distributors used in Russian plants: showers and perforated pipes. The spraying of froth is carried out by sprinklers moving along the front side of the flotation cell. Figure 1.4 shows the photograph of showers for spraying the froth in coal flotation at the Karagandinskaia

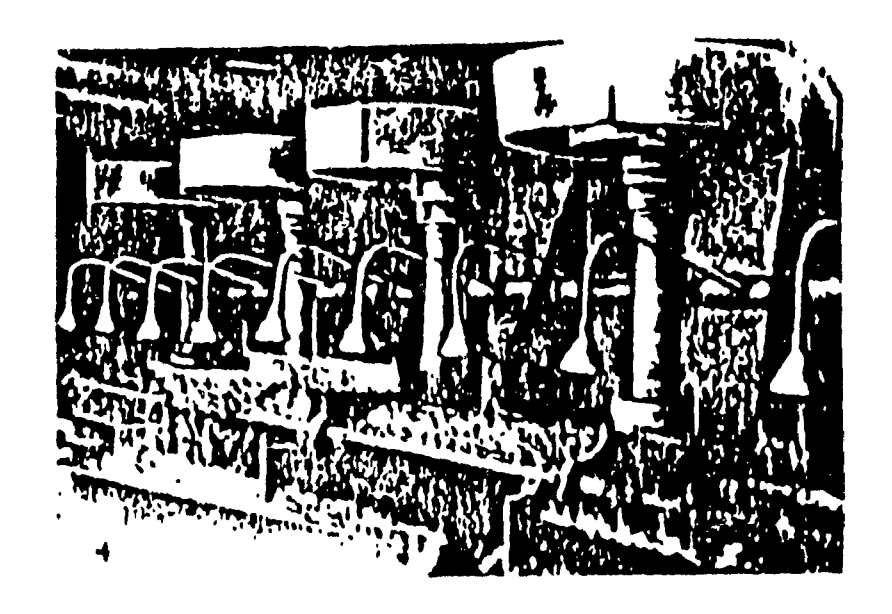


Figure 1.4: Photograph of showers for sprinkling the froth in mechanical flotation cells at Karagandinkaia central concentrator (from Klassen and Mokrousov, 1963).

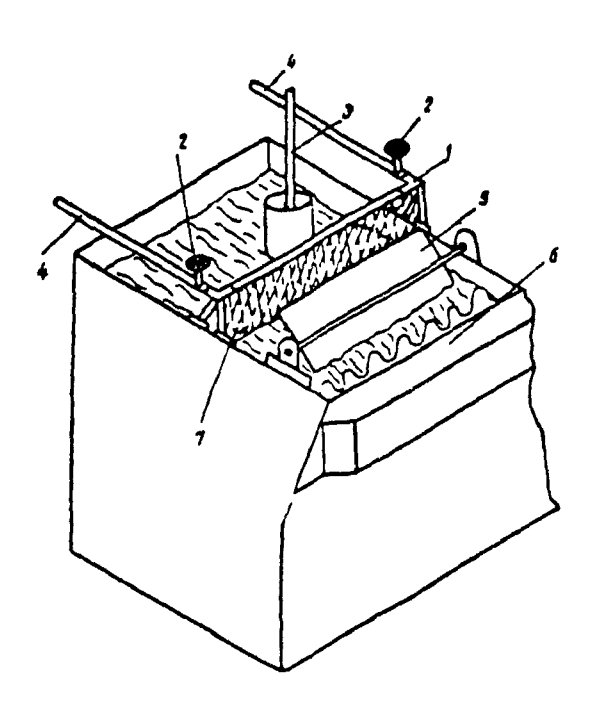


Figure 1.5: Perforated pipe distributor for coal flotation used in USSR (from Klassen and Pikkat-Ordynsky, 1957).

Central Concentration Plant. Water, falling from a very low height, sprays approximately 40% of the front froth surface. In this case concentrate overflows over the cell lip without any paddles (Klassen and Mokrousov, 1963).

Figure 1.5 shows a perforated pipe type spraying mechanism used in coal flotation in Russia. The pipe assemblies were fixed 20 cm above the froth and sprayed 70% of the froth surface. The hole diameter was 1 mm and water flow rate was 6 1/min (Klassen and Pikkat-Ordynsky, 1957). In this application, since the paddles were used, the back part of the froth surface was sprayed with water.

Figure 1.6 shows the effect of water spraying on the stability of a flotation froth, and bubble sizes in the froth. The optimum addition rate is around 12-16 l/min for a 18 cm froth thickness. Unfortunately, no size distribution is given to convert this into a superficial rate to scale up or down. The average bubble diameter in the froth dramatically decreases with increasing water addition rate.

1.3.2 Ore Applications

Significant increases in concentrate grades have been reported by water spraying on froth surfaces. This was first done in the flotation of andalucite ores and led to an increase in concentrate grade by 10-15%. Subsequently, the same process was adopted in USA at an Idaho plant (Klassen and Mokrousov, 1963).

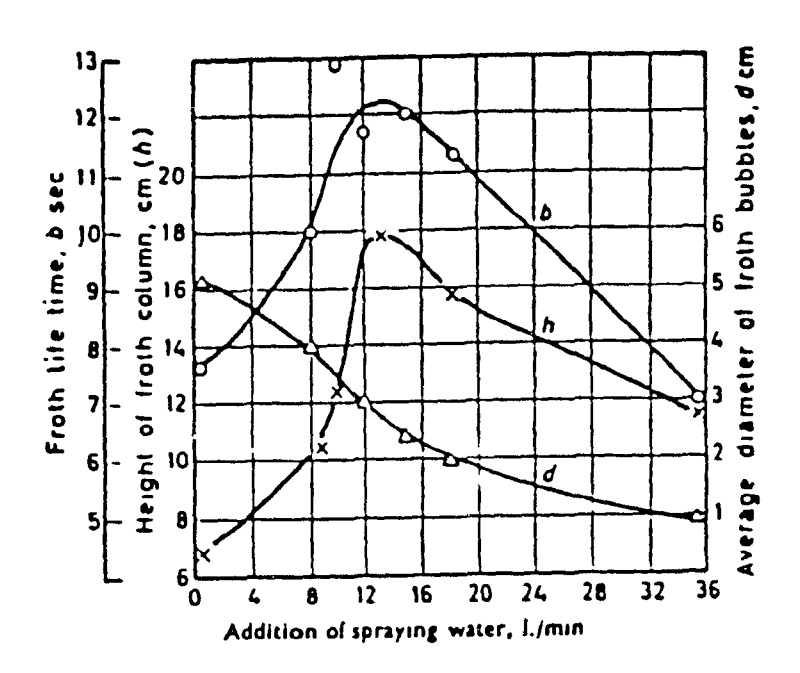


Figure 1.6: Effect of water spraying on the stability of a flotation froth and on the bubble sizes in the froth (from Klassen and Mokrousov, 1963).

Concentrate particle size mm	Weight destribution							
	W almont	Froth speared by nater (1./mm)						
	spraving	5 5	13	16				
~ 0 295 0 160 ~ 0 160 0 104 ~ 0 104 0 074 ~ 0 074	1 85 2 01 1 64 94 50	2 16 3 74 2 10 92 00	2 37 4 37 2 26 91 00	2 55 4 17 1 98 91 30				
TOTAL	100 00	100 00	100 00	100 00				

Table 1.2: Effect of froth washing on the size-by-size scheelite cleaner flotation (from Klassen and Mokrousov, 1963).

Russian experience showed that the degree of concentration was increased up to 3.26 times in scheelite flotation. This feature may be exploited to decrease the number of cleaning stages required in the flotation.

The effect of water addition rate on scheelite cleaner flotation is given in Table 1.2. Size-by-size scheelite recovery increases with increasing water addition rate from 5.5 to 16 1/min for coarse particles and decreases for fine particles. It appears that there is no detrimental effect of wash water on the detachment of coarse valuable particles.

Table 1.3 shows the effect of froth spraying in powellite (tungsten-molybdenum) ore flotation at two different wash water addition rates at the Lyangarska plant cleaner circuit. Increasing wash water addition dilutes the pulp content in the cleaner cells from 34.4% to 21.8%. There is a significant increase in Mo content from 2.7% to 7.2% (2.67 times) with a slightly increased recovery (1.06 times).

The effect of particle size and water flow rate in powellite flotation is given in Table 1.4. Fine particles are washed away, whereas large particles adhere to the froth. An increase in the recovery of floatable minerals is due to the larger amount of coarse particles remaining in the froth. As the froth layer rises to the top of the froth, the bubbles increase in size due to coalescence; this decreases the overall surface area of the bubbles, and leads to a competition for sites on the bubbles and to a displacement of mostly large particles. Water spraying

0 /	Conditions	Solute	in relative units.		
Products	spraving	"	Mo content	Mo recineri	
Feed to cleaning circuit	_	_	1 8	_	
Cleaner concentrate	Without spraying	34.4	2 7	23 76	
Cleaner concentrate	Spraving (7.5.1/mm)	23.4	5 1	24 88	
Cleaner concentrate	Spraving (13.1 /min)	21.8	7.2	25 1	

Table 1.3: Effect of froth washing in powellite ore flotation (from Klassen and Mokrousov, 1963).

	Weight distribution %						
Concentrate particle size	St ithout	3-61 4-1 2-97 4 0 0-62 1-4 92 80 90-4					
	sproying	7.5	13				
-0·295 + 0·160 -0·160 + 0·104 -0·104 + 0·074 -0·074	1·97 1·19 0 49 96 35	2-97 0-62	4·12 4 04 1·44 90-40				
TOTAL	100 00	100 00	100 00				

Table 1.4: Effect of froth washing on size-by-size powellite cleaner flotation (from Klassen and Mokrousov, 1963).

decreases bubble coalescence, increases bubble surface area and decreases the rejection of coarse particles.

Unfortunately, there has not been any published work on Western plant applications yet. The available information relies solely on private communications. However, there is a recently increasing interest to test the effect of wash water addition in mechanical flotation cells. The Zinc Corporation of America, New York, is planning to test it for talcous gangue depression in the cleaner circuits (Kemp, 1988). Les Mines Selbaie is ready to test wash water in their zinc cleaner circuit (Murarka, 1988).

Strong wash water spray is effectively used to increase the selectivity of sphalerite from chalcopyrite in the 4000 tpd Kipushi operation in Zaire (Feron, 1987). In this operation, it was observed that as soon as wash water spray stopped, significant amounts of sphalerite were lost.

In Canada, the Polaris mill is currently spraying wash water to sphalerite cleaner cell lips to remove dolomitic gangue from the concentrate. Some improvements are observed.

In Chile, some plants (e.g. El Salvador of Codelco) are using wash water in the copper cleaning stages, but there is no information available about these operations.

A private communication with Mr. S. Bulotavic from Lakefield Research Centre, who tested the wash water spray in some Russian plants, indicates that grade can be significantly increased. Hot steam was used, which passes through a screen mesh, and generates

hot water droplets.

1.3.3 Coal Applications

Klassen and Mokrousov (1963) and later Miller (1969) are among a number of authors who discuss the effect of froth sprinkling on coal flotation efficiency. They showed the froth sprinkling washes loosely held gangue particles from the froth and compensates for water lost in the upper froth layers, increasing froth stability. Thus, both grade and recovery can be improved. Miller (1969) showed that single stage flotation coupled with froth sprinkling yielded a product comparable to that obtained in a conventional rougher-cleaner combination Substantial savings in flotation volume (35%) were possible.

Results obtained by means of froth spraying in the flotation of coals at the Karagandinskaia Central Plant showed that coal recovery increased from 2.4% up to 11.8% while ash content of the sprayed froth decreased from 14.1% to 1.9%. Thus, wash water spray increased the carrying capacity of the froth (i.e. recovery) at a lower ash content. Table 1.5 shows that water spraying of the froth improves the quality of concentrate in flotation of both coarse and fine sizes of coal. There is an increase in the recovery of coal, particularly with large particles.

Klassen and Pikkat-Ordynsky (1957) applied water spraying on laboratory and plant coal flotation. Table 1.6 shows significant improvement in coal recovery at lower ash contents both plant and laboratory scales. Table 1.7 summarizes the size-by-size coal

recovery with and without wash water addition using two different industrial flotation cells. Coal recovery significantly increases for coarse sizes while there is a reduction in ash content. Comparison of cell #3 and #4 indicates that there is no significant problem using wash water with large cells.

Table 1.5: Size-by-size coal flotation performance with and without wash water (from Klassen and Mokrousov, 1963).

	Size	Without	With spraying			
Product	fraction mm	Recovery	Ash content	Recovery	Ash content	
Concentrate	0-5 -0 07	21 96 36 60	8·74 12 85	36-65 19 25	7·38 11·32	
Boiler fuel	0 5 -0 07	35·16 37·19	37·34 59 01	26 40 46-20	20 44 70-25	

Table 1.6: Effect of froth spraying on coal recovery and ash content.

	WITHO	UT SPRAYING	HTIW	SPRAYING
Products	RECOVERY	ASH CONTENT	RECOVERY	ASH CONTENT
concentrate	41.50	7.2	53.60	8.6
tailing	58.50	24.4	46.40	29.8
concentrate	27.10	8.8	49.80	7.7
tailing	72.90	20.2	50.20	26.8
concentrate	70.90	8.5	85.00	8.5
tailing	29.10	38.5	15.00	68.8
concentrate	46.70	7.3	53.00	6.8
tailing	53.30	24.5	47.00	25.4

			Cell	no+3			re11	no+4	
		Withou	spraving	With	apraving	Without	spraving	With	4prising
PRODUCTS	SIZE (µm)	R.	A.C.	R.	A.C.	R.	A.C.	R.	A.c.
		(1)	(3)	(%)	(*)	(1)	(\$)	(1)	(*)
	+2.0	-	-	-	•	-	-	-	-
	-2.0+1.0	0.5	3.0	2.3	2.9	1.7	3.8	4.8	2,6
CONCENTRATE	-1.0+0.5	14.5		19.8	3, 1	18.0	5.8	25.5	2.6
	-0.5+0.3	19.7	4.6	31.0	5.2	26.3	3.7	28.2	5.7
	-0.3	65.3	9.5	46.9	9.7	54.0	10.0	41.5	10.5
FOTAL		100.0	7.6	100.0	6,8	100.0	7.5	100.0	100.0
	+2.0	1.6	13.5	1.8	17.8	2.2	12.9	1.9	12.5
	-2.0+1.0	12.2		10.9	,.	10.2	16.3	10.5	
	-1.0+0.5	25.5	12.2	28.4	12.5	21.7	14.7	30.1	16,7
	-0.5+0.3	26.7	17.00	27.6	20.0	31.2	21.4	30.3	25,6
	-0.3	34.0	26.0	31.3	31.5	31.7	31.6	27.2	37.7
TOTAL		100.0	18.3	100.0	21.2	100.0	22.1	100.0	24,5

R: Recovery and A.C.: Ash content

Table 1.7: Size-by-size coal recovery with and without wash water using two different industrial flotation cells.

1.4 Temperature Effect in Flotation

On various flotation plants in South Africa (Prieska, Cu-Ni and pyrite) (O'Connor et al., 1985), Canada (Clarabelle, Cu-Ni) (Kerr and Kipkie, 1985), and Finland (Hukki, 1970), experience has shown that during the winter months, significant problems in terms of grade and recovery are experienced in flotation. Changes in ambient temperature fluctuations in the flotation pulp clearly influence the performance of the flotation process.

1.4.1 Objectives of Pulp Heating

Temperature is known to affect the flotation kinetics, since an increase in temperature reduces induction times, often at the expense of selectivity. This has been observed particularly for mixtures ofsphalerite and chalcopyrite. fluorspar and Temperature also affects the pH value, and the viscosity of the pulp, as well as the formation of bubbles. The temperature of the pulp affects the stability of the froth since the lower the temperature, the more stable is the froth. The effects of temperature on the kinetics of reagent adsorption have been studied extensively, much of the work being concentrated on temperatures higher than ambient where the rate of adsorption is higher although desorption is often enhanced (O'Connor et al., 1985).

It is well known that most chemical reactions will be accelerated by the increases in temperature. As a result, the following additional improvements can be expected to take place (Hukki, 1970):

- reduced need for desliming,
- improved floatability of fines,
- reduced conditioning time,
- reduced reagent consumption,
- reduced flotation time,
- reduced energy consumption in all phases of the process, and
- reduced contamination of tailing by excess reagents.

O'Connor et al (1985) showed that the equilibrium recovery of gangue decreased significantly as temperatures increased with sodium ethy xanthate (SEX) (Figure 1.7). A clearer understanding of the gangue flotation or entrainment process can be obtained from plots' of gangue-water recovery (Figure 1.8), which show that more gangue is recovered in the concentrate for the equivalent mass of water as pulp temperature decreases.

1.4.2 Industrial Applications of Hot Flotation

The vast number of papers written on flotation include only exceptional information on the effect of pulp temperature. Similarly, industrial applications at above ambient temperatures are rare. The classical examples are

- molybdenite copper separation
- hematite concentrate cleaning
 - (Cleveland Cliffs Iron Company, Republic Mine, Michigan)
- rare earths flotation
 - (Molybdenum Corporation, Mountain Pass Mill, California)
- sphalerite pyrite or pyrrhotite separation by SO₂ treatment (Brunswick Mining, Noranda, Bathurst)

Heating of pulp may take place before rougher flotation or it may be limited to cleaning of the existing concentrate produced by the conventional methods. In the latter case, one or more of the warmed up middling pulps may be returned to the rougher circuit; this as such can be advantageous.

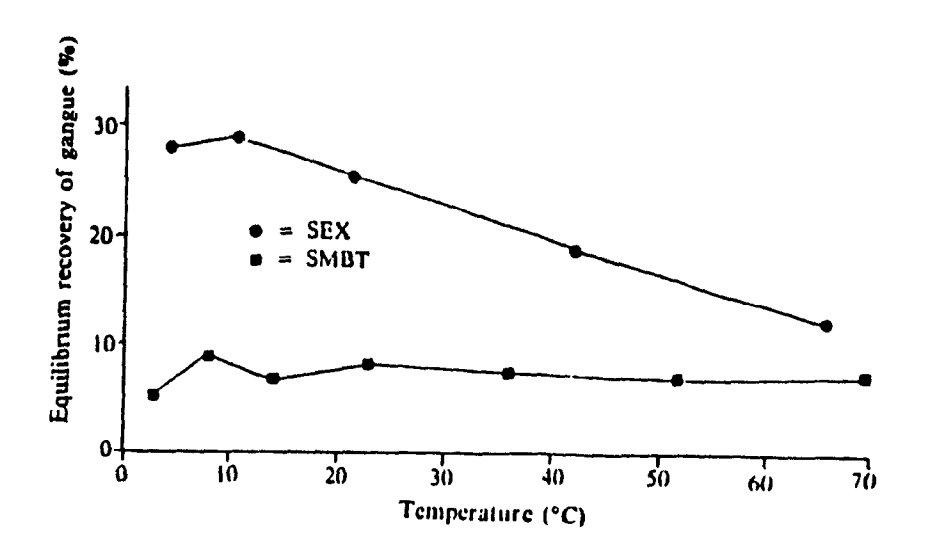


Figure 1.7: Effect of pulp temperature on gangue recovery (from O'Connor et al., 1985).

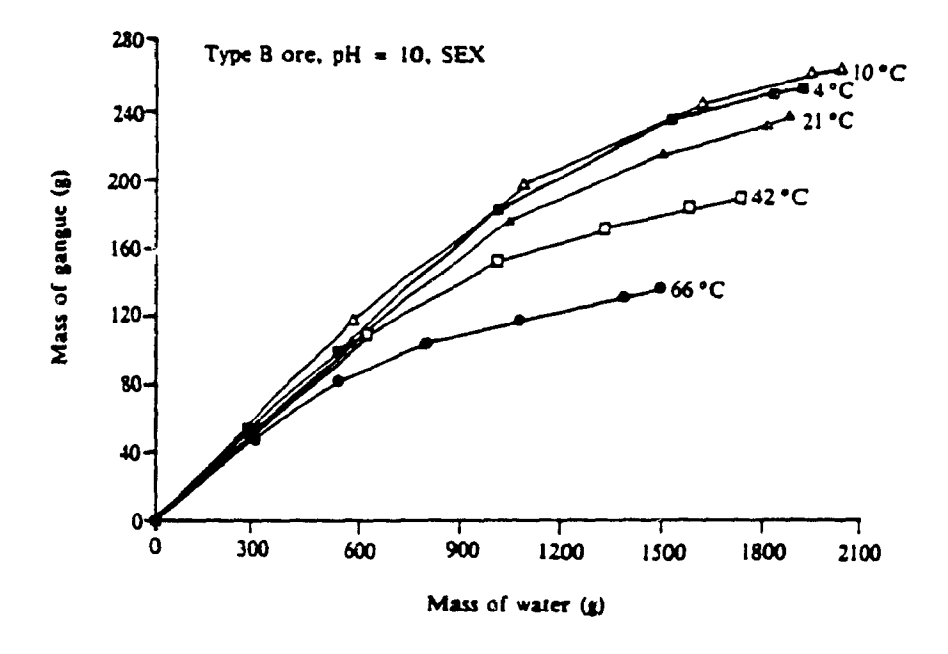


Figure 1.8: Relationship between water and gangue recoveries at different temperatures (from O'Connor et al., 1985).

The most promising fields for hot processing in sulfide flotation are the further cleaning of rougher concentrate, and especially the selective separation of sulphide minerals from bulk concentrate. In a general case the tonnage of such bulk concentrate amounts to a minor part of the initial feed and energy requirements are reduced.

The primary purpose of the treatment of an existing sulphide flotation concentrate is the partial or total removal of xanthate coatings from all sulphide surfaces. The additional purpose that always can be included is the reduction or elimination of the frother content within the concentrate. It is already known that temperatures of 80-100°C are very effective in hydrolyzing xanthates and for desorption of xanthate coatings from sulphide surfaces

After removal of xanthate coatings some difficult sulphide mineral separations from bulk concentrates can be accomplished more selectively than by standard procedures. This allows greater freedom in selecting conditioning agents and possibly eliminate the need for less attractive depressants, such as cyanide and SO_2

Typical examples of separation of sulphide minerals from bulk concentrates after removal of xanthate coatings include (Hukki, 1970):

- galena/chalcopyrite
- pentlandite/chalcopyrite
- cobalt-nickel-sulphides/chalcopyrite
- chalcopyrite/sphalerite
- pyrrhotite/sphalerite
- molybdenite/chalcopyrite

Typical examples of processes where hot flotation should always be considered include:

- final cleaning of concentrates of magnetite, hematite, ilmenite, chromite, rutile, scheelite, cassiterite, columbite-tantalite, monazite, fluorspar, apatite, rare earths, etc., from impurities such as silicates
- selective separation of two oxide minerals from their bulk concentrate typified by separations such as apatite from calcite, and scheelite from calcite.
- separation of feldspar from quartz.

Although heating of the pulp may improve recovery and/or grade, the economics must be carefully evaluated for each plant, since changes in temperature can cause large variations in flotation performance depending on the type of ore being floated as well as the type of collector being used Pulp heating is very costly in the cold Canadian climate. Pulp volume is large; however, froth volume is relatively small. In this study, the effect of wash water temperature on froth washing efficiency will be investigated. The effect of some chemical additives (i.e. depressants) in wash water on gangue entrainment will also be determined.

1.5 Summary

The literature survey showed that wash water sprinkling into the mechanical cells has been widely used for coal (bituminous) and ore mineral (andalusite, powellite, scheelite and molybdenite) flotation in Russia for 25 years. Published data suggest that there is a significant improvement in both concentrate grade and

recovery. From Russian practice, it seems that water might be sprayed 40-70% of the froth surface using perforated pipes or showers (sprinkles).

CHAPTER 2

A STUDY OF THE SLURRY PHASE OF MECHANICAL FLOTATION CELLS

A TWO PHASE SYSTEM

Introduction

The main objective of this chapter is to present some fundamental aspects of the flotation process in a gas-liquid system. The main emphasis is given to the slurry phase where the entrainment problem originates.

Gas holdup and bubble size are two of the most important factors characterizing hydrodynamics in a flotation cell holdup produced in a stirred vessel is a basic measure of the effectiveness of the contacting and mixing Although no universally applicable model to predict gas holdup is yet available, chemical engineering literature suggests a number of empirical correlations Table 2.1 shows a literature survey on gas holdup, interfacial area, and bubble size along with the vessel dimensions, operating conditions, and measuring methods. All investigators measured gas holdup; some attempted to measure interfacial area and bubble size. Therefore, in this study, the main attention was given to gas holdup measurements, due 10 measurement difficulties of bubble size and interfacial area in agitated vessels.

The earliest gas holdup models were derived from experiments with either pure liquids (coalescing systems) or aqueous solutions of electrolytes (non-coalescing systems), it was assumed that gas holdup was proportional to the dissipated energy per unit volume (P/V) and superfictal gas rate (J₀). These are indirect

		Vessel								Variables ?	leasured	
Reference	Vessel	diameter, T	D/T	H/T	ر ع	P/t ₁ V	liquid	gas hold-up	bubble	interfacial	power	measuring
		(m)			(10 ² m/s) (KW/m ³))		diameter	area	consumption	method
Calderbank	STC	0 19,0.51	0.33	EH/T:1	0,3-1.8	0.3-5	vater	x		z	x	light scatering
Westerterp	STC	0 14,0.15 0.19;0.6;0.9	0.2-0.7	EH/T.1	0.2-20	0.2-20	sulphate solution	×		x	×	chemical
Kaueck1	STC	0.191	0.4	H/T:1	1.4-3.1	0.6-7	water	*	×			photography
Reith	STC	0.19;0.45;1.2	0.4	H/T:1	4.7	0.2-20	sulphate solution	×		×	x	chemical
V.Dierendonck	STC	0.17,0.29 0.45;2.60	0.31-0.	55eH/T:1	0.8-5	2-20	water and sulphate solution	x	x			photography
Lee	STC	0.305	0.33	EH/T:1	0.3-0.9	0.1-1	sulphate solution	*		x	*	light scatering
Brown	STC	0.22	0.35-0.	58¢H/T:1	0.2-0.5	0.1-2	Water	x	x		×	photography
Hiller	STC	0.15;0.31 0.69	0.67	H/T:2	0.01-0.1	5	water,CO2	×	*			CO ₂ stripping
fung	STC	0.4	0.225 0.325-0	.45	0 1-2.16		water and ethylene glycol acetone sodium chloride sodium sulphate solutions					pressure gradien

Table 2.1: Literature survey on gas holdup, bubble size and interfacial area.

(STC: stirred tank gas-liquid contactor, D. impeller diamter, T: tank volume, H: power consumption, V: vessel volume, ϵ_1 : liquid holdup in the vessel).

correlations because the aerated power (P_a) is not usually related in any simple way to the power transmitted without gas being present (Mann, 1986).

More recent correlations have sought to avoid this difficulty (so as to provide prediction of gas holdup as a function of truly measurable variables). A recent relation, deduced through dimensional analysis, contains the air flow, the Weber number, and a scale factor (Yung et al., 1979) Some of these holdup equations will be tested for the flotation operation.

Bubble size, bubble rise velocity, spatial bubble distribution, and gas holdup profiles have a direct bearing on flotation. The two most frequent techniques for measuring bubble diameter in a bubble swarm are photography and calculation from holdup and interfacial area measurements. These two methods are compared in this work.

2.1 Theoretical Considerations

Figure 2.1 illustrates a vertically integrated theoretical flotation framework, which relates the fundamental physical phenomena to metallurgical performance, which largely determines the profitability of beneficiation. In order to achieve final metallurgical benefits, i.e. grade, recovery, and selectivity, there should be physical contacting between particles and bubbles The number of such bubble-particle collisions depends on energy dissipation. power input, holdups. gas, and liquid flowrates between the slurry and froth phases. These physical

BENEFITS SELECTIVITY AECOVERY **METALLURGICAL** GRADE **PERFORMANCE** BUBBLE RESIDENCE SURFACE MASS TRANSFER COEFFICENTS AREA MASS TRANSPORT MECHANICS BUBBLE POWER FLOW HOLD-UP ENERGY TION FLOW **PHYSICAL** CONTACTING

FLOTATION FRAMEWORK

contacting phenomena are in turn responsible for determining the capability of the flotation cell as a mass transfer device. Mass transfer in the cell is related to the bubble mechanics (terminal velocity, spatial bubble distribution etc.), available surface (interface) area, kinetic mass transfer rate constants, bubble size distribution, and residence time of gas, liquid, and solid phases.

The flotation process involves the interaction of three phases: solid, liquid, and gas. A flotation cell can be divided into two volumes: the pulp volume in which intimate particle-bubble contact is induced by the turbulent action of the impeller and the froth volume, which acts as a separating medium to segregate and remove the valuable minerals.

Although flotation is a three phase system, it is expedient to consider it first as a two phase system in order to understand basic phenomena taking place in the flotation cell. The pulp and froth volumes can be subdivided in the liquid and air (bubble) phases as well. Table 2.2 shows the summary of the correlations and variables used in this work.

2.1.1 Gas-Liquid Interfacial Area

Some principles of efficient contacting in continuous dispersed-phase flow may be seen by consideration of the relationship.

$$A = \frac{6 \cdot c}{d}$$
 2.1

AUTHOR	PA	RAMETER	VARIABLES	EOU.
Calderbank	A _{lp}	gas-liquid interfacial	Pa,V _{1p} ,J _g ,V _t ,N _{Re} ,N,D,	3,4
Arbiter	P _u	unaerated power	N _p ,N,D,O ₁	5
Michel&Willer	Pa	aerated power	P _u ,N,D,O	6
Luong&Voleski	Pa	aerated power	0,Ν,D,ρ,, σ	7
Pebble&Garber	V _t	terminal rise velocity	g,5 ₁ ,5 g,5	9
Van Dierendonk	$\epsilon_{ m p}$	gas hold-up	u,σ,ρ,Ν,Ν _ο ,D,L	10
Calderbank	ε _p	gas hold-up	$J_g, V_c, P_a, V_{1p}, \rho_p$	11
Rushton	ε _p	gas hold-up	P _a ,V _{lp} ,J _g	13
Yung et al's	ε _p	gas hold-up	0,N,D,L,p,σ	14
Westerterp	'n	min. impeller speed	D,L,p,3	15
Calderbank	o _c	contact time	P _a , K ,J	17
Calderbank	d bP	bubble diameter	Pa, Vlp, W1, Wg, P, Ep	18
Calderbank	^d bp	bubble diameter	$_{a}^{p}$, $_{1p}^{p}$, $_{p}^{p}$, $_{p}^{e}$, $_{\sigma}$	19
Bascur&Herbst	dbp	bubble diameter	$P_a, V_{1p}, CF, \epsilon_p, \rho_p, KI$	20
Graves&Kobbacy	η_{t1}	imp.dis. eff.	N,D,T,O	23
Grave & Kobbacy	η_{r_1}	imp.dis. eff.	т,q,ъ	22

Table 2.2: Summary of correlations used in this work.

where A: interfacial area per unit volume of mixed phase, m⁻¹
c: fractional volumetric gas holdup of dispersed phase
d: equivalent mean spherical bubble diameter, m

i.e. Sauter diameter which is defined as:

$$d_{sm} = \frac{\sum n.d_{bp}^{3}}{\sum n.d_{bp}^{2}}$$
2.2

where d: bubble size in the pulp phase, m
n: number of bubbles at a certain size

The interfacial area may be increased by increasing gas holdup or reducing bubble diameter. Small bubbles are more readily entrained into circulating liquid stream and so give more gas back-mixing than larger bubbles under similar hydrodynamic conditions.

Calderbank (1958) studied the interfacial area of gas bubble dispersions in agitated liquids by light scattering and reflection techniques using a photocell. Those techniques are only applicable in the case of small gas holdups (ε < 0.15). He proposed the following relationship:

$$A'_{1p} = 1.44 \left[\frac{(P_{a}/V_{1p})^{0.4} \rho^{0.2}}{\sigma^{0.6}} \right] \left[\frac{J_{g}}{J_{g}+V_{t}} \right]^{0.2}$$
2.3

where V_{\downarrow} : terminal velocity of bubbles in free rise, m/s

A_{1p}: gas-liquid interfacial area, m⁻¹

J: superficial gas velocity (air flowrate/cell cross-

sectional area), m/s ρ: pulp density, kg/m³

σ: liquid surface tension, N/m

 P_a : aerated power input, W V_{ip} : liquid volume in the cell, m^3

Eq. 2.3 is applicable in the range $N_{Re}^{0.7}(D.N/J_g)^{0.3} < 20000$. For $N_{Re}^{0.7}(D.N/J_g)^{0.3} > 20000$, the interfacial area is increased because suction of air takes place from the free surface. In flotation operation, abstraction of froth into the slurry is the indication of air capture from the atmosphere and is clearly undesirable. The amount of gas picked up at the surface, which increases with increasing impeller speed, can be significant for vessels under 0.25 m³ in size (Miller, 1974). The entrained gas circulates along with the gas introduced in the aerated mass. For flotation, $N_{Re}^{0.7}(D.N/J_g)^{0.3}$ is greater than 20000 and interfacial area in this region denoted by " A_{lp} " is estimated from Eq. 2.4:

$$Log_{10} \left[\begin{array}{c} 2.3 \text{ A}_{1p} \\ \hline A_{1p} \\ \end{array} \right] = 1.95 \ 10 \ N_{Re} \left[\begin{array}{c} N.D \\ \hline J_{g} \\ \end{array} \right]$$
 2.4

where N_{Re}: impeller Reynolds number (D².N. ρ)/ μ

N: impeller speed, rps D: impeller diameter, m

In order to evaluate interfacial area, the aerated power input and terminal bubble rise velocity must be measured or inferred from other operating variables.

Power Consumption: The power consumed in agitation reflects the conversion of tangential velocity at the blade tip to an entire spectrum of turbulent velocities, which dissipate the original rotational kinetic energy through vortex degradation and eventually through viscous resistance to heat.

Flotation is achieved under highly turbulent flow conditions. In the turbulent region $(N_{Re}>10^4)$, the power number is constant for a given cell geometry under a wide range of operating conditions (Rushton et al. 1950). The estimated power consumption is generally 80% of the installed power for industrial practice. The power number for a number of flotation machines operating in water was determined by Arbiter et al. (1969). Unaerated power consumption under the turbulent flow conditions, P_{u} , can be calculated using:

$$P_{u} = N_{p}. \rho_{1}. N^{3}. D^{5}$$
 2.5

where N_p : power number

Power consumption by impellers under aeration condition has been the subject of many studies. Mechanical power input in aerated and agitated systems can be calculated from the most popular and long-standing correlation of Michael and Miller (1962) and Miller (1974).

$$P_{a} = 0.706 \left[\frac{P_{u}^{2}. N. D^{3}}{Q^{0.56}} \right]$$
 2.6

where Q: air flowrate, m3/s

Recently, Luong and Volesky (1979) introduced the use of air flow and Weber numbers for calculating gassed power consumption:

$$\frac{P_a}{P_u} = C \left[\frac{Q}{N.D^3} \right]^n \left[\frac{N^2.D^3.\rho_1}{\sigma} \right]^n$$
2.7

where 0.497 < C < 0.514; m = -0.38; -0.198 < n < -0.18

Terminal Bubble Rise Velocity: The volume fraction of gas in a non-stirred gas-liquid reactor can be considered as the ratio between the superficial gas velocity, J_g , and a characteristic terminal velocity of the bubbles:

$$\varepsilon = \frac{J_q}{V_{\downarrow}}$$
 2.8

Pebbles and Garber (1953) have defined factors affecting the rise velocity of single bubbles in stagnant liquids under turbulent conditions. They found the relationship for the rise of bubbles in the constant velocity region.

$$V_{e} = 1.18 \left[\frac{g. \sigma. (\rho_{1} - \rho_{g})}{\rho_{1}^{2}} \right]^{0.25}$$

where V_{\bullet} : terminal bubble rise velocity, m/s

 ρ_1 : liquid density, Kg/m^3

 $\rho_{\rm d}^{1}$: gas density, Kg/m³

2.1.2 Gas Holdup

Gas holdup is one of the most important parameters characterizing the hydrodynamics of the flotation cell. Air (gas) holdup in the pulp zone, ε_p , expressed as the fraction of air volume in the cell, has also been correlated, for example, by Van Dierendonck et al. (1968) for electrolyte solutions:

$$\varepsilon_{p} = 0.075 \left[\frac{\mu. (N-N_{0}). D^{2}}{L. \sigma} \right] \left\{ \frac{\rho. \sigma^{3}}{g. \mu^{4}} \right\}$$
2.10

where μ : liquid viscosity, Nsec/m²

 N_{Ω} : minimum impeller speed for dispersion, rps

Physical properties represented in Eq. 2.10 were varied in the following range. Viscosity was between 0.0005 and 0.005 Nsec/m², surface tension 0.02 and 0.075 N/m, and pulp density 800 and 1300 Kg/m^3 .

Calderbank (1958) proposed the following equation for gas holdup in aerated vessels:

$$\varepsilon_{p} = \begin{bmatrix} J_{q} \cdot \varepsilon_{p} \\ \hline J_{q} + V_{t} \end{bmatrix} + \begin{bmatrix} 0.000216 & \frac{(P_{a}/V_{lp})^{0.4} \cdot \rho_{p}^{0.2}}{\sigma^{0.6}} \end{bmatrix} \begin{bmatrix} J_{q} \\ \hline J_{q} + V_{t} \end{bmatrix}$$
 2.11

where P: power input in aeration, W

V : slurry volume, m

P/V: power dissipation per unit volume, W/m³

 V_t : terminal bubble rise velocity, m/s

This equation can easily be solved by a computer using the Newton-Raphson root method. When P_a/V_{ip} tends to zero, ε is equal to J_g/V_i , which is a correct deduction and expresses the holdup obtained when air is distributed uniformly over the cell cross-section in the absence of sitation. When P_a/V_{ip} becomes larger, the first term is negligible and Eq. 2.11 yields:

$$\varepsilon_{p} \quad \alpha \left[\begin{array}{c} P_{a} \\ \hline V_{1p} \end{array} \right] \quad . J_{g}^{0.5}$$
 2.12

The above equation agrees fairly well with experimental results obtained by Rushton et al. (1944) for mixing vessel of large capacity:

$$\varepsilon_{p} = \begin{bmatrix} P_{a} \\ \hline V_{1p} \end{bmatrix} \qquad J_{g} \qquad 2.13$$

Calderbank (1958) tested the following variable ranges. Surface tension was between 0.022 and 0.073 N/m; pulp density, 790 and 1600 Kg/m³; effective kinematic viscosity, 0.0005 and 0.028 Nsec/m²; gas rate, 0.003 and 0.018 m³/sec, and power dissipation per unit volume, 0.21 and 4.23 W/m³. These variables are in the order of magnitude of normal flotation operation.

One of the most recent reviews about gas-liquid stirred vessel mixers by Mann (1986) showed that there was no satisfactory unified description of the internal two-phase mixing processes.

He presented a number of correlations for gas holdup in a stirred vessel. Among them, Yung et al's (1979) relationship included the air flow number, the Weber number, and a scale factor on gas hold-up:

$$\varepsilon_{p} = 0.52 \left[\frac{Q}{N.D^{3}} \right]^{0.50} \left\{ \frac{\rho.N^{2}.D^{3}}{\sigma} \right\}^{0.65} \left[\frac{D}{L} \right]^{1.4}$$
 2.14

Minimum Impeller Speed for Air Dispersion: When a gas stream is blown in a liquid under agitation, there is a minimum impeller rotational speed, N_0 , to achieve gas dispersion. Westerterp et al. (1963) suggested the following relationship:

$$N_{O} = \begin{bmatrix} \frac{1}{D} \end{bmatrix} \begin{bmatrix} \frac{\sigma \cdot g}{\rho} \end{bmatrix}^{0.25} \begin{cases} 1.22+1.25 & \frac{L}{D} \end{cases}$$
 2.15

where L: cell diameter, m
D: impeller diameter, m

It can be assumed that the impeller tip (peripheral) velocity must exceed the gas rising velocity a certain number of times in order that all large gas bubbles supplied be broken up into small bubbles. Application to flotation cells show that impeller speeds actually used are higher than this minimum value (Barbery, 1982).

Contact Time: The contact time of a gas with liquid per unit depth, Q_c , is estimated from gas holdup. Denoting the average liquid depth as H, the mean residence time of gas bubbles as τ , and superficial gas velocity as J_c , we have

$$\tau = \frac{\varepsilon}{J_{q}} \quad H \qquad 2.16$$

The contact time per unit depth of liquid is given by:

$$Q_{c} = \frac{\varepsilon}{J_{g}} = K \left[\frac{P_{a}/V_{1p}}{J_{g}} \right]$$
 2.17

where K is a constant, and varies between 1.3 and 1.6 (Calderbank, 1967).

Gas holdup increases with increasing superficial gas velocity, while contact time is decreased. For example, a 50% increase in J_g causes a 25% increase in gas holdup and 17% decrease in contact time per unit depth of liquid.

2.1.3 Bubble Size

Average bubble size results from equilibrium between stresses applied (especially shear stresses) and surface forces. The Weber number is significant, as well as the power dissipated per unit volume, P_a/V_{lp} , which according to Kolmogoroff's theory, controls the size of the smallest eddies in fully developed turbulent flow. Various correlations have been put forward. Calderbank (1958) first suggested:

$$d_{bp} = 2.25 \left[\frac{\sigma^{0.6}}{(P_a/V_{1p})^{0.4} \cdot \rho^{0.2}} \right] \epsilon_p^{0.4} + \left[\frac{\mu_g}{\mu_1} \right]$$
 2.18

where μ_l , and μ_g : liquid and gas viscosities $d_{pp}: \mbox{ Sauter mean bubble diametr in the pulp phase.}$

Later on, Calderbank (1958) proposed the following equation:

$$d_{bp} = 4.15 \left[\frac{\sigma^{0.8}}{(P_{a}/V_{1p}) . \rho_{p}^{0.2}} \right] \varepsilon_{p}^{0.5} + 0.0009$$
 2.19

Miller (1974) tested Calderbank's Equation and found that it gave good estimations if the superficial gas velocity was less than 0.02 m/sec; surface tension was between 0.0217 and 0.0735 N/m; pulp density, 790 and 1600 Kg/m³; and effective kinematic viscosity 0.0005 and 0.028 Nsec/m². Most of these ranges are in the order of magnitude of normal flotation operation. Average bubble diameter can also be calculated from measured gas holdup and calculated interfacial area values (Eq. 2.4) using Eq. 2.1.

Harris (1976) has especially insisted on the importance of frother addition on the control of bubble size in this type of system. Bascur and Herbst (1982), who preferred frother concentration rather than surface tension, used the following equation to calculate average bubble diameter in the slurry phase.

$$d_{bp} = K_{1} \left[\frac{\varepsilon_{p}^{0.4}}{\rho_{p}^{0.2} (P_{a}/V_{1p})^{0.4} CF^{0.344}} \right]$$
 2.20

where K_{i} : constant (function of each system)

CF: frother concentration

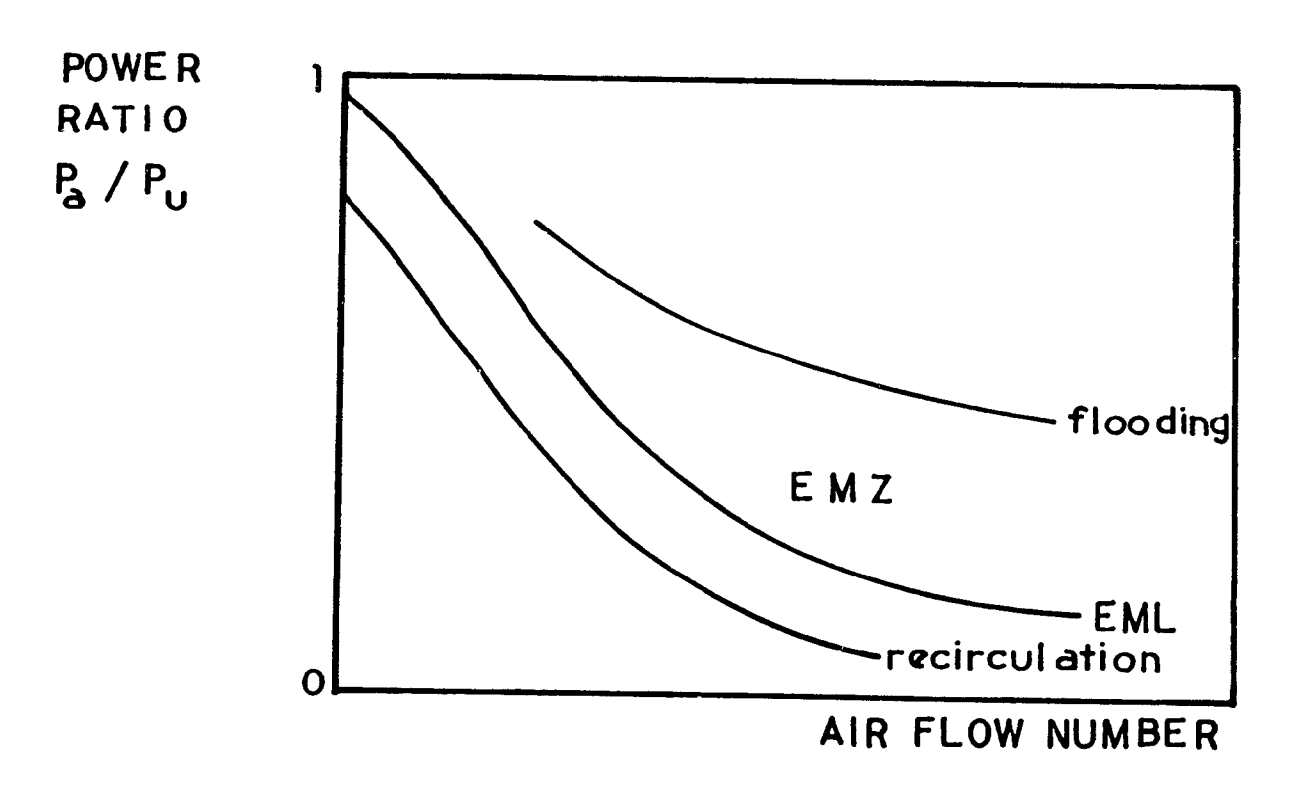
Eq. 2.20 easy to use in plant practice since the frother concentration is used, rather than surface tension. However, this makes it less fundamental than other correlations, and it does require calibration.

2.1.4 Gas Mixing Regimes in Agitated Vessels

There are three different gas mixing regimes described by Nienow et al. (1986) at constant gas flowrate (Figure 2.2). The region lying between the minimum and maximum conditions is called the efficient mixing region, where all of the sparged gas passes through the impeller just once. To the right of the minimum is the flooding region and to the left of the maximum the recirculation region.

The efficient mixing zone (EMZ) is established when all of the sparged gas coalesces with and is dispersed from the cavities behind the impeller blades (Figure 2.3). When recirculation occurs, more gas is transported from the bulk of the tank to the impeller and the rate of gas coalescence with the cavities then exceeds the sparging rate. In the flooding region, the gas cavities are only able to capture part of the sparged gas, while the rest flows more or less vertically to the surface





; 🛊

Figure 2.2: Determination of gas mixing regimes.

EMZ: efficient mixing zone EML: efficient mixing line P: aerated power consumption

 P_{u} : unaerated power consumption



Figure 2.3: Air bubbles attached to trailing edges of impeller blades (high-speed photograph) (from C.C. Harris).

without being dispersed. The flooding region defines the lower limit of the efficient mixing zone.

progression of internal flow regimes observed at increased impeller speed and constant aeration rate is given in Figure 2.4. At a very low impeller speed, gas short-circuits up the shaft forming a partial bubble column shown in Figure 2.4a. condition is called "impeller flooding", as the impeller becomes engorged with gas and is by-passed by excess gas without Under flooding conditions the impeller tip adequate dispersion. speed is less than the bubble rise velocity; therefore not all the air stream introduced can be captured and dispersed into the cell by the impeller. As impeller speed increases, gas is dispersed to form a more homogeneous gas-liquid mixture in the efficient mixing zone (Figure 2.4b). Circulation of gas downward will take place if impeller speed is further increased (Figure 2.4c). Most flotation machines have the conditions shown in Figure 2.4b. of the flotation cell manufacturers prefer to have recirculation to increase intimate contact between particles and gas bubbles, like in Denver DR cells. Recirculation may not be deleterious to metallurgical performance, but flooding is and should be definitely avoided.

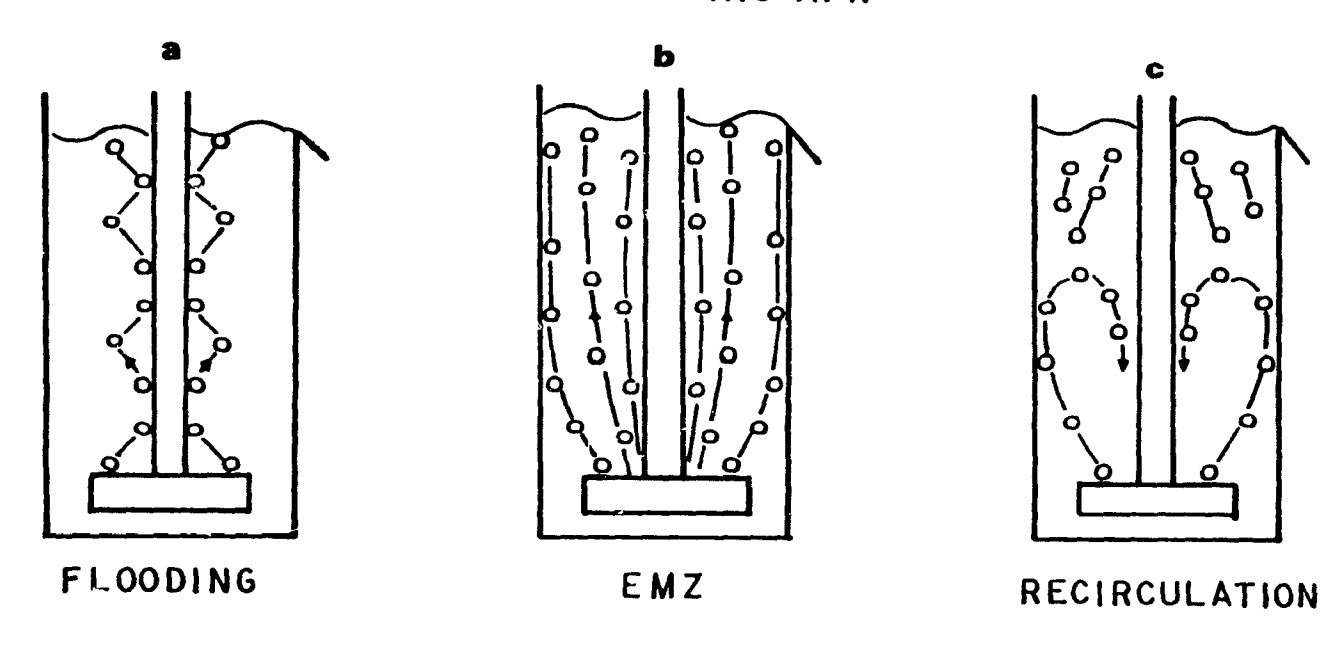
<u>Impeller Dispersion Efficiency:</u> An impeller dispersion efficiency is defined such that:

rate of gas coalescence with impeller cavities

η = _______ 2.21

rate of gas sparging

INCREASING AFR



CONSTANT AFR

Figure 2.4: Flow regimes in a flotation cell.

AFR: air flow rate

EMZ: efficient mixing zone

where $\eta = 1$ in the efficient mixing zone

 η < 1 in the flooding region

 $\eta > 1$ in the recirculation region

Greaves and Kobbacy (1981) give the following equations, for impeller dispersion efficiencies in the recirculation (η_{r1}) and flooding (η_{r1}) zones, respectively:

$$\eta_{r1} = 4.13 \left[\frac{N^{2.53} D^{5.93}}{T^{2.45} Q^{0.33}} \right]$$
2.22

$$\eta_{f1} = 1.52 \left[\begin{array}{c}
0.20 & 0.29 \\
T & Q \\
\hline
D^{1.74}
\end{array} \right]$$
2.23

where T: cell diameter, m
D: impeller diameter, m
N: impeller speed, rps
Q: air flowrate, m / s

If η_{rl} and η_{fl} are calculated for certain points of operation from the above equations, they will satisfy the conditions given below:

 $\eta_{r1} > 1$ recirculation zone

 $\eta_{fl} < 1$ flooding zone

 $\eta_{r1} \leqslant 1 \\
\eta_{f1} \geqslant 1$ efficient mixing

2.2 Experimental

2.2.1 Set-up

The experimental set-up, which was used to measure gas holdup, is shown schematically in Figure 2.5. It consists of a plexiglass modified Denver flotation machine, а (0.15*0.15*0.32 m), water manometers, a Tucessel CD 810 digital conductivity meter, an electrode assembly, and a data acquisition system. Details of the flotation cell and machine are given elsewhere (Kaya and Laplante, 1986). Six pressure taps at 5 cm interval were drilled at the back side of the flotation cell and connected to the water manometers in order to measure pressure Air bubble entry to the water drop at different levels. manometers was prevented by steel wool plugs. Dowfroth 250C at a concentration of 10 ppm was used as a frother unless otherwise All experiments were performed batch wise without feed, tail, and overflow.

The cables from the electrode assembly were connected to an 8-channel multiplexer, which receives timed signals from the master clock card and sends signals to the conductimeter. Temperature corrections can be made automatically with the conductimeter if the temperature probe is used. Conductivity measurements are firstly converted into currents (0-5 volts) by the conductimeter, and then amplified (0-10 volts) by an amplifier. After analog-to-digital conversion by an 8-bit A/D converter, results (i.e. digital signal reading) are stored by an Apple compatible computer.

- 1. Conductivity electrode
- 2. Pressure taps
- 3. Water monometers
- 4. Wash water distributor
- 5. Concentrate launder
- 6. Flotation cell
- 7. Shaft and impeller
- 8. Electronic level control probes
- 9. Varistaltic pumps
- 10. Mixer

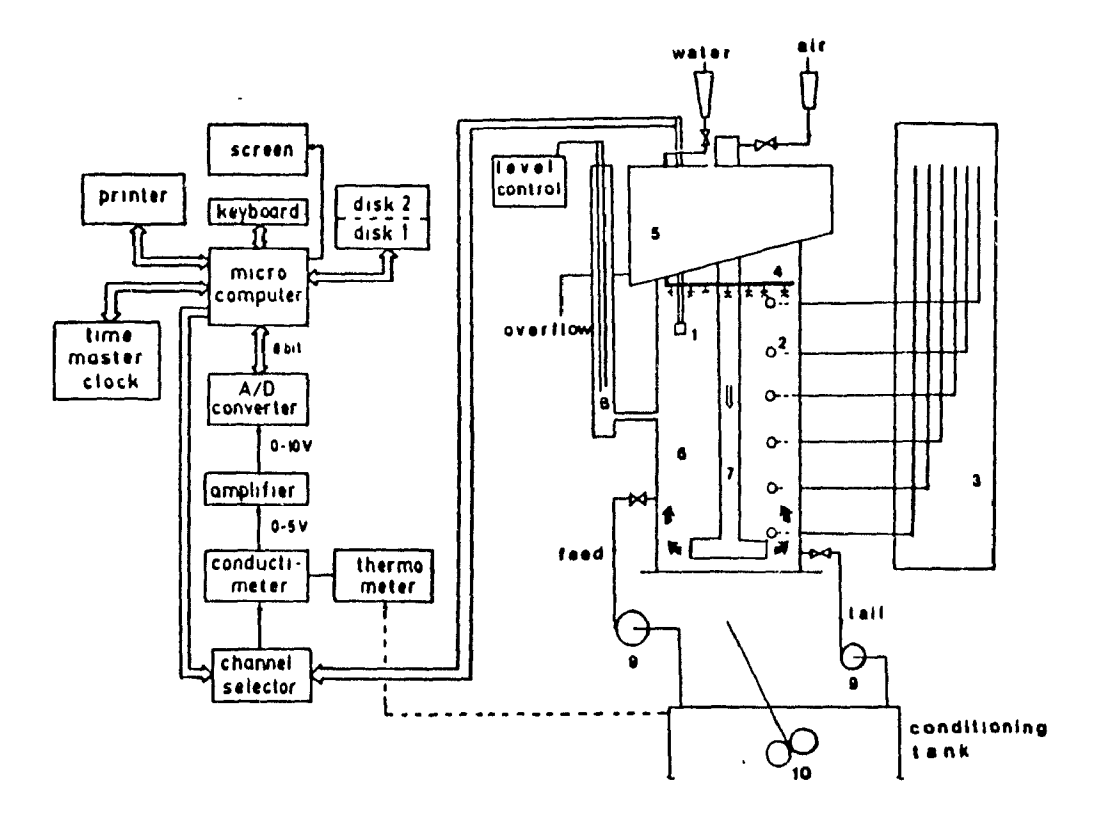


Figure 2.5: Experimental set-up for conductivity and pressure gradient measuremnts.

Two square electrodes (1*1 cm²) made of stainless steel were connected to the conductimeter (measurement reproducibility better than ∓0.3%) These electrodes were fixed in a plexiglass cubic prism cage (1.5*1.5*1.5 cm) open at the top and bottom to allow liquid flow between the electrodes. It was verified that with this geometry, the ion path between electrodes deviates from the cross-section enclosed by the electrodes only 0.5 cm above and below the cage, thus providing a very localised measurement of conductivity.

2.2.2 Overall Gas Holdup Measurements in the Recovery Zone Using Level Rise and Overflow Techniques

Level Rise Technique: A first simple method of measuring overall gas holdup in a flotation cell without solid phase is to measure the height of the aerated liquid height, h_a , and that of clear liquid without aeration, h_u . The average fractional holdup is equal to:

$$\varepsilon_{\mathbf{p}} = \frac{\Delta h}{h_{\mathbf{a}}}$$
 2.24

where Ah: difference in level with and without air, m

The level rise method was used with the modified plexiglass cell in the presence of frother.

Overflow Technique: A second simple method of determining average holdup is to fill the cell up to the cell lip and measure the volume of displaced liquid when air is introduced. The overflow technique was used in order to extend the results to

other laboratory flotation machines and cells. Therefore, two different laboratory flotation machines with three different original (commercial) set of cells were tested. First, the modified Denver flotation machine (D12) was used with three glass Denver cells: second, an Agitair LA-500 flotation machine was used with three original Agitair cells at different sizes. Cell dimensions, effective volumes, and impeller diameters are given in Figure 2.6.

In the overflow technique, a digital balance was placed under the flotation cell to weigh the amount of water in the cell before and after aeration. Both level rise and overflow methods are best suited to systems with a quiescent liquid surface.

2.2.3 Point Gas Holdup in the Recovery Zone Using Conductivity Measurements

The recovery zone of a mechanical flotation cell is extremely complex with respect to the gas phase; however, it is possible to get some valuable information about the internal flow patterns using point holdup measurements with conductivity. The conductivity technique can be used not only for determining the point holdups but also for determining local holdups as a function of height in the cell.

The measured solution conductivity is based on the measurement of resistance. This is usually accomplished by means of a Wheatstone bridge. An alternating current of about 1000 Hertz is used to prevent polarization problems at the electrodes. Direct current produces gas bubbles at the electrodes.

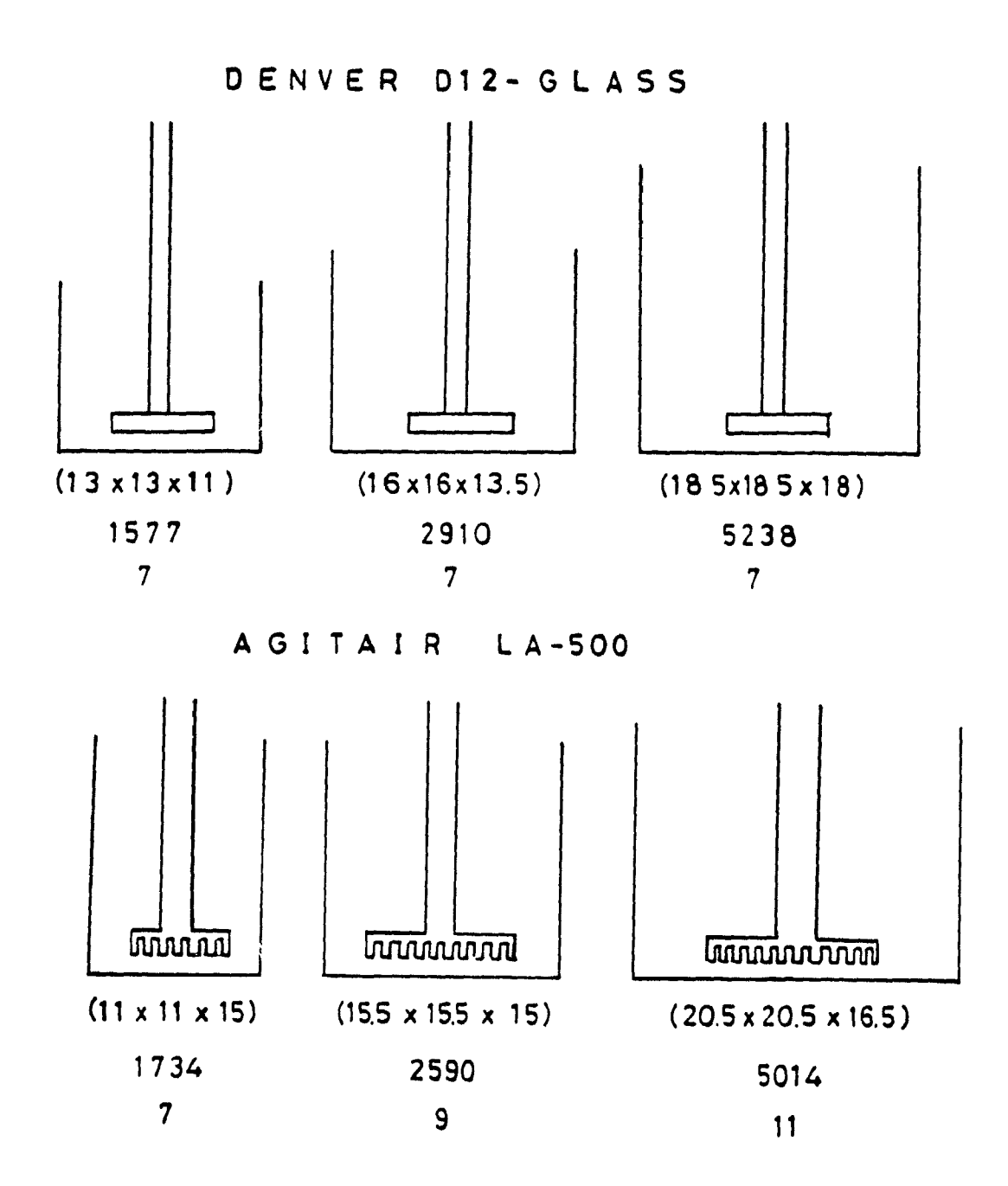


Figure 2.6: Dimensions of the commercial flotation cells and impeller mechanisms tested in this study (scaled drawing).

Cell dimensions are (1, w, and h) in cm. Cell volumes are in cm 3 Impeller diameters in cm.

The resistance of a conductor is proportional to its length

(L) and inversely proportional to its cross-section (A):

$$R = q (L/A)$$
 2.25

Conductivity is reciprocal of the resistivity:

$$C = 1/(qL/A) = K/(L/A)$$
 2.26

where K: specific conductivity

L/A: cell constant

q: specific resistance

Electrolyte solutions, like other conductors, obey Ohm's law. Consider a column of electrolyte of a cross-section 1 m² to which a potential gradient of 1 V/m is applied (Figure 2.7) The current passing will depend on the number, speed, and charge of the ions. All ions present contribute and the total current will be the sum effect of the cations migrating towards the cathode and the complementary effect of negatively charged ions moving in the opposite direction.

The conductivity of a liquid system with a fixed ion concentration at constant conditions is proportional to the length of the path between two electrodes. If the tortuosity factor remains approximately constant, conductivity should be proportional to the liquid holdup in the bed.

$$C = K.(A/L)$$
 2.27

$$C_{\varepsilon} = K. (A(1-\varepsilon)/L_{\varepsilon})$$
 2.28

where C_g: conductivity with aeration

C: conductivity without aeration

L: length between electrodes in the absence of air

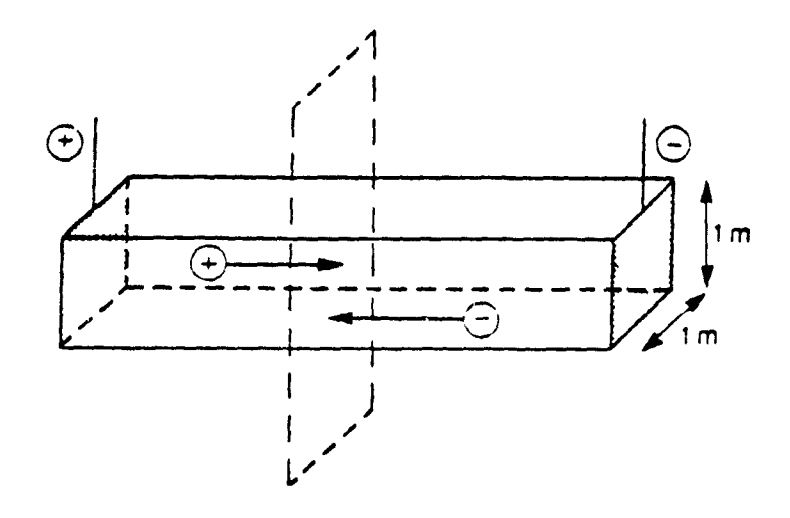


Figure 2.7: Diagrammatic representation of conductivity measurements.

 L_{ϵ} : length between electrodes in the presence of air

A: electrode area

Conductivity can be rendered dimensionless by dividing it by the conductivity obtained in the absence of gas.

$$\begin{array}{ccc}
C_{\varepsilon} & (1-\varepsilon).L \\
\hline
C & L_{\varepsilon}
\end{array}$$
2.29

Yianatos et al (1985) developed a geometrical model of tortuosity in a gas-liquid system, very similar to that of Maxwell (1873):

$$\frac{L_{\varepsilon}}{L} = 1+0.55\varepsilon \qquad 2.30$$

Using this model, gas holdup in the slurry phase is inferred from conductivity with and without gas:

$$\varepsilon_{p} = \frac{C - C_{\varepsilon}}{0.55C_{\varepsilon} + C}$$
2.31

2.2.4 Local Gas Holdup in the Recovery Zone Using Pressure Measurements

The local gas holdup is defined here as the volume occupied by gas bubbles as a function of the clear liquid volume between two pressure taps in the flotation cell. Since the density of the gas is usually negligible compared to that of the aerated liquid it follows that:

$$r_{p} = \frac{\rho_{1} - \rho_{p}}{\rho_{p}}$$
2.32

The bulk density of aerated liquid (ρ_p) was measured by means of pressure taps, which were connected to water manometers to transmit only pressure. From the difference in readings of two separate pressure taps which are open to the atmosphere at the other ends, the bulk density of the aerated liquid was calculated by the following relationship:

$$\varepsilon_{p} = \frac{h}{1}$$
 2.33

where L: vertical distance between two pressure taps
h: difference in the readings of the manometers in terms
of clear liquid head.

2.3 Results and Discussion

2.3.1 Overall Gas Holdup in the Recovery Zone

Effect of Physical Operating Variables: Overall gas holdup as a function of superficial gas rate is shown in Figure 2.8. Average gas holdup increases with increasing superficial air rate. In order to predict overall gas holdup in a stirred flotation cell, Eqs. 2.10, 11, and 12 were tested at different operating conditions. Van Dierendonck's model (1968, Eq. 2.10), which is independent of aeration rate, significantly overestimated the average gas holdup in the recovery zone. However, Calderbank's model (1958, Eq. 2.11) with Luong and Volesky's aerated power

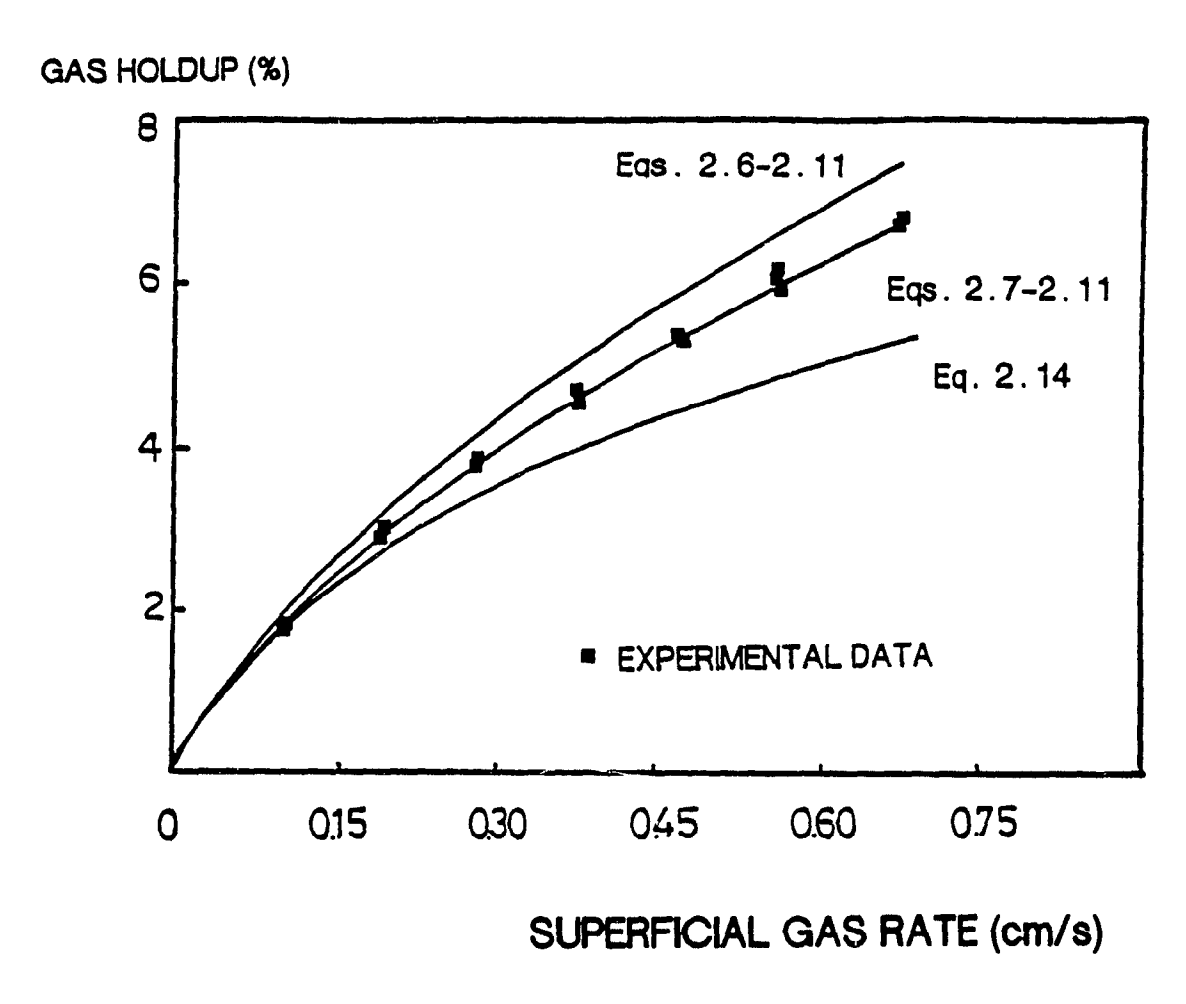


Figure 2.8: Experimental and predicted overall gas holdup in the slurry phase of flotation cell (N: 1500 rpm, 10 ppm frother).

consumption (Eq. 2.7) yielded a very close agreement with experimental data. Michael and Miller's aerated power Eq. 2.6 in conjunction with Eq. 2.11 slightly overestimated the holdup measured, while Yung et al's (1979) dimensional Eq. 2.14 slightly underestimated it.

The effect of impeller diameter (D), impeller speed (N), cell cross-sectional area (S), cell volume (V), and surface tension (σ) calculated from Eq. 2.11 with Eq. 2.7 on the overall gas holdup is given in Table 2.3—Comparison of predicted and measured effects of impeller diameter, impeller speed, slurry volume, and surface tension shows reasonable agreement. The mean gas holdup increases with increasing either impeller diameter or speed or decreasing cell area, cell volume or surface tension of the system.

It should be borne in mind that increasing impeller diameter and speed increases power consumption and impeller wear. An increase in gas holdup with decreasing cell cross-sectional area can be achieved in deep flotation cells. Reducing surface tension with frother to increase gas holdup has the drawback of increased reagent cost; also it is generally preferable to use frother addition rate to control froth kinetics (e.g. the Matagami mill, Konigsmann et al., 1976). It can be readily concluded that aeration is a more effective variable to control fractional gas holdup in the recovery zone than the other five variables investigated here.

Table 2.3: Effect of some physical operating variables on average gas holdup in the slurry zone of the modified cell. D: impeller diameter, N: impeller speed, S: cell cross-sectional area, V: cell volume, and σ surface tension.

	(%) estimated ε_g (from Eqs. 11&7)	(%) experimental ε_g
D(m) 0.05 0.07 0.09	4.76 6.22 8.15	5.98 8.25
N(rpm) 1200 1500 1700	5.59 6.22 6.65	5.50 5.98 6.50
S(cm ²) 105 205 305	10.37 6.22 4.61	
V(cm ³) 0.0036 0.0060 0.0074	6. 62 6. 47 6. 22	6.70 6.50 5.98
σ(N/m) 0.055 0.065 0.072	6. 48 6. 22 5. 57	6.50 5.93 5.50

Effect of Cell Geometry: Table 2.4 compares the experimental and estimated overall gas holdups in three different original Denver and Agitair cells using the overflow technique at different superficial gas rates. There is a very good agreement between experimentally measured and predicted overall gas holdups for the three Denver cells which have the same impeller. For Agitair flotation machines, the impeller diameter increases with

increasing cell volume while cell height remains almost constant. Agitair flotation machines also have a finger type of impeller (Pipsa). Except for the smallest cell, the predicted measured gas holdups are quite different (i.e. Eqs. 2.11 and 2.7 fail to predict the overall holdup). This is mainly related to different scale-up criteria used for Agitair flotation machines. Table 2.5 shows the effect of some Effect of Chemical Additives: inorganic salts on overall gas holdup in the recovery zone. Na SO, NaCl, Na CO, and CuSO, were used as inorganic salts at an arbitrary concentration of 0.1 mole/L. Table 2.5 also shows pH, standard electrode potential (SHE) (mV), solubility, and use of salts in flotation. Comparison of overall gas holdups in the presence of salts with fresh water reveals that there is an increase in gas content due to presence of salts, except for NaCl. Na SO, which significantly increases gas holdup, does not hange the medium conditions significantly (i.e. pH and mV). 250C at a concentration of 10 ppm gives the maximum gas holdup. Na CO and CuSO drastically alter the pH and potential of the medium and are commonly used in flotation as pH regulator and activator, respectively. Thus, they cannot be used as a holdup modifier.

Table 2.4: Comparison of experimental and predicted overall gas holdups (Eq. 2.7 and 2.11) for the commercial flotation cells using the overflow technique. (N: 1500 rpm).

Cell Dimensions	Superficial Gas Rates, cm/s 6 0.4 0.2					
(L*W*H)	- -	_	exp.			calc.
Denver D12 Flotation Machine and Commercial Cells						
(18.5*18.5*18)	5.9 7 0.6	6.3	5.270.5	5.2	3.7∓0.4	3.7
(16*16*13.5)	8.0∓0.7	8.1	7.5∓0.6	7.6	5.4∓0.4	5.6
(13*13*11)	14.5∓1.4	14.7	12.1∓0.9	12.0	8.6∓0.9	8.6
Agitair LA-500 Flotation Machine and Commercial Cells						
(20.5*20.5*16)	22.0∓1.1	7.4	21.175.6	6.0		
(15.5*15.5*15)	16.171.3	10.1	11.3∓1.4	8.2		
(11*11*15)	16.6∓1.6	16.8	13.8∓1.1	13.6		

Table 2.5: Effect of some inorganic salts on overall gas holdup in the slurry phase of a Denver cell (16*16*13.5 cm Glass) using the overflow technique. (Unpurified analytical grade inorganic salts were used).

Chemical additives	ε _q (%)	рН	v(mv)	solubility (at 5°C)	use in flotation
CuSO ₄	10.5	5.3	118	soluble	activator
NaCl Na ₂ SO ₄	8.5 17.0	8.0 8.2	-62 -70	soluble sparingly	
Na ₂ CO ₃	12.2	11.3	-360	sparingly	pH regulator
Fresh water	8.7	8.3	-76		
Dowfroth 250 (10 ppm)	23.4	7.8	-45		frother

The effect of Na₂SO₄ concentration on gas holdup in the recovery zone is given in Table 2.6. There is a very significant increase in gas content with increasing Na₂SO₄ concentration and slight froth formation if the concentration is higher than 0.05 moles/1. Therefore, Na₂SO₄ can be used to reduce coalescence in the slurry phase along with the frother. Lee and Meyrick (1970) reported 2-5 fold increases in gas holdup at higher sodium sulfate dosages than used here.

Table 2.6: Effect of Na₂SO₄ concentration on overall gas holdup in the recovery zone of a Denver cell (16*16*13.5). (N: 1500 rpm and J_a : 0.6 cm/s).

Na ₂ SO ₄ concentration (moles/1)	overall gas holdup $\epsilon_{_{f g}}$ (%)
0.0000	8 .70 ∓ 0.79
0.00 63	9.88 7 1.10
0.0125	10.24 ∓ 0.96
0.0250	11.31 7 1.05
0.0 500	13.42 ∓ 1.38
0.1000	17.08 ∓ 1.81

Since the surface tension of the medium increases with increasing the salt concentration, the main mechanism of increase in gas content in the recovery zone may be due to the adsorption of SO₄ anions at the gas-liquid interface creating an electrical double layer which prevents bubble coalescence. Generally anions are less hydrated (i.e wetted by water) than cations; thus, Na[†] cations most probably are hydrated (energy of hydration: 97 Kcal/gion).

Sodium sulfate can be used in flotation for the following reasons. First, bubble coalescence in the recovery zone is hindered due to electrical repulsion forces generated by the adsorption of sulfate anions at the gas-liquid interface, which creates an electrical double layer (Marrucci and Nicodemo, 1967). Second, frother dosage can be minimized for micro bubble generation (i.e. high gas content), which normally requires relatively large amounts of frother. Probably, the most clear-cut benefits of using the salt flotation technique is an increase in flotation kinetics, with flotation rates 10-15% higher. Youn (1982) found significant improvements in coal flotation with macro bubbles and inorganic salts.

The origin of the frothing action depends on Gibbs' adsorption theory. A solution froths when (-C.do/dC) has a finite value, negative or positive. When do/dC=0, there is no frothing (Wrobel, 1953). When a frother is added to the water do/dC has a large positive value, and therefore -Cdo/dC is large when C is small. Solutions of inorganic salts give, in general, a small positive value for do/dC, and therefore -Cdo/dC has a definite value only when C is large. This is why inorganic salts are used in this study at a relatively high concentration compared to Dowfroth 250.

The introduction of inorganic salt into water usually increases surface tension slightly; the surface layer is consolidated by the electrolyte, which tends to move into the body of the solution. In this case, there is a negative adsorption

(surface deficiency) of the surface inactive electrolytes, which concentrate in the body of the solution, and increase its surface tension, in contrast to positive adsoption (surface excess) of frother. Water dipoles which hydrate the electrolyte molecules (which lie in the liquid phase in the vicinity of the air-water interface) will also form compounds with water dipoles near the surface of such compounds formed if there is sufficient difference between the electrolyte concentration in the bulk of the solution, and consequently where there is a definite difference between the surface tension values of pure water and electrolyte solution. This is the reason for formation of a stable froth in concentrated Frothing in concentrated salt solutions is of salt solutions. prime importance in flotation of soluble salts from their saturated solutions; flotation is possible in these cases without the addition of frothers (Glembotskii et al., 1972).

Tested electrolyte concentrations in this study seem high but sodium sulfate is widespread in occurence and is a common constituent of many alkali lakes and rivers as well as sea water around the world. Many saline lakes throughout the world contain varying amounts of sodium sulfate. In Sackatchewan, Canada, eight major lakes (Ingelbright, Whiteshore, Horseshoe, etc.) and in the United States, two others (Searles and Great Salt) are available for sodium sulphate production. In coastal areas, sodium sulphate bearing sea water could be used.

Russians discovered in the early 1930s that the flotability of coal and naturally hydrophobic minerals can be improved in the presence of inorganic salts. Using solutions with relatively high concentrations (1 to 3%) of inorganic salts, coal flotation was achieved without using either a frother or a collector. Yound (1982) tested 32 different salts for coal flotation and found a better separation efficiency with sulfate salts at a concentration around 0.1 moles than with frother. Ray and Raffinot (1966) reported some successful flotation operations (Pb-Zn, Pb-Zn-Cu, Fe, cryolite, and coal) in pure sea water near the Mediterranean shores.

2.3.2 Local Gas Holdup in the Recovery Zone

The distribution of local gas holdup in a flotation cell is non-uniform. Figure 2.9 shows the observed distribution data from the pressure gradient measurements for 1200 and 1500 rpm, respectively. Cas holdup shows a maximum value just above the impeller and at the slurry-froth interface. After this maximum, local gas holdup decreases with increasing distance from the cell bottom up to 25 cm and then slightly increases again. Holdup in the region under impeller was not measured and is assumed approximatelly equal to the lowest measurement, because of the mixing intensity. It decreases rapidly close to the cell bottom to a zero value at the bottom itself. Figure 2.10 shows a photograph of the recovery zone at a J of 0.6 cm/s. It can be seen that bubble concentration is highest in the middle section of the recovery zone, to increase near the surface.

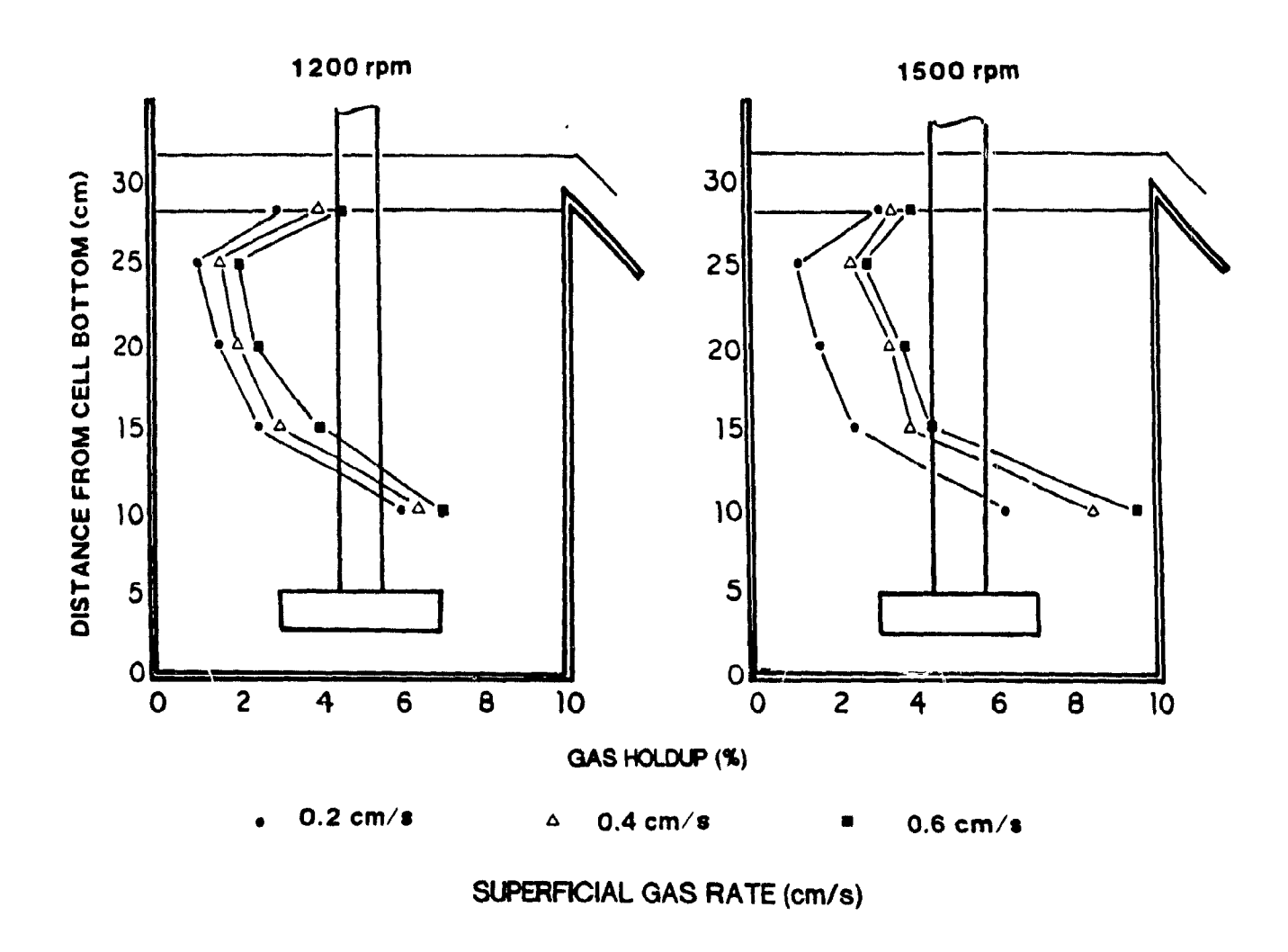


Figure 2.9: Local gas holdup distribution at different pulp levels in the modified cell (10 ppm Dowfroth 250).

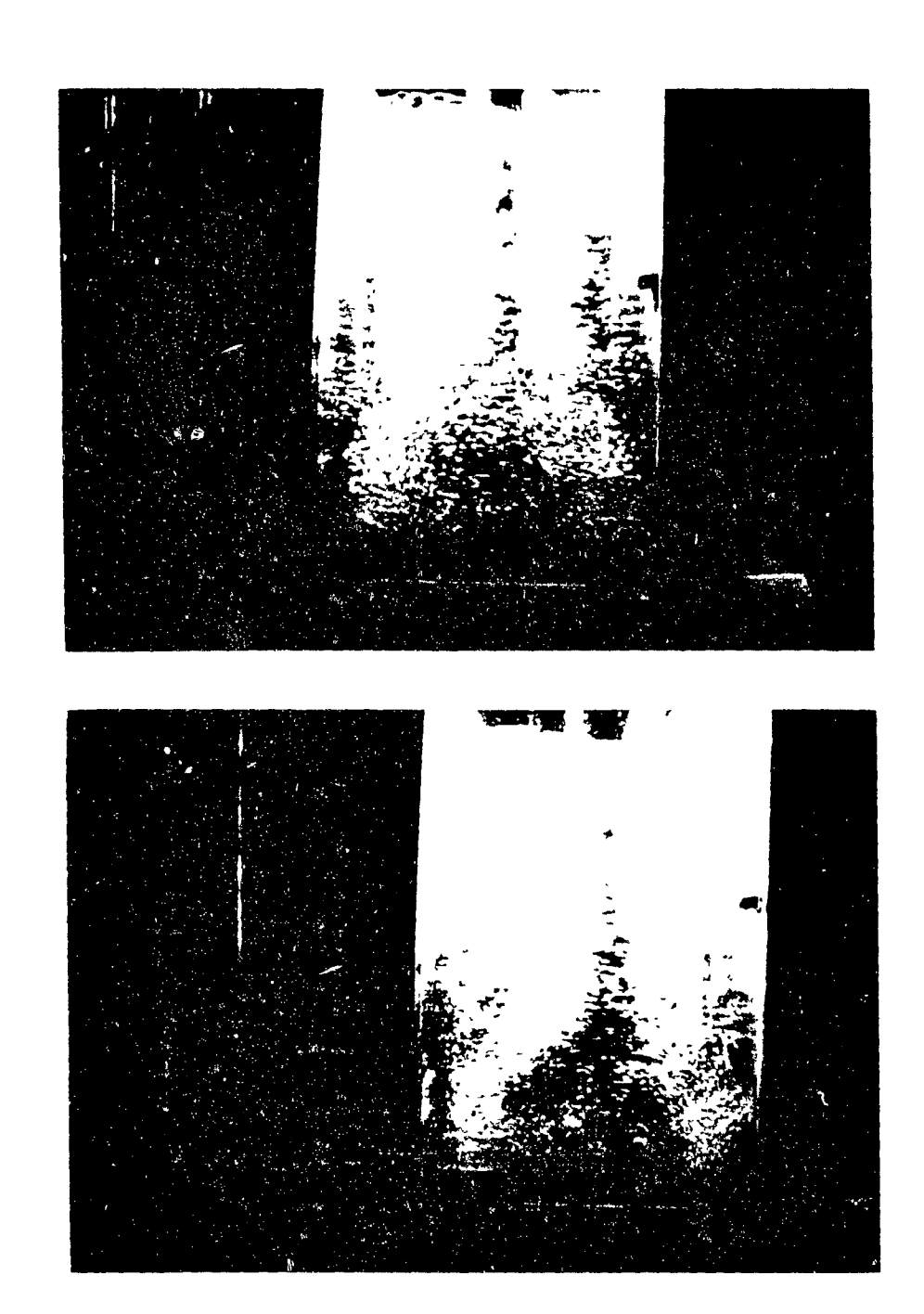


Figure 2 10. Bubble distribution in the clurry phase (N: 1500 rpm and Dowfroin 250: 10 ppm)

Calderbank (1958) investigated the distribution of local gas holdup, and specific interfacial area in the vertical direction of a mixing vessel by a light transmission technique. He observed a similar maximum of the gas holdup in the vicinity of the impeller. Bascur (1982) found the same type of vertical distribution of air in his flotation cell with a two phase system.

Klassen and Makrousov (1963) reported the same type of gas holdup distribution with vertical depth of a Mekhanobr cell at different solid contents (0-50%) in their book. The original investigators a sucking lance to determine the gas used They found a maximum in gas holdup above the impeller holdup. then a decrease, and finally an increase at slurry-froth interface (Figure 2.11). Their holdup values are somewhat higher (10 - 25%) than the present work, most probably due to the effect of increased pulp viscosity, which leads to decreased bubble rise velocities. These results suggest that in three phase systems, gas holdup profiles should show the same trends observed in this two phase system.

Change in air content with the depth of the flotation machine at different percent solids (Figure 2.11) shows that fractional gas holdup increased from 0 to 35% solids because of decreased bubble ascent velocity and increased at high percent solid because of channelling of large air bubbles through the pulp (Harris, 1976). It is also likely that at high pulp density the rheological properties of the slurry were such that biggest bubbles were formed.

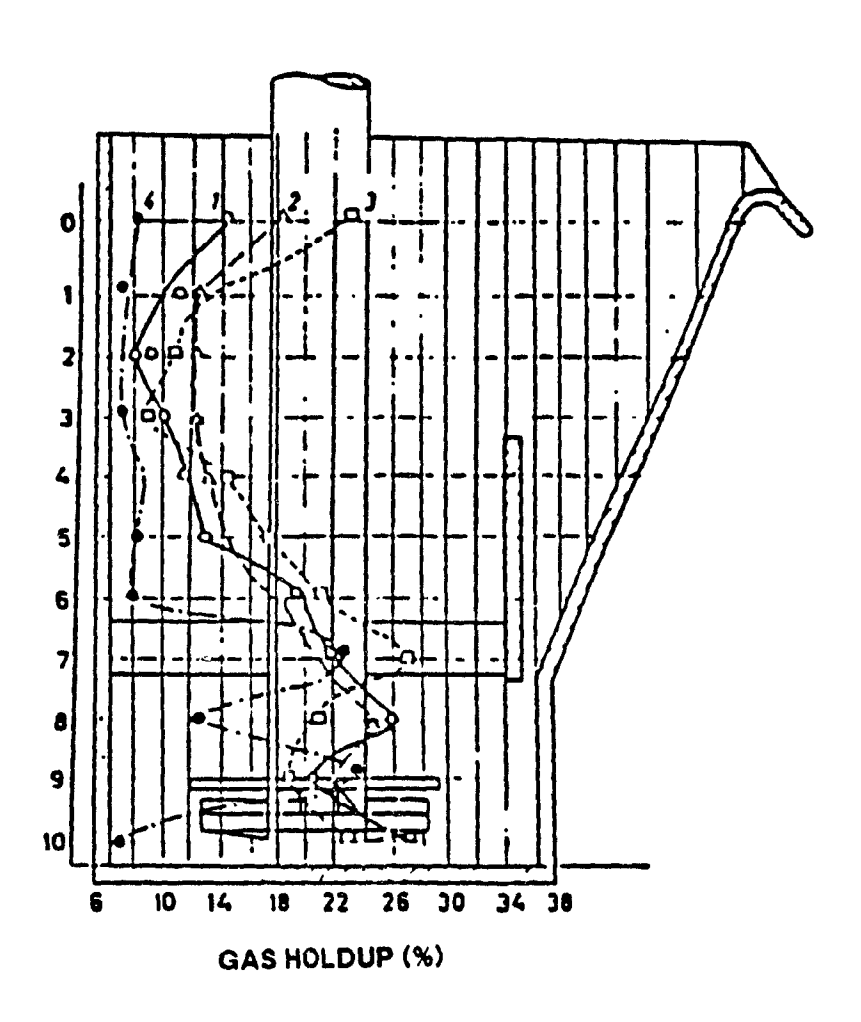


Figure 2.11: Change in air content with the depth of flotation machine at different percent solids (from Klassen and Makrousov, 1963).

curve	% solids	Bubble rise velocity (cm/s)		
1	0	4.1		
2	15	3.4		
3	25	2.9		
4	50	3.7		

These results illustrate that air distribution in industrial pulps is extremely heterogeneous with high concentrations of air in the vicinity of the impeller. Pulp aeration and overall air distribution are optimum between about 15 and 35% solids content in pulp (Harris, 1976)

This study shows that there are two distinct zones within the recovery zone of the flotation cell (Kaya, 1985). The lower part with high gas holdup and turbulence is the active recovery zone where the particles are captured by the bubbles and pulp is recirculated in the cell used. In this work, the active turbulent zone goes up to 15 cm from the cell bottom. Bubble residence time in this zone is increased by the rather helical paths bubbles take to leave the impeller area. Between the active turbulent zone and the froth zone, there is a quiescent buffer (separation) zone where gas holdup is slightly lower as bubbles rise almost vertically, at velocities close to terminal (Kaya, 1985). This zone helps floatable/non-floatable particle separation.

The air-liquid composite density in the zone surrounding the impeller is lower than that of the rest of the cell and is the result of air recirculation within this zone. Around the impeller zone, the aerated slurry is discharged upwards near the cell walls. Recirculation occurs towards the cell center. In the experimental system of this study, the influence of the recirculation flow produced by the impeller on the bubble motion decreases significantly with height. There is a possibility to further restrict these recirculating flow patterns within the

lower section of the cell using special baffles (like in the Leeds cell) to create a stable froth blanket, which is necessary for metallurgical purposes.

The sharp increase in the local gas holdup close to the interface in the presence of froth phase is presumably due to the accumulation of fast rising bubbles at the "fictitious" slurry-froth boundary layer before entering the first froth layer. Hydrodynamic interaction between a bubble and this layer significantly reduces bubble rise velocity.

Effect of Slurry Volume on Gas Holdup: The effect of slurry level (volume) on local gas holdup can be seen from Figure 2.12 at J_gs of 0.4 and 0.6 cm/s. Three different water levels without feed, tail, and overflow (20, 25 and 28 cm from the cell bottom) were tested at 1500 rpm and 10 ppm of Dowfroth. The same maximum in the recovery zone was recognized in each case. The local gas holdup values decrease with increasing water volume (height) in the cell. This is largely due to the decreased energy dissipated per unit volume, which is an important parameter in most of the correlations presented earlier to calculate gas holdup.

2.3.3 Point Cas Holdup in the Recovery Zone

Front and side views of the distribution of gas holdup measured using conductivity probe are given in Figure 2.13. The contour maps indicate four different gas holdup regions in the recovery zone. The higher gas holdup contour is centered around the impeller shaft. Lower contours enclose the higher holdup

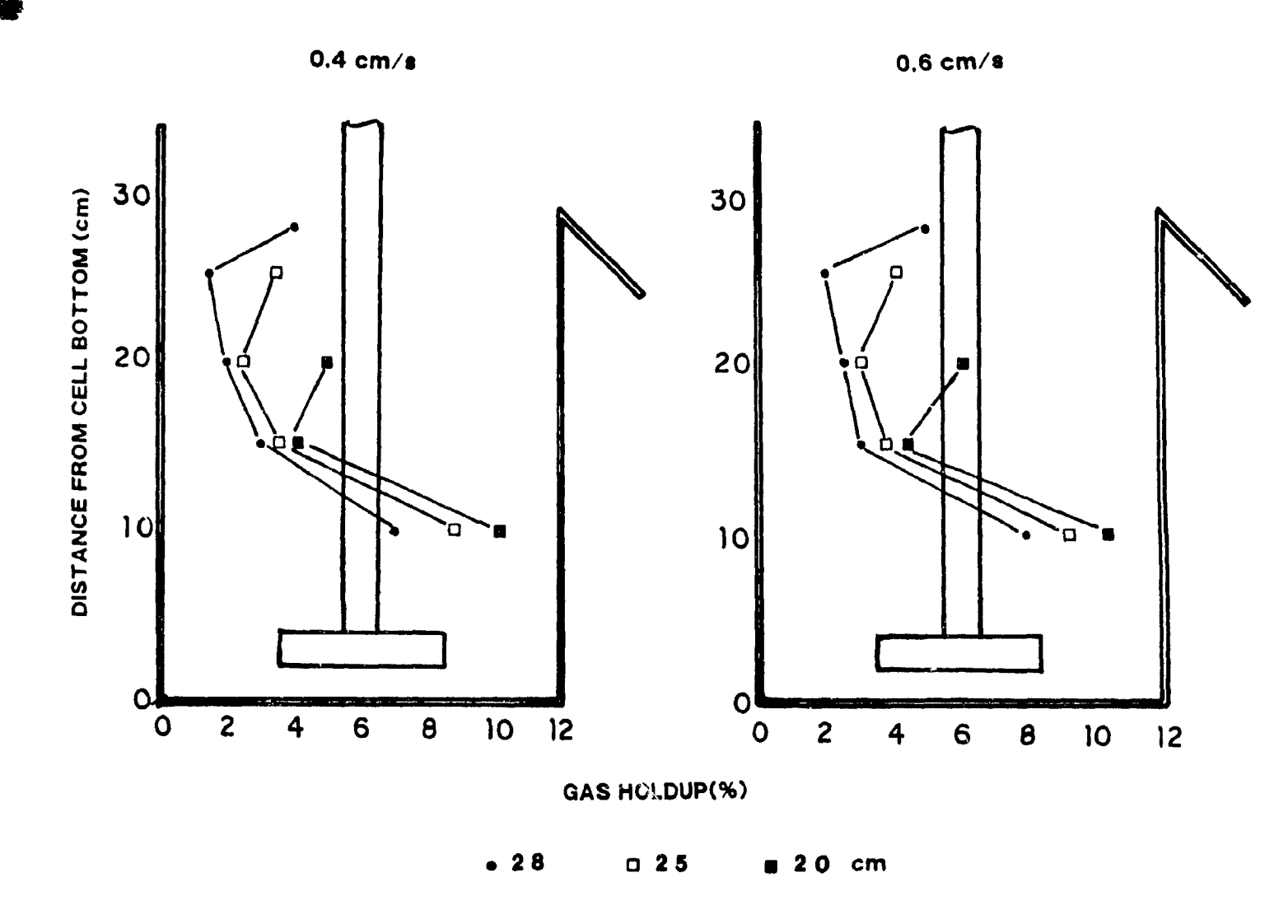


Figure 2.12: Effect of water level (volume) on local gas holdup at two different aeration rates using the modified cell
(N: 1500 rpm, 10 ppm Dowfroth 250).

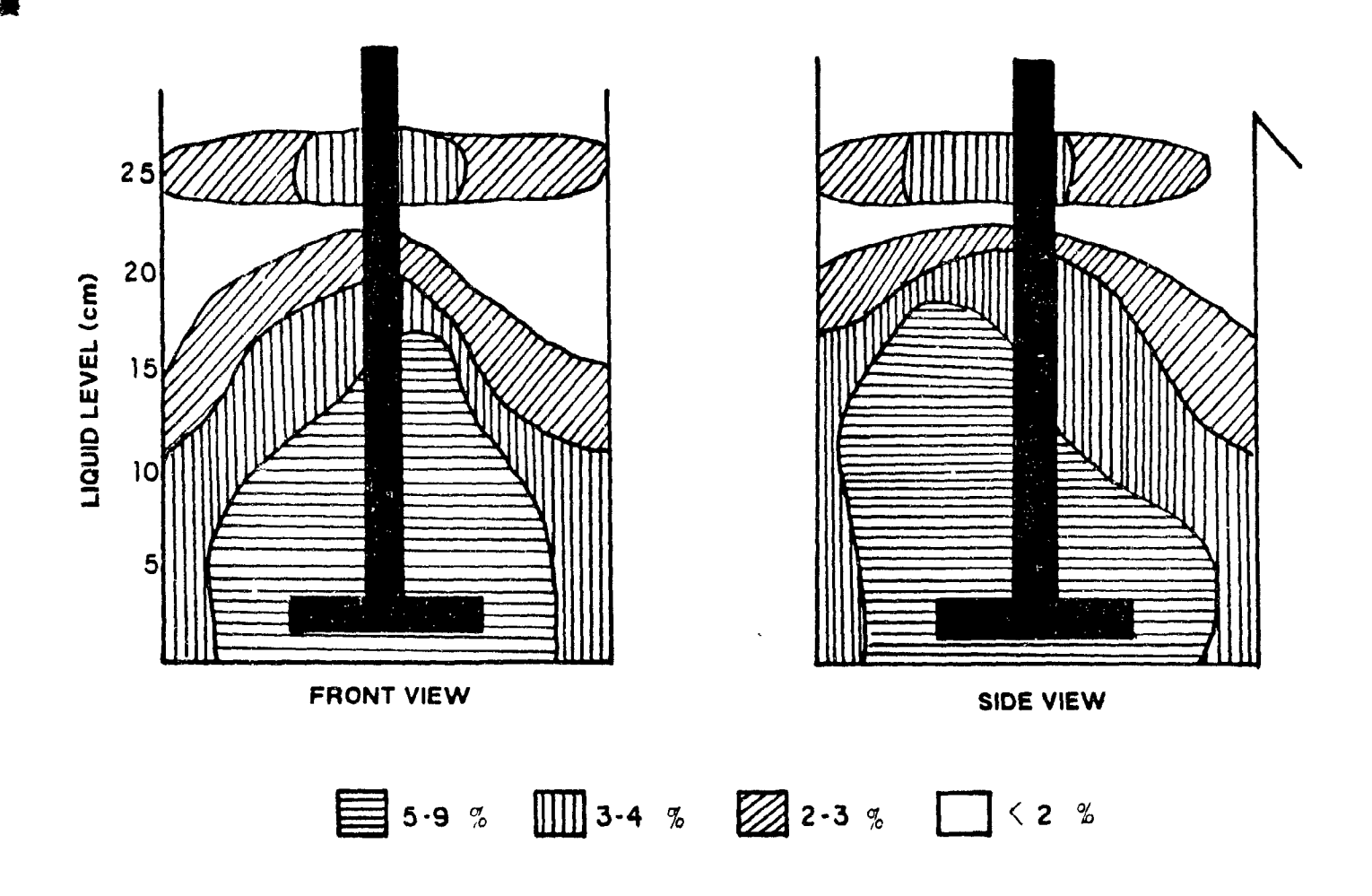


Figure 2.13: Front and side views of vertical holdup distribution in the modified cell (J: 0.6 cm/s, 10 ppm Dowfroth 250, and 1500 rpm).

zones in an upward direction. In the buffer zone, a very low gas holdup region can be seen; close to the interface a higher gas holdup region appears again. The following conclusions can be drawn from the point holdup measurements:

- a. the maximum gas holdup is located near the impeller region which is in good agreement with pressure gradient measurements (see Figure 2.10); this is due to recirculation flow patterns in the active turbulent zone.
- b. from the gas holdup profile and visual observation, it can be seen that there is a tangential swirling flow in the active turbulent zone.
- c. for levels 15 and 25 cm from the cell bottom, most of the gas moves in the middle part of the cell and not around the cell walls (see Figure 2.10). Air bubbles discharge from the impeller rise up along the wall after striking it and are then dispersed over the cross-section of the vessel with bubble coalescence occurring to some degree.

2.4 Bubble Size

In the optimum air flow number range (0.01-0.02), the average Sauter bubble diameter calculated from Eq. 2.1 using the interfacial area and gas holdup estimations is in good agreement with published values (Kaya, 1985) measured photographically with a \(\frac{7}{2}\) error limit. As can be seen from Figure 2.14, the average bubble diameter in the recovery zone increases with increasing aeration rate. Calculation of the average bubble diameter using Eq. 2.19 underestimates measured bubble size and fails to predict the right relationship between superficial gas rate and bubble size. Eq. 2.1 very slightly underestimates the measured bubble size, and predict the right effect for air flowrate.

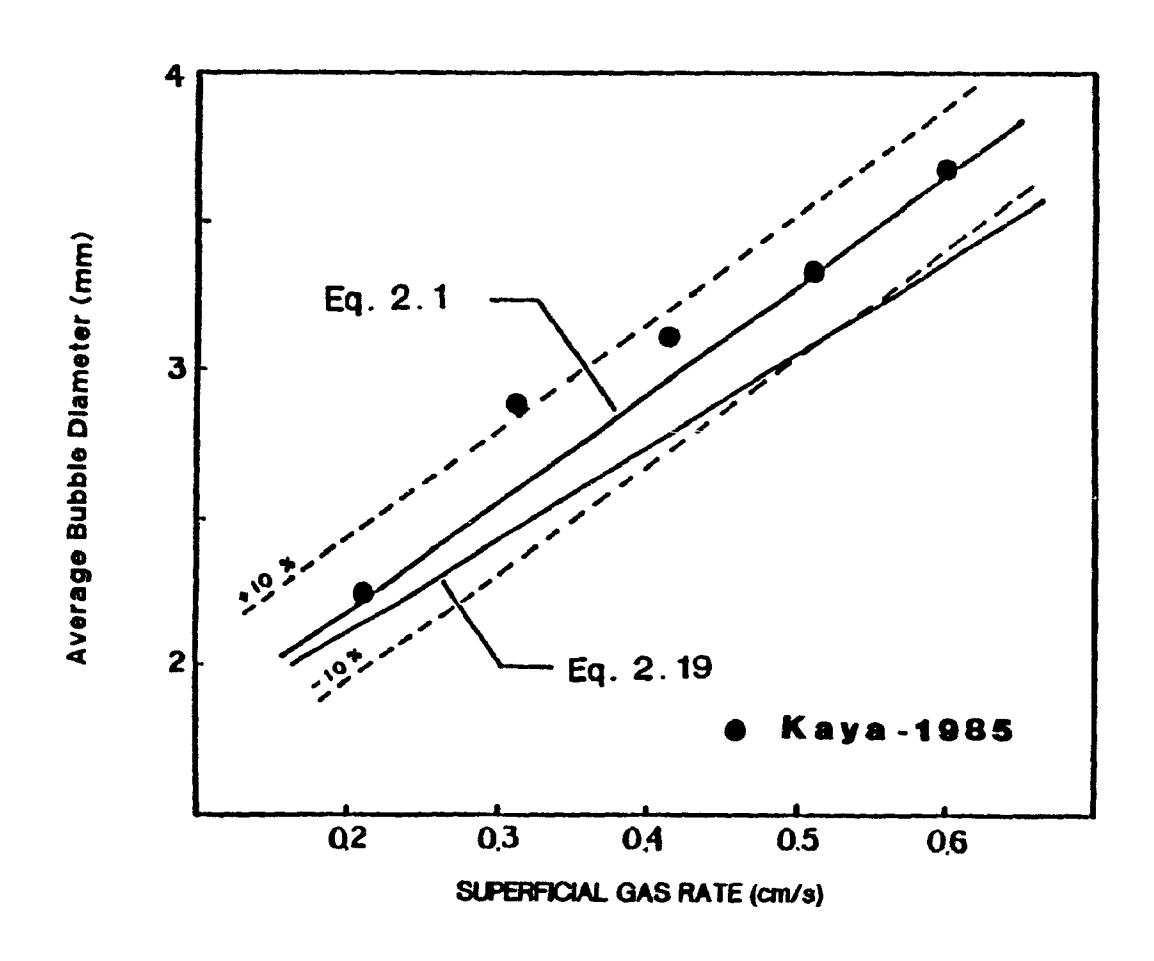


Figure 2.14: Effect of aeration rate on bubble size in the slurry zone of the modified cell (N: 1500 rpm and 10 ppm Dowfroth 250).

2.5 Impeller Dispersion Efficiency

Figure 2.15 shows flooding, EMZ, and recirculation in the present system. Figure 2.16 shows the dispersion mode for different conditions in the present system, s predicted by Eqs. 2.22 and 2.23 (D = 7 cm and T = 15 cm).

In the present system, critical impeller speeds at which transition from flooding to EMZ and EMZ to recirculation occurs are between 600 and 900 rpm. If the impeller speed is less than 600 rpm, the system exhibits flooding for all aeration rates investigated; however, if it is more than 900 rpm, then the system exhibits both EMZ and recirculation. For 600 rpm, EMZ can be seen up to superficial gas rate of 0.8 cm/s; then flooding appears. At 900 rpm, recirculation can be seen up to superficial gas rate of 0.4 cm/s, then EMZ starts. Since the impeller speeds used for this study were 1200 and 1500 rpm, the system clearly exhibits recirculation flow patterns.

The mechanical operating conditions (impeller speed, air flowrate) referring to the modified Denver D12 laboratory flotation machine are charted in Figure 2.17. Full lines indicate constant air flow numbers. The transition between EMZ and recirculation calculated from Eq. 2.22 is also indicated by a thick solid line. The normal operating range of the cell is given by a dashed rectangle is clearly in the recirculation zone.

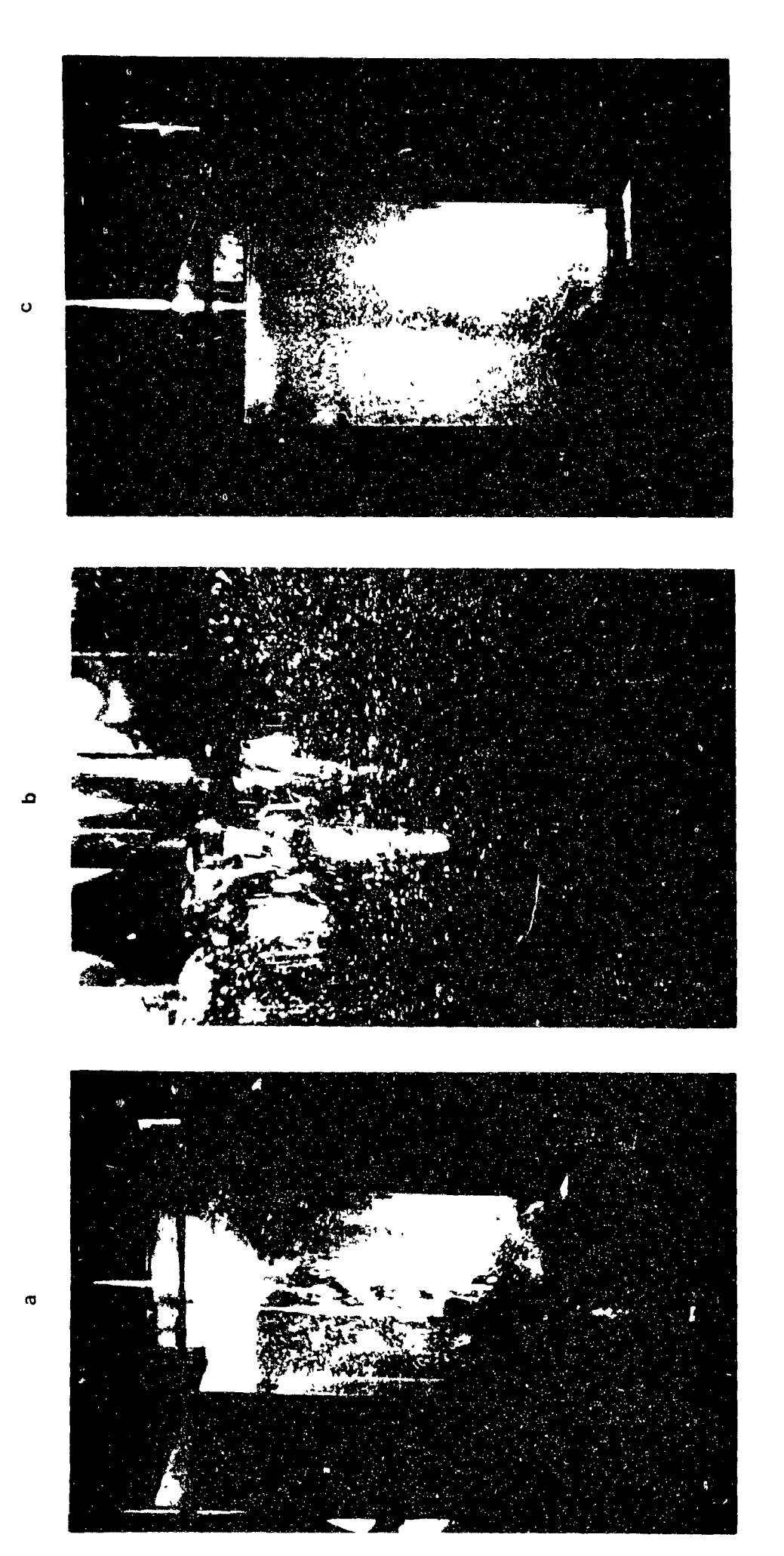


Figure 2.15. Pictures of flooding, recirculation, and IMZ in the modified cell.

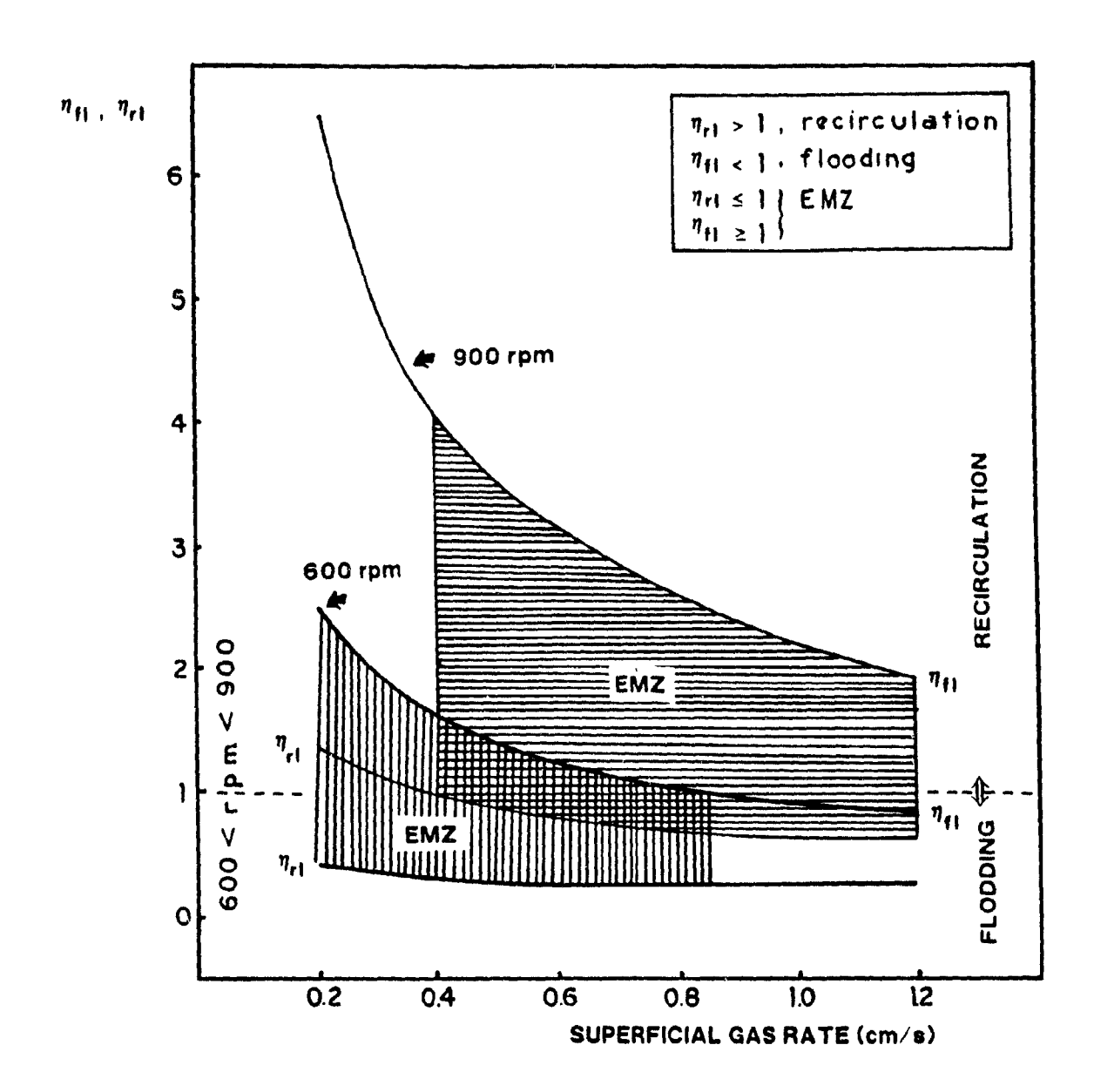


Figure 2.16: Effect of aeration rate and impeller speed on calculated impeller dispersion efficiencies for flooding and recirculation.

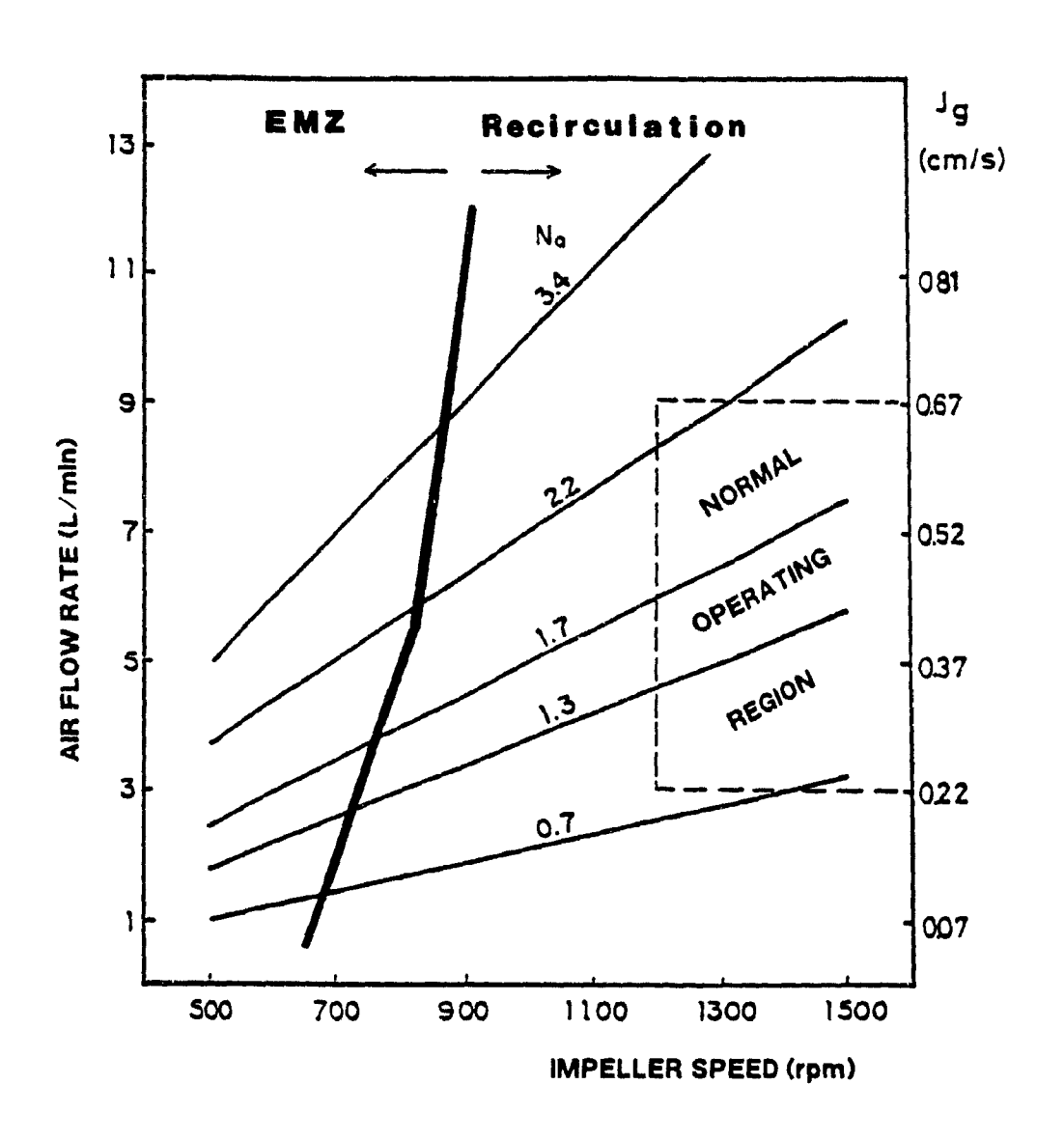


Figure 2.17: The mechanical operating conditions of the modified cell (N_Q : air flow number).

2.6 Summary

Gas holdup and bubble size are important factors characterizing the hydrodynamics of a flotation cell. Here, three different gas holdup concepts were introduced: overall (average), local, and point gas holdups.

Gas holdup in the recovery zone was measured in mechanically agitated flotation cells in the absence of solid particles. Overall gas holdup was determined both from the level rise in the presence of frother and the overflow techniques in the absence of frother. Local gas holdup was measured by using pressure taps connected to the flotation cell. An electrical conductivity method developed by Yianatos et al. (1985) was successfully used to measure point gas holdup of the slurry phase. Gas hold-up profiles were obtained and flow patterns were interpreted from measurements.

Overall gas holdup in a Denver laboratory flotation cell can be estimated using Calderbank's model (Eq. 2.11) in conjunction with Loung and Voleski's correlation for aerated power consumption (Eq. 2.7). It was verified that the model was applicable to all Denver laboratory cells. Local and point gas holdup measurements revealed that the gas phase was not homogeneously distributed in the slurry phase.

Some physical and chemical means of increasing gas content in the recovery zone were investigated. Of the variables investigated, air flowrate proved to influence gas holdup in the

slurry phase most significantly. Inorganic salts (i.e $\mathrm{Na_2SO_4}$), which increase the overall gas content significantly, can be used to minimize frother dosage for fine bubble generation if the chemistry of the flotation environment is suitable.

Average bubble size was predicted using measured gas holdup and the calculated interfacial area. Close agreement was obtained between the predictions and photographic measurements.

Table 2.7 summarizes the agreement between measured interfacial area, gas holdup, and bubble size and the correlations, which were tested in this study.

Table 2.7: Response of the tested equations in this study.

Parameter	Main Eq.	Supplementary Eq.	Result
Interfacial	2.4	3, 5, 7, 9	good
area	2.3	5, 7, 9	underestimate
Gas holdup	2. 10 2. 11 2. 11 2. 14	15 5, 7, 9 5, 6, 9	overestimate good overestimate underestimate
Bubble size	2. 1	4, 11	good
	2. 19	5, 7, 11	underestimate

Different gas mixing zone concepts were introduced. A measure of impeller dispersion efficiency was defined, which can be used to distinguish the different regions of mixing. It provides a basis for estimating the degree of flooding or recirculation. Impeller dispersion efficiency confirmed recirculation in the slurry phase of the modified flotation cell.

CHAPTER 3

A STUDY OF THE FROTH PHASE HYDRODYNAMICS

IN MECHANICAL FLOTATION MACHINES WITH A TWO-PHASE SYSTEM

IN THE PRESENCE AND ABSENCE OF WASH WATER

Introduction

A study of processes occurring in the flotation froth can lead to a clearer insight into the mechanisms important to flotation performance and provide some foundation for new rational operation.

This chapter partly describes the froth (cleaning) zone properties by means of point and local measurements of gas holdup in the froth zone. The ultimate objective is to obtain a detailed description of the washed froths in mechanical flotation cells. Later on, this information will be used to analyze mineral rejection and selection phenomena.

This chapter is structured as follows. First, some fundamentals of froth hydrodynamics are reviewed. The objective is twofold: to describe briefly how froth structure relates to transfer mechanisms and to establish a basis for simple predictive model of water recovery into the concentrate. A second section describes the experimental system and the test program. A third section presents and discusses experimental results.

3.1 Hydraulic Model (Water Balance) in a Flotation Cell

Despite earlier work on the importance of hydraulic entrainment of gangue (Jowett, 1966), early workers of flotation modelling concentrated on the behaviour of valuable particles and tended to neglect the behaviour of gangue particles and water. Recently, investigators have began to recognize the importance of

water behaviour in flotation models. Early entrainment models for gangue recovery have been used by Lynch et al. (1974) and Moys (1981) has given a first approximation model for the distribution of water in flotation cells. The ability of the column to reject feed water from the concentrate has already been identified as the main mechanism whereby columns can achieve better selectivity (Yianatos et al., 1987), as recently demonstrated in a size-by-size study of a laboratory column and cell with a completely hydrophilic feed (Kaya and Laplante, 1986).

One key element controlling water distribution in a flotation cell is the froth phase Unfortunately, there has been very little consideration of water and particle transport in the froth, even though the froth and associated drainage phenomena are considered to have a major impact on overall selectivity.

In order to quantify the interface transfer of water and air (bubbles), superficial rates (i.e. flowrates divided by the cell cross-sectional area) can be useful. The various superficial rates are represented in Figure 3.1. In modelling water transport through the froth, it is assumed that bubbles leaving the pulp carry a sheath (envelope) of water, which moves into the froth (see Figure 3.2a). The size of the bubbles and the water sheath thickness is determined by surface tension and agitation parameters in the pulp. Drainage of water back to the pulp is modelled by analogy with drainage through bubble Plateau borders in foams (Figure 3.2b). Froth height is determined by the froth removal mechanism.

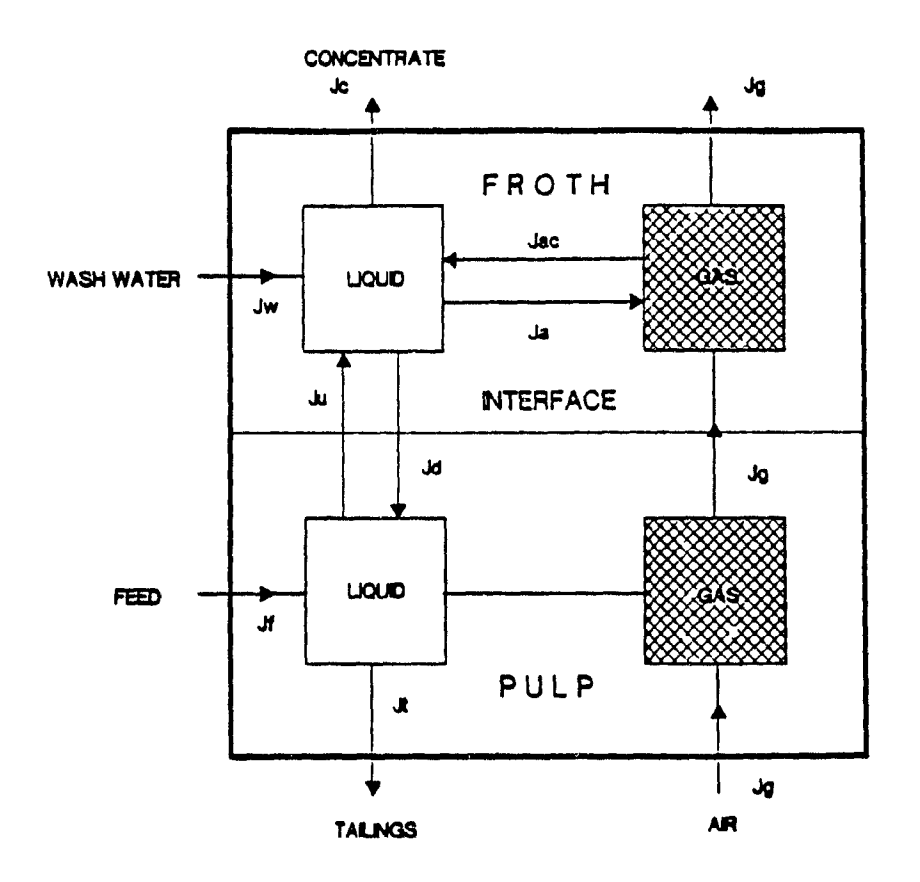


Figure 3.1: Phases in flotation.

(The symbols represent the superficial velocities of water and gas. The subscripts are: f-feed, t-tailing, u-upward, d-downward, w-wash water, c-concentrate, and g-gas).

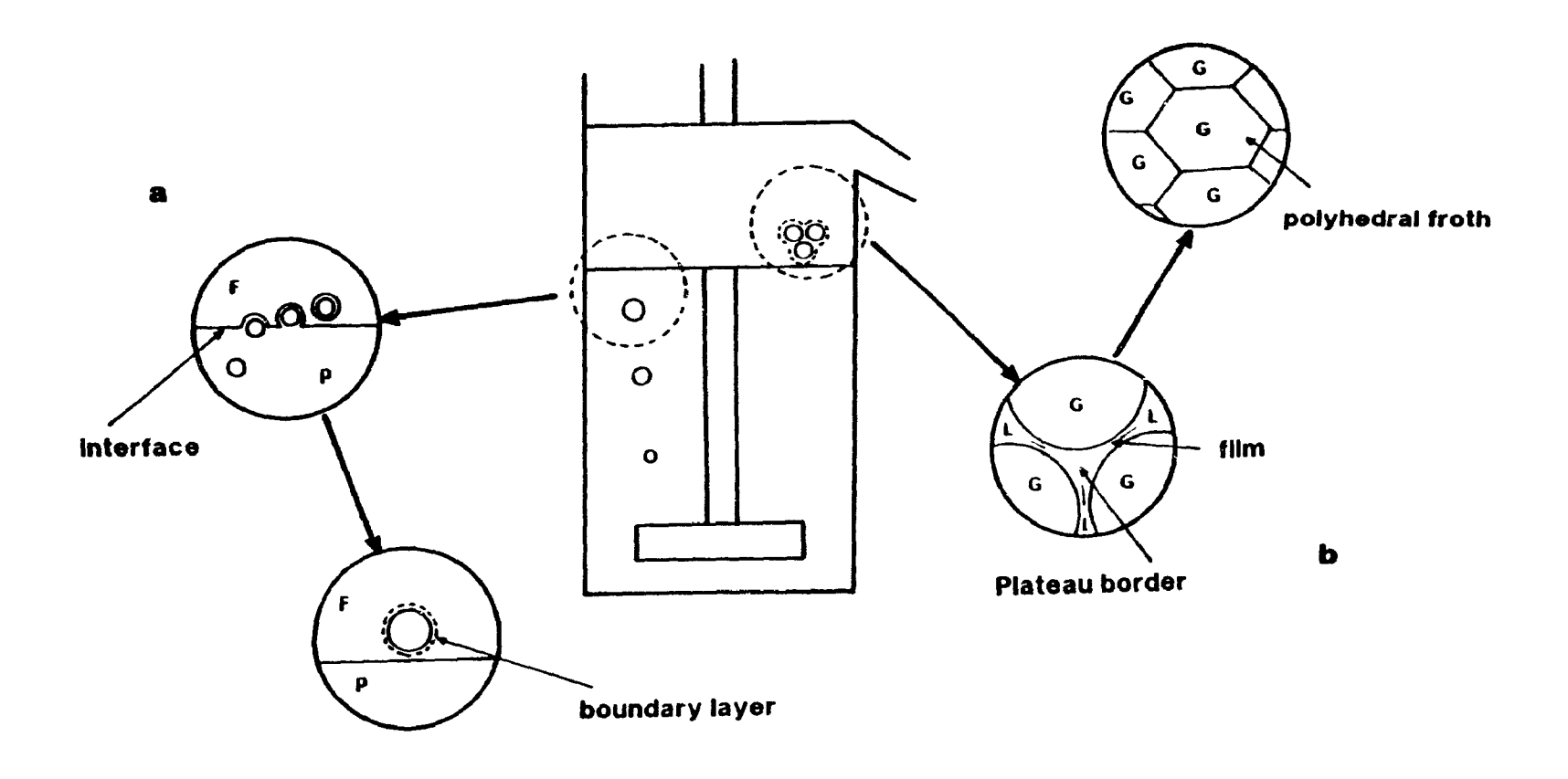


Figure 3.2: Water transport in a flotation cell.

(P: pulp, F: froth, G: gas, and L: liquid).

For the pulp phase, the following water balance can be written (Figure 3.3):

$$J_{f} + J_{d} = J_{t} + J_{u}$$
 3.1

where J_{u} : superficial liquid rate entrained upward, m/s

J_d: superficial liquid drainage rate, m/s

J_s: superficial feed rate, m/s

J.: superficial tailing rate, m/s

Steiner et al. (1977) developed a cellular foam model, which considers that the froth structure as a whole is carried upward by the gas flow while liquid flows down either through the Plateau borders (void spaces between contacts) or films. Their model was slightly modified and adapted to the counter-current column flotation by Yianatos et al. (1985). Since there is no accumulation of liquid in froth layers, the balance of flows any horizontal plane in the system may be written as (Figure 3.4):

$$J_{u} + J_{y} = J_{d} + J_{c}$$
 3.2

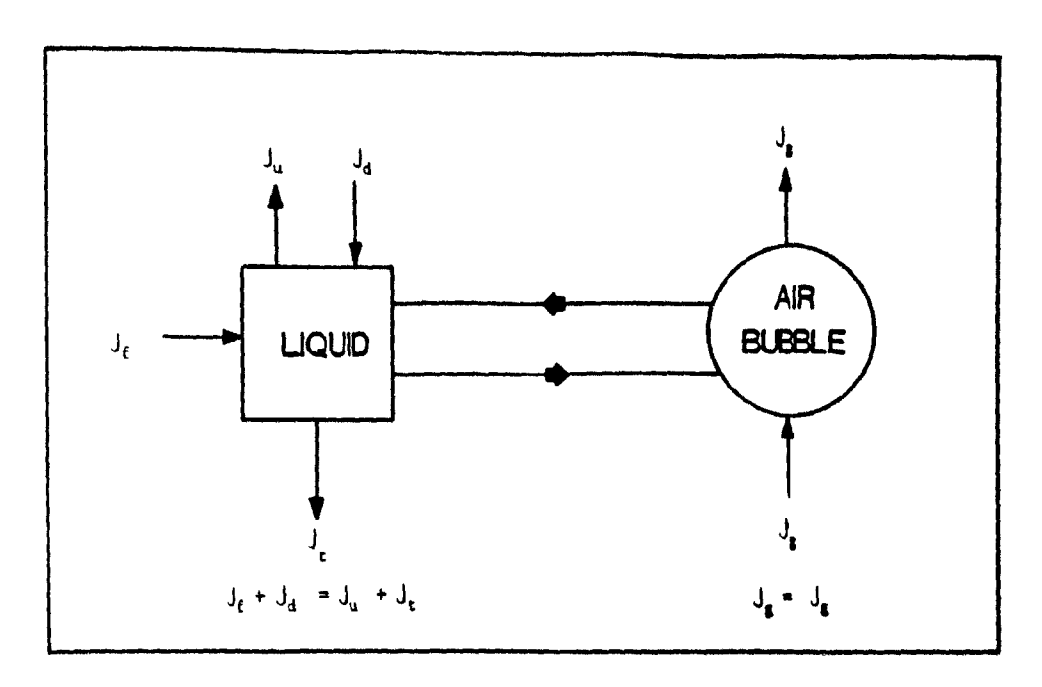
where J: superficial wash water rate, m/s

J: superficial liquid rate going to the concentrate, m/s

Here, J_{u} and J_{c} can be directly measured.

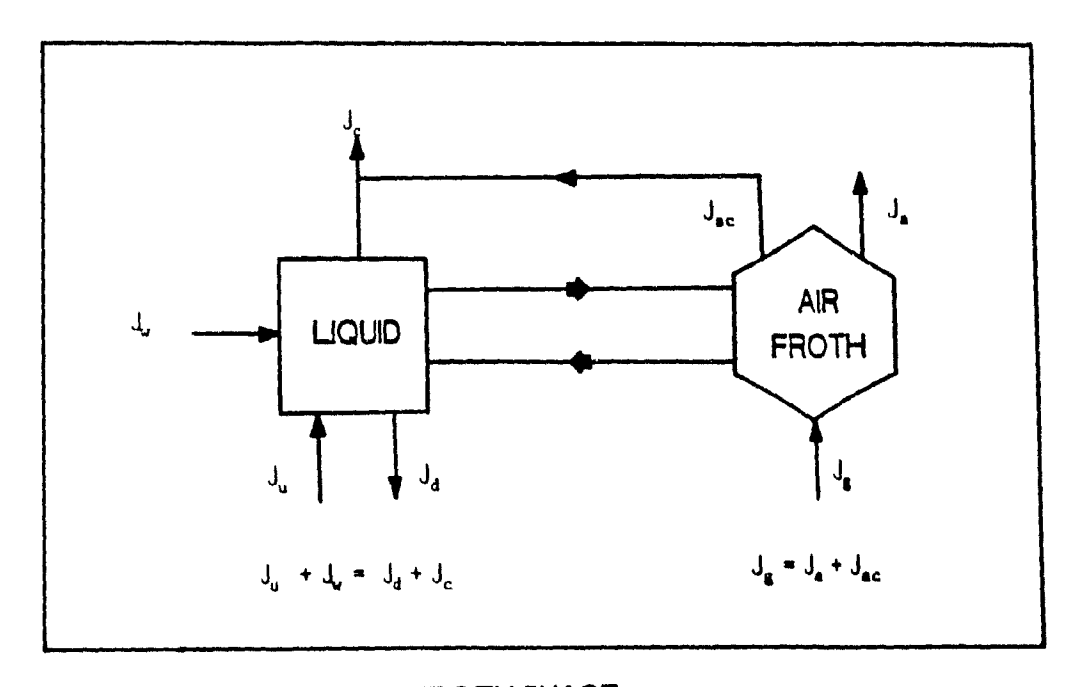
3.1.1 Water Entrainment From the Pulp to the Froth

An attempt to derive an expression for water entrainment rate into the froth, $Q_{\mathbf{u}}$, has been made by Mika and Fuerstenau (1969). They realized that a major proportion of water and gangue fines which cross into the froth are entrapped in a boundary layer (water envelope) of water around the bubble. A similar



PULP PHASE

Figure 3.3: Liquid and gas balance in the pulp phase at steady-state.



FROTH PHASE

Figure 3.4: Liquid and gas balance in the froth phase at steady-state.

approximation was made by Moys in his froth model. The magnitude of this boundary layer is apparently controlled by the hydration effects at the air-water interface and by turbulence levels in the cell (Bascur and Herbst, 1982).

The volumetric flowrate of entrained water can be calculated from the number of bubbles rising per unit time, $6Q_g/\pi$. d_{bp}^{-3} , where Q_g is the volumetric air flowrate and d_{bp} is the mean bubble diameter in the pulp phase. The volume of liquid held by a film surrounding a spherical bubble is π . d_{bp}^{-2} . δ , so that the volume flowrate of water into the froth is:

$$Q_{u} = \frac{6 \cdot Q_{q} \cdot \delta}{d_{bp}}$$
3.3

Estimation of the bubble film thickness, δ , should ideally stem from a rigorous hydrodynamic and physico-chemical analysis of the flotation environment. As a first approximation, δ can be obtained from hydrodynamic boundary layer correlations available in literature. Luis (1983) gives the following empirical equation for boundary layer thickness:

$$\delta = C_1 \left[\frac{\mu^{0.25}}{g^{0.33}} \right] \left[\frac{(Pa/V_{1p})^{0.083}}{V_t^{0.5}} \right] d_{bp}^{0.833}$$
3.4

where μ : liquid viscosity, Nm/sec

ρ: liquid density, kg/m³

P: power input in aeration, W

 V_t : terminal bubble rise velocity, m/s

C₁: adjustable constant

Interstitial upward liquid rate (V_1) , which is the actual liquid rate, is equal to:

$$V_{1} = \frac{J_{q}}{\varepsilon_{bf}}$$
3.5

where J: superficial gas rate, m/s $\varepsilon_{\rm bf}\colon {\rm fractional\ volumetric\ gas\ holdup\ in\ the\ froth\ phase}$

The amount of liquid passing upwards across a unit horizontal plane in unit time is (Steiner et al. 1977):

$$J_{u} = J_{g} - \frac{1 - \varepsilon_{bf}}{\varepsilon_{bf}}$$
3.6

and the volumetric flowrate, $Q_{\mu\nu}$

$$Q_{II} = J_{II} . S$$
 3.7

where S: cell cross-sectional area, m²

3.1.2 Water Drainage From the Froth to the Slurry

Drainage of water from the froth is a complex phenomenon, which has received very little attention in flotation. Mika and Fuerstenau (1969) have emphasized that drainage from the froth is essential to explain secondary concentration in the froth. Considerable efforts have been put into the description of drainage in solids free froths. Assuming the walls of a border in the froth are not completely rigid, the total downward flow can be expressed as (Steiner et al. 1977):

$$J_{d} = \frac{8.845. \, 10^{-3} \cdot \varepsilon_{bf}^{2} \cdot \rho_{1} \cdot g \cdot r^{4}}{\mu \cdot k_{v} \cdot d_{bp}^{2}}$$
3.8

where g: gravity acceleration, m/s²

r: radius of Plateau borders, m

k; velocity coefficient

Without wash water addition, J_d at the interface can be determined from the difference between J_d and J_c .

$$J_{d} = J_{q} \frac{1 - \varepsilon_{bf}}{\varepsilon_{bf}} + (J_{w} - J_{c}) \qquad 3.9$$

Drainage in the froth can be increased by increasing aeration rate, liquid content of froth, and wash water addition rate or decreasing concentrate rate. The volumetric drainage rate, Q_d , can be approximated by:

$$Q_{d} = J_{d} . S 3.10$$

3.1.3 Water into the Concentrate

The flow over a weir can be used to model flowrate of concentrate (Bascur and Herbst, 1982). To model this phenomenon, Francis' equation (Perry and Green, 1984) was used by taking into account the presence of gas in the flotation froths (Figure 3.5).

Velocity over a weir:

$$v^2 = 2 \cdot g \cdot h$$
 3.11

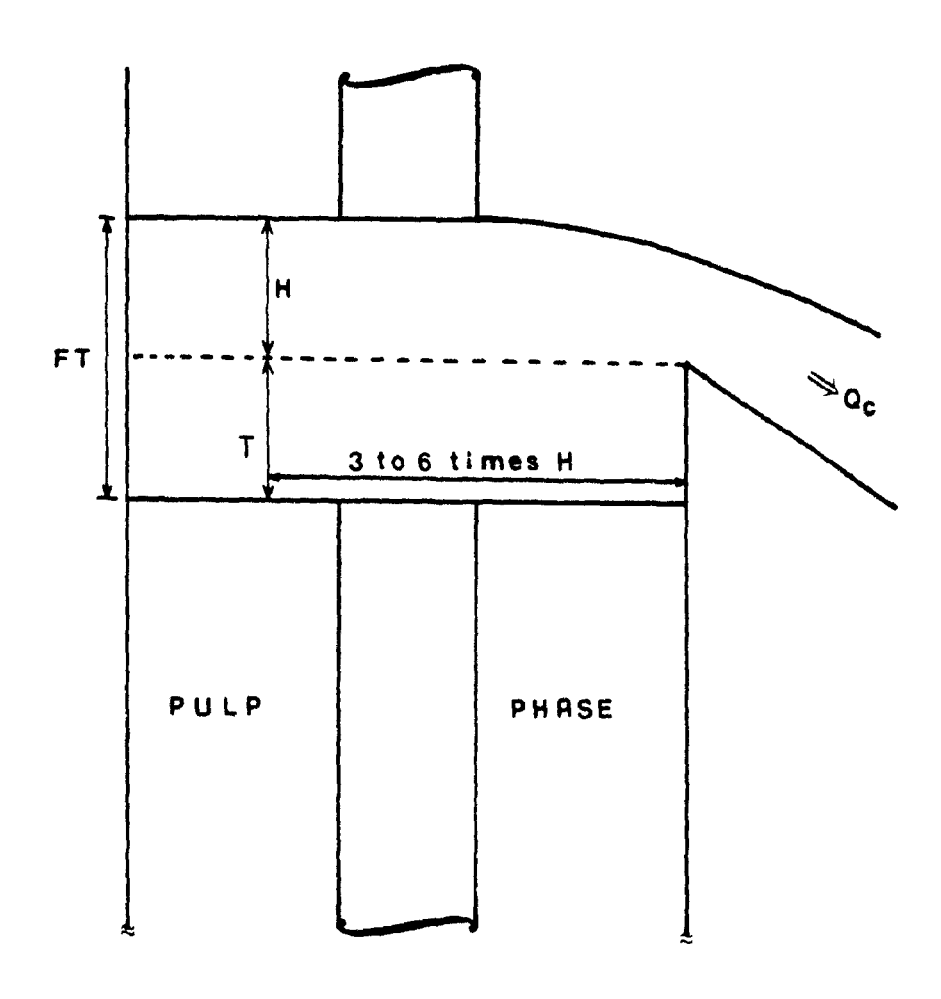


Figure 3.5: Water transport to the concentrate.

The quantity of liquid flowing over the weir is given by:

$$Q_{\alpha} = A \cdot V \qquad \qquad 3.12$$

where A: cross-sectional area of flow above the weir, m^2

By calculus, it can be shown that for a rectangular notch:

$$Q_c = \frac{2}{3} \cdot W \cdot (2 \cdot g \cdot H^3)^{0.5}$$
 3.13

In practice, it is found that because of stream line contraction and frictional losses, Eq. 3.13 over-predicts Q_c . Eq. 3.13 can be rewritten to account for losses and gas holdup:

where W: width of the flotation cell lip, m

H: vertical distance between the cell lip and froth surface, m

Q: volumetric liquid flowrate to the concentrate, m3/s

J : superficial liquid rate going to the concentrate, m/s

K: discharge coefficient, which depends on the type of removal technique used, froth viscosity, % solid, gas holdup, etc.

3.2 Gas Balance in a Flotation Cell

By assuming there is no gas loss in the pulp phase and gas pick up from the froth surface, the following gas balance can be written for the froth phase:

$$J_{g} = J_{ac} + J_{ac}$$
 3.15

where J_{ac} : superficial gas rate associated with liquid transfer to the concentrate, m/s

J: superficial gas rate directly going to the atmosphere by bursting at the top of the froth phase (collapse).

Luis (1983) presented the following equation for superficial gas flowrate associated with liquid transfer into the overflow (J_{ac}) :

$$J_{ac} = J_{c} . \frac{\varepsilon_{bf}}{1 - \varepsilon_{bf}}$$
3.16

and Q :

$$Q_{ac} = J_{ac} * S$$
 3.17

where Q_{ac} : volumetric flowrate (air plus liquid) of the froth flowing over concentrate weir, m^3/s

Q is related to the width, depth, and viscosity of the concentrate stream as it flows over the concentrate weir.

A certain fraction of gas, α , reports to the concentrate, while the rest, 1- α , rises to the top of the froth phase, and then bursts by leaving the carried liquid content into the froth. The froth removal efficiency, α , is defined by (Moys, 1979):

$$\alpha = \frac{J_{ac}}{J_{g}} = \frac{J_{c} (1-\varepsilon_{bf})}{J_{g} \varepsilon_{bf}}$$
3.18

If no bubble breakage occurs on the top of the froth phase, or if the design of the froth chamber forces all froth into the launder, $\alpha = 1$. If no froth is removed, $\alpha = 0$. The former condition can be satisfied under two conditions:

$$J_c = J_g$$
 and $\varepsilon_{bf} = \varepsilon_{1f}$ 3.19
 $J_c = \varepsilon_{bf}$ and $J_g = \varepsilon_{lf}$ 3.20

where $~\epsilon_{_{\text{bf}}};$ fractional volumetric liquid holdup in the froth phase

In general, increasing J_{ac} favours recovery and increasing J_{ac} favours grade. Combining equations 3.2, 3.6, and 3.16.

$$J_{d} = J_{a} \cdot \frac{\varepsilon_{1f}}{\varepsilon_{bf}} + J_{w}$$
 3.21

Drainage rate can be increased by increasing gas escape to the atmosphere (i.e. enhancing bubble collapse at the top of the froth) in order to lessen entrainment. Bubble breakage can be reduced in order to prevent unstable froth generation and valuable particle loss in the shallow froths where particle reattachment is difficult. Clearly, in the absence of wash water, these two objectives are in competition. However, wash water addition both increase water drainage to reduce entrainment and reduces froth instability by increasing inter-bubble water thickness.

3.3 Momentum Conservation Across the Interface and in the Froth Phase

If a gas is introduced at a constant rate (J_g) in a given body of liquid capable of frothing, the liquid becomes covered by froth with increasing thickness until a steady-state is reached Bubble collapse at the top layer of froth occurs at the same rate as gas is introduced. Thus, the maximum froth expansion (FT_{max}) on a certain operating condition is obtained when the bubble rise velocity in the froth (V_g) is equal to gas addition rate (J_g) .

A froth layer grows by adding new bubbles from the below and decays by disappearing of old bubbles at the top. At steady-state, the volumes of gas added and subtracted are equal, but the number of bubbles added is greater than the number of bubbles subtracted at the top because of the bubble coalescence in the froth phase.

The momentum conservation law, which can be applied to the collision of two bubbles at the interface and in the froth phase, states that the sum of the momenta after collision is equal to the sum of the momenta before collision.

$$P_1(before) + P_2(before) = P_1(after) + P_2(after)$$
 3.22
 $P = m \cdot v$ 3.23

where P: momentum, kg. m/sec

m: mass, kg

v: velocity, m/s

1,2: stands for two bubbles

Collisions may be either elastic or inelastic. In an elastic collision, all the kinetic energy of the incoming bubbles reappears after the collision as the kinetic energy of the same bubbles. In the usual inelastic collision, part of the kinetic energy of the incoming bubbles is being lost as heat.

If one bubble moves towards a stationary one and adheres to it after collision, their joint velocity is equal to bubbles together can be calculated from:

$$V_{12} = \frac{m_1 \cdot v_1}{m_1 + m_2}$$
 3.24

where m.: mass of the moving bubble, kg

mg: mass of the stationary bubble, kg

v,: velocity of moving bubble, m/s

v, : velocity of joint bubbles after collision, m/s

A model was developed to predict the bubble rise velocity in the froth phase and the maximum attainable froth thickness at steady-state. The model considers the following assumptions:

- all bubbles are spherical and have the same diameter in the slurry and froth phases,
- average bubble rise velocity is determined from the average gas holdup and bubble size in the slurry phase,
- bubble collisions are elastic.
- water film thicknesses around bubbles are not taken into consideration.

A bubble approaching the interface collides with a previously formed bubble, which is assumed to be stationary (Figure 3.6a). After collision of rising bubble and stationary bubbles in the froth, they adhere and rise at a reduced velocity (Figure 3.6a). Then, these two bubbles collide with the one above them, which is again assumed stationary. Bubble rise velocity is further reduced, and these three bubbles stick together and collide with another one above them. This collision process continues until the bubble rise velocity is equal to gas introduction rate, under that condition the maximum froth expansion is attained.

Figure 3.6b shows average bubble rise velocity as a function of number of bubbles in the froth phase, which determines the froth thickness. At $J_g = v_{\rm bf}$, $FT_{\rm max}$ can be calculated by the multiplication of number of bubbles by average bubble diameter.

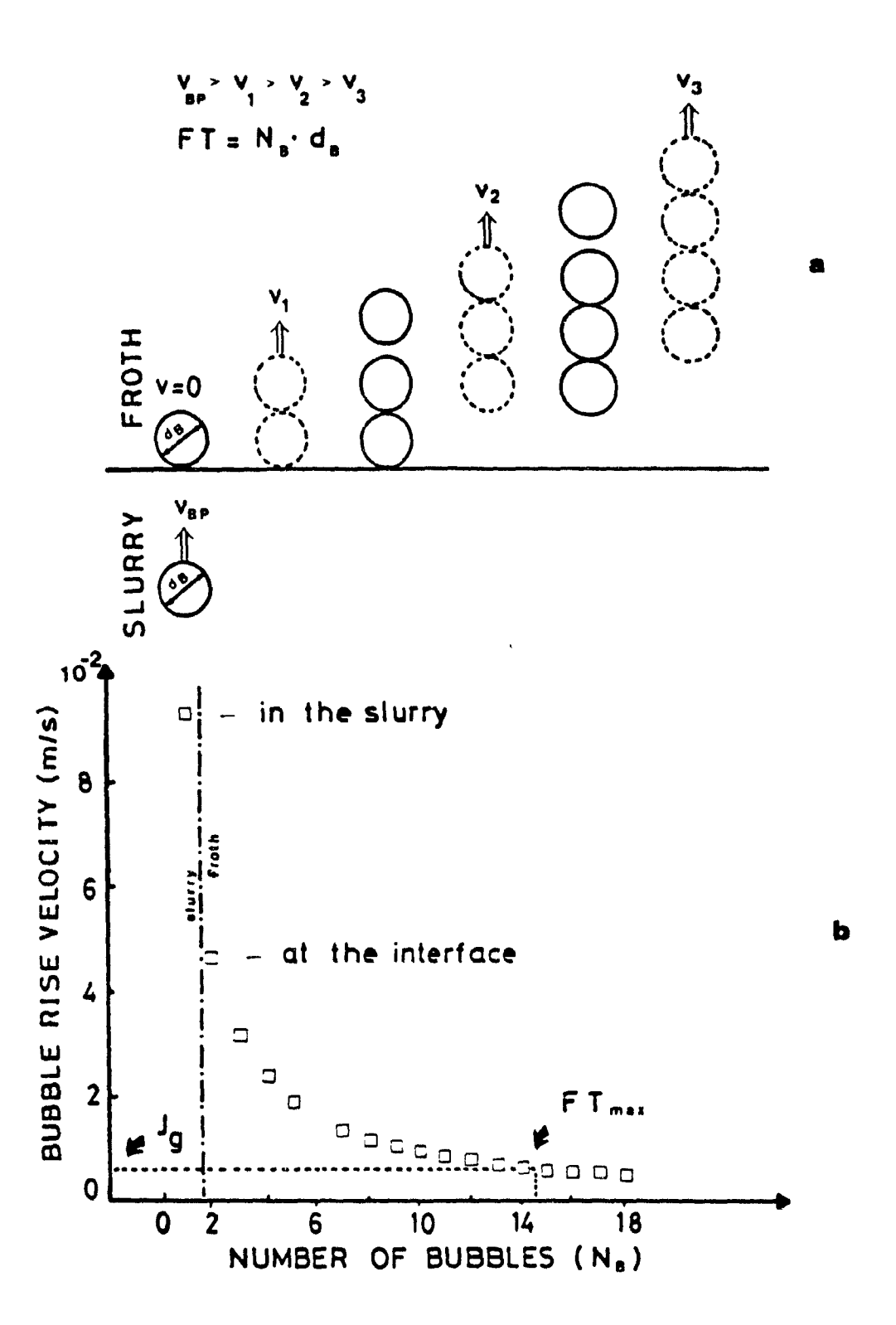


Figure 3.6a: Schematic view of bubble collision at the interface and in the froth phase.

Figure 3.6b: Bubble rise velocity decrease in the froth phase.

3.4 Bubble Surface Loss

The mechanism by which bubbles increase in size upward through the froth is mainly entropic. Although their surface tension has been appreciably lowered by armouring i.e. local change in bubble surface tension, it is still considerable. When several tiny bubbles merge, the total air volume remains the same but the total bubble surface shrinks considerably; stated mathematically, n bubbles, each of the same radius and having a combined area A, will then merge to form one new spherical bubble of volume equal to their combined volume and of area A':

$$\frac{A'}{A} = \frac{1}{\sqrt[3]{n}}$$
3.25

Merging two identical bubbles into one bubble will reduce the available surface to about 79% of the original surface. The surface loss increases substantially as the number of coalescing bubbles increases, as shown in Figure 3.7. Bubble surface shrinkage adversely affect the carrying capacity of the froth.

3.5 Froth Structure

The froth phase in mechanical flotation cells can be schematically divided into three sections (Figure 3.8). Section 1 is the bottom part of the froth phase between the slurry-froth interface and the cell overflow lip. The vertical distance between interface and the cell lip level (T) determines the concentrate grade and selectivity between valuable and gangue

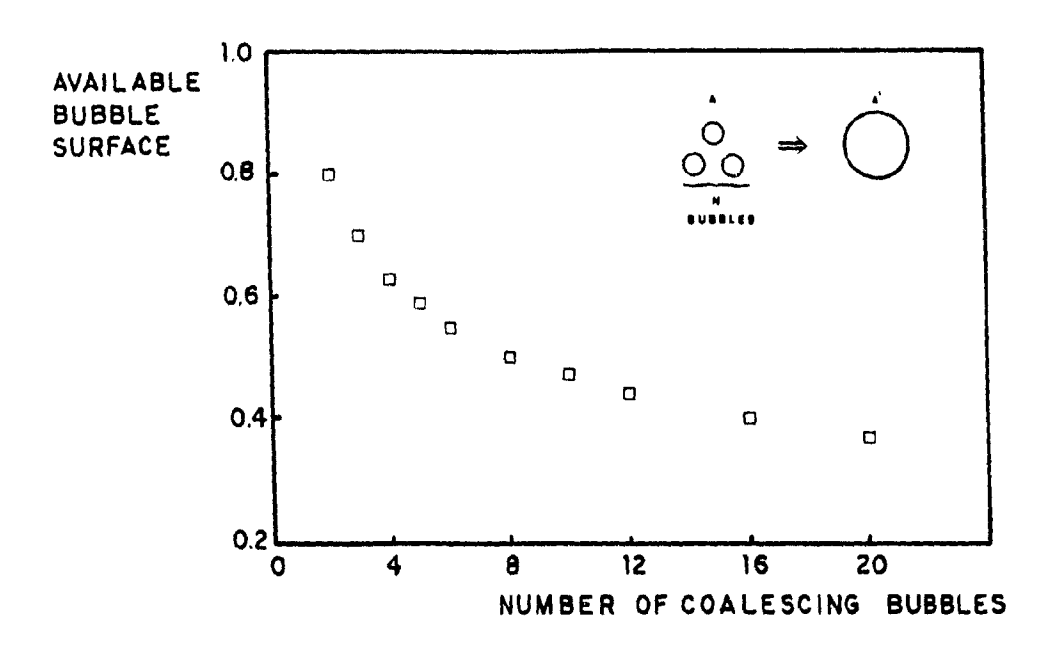


Figure 3.7: Available bubble surface as a function of coalescing number of bubbles.

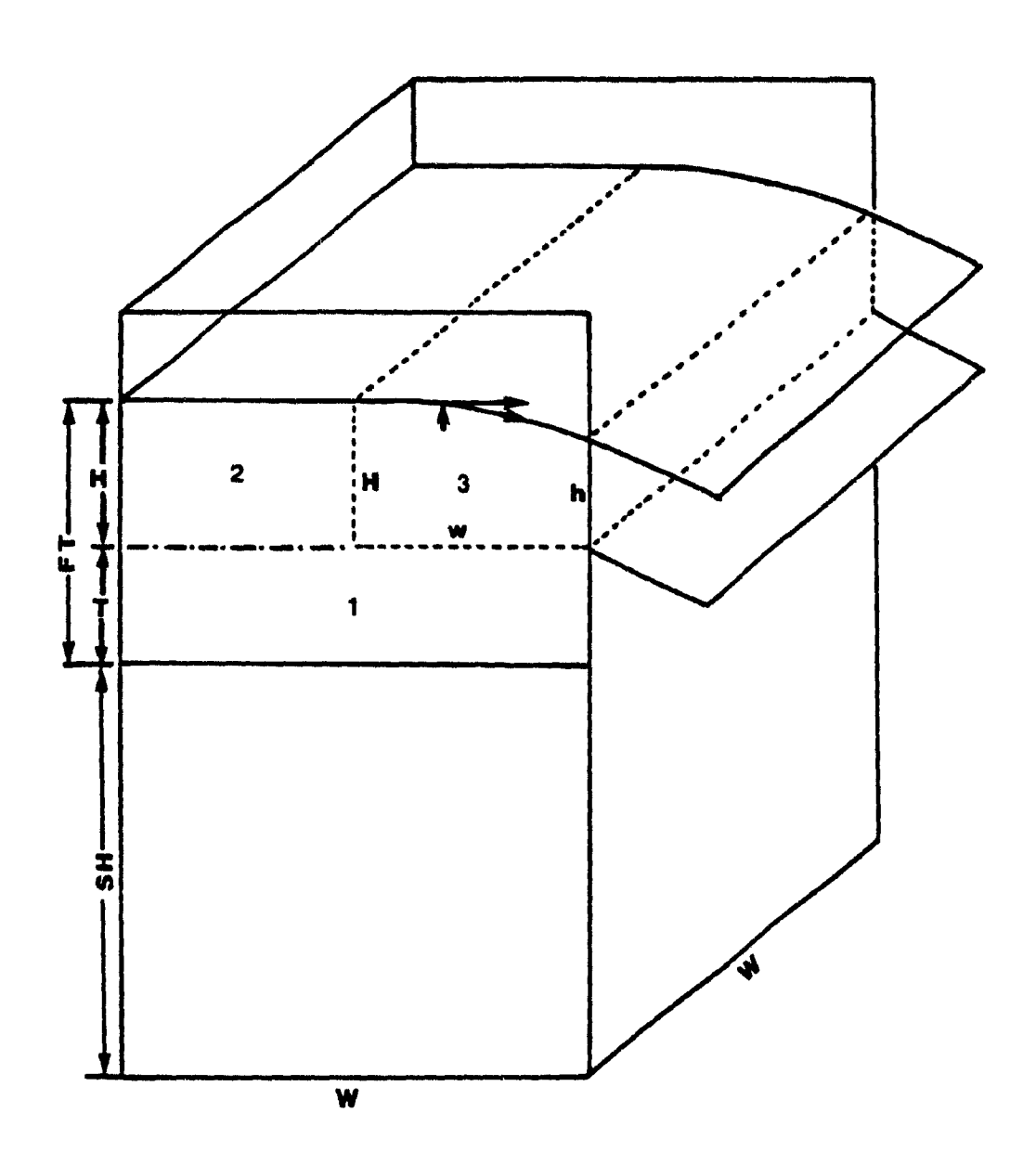


Figure 3.8: Froth phase in mechanical flotation cells.

particles. The higher T, the better the gangue rejection at the expense of the production rate.

Sections 2 and 3 are above the section 1. Section 2 is at the back part of the cell. This section cannot be utilized for production due to design constraints in the single sided overflow cells. The vertical height (H) is almost constant throughout this section. Bubbles along with liquid rise vertically like plug flow in section 1 and 2. After reaching the froth surface, bubbles burst and liquid drains back first into section 1 and then into the slurry phase.

Section 3 is at the top front part (i.e. overflow side) of the cell. This section determines the recovery from the cell. The vertical thickness decreases from H to h at the cell lip due to frictional losses and stream line contraction.

In flotation, recovery can be increased by increasing cell lip length (W) and H. Lip length is generally determined by the manufacturers. For existing plants, H, which is mainly affected by J_{q} , J_{w} , T, rpm, and frother dosage, is the only operating variable to increase recovery.

A structural model of a countercurrent water-bubble bed was derived from local gas holdup and bubble size measurements in flotation column by Yianatos et al. (1986). They observed three different zones in column froths with wash water addition a few centimeter below the overflow lip: an expanded bubble bed, a packed bubble bed, and a conventional draining froth.

The conventional draining froth section at the top did not occur in this system because wash water is added above the froth phase. From experimental holdup measurements and observations, the presence of two distinct sections can be distinguished (Figure 3.9). The first zone is an expanded bubble bed where the gas holdup is less than 74% and bubbles are quite small and spherical. The thickness of this zone (1-1.5 cm) depends on air and water rates.

The second section, which extends until the top of the froth, is the packed bubble bed. The maximum fractional liquid holdup that can be supported in a homogeneous packed bubble bed of spheres is 26%. Generally the packed bubble bed is thicker than the expanded bubble bed.

In general, froth can be divided into two extreme types. These are wet (high liquid content) froths, with spherical bubbles and dry (low liquid content) froths, with polyhedral bubbles. Three different froth structures are encountered in flotation practice: conventional draining froth, polyhedral froth, and washed froth (Figure 3.10).

Entrainment occurs when particles enter the base of the froth phase suspended in the inter-bubble water occupying the spaces between bubbles. The wetter the froth, the greater the proportion of particles in the concentrate that will be recovered by entrainment rather than by true flotation. This is partly because

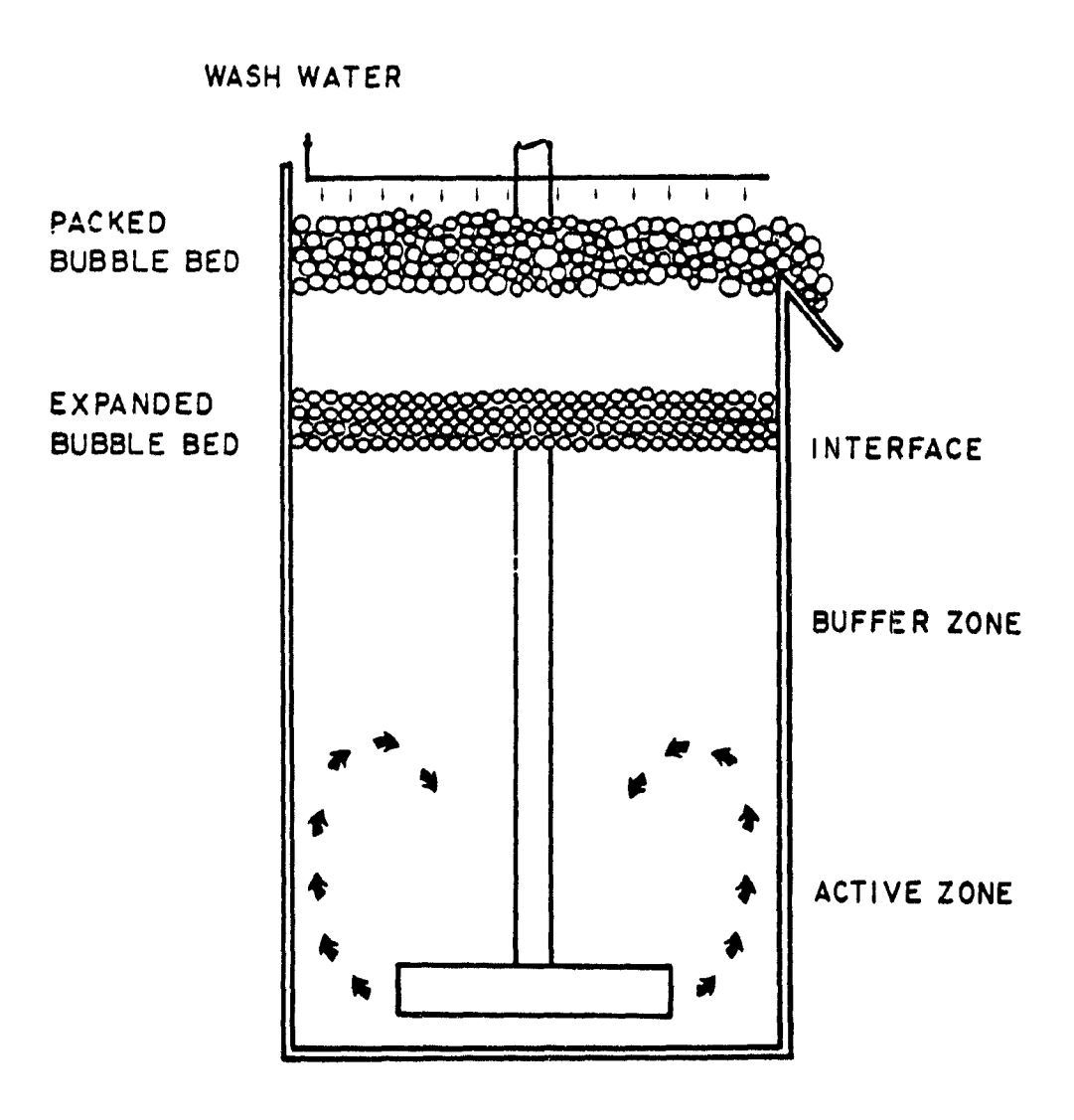


Figure 3.9: Different froth zones in the modified cell.

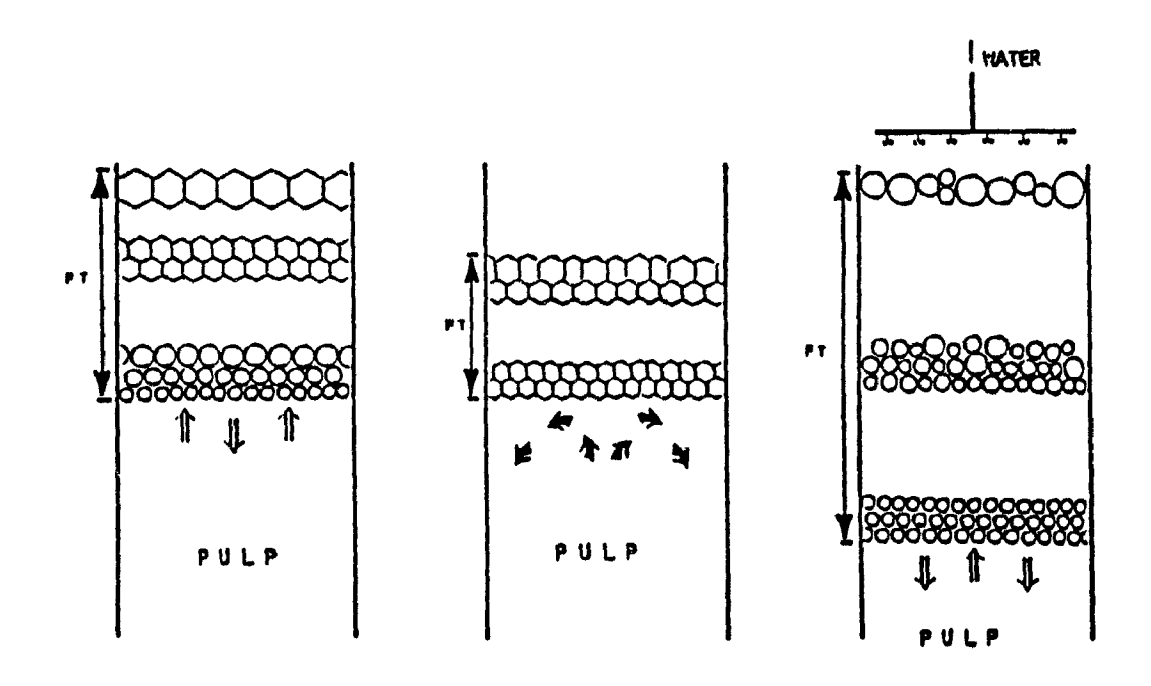


Figure 3.10: Three different froth structure encountered in flotation.

Draining Froth	Polyhedral Froth	Washed Froth
more entrainment	less entrainment	less entrainment
more coalescence	more coalescence	less coalescence
more drainage	less drainage	more drainage
not very stable	not stable	very stable
difficult to remove	difficult to remove	move easily
easy to produce	difficult to produce	produced easily
shallow froth	shallow froth	deep froth

in wetter froths, bubbles are spherical and fill the available space less efficiently than the larger polyhedral bubbles of drier froths, thus increasing entrainment of gangue in the inter-bubble water (Koh and Warren, 1979).

In conventional draining froths, which are commonly encountered in mechanical cells without wash water addition, spherical bubbles do not normally exist at distances higher than two or three bubble diameters above the pulp zone. Then, due to water drainage between bubbles and compression, spherical bubbles assume a polyhedral shape. In these type froths, the net liquid velocity is upward; this is one of the main causes of fine particle entrainment.

Thin polyhedral froths, which may be produced in ultrafine flotation at low agration rates and are not usually good for mass transfer, fill the available space more efficiently than small spherical bubbles and limit liquid penetration (entrainment) into the froth phase. Allowable froth is often limited by bubble coalescence. Generation of polyhedral froths is generally difficult in normal flotation operations.

In a washed froth, bubbles are well separated from each other and gangue drainage between bubbles is promoted by a net downward water flowrate. Froth can expand significantly with a good stability if there is a positive bias. Penetration of feed water can easily be suppressed and returned back to the pulp zone through drainage channels. A polyhedral bubble zone can be

generated at the top of washed froths, if wash water is added a few centimetres below the top of the froth surface, but this may not be advantageous. If it is added above the froth surface, then polyhedral bubbles cannot be seen.

Figure 3.11 shows the washed froth in the modified Denver cell. Bubble size significantly increases towards the froth surface but bubbles still remain spherical.

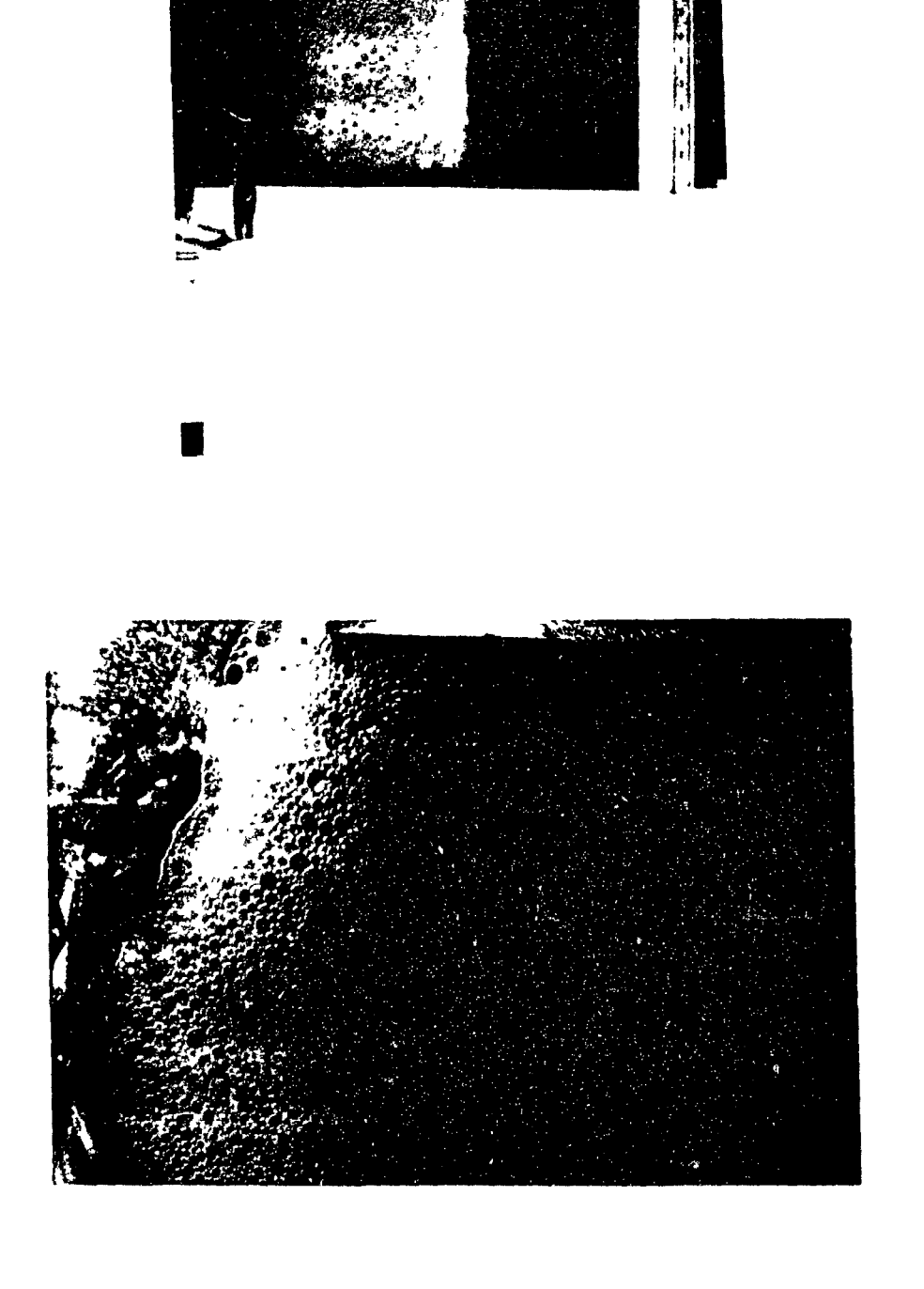
What is a good froth from flotation point of view? A good froth could be considered to contain mostly spherical bubbles grading upwards into large bubbles with little water. However, from an entrainment point of view polyhedral froths are desirable. In mechanical cells with wash water addition, an expanded and washed froth, which approaches flotation column froths, can be created. Comparing of the three froth structures reveals that washed froths yield the good mass transfer properties of small spherical bubbles, without the penalty of higher entrainment.

3.6 Experimental

3.6.1 Set-up

The general set-up has been discussed in Chapter 2; specific to this study is the measurement of gas hold-up in the froth phase which will now be discussed.

Dowfroth 250C at a concentration of 10 or 15 ppm added to the conditioning tank was used as a frother. Experiments were performed with and without froth overflow. Continuous



Ţ

Washed froth in the modified coll inote that bubbles are spherical). Figure 3 11

experiments were carried out in a close circuit-i.e. feed and wash water coming from a conditioning tank (50 L) to which tails and concentrate are pumped. Impeller speed was 1500 rpm, unless otherwise stated.

It was observed that some of the gas bubbles in the present cell were discharged from the tailings stream due to the location of the tailing discharge outlet. This problem was minimized by putting a vertical barrier in front of the tailing discharge outlet.

3.6.2 Conductivity Measurements to Determine Gas Holdup in the Froth Phase

Gas holdup in the froth phase was determined by measuring the conductivity between electrode plates at different vertical locations. Assuming a cellular bubble shape with the ions preferentially migrating along the borders, a simplified geometrical tortuosity model relates conductivity and gas holdup (Yianatos et al., 1986):

$$\varepsilon_{\rm bf} = \frac{C}{2.315 * C_{\varepsilon} + C}$$
3.26

where $\varepsilon_{\rm hf}$: fractional gas holdup in the froth

 C_{ε} : conductivity with air

C: conductivity without air

Table 3.1 shows the reproducibility of conductivity measurements. 60 to 260 readings were taken at 3 sec intervals (conductimeter response time is around 2 sec) and then average

readings and standard deviations were calculated. As can be seen from Table 3.1, most data have less than \$10% error limit.

When first measuring conductivity in this system, one problem was encountered. In a conventional flotation cell, there is a metallic standpipe in the cell, which may work as an electrode with one electrode connected to the conductivity meter, a conductivity measurement could be obtained, without connecting the second electrode ground to the conductimeter. Thus, the standpipe worked as ground. After realization of this problem, metallic (electrical) contact between impeller motor and standpipe was prevented by using teflon insulators.

Table 3.1: Reproducibility of conductivity measurements.

Number	Ave. Cond.	St andard	Location Above	Froth
of Read.	Reading	Deviation	Interface	Thickness
92	15.2	1.1	3.7	4.2
260	15.0	1.2	3.7	4.2
92	36.6	1.8	2.6	4.2
187	36.7	1.6	2.6	4.2
152	78.3	3.4	1.6	4.2
88	79.4	4.5	1.6	4.2
63	169.3	17.8	0.5	4.2
128	156.8	13.2	0.5	4.2
205	14.1	1.3	3.5	4.0
69	13.6	1.6	3.5	4.0
168	46.3	5.0	2.5	4.0
76	44.2	3.3	2.5	4.0
67	78.1	3.0	1.5	4.0
114	90.2	4.3	1.5	4.0
178	260.0	27.0	0.5	4.0

3.6.3 Electrode Assemblies

For this study, three different types of electrodes were designed: single, quadruple, and open. The single electrode was used to measure point gas holdup in the froth. The quadruple-electrode assembly was used to measure local gas holdup at the same horizontal level. Square plate electrodes (1*1 cm²) made of stainless steel were connected to the conductimeter. These electrodes were fixed in a plexiglass cubic prism cage (side: 1.5 cm) open at the top and bottom to allow vertical liquid flow between electrodes. The quadruple electrode assembly was fixed in a plexiglass frame; it was positioned in such a way that the water spray did not directly affect measurements. Figure 3.12 shows the dimensions of the two electrode assemblies.

The open electrode was used to take measurements at the surface of the froth near the overflow lip. Two stainless steel electrodes (1*2 cm) were placed 1 cm apart from each other not to disturb both horizontal and vertical flow and the effect of pulp level change on conductivity is minimized. The data acquisition system described in Figure 2.5 was used for the quadruple assembly, conductivity being read sequentially.

3.6.4 Test Program

Gas Holdup Profile in the Froth Phase: Preliminary test work focussed on the effect of superficial gas and liquid rates and frother concentration on the gas holdup profile, which was determined using the single electrode system in the absence of froth overflow. Wash water was added 4 cm above the froth surface

t

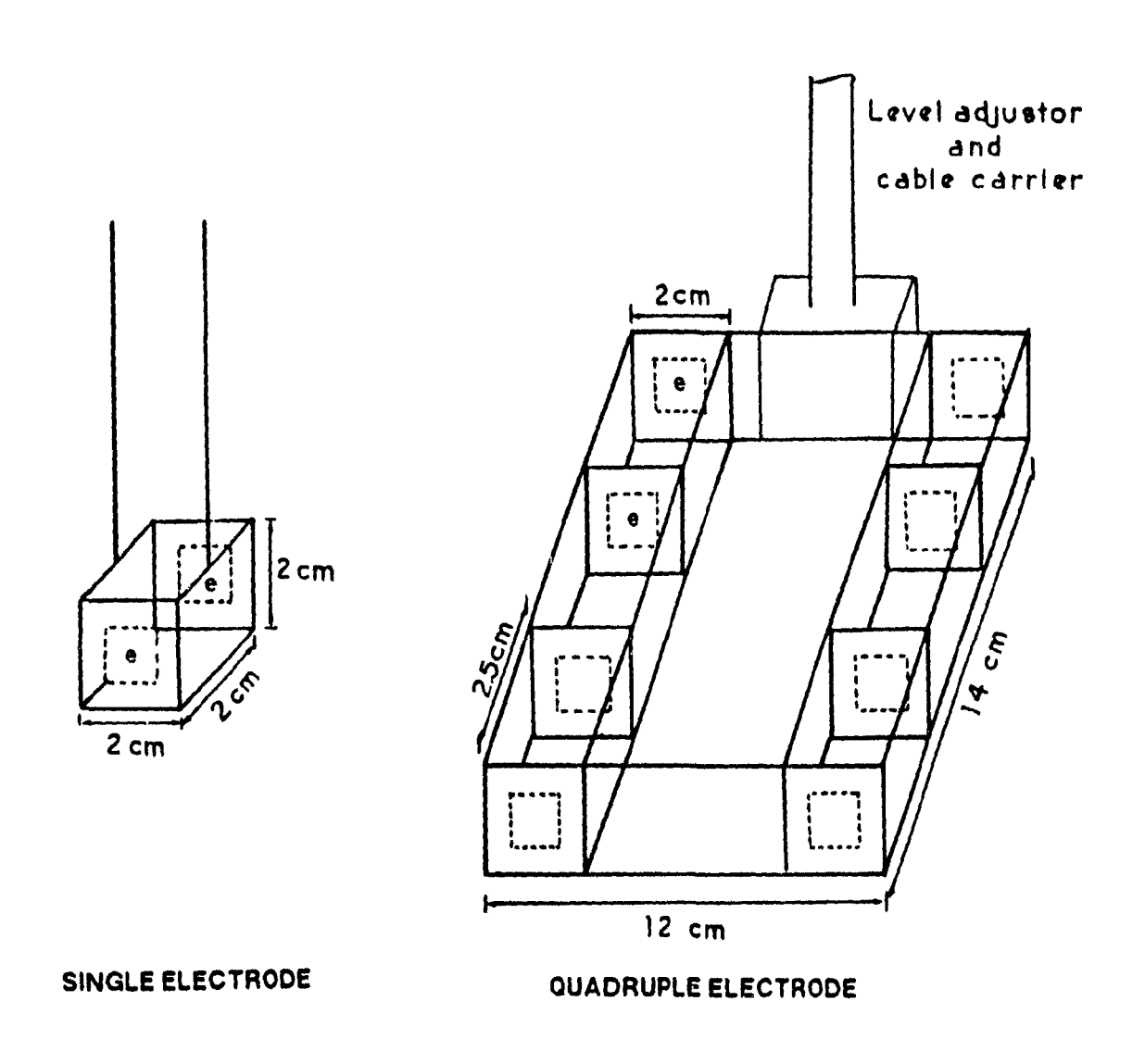


Figure 3.12: Electrode assemblies used in this work (e. electrode).

The test program is summarized in Table 3.2. The main objective in these tests was to determine the effect of superficial gas rate on the gas holdup profile and water balance.

In the first test series, J_f , J_w , and J_t were kept constant at three different gas rates. The aim here was to determine the effect of sudden change in aeration rate if there is no control action taking place. The single electrode was used to measure the gas holdup.

Table 3.2: Experimental test conditions. (J's are in cm/s and FT, T, and H are in cm).

Test series	constant	V A R I A I dependent	B L E S contro input	lled output	electrode type
I	J, H, J, (0.14)	J _e н Т	-	-	single
II	J _f , H _w J _w (0.14)	H J	T(2)	Jŧ	single
III	J f J _w (0.06)		FT(4) H(2)	H.	quadruple
IV	H T L	J _c H	T(2)	J	open

In the second test series, the slurry level (SH) was maintained constant by adjusting the tailing flowrate at constant J_f and J_w . The single electrode system was also used. This series is meant to illustrate the effect of changing superficial gas velocity at constant slurry level.

In the third test series, the effect of J_g was investigated at a much lower J_w (0.06 cm/s). Slurry level was maintained constant by adjusting tailing flowrate and FT was maintained constant by adjusting the distributor height (H_j).

In the fourth test series, J_{w} was used to keep slurry level constant and J_{g} was varied. This scheme corresponds to a possible approach to column flotation control.

Test series five was carried out to determine the J_c by changing the J_g , J_w , H, and T (Table 3.4). Gas holdup was measured using the open electrodes.

Local Gas Holdup in the Froth Phase: The effect of wash water flowrate, impeller speed, and froth thickness on local gas holdup was determined using the quadruple-electrode assembly. For the gas holdup calculation, the average of the quadruple electrode readings was used. In the froth thickness test (Table 3.6), the electrode assembly was fixed at the cell lip level for two FTs.

3.6.5 Determination of the Amount of Water in the Concentrate (J_c)

In a two phase system, water recovery to the concentrate was estimated using the weir equation. A comprehensive model was developed for prediction of J. The calculation algorithm is shown in Table 3.3. The model requires the measurement of conductivity in the slurry and froth phases to determine the gas holdup. At the beginning, it is also necessary to determine the cell discharge coefficients by measuring the H and actual J. Once the K was determined for a certain cell, it will be constant if the slurry level is maintained constant. There two ways to calculate FT : the momentum conservation model or direct use of Eq. 3.27. The discharge coefficient, K_{c} , can be calculated from measurements of the gas holdup at the cell lip level using the open electrode system and the actual water recovery. Then J_{α} is calculated from Eq. 3.14. If K_{α} is not constant due to variation in SH, the use of Eq. 3.29 is necessary. In order to compare the experimental calculated J_c values, experiments were performed at various J_c , J, J, H, T, and FT. Table 3.4 shows the operating variable ranges for the test series five.

Table 3.3: Algorithm for the water recovery calculations

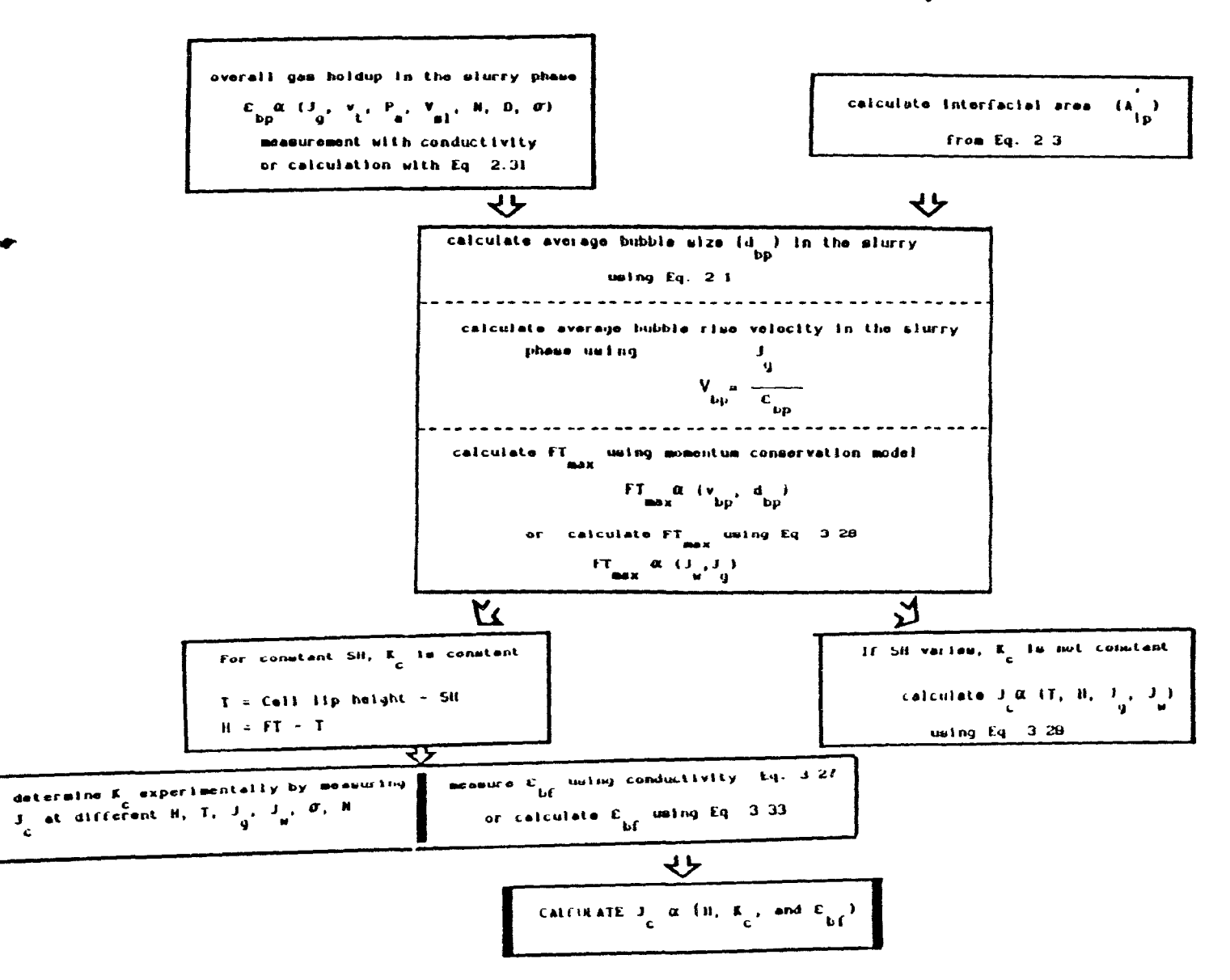


Table 3.4: Operating range of test series five to determine J_c .

(J's are in cm/s and T, FT, and H are in cm).

Variables	Range
J	0.11
J a	0.4 - 0.7
J ^m J ^d	0.03 - 0.14
J _e	0.16 - 0.2 4
J	0.001 - 0.050
FT	2 - 2.4
H T	1 - 2 1 - 2.5
	1 - 2.5

3.7 Results and Discussion

3.7.1 Froth Expansion

Figure 3.13 shows the froth expansion in the modified cell as a function of wash water superficial rate at different superficial gas rates. During these experiments, there was no froth overflow. Equivalent air flow numbers, N_Q , are also indicated in the same figure. As superficial wash water and gas rates increase, froth thickness increases. The higher the superficial gas rate, the higher will be the rate of increase in the froth thickness.

A number of empirical relationships were tested to estimate FT_{max} using polynomial regressions. The following equation proved to give best fit at a correlation coefficient of 0.94:

$$FT_{\text{max}} = -0.34 - 308.6J_{\text{w}}^2 + 6.4J_{\text{g}} + 1078.1J_{\text{w}}^2.J_{\text{g}}$$
 3.27

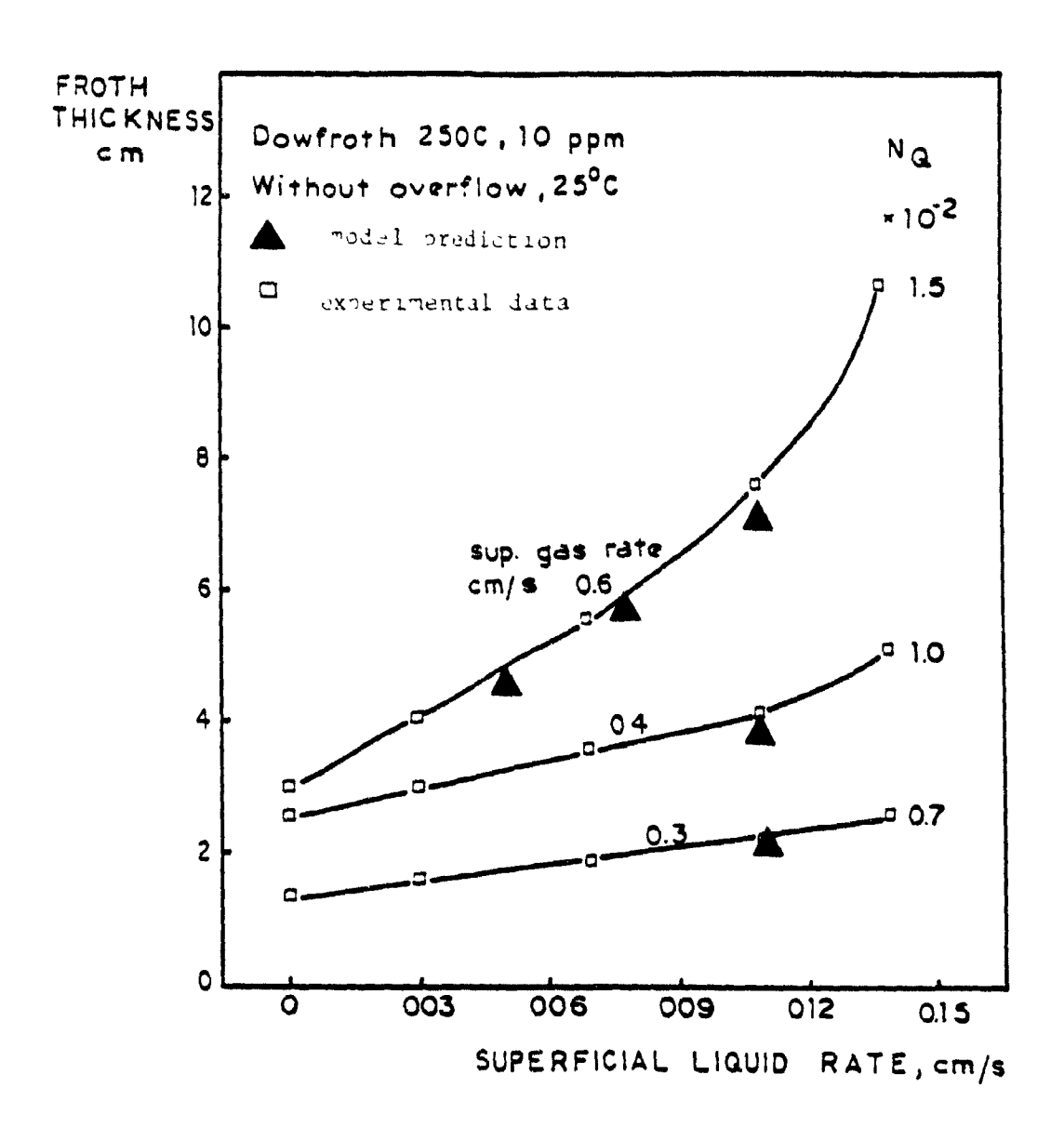


Figure 3.13: Froth expansion without overflow $(N_0 - air flow number)$.

(Model: momentum conservation predictions)

where FT is in cm and superficial rates are in cm/s.

Estimation of Maximum Froth Expansion Using Simple Momentum Figure 3.13 also shows the predicted maximum Conservation: attainable froth thicknesses using the simple momentum conservation model. There is a reasonably good agreement between experimentally measured froth thicknesses and predicted values. Therefore, the model can be used to estimate the maximum froth thickness by knowing average gas holdup and bubble size in the slurry phase. The slight underestimation of experimental data is most likely due to not taking into account the effect of liquid films around the bubbles in the simplified model.

Figure 3.14 shows the effect of impeller speed and aeration rate on froth expansion along with gas holdup in the slurry phase at a constant water volume (height) in the modified cell. Increasing superficial gas rates and impeller speed leads to thicker froths in the absence of froth overflow mainly due to increased gas content in the slurry phase.

Effect of Wash Water Addition Level on Froth Expansion: The effect of wash water addition level on the froth expansion with froth overflow at constant tails flowrate is given in Figure 3.15. In this graph a minus sign indicates that the wash water is added below the slurry-froth interface, zero means that addition is just at the interface and positive values stands for addition above the froth surface. The upper curves, FT, show the total froth expansion i.e. the distance between the slurry-froth interface,

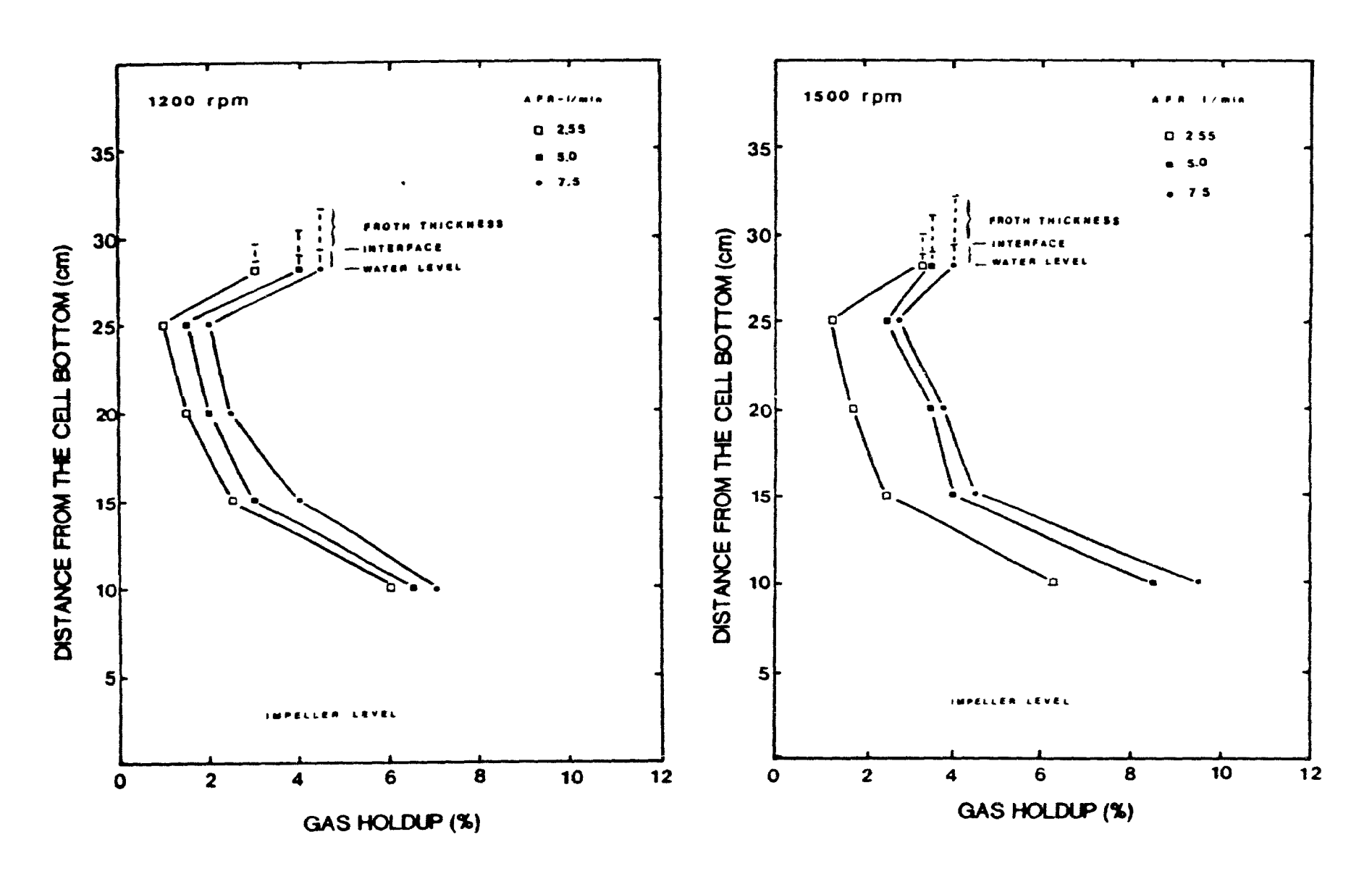


Figure 3.14. Froth expansion and gas holdup in the slurry phase

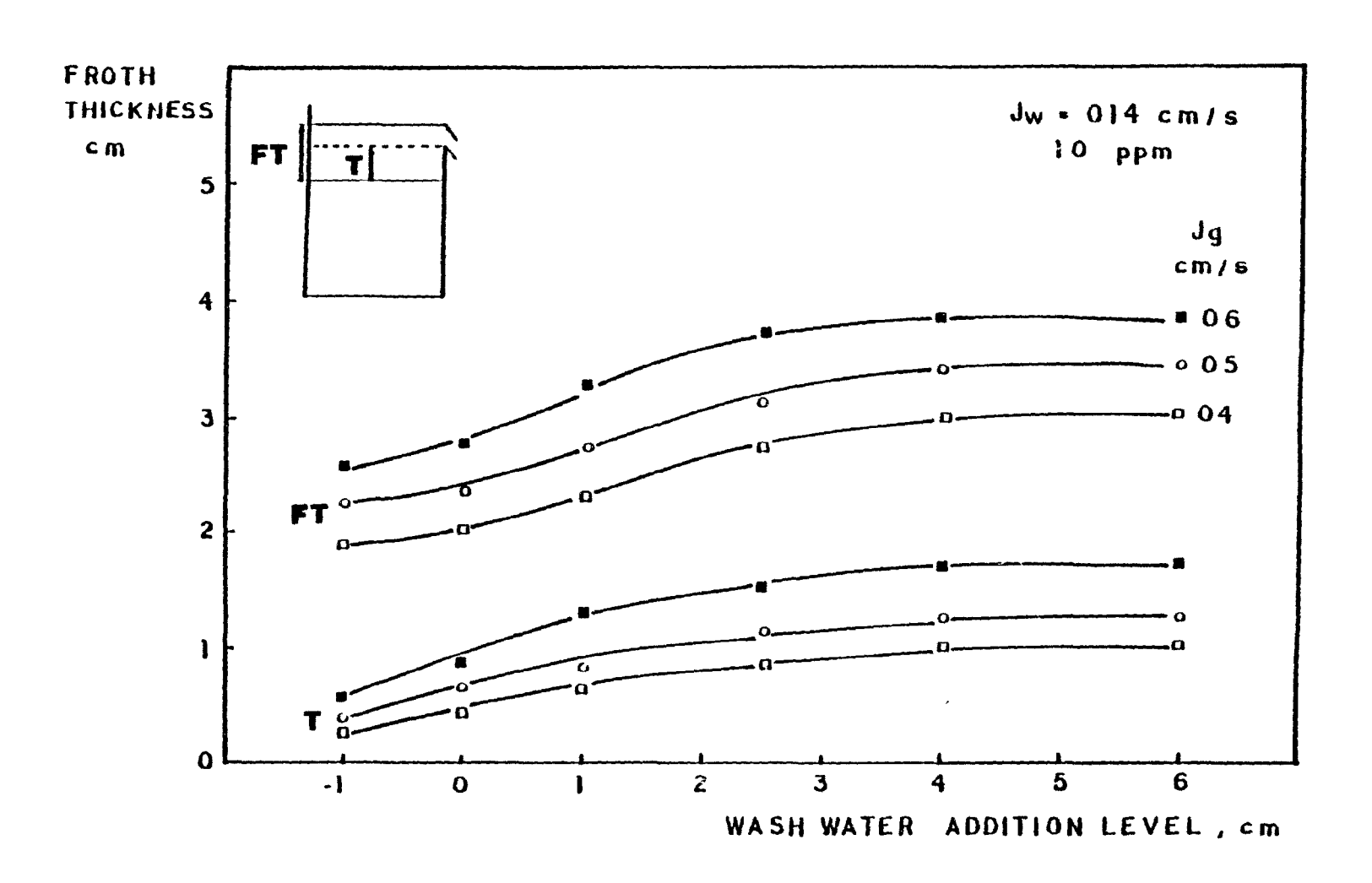


Figure 3.15: Effect of wash water addition level on froth expansion.

and the froth surface while the lower curves, T, indicate the distance between slurry-froth interface and the overflow lip. As can be seen from the graph, froth thickness increases as the wash water addition level rises up to 4 cm above the froth; the expansion then levels off.

Froth also expands more with increasing gas superficial rate. In the presence of overflow the froth cannot expand as much. It should be noted that when wash water is added below the slurry-froth interface, the froth cannot expand but if it is added at the interface or above the froth zone, there is a significant expansion in the froth thickness. The expansion of froth with increasing addition height above the froth surface is related to wash water penetration depth, distribution, and residence time in the froth. Since froth expansion is beneficial, it is concluded that wash water addition should be at least 4 cm above the cell lip to reach its full benefit.

3.7.2 Point Gas Holdup Profile and Water Balance in the Froth Phase

Gas Holdup Profiles: Figures 3 16, 3.17, and 3 18 show typical axial profiles of gas holdup as a function of vertical distance from the slurry-froth interface in the absence of froth overflow. Figures 3 16 and 3 17 show that increases either in gas or wash water rate significantly decreases the gas content of the froth zone. An increase in aeration rate for a given frother concentration and impeller speed produces an increase in water entrainment due to the larger bubble production, which carry more

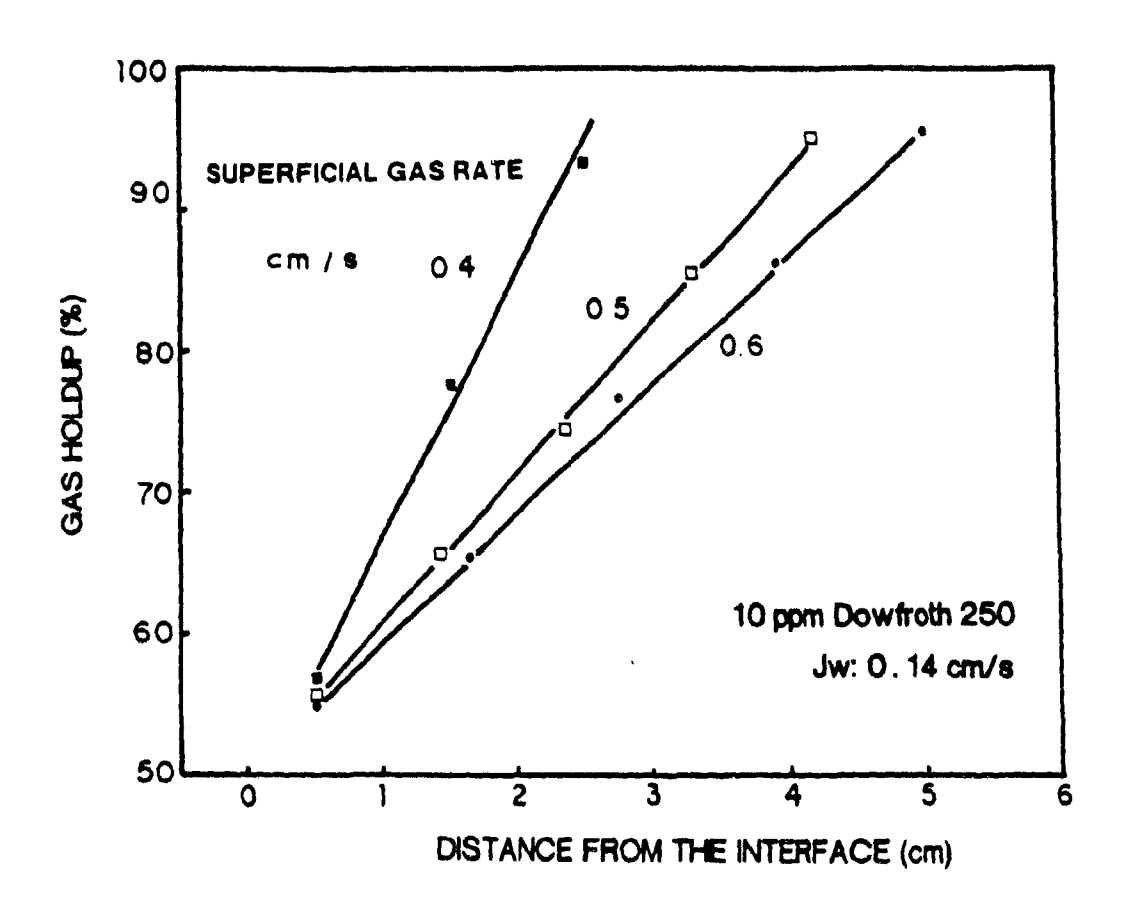


Figure 3.16: Effect of aeration rate on gas holdup (FTs are 3, 4.7, and 5.5 cm).

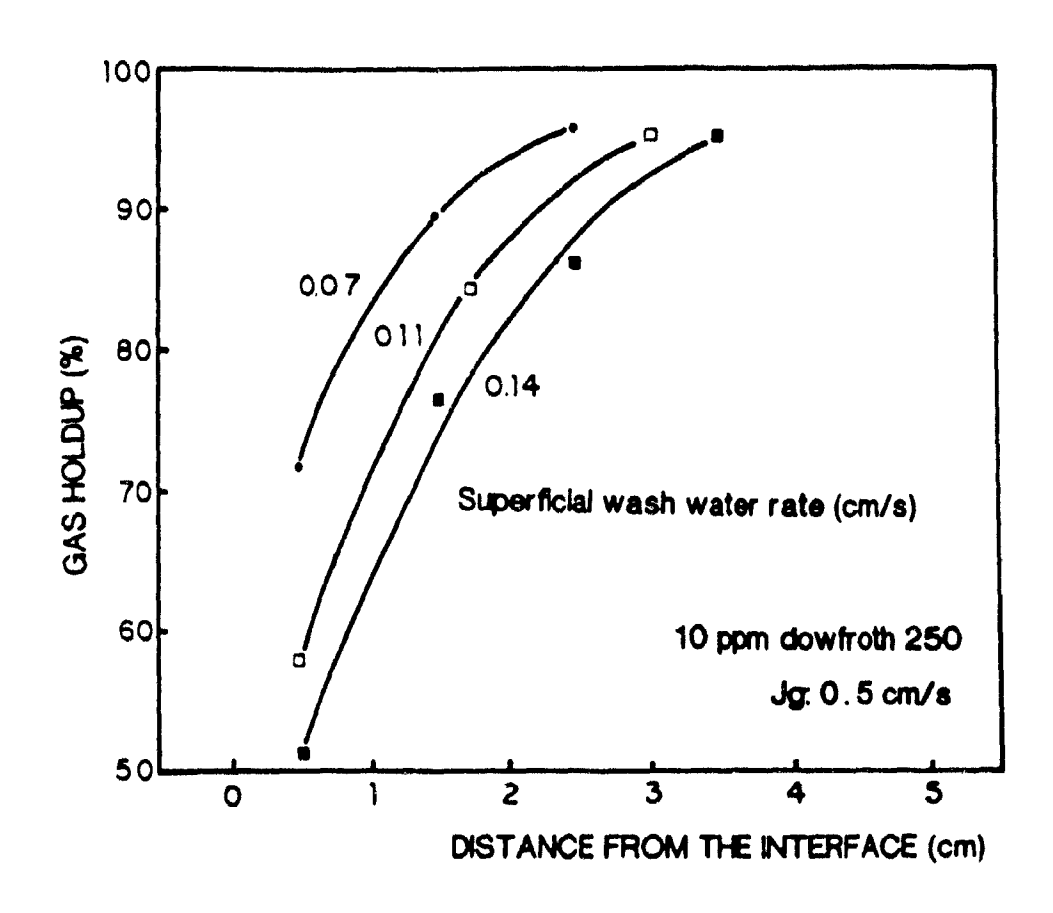


Figure 3.17: Effect of superficial wash water rate on gas holdup (FTs are 3, 3.5, and 4 cm)

water to the froth phase (the number of bubbles and their diameter increases). The following equations can be used to calculate percent gas holdup in the froth phase at different heights as a function of gas and wash water rates.

$$\varepsilon_{g} = 79.54 + 9.79.Z - 56.67. J_{g}$$
 3.28

$$\varepsilon_{q} = 0.778 + 0.113.Z - 1.573.J_{w}$$
 3.29

where Z: distance from the slurry-froth interface, cm

J: superficial gas rate, cm/s

J: superficial wash water rate, cm/s

Figure 3.18 shows that increasing frother dosage leads to significant increases in the liquid content in the froth zone, especially close to the interface, because of the decreased bubble size and the increased thickness of the water film surrounding the bubbles. The percent gas holdup was correlated to frother concentration and distance from the slurry-froth interface using the following equation:

$$\varepsilon_{g}$$
: 56.21 + 10.21.Z - C 3.30

where C: frother concentration in ppm

Klassen and Tikhonov (1964) concluded that aeration rate, impeller speed, and frother dosage increased water entrainment, the more effective variable being frother concentration in their system.

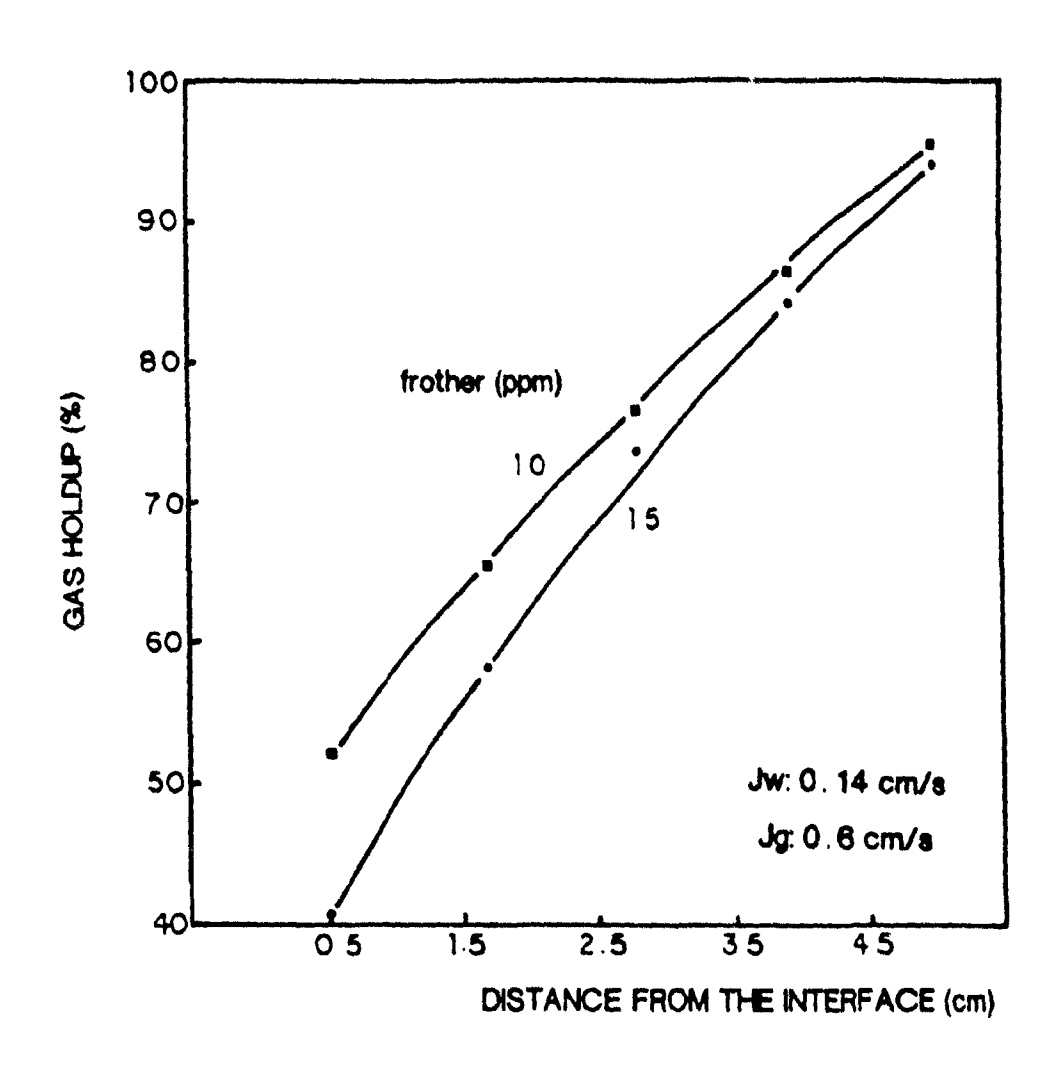


Figure 3.18: Effect of frother dosage on gas holdup

(FT is 5.5 cm and frother is Dowfroth 250)

Water Balance: In the presence of froth overflow, the gas and liquid holdups are significantly changed. Table 3.5 summarizes the water balance for the four test series.

In the first test series, although the tailing flowrate was not changed, J_t decreased with increasing aeration rate, because of gas entrainment in the tailing line. As a result, Jc increased slightly with increasing J_g . H and T increased with J_g , because of a significant increase in J_u : as more water is entrained in the froth phase, it needs a longer residence time (i.e. a thicker froth) to drain back to the slurry. Gas holdup profile is shown in Figure 19a.

In the second test series, the interface level was kept constant by varying tailings discharge flow rate at again three different gas rates (Figure 3.19b). Increasing J_{q} increased the liquid overflow rates because of the increasing FT and the resulting increase in the froth height above the cell lip, H.

For the first and second test series, the following equations can be used to calculate gas holdup in the froth phase:

$$\varepsilon_{g} = 77.52 + 9.60.2 - 30.23. J_{g}$$
 3.31

$$\varepsilon_{g} = 76.78 + 12.56.2 - 39.79.J_{g}$$
 3.32

If the data from test series one and two are combined, then the following equation can be developed:

$$\varepsilon_a = 77.17 + 11.26.Z - 35.71.J_a$$
 3.33

FI	21	j	J_t	j	J.	Je	j,	J,	$J_4 - J_a$	J., / J.	J ₄ / J ₄
(cm)	(cm)				(c a	/ =)				diacasi	onless
4.2	30,6	0.6	0.113	0.227	0.14	0,026	0.473	0,359	0.114	3,18	2,08
2.5	31.3	0.4	0.113	0,232	0,14	0,021	0,313	0,194	0.119	1.72	1.35
1.7	31.8	0.2	0,113	0.243	0,14	0,011	0.196	0,067	0.129	0.59	0,81
4.0	30.0	0.6	0.113	0.238	0.14	0.015	0.524	0,393	0.125	3,53	2,20
3.4	30.0	0,5	0,113	0.245	0.14	0.013	0,433	0.300	0.133	2,65	1.77
3.0	30.0	0.4	0.113	0,243	0.14	0.05	0.328	0.193	0.135	1.71	1.32
4.0	30,0	0,6	0.113	0,160	an,0	0.013	0,323	0.282	0.035	2.59	2.05
4.0	30,0	0.5	0.113	0,162	0,06	0.011	0.294	0.245	0.00	2.17	1.81
4 3	30.0	0.4	0.113	0.167	9,06	0.006	0.261	0.297	0,054	1.83	1.56
4,0	n.0	0.6	9,113	J'ItJ	1,761	1,113					
3.2	51.9	9.5	1,113	1,161	9.955	9,978					
3,9	₹), ე	9.4	9.113	1,153	า.ชา	1,713					

Table 3.5: Water balance around the flotation cell.

J: calculated from Eq. 3.6

J: calculated from J=J+J-Jc

J-J: bias

J/J: entrainment factor

J/J drainage factor

FT: froth thickness

SH slurry height

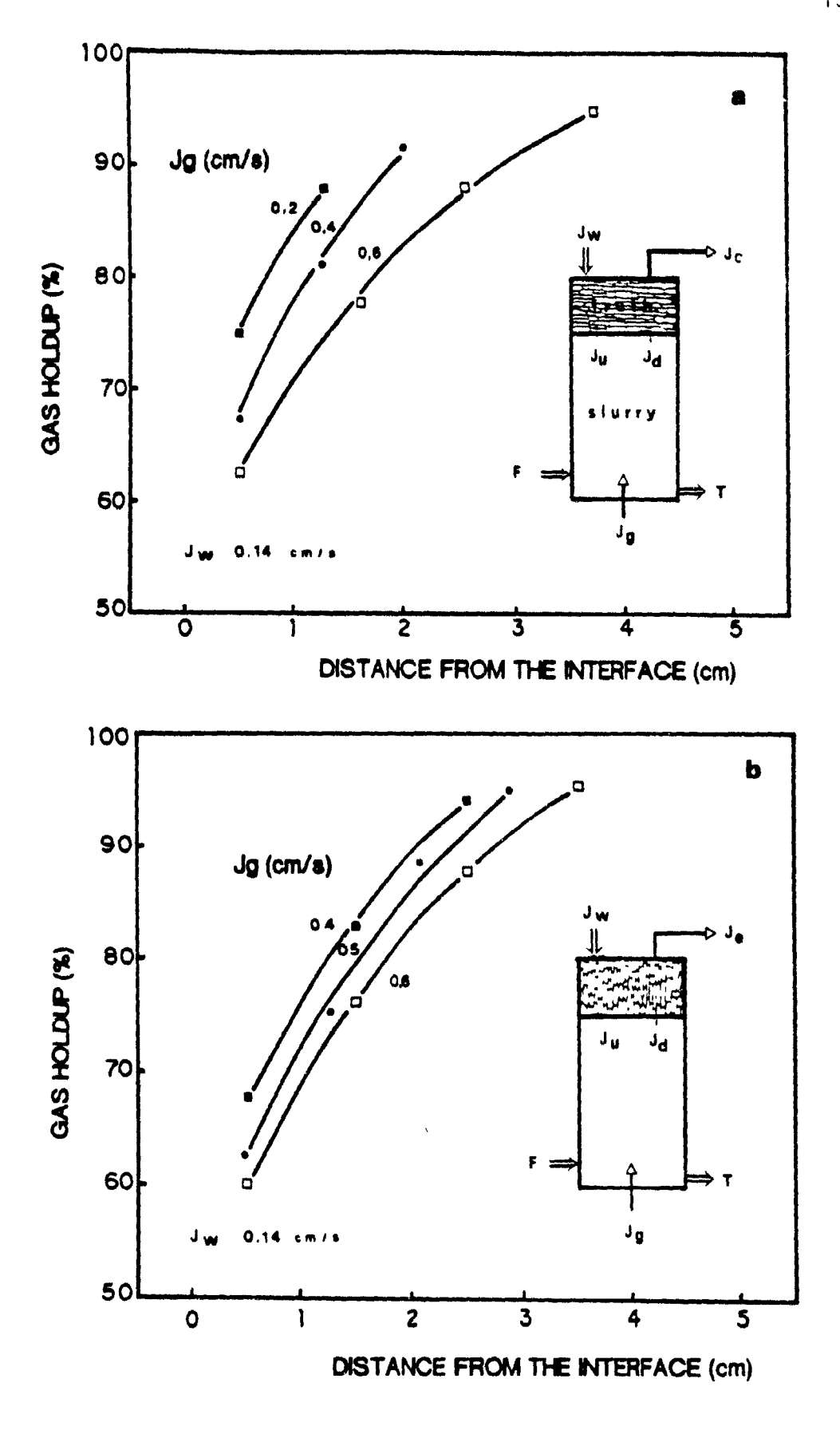


Figure 3.19: Gas holdup profile for the first two test series.

In the third test series, the effect of aeration was investigated at a much lower wash water addition rate ($J_u = 0.06$ cm/s) at a constant T and H. Thus, upward and downward liquid rates are lower than for the previous two cases. Again J_c , J_d , and J_u increase with increasing aeration rate. Since both H and T are constant, the increase in J_c can only be caused by an increase in ε_{bc} .

The four test series confirm that irrespective of the control scheme, gas rate can affect water recovery significantly, at constant slurry height. Liquid holdup increases significantly throughout with J_q ; consequently, all superficial liquid rates in the froth increase substantially: J_q , J_d , and J_c .

Figure 3.20 shows the overall gas holdup profile in the modified cell as a function of cell depth, with the horizontal axis in logarithmic scale. Gas holdup drastically increases near the slurry-froth interface due to the accumulation of fast rising bubbles before entering into the froth phase. Bubble rise velocity decreases because of collision of bubbles with the previously formed bubbles. Gas holdup parabolically increases in the froth phase.

Figure 3.21 shows the effect of $J_{\underline{u}}$ on gas holdup profile in a relatively deep froth. The higher the superficial wash water rate, the wetter the froth. The difference in froth wetness is more significant at the interface than at the top of the froth.

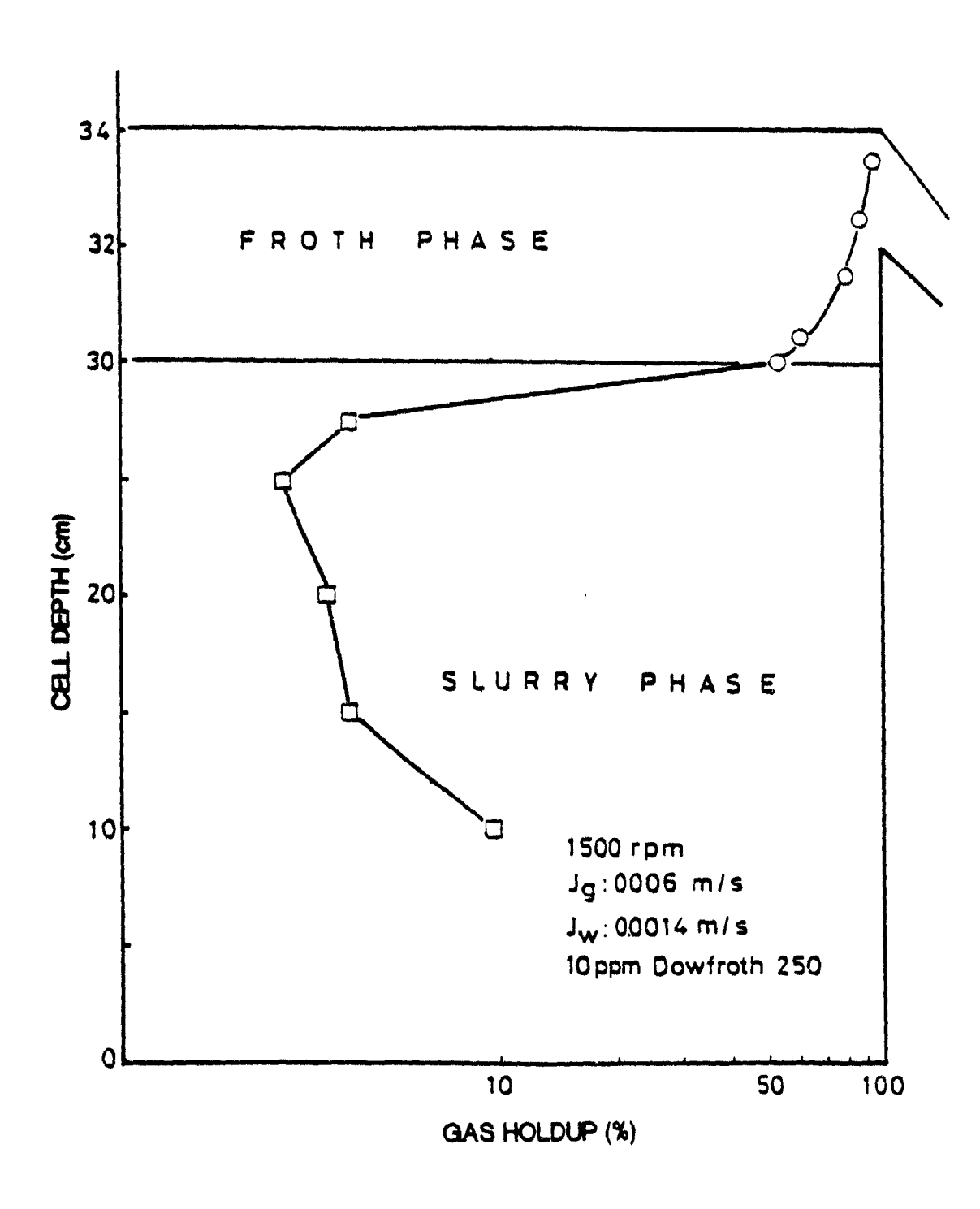


Figure 3.20: Gas holdup distribution in the modified cell.

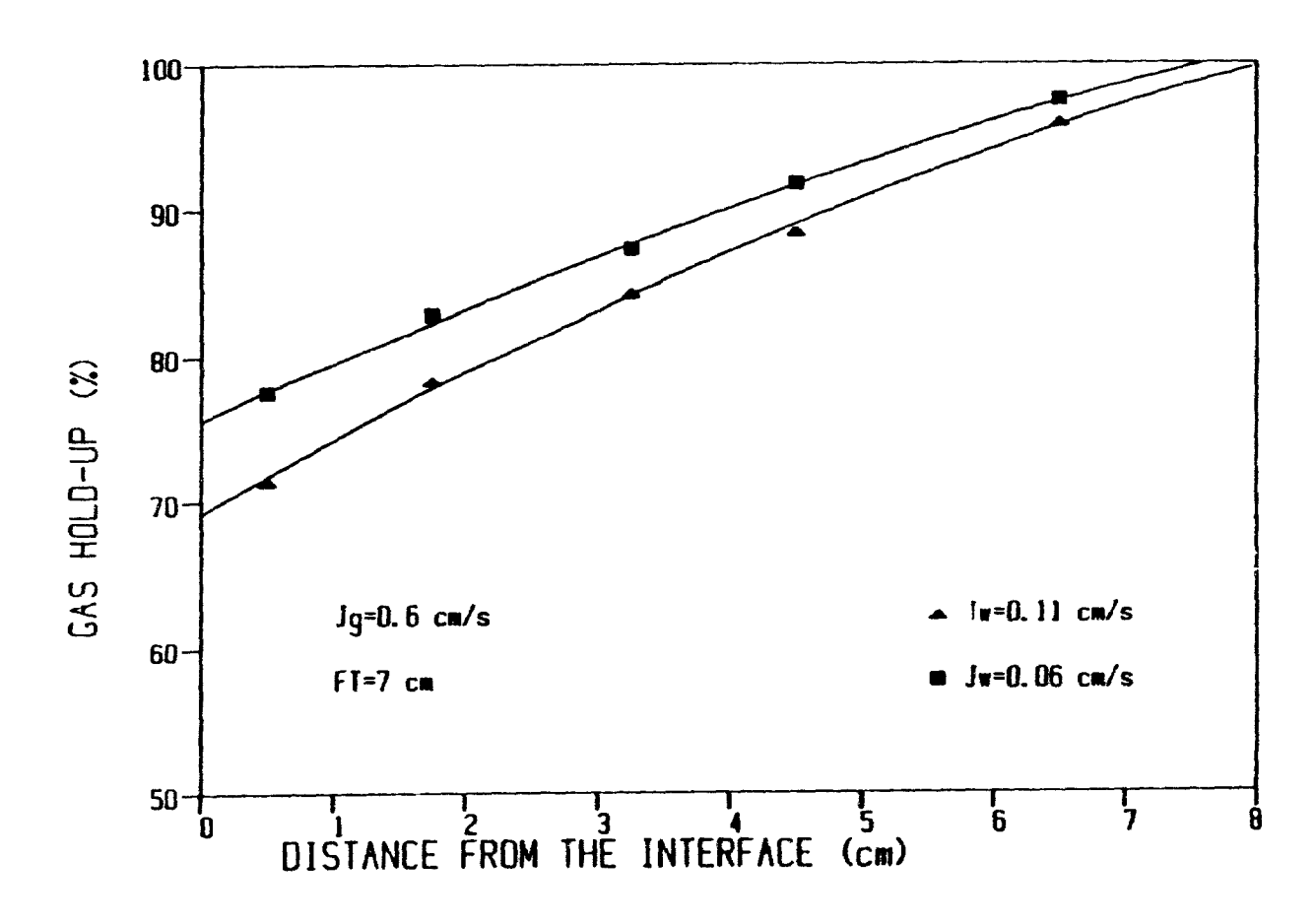


Figure 3.21: Gas holdup profiles at two different superficial wash water rates.

Entrainment and cleaning factors are introduced here in order to understand the effect of aeration rate. J_u/J_f is used as an entrainment factor while J_d/J_f is used as a cleaning (drainage) factor. J_u and J_d were calculated at the interface level. A higher drainage factor and a lower entrainment factor are desirable in flotation operation to achieve low hydraulic entrainment. Both entrainment and drainage factors increase with increasing aeration rate.

The change in upward and downward superficial liquid velocities as a function of distance above the slurry-froth interface at different wash water addition rates are given in Figure 3.22. Both upward and downward liquid rates significantly decrease with increasing distance above the interface. It should be noted that $(J_d - J_u)$ increases with increasing wash water addition rate and is constant throughout the froth phase. A higher bias $(J_d - J_u)$ means less entrainment due to suppression of feed water with wash water and a better cleaning action in the froth.

3.7.3 Prediction of Superficial Concentrate Rate (J c)

At constant SH and T, K_c is constant and J_c can be determined from the weir equation by measuring only H and ε_{lf} , which is obtained from conductivity measurements. Figure 3.23 shows Q_c as a function of W.H^{1.S}. ε_{lf} . In the normal operating range, K_c was calculated to be 0.00887 for the modified laboratory cell. A plot of experimental Q_c versus predicted Q_c is given in

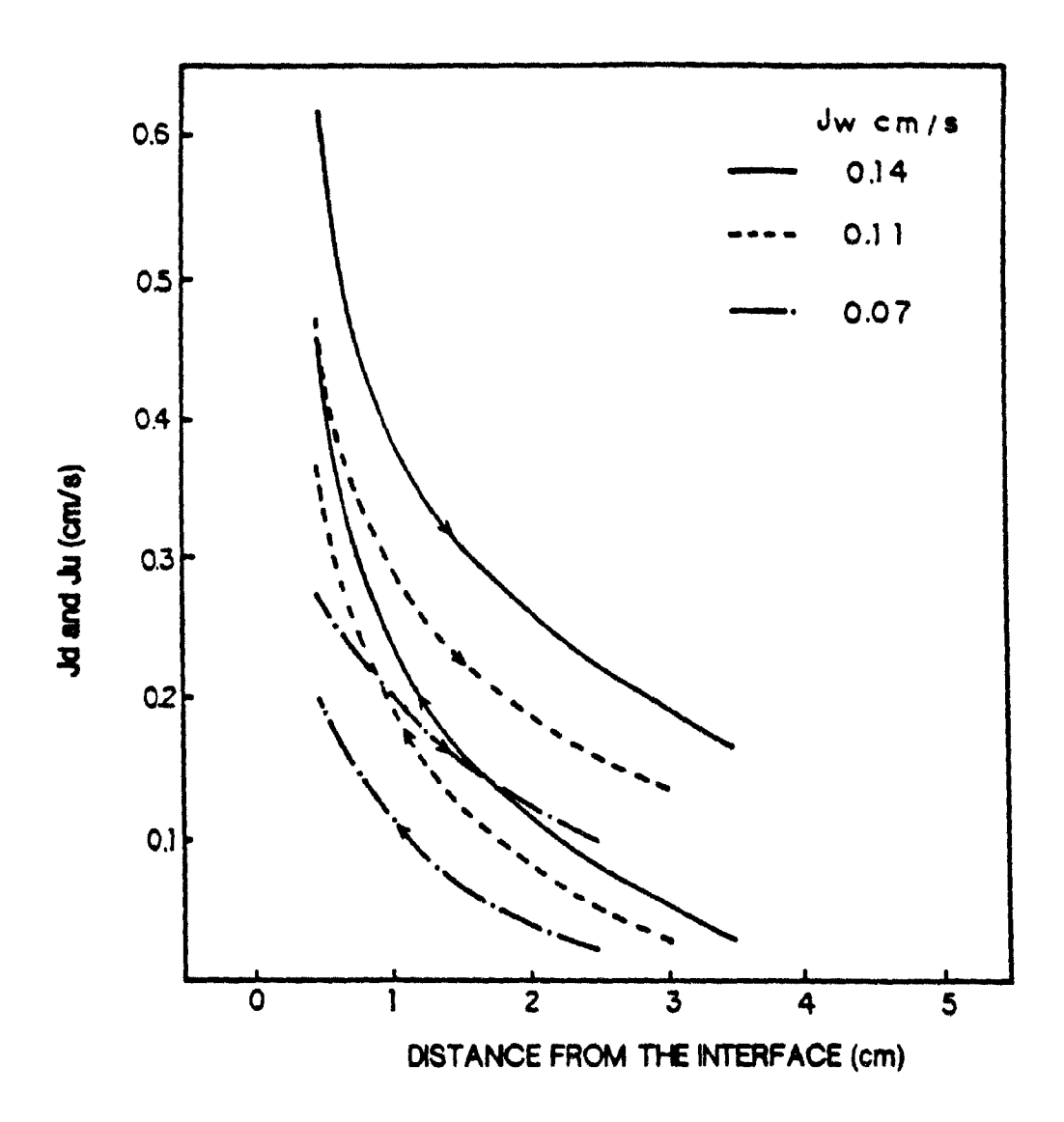


Figure 3.22: Change in upward (J_u) and downward (J_d) liquid velocities with distance from the interface at different superficial wash water rates. $(J_u$ is identified by the upward arrows and J_d by the downward arrows).

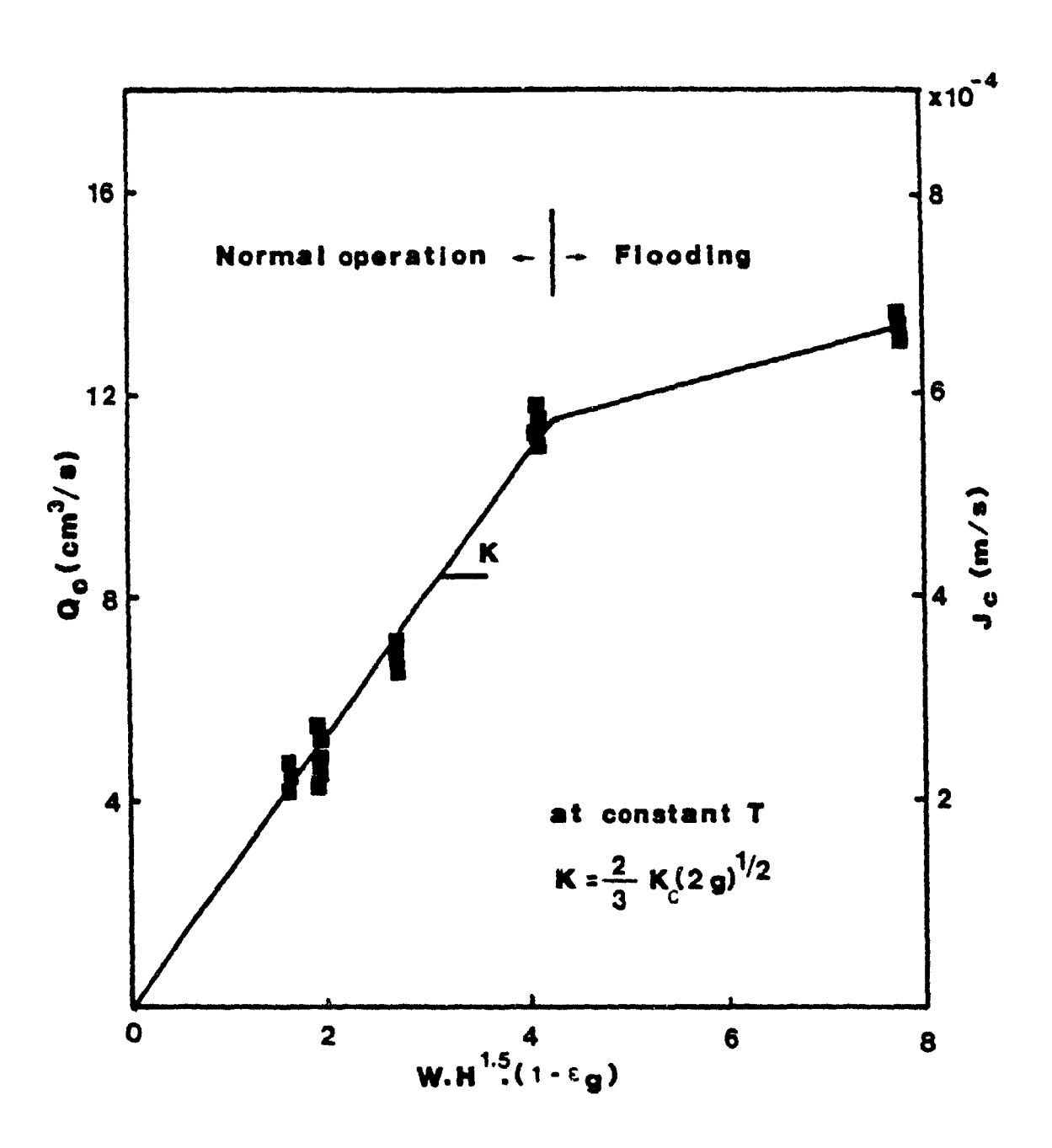


Figure 3.23: Estimation of the discharge coefficient ($\frac{K}{c}$) for the modified cell.

Figure 3.24. There is a reasonably good agreement between experimental and predicted water recoveries within 715% error limits.

If slurry level (SH) is not maintained constant both T and H vary with operating conditions and the cell discharge coefficient (K_c) changes. The following empirical equation was obtained from laboratory cell data with a correlation coefficient of 0.98.

 $J_c = 0.00061-0.0088T+0.00196H^{1.5} + 0.0408J_q+0.01899J_w 3.34$ where T varies from 0.2 to 2 cm, H from 1 to 3 cm, J_q from 0.2 to 0.6 cm/s, and J_w from 0.05 to 0.14 cm/s. According to the above equation, the most important factors affecting J_c (or Q_c/S) are J_q and T.

The water film thickness associated with each bubble can be roughly predicted using a gas holdup value at the base of the froth (boundary condition) (Moys, 1979). Using Eqs. 3.3, 3.6, and 3.7 film thickness around bubbles was estimated and plotted as a function of aeration rate at a superficial liquid rate of 0.14 cm/s in Figure 3.25. Gas holdups were taken from Figure 3.19 at 0.5 cm above the interface while average bubble sizes were taken from Kaya (1985). Film thickness around bubbles increases from 14µm to 40µm with increasing aeration rate from 0.2 to 0.6 cm/s; more water is entrained into the froth from the slurry phase.

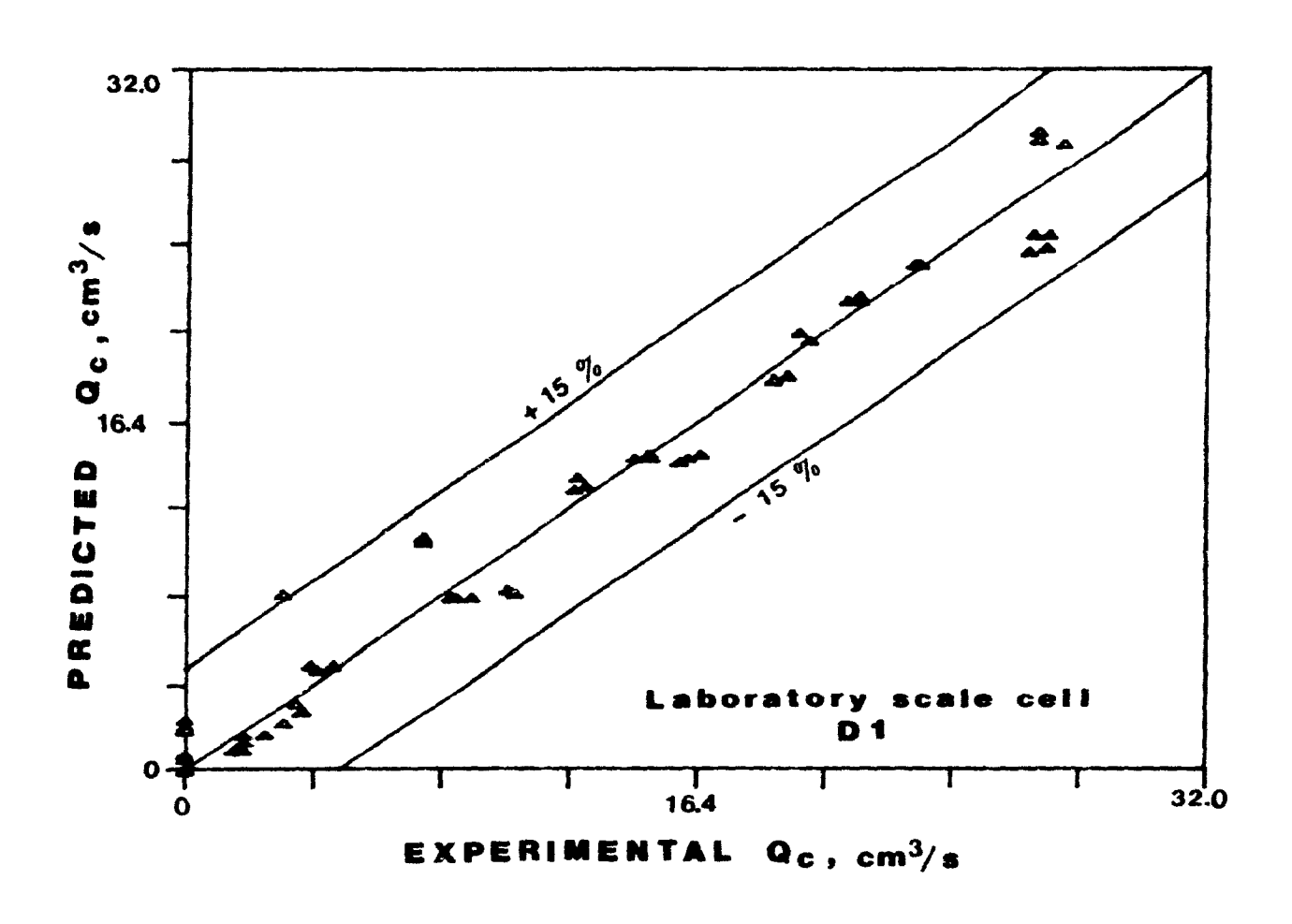


Figure 3.24: Comparison between estimated and measured water recoveries in the modified cell.

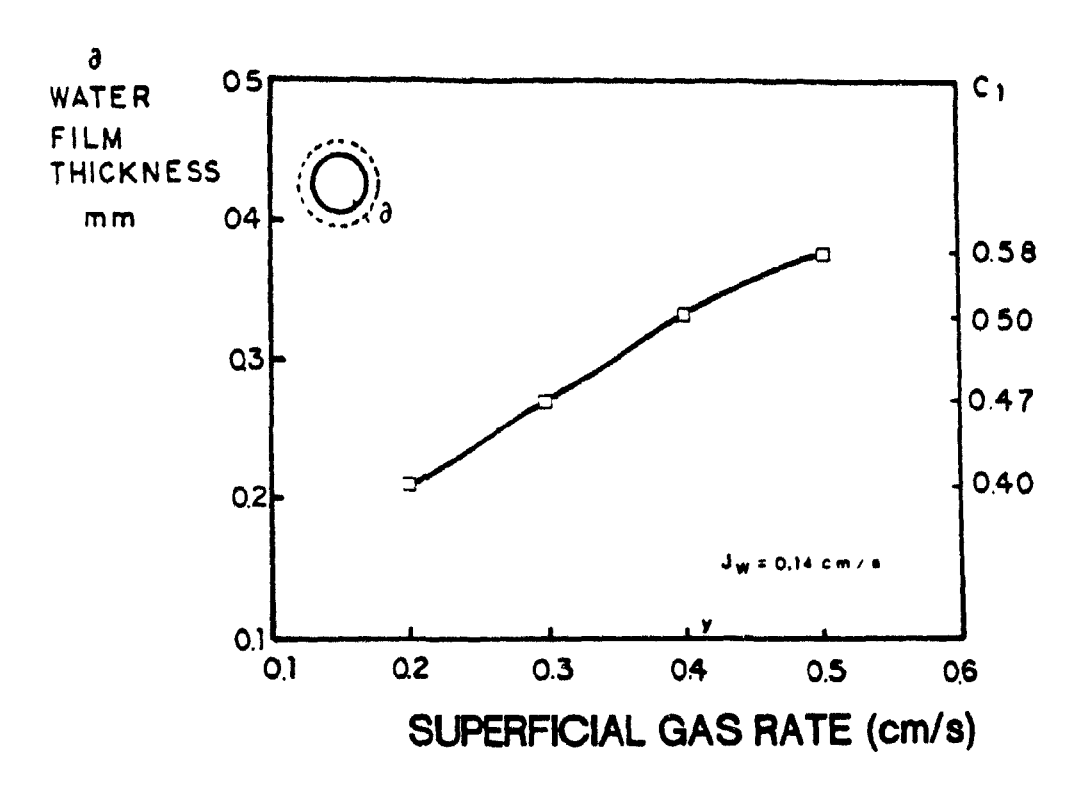


Figure 3.25: Effect of aeration rate on water film thickness.

The parameter C_1 in Eq. 3.4 was also estimated using Eqs. 3.3 and 3.4. Aerated power input per unit volume (energy dissipation) was calculated using Luong and Voleski's equation (2.7) and terminal bubble rise velocity was determined using Pebble & Garber's equation (2.9). C_1 increases from 0.25 to 0.52 when aeration rate increases from 0.2 to 0.6 cm/s. Since C_1 varies, it is difficult to estimate the exact water film thickness around bubbles; a rough estimate can be calculated using Eq. 3.4.

3.7.4 Local Gas Holdup in the Froth Phase

The effect of wash water addition flowrate on local gas holdup at four different points on the same horizontal level using the quadruple-electrode assembly is given in Figure 3.26. Although the electrodes were all at the same horizontal plane in the froth, the gas holdup significantly varied. The front electrodes (1 and 2) showed higher gas holdup than back electrodes (3 and 4). The change in gas holdup in the froth phase was correlated with superficial wash water rate as below:

$$\varepsilon_{\rm q} = 72.62 - 67557. J_{\rm w}^4$$
 3.35

The effect of impeller speed at FT of 5 cm and the effect of FT (3 and 6 cm) at 1500 rpm on local gas holdup in the froth was also investigated using the quadruple-electrode assembly. Gas hold-up decreased with increasing impeller speed or decreasing froth thickness (Table 3.6). Increasing impeller peripheral speed

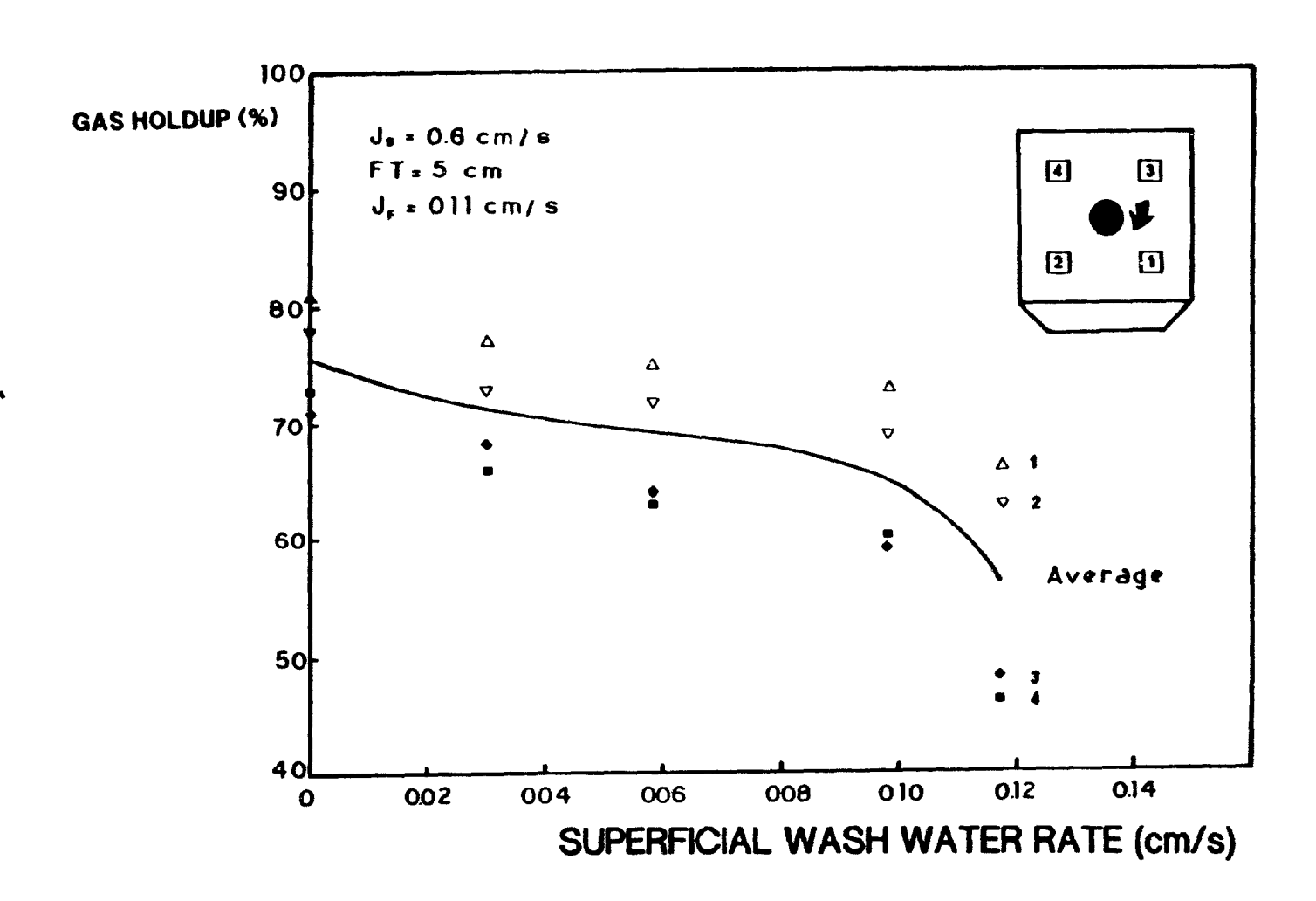


Figure 3.26: Effect of wash water flow rate on local gas holdup using the quadruple electrode assembly.

creates finer bubbles with larger interfacial area which increases the volume of interstitial bubble water in the froth. In froth thickness tests, the electrode assembly was fixed at the cell lip level for both tests. FT was decreased by increasing SH. As expected, a lower gas holdup was measured.

Table 3.6: Effect of impeller speed and froth thickness on local gas holdup in the froth phase.

	Local Gas	-
Electrode	1200 rpm	1500 rpm
1	0.84	0.73
2	0. 63	0.60
3	0.72	0.69
4	0.66	0.59
	(J _g : 0.6 cm/s, J _w : 0.098 cm/s, and F	T: 5 cm)
1	(J _g : 0.6 cm/s, J _w : 0.098 cm/s, and F	T: 5 cm)
1 2	(J _g : 0.6 cm/s, J _w : 0.098 cm/s, and F FT: 3 cm	T: 5 cm) FT: 6 cm
1 2 3	(J _g : 0.6 cm/s, J _s : 0.098 cm/s, and F FT: 3 cm 0.81	T: 5 cm) FT: 6 cm 0.88

3.8 Summary

On the basis of insights gained from this chapter, a number of conclusions can be stated:

a. Two different zones in a washed conventional froth were recognized. In the expanded bubble bed, where the gas holdup is less than 74%, all bubbles are well separated from each other by draining water films. Above the expanded bubble bed, gas holdup is

higher than 74% and thinner water films occasionally collapse creating bubble coalescence. This zone is called packed bubble bed.

- b. Comparison of three different types of froth structures showed that washed froths have the best properties required for flotation.
- c. The general trend of holdup profile strongly depends upon gas rate, liquir rate, and frother concentration. The liquid holdup at the top of the froth was found to increase drastically with increasing gas flowrate, water flowrates, and frother dosage.
- d. A froth hydraulic model, which includes a water and gas balance in a conventional flotation cell with wash water addition, was introduced. A predictive model for water recovery was established.
- e. It was found that froth thickness increased with increasing both gas and water addition rates. Maximum froth expansion was obtained when wash water was added 4 cm above the froth.

This type of information will assist in deciding the use of wash water in conventional flotation machines. Insights gained can lead to the development of better operation conditions for the existing flotation systems, which may produce an improvement in their performance.

CHAPTER 4

DETERMINATION OF RESIDENCE TIMES
IN
THE LABORATORY FLOTATION CELLS

Introduction

Mean residence time (MRT) is an important factor in determining metallurgical performance. An inadequate MRT may lead to losses of valuable species; particles with low flotation kinetics, such as fines or middlings, are particularly vulnerable. An excessive MRT will lead to increased recoveries for water, gangue particles, and weakly floatable particles. Strongly floatable particles may also suffer deactivation, and some gangue sulfides activation through surface oxidation. This study investigates the effect of operating variables on the MRT of gas, liquid, and solid in the slurry and froth phases in the presence of wash water. Variables affecting gangue entrainment, such as the fraction of feed water recovered in the concentrate, are also quantified.

The mixing behaviour of the small-scale modified laboratory flotation cell was investigated experimentally. Impulse tracer tests were performed with both liquid and solid tracers. The liquid residence time is significantly affected by wash water addition flowrate in the slurry phase and froth thickness in the froth phase. Froth thickness and aeration rate are the major variables affecting residence time in the froth phase.

4.1 Experimental

Most of the experiments were performed in a two-phase system (air-water) where feed flowrate and impeller speed were always kept constant, unless otherwise stated. The slurry level was

maintained at a set point by varying the tailing flowrate, a common control strategy in plant practice. Different results would be obtained if other types of level control strategies are employed. Some results from a previous three-phase study (Kaya, 1985) are also included to relate the results to actual flotation conditions.

At constant feed rate, the effect of superficial gas rate, froth thickness, superficial wash water rate, and impeller speed on the MRT in the slurry and froth zones was investigated. In the three phase study, silica was the solid phase at 10% by weight.

4.1.1 Measurement Techniques

Liquid Mean Residence Time in Slurry: Two different methods were used. For the first method, a water soluble tracer was added into the feed stream; samples were collected from the tailing stream periodically. The RTD was determined from the tracer response curve and MRT was estimated. LiCl was used as a liquid tracer, because of its low cost, unreactiveness, solubility in water, and ease of analysis by atomic absorption (AA). For each test, 1 gram of dissolved LiCl was injected as an impulse tracer using a 50 mL syringe. As the times of injection and collection of the tracer material were very short, 10 and 5 sec respectively, in comparison to the residence time in the cell (2 to 4 min), the observed concentration-time curve in tail stream could reasonably be considered that of an instantaneous response to a perfect impulse.

For the second method, the gas holdup and tailing flowrate were measured. Average gas holdup was determined measuring conductivity with the quadruple-electrode assembly, which is placed in the middle of the slurry phase.

The results of the second method are best understood considering that the MRT of the liquid in the slurry zone, τ_{lp} , is equal to

$$\tau_{1p} = \frac{V_{p} \cdot \varepsilon_{1p}}{Q_{t}} = \frac{SH \cdot \varepsilon_{1p}}{J_{t}}$$
4.1

where Q_t: tail flowrate, m³/s

V: slurry volume, m³ ϵ_{lp} : volumetric liquid holdup in the slurry phase

SH: slurry height, m

J_t: superficial tailing rate, cm/s

Solid Mean Residence Time in Slurry: In flotation, it is the MRT of solids that is of prime importance. The use of solid tracers, though by no means impossible, does tend to add both complexity and cost to a test. Thus, the industrial practice is 'a use liquid tracers and to make the assumption that the liquid phase of the slurry closely approximates the behaviour of the solid phase. Dobby (1985) has shown that the validity of this approximation in a flotation column is a function of particle size and improves with decreasing particle diameter. RTDs of solid

particles were determined by radioactive tracing in the same system previously (Kaya, 1985). Detailed theoretical background and results are found in the above reference.

The following equations for perfect mixing were used to calculate the slope of lnA vs t plot, which is the inverse of the MRT:

$$E(t) = \frac{C(t)}{\int C(t).dt} = \frac{1}{\tau} e^{-t/\tau}$$

$$\ln A = \ln \left(\frac{1}{\tau} - \frac{t}{\tau} \right) \tag{4.3}$$

Gas and Liquid Residence Time in Froth: Assuming a constant gas holdup in the froth phase, the mean residence times of gas and liquid in the froth phase $(\tau_{bf} = \tau_{if})$ is equal to:

$$\frac{V_{f} \cdot \varepsilon_{bf}}{V_{f}} = \frac{FT \cdot \varepsilon_{bf}}{J_{g}}$$
4.4

$$V_{\rm bf} = \frac{\rm FT}{\tau_{\rm bf}}$$
 4.5

where V_f : froth volume, m^3

 $\epsilon_{bf}^{}\colon$ fractional gas holdup in the froth phase

Q: air flowrate, m3/s

 $V_{\rm bf}$: average bubble rise velocity in the froth phase, m/s

The average gas holdup in the froth was assumed to be equal to the mean of local gas holdups in the middle of the froth, measured using the quadruple-electrode assembly. Since the horizontal transport was neglected here the residence time is the minimum time spent in the froth phase.

Feed Water Split: Laboratory scale tests were performed to measure the amount of feed water in the concentrate stream at different superficial gas and water rates, froth thicknesses, impeller speeds, and feed flow rates. A material balance of the tracer (i.e. water split between the tailings and concentrate streams) was obtained using the following equations:

$$A_{c} = \frac{\int_{Q_{c}, C_{c}(t).dt}}{\int_{Q_{c}, C_{c}(t).dt}}$$

$$4.6$$

$$A_{t} = \frac{\int_{Q_{t}.C_{t}(t).dt}}{\int_{Q_{t}.C_{t}(t).dt} + \int_{Q_{c}.C_{c}(t).dt}}$$
4.7

where Q: concentrate flowrate, m3/s

Q: tailing flowrate, m³/s

C: concentrate tracer concentration, kg/m³

C: tail tracer concentration, kg/m³

 A_{c} : amount of tracer reporting to the concentrate, kg

A.: amount of tracer reporting to the tails, kg

One gram LiCl dissolved in water and injected into the feed stream. Tail and concentrate streams were collected in different pails for 5 minutes. Their volume was measured and Li concentration was determined. Experiments were repeated at different operating conditions.

4.2 Results and Discussion

4.2.1 Liquid and Solid Residence Times in the Slurry Phase Table 4.1 summarizes the effect of J_g , J_w , FT, and RPM on the MRT of liquid in the slurry phase. Figure 4.1 shows the fit of typical experimental data to the perfectly mixed model. The effect of operating variables will be discussed separately.

Table 4.1: Effect of superficial gas and wash water rates, froth thickness, and impeller speed on the liquid residence time in two and three phase systems. (Three phase results are from Kaya, 1985).

J (cm	g /s) (J cm∕s)	FT (cm)	T (cm)	SH (cm)	Residence Tailing	time I	Phase
	. 4 . 6	0 0	3	2	30 30	3.83 4.06	4.04	3
		0. 14 0. 14	3 1.5	2	30 31	2.26 2.78	2.36	2
0 0 0	. 6 . 6 . 5	0 0.03 0.08 0.14 0	3 3 3 3 3	2 2 2 2 2 2	30 30 30 30 30 30	4.06 3.83 2.97 2.26 3.83 3.47	2.36 4.04	3 3 2 2 3 3
J (cm/s)	J (cm/s)	FT (cm)	T (cm)	SH (cm)	ε _{bp} (%)	τ lp (min)	RPM	
0.4	0.11 0.11	2 2	1 1	31 31	5.5 7.2			

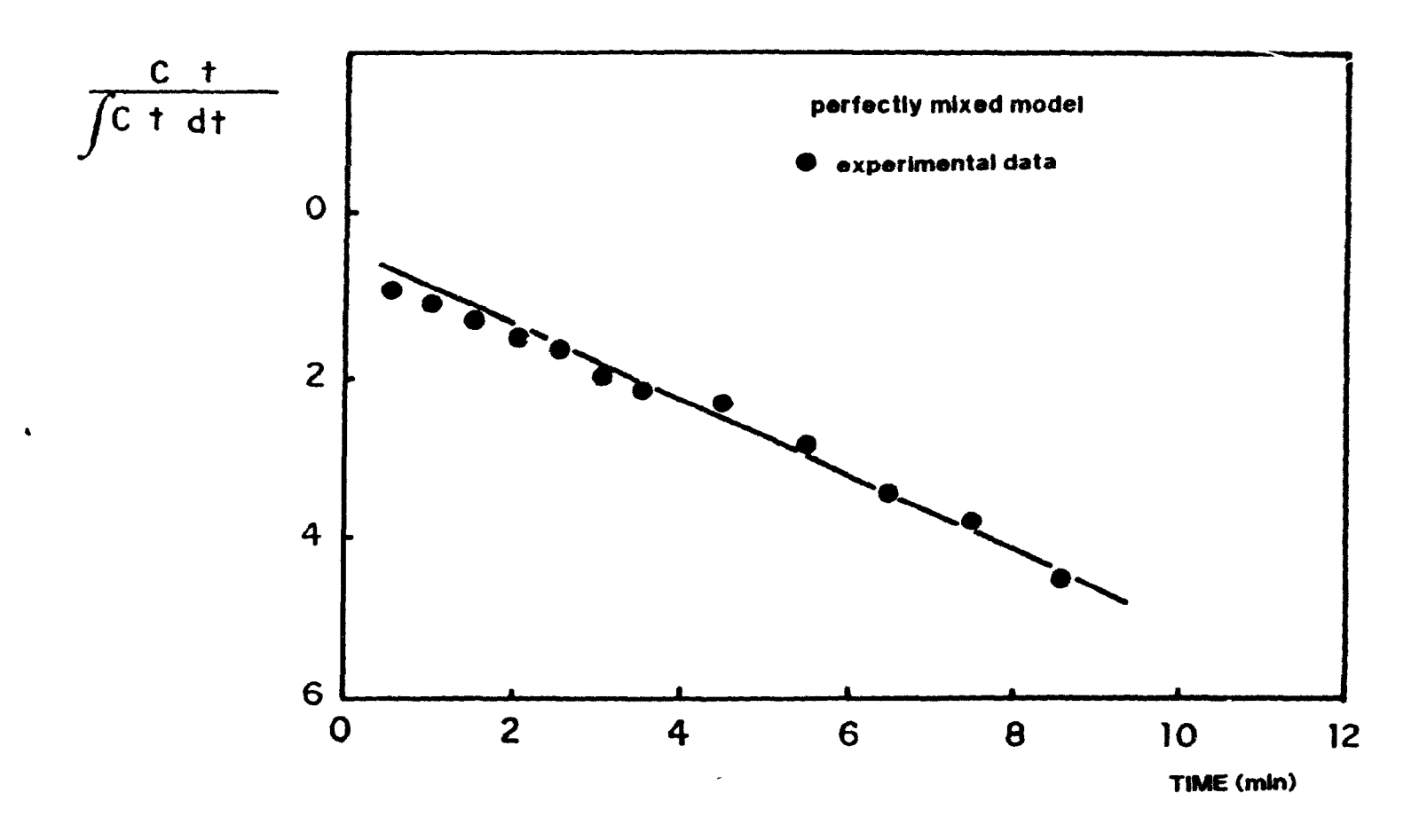


Figure 4.1: Fit of experimental data to the perfectly mixed model.

Effect of Gas Rate: In the absence of wash water addition, it was found in the three phase system that liquid MRT in the slurry phase slightly increases with increasing superficial gas rate (Table 4.1). Increasing J decreases both the liquid holdup in the slurry zone and tails volumetric flowrate. Figure 4.2 shows that the decrease in Q_t is more important than that of ε_{lp} measured by the quadruple electrode assembly in the two phase system. The net result is an increase in the MRT of liquid in the slurry phase.

Effect of Froth Thickness: At constant J_q and J_u , rising the slurry/froth interface leads to an increase in the liquid residence time in the slurry phase (Table 4.1). This only partially stems from the increase in the slurry volume (here only 5%). The main cause is the much increased water recovery in the concentrate, resulting in an equivalent decrease in Q_{\downarrow} .

Effect of Wash Water Addition Rate: At constant J_q and FT, the liquid residence time in the slurry significantly decreases with increasing wash water addition rate, as shown in Figure 4.3. It also shows that samples collected from concentrate stream have a slightly higher residence time than samples taken from the tailings streams, as the froth zone has its own residence time, which can be estimated by the difference between MRTs of the concentrate and tailing streams. The MRT in the froth is in the order of 6 to 12 seconds.

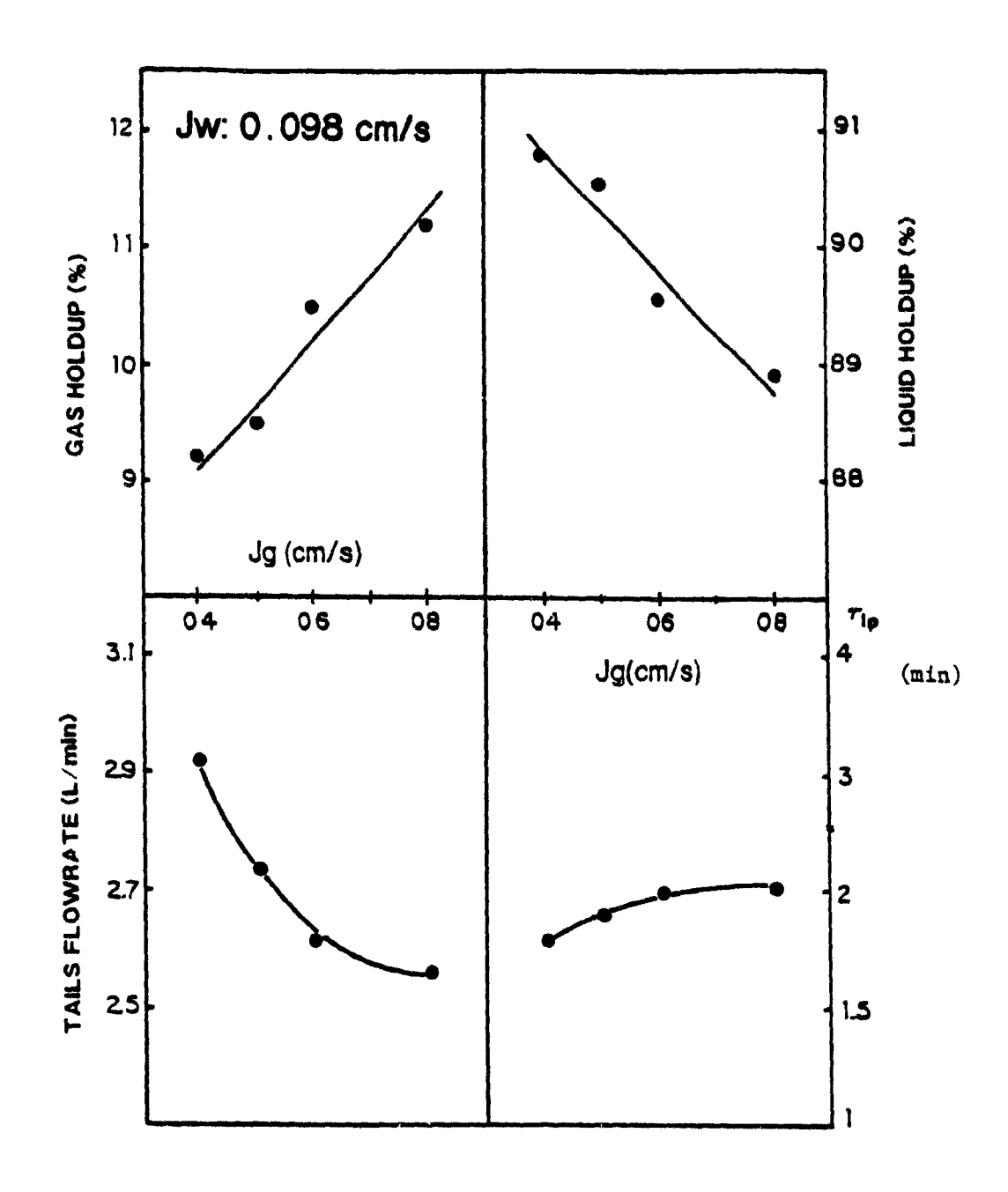


Figure 4.2: Effect of aeration rate on gas and liquid holdups, tailing flow rate and liquid residence time in the slurry phase.

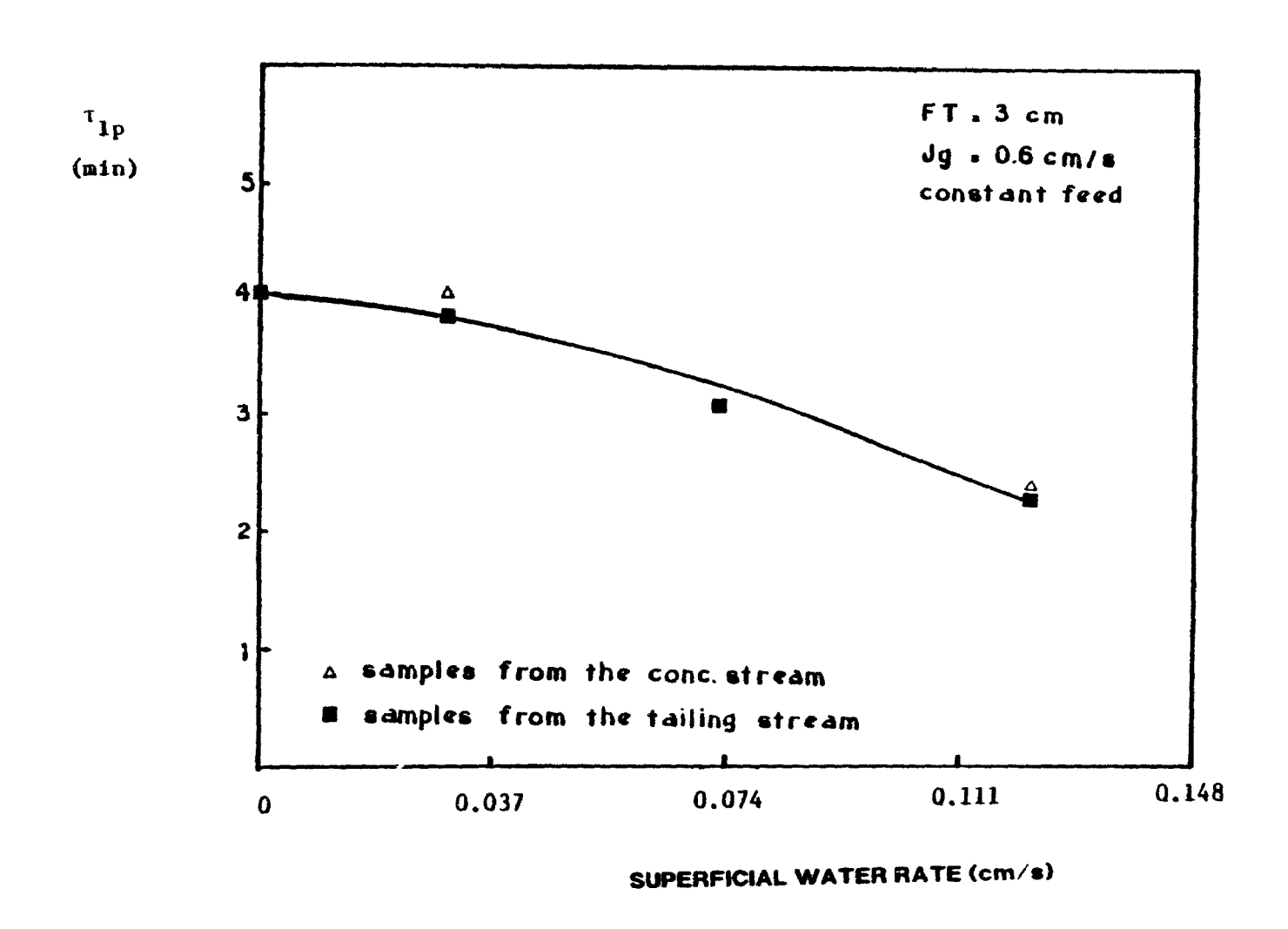


Figure 4.3: Effect of wash water addition rate on liquid residence time in the slurry phase.

The decrease in the MRT in the collection zone with increasing wash water rate is by far the most undesirable side effect of using wash water. Clearly, J must be minimized to reduce not only water consumption, but also the decrease in flotation time and circuit capacity.

Effect of Impeller Speed: Table 4.1 shows that as impeller speed increases, gas holdup in the slurry phase increases, because smaller bubbles with lower rise velocities are generated. Therefore, liquid holdup decreases and so does the residence time in the slurry zone.

4.2.2 Comparison of Solid and Liquid Residence Times in The Slurry Phase

Results of solid and liquid residence time study are given in Table 4.2a. For these tests, samples were collected from the tailing stream without wash water addition. The liquid residence time in the slurry phase is slightly higher than that of the solids, but the difference is within experimental error.

4.2.3 Presence of Perfect Mixing

An experiment done without froth phase showed that the residence time calculated from tail and concentrate streams were very similar (Table 4.2b). This means that the solid phase is perfectly mixed in the slurry phase, i.e. its contration is almost same throughout the slurry volume in the absence of froth phase. This will be further investigated in the next chapter.

4.2.4 Cas and Liquid Residence Time in the Froth Phase

Table 4.3 summarizes the effect of superficial gas rate, water rate, froth thickness, and impeller speed on $\epsilon_{bf}^{},~\tau_{bf}^{},$ and $V_{bf}^{}.$

Table 4.2: Comparison of solid and liquid residence times in the pulp zone (a), and the presence of perfect mixing (b). (Results were obtained from radio-active tracer tests using Mn-56).

	J	J	FT	T	SH		ce time (min)
	(cm/s)	(cm/s)	(cm)	(cm)	(cm)	solid	liquid
a	0.5	0	3	2	30	3.75	3.83
						tails	(min)
b	0.5	0.098	0	0	32	2.97	2.95

Superficial Gas Rate: Mean gas residence time in the froth, $\tau_{\rm bf}$, decreases with increasing superficial gas rate. Bubble rise velocity in the froth is very low (0.5 - 1.1 cm/s) as compared to in the slurry phase (4 - 10.5 cm/s). The implication is that increasing residence time in the froth leads to increased drainage and a drier froth.

Table 4.3: Effect of superficial gas rate, wash water rate, froth thickness, and impeller speed on the gas residence time in the froth phase.

J g (cm/s)	J (cm/s)	FT (cm)	T (cm)	SH (cm)	ε bf (%)	τ bf (sec)	V bf (cm/s	N)(rpm)
0.6 0.6 0.5 0.5	0.098 0.098 0.098 0.098	4 4 4 4	2 2 2 2 2	30 30 30	56.9 56.5 57.7 57.4	3.8 3.7 4.6 4.6	1.1 1.1 0.9 0.9	1500 1500 1500 1500
0.4	0.098	4	2 2	30	58.7	5.8	0.7	1500
0.4	0.098	4		30	58.3	5.8	0.7	1500
0.3	0.098	4		30	59.0	7.8	0.5	1500
0.4	0.140	2.5	1.5	30.5	83.0	4.9	0.5	1500
0.4	0.140	3	2	30	81.0	6.0	0.5	1500
0.6	0.090	3	2	30	70.2	3.5	0.9	1500
0.6	0.090	5	3	29	65.2	5.4	0.9	1500
0.6 0.6 0.6 0.6	0 0.030 0.058 0.090 0.120	5 5 5 5 5	3 3 3 3	29 29 29 29 29	75.5 71.1 68.5 65.0 55.5	6.2 5.9 5.7 5.4 4.6	0.8 0.8 0.9 0.9	1500 1500 1500 1500 1500
0.6	0.090	5	3	29	71.2	5.9	0.8	1200
0.6	0.090	5		29	65.0	5.4	0.9	1500

(FT: froth thickness, T: distance between slurry-froth interface, and cell lip level, SH: slurry height)

Figure 4.4 shows the calculated average bubble rise velocity in the froth phase as a function of distance from the interface using the momentum conservation model in Chapter 3 (Eq. 3.24). The following data were used in calculations:

Table 4.4: Variable ranges used in FT calculations.

J _g (cm/s)	ε _{bp} (%)*	V _{bp} (cm/s)	d _{bp} (cm)
0.6	8.67	6.9	0.364
0.5	6.94	5.7	0.336
0.4	4.98	4.0	0.306

* : measured with conductivity

d : from Kaya-1985

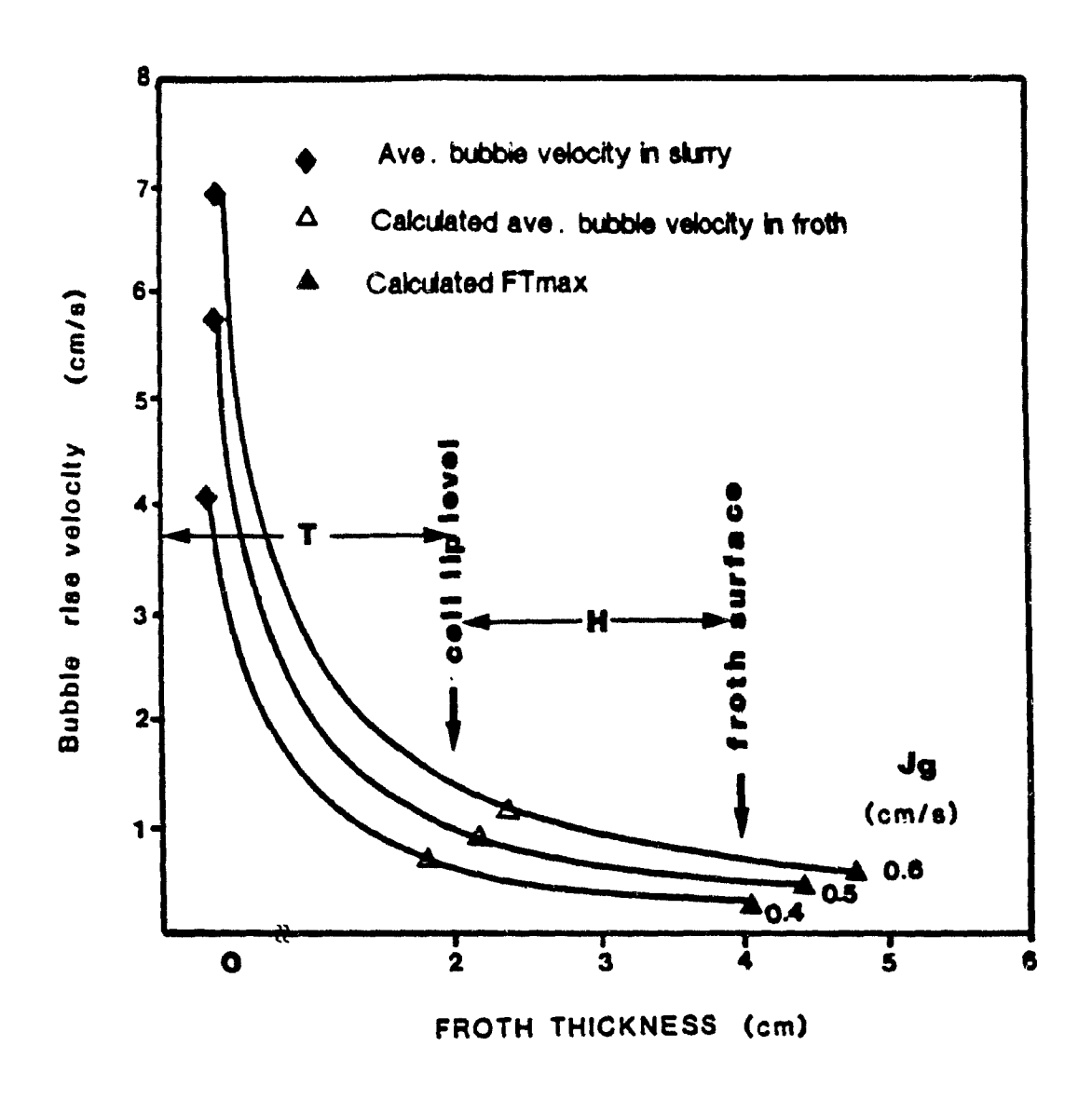


Figure 4.4: Change in bubble rise velocity in the froth phase.

(Calculated from the momentum conservation model)

Average bubble rise velocity in the froth phase drastically decreases towards the froth surface. The higher the gas rate, the higher the average bubble rise velocity in the froth. The decrease in average bubble rise is maximum at the interface, and lessens with height above the interface. Above the lip level, the decrease is more gradual, due to the initiation of horizontal velocity, which forces froth towards the overflow weir.

Figure 4.4 also indicates the calculated FT_{max} , which depends on the no froth overflow condition and calculated average bubble rise velocities from Table 4.3.

Froth Thickness: Table 4.3 shows the effect of froth thickness at two different gas and wash water rates. Gas residence time in the froth significantly increases with increasing froth thickness. Higher residence times lead to drier froths, because of increased drainage and bubble coalescence.

Wash Water Superficial Rate: Gas residence time in the froth increases slightly with decreasing wash water rate, because of the ensuing increase in the gas content of the froth phase (Table 4.3).

Impeller Speed: Gas residence time in the froth decreases slightly with increasing impeller speed (Table 4.3). This is a direct result of the increased liquid content of froth, as higher impeller speeds produce finer bubbles, with larger interfacial area and higher volume of interstitial water.

4.2.5 Feed Water Split

In this study, feed water penetration into the froth, which corresponds to the worst conditions of fines entrainment, was determined. A material balance of the tracer split and hence feed water split between tailings and concentrate streams was obtained.

Superficial Gas Rate: Experiments done at constant FT, $J_{\rm w}$, and $J_{\rm f}$ showed that feed water reporting to the concentrate stream slightly decreases with decreasing $J_{\rm g}$ (Table 4.5). At high gas rates, more water is entrained into the froth by large bubbles.

Table 4.5: Effect of gas rate, froth thickness, feed rate, and impeller speed on feed water recovery at constant wash water rate.

J	FT	J	O ^t	N	Feed Water Recovery	τ
(cm/s)	(cm)	(cm/s)	(L/min)	(rpm)	(%)	(min)
0.4	3.0	0.14		1500	6.8	
0.6	3.0	0.14		1500	7.5	
0.6	1.5	0.14		1500	12.3	
0.6	3.0	0.14	0.48	1500	18.8	4.7
0.6	3.0	0.14	1.24	1500	7.5	2.8
0.6	3.0	0.14	2.08	1500	6.6	2.3
0.6	3.0	0.098		1300	1.5	
0.6	3.0	0.098		1500	2.2	

Froth Thickness: At constant J_g , J_w , and J_f , there was a significant increase in the amount of water reporting to the concentrate with decreasing FT (Table 4.5). These results show that a 50% decrease in FT increases the feed water reporting to the concentrate stream about 39%, while a 33% increase in aeration rate increases the feed water reporting to the concentrate stream about 9%. Therefore, feed water split can be more closely controlled by adjusting FT rather than J_a .

Wash Water Superficial Rate: Figure 4.5 shows the percent feed water reporting to the concentrate stream. A minimum penetration of feed water was found at an intermediate J_w A five-fold decrease (from 11% to 2 2%) in water reporting to the concentrate was achieved by wash water addition 4 cm above the froth surface. Wash water promotes froth stability and largely eliminates feed water from the concentrate. Elimination of feed water prevents fines recovery by mechanical and hydraulic entrainment in the froth phase.

The increase of feed water reporting to the concentrate after minimum is presumably due to the mixing effect induced by strong wash water addition in shallow froths (i.e. 3 cm). In deep froths, mixing may not be a problem. This will be further investigated in the following chapters.

Feed Rate: Feed water recovery to the concentrate increases significantly with decreasing feed flowrate due to increased liquid residence times in the slurry phase. Mean residence times are 4.66, 2.78, and 2.28 min for feed flow rates of 0.48, 1.24, and 2.08 L/min, respectively. Since water resides short time at probability of concentrate high feed flowrate, the contamination by feed water is lower. Therefore, it seems that the liquid residence time in the slurry plays a very important role in the entrainment mechanism and that it should be closely controlled. Frew and Trahar (1982) found that Cu grade significantly decreased with decreasing feed flowrate in bornite and quartz flotation.

SUPERFICIAL WASH WATER RATE (cm/s) 007 011 014 0 FEED NOT OF THE TENT OF THE TE FT = 3 cm Jg = 06 cm/s constant feed CONCENTRATE 8 6 THE 10 WATER 2 83 1500 1000 500 0

Figure 4.5: Effect of wash water superficial rate on feed water entrainment to the concentrate.

WASH WATER FLOWRATE (mL/min)

Impeller Speed: Feed water reporting to the concentrate decreased from 2.2% to 1.5% by decreasing impeller speed from 1500 rpm to 1300 rpm (Table 4.5). Because increasing impeller speed will create finer bubbles and higher gas holdup in the slurry phase, which results in higher water transport to the froth and therefore to the concentrate stream.

4.3 Summary

Since the recovery of gangue particles is related to feed water reporting to the concentrate, a longer liquid residence time in the froth and a shorter liquid residence time in the slurry are necessary to lessen entrainment problem or to achieve higher grades in cleaner circuits. The results are summarized in Table 4.6 where + and - refer to the direction of change in the controlled variables resulting from an increase in manipulated variable. The response for J and rpm is very fast, while for FT and J_{ij} , it is relatively slow. A decrease in liquid residence time in the slurry is achieved by increasing FT, J, and rpm; however, an increase in liquid residence time in the froth is accomplished just by increasing FT. It can be concluded that the control of FT can easily achieve the desired purpose, while the beneficial effects of impeller speed and $J_{\underline{\ }}$ in the slurry phase are compensated to some extent in the froth zone. Therefore, it is necessary to find an optimum J and FT combinations.

Mineralized bubbles should not remain in the pulp an inordinately long time because of the increasing probability of demineralization. On the other hand, air bubbles should not rise excessively fast in the pulp, otherwise they will not have time to pick up a suitable load of mineral particles. The optimum life of bubbles in the pulp and the rate of rise depends on the properties of the floated minerals, reagent additions, density of pulp and finally the size of mineral particles.

Table 4.6 also shows the response of froth (gas and liquid) residence time in the froth phase to changes physical manipulated variables. An increased gas residence time in the froth phase leads to an increased probability of coalescence, which may reduce entrainment problems depending on the possibility of reattachment in the froth. Coalescence also reduces interfacial area and thus solids carrying capacity. Therefore, to prevent a major release of collected particles, coalescence of the gas bubbles must be minimized. Thus, what is desired from the gas bubbles in the froth is system and purpose dependent.

The amount of feed water reporting to the concentrate should be minimized in order to lessen entrainment and increase product grade. Increasing FT and feed rate reduces feed water recovery to the concentrate. However, increasing J_q and rpm leads to increased feed water recovery and entrainment. There is an optimum J_m at an intermediate addition rate (0.08 - 0.1 cm/s), which reduces the feed water penetration—five fold than without wash

water addition. Feed water penetration to the concentrate should be minimized, but at a reasonable concentrate flowrate; otherwise recovery will suffer significantly.

Table 4.6: Effect of some physical manipulated variables on liquid and gas residence times and feed water recovery (R_{fw}) .

PHYSICAL MANIPULATED	CONTROLLED VARIABLES					
VARIABLES	$\tau_{_{1}}$		τ	R fw to conc.		
(increase in)	slurry	froth	froth			
Superficial gas rate	+	-	+	+		
Froth thickness	-	+	+	-		
Superficial wash water rate	-	-	-	+ - +		
Impeller speed	-	-	-	+		
Feed rate				-		
Desired	-	+	+,-	-		

CHAPTER 5

DETERMINATION OF GANGUE PROFILES

IN

THE SLURRY AND FROTH PHASES

Introduction

An appropriate first step towards understanding entrainment mechanisms is to determine the factors responsible for the presence of gangue immediately below and above the slurry-froth interface. The approach taken here was to systematically determine gangue profiles in the slurry and froth phases at different superficial gas rate and superficial wash water rate at constant froth thickness and feed rate.

An attempt was made to estimate gangue content in the froth phase. A classification coefficient was defined based on interstitial bubble rise velocity and particle settling velocity in the froth phase.

- 5.1 Theoretical Concepts of Mass Transfer and Particle Rejection in Flotation Cells
- 5.1.1 Mass Transfer to the Slurry-Froth Interface

If the mass of gangue of size i in the slurry phase is x_i , the gangue content change in a flotation cell can be calculated from the following equation assuming a perfectly mixed pulp phase:

$$\frac{dx_i}{dt} = -k_e^i \cdot x_i$$
 5.1

where k_e^i : entrainment rate constant of species i, \sec^{-1}

The rate constant due to entrainment (k_e) can be derived by considering the probability of entrainment P_e . The number of particles recovered by entrainment per unit time is then given by (Luttrell et al., 1987):

$$N = P_e Q_g V_w \frac{N_t}{V_c}$$
 5.2

where V: dimensionless wake volume defined as the ratio of the wake volume to the bubble volume.

V: cell volume, m³

 N_{\bullet} : total number of particles in the cell

Q: air flowrate, m³/s

Dividing equation by total number of particles in the cell and considering a square cell with a length of S and height of H, k is given by:

$$k_e = \frac{P_e \cdot Q_g \cdot V_w}{S^2 \cdot H}$$
5.3

Combining Eqs. 5.1 and 5.3

$$\frac{dx_1}{dt} = \begin{bmatrix} -P_e \cdot Q_g \cdot V_w \cdot x_1 \\ \frac{2}{S \cdot H} \end{bmatrix}$$
 5.4

This final equation for the slurry phase suggest that one can reduce entrainment problem by reducing aeration rate, bubble wake volume to bubble volume ratio, percent solid, and the probability of entrainment or by increasing cell height, cell length, and feed

flowrate (i.e. reducing pulp residence time). Wash water addition most probably affects the dropback rate constant and residence time in the cell and reduces the fraction of feed water in the concentrate. This analysis strongly suggests that processing fine particles in deep flotation cells is beneficial.

Luttrell et al. (1987) found that decreasing bubble size or increasing flotation cell height resulted in improved recovery and selectivity of fine particles. The size of the turbulent wake increases with increasing bubble diameter. Bubbles less than approximately 0.3 mm in diameter carry no wakes while larger bubbles exhibit a substantial wake. Bubble size determines whether or not wake (hydraulic) entrainment occurs, while particle size determines the degree of entrainment.

A bubble wake model developed to estimate the net downward velocity of particles in a slurry contacted counter-current with bubble swarm by Yianatos et al. (1987). The concentration of particles in the liquid rising in the bubble water relative to the concentration in the descending liquid is the major factor affecting gangue entrainment in the slurry phase. Thus, the ratio $\varepsilon_{\rm sw}/\varepsilon_{\rm s}$, i.e. the gangue particles holdup in the drift flux to the total particle holdup, will be equal or smaller than the corresponding liquid ratio $\varepsilon_{\rm lw}/\varepsilon_{\rm l}$ and they can be related as:

$$\frac{\varepsilon_{sw}}{\varepsilon_{s}} = \alpha \frac{\varepsilon_{lw}}{\varepsilon_{l}}$$
5.5

where α is a distribution coefficient describing the relative entrainment of solid and liquid into the wake of bubble. $\alpha=1$ corresponds to a perfectly mixed slurry i.e. the solid content of pulp volume and bubble wakes are exactly same. $\alpha=0$ represents the limiting conditions where there is no entrainment of gangue particles in the bubble wakes (i.e. no hydraulic entrainment). In this case, there may be some mechanical entrainment due to internal flow patterns and turbulence.

The average α value can be calculated using (Yianatos et al. 1987):

$$\alpha_{\text{ave}} = \frac{J_{\text{g}}}{5.16. \, \epsilon_{\text{g}}^{0.67} \, U_{\text{ps}}} \left[1 - \left[\frac{-5.16.U_{\text{ps}} \, \epsilon_{\text{g}}^{0.87}}{J_{\text{g}}} \right] \right]$$
 5.6

and can be used to compare mechanical cells and flotation columns with respect to hydraulic entrainment in the slurry phase. (U is the particle settling velocity given by Eq. 5.17).

Figure 5.1 shows that the calculated α_{ave} decreases with increasing particle size for both column and mechanical flotation. From this graph, it can be concluded that the entrainment of coarse particles is difficult and fine particles behave like water. It appears that hydraulic entrainment (i.e. wake entrainment) is higher in flotation columns than conventional cells due to a longer residence time of particles in the slurry phase.

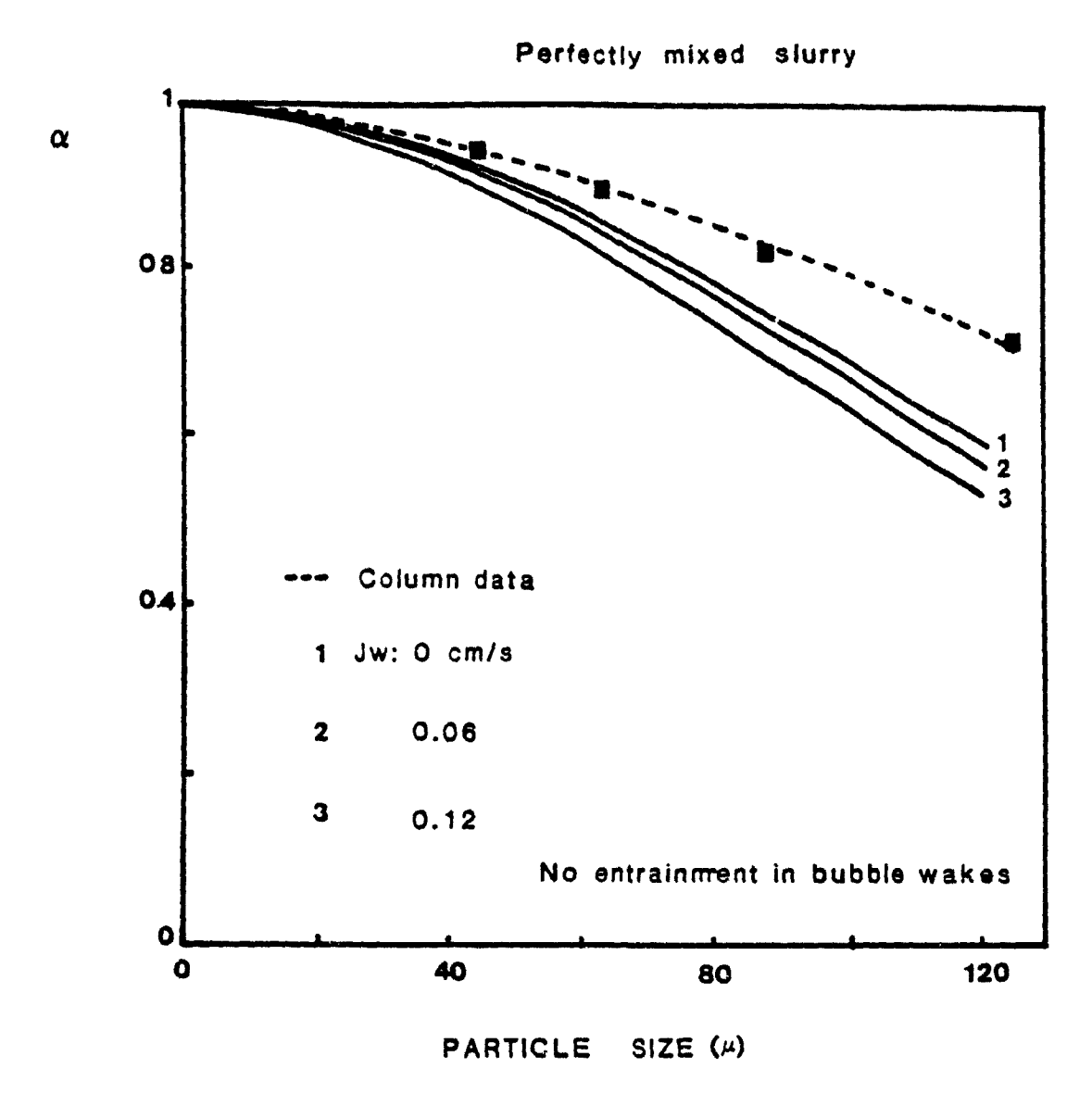


Figure 5.1: Comparison between mechanical cells and flotation columns for entrainment in the slurry phase.

	Industrial column	Laboratory cell
$\rho_{p} (g/cm^{3})$	5.19	2.65
% solid by weight τ (min)	2.50 12.60	10.00 2. 25-4
J _g (cm/s)	1.40	0.6
J (cm/s)	2.29	0-0.12

5.1.2 Mass Transfer in the Froth Phase

Moys (1978) developed a comprehensive model for flotation froth behaviour using the concept of plug-flow initially introduced by Cooper (1966). Recently, Yianatos et al. (1987) successfully applied the same principles to predict the mass transport of valuable particles from the selectivity point of view through the column flotation froths.

Here, a plug-flow model based on Moys' is developed to describe the behaviour of the entrained gangue particles in the froth phase of a mechanical flotation cell. Figure 5.2 shows schematically the mass flowrates in the froth phase. The following assumptions are made:

a. Hydrophilic particles of species "i" do not attach to the bubbles in the slurry zone (i.e. all hydrophilic particles are mechanically and/or hydraulically entrained into the froth). Bubbles entering the froth carry a thin layer of water, which preferentially entrains fine gangue particles. The relative interstitial velocities of air, liquid, and solid in the froth determine transfer rates. Slurry is entrained between the bubbles in the froth phase and containing gangue particles in the same concentration as that in the cell. The initial flowrate of water along with gangue particles, $Q_{\underline{i}}(0)$, is obtained by assuming that each bubble carries a thin layer of slurry (i.e water plus solid) of thickness δ , into the base of froth.

$$Q_{1}(0) = \frac{6 \cdot Q_{g} \cdot \delta}{d_{h}}$$
5.7

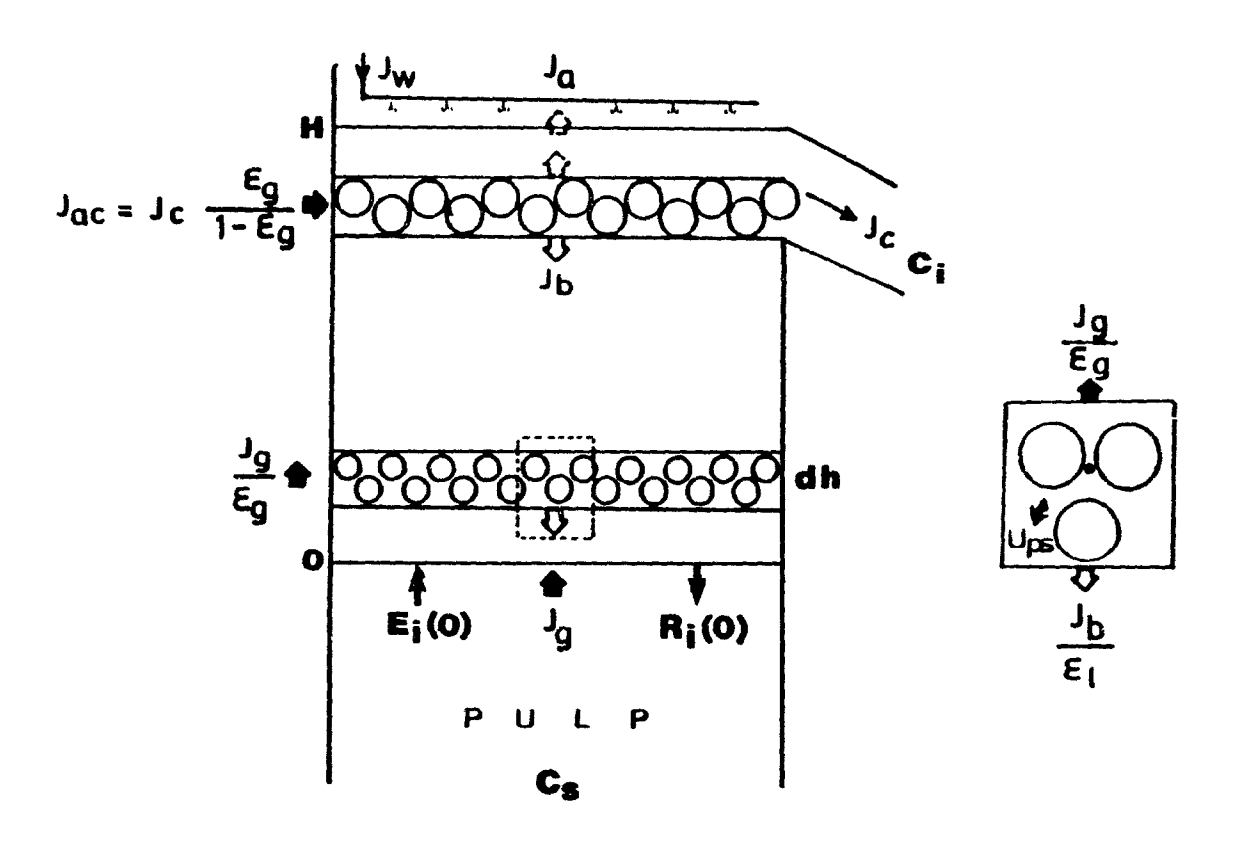


Figure 5.2: Notation for the mass transfer calculations in the froth phase.

where $Q_{i}(0)$: initial upward slurry flowrate at the interface,

Q: aeration rate, m³/sec

 δ : water film thickness, m d $_{\rm bp}$: average bubble diameter in the slurry phase. m

The mass flowrate of gangue particles can be obtained from:

$$E_{i}(0) = Q_{i}(0).C_{g}$$
 5.8

where E_i(0): upward solid mass flowrate, kg/sec

 C_s : pulp gangue concentration near the interface, kg/m³

Both water and entrained particles rise at a rate E (h) and velocity V(h) towards the top of the froth. The interstitial upward liquid rate at a certain height in the froth is equal to:

$$V(h) = \frac{J_g}{\varepsilon_g(h)}$$
 5.9

where V(h): bubble film rise velocity in the froth, m/sec

 $\varepsilon_{_{_{\mathrm{C}}}}$: fractional gas holdup in the froth phase

b. At the top of the froth, a fraction of the froth is removed. while the rest collapses and enters the downward flowing stream. The upward interstitial liquid velocity at the overflow lip can be calculated using:

$$V(H) = \frac{J_c}{\varepsilon_1(H)} = \frac{J_{ac}}{\varepsilon_a(H)}$$
5. 10

where $J_{\hat{a}}$: superficial concentrate rate, m/sec

 $\boldsymbol{J}_{\text{ac}}$: superficial gas rate associated with liquid transfer to the concentrate, m/sec

H: froth thickness between the slurry-froth interface and froth surface, m

c. Particles may drain through the Plateau borders and enter the downward liquid flow in the froth by drainage bubble coalescence, collapse or froth washing. The rate of drainage is proportional to the concentration of component in question. Taking the mass balance over a differential element yields:

$$\frac{dE_{i}(h)}{dh} = \frac{-k_{i} E_{i}(h)}{V(h)}$$
5.11

where k_i : dropback rate constant, \sec^{-1}

Combining Eqs. 5.9 and 5.11 yields:

$$\frac{dE_{i}(h)}{dh} = \frac{-k_{i} E_{i}(h) \varepsilon_{g}(h)}{J_{g}}$$
5.12

The solution to the above equation is:

$$E_{i}(h) = E_{i}(0) \exp(-k_{i}\tau(h))$$
 5.13

where $\tau(h)$: minimum bubble residence time in the froth and is equal to:

$$\tau(h) = \frac{\int_{0}^{z} \varepsilon_{g}(h) \cdot dh}{\int_{g}^{J}}$$
5.14

d. It is assumed that hydrophilic particle re-entrainment does not occur in the froth. The dropback rate constant includes both drainage and washing rate constants for entrained particles.

Therefore, k_i represents the net loss of mineral from the ascending bubbles and can be estimated from:

$$k_{i} = \frac{-\ln(C_{i}/E_{i}(0)) J_{g}}{\varepsilon_{g}. H}$$
5.15

where C_i : mass flowrate of species i at the concentrate level, kg/sec

e. A particle descending in the downward flowing water without contacting gas bubbles will move with a velocity equal to the interstitial liquid velocity plus the relative particle-fluid settling velocity in hindered settling regime (Upp). Bubbles in the froth was assumed the cause of hindrance. Then, the net interstitial downward liquid rate can be calculated from:

$$U_{1} = \frac{J_{b}}{\varepsilon_{q}} = \frac{J_{w} - J_{c}}{\varepsilon_{1}}$$

$$5.16$$

where U_i : interstitial downward liquid rate, m/s

The relative particle-fluid settling (slip) velocity can be estimated from the general equation proposed by Masliyah (1979) using a momentum balance for the particles and fluid:

$$U_{ps} = \frac{g.d_{p}^{2} \varepsilon_{1}^{2.7} (\rho_{p} - \rho_{susp})}{18 \mu_{1} (1+0.15 \text{ Re}_{p}^{0.0687})}$$
5.17

where $d_{\mathbf{p}}$: particle diameter, m

 $\epsilon_{_{1}}$: fractional liquid holdup in the froth

 $\rho_{\rm p}$: particle density, kg/m³

 μ_{i} : liquid viscosity, centipoise

Re : particle Reynolds number, dimensionless

The above equation is valid for hindered settling systems containing particles of different size and density.

The net downward interstitial velocity is calculated from:

$$\frac{J_{\text{W}} - J_{\text{C}}}{\varepsilon_{1}} + U_{\text{ps}}$$
 5.18

The drainage rate is given by:

$$R_{i}(h) = E_{i}(h) - C_{i}$$
 5.19

f. The mass fraction of hydrophilic particles between h and $h+\Delta h$ is equal to:

$$dM_{i}(h) = \begin{bmatrix} E_{i}(h).\varepsilon_{g}(h) & R_{i}(h).\varepsilon_{l}(h) \\ \hline J_{g} & J_{b}+U_{ps} \end{bmatrix} dh \qquad 5.20$$

and gangue concentration (i.e. ratio of solids to the total weight of material suspended in the froth at a given location) is G_i :

$$G_{i}(h) = \frac{dM_{i}(h)}{\sum M_{i}(h)}$$
5.21

From G_i , it is possible to calculate fractional volumetric solid holdup, $\epsilon_{\rm g}$, in the froth at certain level:

$$\varepsilon_{s}(h) = \frac{dM_{i}(h)}{\rho_{s} A_{c} dh}$$
5.22

where ρ_s : solid density, kg/m³

A: cell cross-sectional area, m²

5.1.3 Particle Rejection Mechanisms in the Froth Phase

The residence time of froth elements (air, water or particle species) passing through the froth phase in mechanical flotation cells is distributed over a wide range. Elements entering near the overflow weir are removed rapidly while elements entering near the back of the cell may in fact never be removed and fall into the pulp phase due to long horizontal travel distances. Therefore, the residence time distribution, $E_c(\tau)$, will be an important factor determining the recovery of water, gangue, and weakly floatable particles. $E_c(\tau)$ is a function of the properties of the component (e.g. hydrophobicity), froth stability, cell design, and operating variables.

The bubble residence time is always smaller than or equal to the particle residence time and all liquid in froth is recovered in the concentrate. Minimum and average bubble residence times in froth can be calculated respectively from:

$$\tau_{\text{bfmin}} = \frac{\text{H. } \varepsilon_{\text{bf}}}{\text{J}_{\text{a}}}$$
 5.23

$$\bar{\tau}_{\rm bf} = \frac{H.\,\varepsilon_{\rm lf}}{J_{\rm c}}$$
 5.24

Bubble residence time distribution is given by (Moys, 1984):

$$E_{c}(\tau_{b}) = \frac{1}{\bar{\tau}_{bf}} \exp \left[-(\tau_{bf} - \tau_{bfmin})/\bar{\tau}_{bf}) \right] \quad \text{for } \tau_{b} > \tau_{bfmin}$$
5.25

$$E_c(\tau_b) = 0$$
 for $\tau_b < \tau_{bfmin}$

Upward bubble rise velocity in the froth is calculated using:

$$V_{bf} = \frac{H}{\tau_{bf}}$$
 5.26

$$V_{\text{bfmin}} = \frac{H}{\tau_{\text{max}}}$$
 5.27

$$V_{\text{bf}} = \frac{H}{\tau_{\text{bf}}}$$
 5.28

$$E_{c}(V_{bf}) = \frac{1}{\bar{v}_{bf}} \exp \left[-(V_{bf} - V_{bfmin}) / \bar{V}_{bf} \right]$$
 5.29

$$U_{\rm bf} = \frac{V_{\rm bf}}{\varepsilon_{\rm bf}}$$
 5.30

Gangue contamination of froth will occur if the interstitial upward bubble velocity exceeds the particle settling velocity. Therefore, hydrophilic particles will be rejected or retained depending on following conditions:

For a given particle size, classification coefficient (Z_i) , i.e. weight fraction of the gangue particles of size i entering the froth which is recovered in the concentrate, can be calculated at $U_{ps} = U_{bf}$:

$$Z_{i} = \frac{E_{c}(U_{bf})}{\sum E_{c}(U_{bf})}$$
 5.31

5.2 Experimental Procedure

Summary of experimental conditions is given in Table 5.1..

Table 5.1: Summary of experimental conditions.

	J	J	FT		Cell	Type
Gangue	profile in	n the sl	urry phase			
silica silica	0 0.6	o 8. 061	0		modified modified	batch continuous
	profile i	0.123				
J	•		•			
tails	0.6	0 0.076	4		modified	continuous
tails	0.6 0.4	0 0	4 4		modified	continuous
N: 150	O rpm,	Frother:	Dowfroth	250,	10 ppm,	10% solid,

N: 1500 rpm, Frother: Dowfroth 250, 10 ppm, 10% solid, and distributor: spiral

5.2.1 Set-up and Material

Most of the experiments were performed continuously using the modified cell. Particle size distributions were determined by a sedigraph 5000D. Li concentrations for tracer tests were measured by atomic absorption. The distributor was fixed 4 cm above the froth phase. Residence time was adjusted by tailings flowrate and slurry level by feed flowrate at constant water addition rate.

Two different solid samples were used to characterize gangue entrainment: silica flour (from Indusmin) and a reject (slimes) from Niobec (St-Honoré, Quebec, Canada); their size distribution is given in Figure 5.3. Niobec slimes contain 65% carbonates (dolomite and calcite), 21% silicates, 7% hematite, 2 % apatite and less than 1% pyrite. Both samples are hydrophilic when conditioned by frother alone.

5.2.2 Determination of Gangue Profile in the Slurry Phase

A sampler was developed to measure the gangue concentration profile in the slurry phase. Samples were drawn from the slurry phase at different levels by a sampling probe consisting of a 50 mL glass pipette connected through a flexible tubing to a peristaltic (Masterflex) pump. A variable speed controller provided satisfactory control of sucking and facilitated easy manipulation as required for the sampling procedure. The tip of pipette was cut in order to enlarge the sucking orifice to 3 mm which is at least four times larger than the coarsest particles present in the feed, but small enough to prevent bubbles from

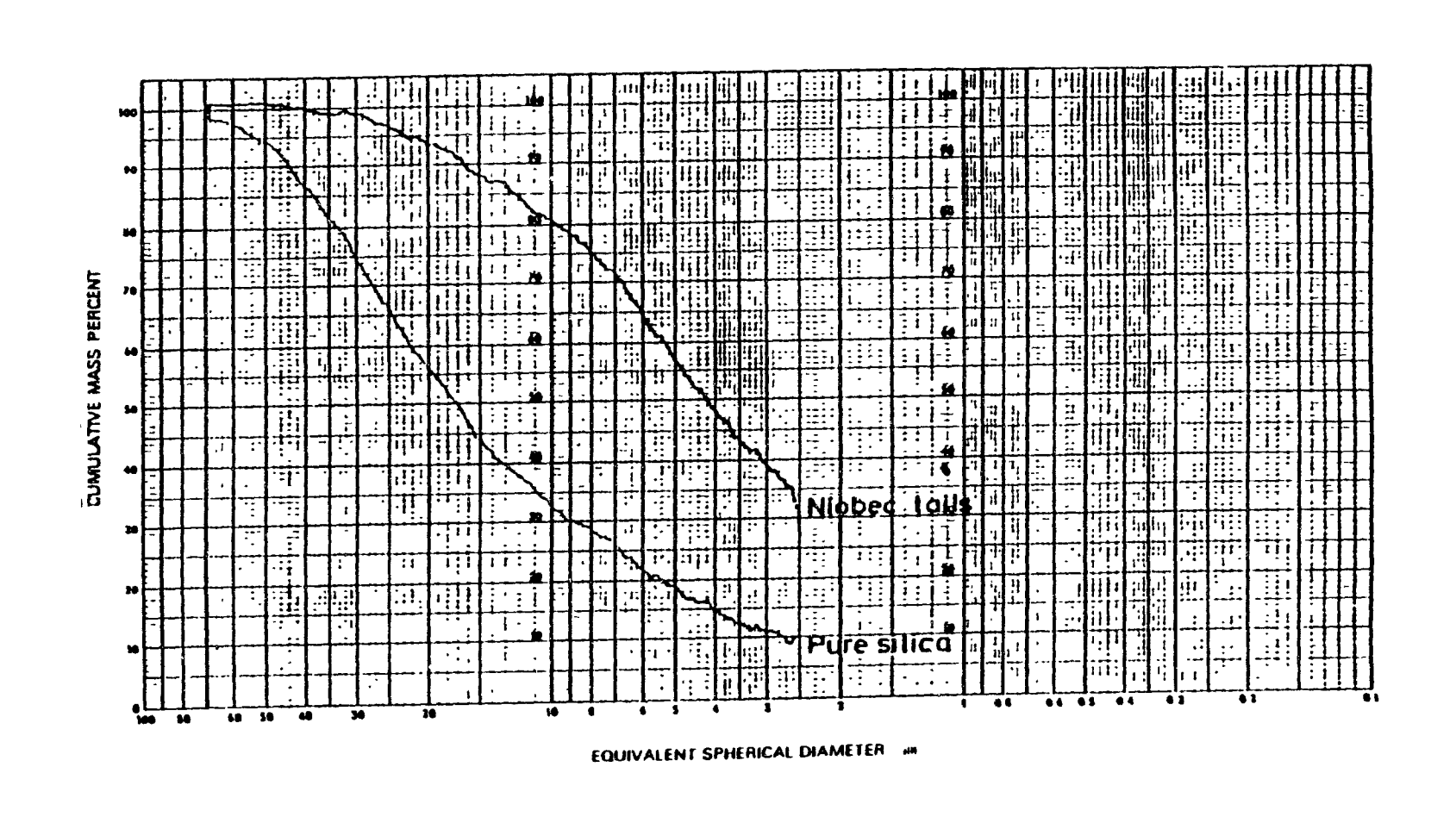


Figure 5.3: Particle size distributions of the samples used.

entering. Since just a small tube is plunged into the cell, the actual flow patterns and hydrodynamic conditions of the slurry phase are not disturbed. A 50 mL sample is an adequate in size to determine "solid and the particle size distribution. Statistical fluctuations in the resulting particle size concentration were reduced by taking a minimum of three samples and averaging concentrations.

The top view of the cell (see Figure 5.6) shows the sampling points (B and F) which are on the tailing discharge side of the cell. Sampling from the feed side was practically impossible due to the confined space and could have introduced bias. Since tailings are discharged from the cell bottom, the samples from the lowest sampling depth, 10 cm above the cell bottom, will not be affected by the tailing discharge.

Samples were taken during continuous operation. After the last sample was taken, the system was allowed to run 3 minutes; the feed and tailing pumps and rotor were then turned off immediately. The slurry in the flotation cell was discharged, weighed, filtered, dried and reweighed. An ideal mixing line was determined from the cell inventory.

First, the effect of agitation on gangue profile was investigated to characterize mechanical entrainment. In the presence of frother, the gangue concentration profile was determined without aeration and wash water addition in batch

operation. Second, similar profiles were determined at three different J_{w} at a constant J_{g} , FT and RPM with a feed of 10% silica by weight. This second series of tests show the effect of wash water on mechanical and hydraulic entrainment together.

Mechanical entrainment in a flotation cell is mainly influenced by the impeller pumping capacity (Q_i) , i.e. the volume of fluid it discharges per unit time. It is proportional to the impeller peripheral (tip) speed and its discharge area.

The calculation of pumping capacity for impellers with radial flow is analogous to that of centrifugal pumps (Azbel and Cheremisinoff, 1983).

$$Q_1 = \pi^2. N. b. D^2$$
 5.32

where N: impeller speed, rps

D: impeller diameter, m

b: impeller thickness, m

The superficial fluid pumping rate (J_i) , i.e. the liquid flow per unit cell area, depends on the impeller aspect ratio (D/T) for square cells:

$$J_1 = \pi^2. \text{ N. b. } (D/T)^2$$
 5.33

where T: cell lenght, m

 J_i : superficial fluid pumping rate, m/s

The flowrate per unit cell volume (V) is based on both the impeller aspect ratio and inverse of cell height:

$$\frac{Q_1^2}{V} = \pi^2. N. b \left[\frac{D}{T} \right] \left[\frac{1}{H} \right]$$
 5.34

where H: cell height, m

Q_i/V is also defined as a tank turnover rate i.e. the number of turnovers per unit time. The mechanical entrainment component of gangue recovery can be lessened by decreasing superficial fluid pumping rate (i.e decreasing impeller diameter or increasing cell length). For a given volume, an increase in the impeller aspect ratio (D/T) will significantly increase mechanical entrainment. For a constant cell cross-sectional area, an increase in the cell height (i.e. deep cell) leads to reduced mechanical entrainment. The use of baffles and different impeller types has some effect on mechanical entrainment.

The pumping capacity of the impeller entrains considerably more fluid as it passes out into the tank (Figure 5.4) (Oldshue, 1979). There is a nearly constant D/L ratio for the different-sized members of the same family (design). Most of the industrial families are given ratios falling in the range of 0.3 to 0.5 (Denver, Wemco, Fagergren, Soviet, and Agitair flotation machines). As the D/T ratio approaches 0.6, there is a little room for mechanical entrainment to take place. For the present laboratory study, the D/L ratio was 0.47.

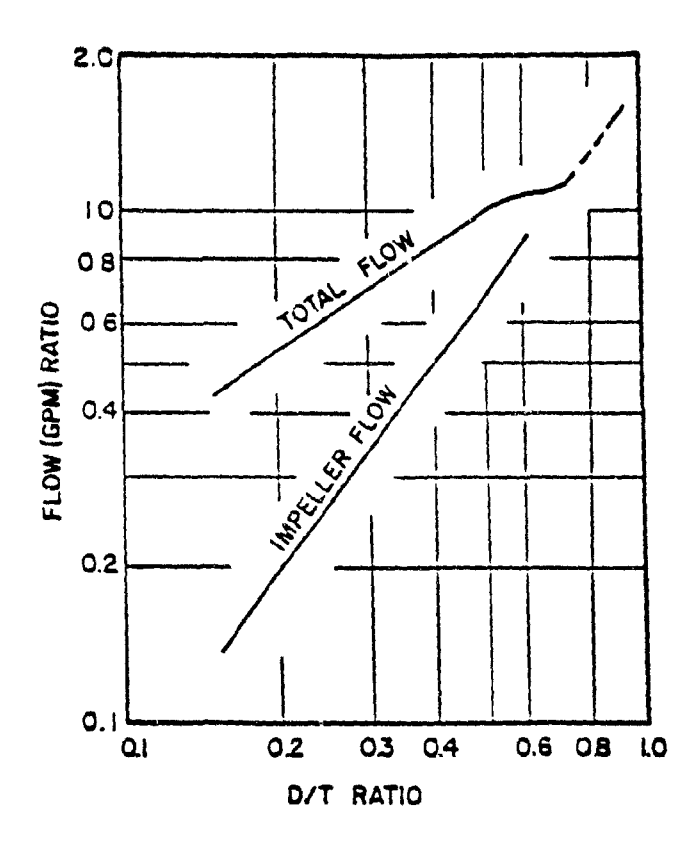


Figure 5.4: Effect of D/T ratio on mechanical entrainment due to impeller flow.

(from Oldshue, 1579).

5.2.3 Froth Sampling Techniques and Gangue Holdup Profiles

There are various methods of obtaining known volumes of froth sample (slurry and air) in the flotation literature: slicing, ports and multi-point sampling lance.

The most accurate method of obtaining the variations of froth properties with height would be that of Watson and Grainger-Allen (1974) i.e. using horizontal slides to partition the froth phase into a number of segments and removing the samples by sucking. In our experimental set-up, slicing the froth phase is impossible because of the impeller shaft.

In the port method, a stopper from a hole on the side of the cell is removed to allow a sample to flow into a beaker. Since a sample of large volume removed from a hole would not necessary be characteristic of the froth at that level (in the limit, all the froth above any hole could removed through it). Small samples are usually taken and this process is repeated at intervals long enough to allow the froth to reestablish itself until a sufficient amount of sample was obtained at each level. If there is a horizontal concentration gradient, this technique may give unrealistic results.

A multi-point sampling lance was used to extract froth samples for pulp density and grade analysis by Cutting et al. (1981). A similar technique was used to suck samples simultaneously at different froth levels by vacuum (Yianatos et al., 1987). This sampler is more convenient for sampling thick froths as in column flotation.

None of the above sampling methods were found adequate for our experimental set-up with FTs up to 5 cm, and eventually a small sampler was designed and constructed to determine the average solid, liquid, and gas holdups in the froth phase. Figure 5.5 shows the froth sampler, which is made of plexiglass (1.8, 1.8, 1.6 cm). Two sliding stainless steel plates can open and close the sampler box at the top and bottom. Two 0-rings assist closing. The sampler in open position is plunged into the froth phase as soon as it is full of froth, the sliding plates are closed. It is then removed from the cell, washed, weighed, dried, and weighed again.

5.2.3.1 Test Work

Solid, liquid, and gas content of the froth phase were determined at two different aeration rates (0.4 and 0.6 cm/s) without wash water and at a constant gas rate (0.6 cm/s) with two different wash water addition rates (0 and 0.076 cm/s). For each test, two samples in the froth and another one 1 cm below the slurry-froth interface were taken (this sample is assumed to represent the gangue concentration at the interface). At the end of each test, the cell content was also measured to estimate average solid holdup in the slurry phase.

5.2.3.2 Calculation Procedure

In order to simulate gangue holdup profile in the froth:

- a. input J_{q} , J_{w} , J_{c} , A_{c} , H, C_{s} , and C_{i} from three phase tests
- b. input d_{b} and δ from two phase tests. The average bubble

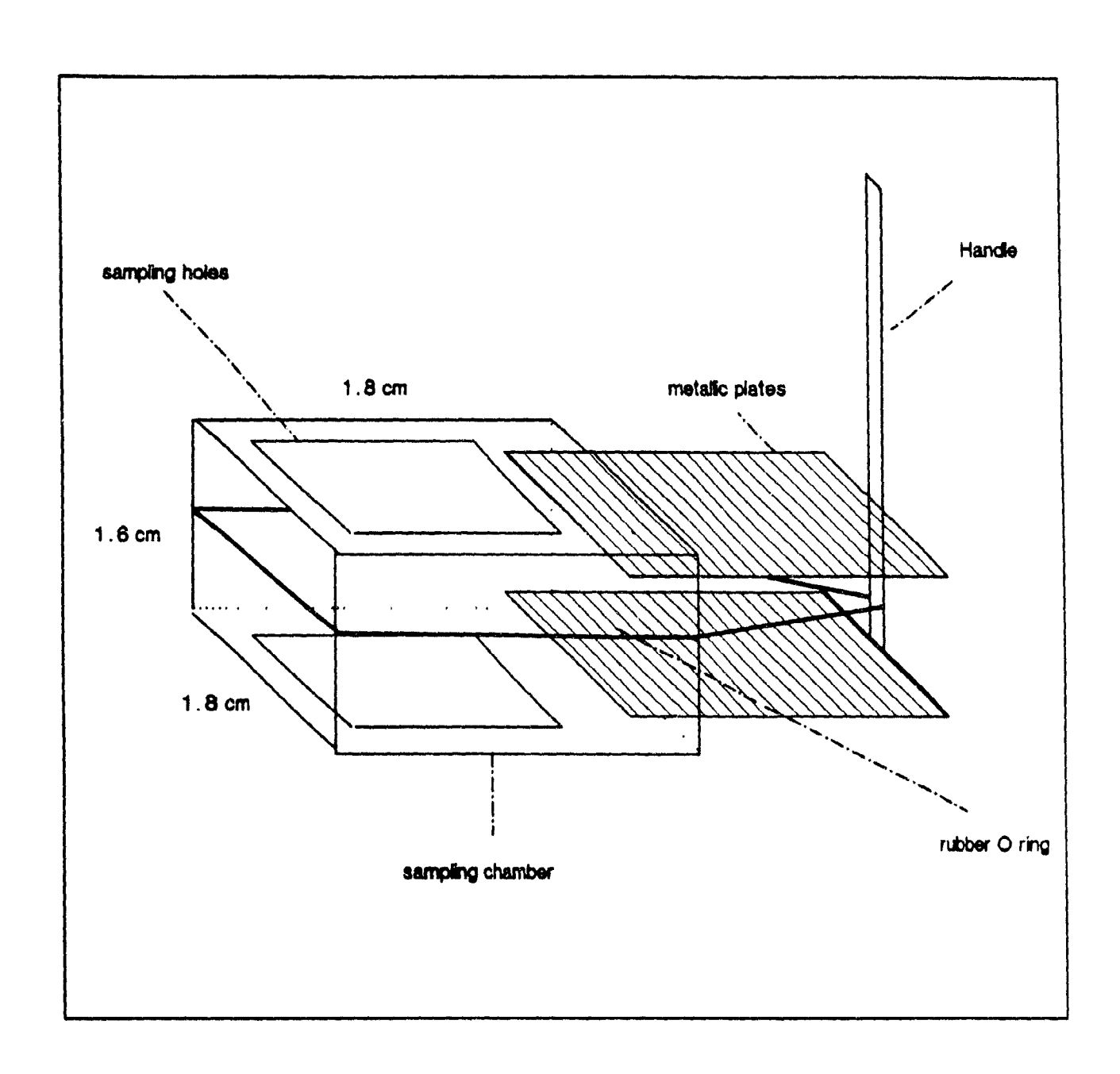


Figure 5.5: Schematic diagram of the froth sampler.

diameter in the slurry phase was assumed not to be affected by wash water.

- c. input parabolic gas holdup profile in the froth phase from two phase measurements as a function of distance from the slurry-froth interface (H).
- d. input d. Particle settling velocity can be calculated for a 10 μ m particle since the gangue particles entrained are finer than this size. (Settling velocity, at dp=10 μ m, has a negligible effect).
- e. input $\varepsilon_{\rm g}$ at the interface level from pulp sampling.

A printout of the computer program can be found in Appendix 5.1.

5.2.4 Hydrophilic Particle Rejection in the Froth Phase

Gangue particle settling velocity in the froth phase were calculated using free settling in the Stoke's range and hindered settling equations (5.17). In this calculations, ε_g , ε_s , J_c , J_g , and J_w were taken from the froth sampling tests. Size-by-size classification coefficients were calculated using Eq. 6.31.

5.3 Results and Discussion

5.3.1 Gangue Concentration Profiles in the Slurry Phase

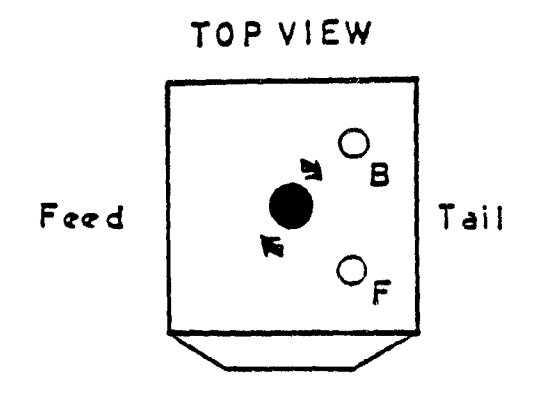
Gangue concentration profiles in the slurry zone were first determined in the absence of aeration in order to characterize mechanical entrainment and then with air, to assess mechanical and hydraulic entrainment together.

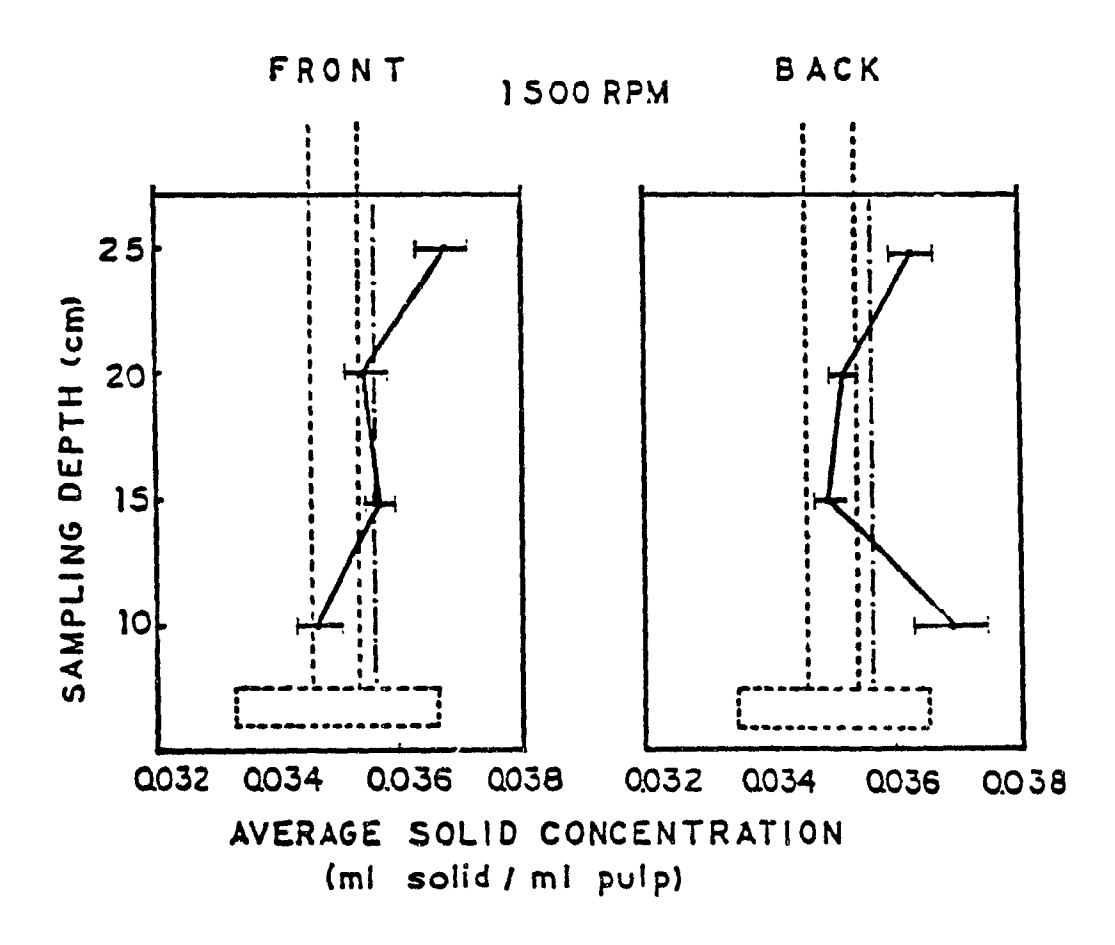
Mechanical Entrainment: Figure 5.6 shows silica concentration profile and sampling locations in the laboratory flotation cell. Samples taken from the front (F) and back (B) parts of the flotation cell slightly deviate from the ideal mixing line in the absence of aeration. The recycle flow around the impeller-stator assembly can account for the observed deviations from ideal mixing (Harris et al, 1975). The average solid concentration in the upper-most pulp layer (close to the interface) is higher than average, which is undesirable.

Ideal mixing of gangue particles provides no selectivity. It implies complete particle suspension and dispersion throughout the slurry volume. It is one factor responsible for gangue contamination of the concentrate.

Since there is no aeration in these tests, all of the silica particles should practically be carried by mechanical entrainment rather than hydraulic entrainment.

Table 5.2 shows the particle size distribution of the feed and at different depths in the slurry phase. Samples taken at levels 10 and 25 cm from the cell bottom have the finest size distribution. At 15 and 20 cm from the bottom, the particles are much coarser. In the upper levels, coarse particles are more difficult to suspend. At the lower level, they are centrifuged out by the recycle action. Here, the flotation cell works like an inverted hydrocyclone in which fine particles are pushed towards





(10% Solid by weight, 10 ppm Dowfroth 250 C no aeration and wash water addition.)

- Average silica (gangue) concentration
- __ Ideal mixing line

Figure 5.6: Gangue (silica) concentration profile without aeration and sampling locations in the modified cell (batch test).

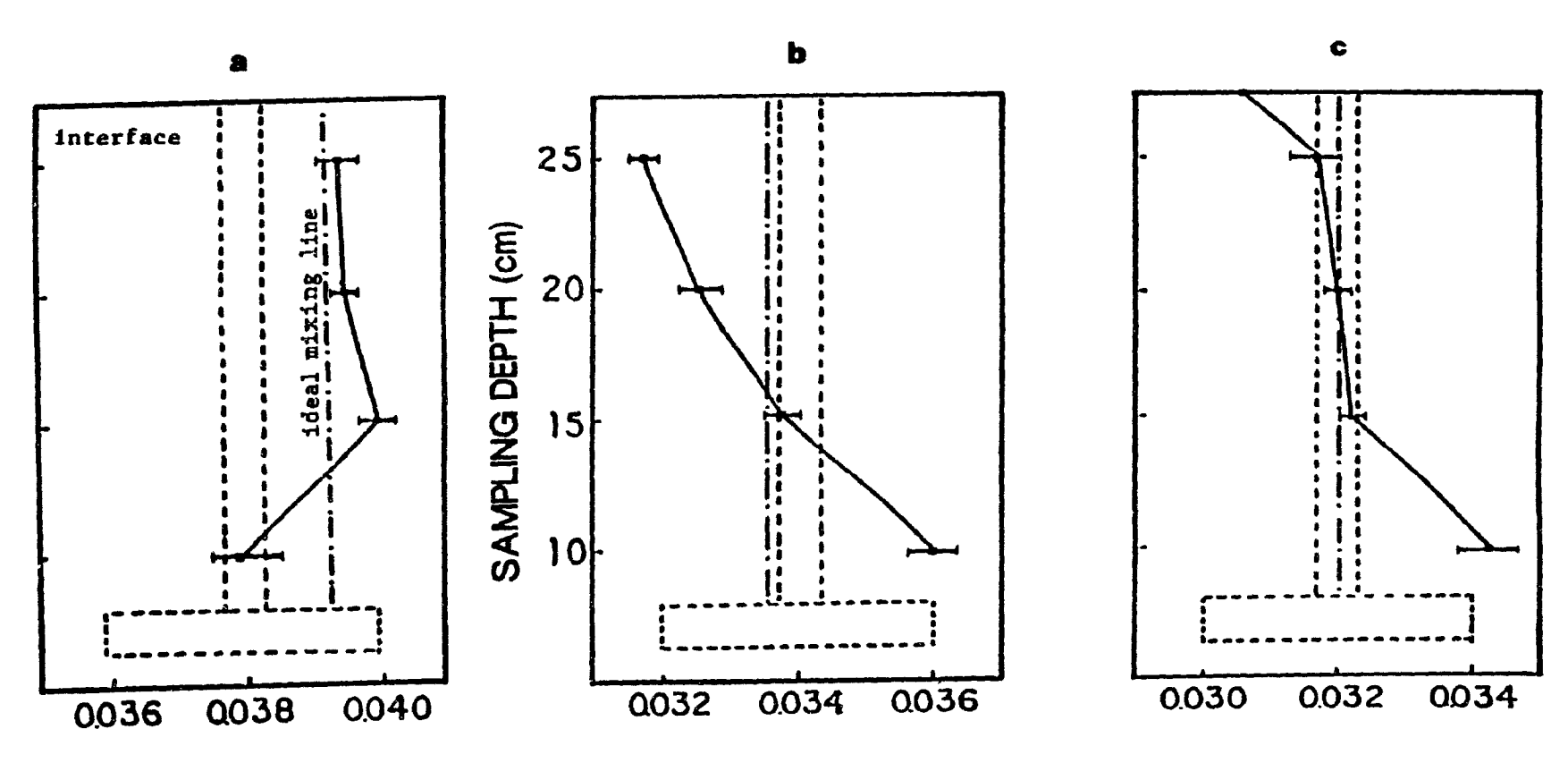
underflow (upward) in the centre of the cell due to a high centrifugal force.

Table 5.2: Particle size distribution of samples extracted at different levels. (Cumulative mass percent finer than the specified particle size).

Particle size (μm)	Sampling Depth (cm)							
	Feed	10	15	20	25			
70	95	99	97	95	98			
60	92	97	94	92	96			
50	90	95	90	89	93			
40	83	87	80	80	83			
30	69	70	60	61	70			
20	46	52	41	41	47			
10	17	24	18	17	24			
8	13	17	12	12	16			
6	6	10	5	4	8			

Harris et al. (1983) also observed departures from the ideal mixing in unaerated pulps in a laboratory Denver flotation machine. They found that increasing impeller speed and impeller-stator clearance caused less departures from ideal mixing.

Hydraulic and Mechanical Entrainment: Figure 5.7a shows the average silica concentration in the slurry zone in the presence of air, but without wash water addition. The gangue concentration appears to be maximum at 15 cm from the cell bottom. In the upper part of the cell, gangue concentration is very close to ideal mixing, a serious problem from an entrainment point of view.



AVERAGE GANGUE CONCENTRATION (mL gangue/mL pulp)

Figure 5.7: Gangue (silica) concentration profile in the slurry phase with agitation and aeration (continuous flotation and J: 0.6 cm/s)

(a: J = 0 cm/s, b: 0.061 cm/s, and c: 0.12 cm/s)

Arbiter et al. (1969) showed that the degree of particle suspension and dispersion depends directly on impeller speed and inversely on air rate and particle size.

Figures 5.7b and 5.7c show the gangue profiles throughout the slurry phase at J_{w} 's of 0.061 and 0.123 cm/s, respectively. In the presence of wash water addition, the gangue concentration decreases towards the slurry-froth interface. The deviation from the ideal mixing line is more significant at the intermediate than high wash water rate.

Decreased gangue concentration at the top of the slurry assists in decreasing the entry of fine free gangue into the froth. The effect, however, is small.

5.3.2 Solid, Liquid, and Gas Contents of the Froth Phase

Table 5.3 shows experimental solid, liquid, and gas holdups at ferent levels in the froth phase along with average values. In the absence of wash water, increasing J_g will increase the average solid and liquid content of the froth phase. Adding wash water decreases the hydrophilic solid content and increases the liquid content of the froth.

Figure 5.8 shows predicted and measured volumetric gangue holdup as a function of froth depth with and without wash water.

The gangue content of the froth significantly decreases from the slurry-froth interface to the top of the froth phase.

Gangue holdup is higher in the absence of wash water and there is

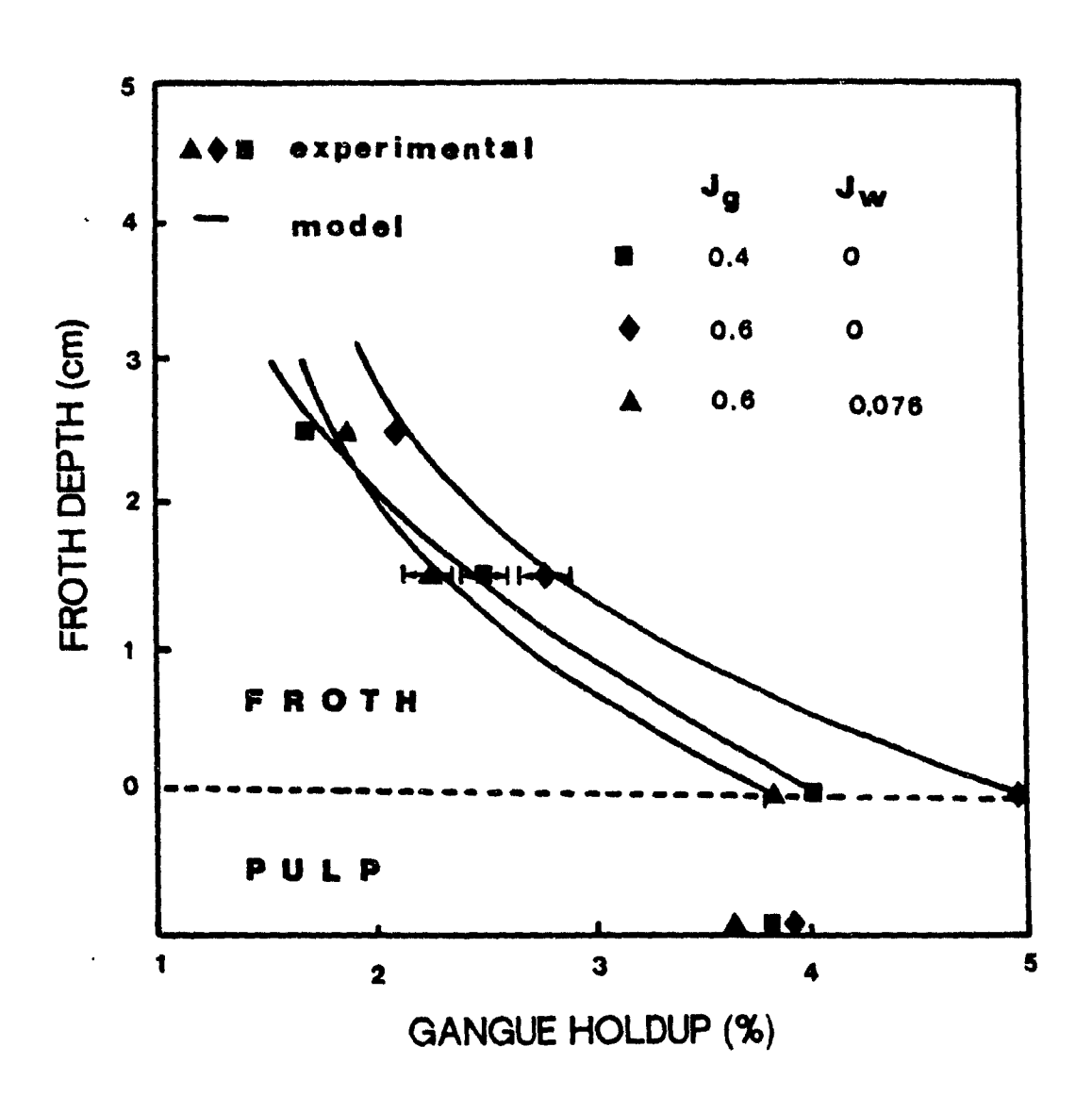


Figure 5.8: Gangue holdup versus froth depth in the presence and absence of wash water at different aeration rates.

a good agreement between measured and predicted gangue holdups in the froth phase. Dropback rate constants (k_i) are 0.34 and 0.86 without wash water at J_g of 0.4 and 0.6 cm/s and 0.55 with wash water.

Table 5.3: Solid, liquid, and gas holdups of the froth phase using the froth sampler. (FT = 4 cm)

			Hold	Holdups in the Froth					
	J (cm/s)	J (cm/s)	ε _s (%)	ε, (%)	ε _g (%)				
pulp interface H=1.5 cm H=2.5 cm average	0	0.4	3.70 3.97 2.25 1.84 2.37	12.03 4.50 2.25 10.63	84.00 93.00 96.00 87.00				
pulp interface H=1.5 cm H=2.5 cm average	0	0.6	3.90 4.94 2.81 2.21 2.91	13.06 6.19 3.79 12.09	82.00 91.00 94.00 85.00				
pulp interface H=1.5 cm H=2.5 cm average	0.076	0.6	3.55 3.78 2.72 1.80 2.51	20.22 13.28 6.20 19.49	76.00 84.00 92.00 78.00				

3.5.3 Hydrophilic Particle Rejection in the Froth Phase

Figure 5.9 shows classification coefficients calculated for free settling in the Stoke's regime and hindered settling using Masliyah's equation (5.17) as a function of particle size with and without wash water. If free settling dominates, particles

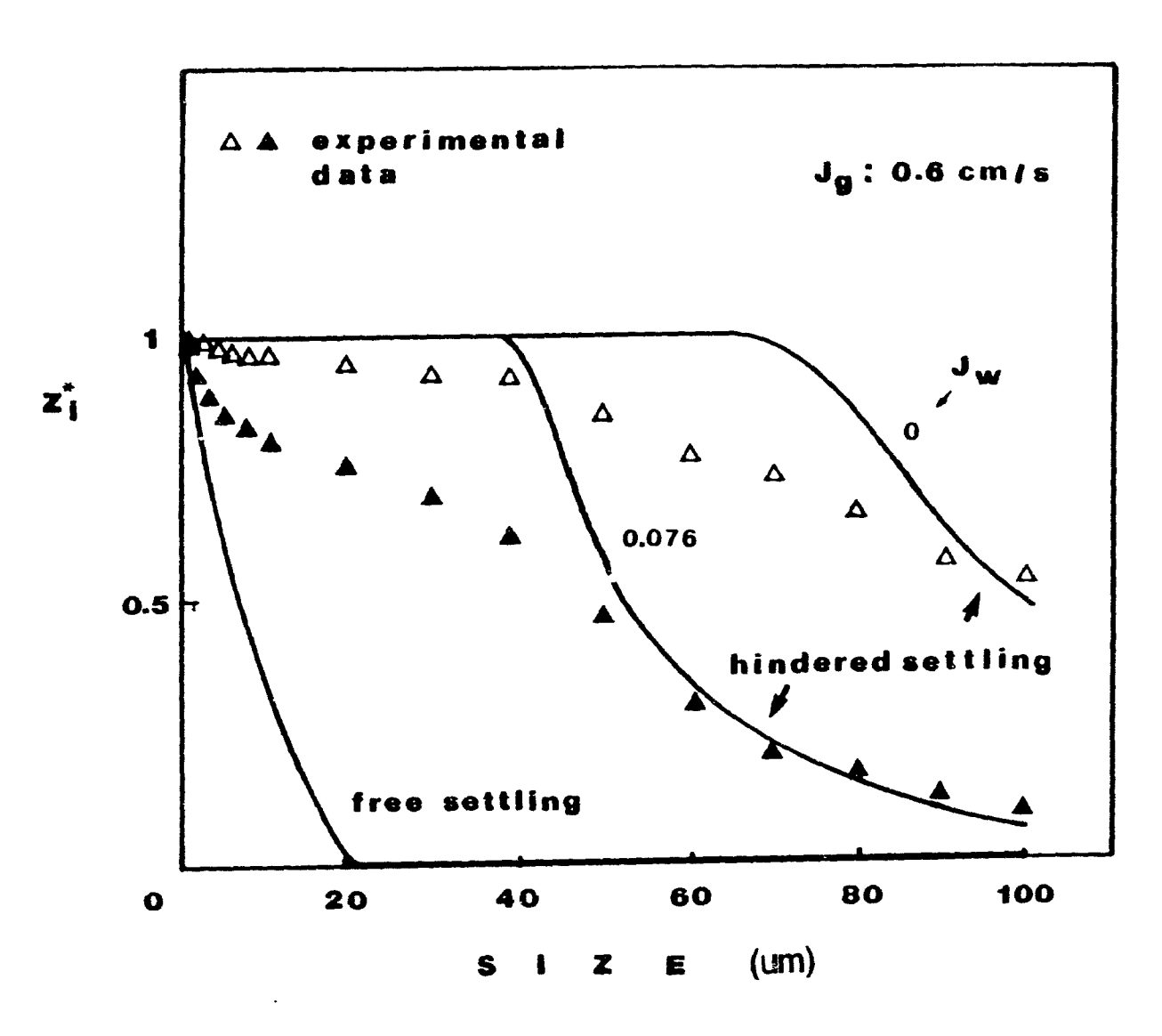


Figure 5.9: Calculated and experimental 2 values as a function of particle size with and without wash water.

coarser than 20 µm should be rejected back to the pulp phase. If hindered settling dominates, particles finer than 40 and 70 µm should be entrained and the rest of them should be classified in the presence and absence of wash water, respectively. However, experimentally determined classification coefficient values do no fit to free or hindered settling conditions very well. With wash water, the fit of data to free settling calculations at the fine end and to hindered settling calculations at the coarse end is good. At the intermediate size range, both settling equations do not represent the experimental data. Without wash water, hindered settling represents the experimental data better than free settling.

Particle settling in the froth phase is very complex, and hindered settling conditions are more realistic than free settling in the presence of wash water. Therefore, it was decided to use the Masliyah's equation for particle settling.

From these results, it can be concluded that fine particles (>10 µm) follow water and freely fall in the Plateau borders and water films without bridging. However, well drained froths hinder the settling of coarse particles.

The effect of superficial wash water and gas rates on the insterstitial particle settling velocity in the froth was calculated using equation 5.17 and plotted as a function of particle size in Figure 5.10. Particle settling velocity

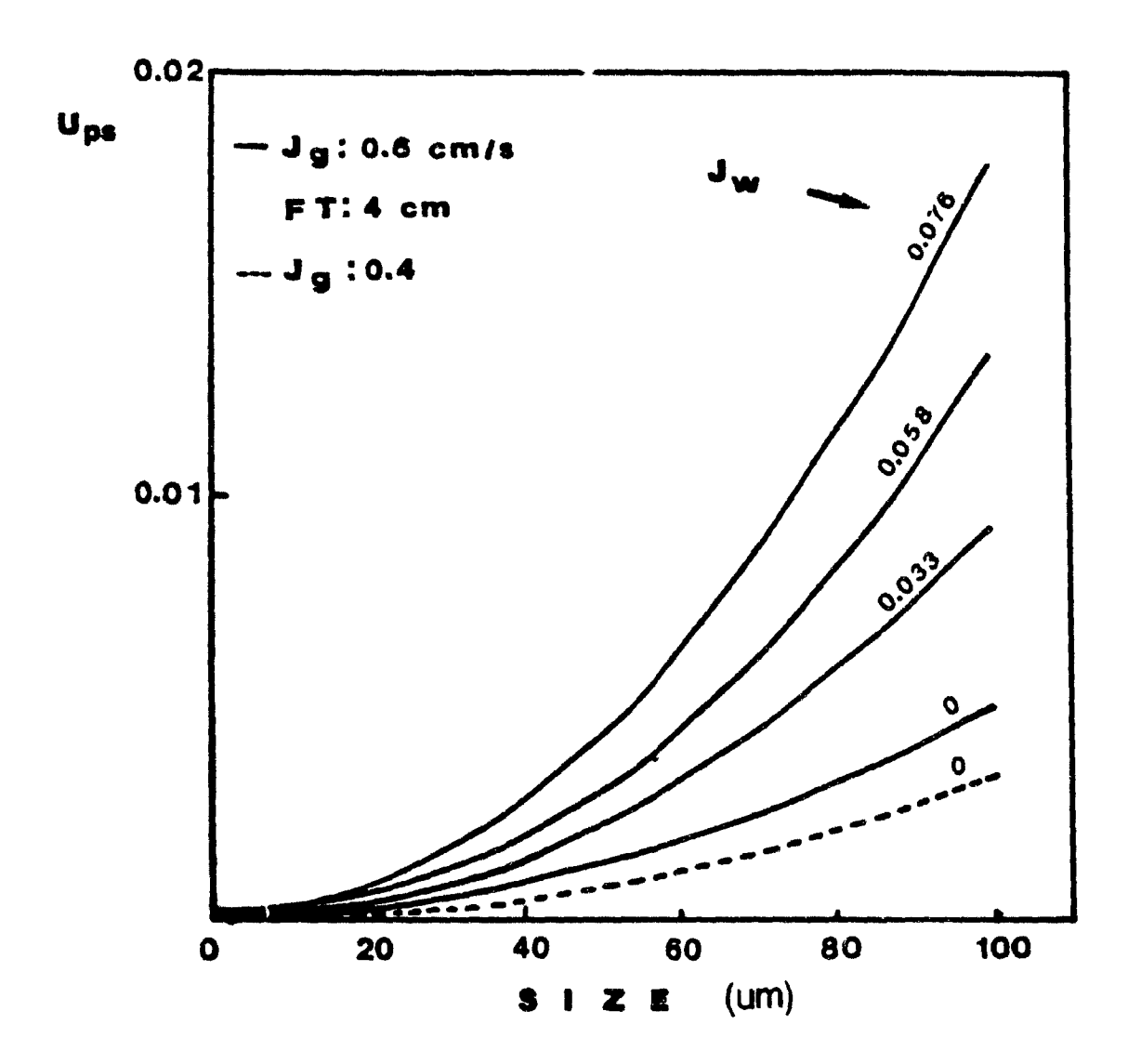


Figure 5.10: Interstitial particle settling velocity versus particle size at different wash water and gas rates.

increases with increasing both gas and wash water rates. The effect of wash water is more significant than gas rate.

Figure 5.11 shows the calculated classification coefficients versus particle size at different depths in the froth phase with and without wash water. Particle classification in the froth is much sharper with wash water than without it. The sharpest classification occurs at the interface and its sharpness decreases towards the froth surface, which makes it possible to reject fine particles. Particles not rejected near or within 1.5 cm of the surface have a high probability of being entrained into the concentrate, because the froth at this level is well drained and the settling of interstitial particles is strongly hindered.

These findings confirm that the main cleaning action takes very close to the interface. Mainly, the fine hydrophilic particles (< $10\mu m$), which have insignificant settling velocities and follow water, are entrained. The only way of rejecting them is to replace slurry water coming from the pulp with wash water using a sufficiently high bias rate (J-J).

Moys (1978) found that the gangue grade decreased markedly at the base of the froth due to settling of the larger particles in the slurry entering the froth phase. Above a certain height the concentration remains constant.



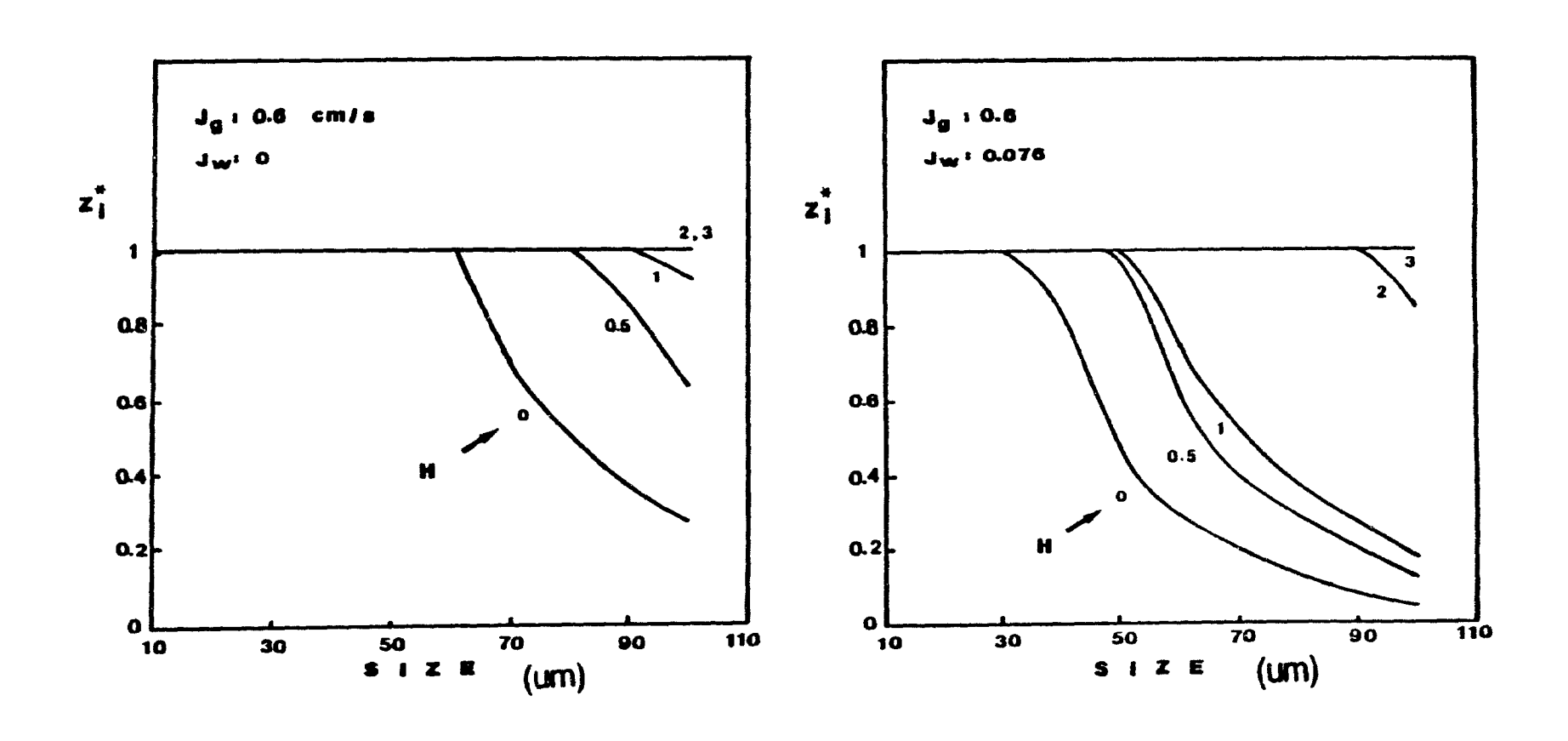


Figure 5.11: Size-by-size calculated 2_i^{\bullet} values at different froth depths with and without wash water.

(H: distance from the interface in cm)

5.4 Summary

Following conclusions can be stated from this chapter:

- a. Gangue concentration is not homogeneous in the slurry phase.

 Wash water slightly dilutes the pulp phase and decreases gangue content near the interface. The effect, however, is small.
- b. Gangue content in the froth phase decreases with increasing wash water rate or decreasing gas rate. The location of cleaning action is near the interface. Estimation of gangue content is possible using the froth model presented in this chapter.
- c. A criterion was developed to calculate the classification coefficient for hydrophilic particle rejection. It was found that particle settling velocity is negligible for fine particles. Therefore, the only way to reject them is to provide a sufficient downward water flowrate, which can be only achieved by wash water.

CHAPTER 6

THE EFFECT OF WASH WATER ADDITION AND FROTH VERATION
ON

GANGUE ENTRAINMENT AT LABORATORY SCALE

Introduction

The applicability of froth washing and vibration in mechanically agitated flotation cells to lessen gangue entrainment was studied at laboratory scale. In this chapter, the main objective is to explore how, where, and how much wash water should be added in mechanical flotation cells. The effect of superficial air rate, froth thickness, impeller speed, wash water superficial rate, distributor design (geometry), and froth vibration generated mechanically and ultrasonically on gangue entrainment was investigated. At the end of this chapter, there is a comparison between a laboratory cell and column with respect to entrainment.

6.1 Modelling the Entrainment Process

There is a strong correlation between the recovery of water to the concentrate and that of hydrophilic particles. The description of entrainment mechanisms by a classification matrix has been postulated by Johnson et al. (1974). This diagonal matrix is made of $\mathbf{Z}_{\mathbf{i}}$ elements such that for the \mathbf{i} th size fraction.

(mass of free gangue per unit weight of water) conc.

Zi= (mass of free gangue per unit weight of water) pulp

Gangue recovery is related to particle size and water recovery. Laplante (1980) derived a model for the entrainment of gangue particles in continuous flotation based on water recovery and classification coefficient. In the present work, his model was slightly modified to take into account wash water addition.

At steady-state, assuming perfectly mixed slurry zone, the following mass balance can be used:

$$0 = F_i - \frac{x_i}{\tau} - \frac{x_i}{x_w} = \frac{x_i}{2} \cdot Q_{gc}$$

$$6.2$$

where x_i : mass of the gangue mineral of size i in the slurry phase (kg)

F: what flows in the slurry in the feed stream , kg/s

 τ : residence time of the slurry in the cell, sec

x: total weight of water in the cell, kg

Z_i: classification coefficient, i.e. weight fraction of the gangue particles of size i entering the froth, which is recovered in the concentrate.

Q : slurry water flowrate at the concentrate, kg/s

Gangue recovery is given by:

$$R_{i} = \frac{\left(x_{i}/x_{M}\right) Z_{i}Q_{mc}}{\left[\left(x_{i}/x_{M}\right) Z_{i}Q_{mc}\right] + \left(x_{i}/\tau\right)}$$

$$6.3$$

Similarly for water:

$$0 = F_{W} - \left[\frac{x_{W}}{\tau} \right] - Q_{SC} + F_{WW} - Q_{WC}$$
 6.4

where F .: feed water rate, g/s

 $\mathbf{Q}_{\mathbf{u}\mathbf{r}}$: wash water mass flow rate going to the concentrate, g/s

 F_{uu} : wash water addition rate, g/s

Water recovery can be expressed as:

$$R_{w} = \frac{Q_{sc} + Q_{wc}}{(Q_{sc} + Q_{wc}) + (x_{w}/\tau)} = \frac{(Q_{sc} + Q_{wc})/x_{w}}{[(Q_{sc} + Q_{wc})/x_{w}] + (1/\tau)}$$
6.5

Rearranging:

Let us assume that the fraction of water in concentrate from the slurry is $\boldsymbol{\beta}$:

$$\beta = \frac{Q_{sc}}{Q_{sc} + Q_{wc}}$$
6.7

rearranging:

$$Q_{sc} = \frac{(R_w/\tau).\beta.X_w}{1 - R_w}$$

 R_{ij} may be expressed as a function of water recovery as:

$$R_{i} = \frac{(Z_{i} \cdot R_{i}/\tau)/(1 - R_{w})}{\begin{bmatrix} Z_{i} \cdot R_{w}/\tau & 1 \\ \hline 1 - R_{w} & \tau \end{bmatrix}} = \frac{\beta \cdot Z_{i} \cdot R_{w}}{1 + R_{w}(\beta Z_{i} - 1)}$$
6.9

If we assume that Z_i^{\bullet} is equal to $\beta.Z_i^{}$, the slope of gangue recovery versus water recovery curve is roughly equal to Z_i^{\bullet} , which is a good parameter to compare different operating conditions. If Z_i^{\bullet} is close to one, there is no classification in the froth (i.e. gangue particles entrained to the concentrate). The lower the Z_i^{\bullet} , the better the gangue rejection.

The cumulative recovery obtained from a distribution of $\mathbf{R}_{\mathbf{i}}$ over the entire size range:

$$R_{t} = \sum_{i=1}^{n} W_{i}R_{i}$$

$$6.10$$

where R: total gangue recovery

 W_i : weight of gangue particles in size class i.

6.2 Experimental

6.2.1 Set-up

Most of the experiments were performed continuously using the modified and Denver 5L original cells. A plexiglass laboratory flotation column was also used. Operating details are given in Table 6.1.

The design of wash water distributor for homogeneous additions was a serious problem. Different materials (e.g. cloth, sponge, sparger, screen mesh, perforated funnel etc.) were tested to create water droplets for gentle and even water addition. At high flow rates, commercial garden sprinkles (e.g. Malnor), which may be used for pilot-plant and plant applications, can be used to create mists. A perforated copper pipe (2 mm, inner diameter and 4 mm, outer diameter) with holes 1 mm in diameter at 1 cm intervals was found to be the best distributor for low flowrates.

Figure 6.1 shows the wash water distributor designs developed and evaluated for this study. First, a U-type distributor with one water entrance port was used. Since water spraying was not homogeneous, square and circle geometry with two water entrance ports were developed. However, these designs did not cover the whole froth surface. A spiral shape with two entrance ports (one from the outer circle and another from the inner circle) was then designed. However, loss of pressure throughout the pipe

0V TE	OFFICIAL OL LE LESS	J (C2/8)	J ₂ (ca/e)	'T(ca)	:selid	Samela	/454 ×41.	Diet.	Lee.	300.	71
	EFFECT OF FT, J and J ON GARGE	AND -ATE	1 140791								
1	determine the effect of 'T and J on gampus settainment at constant siurry height	2 4	3.^33 ta 335	3 - 4	13	*:lica	celá		٨		-
2	determine the effect of J and J on gangue entrainment at varying siurry neight.	0 5 13 2.7	1.133 12 1.114	4.5	20	stlice	cold	10.	•		
1	determine starty rater recovery and gampus recovery to the conc. As a function of J	9.6) to 0.116	4	19	talia	cold water	19.	•		
•	determine effect of EPF on gangue entrainment.	0.4	0.136	3	10	silica	co14	19.	Å		
	EFFECT OF DESTRUMENTS PECHANISH OF	. व्यव्य	700 ±7533 ;	COVERT			·				-
3	determine the effect of dist. goometry on gampa entraigment.	0.6	9.3 12	4.3	10	catle	ceid	87. 10.444.		**********	
6	determine the effect of dist. geometry on tangua entrainment as a function of J	0.5	7.237 	5	15	talla	celd	n. n im.	. A.S		
,	determine the effect of dist. location on gamps and wash water spilt.	1 &	3.272	3	10	tails	cotq	40. 19.	3		
•	determine the effect of dist. location on weter and gampus recovery.	3.4	9.972	5	19	taile	celá	09. 09.400. 09.400.			
· , ,	EFFECT OF PROTE VIRIATION ON GAR	EL YED A	ALEX REGIM	w							
,	using flow modifier and constant speed vibrator.	0.6	0 0.071	3	10	talls	co14	sp.	A		
10	using screen mesh and variable speed vibrator.	0.6	0 0.373	3	10	talla	celd	sp.	A		
u	ming ultrasonic translator	0,6	5 0.021 0.250	4	5	cails	cold	ŋ.	•		
13	wing two ultranguic transducer	0.6	0.076	3	10	tails	celd	ep.	A		,
	EFFECT OF GASE VALUE TEMPERATURE	um depar	YAAY AME	7,00 0							
ប	determine the effect of wash water temperature on gampus occurrence.	0.6	0.093	5	10	talls	ee14 ***********************************	rp.	4		
14	determine the effect of sodium milicate and cammic said on graque entraisment.	0.6	0.393	3	10	taila	MIN MIN	.	A	763	
	EFFECT OF MASH WATER QUALITY OF	ETTALES	DT .								
			9		10	talla	cold	89	4		
15	metricomme rate constant	0.6	0. 076	-			VARM				

(spr spiral, sqr square, cur cube. At above, Sr balow, J. seperficial gas rece, J. seperficial wash water race, FT1 frech chickness, Sep.: depressent, Fib., sibration, Dist., discributor, Location and EP41 ignoider speed)

Table 6.1: Experimental conditions.

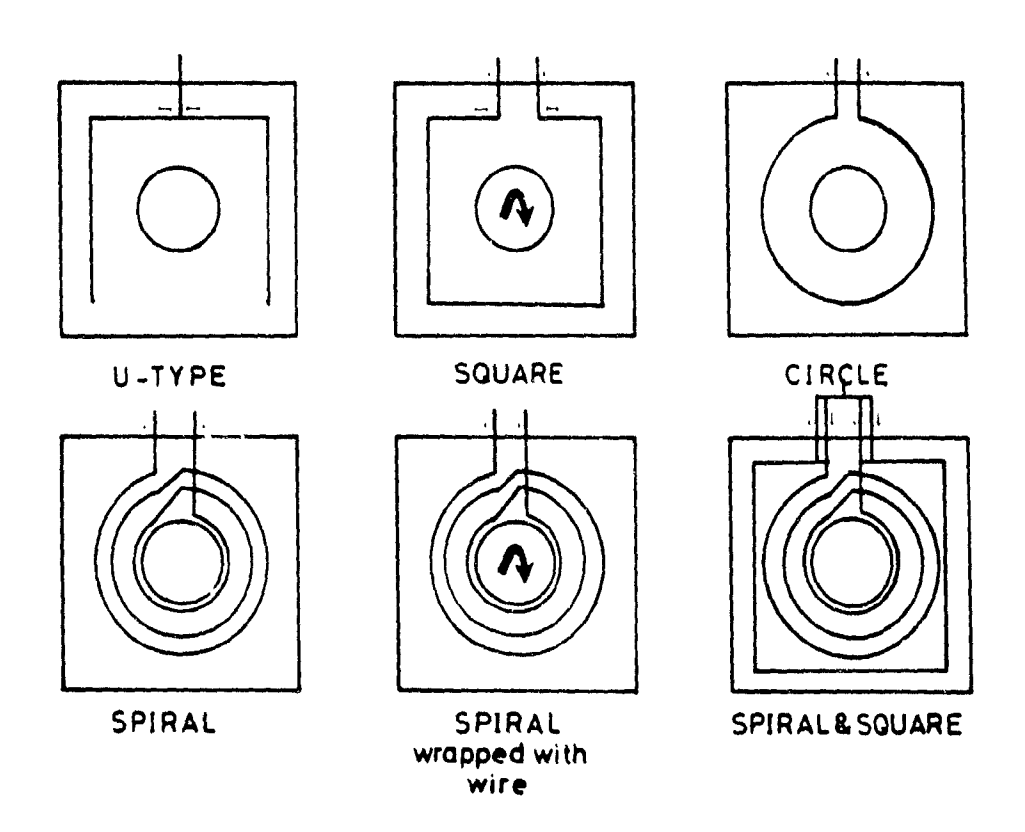


Figure 6.1: Evaluation of wash water distributor designs for laboratory flotation machines.

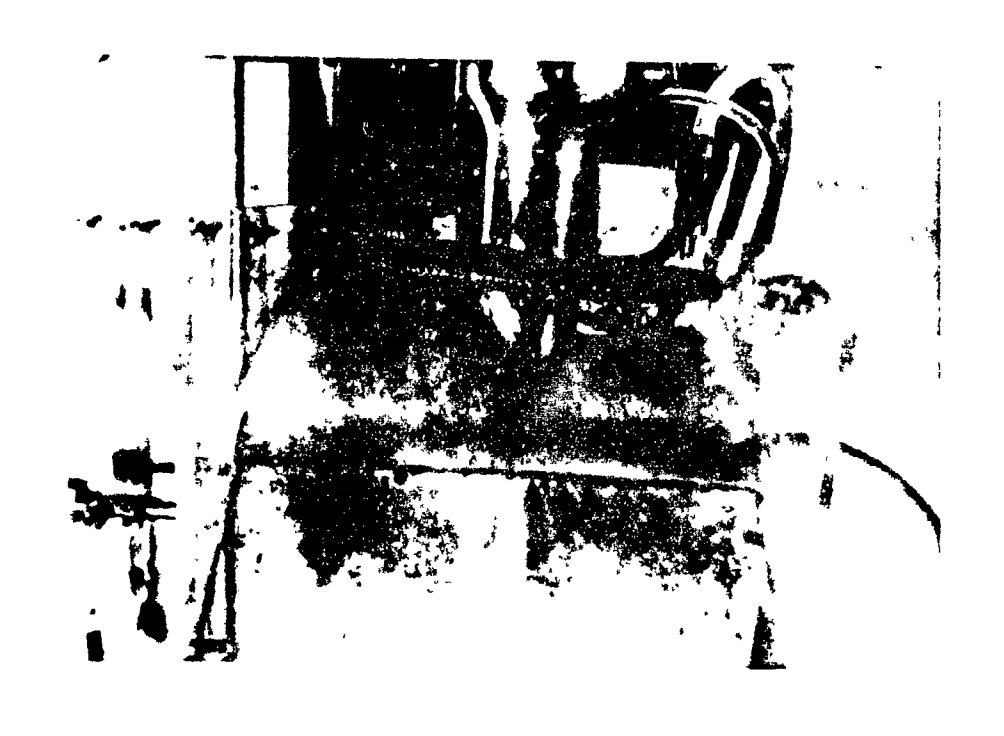
caused uneven water flow. To solve this problem, the distributor was wrapped with electrical wire; water then falls between adjacent wires like droplets (Figure 6.2). The whole froth surface can be covered using the spiral and square distributors together. The number of holes, hole diameter, and spacing are important to minimize pressure drop in the pipe. The U and square distributors have another disadvantage, which is the significant pressure drop due to sharp corners.

A linear wash water distributor, not shown in Figure 6.1, was used to prevent short-circuiting from the front (overflow) side of the cell. It is a 14 cm long stainless steel pipe fed at one end, 0.5 cm in diameter, with 10 manifolds, each 1 cm long with 1 mm inner diameter. Since the front part of the froth is drier than the back part, water addition with a linear distributor may increase the wetness of froth and remove gangue particles.

6.2.2 Methodology

Effect of Cell Size on Entrainment: The effect of cell dimensions on gangue entrainment was determined at constant feed flowrate, feed density, FT, J_{M} , J_{g} , impeller speed, impeller diameter, and cell cross-sectional area.

Determination of Water and Gangue Recoveries: Pure silica and Niobec tails were continuously floated with only frother at a J of 0.6 cm/s and an impeller speed of 1500 rpm, unless otherwise



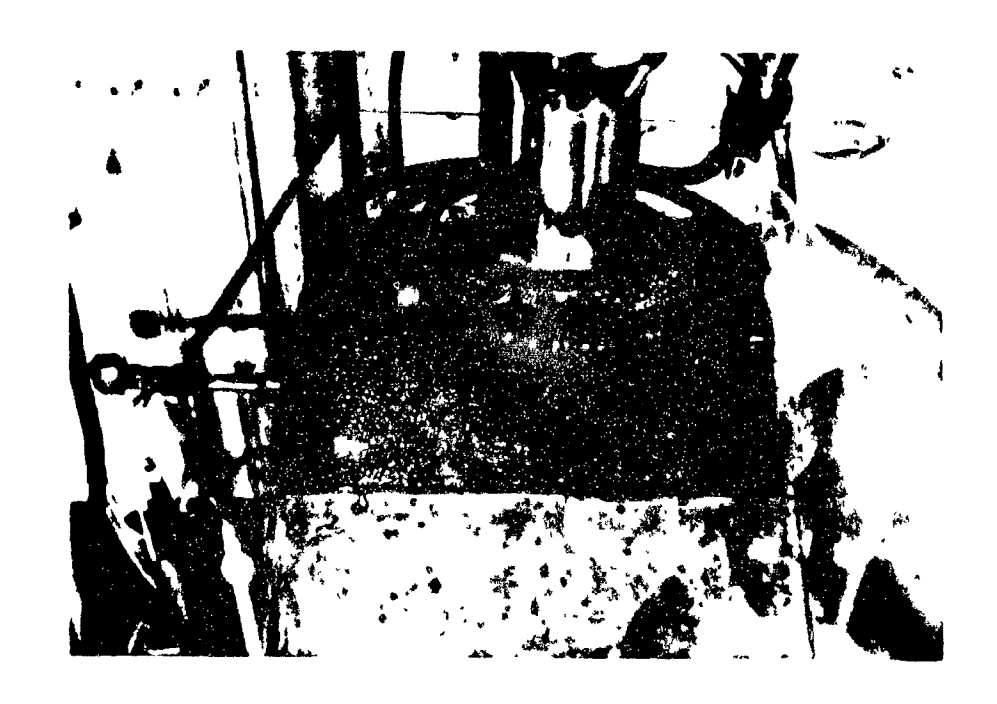


Figure 6.2: Spiral wash water distributor wrapped with electrical wire for droplet generation.

specified. Feed flowrate was always kept constant while tails flowrate was adjusted to achieve the desired FT. Timed samples from the concentrate and tail streams were collected at different operating conditions. At the end of each experiment, the samples were weighed, filtered, dried, and weighed again to determine the amount of gangue and water. For most runs, the content of the cell was also collected and treated as above. For some experiments, size-by-size classification coefficients (Z_i) were determined from the size distributions and flowrates of concentrate and tailing. Table 6.1 summarizes the experimental conditions for all tests.

Entrainment Rate Constant Determination: In continuous flotation, entrainment rate constants in the slurry phase were determined using cold (25°C) and warm wash water (50°C). The experimental and calculation procedure is from Kaya and Laplante (1986). Final pulp temperature with warm wash water was 32°C (Test 14).

The effect of pulp water quality on entrainment was also determined by semi-batch tests, the pulp water was cold (24°C), warm (42°C) or sonified (i.e ultrasonically treated in a ultrasonic bath for 10 minutes). Water flowrate to eliminate froth formation was 0.061 cm/s (Test 15).

Effect of Superficial Wash Water and Gas Rates and Froth Thickness on Gangue Entrainment: Tests 1 and 2 were carried out to determine the effect of FT and J_g as a function of J_g on gangue recovery using silica. First, FT and slurry height (SH) were maintained constant by adjusting tailings flowrate at constant J_g . Second, feed and tailings flowrates were kept constant at two different J_g , and at a higher initial pulp density.

Slurry water and gangue recoveries were determined using cold (22°C) and warm (36°C) wash water (Test 3). Initial pulp temperature for both tests was 22°C and the final pulp temperature with warm water addition was 32°C. 10 grams of dissolved LiCl were added to the feed tank. Samples from the tail and concentrate streams were collected, weighed, filtered, dried, and weighed again. The filtrate was analyzed for Li. Gangue recovery and slurry water reporting to the concentrate, which is the main cause of entrainment, were determined.

The effect of impeller speed (rpm) on gangue and water recoveries was determined at constant J_g , J_w , FT, and SH using silica (Test 4).

Effect of the Water Distributor Geometry on Gangue Entrainment:

In these tests, three different distributors were used: spiral,
square, and linear. Distributors were fixed 4 cm above the froth
surface and/or 1 cm below the slurry-froth interface.

The effect of the distributor mechanism on gangue recovery was determined using the spiral and spiral-square distributors combinations (Test 5). J_a , J_a , and FT were kept constant.

The effect of J_w on gangue recovery was also determined during two different distributors above the froth. Spiral and linear distributors were used for above and front additions. The tube distributor was placed at the interface directed 45° towards the cell bottom (Test 6).

Distributor Location: The effect of wash water addition location on wash water and gangue recovery was determined at a constant J_g , J_w , and FT (Test 7). The spiral distributor was placed below the interface or above the froth surface. 2 grams of dissolved LiCl was added to the wash water close to the distributor entrance with a 50 cm³ syringe. Timed concentrate and tail stream samples were collected. Cell content was also collected. Gangue and water recoveries; concentrate and tail flowrates; % solids for concentrate, tailing, and cell content; and residence time in the slurry phase were determined.

The effect of wash water addition location was also determined using spiral and spiral-square distributor combinations at a constant J_g , J_w , and FT (Test 8). Three different types of addition were tested: below the interface with the spiral distributor; below the interface with spiral distributor and above the froth with the square distributor; and

above the froth with the spiral-square distributors.

Effect of Froth Vibration on Gangue Entrainment

Mechanical Vibration: Gangue and water draining from the froth may be regulated by vibrating a flow modifier or a screen mesh. In this study, two different types of vibrators and vibrating assemblies were used. Both vibrators were electromagnetic. The first has a constant speed (Frantz Isodynamic Magnetic Separator Type) and the other is a variable speed Syntron (FMC) Model 4. The Syntron vibrator has a rectified controller and operates at frequencies up to 3600 vibrations per minute (vpm).

A plexiglass flow modification mechanism was designed to prevent short circuiting near the concentrate weir and to facilitate froth horizontal transport towards the cell lip for particles entering the froth at the back part (Moys, 1984). The objective is to minimize gangue recovery by increasing particle residence time in the froth for the front part and by decreasing travel distance for the back part of the froth.

Two parallel flow modifiers for the front part and one froth crowder for the back part were mounted in a plexiglas; frame (Figure 6.3). The flow modifiers force all bubbles to rise in the centre of the cell by diverting the flow patterns (see Figure 6.4). The froth formed then flows across the cell towards the froth lip. The crowder mounted at the back part of the flow

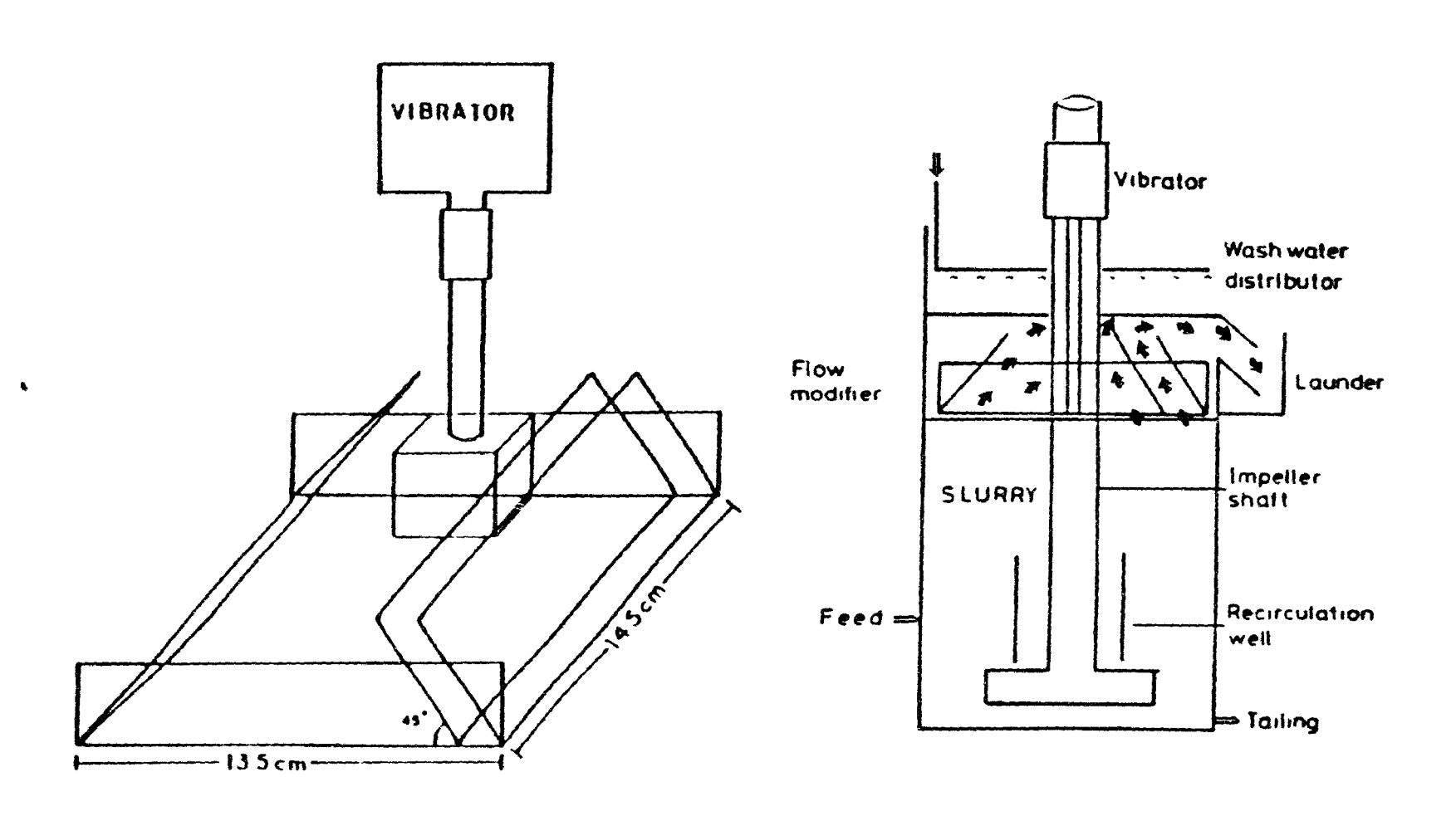


Figure 6 3: Flow modifier mechanism with vibrator connection.





Figure 6.4: Diversion of flow patterns with flow modifier in the froth phase.

modification mechanism forces the froth towards the froth lip, facilitates horizontal froth movement and prevents froth accumulation at the back part of the cell (subduction). Therefore, all froth is subjected to a more uniform residence time and is better drained. The mechanism does not significantly reduce froth volume.

A screw type shaft was used to connect the vibration source and froth mechanism. Very gentle vibrations were applied to facilitate gangue drainage and increase residence time in the froth. The effect of vibration with and without wash water addition was determined at a constant J., J., and FT (Test 9).

A screen mesh (0.5 cm) placed at the slurry-froth interface was also vibrated using the variable speed vibrator at a constant J_g , J_w , and FT in the absence and presence of wash water (Figure 6.5, Test 10). The aim here is to deccelerate the fast rising bubbles before entering the froth to increase particle residence time in the froth.

Ultrasonic Vibration: The effect of ultrasonic vibration on gangue recovery was first determined using Niobec tails (5% solids by weight) at constant FT and J_g An ultrasonic transducer (Vernitron cylindrical type lead-zirconate-titanate plezoelectric crystal, diameter: 5 08 cm, thickness 0 5 cm, and intensity 0.4 W/cm²) was placed in a waterproof plexiglass box. Ultrasonic

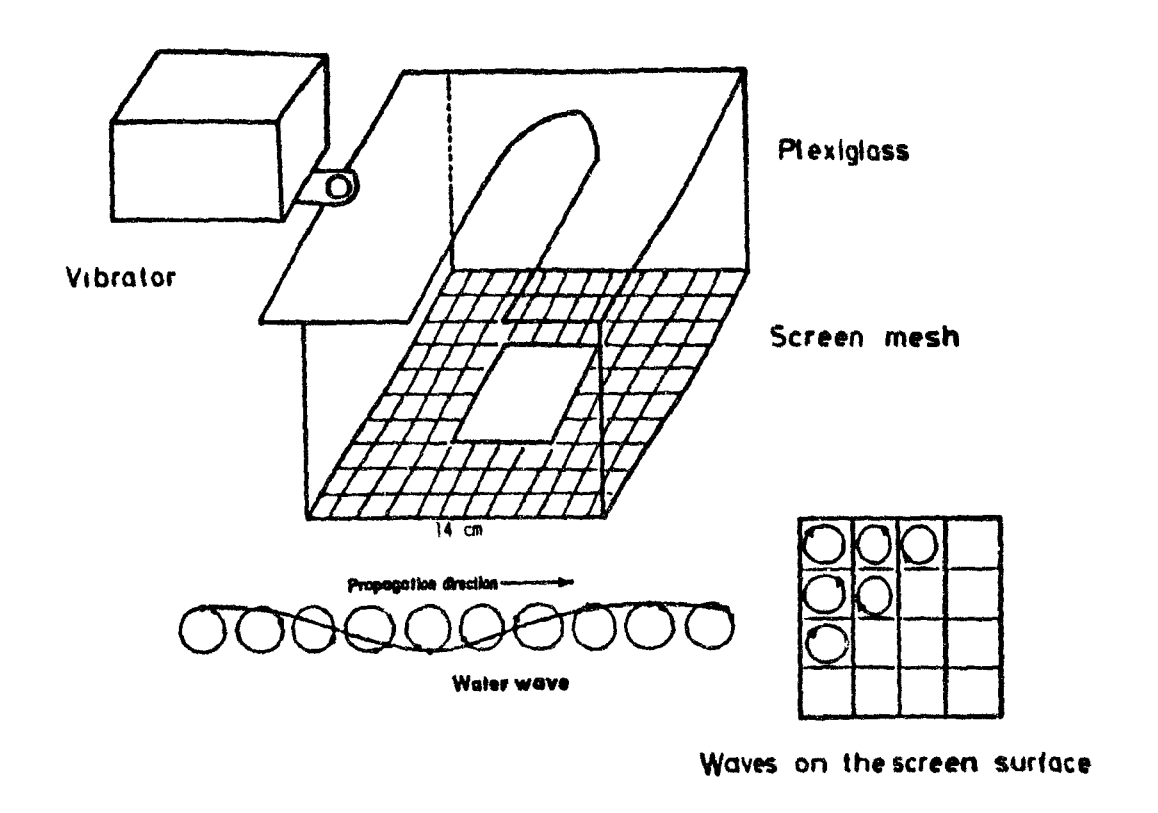


Figure 6.5: Screen mesh assembly for vibration.

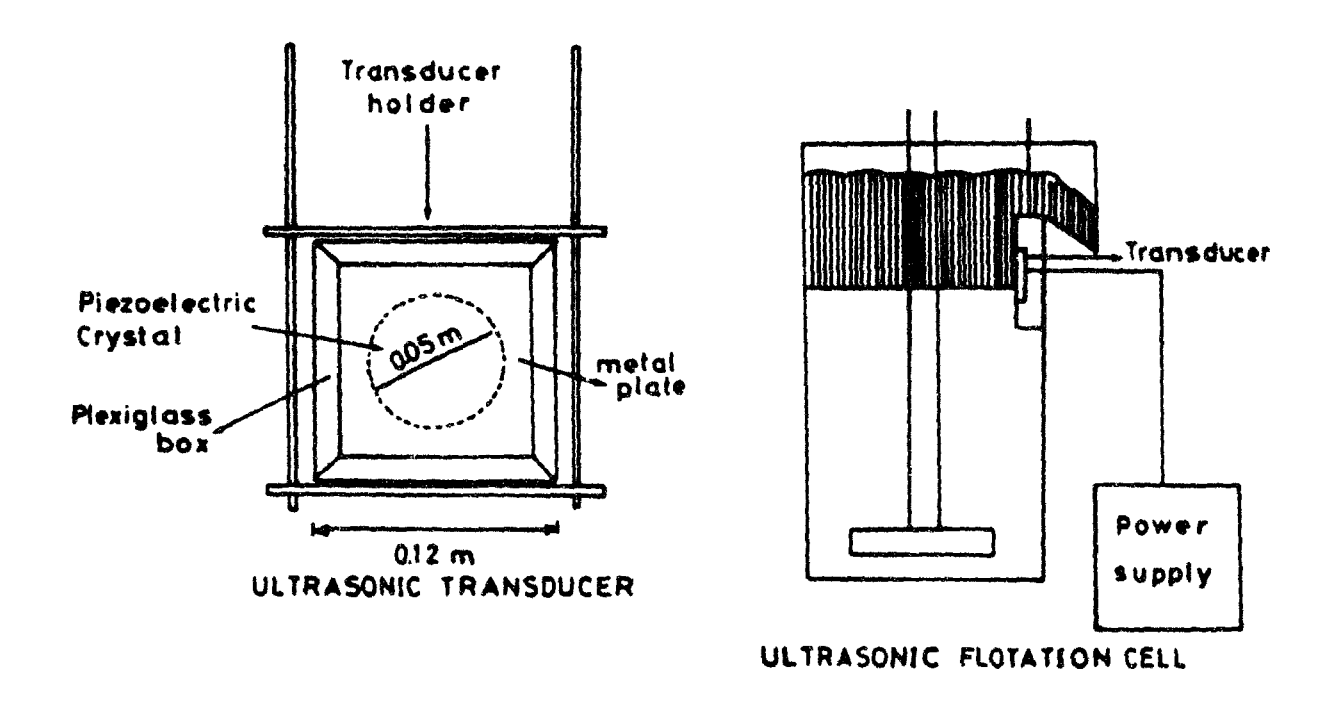


Figure 6.6: Single ultrasonic transducer and flotation cell.

waves dissipate through the front face of the box where the crystal was fixed (Figure 6.6). The power supply of a Brunsonic 12 ultrasonic bath was used. The intensity of the ultrasonic field in the froth phase was not measured.

The ultrasonic transducer transforms low frequency AC voltage into high frequency sound waves (40-60 Khz, beyond the audible range). Waves are set in motion by the process of cavitation (i.e. disruption of the inner liquid cohesion and the formation of cavities). These ultrasonic waves create and violently collapse millions of minute bubbles in the cleaning solution, gently scrubbing every surface the solution touches by the capillary action. The use of ultrasonics seems to be promising in reducing entrainment and selectivity.

The ultrasonic transducer was placed under the overflow lip in the froth phase. The front side of the cell was chosen due to presence of short-circuiting of some material in this area. Ultrasonic waves propagate from the crystal surface towards the centre of the cell. The effect of ultrasonic vibration was investigated at two different Js, a thicker FT was used in order to dissipate all vibrations into the froth phase. Low percent solids and J were used because at high percent solids the dissipation of vibration may be difficult.

Second, two ultrasonic transducers were mounted on both side of the flotation cell at froth level (Figure 6.7). A Bransonic 220 power supply was used. The effect of ultrasonic vibration generated by the two transducers and wash water was determined at J of 0.076 cm/s. For these tests, 10 grams of LiCl was added into the feed tank to determine the feed water recovery (Test 12).

Effect of Wash Water Temperature and Depressant Addition: The effect of wash water temperature and depressant (sodium silicate and tannic acid) addition in the wash water on gangue and water recoveries were determined at constant J_q , J_w , and FT. Initial pulp temperature was $12^{\circ}\mp$ 2° C for these tests.

Comparison Between Modified Cell and Laboratory Column: Flotation columns are known to be entrainment free. Comparison of laboratory cell with wash water and laboratory column helps to understand the entrainment problem in detail. Continuous tests were performed at ideal operating conditions for both units. Pulp residence time was changed by tailing flowrate for both units, while slurry level is controlled by feed flowrate at constant wash water superficial rate. Size-by-size classification coefficients were also determined.

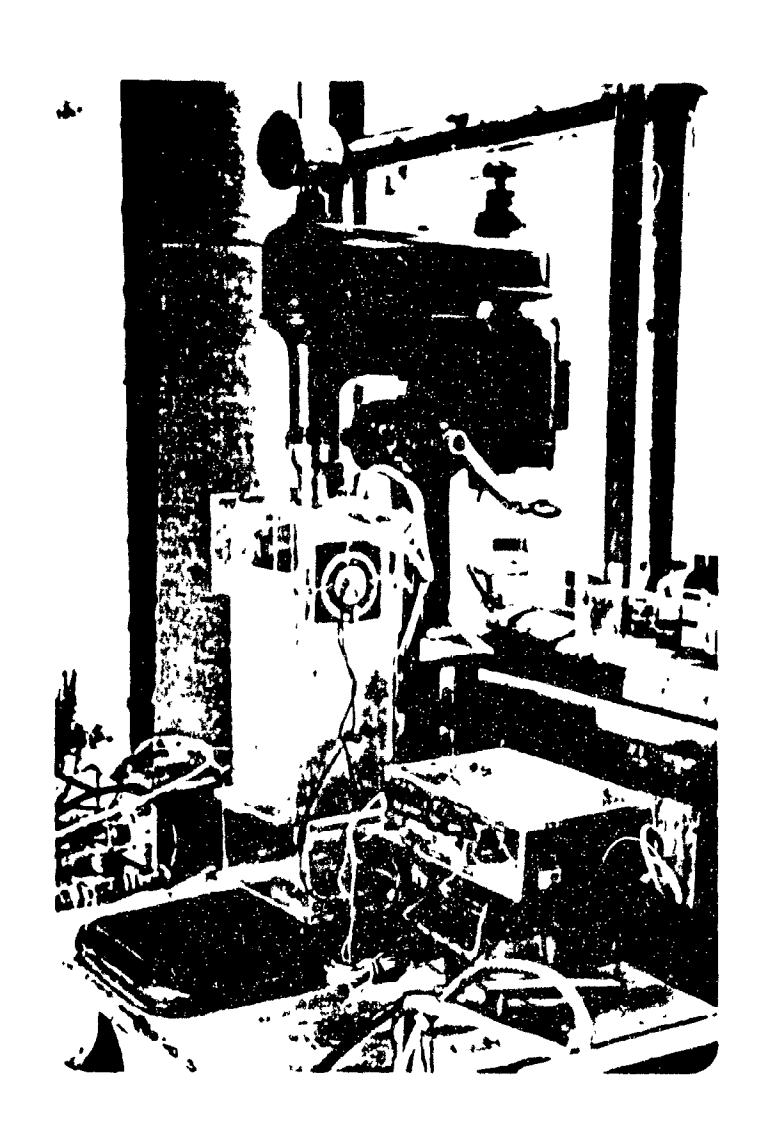


Figure 6.7: Two ultrasonic transducers mounted on the flotation cell walls and power supply.

6.3 Results and Discussion

6.3.1 Effect of Cell Dimensions on Entrainment

Figure 6.8 shows the effect of cell size on gangue entrainment using the modified and 5L Denver cells. Gangue particles stay in the deep modified cell at a longer time (3.85 min) than the original cell (2.32 min). Significantly higher gangue and water recoveries were obtained in the modified cell due to the increased residence time and decreased turbulence. The net downward bias rate is lower in the modified cell (0.027) than the original cell (0.054 cm/s). A higher bias rate reduces entrainment and dilutes the pulp in the cell. Modified cell was chosen for the following tests to study gangue entrainment.

6.3.2 Visual Evidence of Cleaning Action in the Froth Phase

Niobec tails have a brown color, yielding a brown looking froth. The froth overflowing on the cell lip has white and brown color strips depending on how uniformly water is distributed. The cleaning action taking place in the froth can be visually seen from Figure 6.9. Here, black froth is contaminated; white froth is gangue free. In Figure 6.9a, there is no wash water addition and the froth phase is completely dark; entrainment is severe. Figure 6.9b shows the froth shortly after wash water was turned on; it is possible to see local cleaning yielding a white froth, almost free of gangue, just above the interface. In Figure 6.9c, the cleaning action is progressing. Figure 6.9d and 6.9e show the

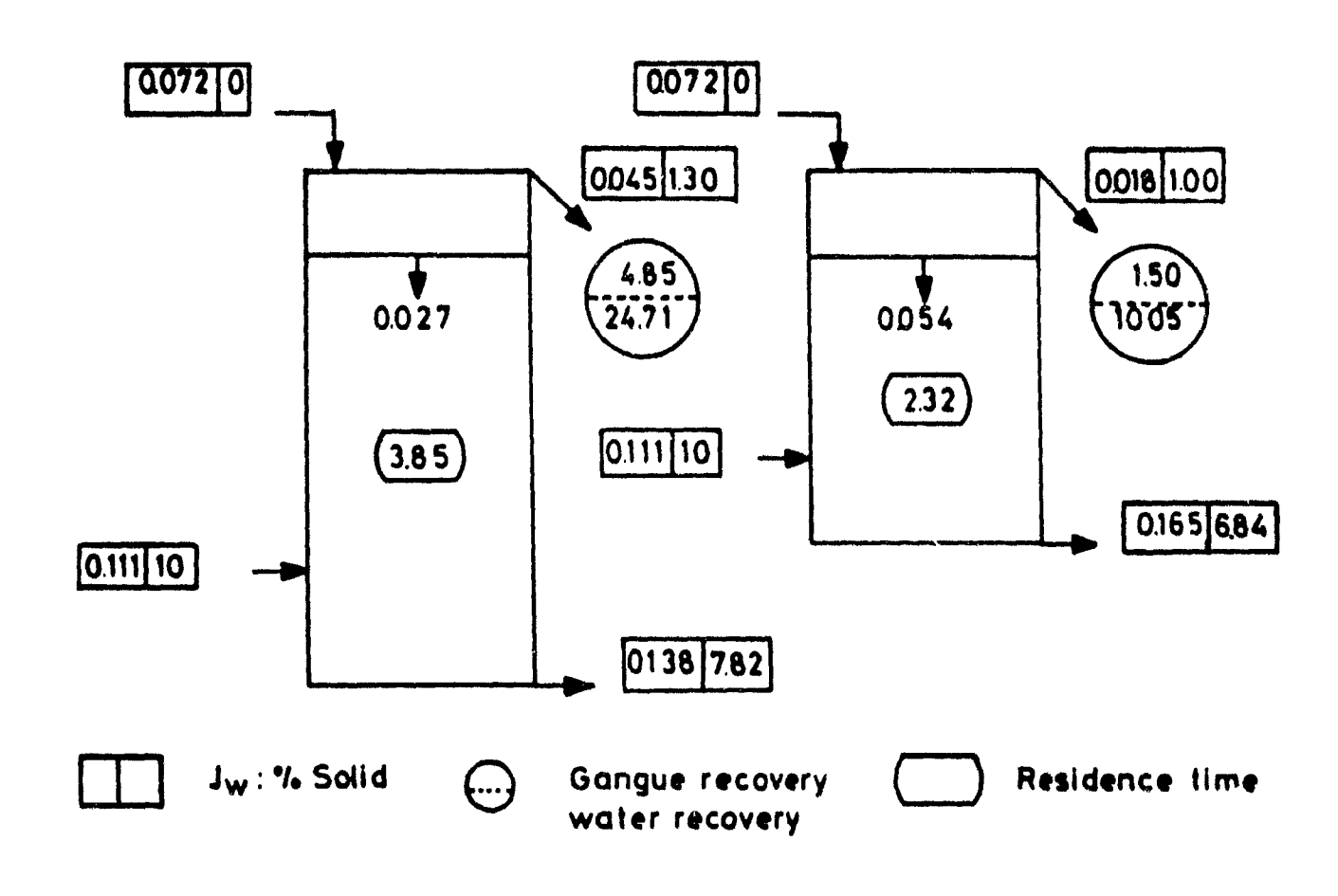


Figure 6.8: Effect of cell size on entrainment.

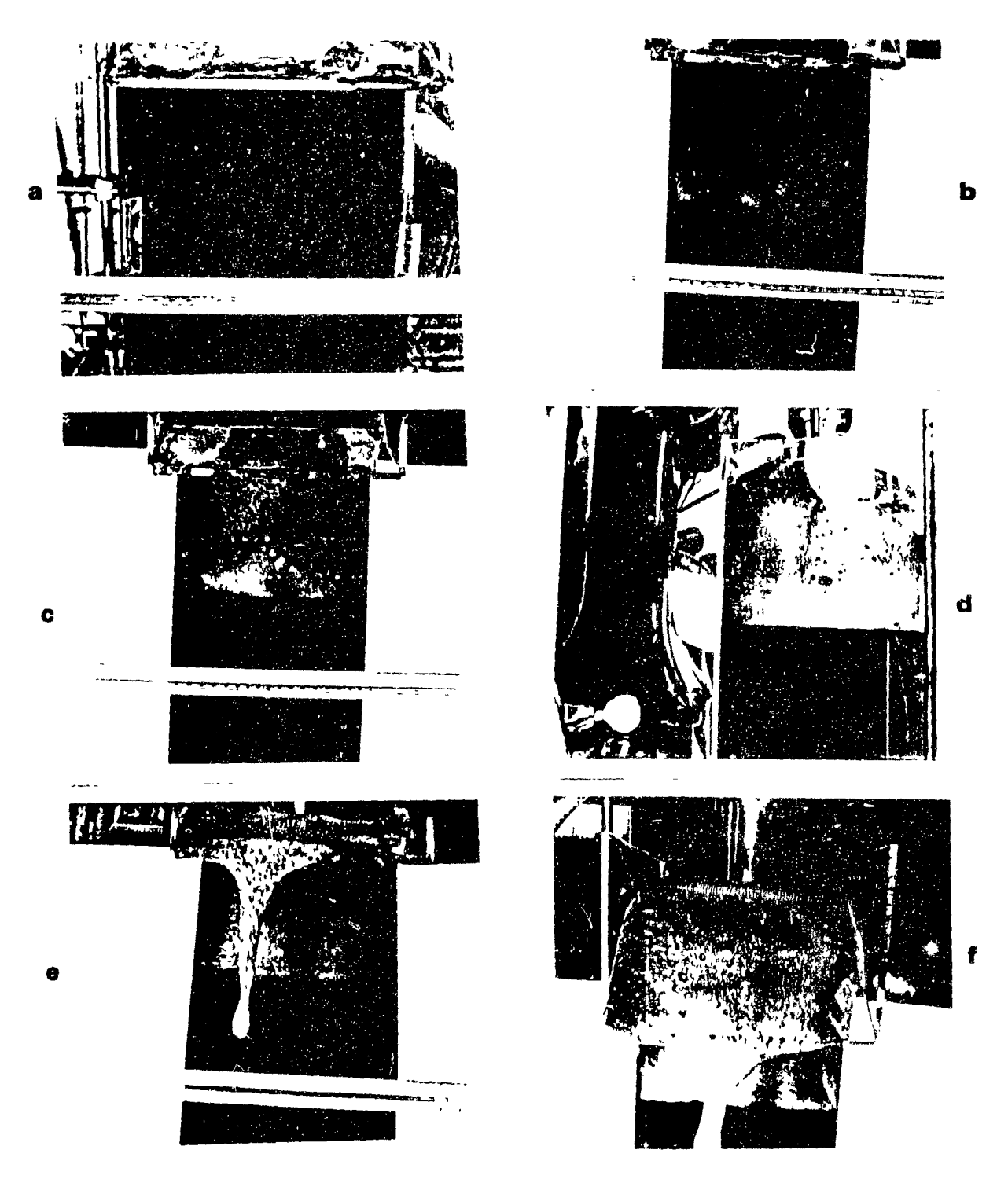


Figure 6.9 Cleaning action in the froth phase with wash water addition.

- a. without wash water addition
- b. start of wash vater addition
- c. progression of cleaning action in the froth
- d. side view of cleaned froth with wash water
- e. front view of cleaned froth with wash water
- f. overflow of cleaned froth (Black froth means contaminated froth, white froth means cleaned froth or gangue free froth).

1

side and front views of the cleaned froth. Finally, it is possible to see the whiteness of overflowing froth from Figure 6.9f.

6.3.3 Effect of Wash Water Superficial Rate and Froth Thickness on Gangue Recovery

Figure 6.10 shows the effect of $J_{_{\rm M}}$ on silica recovery at three FTs. Gangue recovery first decreases with increasing $J_{_{\rm M}}$ after reaching a minimum between 0 06 and 0 08 cm/s, it increases again. There is also a decrease in silica recovery with increasing FT. The location of the minimum shifts towards a higher $J_{_{\rm M}}$ with increasing FT, making it possible to add more water to thicker froths.

At constant tailings discharge rate (i.e. FT and SH vary with J_{w}), gangue recovery significantly increases with increasing J_{w} and J_{g} (Figure 6.11). From these results, it can be concluded that level control in the flotation cell is necessary. Otherwise, wash water cannot decrease gangue entrainment. Comparison of Figure 6.10 with 6.11 shows that the initial pulp density also has a dramatic effect on gangue recovery.

6.3.4 Effect of Feed Size

Figure 6.12 shows the gangue recovery as a function of superficial wash water rate for Niobec tails and pure silica flour. There is a minimum in gangue recovery at an intermediate



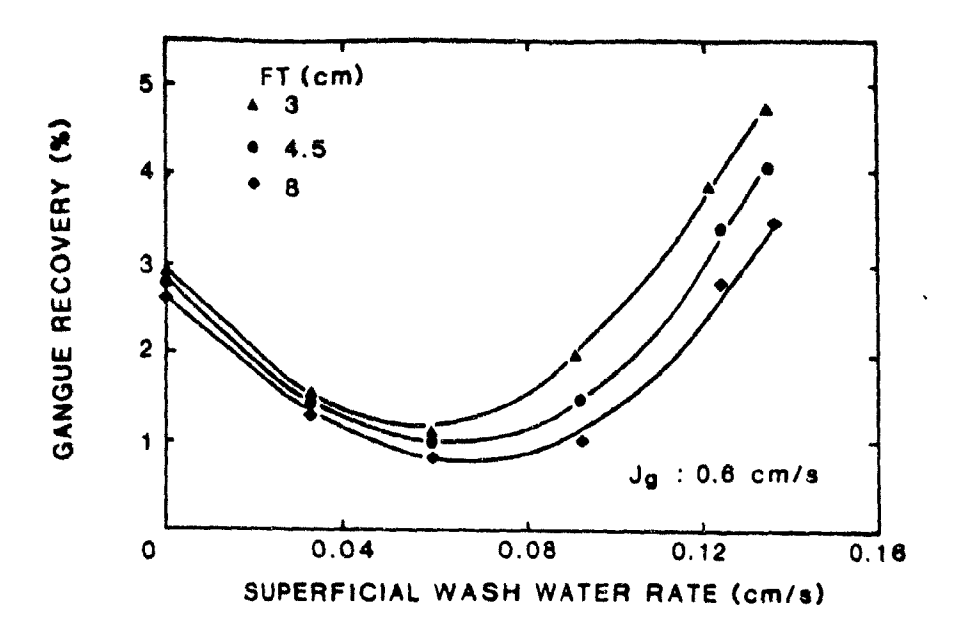


Figure 6.10: Effect of wash water addition rate on silica recovery at constant FTs.

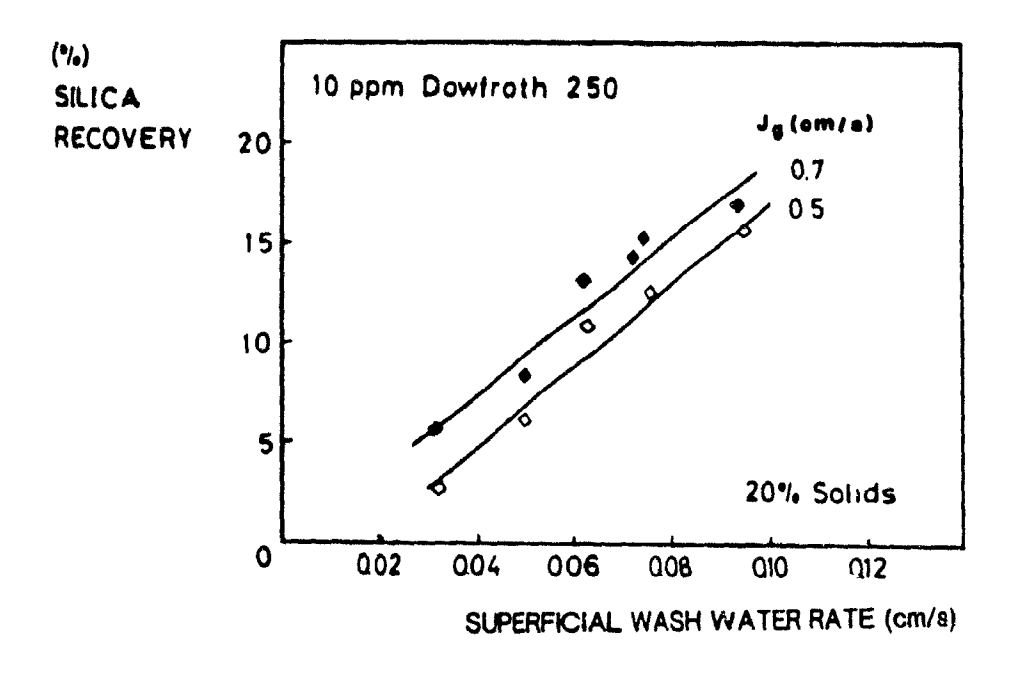


Figure 6.11: Effect of wash water addition rate and gas rate on silica recoveries at constant tailing discharge rate.

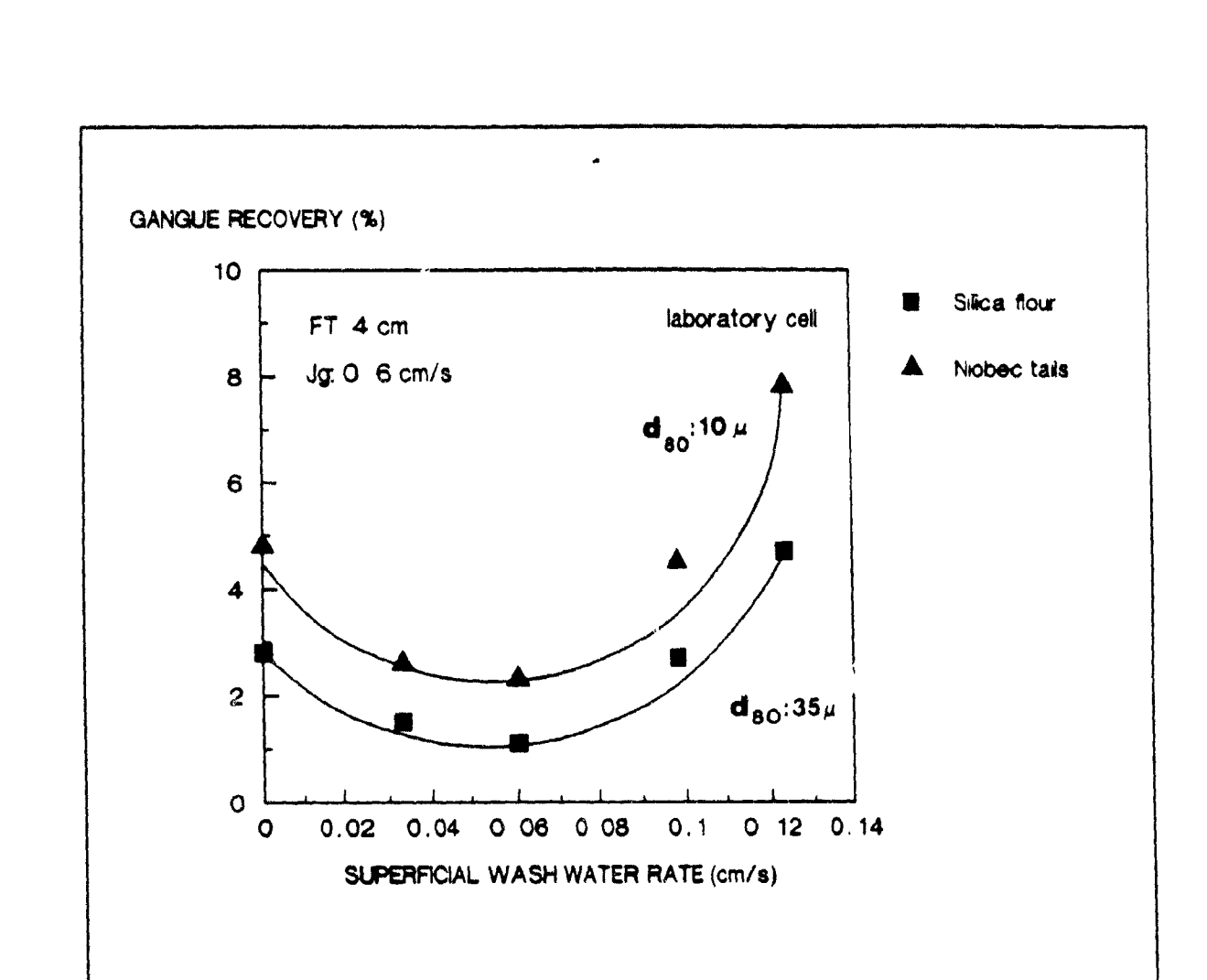


Figure 6.12: Effect of sample size on gangue recovery.



J for both cases. Due to the fineness of the Niobec tails (see Figure 5.3), the cleaning action in the froth is sharper and more distinct than for pure silica.

6.3.5 Feed Water and Cangue Recovery

Figure 6.13 shows gangue recovery versus feed water recovery using cold and warm wash water. Gangue recovery drastically increases with increasing feed water recovery. The effect of wash water temperature on gangue entrainment is discussed in detail in Section 6.3.11. At zero feed water recovery, the gangue recovery is not zero because of entrapment. The contribution of entrapment could be constant for both tests since the impeller and cell diameters, cell height, and impeller speed are constant. Further test work is needed to clarify this point.

Figure 6.14 shows feed water recovery versus J_{w} . Bias ratio (i.e. tails flowrate/feed flowrate) is also indicated. A similar minimum was found at intermediate J_{w} . The same type of relationship was also obtained in the two-phase system (Figure 3.5). At the same J_{w} , feed water recovery is 2-3% higher in the three-phase system than the two-phase system.

Schematic flow patterns are shown in Figure 6.15 at low, intermediate, and high $J_{\rm w}$. Without wash water addition, the upward water flowrate is significantly higher than the downward flowrate, yielding a high entrainment. This condition is

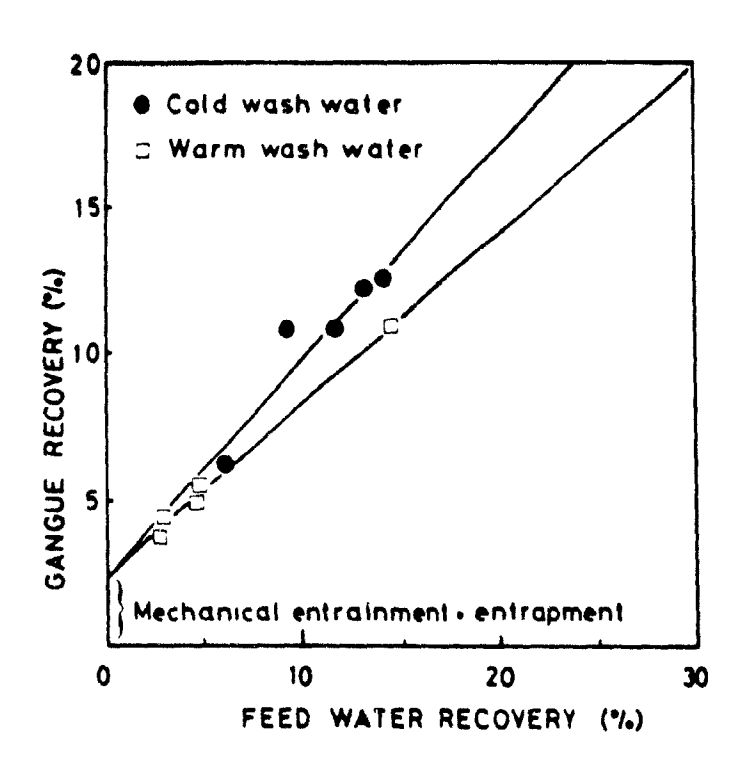


Figure 6.13: Gangue recovery versus feed water recovery using cold and warm wash water.

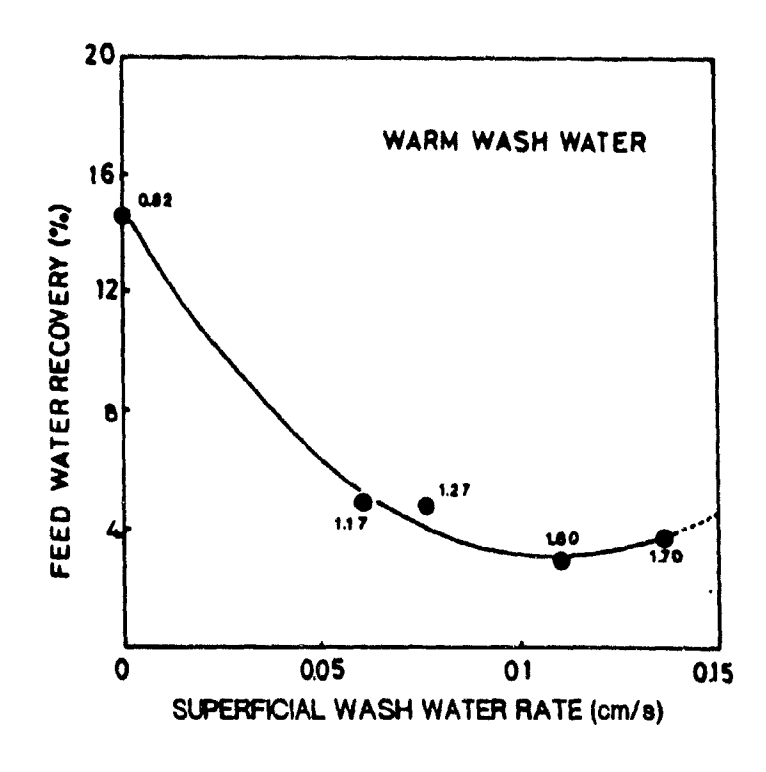


Figure 6.14: Feed water recovery as a function of superficial wash water rate (Numbers represent bias ratios).

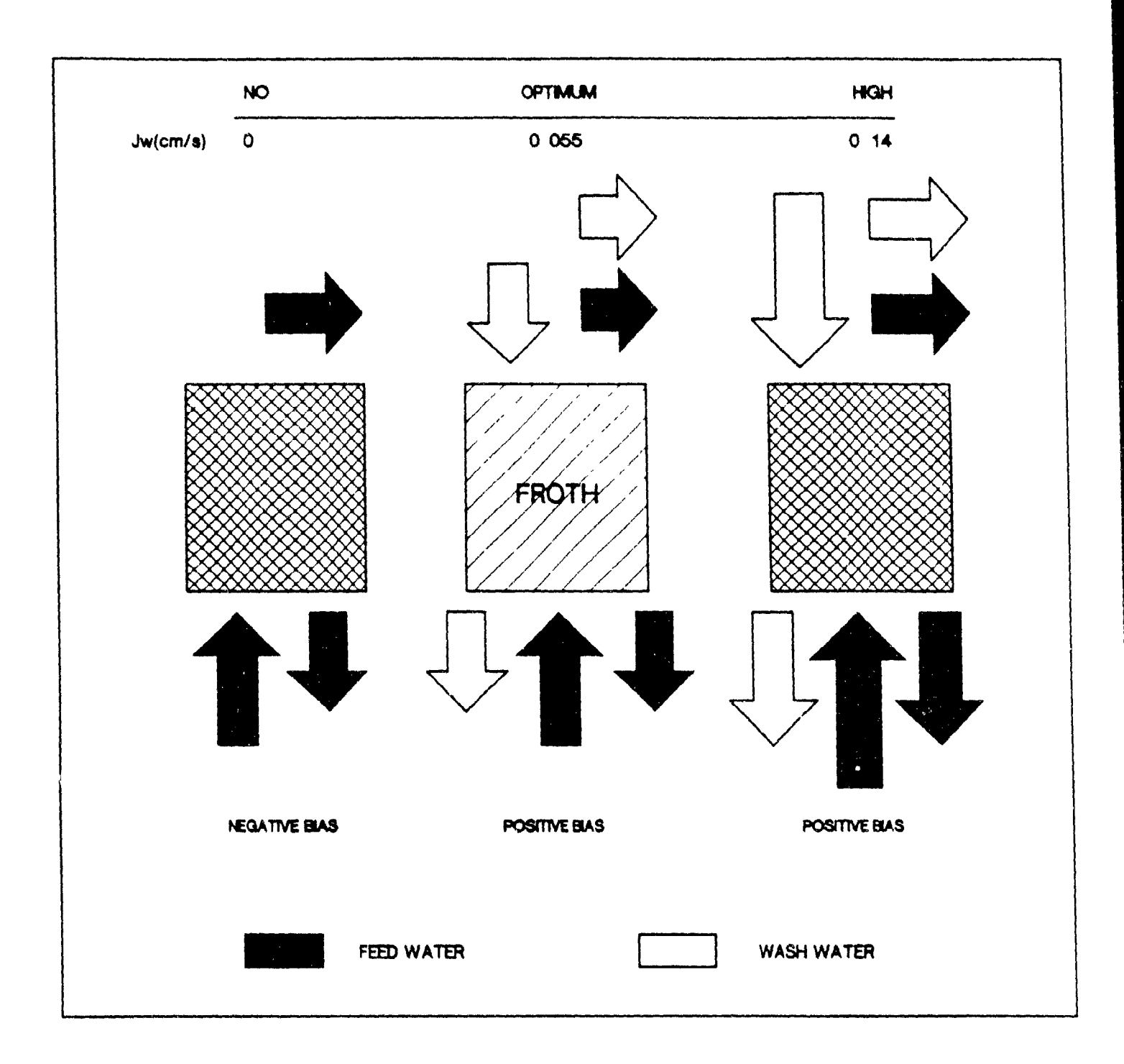


Figure 6.15: Schematic flow patterns at different wash water addition rates.

called negative bias. At low J_w , there is a negative, zero or very small positive bias. Under this condition entrainment is lower than without water addition.

In the intermediate J's, the downward water flowrate exceeds the upward water flowrate (positive bias). A significantly lower feed water penetration into the froth yields minimum gangue entrainment. As J increases, water recovery increases and mixing is induced in the froth. Material is short circuited from the bottom of the froth into the concentrate; gangue recovery increases. Slurry sampling close to the interface also supports this finding (Figure 5.7). Liquid holdup, bubble rise velocity, particle settling velocity, and superficial concentrate rate significantly increase, and bubble residence time in the froth decreases with increasing J.

6.3.6 Effect of Impeller Speed

Table 6.4 shows the effect of impeller speed. Gangue and water recoveries increase with increasing impeller speed from 1500 to 1700 rpm. Finer bubbles with higher interfacial area are produced at higher impeller speeds, which increases hydraulic entrainment.

, A

Table 6.4: Effect of impeller speed on gangue entrainment (Test 4).

Ją (cm/s)	FT (cm)	SH (cm)	N (rpm)	R g (%)	R (%)
0.6	3	30	1500	4.95	13.73
0.6	3	30	1700	6.10	19.25

6.3.7 Effect of Distributor Geometry

Table 6.5 summarizes results obtained with two different distributor designs (spiral and spiral-square). Cangue recovery is slightly higher with the spiral distributor at a significantly higher water recovery. A combination of spiral-square distributors, which covers the whole froth surface, does not suppress gangue. Thus, the effect of distributor geometry on gangue entrainment and washing efficiency is small

Table 6.5: Effect of water distributor mechanism on gangue and total water recoveries (Test 6).

Spiral Di	stributor	Spiral-Square	Distributo rs
R _G	R	R G	R w
8.56	33.36	7.72	25.76

6.3.8 Effect of Distributor Location

Table 6.6 shows that water recovery is strongly affected by distributor location: it increases from 14.8 to 27.3% with water addition above the froth. Adding water above the froth stabilizes it and increases water flowrate into the concentrate, whose density is decreased. Conversely, slurry and tailing density is increased, compared to that obtained with addition below the interface. Water added below the interface mostly reports to the tailing and decreases residence time more.

Table 6.6: Effect of wash water addition location on water and gangue recovery using Niobec tails (Test 7).

Ве	low the froth	Above the froth	
Conc. Flowrate (1/min)	0.24	0.53	
Tailing flowrate (1/min)	1.89	1.58	
Water to Conc. (%)	14.83	27.31	
Water to tailing (%)	85. 17	72.69	
% Solid in tailing	6.50	7.00	
% Solid in Conc.	1.66	1.29	
% Solid in Cell	6.50	7.00	
Residence time in slurry (min)	3.46	4. 12	

 $(J_a: 0.6 \text{ cm/s}, J_a: 0.072 \text{ cm/s}, FT: 3 \text{ cm}, using spiral distributor})$

Figure 6.16 shows gangue recovery versus water recovery for three different water addition locations: below the froth phase with the spiral distributor, below and above the froth with the

spiral and square distributors, and above the froth with a combination of spiral-square distributors. Each point represents the average of a number of samples, with 95% confidence intervals for gangue and water recoveries.

The format of Figure 6.16 will be used extensively from now on to compare different water addition schemes and deserves more attention. For a given scheme, it is expected that gangue recovery will be proportional to water recovery. Thus, each scheme will yield a line approximately straight (i.e. Eq. 6.9 for low $R_{\rm w}$), which goes through the origin. A superior scheme is one which yields, at constant water recovery, the lowest gangue recovery possible. It follows that if we draw a line between any point on the graph and the origin, the line with the lowest slope identifies the best operating point i.e. the lowest value of the $Z_{\rm i}^{\rm e}$.

Minimum gangue recovery is obtained with wash water addition above and below the froth using the spiral and square distributors, respectively. Wash water below the froth with the spiral distributor gives less gangue entrainment than above the froth with the spiral-square distributors. However, water recovery is significantly lower if wash water is added below the interface. Wash water addition either above the froth or below the interface using any distributor reduced entrainment significantly

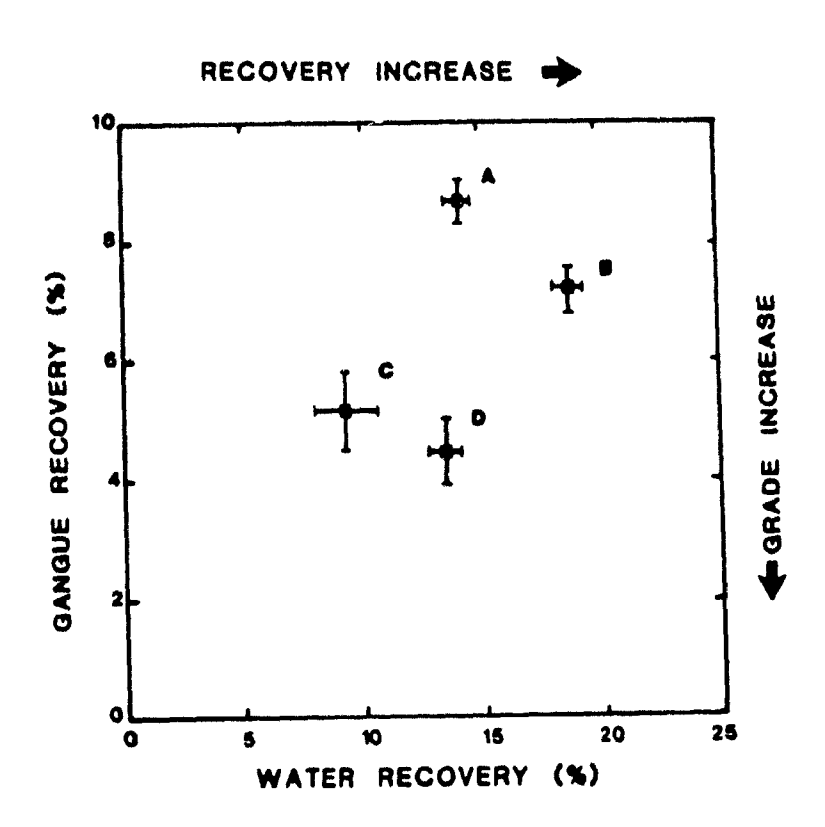


Figure 6.16: Effect of wash water addition location on gangue and total water recoveries.

- A: without wash water addition.
- B: above froth with spiral&square distributors
- C: below froth with spiral distributor
- D: below froth with spiral and above froth with square distributor.

as compared to no wash water addition. It appears that above additions decrease Z_i^{\bullet} while below additions affect water recovery and dilute the pulp phase. There was a plugging problem with wash water addition below the interface. Valuable particle recovery (i.e. production rate) and concentrate grade increase directions are also shown on the same figure. Addition of wash water both above and below and only above is best due to a lower gangue recovery at a higher throughput rate (recovery).

Table 6.7 shows the result of two different types of additions at three J. Generally, water recovery is higher when wash water is added above the froth with both distributors. At low and intermediate J.s., gangue recovery with the above addition is lower than with the two additions. The linear distributor was not working sufficiently (i.e. wash water cannot create water jets to wash bubble wakes). At high wash water superficial rate, there is very good water jetting from tube manifolds, which can reach half of the cell length and wash bubble wakes, which carry gangue particles to the froth.

Table 6.7: Effect of superficial wash water rate on gangue recovery using spiral and spiral-linear distributors (Test 6).

J (cm∕s)		R _C		R _u
	Above	Above-Front	Above	Above-Front
0.050	2.50	4.84	33.30	33.27
0.093	3.67 4.80	9. 08 8. 36	33.46 33.93	32.61 29.40
	2.88	8.92	36.49	33.27
0.136	8.71 7.11	6.06 6.81	37.90 37.78	29.06 30.63

 $(J: 0.6 \text{ cm/s}, FT: 5 \text{ cm}, above with spiral distributor and front with linear distributor)}$

Addition of wash water above the froth is simple and has some advantages. First, there is an additional froth expansion capability, which is beneficial to increase valuables recovery. Second, the water distributor is maintainance free (i.e. no plugging problem). Third, poor distribution can be readily detected and corrected. One possible disadvantage may be the kinetic energy of water due to gravitational acceleration, which may induce some mixing in froth, since water drops some distance above the froth. This problem can be minimized with location. One of the side effect of adding the wash water above the froth is short-circuiting to the concentrate stream, which may be considered advantageous or disadvantageous.

In column flotation practice, the wash water distributor is generally placed a few centimeters below the overflow lip level (i.e. in the froth). This type of addition minimizes wash water short-circuiting. However, it should be borne in mind that flotation columns have at least a 1-2 m froth, whereas mechanical cells have a maximum 10-40 cm froth

6.3.9 Effect of Froth Vibration on Gangue Entrainment

Mechanical Vibration. Figure 6.17 shows that without wash water addition and vibration, entrainment is 12.4%. With froth vibration but no wash water, entrainment is reduced to 10.4%. However, with wash water addition and without vibration. Both with wash water entrainment is almost halved to 6 5%. vibration, the minimum entrainment, 4.9%, was achieved (a 60.5% reduction). Wash water has a more pronounced effect to lessen entrainment than vibrations, which can be used as an auxiliary method to achieve 15-20% more reduction in gangue recovery. an increase in water recovery with wash water addition. Vibrations slightly reduce water recovery.

The results of froth vibration using the screen mechanism are given in Figure 6.18. Percent reduction in entrainment for each point is given on the right vertical axis. Gangue recovery is 13.3% in the absence of wash water and vibration. With only wash water addition, 8% gangue recovery was obtained. Vibrations alone

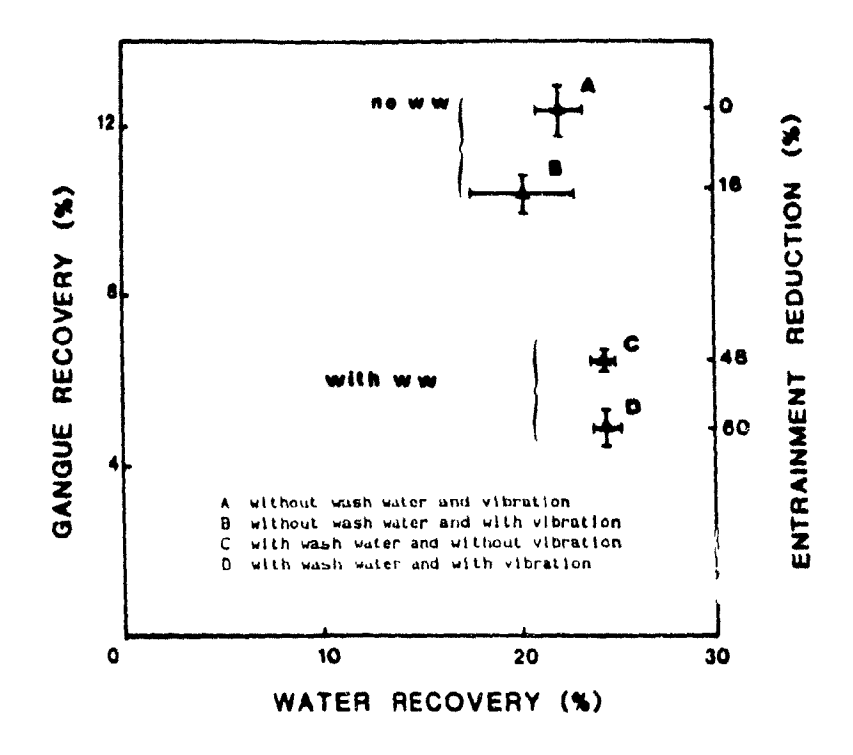


Figure 6.17: Effect of wash water and vibration on gangue and total water recoveries using flow modifier.

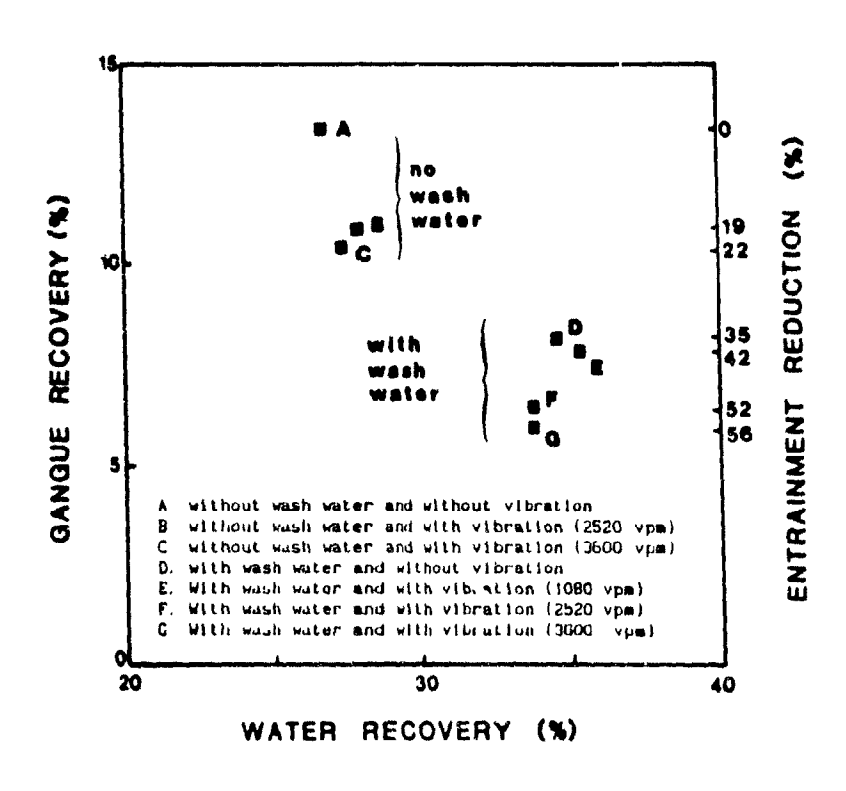


Figure 6.18: Effect of vibration and wash water on gangue and total water recovery using screen mesh mechanism.

at two different frequencies reduced entrainment down to 10.4%. Combining of wash water and vibration yields slightly better gangue rejection. From the three vibration frequencies tested, the highest one has the lowest gangue recovery, with a 56% reduction in entrainment Wash water significantly increases water recovery while vibration has a little effect on water recovery. The effect of wash water and vibration is approximately additive. The flow modifier appears to reduce gangue recovery better than the screen mesh and provides a constant water recovery.

The cleaning action with vibration is related to wave motion, which is the means by which vibration energy is propogated from one screen bar to another. Although the waves travel, water which makes up the waves does not move in the direction of the wave motion. When the screen mechanism was vibrated on the water surface, ripples were observed. These ripples are the combination of longitudinal and transverse waves. Between each square openings, circular ripples spin very fast and create a new rough surface with waves (see Figure 6.4). This means that wave interference is destructive (i.e. the peaks and valleys of each wave coincide and the amplitudes of the waves are added together and the combined wave has larger peaks and valleys) rather than constructive (i.e. the peak of one wave arrives at the same time as the valley of the other, result is cancellation or constructive interference). It is expected that the destructive interference creates a kind of jigging action to remove hydrophilic gangue particles from bubble wakes near the interface.

The particle size distribution of the washed and vibrated gangue particles recovered in the concentrate stream is given in Table. 6.8. Particle size becomes coarser with increasing vibration from 1080 to 3600 vpm. Vibrations reject finer particles (-10μ) more effectively, which is desirable to reduce entrainment.

Table 6.8: Effect of vibration on particle size of recovered gangue particles using the screen mesh mechanism.

Size	No WW	With WW	With WW	With WW
(µm)	No Vib.	1080 vpm	2520 vpm	3600 vpm
70	100	100	100	00
70	100	100	100	98
60	100	100	100	98
50	100	100	100	98
40	100	99	99	97
30	98	98	98	96
20	95	95	95	94
10	87	86	86	84
8	84	83	81	79
6	76	74	70	69
5	69	65	63	61
4	60	56	53	53
3	48	46	42	41
2	35	33	30	30
<u></u>	18	16	12	10

The effect of wash water and vibration on gangue and water recoveries is summarized in Figure 6.19. Without wash water and vibration, Z_i^{\bullet} values are between 0.4 and 0.6. In the absence of wash water, vibrations alone do not improve the overall classification coefficient significantly. In the presence of wash water, there is a significant reduction in Z_i^{\bullet} . A further decrease in Z_i^{\bullet} can be achieved by combination of wash water and vibrations.

8.3.10 Ultrasonic Vibration

Figure 6.20 shows that in the absence of wash water addition, ultrasonic froth vibration with a single piezo-electric transducer alone reduces gangue entrainment about 29%. A small amount wash water addition (0.05 cm/s) will reduce entrainment more significantly than ultrasonic vibration. Both ultrasonic vibration and wash water addition will reduce entrainment by about 53% at a wash water recovery rate of 14%. It should be noted that wash water addition increased the total throughput at a lower gangue recovery.

Better cleaning was achieved at a reduced wash water addition rate (0.024 cm/s) along with ultrasonic vibration. The optimum water flowrate and vibration intensity must be jointly determined. Ultrasonic vibration may be used to reduce J to a mechanical cell.

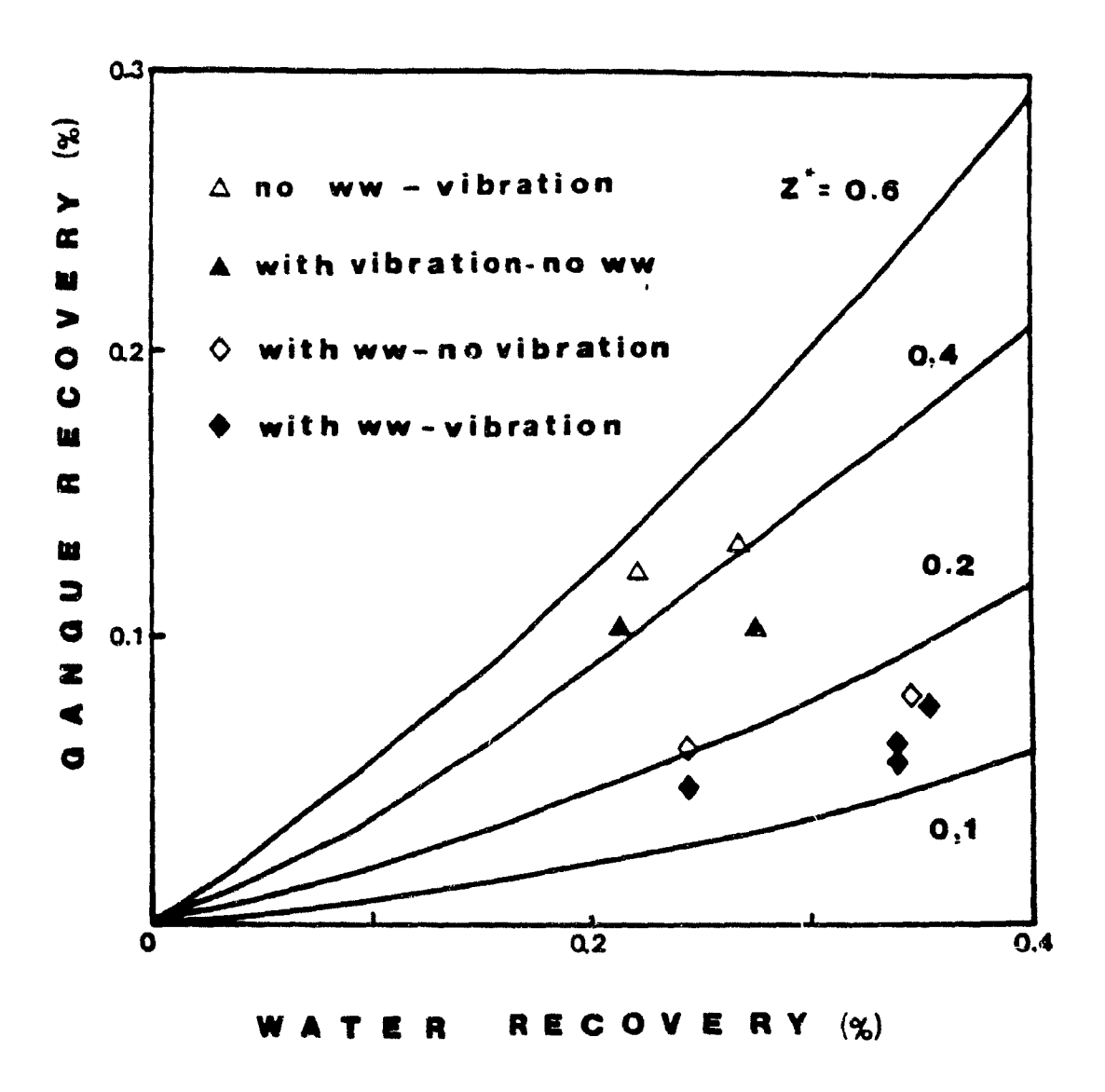


Figure 6.19: Effect of wash water and vibration on overall classification coefficient.

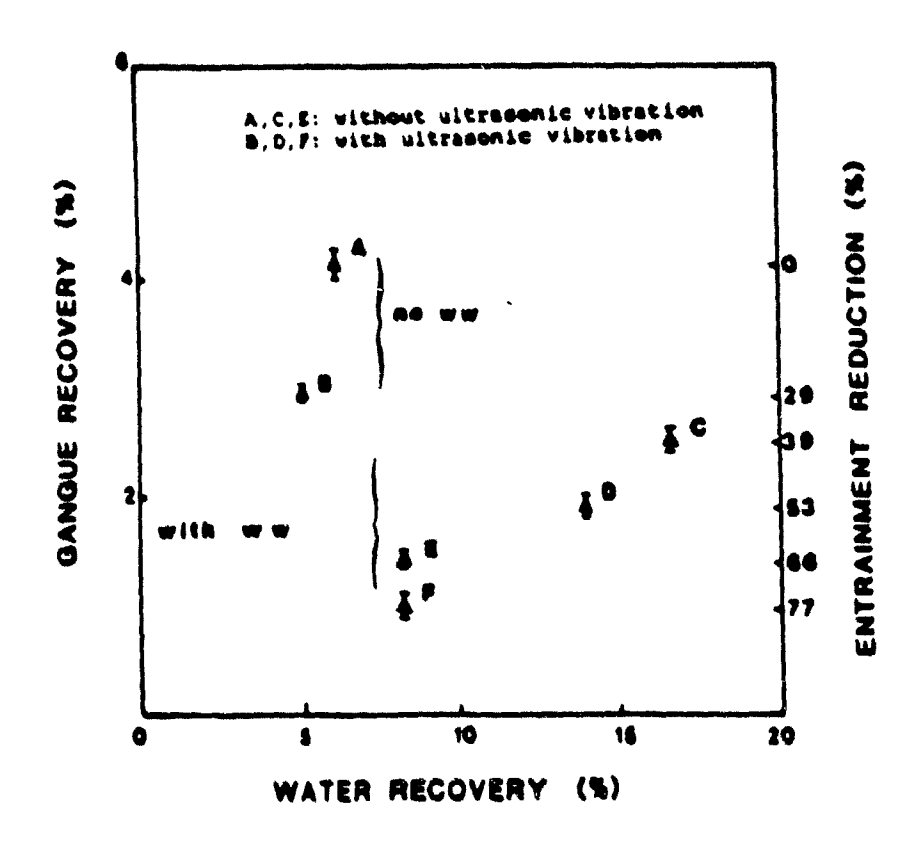


Figure 6.20: effect of ultrasonic vibration and wash water on gangue entrainment.

Figure 6.21 shows the classification coefficient versus particle size. Z_i decreases with increasing particle size. Without wash water, ultrasonic vibrations can reduce Z slightly. Wash water significantly lower the classification in the function values, which shows that the most effective factor to reduce entrainment is wash water. Ultrasonic vibrations with wash water shows the lowest classification coefficient.

Figure 6.22 shows the effect of ultrasonic vibration using double transducer and wash water addition at 10% solids. Without wash water addition, gangue recovery is 12.7% at 17.3% total water recovery. Ultrasonic vibrations alone reduce entrainment by about 23% and wash water alone by 38%. The combined effect of wash water and ultrasonic vibrations is most effective. Feed water recoveries, in parantheses, show significant decrease with wash water and ultrasonic vibration.

6.3.11 Effects of Wash Water Temperature and Depressant Addition

The warmer the wash water the better the gangue rejection
and the lower the water recovery. (Figure 6.23). A slight
temperature difference between pulp and wash water appears to be
beneficial to enhance froth washing efficiency significantly.

Depressants are not effective in both cold and warm water because of very short residence times in the froth phase. Both deprassants (i.e. tannic acid and sodium silicate) increase water

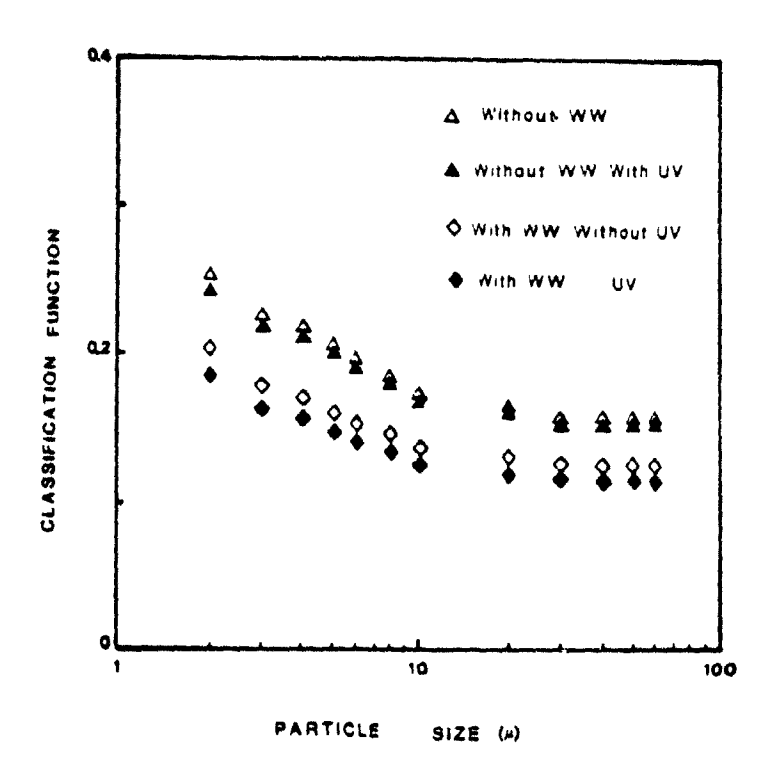


Figure 6.21: Effect of ultrasonic vibration and wash water on classification coefficient.

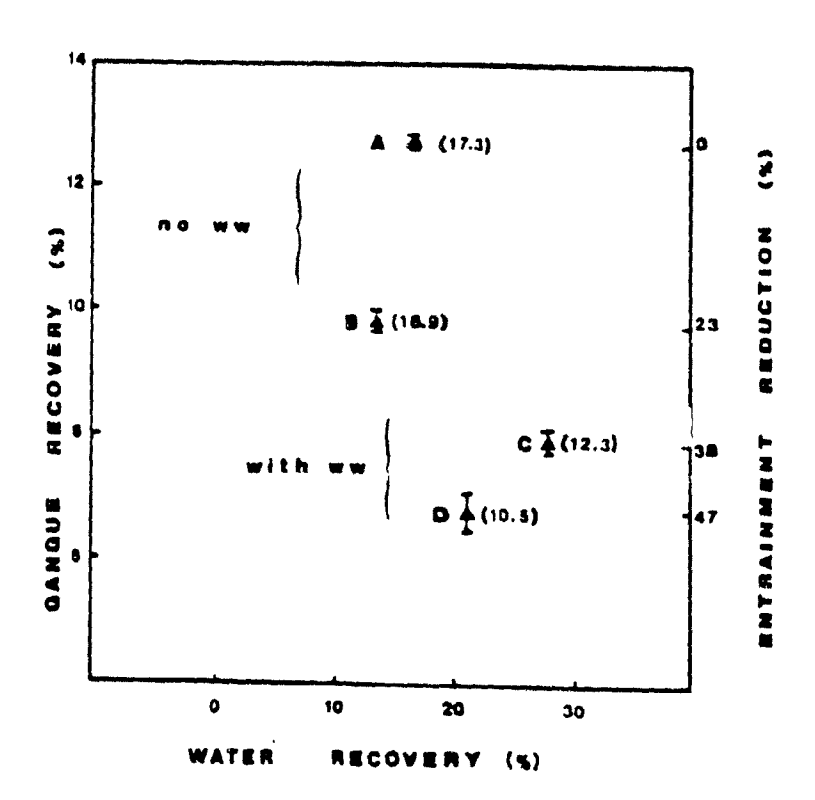


Figure 6.22: Effect of ultrasonic vibration and wash water on gangue entrainment using two transducers.

A: no wash water and ultrasonic vibration

B: with ultrasonic vibration without wash water

C: without ultrasonic vibration with wash water

D: with ultrasonic vibration and wash water

(numbers are feed water recoveries to the concentrate)

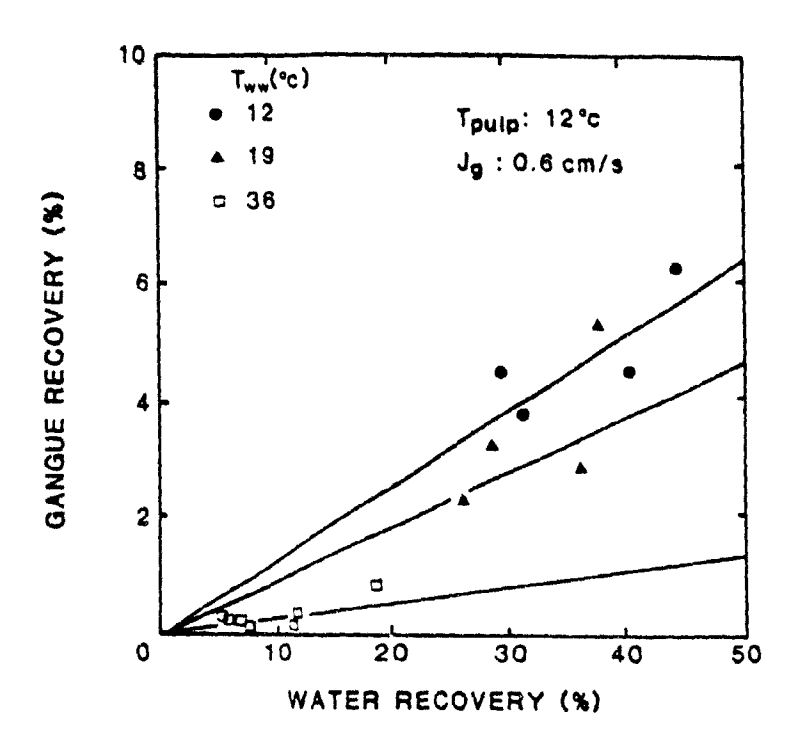


Figure 6.23: Effect of wash water temperature on gangue and water recoveries.

	Water		Air	
Temperature °C	Viscosity, μ N·sec/m²	Kinematic Viscosity, v m²/sec	Viscosity, μ N·sec/m²	Kinematic Viscosity, ν m²/sec
0	1.781×10^{-3}	1.785 × 10 ⁻⁶	1.717×10^{-1}	1.329 × 10 ⁻⁵
5	1.318 × 10-3	1.519 × 10 ⁻⁴	1.741×10^{-5}	1.371×10^{-5}
10	1.307×10^{-3}	1.306 × 10 ⁻⁶	1.767×10^{-3}	1.417×10^{-5}
15	1.139×10^{-3}	.1.139 × 10 ⁻⁴	1.793×10^{-1}	1.463 × 10 ⁻⁵
20	1.002×10^{-3}	1.003 × 10 ⁻⁶	1.817×10^{-5}	1.509 × 10 ⁻⁵
25	0.890×10^{-3}	0.893 × 10 ⁻⁴	1.840×10^{-3}	1.555 × 10 ⁻⁵
30	0.798×10^{-3}	0.800 × 10 ⁻⁴	1.364×10^{-1}	1.601 × 10-3
40	0.653×10^{-3}	0.658 × 10 ⁻⁴	1.910×10^{-3}	1.695 × 10 ⁻³
50	0.547×10^{-3}	D.553 × 10 ⁻⁴	1.954×10^{-5}	1.794 × 10 ⁻⁵
60	0.466 × 10 ⁻¹	0.474×10^{-6}	2.001 × 10 ⁻⁵	1.886×10^{-3}
70	0.404×10^{-3}	0.413 × 10 ⁻⁶	2.044×10^{-3}	1.986×10^{-5}
80	0.354×10^{-3}	0.364 × 10 ⁻⁶	2.088 × 10 ⁻³	2.087×10^{-5}
90	0.315×10^{-3}	0.326 × 10 ⁻⁴	2.131×10^{-5}	2.193 × 10 ⁻³
100	0.282×10^{-3}	0.294×10^{-6}	2.174 × 10 ⁻³	2.302 × 10 ⁻⁵

Table 6.9: Viscosity of water and gas at different temperatures.

recovery with cold and warm wash water. Tannic acid seems to have more frothing characteristics than sodium silicate in both cold and warm water.

The effect of wash water temperature on gangue and water recoveries can be explained by viscosity effect and gas expansion. The viscosities of water and air (froth) at atmospheric pressure significantly depend on temperature. Table 6.9 shows the water and air viscosities as a function of temperature. Note that for gases at low density, viscosity slightly increases with increasing temperature, whereas for water it significantly decreases. With warm wash water, the viscosity of the inter-bubble water significantly decreases, which increases the downward mobility of interstitial water.

Warm wash water also increases gas holdup in the froth phase (this will be verified in Chapter 7), which leads to a higher coalescence probability—and water drainage through Plateau borders. Smelter steam or any other source of waste heat can be used to elevate wash water temperature to 30-40°C.

6.3.12 Comparison Between Mechanical Cell and Flotation Column

Figure 6.24 compares the modified cell and laboratory column.

Gangue recovery, in both systems, increases with increasing residence time in the recovery zone due to increase in water

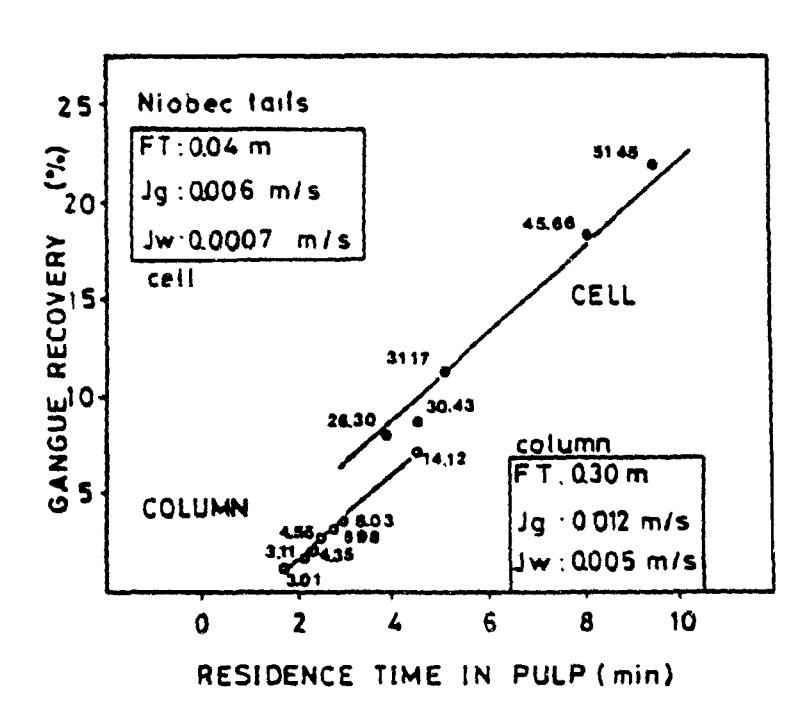


Figure 6.24: Effect of pulp residence time on gangue entrainment in the modified cell and flotation column.

recovery shown in brackets for each data points. Gangue and water recoveries are lower for the column.

Size-by-size Z_i^{\bullet} for laboratory cell and column is shown in Figure 6.25 at different pulp residence times. For the flotation column, Z_i^{\bullet} sharply decreases with increasing size up to 20 μm and then levels off. For the mechanical cell with a 4 cm froth, the decrease in Z_i^{\bullet} is not nearly as sharp as in flotation column with a 30 cm froth thickness. Z_i^{\bullet} significantly decreases with decreasing pulp residence time.

6.3.13 Testing the Proposed Entrainment Model

The proposed gangue recovery model (Eq. 6.9) was tested with data from the present system, Laplante (1980), Lynch et al.(1974), and Engelbrecht and Woodburn (1975). The objective is first to evaluate the range of Z_i^{\bullet} obtained, and then assess the effect of scale and wash water.

Data from Present System: Gangue recovery was plotted as a function of water recovery at different Z_i^{\bullet} values from 0.2 to 0.6 (Figure 6.26). Most of the data obtained from the present system fall between Z_i^{\bullet} values of 0.1 and 0.3. Water recovery changes from 10% to 50% while silica recovery varies from 2% to 25%.

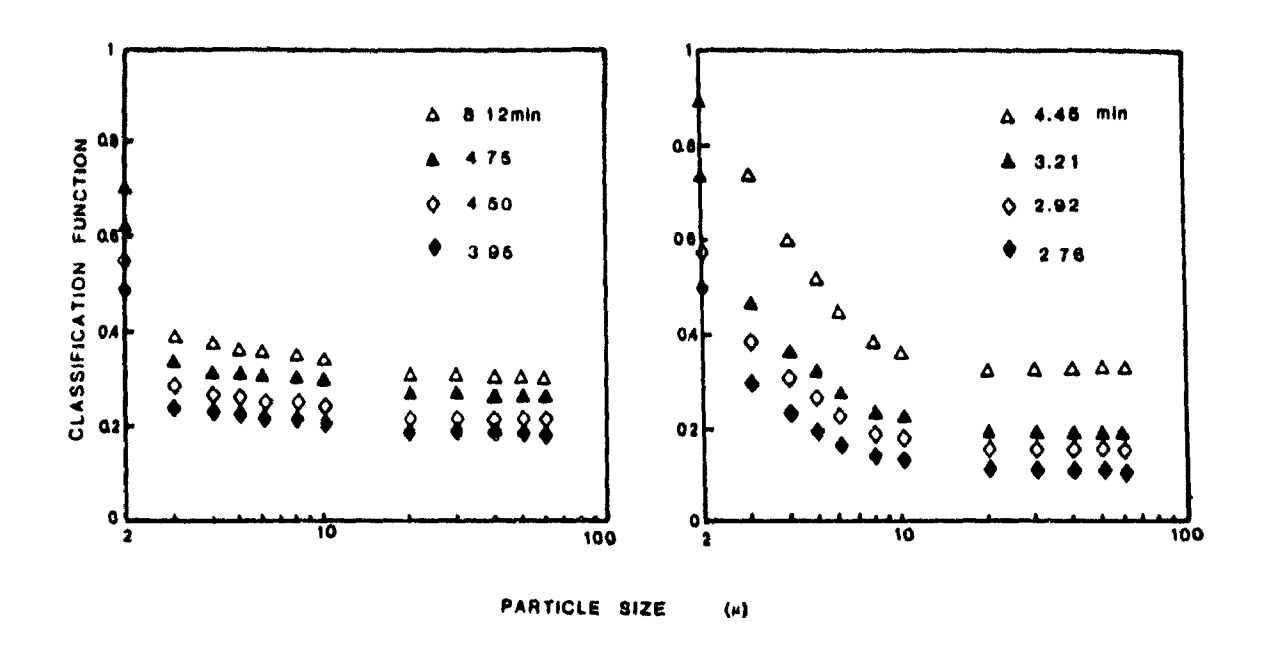


Figure 6.25: Effect of pulp residence time on the size-by-size Z_i^{\bullet} for the modified cell and flotation column.

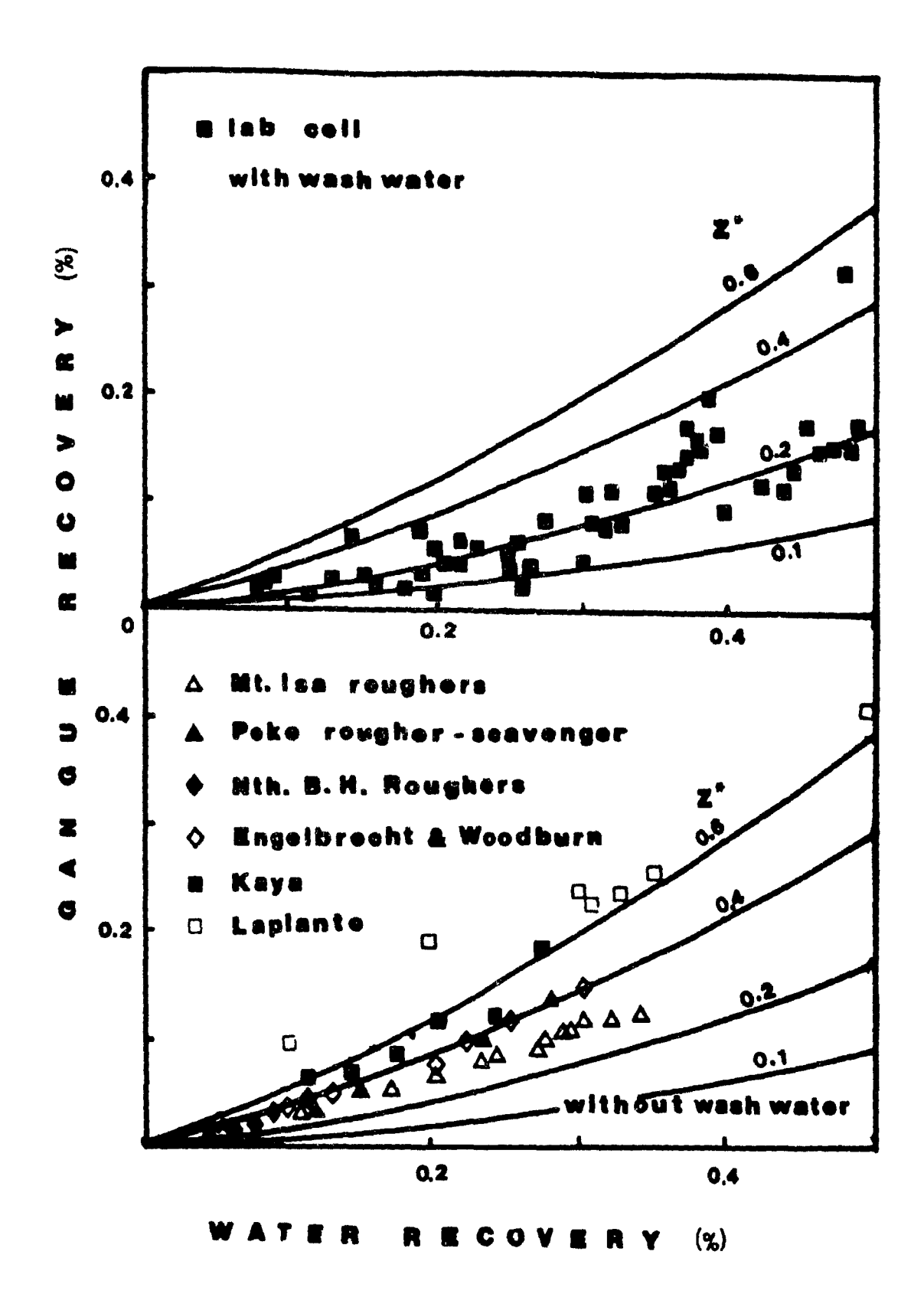


Figure 6.26: Cangue recovery versus water recovery for the present, plant, and pilot-plant systems.

Data from Kaya (1985): An artificial mixture of sphalerite and silica flour was floated continuously in the 6.5L laboratory cell of the present study. 2 values vary between 0.4 and 0.6 (Figure 6.26).

Data from Laplante (1980): He used 2L shallow laboratory cell with froth paddles. Sphalerite and quartz were continuously floated at different gas rate and froth thickness. The Z_i^{\bullet} values are between 0.6 and 0.7.

Data from Lynch et al. (1974): They determined the relationship between recovery rates of non-sulfide gangue and water in several chalcopyrite and galena flotation stages in Australia. The data from Mt Isa Rougher, Peko Rougher-Scavenger and North Broken Hill Rougher sections are given in Figure 6.26. These sections are flotation banks rather than a single cell operated without wash water. Most plant data fall between $Z_1^{\bullet} = 0.2$ and 0.4. In plant study, water recovery varies from 0 to 30% while gangue recovery changes from 1 to 13%.

Data From Engelbrecht and Woodburn (1975): They studied the effect of froth height, aeration rate, and gas precipitation on flotation. They determined the gangue recovery at different water recoveries in a continuous pilot-plant flotation cell without wash water. Maximum water recovery was around 32% at 18% gangue recovery. These data all show a Z_i very close to 0.4.

 Z_i^{\bullet} varies between 0.1 and 0.7, depending on cell size, and geometry, use of wash water or paddles. At one extreme, very small cells with froth paddles may yield a very small residence time in the froth with virtually no cleaning and Z_i^{\bullet} values are in excess of 0.6. Similar full scale operations yield Z_i^{\bullet} equal to about 0.3; Engelbrecht and Woodburn's 30L cell yielded intermediate values, close to 0.4, and Kaya (1985), with a slightly smaller cell, yielded values around 0.4 to 0.6. The effect of wash water in the same system was to reduce Z_i^{\bullet} values down to 0.1 to 0.3, equal to or better than full scale results. Full scale testing is required to assess the applicability of wash water when Z_i^{\bullet} values are already below 0.4.

The suggested model can represent well laboratory, pilotplant, and plant scale results, provided that an appropriate value of Z_i^* is selected. It varies between 0.1 and 0.7 for wide operating range. Z_i^* in the plant is sharper than at laboratory scale. Figure 6.27 shows the comparison of classification coefficient of laboratory and plant scales. Z_i^* decreases slightly with increasing particle size both for the present study and for the data of Johnson et al. (1974). However, it decreases more sharply for plant tests. This difference in Z_i^* at coarse particle sizes could be related to the different particle residence time in the froth phase, usually much higher in industrial cells due to longer horizontal travel distances.

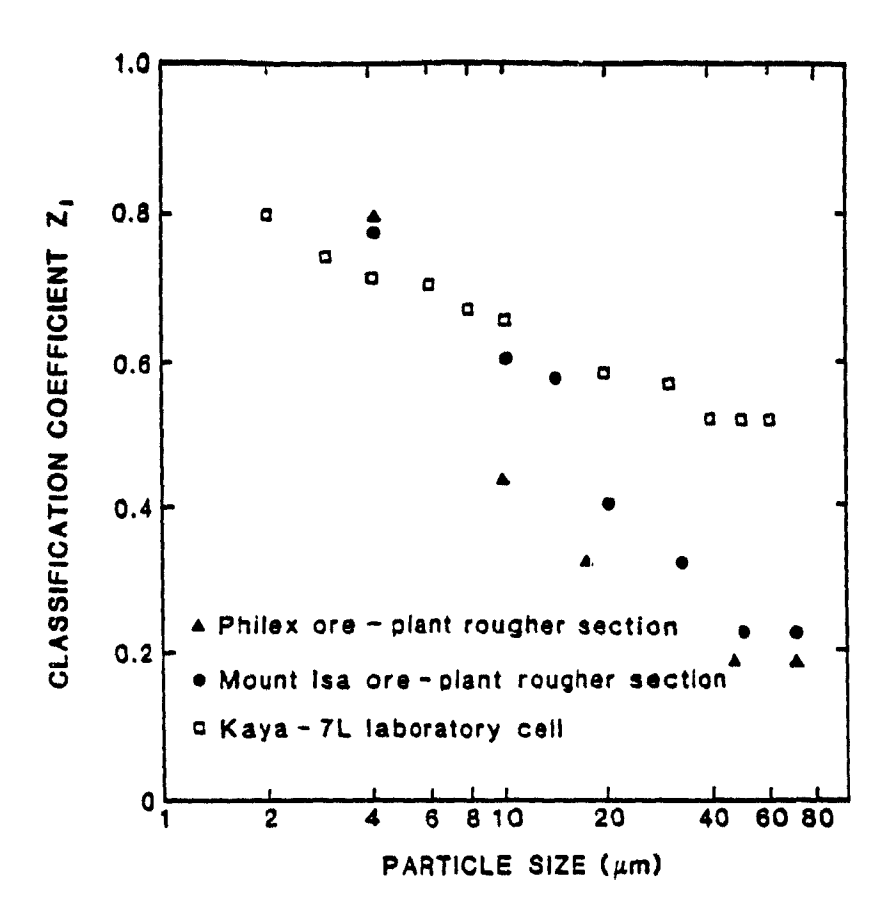


Figure 6.27: Comparison between laboratory and plant scale flotations with respect to the classification coefficient.

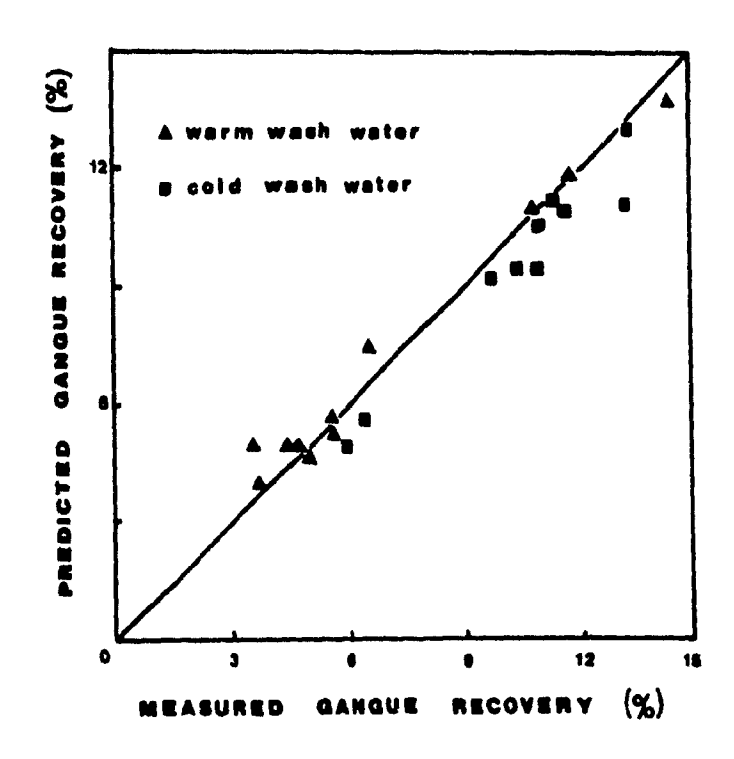


Figure 6.28: Comparison between predicted (from Eq. 6.9) and measured gangue recoveries.

نية

Figure 6.28 shows a good agreement between the predicted gangue recovery from Eq. 6.9, using measured feed water recovery, and an overall Z_i^{\bullet} determined for a 10 μ m particle and experimentally measured gangue recovery (Test 3). Proposed entrainment model can be used to estimate gangue recovery by knowing the overall Z_i^{\bullet} and feed water recovery.

6.4 Summary

- 1. The cleaning action taking place in the froth was visually observed and verified using a colored sample. There is an optimum wash water addition rate, at which the gangue recovery is minimum, between 0.06 and 0.08 cm/s in the present system.
- 2. One of the most important requirements of an effective wash water distribution is that it must ensure uniform water distribution throughout the distributor. Uneven distribution or channelling of flow will lead to excessive water bypassing in some parts of the froth phase and poor cleaning in others. Uniform froth washing was achieved using the spiral distributor and yielded the better gangue rejection at higher production rates.
- 3. Adding wash water above and below the froth is as effective as only above. However, below the interface addition requires additional piping and maintainance, is difficult to monitor, and does not contribute to froth stability.

- 4. The most effective way to reduce gangue entrainment is froth washing. Wash water can reduce entrainment around 50%. Mechanical and ultrasonic froth vibrations in conjuction with wash water can be used as an auxiliary method to further lessen entrainment (around 15-30%). Ultrasonic vibrations do not require any type of obstacle in the froth. The use of froth vibration in plant scale seems to be difficult.
- 5. A slight temperature difference between pulp water and wash water affects the entrainment mechanism significantly. Warm wash water can be used to minimize water addition requirement. Depressant addition in the wash water does not affect significantly gangue recovery because of short residence times in froth.
- 6. The proposed entrainment model was used and tested with laboratory, pilot plant, and plant scale data available. It was found that the overall Z_i^* values fall between 0.2 and 0.4 in most cases. For laboratory scale, the average Z_i^* is 0.2, for pilot-plant and plant scale 0.3. Thus, by knowing overall Z_i^* , and total water recovery, the gangue recovery (entrainment) can be estimated using the suggested Eq 6.9.

CHAPTER 7

EVALUATION OF WASH WATER ADDITION

IN A PILOT-SCALE FLOTATION CELL

USING TRACER TECHNIQUES IN A TWO-PHASE SYSTEM

Introduction

The main objective of this chapter is to evaluate the effect of wash water addition on a pilot-plant scale flotation cell using tracer techniques. Tracers were added into the wash water to determine wash water split, into the cell to determine slurry water rejection, and into the feed tank to determine feed water suppression using continuous conductivity measurement and sample collection.

Two different electrode assemblies were designed to monitor horizontal and vertical conductivity variations. Perforated pipes and spray nozzles were used to distribute wash water on the froth surface.

All tracer tests confirmed that there was a minimum gangue recovery at intermediate wash water addition rate. It was found that continuous conductivity measurements are a powerful technique to monitor the washing efficiency in the froth phase.

7.1 Theoretical Background

Wash water is divided into three streams when it is added above the froth phase (Figure 7.1). A very small fraction of wash water directly short-circuits to the concentrate (a), depending on wash water distributor location and design. A major fraction of wash water (b) suppresses slurry water coming from the pulp and then goes to the concentrate and the rest of the wash water (c) goes to the pulp phase diluting the slurry in the cell. The main objective of wash water is to maximize (b) at minimum (a) and (c).

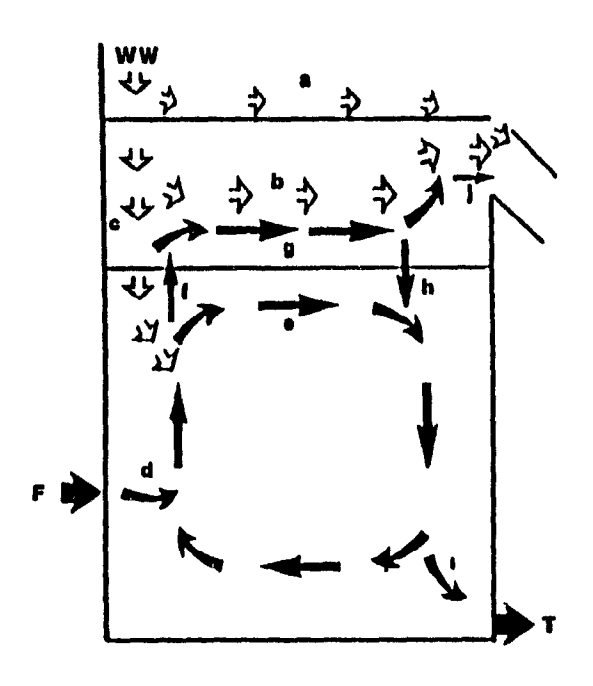


Figure 7.1: Water split in a flotation cell.

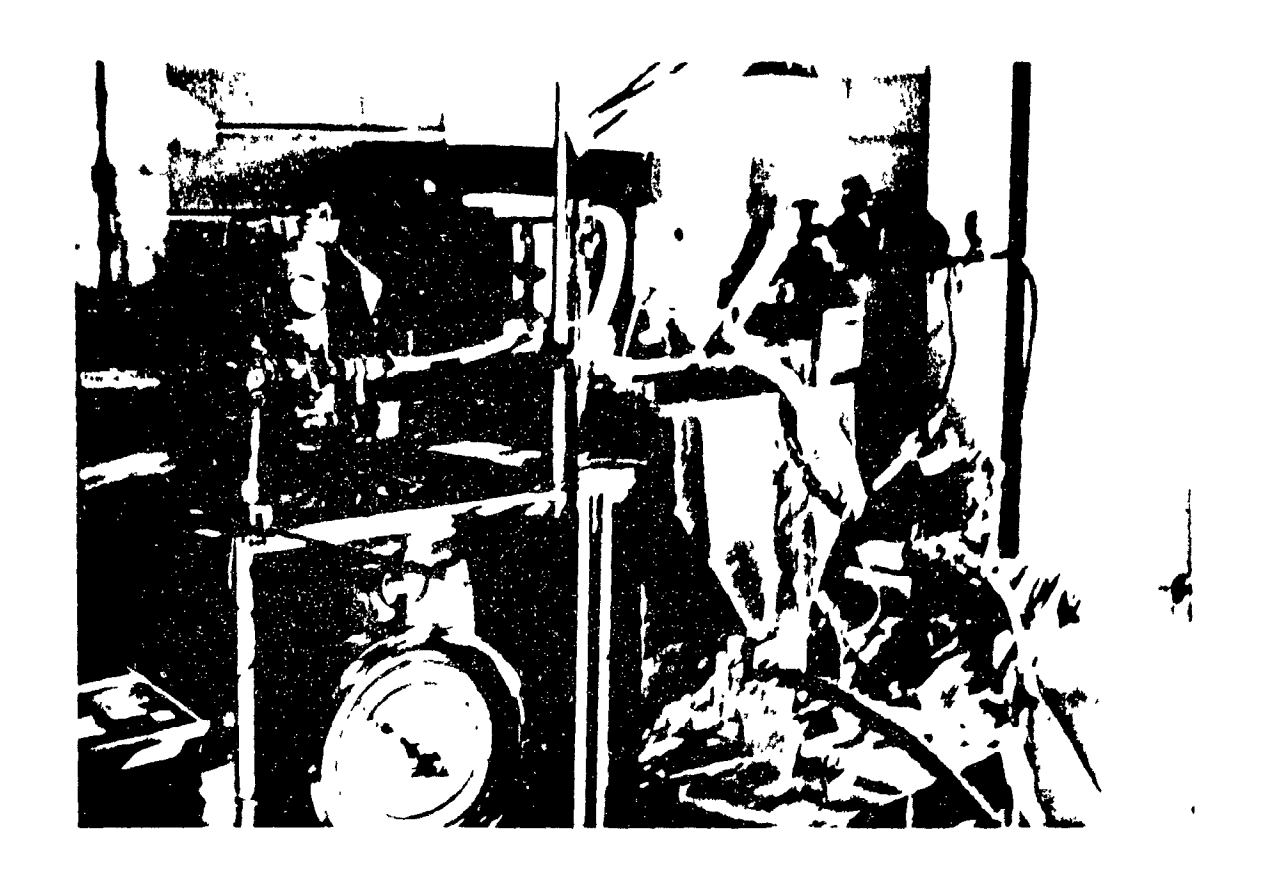


Figure 7.2: Overal view of pilot-plant scale set-up.

At steady state, feed water (d) and wash water draining to the slurry (c) called slurry water from now on, mix perfectly. Some is swept into the froth by hydraulic and/or mechanical entrainment (f). If there is no wash water (b) addition, all of water in the concentrate is from the feed. With wash water addition, then some of the feed water that would be recovered is displaced with wash water and drains back to the slurry phase (h) while the rest goes to the concentrate (j). Thus, the froth cleaning efficiency is determined by the exchange between (g) and (b).

7.2 Experimental

7.2.1 Set-up

The dimensions and operating ranges of the pilot-plant scale flotation machine and cell used in this study are given in Table 7.1. The main experimental set-up consists of a Denver D8 flotation machine, a 65 L plexiglass flotation cell, a 200 L plastic feed tank with a variable speed Lightnin mixer (1 HP), a Ramoy progressing cavity pump with a Brooke motor (1.1 HP) for feed, two 50L plastic wash water tanks, one Ramoy progressing cavity pump and one Masterflex peristaltic pump for wash water addition, and one 200 L plastic drum as a thickener (Figure 7.2). All experiments were performed continuously.

Table 7.1: Dimensions of the pilot-plant flotation machine and operation variable ranges.

Flotation Machine : Denver D8

Impeller : Stainless steel, 20.23 cm in diameter

Stator : Stainless steel

Cell : Plexiglass (40, 40, 45 cm)

Effective Area : 1600 cm²
Nominal Volume : 65 L
Motor Drive : 1.5 HP
Impeller Speed : 600 rpm
Froth Removal : free flow

Frother : Dowfroth 250, 10 ppm : 0.005 - 0.01 m/s (30 psi)

Jw : 0.0004 - 0.0009 m/s

FT : 0.10 - 0.15 m T : 0.08 m

H : 0.025 - 0.07 m

Wash Water Distributors: Two different water distributors were used in this study: perforated pipe and spray nozzle.

Perforated pipe distributor (PPD) was made of four 50 cm long copper pipes (dia: 1.27 cm), with 1 mm diameter holes 1 cm apart. Both sides of the copper pipes were closed with removeable rubber caps. T-fittings were connected in the middle of pipes for water entrance. Two of the pipes were at the back and the other two in front (Figure 7.3). Pipes were fixed together by a frame, which was placed on top of the cell. Pipes can easily be cleaned by removing rubber caps.

A four-way copper pipe splitter divides the wash water equally to each perforated pipe, via plastic hoses. A Ramoy progressing cavity pump was used to deliver wash water whose flow rate was adjusted using a by-pass pipe and two manual valves.

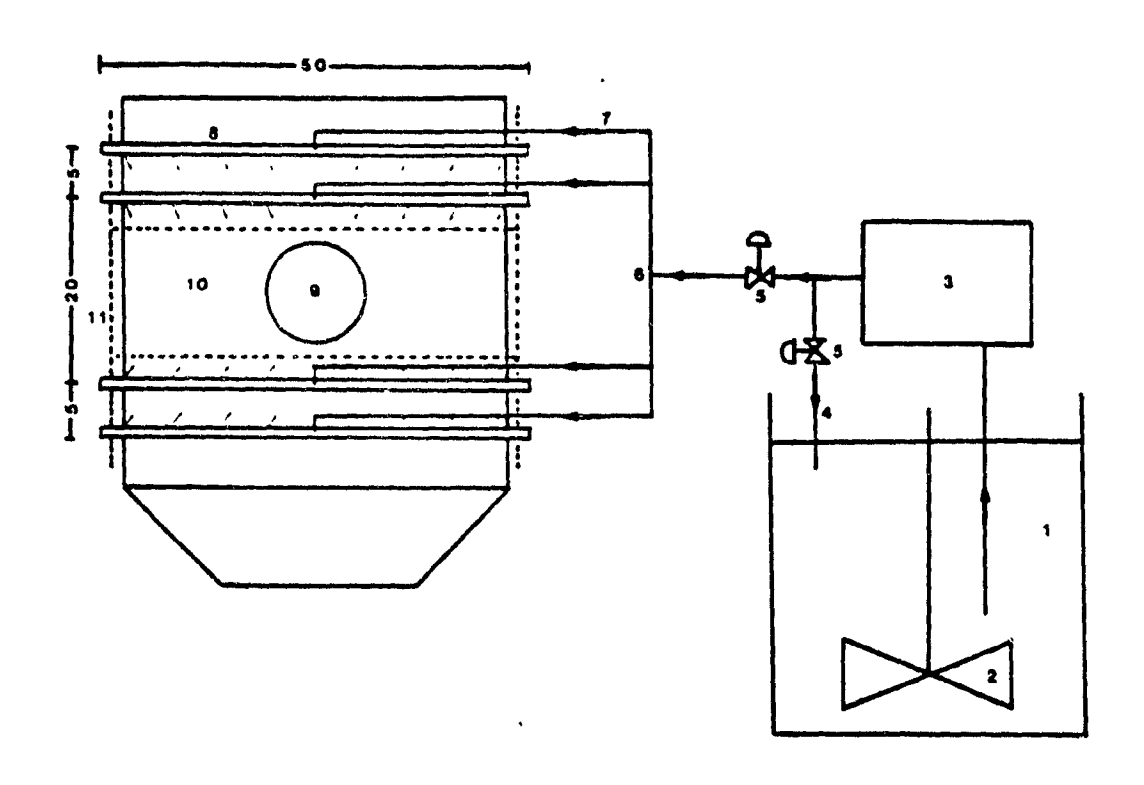


Figure 7.3: Wash water distribution system for pilot-plant scale flotation cell (dimensions are in cm).

- 1. wash water tank
- 2. agitator
- 3. cavity pump
- 4. by-pass pipe
- 5. valves
- 6. wash water splitter
- 7. hoses
- 8. perforated copper pipes
- 9. stator
- 10. flotation cell
- 11. plexiglass cell

A Malnor plastic garden water spray nozzle (SN) was used as an additional wash water source for some experiments. Wash water delivered by a Masterflex pump can be sprayed over almost the whole froth surface with a single nozzle. The spray nozzle creates a round full cone spray pattern and was fixed 15 cm above the froth surface. Coverage diameter can be adjusted by changing the distance between froth surface and spray nozzle level.

For some tests, the perforated pipe and spray nozzle were jointly used to increase wash water superficial rate. Both distributor mechanisms have separate pumps and wash water tanks. Maximum superficial wash water rates with the perforated pipes and spray nozzle are 0.066 and 0.023 cm/s, respectively.

Electrode Assemblies: Two different electrode assemblies were designed to measure the froth conductivity vertically and horizontally. Each electrode assembly has four electrode pairs.

The horizontal electrode assembly (HEA) was used to measure froth conductivity at four different locations on the same level. Stainless steel electrodes are square (1*1 cm) and fixed in plexiglass cubic prism cages (1.5*1.5*1.5 cm) open at the top and bottom to allow vertical liquid flow. These four electrode cages are fixed at the corners of a large plexiglass frame (14*12*1.5 cm). Two 30 cm screws were connected to the frame to adjust the assembly location shown in Figure 7.4a and 7.4b.

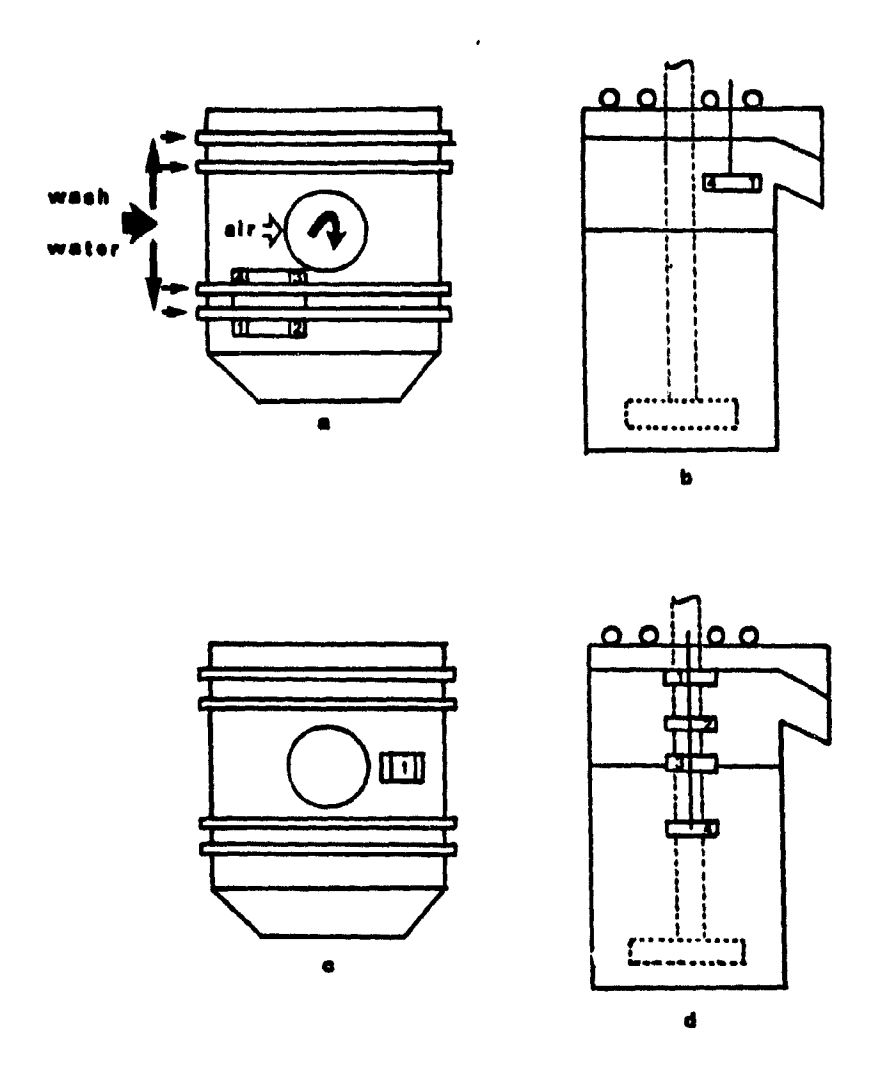


Figure 7.4: Vertical and horizontal electrode assemblies for conductivity measurement in the pilot-plant scale flotation cell.

Another quadruple electrode assembly was designed and constructed to measure the vertical conductivity profile in the froth, in the slurry, and at the interface. Copper electrodes (1.5*2*2.5 cm) were fixed in plexiglass boxes open at the bottom and top to allow slurry flow. Four electrode boxes were connected vertically by two 30 cm screws on both sides (Figure 7.4). Electrodes can thus be set at any level. This assembly was placed on the right hand side of the cell. The use of the left hand side was not possible due to the presence of the air entrance inlet to the standpipe and feed pipe entrance into the cell.

Conductivity Measurements: Slurry and froth conductivities were measured with the data acquisition system described above. Conductivity measurements were transformed into gas holdups. Gas holdup at the interface is assumed to be the average of gas holdup in the slurry and froth phases.

In this study, KCl and LiCl were used as electrolytes to increase the conductivity of the liquid. The conductivity of an electrolyte increases with increasing concentration. The increase in ionic concentration may be the result of an increase in the electrolyte concentration or changes in the extent of ionization of the electrolyte. There are two groups of electrolytes: strong and weak. Salts of alkali metals are strong electrolytes, which are completely ionized. In water, ions become hydrated and the hydrated ions disperse in the medium. The conductance of electrolyte solutions increases by more than 2% per degree, thus

close temperature control is essential. KCl is a stronger electrolyte than LiCl. For conductivity measurements KCl is better; however, its analysis with AA is more difficult due to partial ionization in the flame.

7.2.2 Methodology

Three different types of tracer tests were performed to evaluate the wash water distribution and determine the effect of wash water and air flowrates on wash water split, slurry water rejections using the pilot-plant cell at a constant feed rate. Tracers were added into:

- a. the wash water tank to determine wash water split,
- b. the flotation cell to determine slurry water recovery,
- c. the feed tank to determine feed water recovery.

Slurry height (SH) was maintained constant at 37 cm from the cell bottom by adjusting tailing flowrate. Experimental conditions are summarized in Table 2.

Electrode Calibration: The effect of water height above the electrode cage and container size used on conductivity was determined using an electrode box.

The effect of water height above the electrode cage was determined in a 500 cm³ graduated cylinder. It was filled with tap water and the electrode cage was immersed in the cylinder at different depths from 1 cm to 30 cm from the top of water surface.

Test N	6 J	J	H	τ	SII	Tracer	Distributor	Electrode	Tracer	addition	Wash water
	(cm/s	(cm/s)		(cm)		(g)	Туро	assembly	location	type	Temperature
Effect	of una	th water	£1owr	ate and	tempe an	ture on condu	etlylty				
Tost s	0 089	1 03	8	8	37	no	กาอ	REA			12-45
ompar	ison of	wish wi	ler d	latribut	OI II						
iest b	0 023	1 03	4	8	37	40g LICI	1710 SN	REA	wash water tank	continuous	12
Effect	of J	and J o	n was	h water	dinti ib	ut Ion					
Test 1	0 046	0 78	8	٤	31	40g LICI	rrn	HEA	wash water	continuous	12
	0 000						PPD+SN		tank		
Test 2	0 066	0 78 1 03	8	8	31	40g LICI	เมอ	HEA	wash water _tank	continuous	12
	0 089		6	8	31		PPD+SN		, cente		
Effect	ol 1° (on wash	mter	spilt							
Test 3	0 045 0 066 0 089	1 03	6	8	3/	40g KCl	i'i'd Pi'd Pi'd+Sn	VEA	wash water tank	continuous	12
Effect	ot j" (on slurry	wate	r recov	ery						
Test 4			6	8	37	10g KC1		VEA	pulp phase	impulse	12
Effect	of 1°	on feed v	ater	recover	y						
lest 5	0 045 0 066 0 089	1 03	8	8	37	15g KCl	PPD PPD PPD+SN	VEA	feed tank	cont l nuous	12
	0 066 : 0 078 0 65	1 03	8	8	37	15g KCI	ero ero ero	VEA	feed tank	continuous	12

NEA: horizontal electrode assembly, VFA vertical electrode assembly, PPD perforated pipe distributor, SN: spray nozzle

Table 7.2: Summary of experimental conditions.

Conductivity was also measured using another electrode in 100, 250, 500, and 1000 cm³ beakers filled with tap water, the electrode cage always immersed in the center of beaker at half-depth. Once conductivity was measured in each beaker, then repeat measurements from each beaker were taken for reproducibility. This time, location of the electrode in the beaker changed on the same horizantal plane at half-depth.

Effect of Wash Water Flowrate and Temperature on Froth Conductivity: Before starting tracer tests, the effect of a step change of wash water flowrate on conductivity was determined with HEA in the absence of any tracer at a Jg of 1.03 cm/s. Cold and warm wash water temperatures were 12°C and 45°C (Test series a).

Effect of Wash Water and Air Flow Rates on Wash Water Distribution

Using Horizantal Electrode Assembly: 40 grams LiCl dissolved in

water were added in the wash water tank in order to evaluate the

wash water distribution in the froth phase of the pilot-plant

scale cell (Test series 1).

First three different wash water addition flow rates were tested (0 046, 0.066 and 0.089 cm/s) at J_g of 0.78 cm/s. Conductivity of the froth phase was measured using the HEA in the middle of froth. For low and intermediate addition rates, the perforated pipe distributor was used. At high addition rate, the perforated pipe and spray nozzle were used together. Samples from concentrate, tailing, and wash water were taken for lithium analysis and flowrate measurements.

Second, the effect of air flowrate on wash water distribution was evaluated at two different air rates (0.78, and 1.03 cm/s) by continuous froth conductivity measurements with the HEA (Test series 2).

Effect of Wash Water and Air Flow Rates on Wash Water Split: Wash water split was determined by adding 40 gram KCl into the wash water tank in order to create a sharp conductivity difference between wash water and water coming from slurry phase (Test series 3). Conductivities were measured using the vertical electrode assembly (VEA). The first electrode was 7 cm below the interface, the second at the interface (8 cm below the cell lip level), the third 2 cm below the cell lip level, and the fourth at the top of the froth. The effects of wash water flow rate and air flow rate were investigated by continuous conductivity measurements. Samples from concentrate, tailing, and wash water were taken to determine flow rates and K content in each stream.

Wash water (tracer) split (R_m) was determined by taking a sample from concentrate at the beginning of each experiment (i.e. first 30 second after wash water is introduced):

$$R_{WW} = Q_c \cdot C_c / Q_w \cdot C_{WW}$$
 7.1

where Q: concentrate flowrate (cm3/s)

C: tracer concentration in concentrate (g/cm³)

Q : wash water flowrate (cm3/s)

C: tracer concentration in wash water (g/cm³)

then,

$$Q_{MC} = Q_{MN} \cdot R_{MN}$$
 7.2
 $Q_{MS} = Q_{MN} - Q_{MC}$ 7.3
 $Q_{SC} = Q_{C} - Q_{MS}$ 7.4

where Q_{wc} : wash water flowrate going to concentrate (cm^3/s) Q_{ws} : wash water flowrate going to slurry (cm^3/s) Q_{sc} : slurry water flowrate going to concentrate (cm^3/s)

Figure 7.5 shows diagrammatically the notation for flowrates, and concentrations. The transient mass balance of tracer in the slurry phase:

$$Q_{WS}, C_{W} - (Q_{SC} + Q_{t}), C_{t} = V_{2}, (dC_{t}/dt)$$
 7.5

$$\int_{0}^{t} dt = \int_{Q_{ws}}^{C_{t}} \frac{V_{2} \cdot dC_{t}}{Q_{sc} + Q_{t} \cdot C_{t}}$$
7.6

$$t = \frac{V_2}{-(Q_{sc} + Q_t)} \ln(Q_{ws} \cdot C_w - (Q_{sc} + Q_t) \cdot C_t) \mid {c \atop 0}$$
 7.7

$$\frac{-(Q_{sc}+Q_t).t}{V_2} = \ln \left[\frac{Q_{ws}.C_{w}-(Q_{sc}+Q_t).C_t}{Q_{ws}.C_{w}} \right]$$
 7.8

$$Q_{wg} \cdot C_{w} - (Q_{gc} + Q_{t}) \cdot C_{t} = Q_{wg} \cdot C_{w} \cdot \exp(-t/\tau)$$
 7.9

and $C_{\underline{t}}$ can be calculated from

$$C_{t} = \frac{(Q_{ws}.C_{w}(1-\exp(-t/\tau)))}{Q_{sc} + Q_{t}}$$
7.10



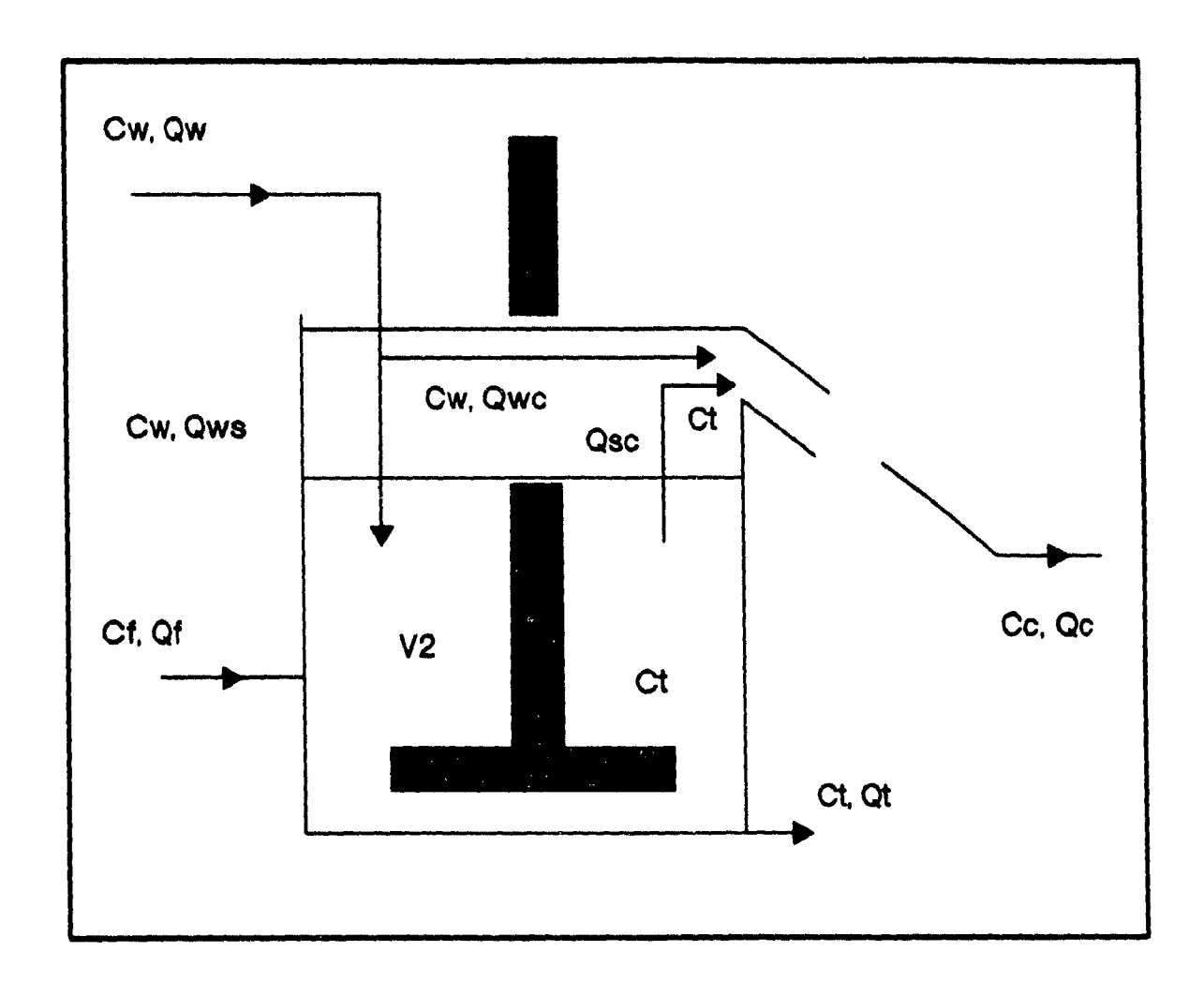


Figure 7.5: Definition of concentrations and flowrates for calculations.

where
$$T = (V_2/(Q_{sc} + Q_t))$$
 7.11

then, C is given by

$$Q_{MC} \cdot C_{M} + Q_{MC} \cdot C_{L}$$

$$C_{C} = \frac{Q_{MC} + Q_{MC}}{Q_{MC}}$$
7.12

Effect of Wash Water Flowrate on Slurry Water Suppression: The effect of wash water flowrate on slurry water suppression was determined by impulse tracer tests (Test series 4). 10 grams of KCl were introduced into the flotation cell near the impeller by an inclined plexiglass pipe. The vertical electrode assembly was used to measure conductivity profiles and samples were taken from tailing and concentrate streams at known time intervals for K analysis.

Conductivity measurements were corrected for tracer:

$$K(t,z) = (K(t,z,\varepsilon)_{g \text{ with tracer}} - K(t,z,\varepsilon)_{g \text{ without tracer}})$$
 7.14

In order to quantify and compare results at different operation conditions, tracer recovery, which corresponds to slurry water recovery, was defined as follows:

$$R_{sw} = \frac{\int K_{c}(t,z).Q_{c}.dt).100}{\int K_{c}(t,z).Q_{c}.dt) + \int K_{t}(t,z).Q_{t}.dt}$$
7.15

where $K_c(t,z)$: measured conductivity by electrode number 3 $K_t(t,z)$: measured conductivity by electrode number 1

Slurry water recoveries were calculated using electrodes is and 3, which are in the slurry and froth, respectively. The conductivity in the slurry phase assumed to be equal to the conductivity in the tailing stream considering a perfectly mixed liquid phase. Due to reading variations from electrode number 4, electrode 3 is used as a representative of the froth phase. Experiments started with conductivity measurements without tracer addition in the presence of wash water.

Effect of Wash Water and Air Flow Rates on Feed Water Rejection:

15 gram KCl was added into the feed tank (200 L) at the beginning of the test and well mixed with the agitator (Test series 5 and 6). The cell was filled with this water. Conductivities were measured continuously with the VEA. Samples were taken from tailing and concentrate to determine flow rates and K* content. First, the effect of J (0.045, 0.066, and 0.089 cm/s) was determined at J of 1.03 cm/s. Second, J was kept constant at 0.066 cm/s at three different J (1.03, 0.78, and 0.65 cm/s). Feed water recovery was calculated as follows:

At $t = 0^+$, $C_f = C_t$ and it can be assumed that

$$C_c = (Q_{ac}/Q_c).C_t$$
 7.16

Q can be calculated from the samples collected from the first 30 second.

$$Q_{_{\rm MC}} = Q_{_{\rm C}} - Q_{_{\rm SC}}$$
 7.17

$$Q_{we} = Q_{w} - Q_{we}$$
 7.18

Transient mass balance for the slurry phase:

$$Q_f \cdot C_f - (Q_{sc} + Q_t) \cdot C_t = V_2 \cdot (dC_t/dt)$$
 7.19

$$\int_{0}^{t} dt = \int_{c_{f}}^{c_{t}} \frac{V_{2}}{Q_{f} \cdot C_{f} - (Q_{c} + Q_{c}) \cdot C_{c}} dC_{c}$$
7.20

$$t = \frac{-V_2}{Q_{sc} + Q_t} \ln(Q_f \cdot C_f - (Q_{sc} + Q_t) \cdot C_t) \begin{vmatrix} C_t \\ C_f \end{vmatrix}$$
 7.21

$$\frac{-t}{\frac{(V_2/(Q_{sc} + Q_t))}{(Q_f, C_f - (Q_{sc} + Q_t), C_f)}} = \ln \left[\frac{Q_f, C_f - (Q_{sc} + Q_t), C_t(t)}{Q_f, C_f - (Q_{sc} + Q_t), C_f} \right]$$
 7.22

$$e^{-t/\tau} = \ln \left[\frac{Q_f \cdot C_f - (Q_{sc} + Q_t) \cdot C_t}{(Q_f - Q_t - Q_s) \cdot C_f} \right]$$
 7.23

$$C_t = C_f - (Q_f - Q_t - Q_{sc}) \cdot e^{-t/\tau}$$

$$Q_{sc} + Q_t$$
7.24

and

$$Q_{sc} \cdot C_{t}$$

$$C_{c} = \frac{Q_{sc} \cdot C_{t}}{Q_{wc} + Q_{sc}}$$
7.25

Feed water recovery (R_f) is calculated from:

$$R_{f} = \frac{\int Q_{c}.C_{c}.dt}{\int Q_{c}.C_{c}.dt + \int Q_{t}.C_{t}.dt}$$
7.26

Some of the tests done were used to determine the amount of water going to the concentrate (Q_c) . Continuous conductivity measurements were converted into average gas holdups in the froth phase. The distance between the interface and the cell lip (T) and between the cell lip level and the froth surface (H) were measured. Timed samples from concentrate and tailing were collected. For these calculations, slurry height (SH) in the cell was always kept constant (37 cm) (i.e. T is constant). The discharge coefficient (Kc) (Eq. 3.14), was evaluated using the procedure outlined in section 3, depends mainly on H and T.

7.3 Results and Discussion

7.3.1 Electrode Calibration

As can be seen from Figure 7.6, there is almost no effect of water height above the electrode from 1 cm up to 30 cm on conductivity measured. The ion path between electrodes is almost horizontal due to short distance between electrode plates.

Conductivity measurements in different beakers, which contains different amount and height of water, are almost identical as shown in Figure 7.7.

7.3.2 Effect of Wash Water Flowrate and Temperature on Conductivity

The effect of wash water on gas holdup and water balance is shown in Table 7.2. Liquid content in the froth increases significantly with wash water addition. There is also a slight

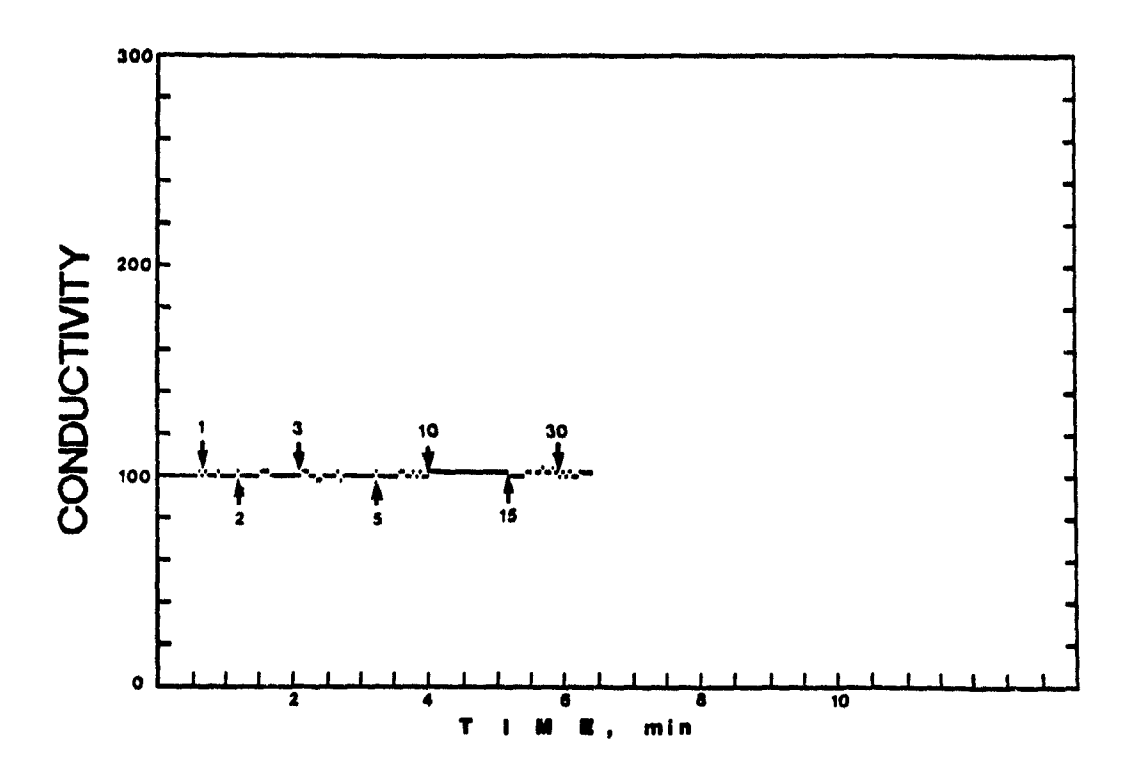


Figure 7.6: Effect of water height above the electrode box on conductivity measurements (Numbers represent water height above the electrode box in cm).

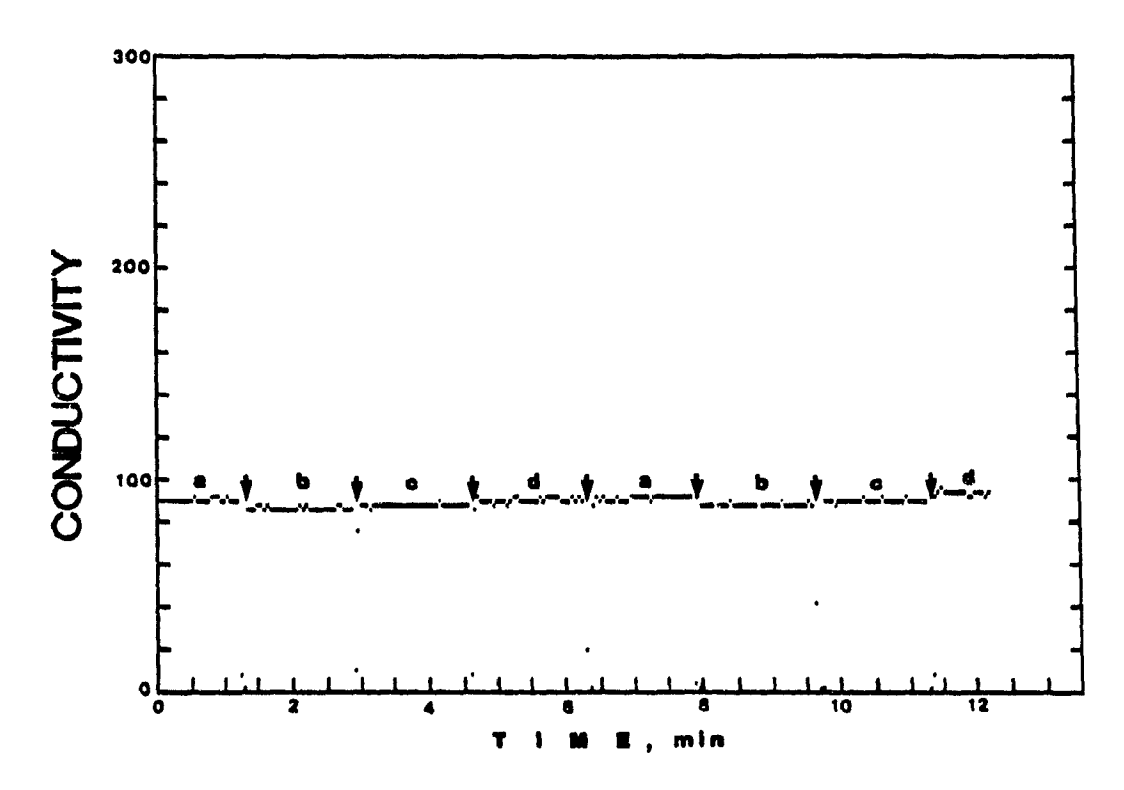


Figure 7.7: Effect of container size on conductivity measurements.

a) 100 cm³ beaker

c) 500 cm³

b) 250 cm³

d) 1000 cm^3

increase in the liquid content of the slurry phase with wash water. In the presence of wash water, upward and downward water superficial rates are higher. Without wash water, there is a significant negative bias; with wash water, there is a small positive bias.

Figure 7.8 shows the conductivity versus time response curve for a step change in wash water addition. At the beginning, there is no wash water addition; therefore, conductivity is lowest (i.e. liquid holdup is low). With wash water, conductivity increases (i.e. liquid content increases). A step increase in wash water during operation leads to an additional increase in conductivity. The warmer the wash water, the lower the froth conductivity. Water drainage between bubbles is higher with warm wash water because of decreased inter-bubble water viscosity. Bubble expansion (gas holdup increase) due to warm wash water also reduces the liquid content in the froth (i.e. lower conductivity). Correcting conductivity for temperature would further increase the difference between cold and warm wash water.

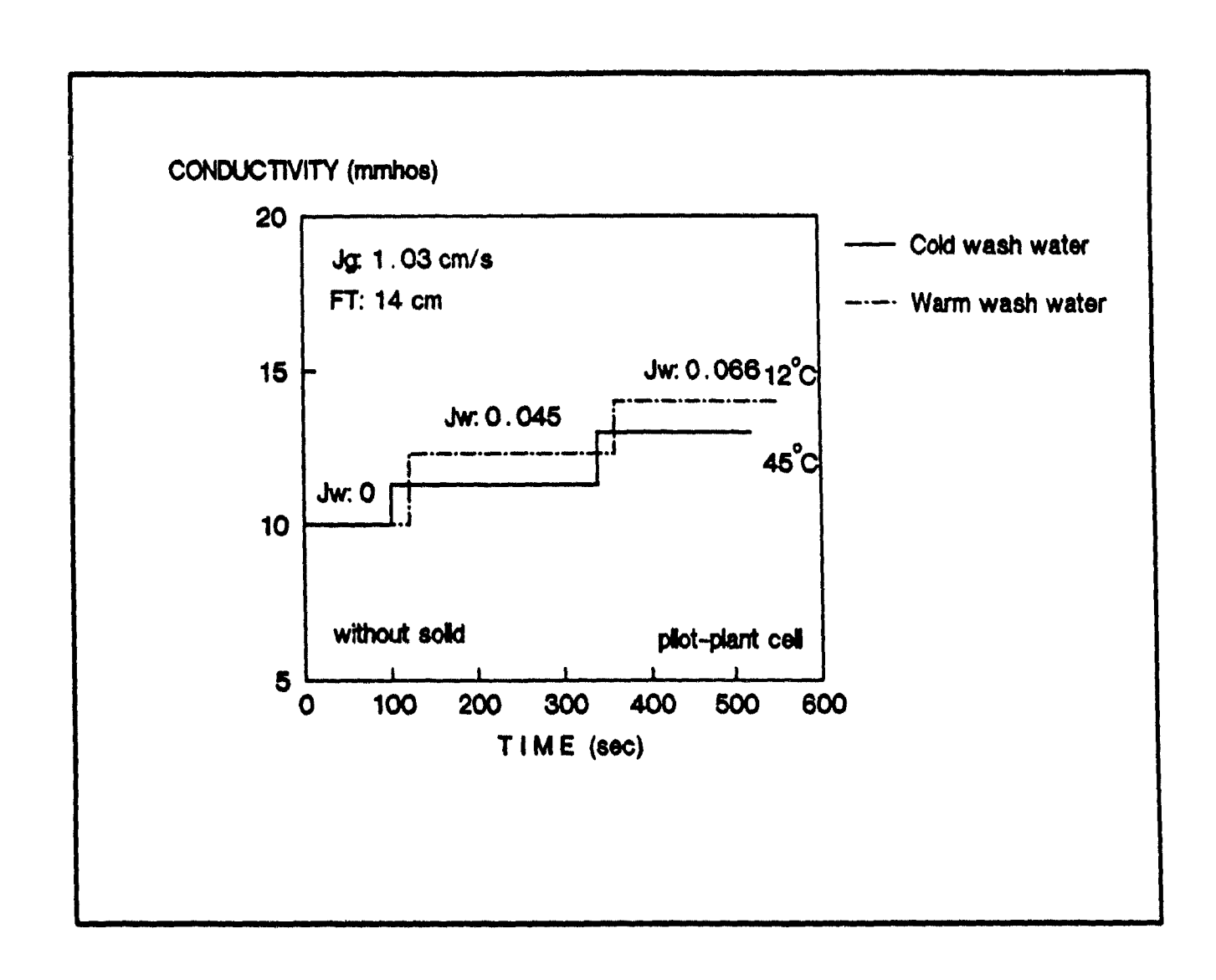


Figure 7.8: Effect of wash water flowrate and temperature on froth conductivity (HEA, average of four electrodes).

(lines are average responses from four electrodes)

TABLE 7.2: Effect of wash water on gas holdup and water balance.

	J_=0.066 cm/s	J_=O cm∕s
	FT=14 cm SH=37 cm	FT=12 cm/s SH=37 cm
e.Reading	ELECTRODE 4 (at the 6.48	cell lip level) 4.25
(%)	75.56	82.56
(cm/s)	0.357	0.218
(cm/s)	0.366	0.177
(cm/s)	0.057	0.041
	ELECTRODE 3 (in the	
ve.Reading (%)	12.90 59.39	9.50 68.91
(cm/s)	0.684	0.451
(cm/s)	0.693	0.410
	ELECTRODE 2 (at t	he interface)
ve.Reading	31.48 45.31	29.00 50.31
(%) g (cm/s)	1.243	1.017
d (cm/s)	1.252	0.976
	ELECTRODE 1 (in the	e slurry phase)
ve. Reading	48.03	47.00
g (%)	31.70	31.23
(cm/s)	0.132	0.12
f (cm/s)	0.123	0.123

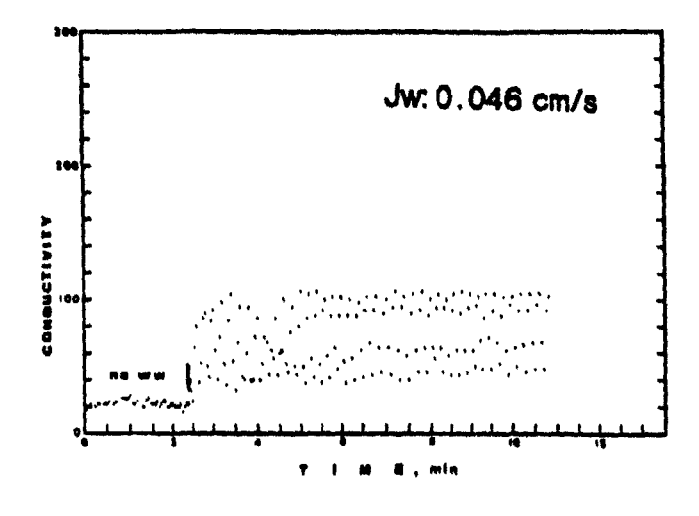
7.3.3 Evaluation of Wash Water Distributor for Homogeneous Addition

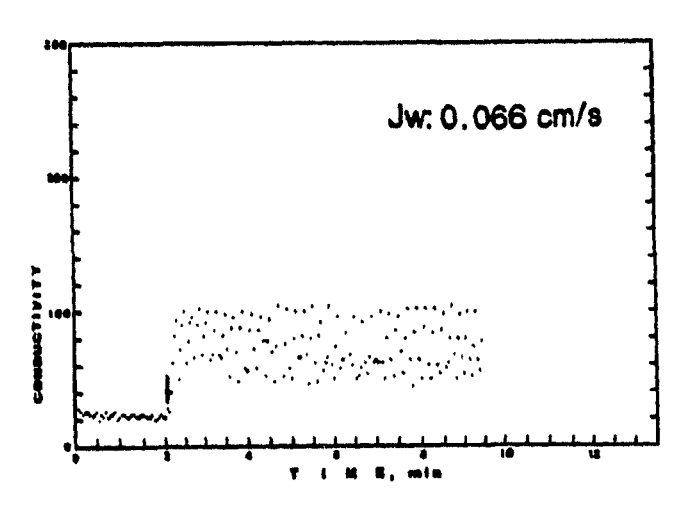
Effect of Wash Water Addition Rate: Figure 7.9 shows conductivity versus time at three different wash water addition rates. Electrolyte was added to the wash water. The increase in conductivity with wash water stems both from the increased liquid holdup and liquid conductivity, due to the electrolyte. Thus, the effect of wash water on froth conductivity is extremely striking. Conductivity in the froth is low and measurements from the four electrodes are quite close in the absence of wash water. When the wash water was introduced, froth conductivity significantly increased due to presence of salt in the wash water (Test series 1). The maximum increase in conductivity was achieved at the highest wash water addition rates, froth conductivity is lower and measurements spread widely. The higher the froth conductivity, the higher the liquid content of froth phase.

The wider the conductivity measurements from four electrodes, the less homogeneous the water distribution in froth. The smoother the conductivity readings from one electrode, the more gentle the addition (i.e. less froth mixing) and the more stable the froth phase (i.e. less froth disturbance).

Table 7.3 summarizes of flowrates and tracer concentrations.

At constant feed rate and slurry height, concentrate and tailing flowrates increase with increasing wash water rate.





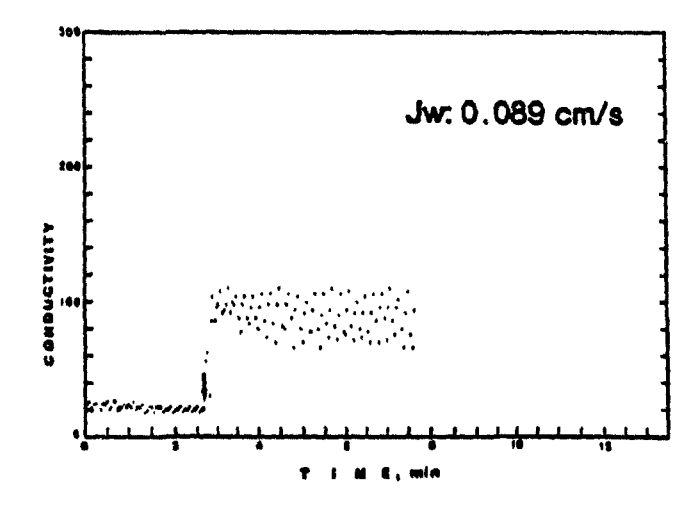


Figure 7.9: Effect of wash water flowrate on water distribution in Denver D8 cell using the HEA.

TABLE 7.3: Effect of wash water flowrate on water distribution.

	Q (cm ³ /min) J (cm/s)				
	4378(0.046)	6378(0.066)	8636(0.089)		
۵ ^۲ (۹ ^۲)	11420 (0.119)	11420 (0.119)	11420 (0.119)		
g (J)	4941 (0.051)	6245 (0.065)	6477 (0.067)		
ດ້ (ງ້)	10857 (0.112)	11553 (0.120)	13571 (0.141)		
Q,	-563	+133	+2159		
H (cm) T (cm) SH (cm) Q/Q_	6 8 37 0.38	6 8 37 0.56	6 8 37 0.73		
τ (min)	4.42	4. 15	3.54		
Li (ppm)					
Concentrate	107.40		114.82		
Tailing Wash water	27.49 141.52		33.32 141.52		

Concentrate and tailing lithium assays show that the transient lithium content of the concentrate is much closer to that of wash water than that of tailings. As wash water flowrate increases, the lithium content in both the concentrate and tailing increases. An increase in wash water addition rate results in a decrease in gas holdup and bubble residence time in the froth. Therefore, bubbles rise much faster in the froth and carry more inter-bubble water into the concentrate. Feed water recovery may then decrease or increase depending on wash water.

Effect of Air Flowrate on Wash Water Distribution: The effect of air flowrate on wash water distribution can be seen from Figure 7.10 where froth conductivity is plotted as a function of time. There is a significant increase in conductivity with wash water

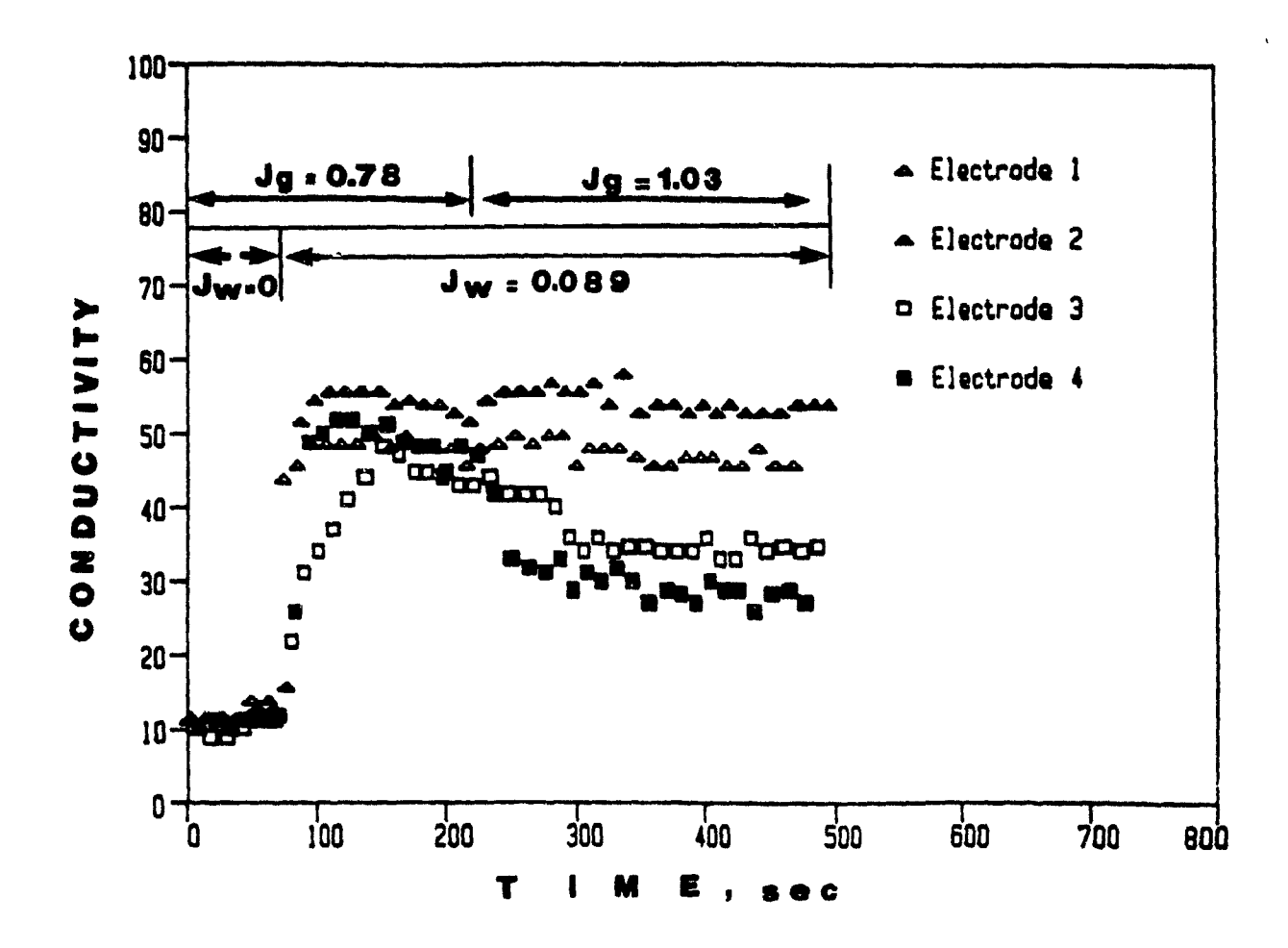


Figure 7.10: Effect of air flowrate on wash water distribution in Denver D8 cell using HEA located in the middle of the froth (Li tracer is added to wash water).

addition due to presence of tracer in wash water (Test series 2). An increase in J_g from 0.78 to 1.03 cm/s causes significant variation (i.e. spread) in conductivity. The higher the aeration rate, the less homogeneous the wash water distribution in the froth phase. The conductivity of the froth phase decreases because more slurry water is carried into the froth. Slurry water is combination of feed water, which does not contain any salt tracer, and some of the wash water, which trickled down to the slurry. Thus, slurry water penetration into froth increases with increasing aeration rate, which leads to an increased liquid holdup in the froth. Variations in conductivity on the same horizontal plane confirm that wash water distribution is less homogeneous at higher J_w . It appears that aeration increases froth mixing more than wash water.

Average Li concentrations of these tests are given in Table 7.4.

TABLE 7.4: Average Li assays at different air and wash water flowrates.

Stream	J _g (cm∕s)	J (cm/s)	Li(ppm)
II b A	0.70	0.000	450.55
Wash water	0.78	0.089	159.55
Concentrate	0.78	0.089	129.41
Tailing	0.78	0.089	25.29
Wash water	1.03	0.089	159.55
Concentrate	1.03	0.089	121.53
Tailing	1.03	0.089	31.12
Wash water	0.78	0.066	159.55
Concentrate	0.78	0.066	112.87
Tailing	0.78	0.066	
rarring	0.76	0.000	24.83

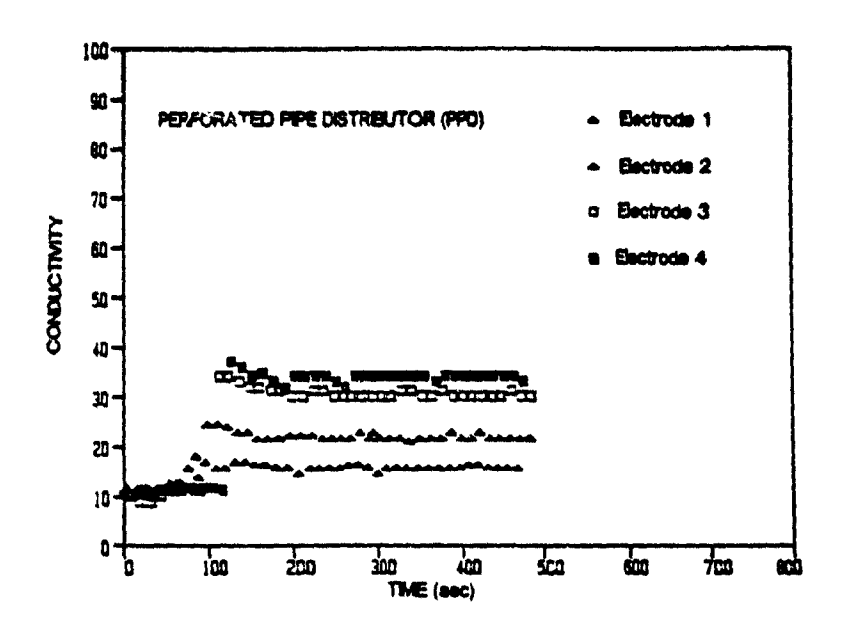
The tracer content of the concentrate is much closer to wash water than that of tailings. Therefore, most of the water going to the concentrate should come from wash water. At constant wash water addition rate, an increase in aeration rate causes an increased penetration of slurry water into the froth.

7.3.4 Comparison of Wash Water Distributors

Water distributors can be compared by measuring the conductivity as a function of time using the HEA (Test series b). Figure 7.11 shows the conductivity vs time curves for the PPD and the SN at a J of 0.023 cm/s. With the PPD, froth conductivities are smoothly changing with time. However, the SN gives very noisy data due to pulsating nature of spraying operation.

Conductivity readings from the four electrodes are slightly spreaded with SN because of more uniform wash water addition. The SN can cover almost whole froth surface while the PPD cannot.

It can be concluded that addition of wash water by the PPD is more gentle but less homogeneous than the SN, which may disturb the froth. The use of PPDs for thin and brittle froths and SNs for thick and persistant froths is advisable. It should be borne in mind that SNs may be easily plugged with recycled water.



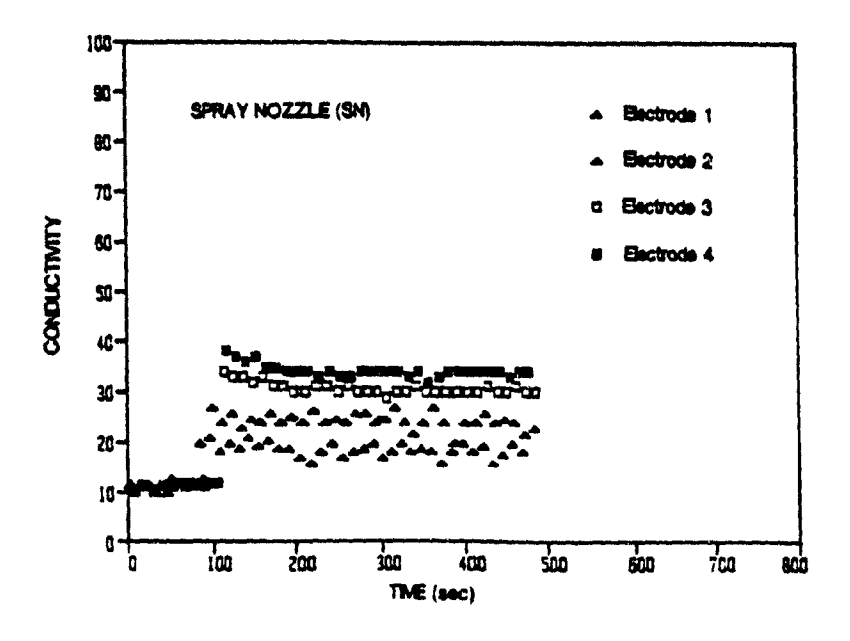


Figure 7.11: Conductivity versus time response curves with HEA for perforated pipe distributor and spray nozzle (Li tracer in wash water).

7.3.5 Wash Water Split

Figure 7.12 shows typical transient conductivity versus time response curves using the VEA at a $J_{\rm w}$ of 0.045 cm/s. At the beginning of the experiments, there is no wash water addition; therefore, conductivities are low for electrodes 3 and 4, which are in froth. As soon as wash water with KCl is added, conductivity measured by electrodes 3 and 4 increases drastically, while conductivity measured by electrode 1 in the slurry increases exponentially. The sharp conductivity increase in the froth is related to suppression of slurry water, which does not contain any KCl. The exponential increase in the slurry is due to the slow accumulation of KCl in the slurry, which follows first order kinetics (time constant: MRT in the slurry).

It also corresponds to pulp dilution in actual flotation operation after wash water is introduced. The response of electrode 2 could be used to control interface level. If there is a slight change in the slurry level, conductivity changes immediately in the response curve. There is a good potential to monitor slurry level by this type of conductivity measurements in two phase systems. Sudden conductivity increases for electrodes 3 and 4 yields important information regarding froth cleaning. It appears that conductivity measured by electrode 3 increases exponentially with time, since KCl concentration in the pulp increases. Conductivity measured by electrode number 4 seems to be remain constant with time, which means that the cleaning action is largely taking place below this electrode level.

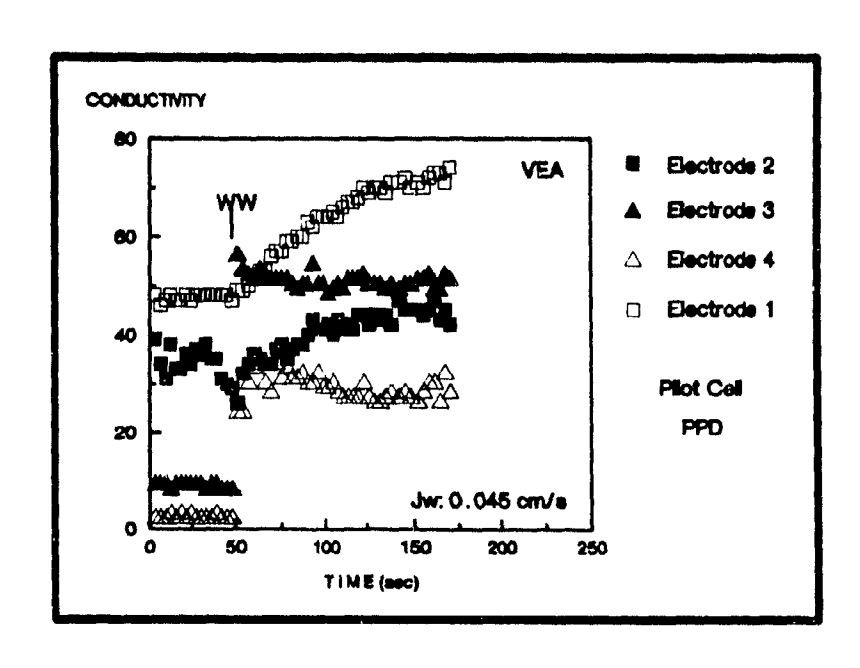


Figure 7.12: Conductivity response curve using the VEA (tracer is in the wash water).

Wash water split at two different air flowrates is shown in Table 7.5. At both air flowrates, tailing and concentrate flowrates increase with increasing wash water addition rates. Slurry residence time decreases slightly with increasing J.

Net bias flowrate (Q_b) and bias ratio $(Br = Q_t/Q_f)$ increase with increasing wash water superficial rate. Upward water flow is considered as a negative bias and downward water flow as a positive bias.

In the absence of wash water, tailing and concentrate flowrates are minimum and feed water penetration into the froth and then into the concentrate is maximum. Minimum feed water penetration was achieved at the intermediate wash water rate. Therefore, the effect of wash water is confirmed.

Even if percent wash water recovery $(R_{_{\mathbf{W}\mathbf{W}}})$ to the concentrate decreases with increasing $J_{_{\mathbf{W}}}$, the amount of wash water going to the concentrate increases. Wash water flowrate going to the slurry phase also increases with increasing $J_{_{\mathbf{W}}}$. Interestingly, slurry water penetration to the concentrate is minimum at the intermediate $J_{_{\mathbf{W}}}$ at both air flowrates. This is why maximum gangue rejection is achieved at the intermediate $J_{_{\mathbf{W}}}$'s.

Table 7.5: Effect of wash water flowrate and gas rate on wash water split and water balance.

/min (cm/	s)	0		(0.045)	6378	(0.066)	8636	(0.089)
			Jg: 0.78					
(1 ⁻)	13390	0.139		0.139	13390	0.139	13390	0.139
(J,)	11286	0.118	12490	0.130	14205	0.148	15503	0.161
(J _e)	2104	0.022	5250	0.055	5563	0.058	6523	0.068
ww			75	. 77	73	. 39	65	. 23
(J)			3302	0.034	4681	0.049	5175	0.054
(J)			1056	0.011	1697	0.018	3461	0.036
(J)	2104	0.022	1948	0.020	882	0.092	1348	C.014
(1)	-2104	-0.022	-892	-0.009	+815	0.008	+3661	0.038
r (min)		. 8 4 . 25	3.	. 93 . 84	3.	. 06 . 38	3.	. 16 . 10
l vQ f			0.	32	0.	48	0.	86
T (min) (cm)		12 7	•	1 4 7	:	1 4 7	:	14 7
^				المستريب سنهي مشهوسه الرسسان				· · · · · · · · · · · · · · · · · · ·
n ³ /min)(cm	n∕s)		4389		6378	(0.066)	8636	(0.089
	u/s)		Jg: 1.03	3 cm/s				-
) (1 ^t)	n∕s)		<u>Jg: 1.03</u>	3 cm/s 0.172	16501	0. 172	16501	0. 172
ງ້(ຖ້) ງ້(1້)	n/s)		Jg: 1.03 16501 15437	0.172 0.161	16501 16919	0.172 0.176	16501 18226	0. 172 0. 190
ີ(1້) ໂ(1້) _ໄ (1້)	n/s)		J ₉ : 1.03 16501 15437 5453	0.172 0.161 0.057	16501 16919 5960	0.172 0.176 0.062	16501 18226 6911	0.172 0.190 0.072
ງ ^{າທ} ີ່ ງີ (ຊຶ່) ງ [‡] (ຊຶ່)	n/s)		Jg: 1.03 16501 15437 5453	0.172 0.161 0.057	16501 16919 5960	0. 172 0. 176 0. 062 0. 19	16501 18226 6911	0. 172 0. 190 0. 072 3. 96
) ^{MC} (n/s)		Jg: 1.03 16501 15437 5453 68 2867	0.172 0.161 0.057 5.32 0.030	16501 16919 5960 60 3839	0.172 0.176 0.062 0.19 0.040	16501 18226 6911 53	0. 172 0. 190 0. 072 3. 96 0. 049
) ^{Ma} (1 ^{Ma}) Ma (1 ^{Ma}) J ^{MM} ງ ⁽ (1 ⁽) ງ ⁽ (1 ⁽)	n/s)		J ₉ : 1.03 16501 15437 5453 65 2867 1522	0.172 0.161 0.057 5.32 0.030 0.016	16501 16919 5960 60 3839 2539	0.172 0.176 0.062 0.19 0.040 0.026	16501 18226 6911 53 4660 3976	0.172 0.190 0.072 3.96 0.049 0.041
ງ ac ac) ງ ac ac) ງ ac ac) ກາ ງ (1°) ງ (1°) ງ (1°)	n/s)		Jg: 1.03 16501 15437 5453 65 2867 1522 2586	0.172 0.161 0.057 5.32 0.030 0.016 0.027	16501 16919 5960 60 3839 2539 2121	0.172 0.176 0.062 0.19 0.040 0.026 0.022	16501 18226 6911 53 4660 3976 2251	0.172 0.190 0.072 3.96 0.049 0.041 0.023
ງ" (ງ") ງ" (ງ" ;) ງ" (ງ" ;) ງ" (ງ" ;) ງ" (ງ" ;) ງ" (ງຶ) ງ້ (ງຶ)	n∕s)		Jg: 1.03 16501 15437 5453 68 2867 1522 2586 -1064	0.172 0.161 0.057 5.32 0.030 0.016 0.027	16501 16919 5960 60 3839 2539 2121 +418	0.172 0.176 0.062 0.19 0.040 0.026 0.022 0.004	16501 18226 6911 53 4660 3976 2251 +1725	0. 172 0. 190 0. 072 3. 96 0. 049 0. 041 0. 023 0. 018
ງ ^ສ ເ ສ ເ ງ ^{ສຂ} (ງ ^{ສ ສ}) ງ ^{ສເ} (ງ ^{ສ ຂ}) ງ ^{ສເ} (ງ ^{ສ ເ} ງ ^ເ (ງ ^ເ) ງ ^ເ (ງ ^ເ)	n/s)		Jg: 1.03 16501 15437 5453 65 2867 1522 2586 -1064	0.172 0.161 0.057 5.32 0.030 0.016 0.027	16501 16919 5960 60 3839 2539 2121 +418	0.172 0.176 0.062 0.19 0.040 0.026 0.022	16501 18226 6911 53 4660 3976 2251 +1725	0.172 0.190 0.072 3.96 0.049 0.041 0.023
3. 3. (1°) 3. (1°) 3. (1°) 3. (1°) 3. (1°) 5. (1°) 5. (1°)	n/s)		Jg: 1.03 16501 15437 5453 65 2867 1522 2586 -1064	3 cm/s 0.172 0.161 0.057 6.32 0.030 0.016 0.027 -0.011	16501 16919 5960 60 3839 2539 2121 +418	0.172 0.176 0.062 0.19 0.040 0.026 0.022 0.004	16501 18226 6911 53 4660 3976 2251 +1725	0. 172 0. 190 0. 072 3. 96 0. 049 0. 041 0. 023 0. 018

Concentrate and tailing flowrates increase with increasing air flowrate at constant T and FT. The higher the aeration rate, the lower the amount of wash water going to the concentrate and the higher the wash water going to the slurry. Thus, the amount of slurry water going to the concentrate is higher at high air flowrates for a constant J_{μ} . Lower $Q_{\mu\nu}$ at lower aeration rate is related to a higher $Q_{\mu\nu}/Q_{\Gamma}$ ratio and a higher net bias flowrate (Q_{μ}) . Bias ratio appears to be similar for both feed flowrates.

Figure 7.13 shows K⁺ concentration versus time at three different wash water addition rates. K⁺ content of concentrate and tailing increases with increasing wash water addition rate at the beginning of experiments (i.e. transient response). The tracer concentration of the concentrate is much higher than that of tailing. There is a very good agreement between predicted tracer contents from Eqs. 7.10 and 7.12 and experimentally measured tracer contents for all water flowrates.

Calculated fractional tracer or wash water recoveries versus time are shown in Figure 7.14. The lower the wash water addition rate, the higher the wash water recovery. As time increases, wash water recovery approaches a constant value (i.e. system reaches to a steady-state condition), which is the actual wash water recovery in the concentrate. In plant operation, this corresponds to dilution of cell content with wash water. After a certain time, which depends on operating conditions, dilution becomes negligible and the system reaches steady-state. In pilot-plant scale tests.

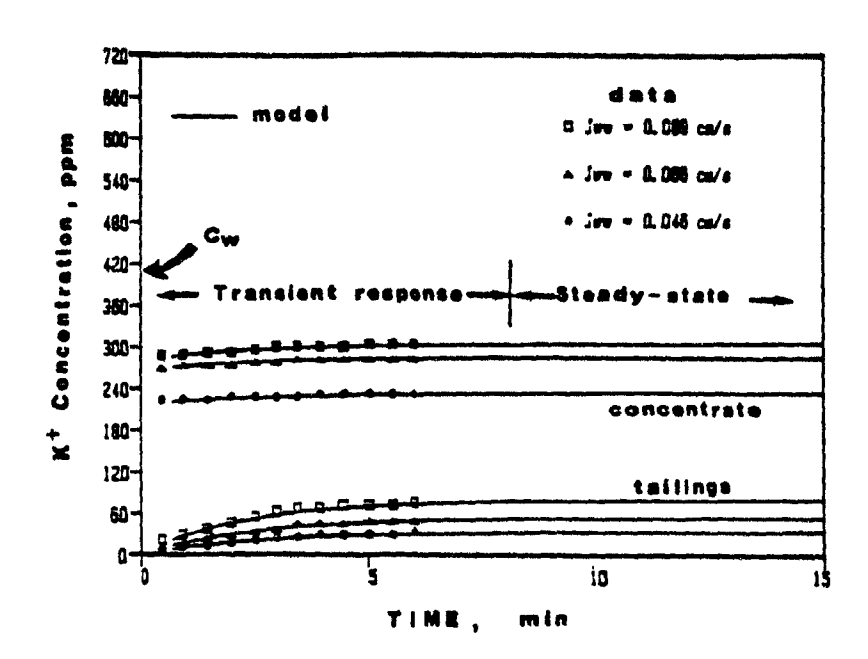


Figure 7.13: Concentrate and tailing K+ concentration versus time at three different Jws (Curves: Eqs. 7.10 and 7.12).

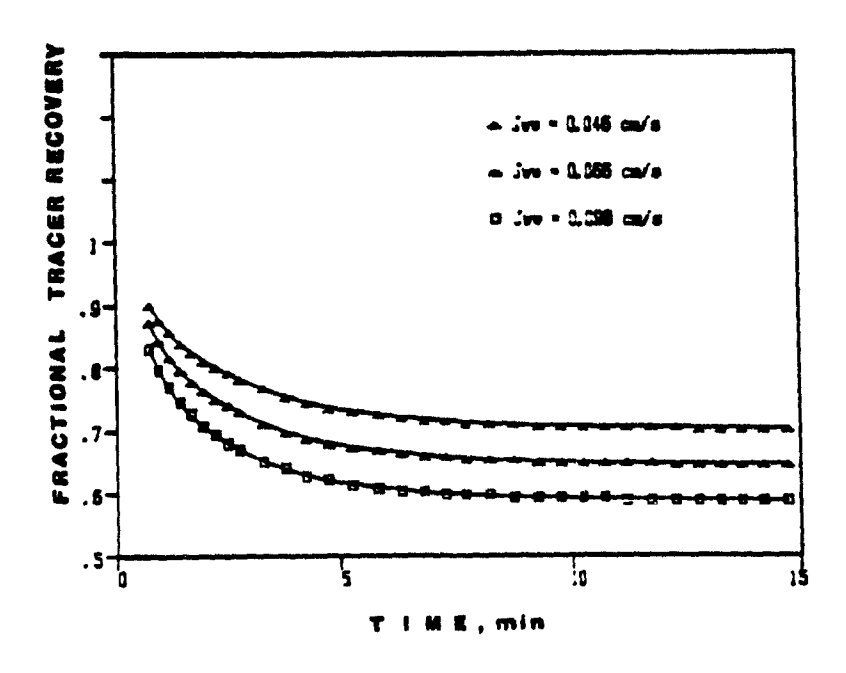


Figure 7.14: Wash water recovery versus time at three different Jws.

(points are calculated values)

it was impossible to reach actual steady-state condition even with the 200 L feed tank used in this study. Therefore, results given here are the transient responses of the system.

7.3.6 Effect of Wash Water on Slurry Water Rejection Using the VEA A typical conductivity versus time response curve is shown in Figure 7.15, for an impulse tracer addition in the slurry phase. The response of electrode 1 shows a perfectly mixed slurry phase with respect to liquid phase. Electrode 2 shows a similar response. Electrodes 3 and 4 are in the middle and top of the froth phase, and show only a very slight increase in conductivity after tracer introduction (Test series 5). Slurry water penetration into the froth is very small.

Figures 7.16a and 16b show conductivity versus time responses for four different J s for the concentrate and tailing streams. For these tests, unfortunately, the sensitivity was very poor, as the mass of tracer added was insufficient to yield large conductivity increases. Tailing conductivity decreases exponentially with time. Without wash water addition, the conductivity decreases slowly due to a high residence time (i.e. tailing flowrate is lower). The fastest decrease in conductivity (i.e. fastest rejection of slurry water) was achieved with the intermediate wash water addition rate. As can be seen from Figure 7.16b, maximum conductivity was achieved without wash water addition in the concentrate. The maximum tracer (slurry water) recovery is obtained in the absence of wash water. The lowest conductivity values were measured at the intermediate J. At low

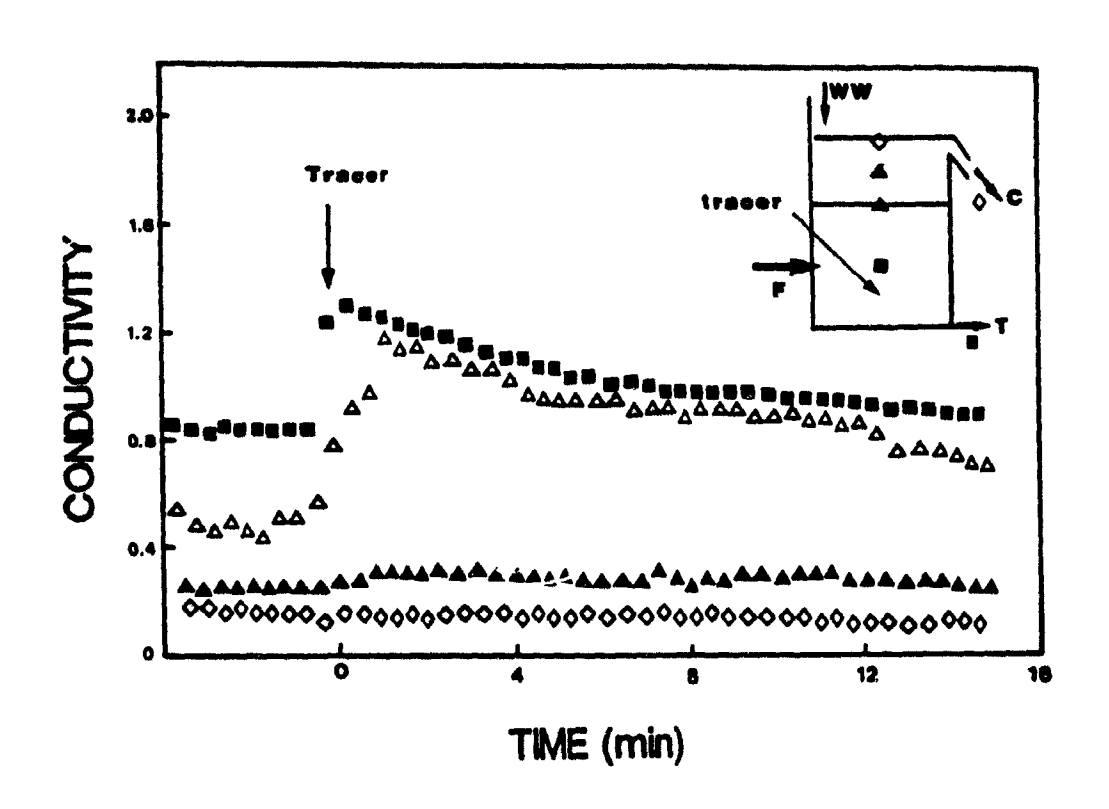
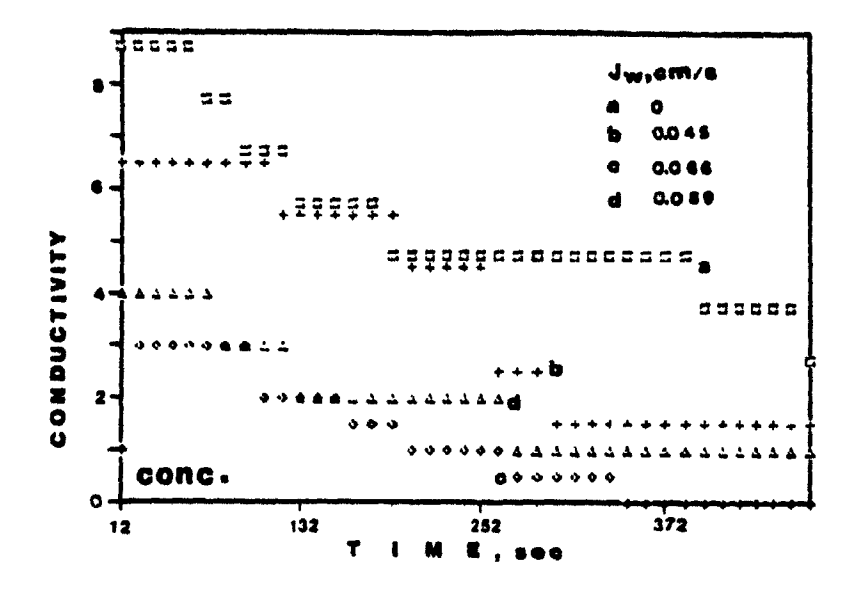


Figure 7.15: Conductivity versus time with the HEA in the impulse test.



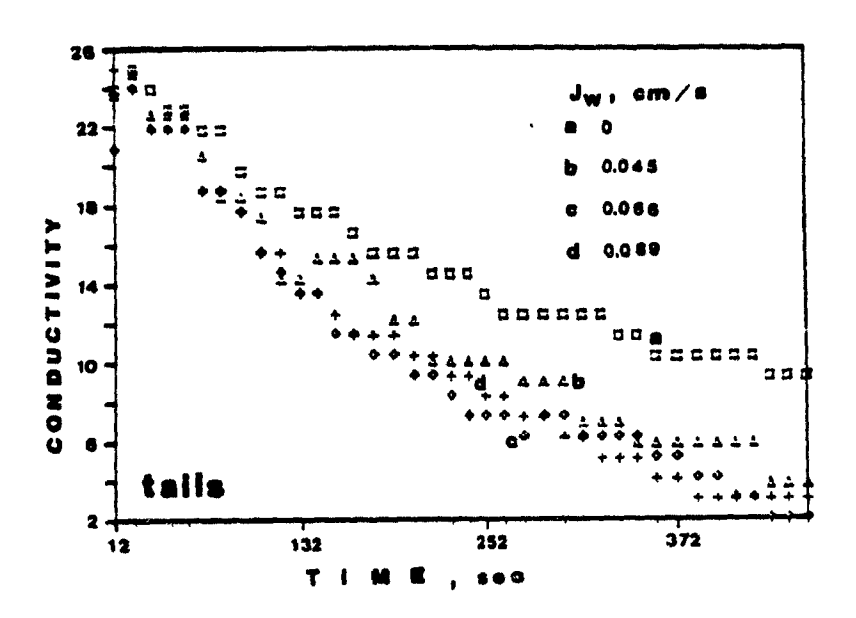


Figure 7.16: Conductivity versus time response curves at different Jws.

and high J_{w} s, the conductivity is slightly higher than the intermediate J_{u} , but significantly lower than without wash water.

7.3.7 Effect of Wash Water and Air Flowrates on Feed Water Rejection

A plot of feed water recovery versus J_{w} at three different J_{q} 's is given in Figure 7.17 (Test series 6). Feed water recovery decreases with increasing J_{w} ; after reaching a minimum, it increases again with increasing J_{w} . Gangue recovery is minimum at the intermediate J_{w} . The lower the J_{q} , the lower the feed water recovery to the concentrate. In the absence of wash water, the feed water penetration is always higher.

Table 7.6 shows the average conductivity readings for some experiments:

Table 7.6: Conductivity readings using the VEA at different wash water and gas rates.

			Electrode		
J _w	J	1	2	3	4
0.045	1.03	64.00	20.13	14.54	5. 13
0.066	1.03	62.52	19.16	12.25	4.82
0.089	1.03	59.80	18.00	14.55	5.63
0.066	0.78	63.76	17.77	11.81	3.62
0.066	0.65	64.96	16.06	10.94	2.35

At constant J_g , the conductivity measured by electrodes 1 and 2 decreases with increasing J_w , which dilutes the pulp tracer content. The minimum conductivity, which corresponds to the lowest feed water penetration, was measured in the froth at the intermediate J_{\perp} .

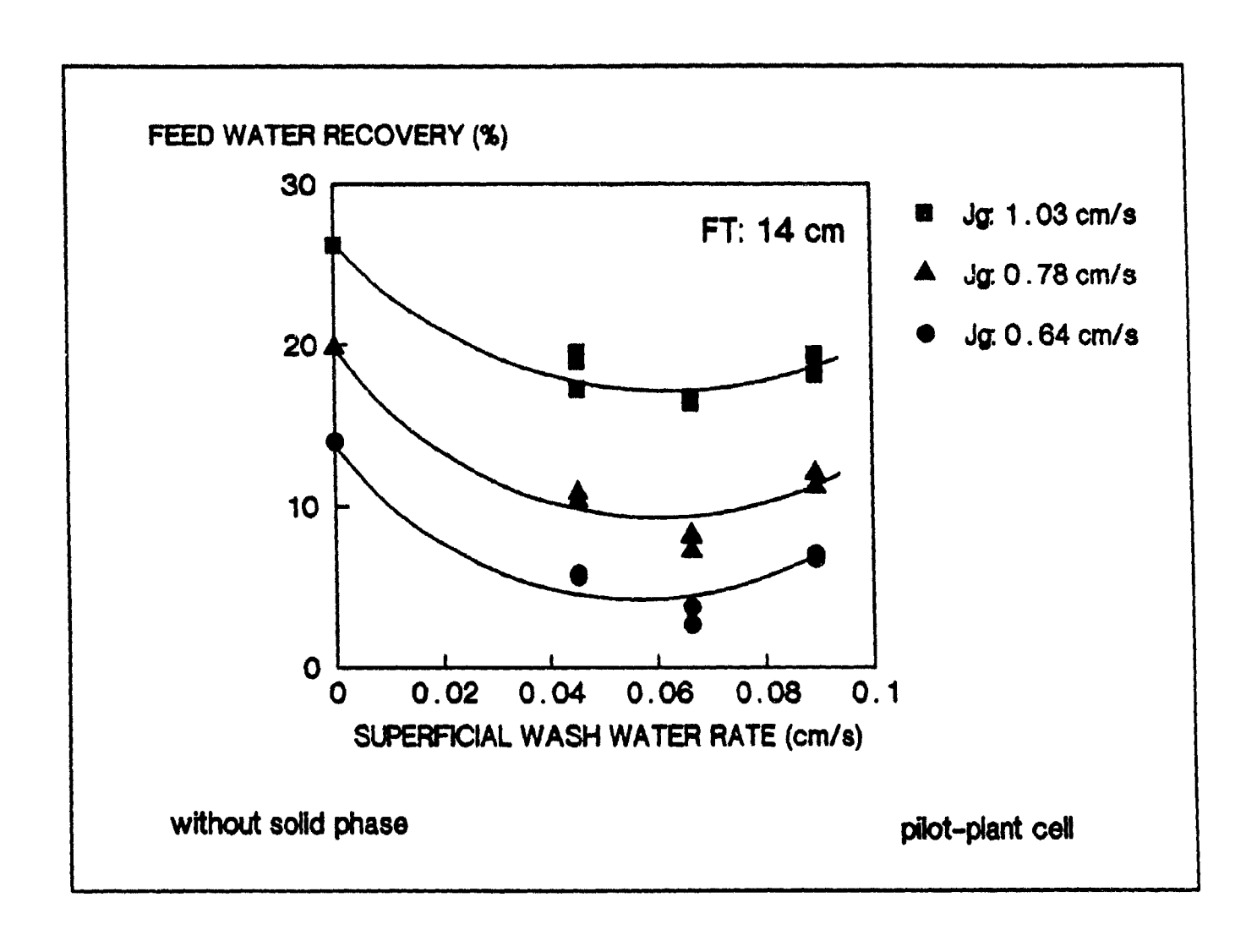


Figure 7.17: Feed water recovery versus superficial wash water addition rate at different aeration rate (from Li assays by AA).

At constant J_w , the higher the J_g , the lower the conductivity in the slurry phase because of increased gas holdup. However, the opposite was observed in the froth, due to increased feed water entrainment with increasing J_g s; at the interface, the same effect is felt, but to a lesser extent.

Figure 7.18 shows concentrate and tailing K^+ concentration as a function of time at three different J_w 's. Full lines were calculated from Eqs. 7.24 and 7.26. Slurry water dilution by wash water occurs very fast at the beginning of the experiment and is then more progressive. The higher the J_w , the lower the tracer concentration in the concentrate and tailing. The agreement between calculated and experimentally measured tracer concentrations is very good.

7.3.8 Estimation of Water Recovery (Q_) in the Pilot-Plant Cell

At constant SH and T, K is constant and J can be determined from the weir equation (3.14) by measuring H and ε_1 , obtained from conductivity measurements.

For the pilot-plant scale cell, K_c determined from the slope of Q_c versus WH^{1.5}. ϵ_1 was 0.0125. Figure 7.19 shows experimentally measured versus predicted J_c s. There is again a reasonably good agreement between experimental and predicted J_c s within a $\mp 15\%$ error limit. A similar agreement was obtained for the laboratory cell in Chapter 3.

K CONCENTRATION (ppm)

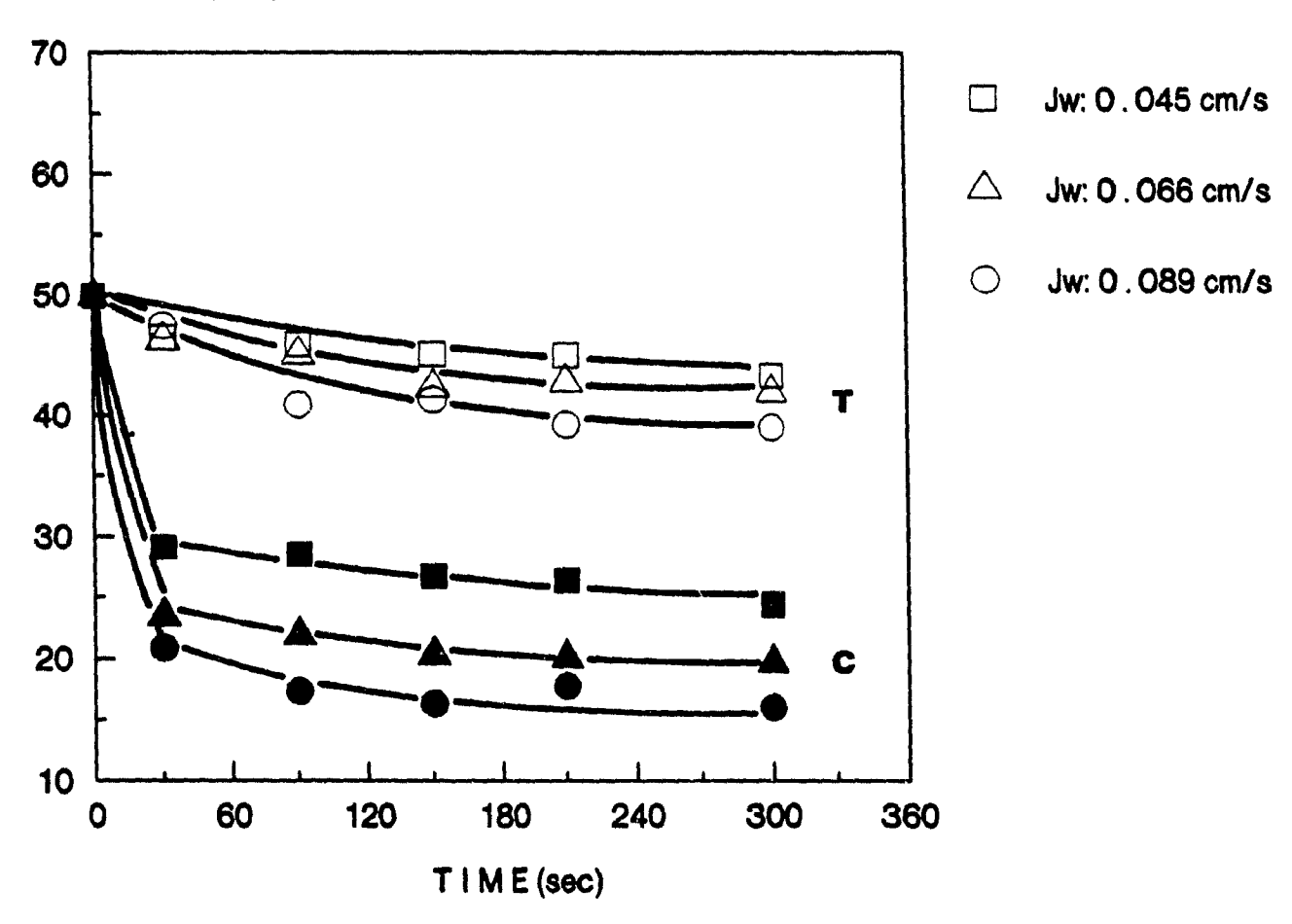


Figure 7.18: K+ concentration versus time at three different Jws.

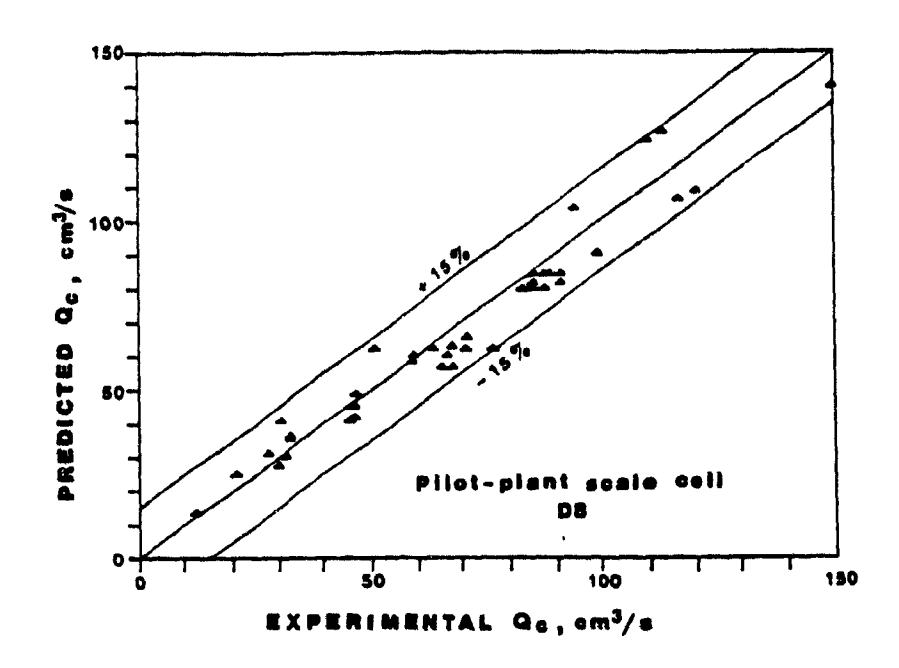


Figure 7.19: Experimental versus predicted Qc for the pilot-plant scale cell.

4. Conclusions

- a. Wash water significantly increases liquid content of the froth phase. The warmer the wash water, the higher the liquid drainage in the froth phase. Warm wash water decreases gangue entrainment more than cold wash water due to increased inter-bubble water mobility.
- b. Measurements with the HEA revealed that froth conductivity increases with increasing $J_{\underline{w}}$ due to an increased liquid content in the froth phase and more homogeneous wash water distribution.
- c. At constant J_w , increasing J_g increases liquid content in the froth and yields a less homogeneous wash water distribution.
- d. The HEA can be used to compare on-line wash water distributors and monitor froth washing efficiency. Noise in conductivity readings are due to froth disturbances.
- e. Slurry water penetration into the froth and then into the concentrate is minimum at the intermediate J_w . The higher the J_w , the higher the amount of wash water going to the concentrate and slurry. Increasing J_g at constant FT and J_w leads to significantly higher feed water recovery in the concentrate.
- f. Impulse tracer tests verified that slurry water rejection is maximum at intermediate $J_{\rm w}$ (0.05-0.07 cm/s) and minimum in the absence of wash water.

- g. Transient tracer concentrations in the tailing and concentrate can be predicted by Eqs. 7-10 and 7-12, and 7-24 and 7-25 for tracer tests.
- i. Water recovery in the pilot-plant cells can be predicted reasonably well with the weir Eq. 3.14. Two parameters (K and ε) must be determined experimentally.

CHAPTER 8

LABORATORY AND PILOT-SCALE FLOTATION TESTS
WITH THE STRATHCONA CU-NI ORE TO ASSESS THE POTENTIAL
OF WASH WATER ADDITION IN MECHANICAL FLOTATION CELLS

Introduction

In previous chapters, laboratory scale results using pure gangue were reported. Successful cleaning of froth by wash water addition improved the flotation process and reduced gangue entrainment up to 60%.

This chapter assesses the potential of wash water addition in laboratory and pilot-plant scale mechanical flotation cells using the Strathcona Cu-Ni ore. Results will be used to select the plant stream most likely to respond to froth washing.

8.1. Defining the Problem

One of the major problems for the Strathcona concentrator appears to be the separation efficiency between Cu/Po, Ni/Po, and Ni/Cu. It is expected that even small improvements in separation efficiencies would generate significant savings.

Concern for the environment as a result of damage caused by acid rain has focussed a lot of attention on the SO_2 emissions; governmental regulations are increasingly stricter. Reduction of SO_2 emissions from the smelter can be primarily achieved by rejecting more pyrrhotite (Po) to the mill tailings. Non-sulfide gangue reduction is also important. The cost of additional nickel losses is then partially offset by savings in smelting costs.

8.1.1 Geology of the Ore Body

The Cu-Ni deposits of the Sudbury basin in north-eastern Ontario represent the largest single source of Ni in the world as well as being one of the richest complex sulfide ore bodies. Besides Cu and Ni, the ore also contains significant amounts of cobalt and precious metals and is the largest source of platinum in the Western hemisphere outside of South Africa. The Cu and Ni sulfides represent only one quarter of the total sulfides present; the balance consists of nickelliferrous Po, which contains 12% of the total Ni and about 75% of the total sulfur in the ore.

8.1.2 Falconbridge's Nickel Operations in Sudbury

Ore extracted from five mines in the Sudbury area contains between 1 and 2% Ni and 0.8 and 1.1% Cu. The Strathcona mill processes a Cu-Ni sulfide ore whose major mineral constituents are given below.

Primary Minerals:

Pentlandite (Fe, Ni)₉.S₈ Chalcopyrite CuFeS₂

Nickelliferrous Pyrrhotite (Fe₇S₈)

contains 0.2 to 1.2% Ni

monoclinic pyrrhotite (magnetic)-----magnetic separation hexagonal pyrrhotite (non magnetic)-----floats well in natural pH

Pyrite FeS₂

Secondary Minerals:

Cobalt, selenium, silver, platinum, palladium, rhodium, iridium, and ruthenium.

Gangue Minerals:

Feldspar, quartz, mica, talc, and chlorite.

All these may occur as disseminations in the host rock, as stringers, or as massive sulfides with varying amounts of rock inclusions.

8.1.3 Strathcona Mill

The Strathcona mill flowsheet is shown in Figure 8.1. It consists of three separate grinding circuits, feeding two flotation circuits. Each flotation circuit treats approximately 4100 ton per day. The crushing, concentrator, and tailing fill plants are operated from one central control room making use of numerous sensors and actuators, an X-ray fluorescence analyzer, and an on-line digital computer.

Ore is ground to 60% -74 µm (200 mesh) to achieve liberation. A simplified flotation flowsheet is shown in Figure 8.2. In this operation, a bulk Cu-Ni concentrate is obtained from the primary rougher circuit using 14 g/t (0.031 lbs/t) Dowfroth 250 and 25 g/t (0.056 lbs/t) NaIPX at a pH of 9.2 adjusted with lime. The main objective is to recover a good bulk Cu-Ni concentrate, and leave as much Po behind as possible.

The Cu-Ni concentrate is separated into Cu and Ni concentrates by floating the Cu minerals, while depressing Ni and iron sulfides with lime at a pH of 12 and small amounts of cyanide. The Cu cleaner circuit produces a final Cu concentrate at 29-30% Cu. The Ni content should be less than 0.6%, and there should be virtually no Po.

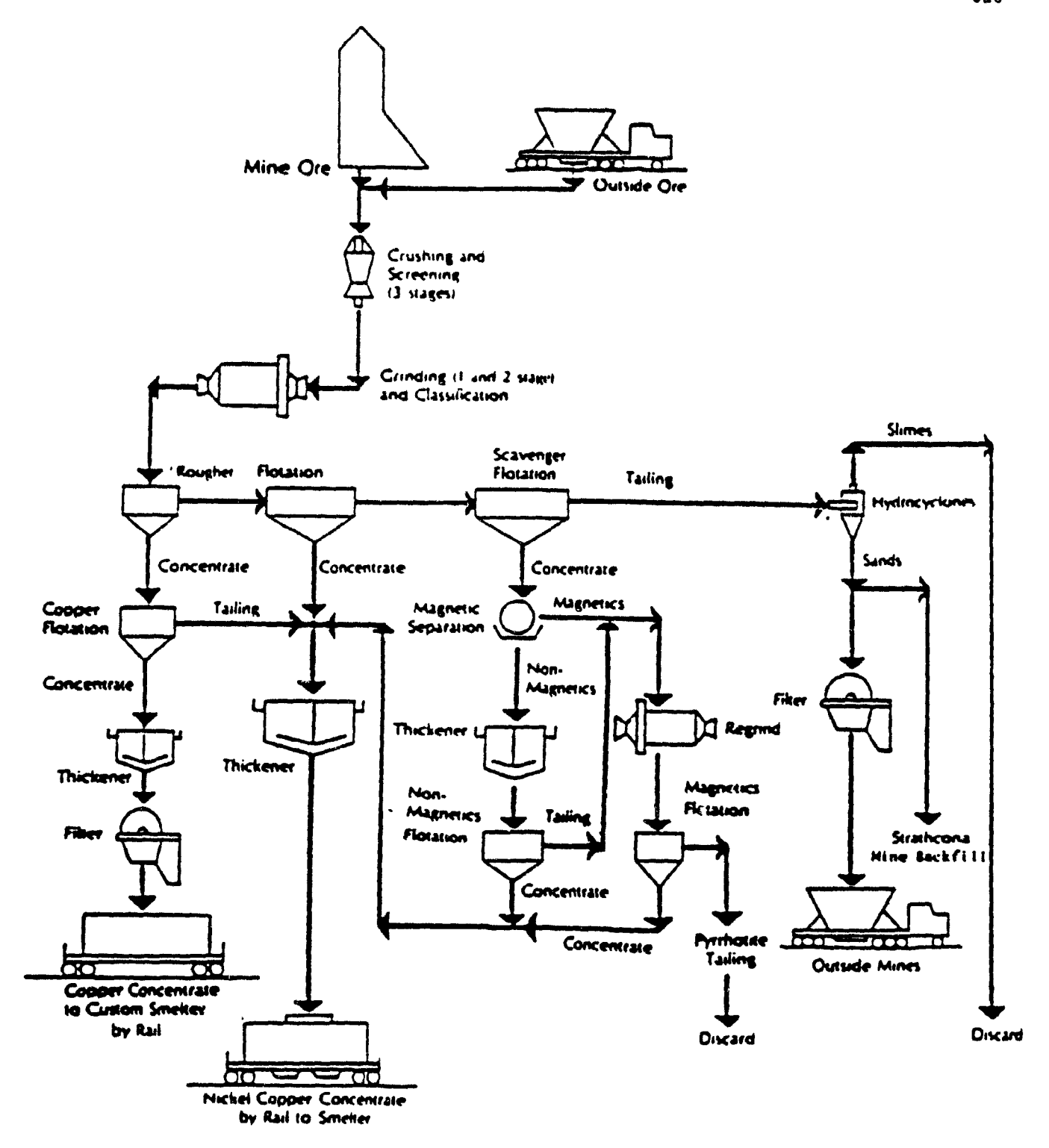


Figure 8.1: Overall Strathcona concentrator flowsheet.

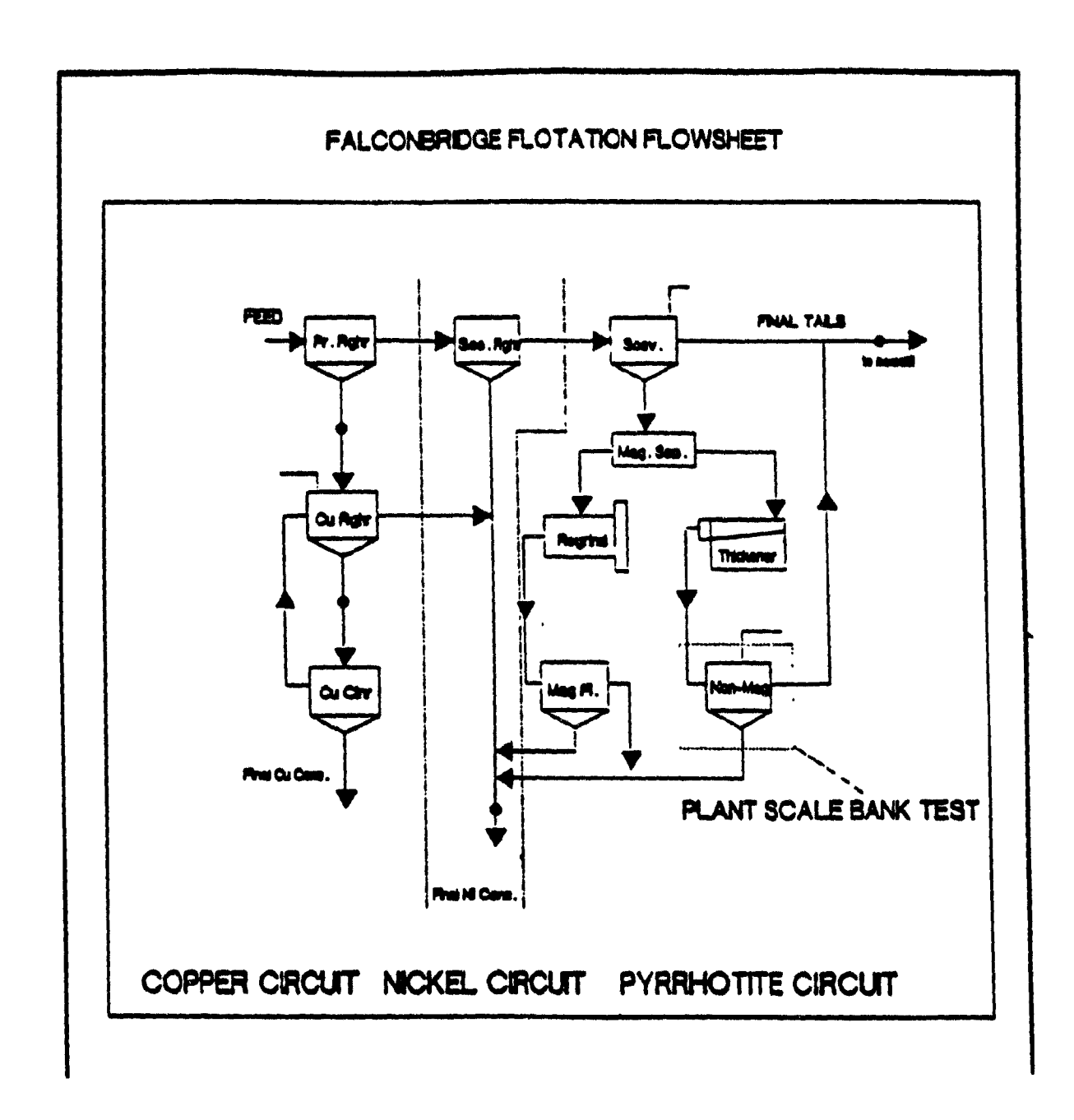


Figure 8.2: Simplified flowsheet of the Strathcona flotation circuit.

(Circles show feed sample points)

The primary rougher tails are floated for Ni in the secondary rougher circuit at a pH of 9.2. Its concentrate, which should contain little Cu and Po, is combined with the Cu rougher tails and shipped to the Falconbridge smelter by truck, after thickening.

The secondary rougher tails are scavenged for nickelliferrous Po at a pH of 8.2 adjusted by H_2SO_4 . In this circuit Po is activated by $CuSO_4$. The scavenger concentrate is fed to two banks, each with 1000 gauss Eriez magnetic separators (0.9m*1.8m). The magnetic product is reground to 80% $-45\mu m$ (325 mesh) and then floated in the mag circuit. The concentrate is combined with the Cu-Ni concentrate and the tails are discarded.

The non-magnetic fraction is first thickened and then floated to recover nickelliferrous Po at a pH of 8.2 using NaIPX; the tails are sent to the backfill plant. The non-magnetic circuit contains large amounts of easily floating gangue particles, some of which are recovered into the non-magnetic concentrate.

8.2 Experimental

8.2.1 Set-up

In this study, a laboratory scale flotation cell (6.5 L), a flotation column (2.3 L), and a pilot-plant scale flotation cell (65 L) were used to evaluate the potential of wash water addition for the Strathcona mill. Experimental conditions are summarized in Table 8.1.

TABLE 8.1: Operating conditions of the flotation cells, and column.

LABORATORY FLOTATION MACHINE

Machine : Modified Denver D1

Cell : Plexiglass, (15*15*32 cm)

FT : 4 cm SH : 30 cm RPM : 1500 J : 0.6 cm/s

J : 0 - 0.11 cm/s

Distributor : Spiral

LABORATORY FLOTATION COLUMN

Column : Plexiglass, (dia: 3.81 cm; height: 200 cm)

FT : 30 cm

SH : 170 cm

J : 1.2 cm/s

J : 0.8 cm/s

Sparger : Ceramic

Distributor : Circular copper pipe

PILOT-PLANT SCALE FLOTATION MACHINE

Machine : Denver D8

Cell : Plexiglass, (40*40*45 cm)

FT : 9 - 15 cm

SH : 37 cm

RPM : 600 rpm

J : 1.03 cm/s

J : 0 - 0.089 cm/s

Distributor : Perforated pipe and/or spray nozzle

8.2.2 Samples

For this study, four different samples were provided by Falconbridge's Strathcona mill (see Figure 8.2).

- a. Primary rougher concentrate (PRC)
 (combined concentrate from first 2 banks A, B, C, and D rows at #5 surge tank)
- b. Combined (final) Ni concentrate (CNC of FNC) (#4 thickener U/F going to #13 tank)
- c. Final tails (FT)
 (cyclone O/F)

d. Cu rougher concentrate (CRC)

Samples were received from the Strathcona concentrator in pails. Wet samples were kept in closed double-plastic bags to minimize the oxidation of Pe, which happens easily oxidize in air. Before each laboratory test, the required mass of feed was dried in the oven and then repulped to the desired density. For the pilot-plant scale tests, the copper rougher concentrate sample as received was well agitated and then split in two, to be used for two test series; before each series, percent solids was adjusted in the feed tank.

Samples were assayed by the Metallurgical Technology Centre (MTC) of Falconbridge. Ni, Cu, S, and Gn assays of the feed samples are given in Table 8.2.

Elemental grades were converted into mineral grades using the following empirical equations developed at Falconbridge:

```
Pentlandite = 2.8*Ni(%) - 0.045 (S(%) - Cu(%))

Pyrrhotite = 2.55*S(%) - 2.58*Cu(%) - 2.33*Ni(%)

Chalcopyrite = 2.9*Cu(%)

Nonsulfide Gangue = 100 - (pent. + chalco. + pyrrho.)
```

The particle size distributions and sample densities used in this study were determined using a cyclosizer and a null picnometer, respectively; they are shown in Table 8.3.

TABLE 8.2: Ni, Cu, and S assays of feed samples.

	N1 (%)	Cu(%)	S(%)	Gn(%)
Primary Rougher Conc. (PRC)	12.3	10.4	31.2	12.3
	12.1	10.4	30.1	15.1
Combined Ni Conc. (CNC of FNC)	6.9	1.2	25.0	33.7
	6.5	0.8	26.6	30.1
Cu Rougher Conc. (CRC)	3.0	22.8	29. 4	16.6
	3.0	22.6	29. 1	17.4
Final Tails (FT)	0.2	0.1	0.6	98.4
Artificial Mixture (calc.) Artificial Mixture (exp.) (PRC + FT)	10.1	8.5	25.6	27.9
	11.4	8.7	25.5	27.6
Artificial Mixture (exp.) (PRC + FT)	10.4	8.8	23.3	28.6

TABLE 8.3: Particle size distribution and density of the samples used.

Size (μm)	% retained	% finer	density (g/cm ³)
	Primary Rougher	Concentrate	(PRC)
+ 34.7	17.42	82.58	
- 34.7 + 21.5	27.40	55. 18	
- 21.5 + 14.9	12.98	42.20	4. 18
- 14.9 + 10.1	9.68	32.52	
-10.1 + 7.3	6.28	26.24	
- 7.3	26.24		
	Combined Ni	Concentrate (CNC)
+ 37.1	19.74	80.26	
- 37.1 + 22.9	26.40	53.86	
- 22.9 + 16.1	10.68	43.18	3.87
- 16.1 + 10.8	8.02	35.16	
-10.7 + 7.8	5.40	29.76	
- 7.5	29.76		
	Final	tails (FT)	
+ 39.6	2.88	97.12	
- 39.6 + 24.5	3.83	93.29	
- 24.5 + 17.1	10.83	82.46	3.50
- 17.1 + 11.5	17.03	65.43	
- 11.5 + 8.4	13.53	51.90	
- 8.4	51.90		

8.2.3 Test Procedure

8.2.3.1 Laboratory Scale Tests

Two different types of experiments were performed using six different samples:

a. determine the effect of superficial wash water rate on overall metallurgical performance at constant feed rate; the tails flowrate was used to keep slurry level constant.

b. generate grade-recovery curves by changing residence time at constant wash water rate; slurry level was controlled by feed rate.

Table 8.4 shows the experimental conditions for test 1 to 4. In test 1, the effect of wash water superficial rate and wash water temperature on overall metallurgical performance was determined using the artificial mixture of primary rougher concentrate and final tails with the laboratory flotation cell.

The main objective was to understand better the effect of wash water on the flotation behaviour of each individual mineral. Experiments were started without wash water addition, then wash water flow rate increased to the desired level. Timed concentrate and tailing samples were collected to determine grade and recovery of each mineral. None of the minerals were depressed in these tests, as the main objective of the corresponding plant stage is to achieve a good bulk Cu-Ni flotation.

In test 2, grade-recovery curves were determined with and without wash water in the laboratory cell and compared with the laboratory flotation column using the artificial mixture. The main objective of this comparison is to evaluate the performance of units in parallel for different minerals. For each unit, the best operating conditions were used (i.e. J_q , J_w , FT, etc). Residence time can be increased by decreasing tailing flowrate. Since the slurry level was kept constant and adjusted by feed flowrate, an increase in residence time required a reduction in feed flowrate. Solid and water recoveries increase with increasing residence time in the cell.

TABLE 8.4: Experimental conditions for laboratory tests (1-4).

TEST 1 : 4.5 kg PRC + 1 kg FNC Percent Solid: 10% : 9.2 with lime pН J : 0.6 cm/s FT : 4 cm Frother : 14 g/t Dowfroth 250 : 25 g/t NaIPX, : 23°C Collector Tpulp : 23°C and 45°C Tww TEST 2 : 2.25 kg PRC + 0.5 kg FNC Percent Solid: 5.2% рH : 9.2 J : 0.6 cm/s Jw : 0.04 cm/s FT : 4 cm : 25 g/t NaIPX Collector : 14 g/t Dowfroth 250 Frother TEST 3 Sample : FNC Percent Solid: 5% : 9 - 9.2 pН J : 0.6 cm/s Jw : 0 - 0.076 cm/sFT : 4 cm SH : 30 cm Collector : 25 g/t NaIPX Frother : 14 g/t Dowfroth 250 TEST 4 Sample : FNC Percent Solid : 5% : 9 - 9.2 pН J : 0.6 cm/sJ : 0.05 cm/sFT : 4 cm

SH

Collector

Frother

: 30 cm

: 25 g/t NaIPX

: 14 g/t Dowfroth 250

The effect of J_{w} on final Ni concentrate flotation was investigated at constant feed flowrate (Test 3). pH was 9.2 to favour Pe flotation. In test 4, The grade-recovery curve was determined using the final Ni concentrate as feed.

8.2.3.2 Pilot-Plant Scale Tests

The effect of wash water was investigated using PRC, CRC, and FNC as feed. Experimental conditions are summarized for test series 5 to 8 in Table 8.5. Percent solids were much lower than the corresponding plant operation. In test 9, the effect of superficial wash water rate on gangue recovery was determined using silica flour.

TABLE 8.5: Conditions for pilot-plant test series 5 to 9.

TEST 5 : 28.5 kg PRC Percent Solid: 7.2% : 12.19 with lime (sample as received 7.2) pН J : 1.03 cm/s FT : 9 cm : 25 g/t NaIPX Collector Frother : 14 g/t Dowfroth 250 Depressant : 350 g/t NaCN TEST 6 Sample : CRC Percent Solid: 8.9% : 11.8 pН Ĵ : 1.03 cm/s FT : 15 cm Frother : 14 g/t Dowfroth 250 TEST 7 Sample : CRC Percent Solid: 14.68% : 11.8 pН J : 1.03 cm/s FT : 15 cm Frother : no TEST 8 Sample : FNC Percent Solid: 5% : 9.2 with lime (sample as received 8.3) рH Jg : 1.03 cm/s FT : 12 cm Collector : 25 g/t NaIPX Frother : 28 g/t Dowfroth 250 TEST 9 Sample : silica flour Percent solid: 10% J : 1.03 cm/s J $: 0 - 0.09 \, \text{cm/s}$ FT : 9 cm Frother : 10 ppm Dowfroth 250

8.3 Results and Discussion

8.3.1 Laboratory Scale Tests

Table 8.6 shows the effect of wash water on metallurgical performance for test 1. Without wash water addition, Ni and Cu recoveries are very low. The concentrate Ni grade is lower—than the feed; however, the Cu grade is almost doubled. Wash water significantly increases—Ni, Cu, and Po recoveries, which indicates that all sulfides are hydrophobic, but gangue is not. Despite a decrease in residence time with increasing wash water, recovery increases due to froth stabilization. The overall effect is an increase in Ni and Po grade, a slight decrease in Cu grade and a significant drop in non-sulfide gangue content. The gangue profile confirms the previous results. In these tests, the main objective is to achieve good bulk Ni-Cu flotation—i.e. good Ni and Cu recovery. Bulk Ni-Cu recovery significantly increases with wash water addition.

Table 8.7 shows the effect of superficial wash water rate and temperature. In the absence of wash water, Ni and Cu recoveries are again very low; Cu grade is maximum and Ni grade minimum. The recovery of pentlandite almost triples with wash water addition; that of chalcopyrite more than doubles. The net effect is a slight increase in the concentrate Ni grade and a slight decrease in Cu grade. Cangue recovery is halved with wash water. The effect of wash water flowrate is small between 0.076 and 0.110 cm/s; the higher rate would not be attractive, because of the increased water requirement and slurry dilution. The

effect of wash water temperature is also small: warm water slightly increases the recovery of all hydrophobic species. Heating wash water is not attractive for this feed.

TABLE 8.6: Effect of wash water addition on metallurgical performance. (Po: pyrrhotite, Gn: non-sulfide gangue).

			GRADE			RECOVERY			
	J	Ni	Cu	Po	Pe	Ch	Po	Gn	
-	cm/s	(%) (%) (%) (%)	(%)	(%)	(%)				
FEED (calc)	10.1	8.5	19.9					
Conc.	0	9.9	17.4	17.8	24.0	44.0	21.0	5.1	
Conc.	0.061	12.0	15.3	19 5	35.5	59.0	32.5	2.7	
Conc.	0.076	12.9	14.5	20.2	49.0	68.5	46.0	2.5	
Conc.	0.110	13.2	13.6	20.8	51.0	69.0	47.0	4.1	

TABLE 8.7: Effect of wash water addition rate and temperature on metallurgical performance. (c: cold wash water 23°C, w: warm wash water 45°C, Tpulp: 23°C).

		GRADE		R	ECOVERY		
J	Ni	Cu	Po	Рe	Ch	Po	Gn
cm/s	(%)	(%)	(%)	(%)	(%)	(%)	(%)
FEED (exp)	11.4	8.7	16.0				
Conc. 0	9.5	18.5	16.8	15.0	30.5	14.0	5.0
Conc. 0.076c	12.9	15.1	16.9	41.0	57.0	34.5	2.1
Conc. 0.076w	11.5	16.6	17.7	42.0	61.0	38.5	2. 1
Conc. 0.110c	13.1	14.8	18.7	43.0	62.0	38.5	1.9

The low Cu and Ni recoveries are due to a low residence time in a single flotation cell --i.e. with much short-circuiting. The amount of solid and water going to the concentrate increases with

increasing wash water addition rate, which leads to an increased recovery, despite the lower residence time. Percent solids in the concentrate and tailing are lower with wash water (Table 8.8).

Figure 8.3 shows Ni and Cu grade-recovery curves along with Pe and Po/Gn recoveries with and without wash water. Wash water increased both the Ni and Cu recoveries at a higher Ni and lower Cu grade. In the insert recovery-recovery graph, the diagonal line shows no separation between species. Since the Po data points show little separation, either there is a locking or selectivity problem. Gn is mainly free due to the presence of artificially mixed final tails.

TABLE 8.8: Effect of wash water on slurry residence time (τ) , % solid and solid and water recoveries.

				CONCENTRATE				
J cm/s	τ	% so	% solids		water rec			
	min	Conc. Tail		(%)				
Feed		1	0					
0.000	2.86	39.5	8.0	15.0	4.0			
0.061	2.60	25.0	6.0	31.5	11.5			
0.0 76c	2.58	18.8	5.5	41.0	16.3			
0.076w	2.38	15.5	4.5	38.5	9.5			
0.110c	2.37	15.5	4.5	42.7	17.0			
0.110w	2.28	12.0	3.7	39.5	12.0			

Figures 8.4a and 4b show grade-recovery curves for the laboratory column and cell with and without wash water addition for test 3. Cu and Ni grade-recovery curves are given in Figure 8.4a. The best Cu grade-recovery curve was obtained with the

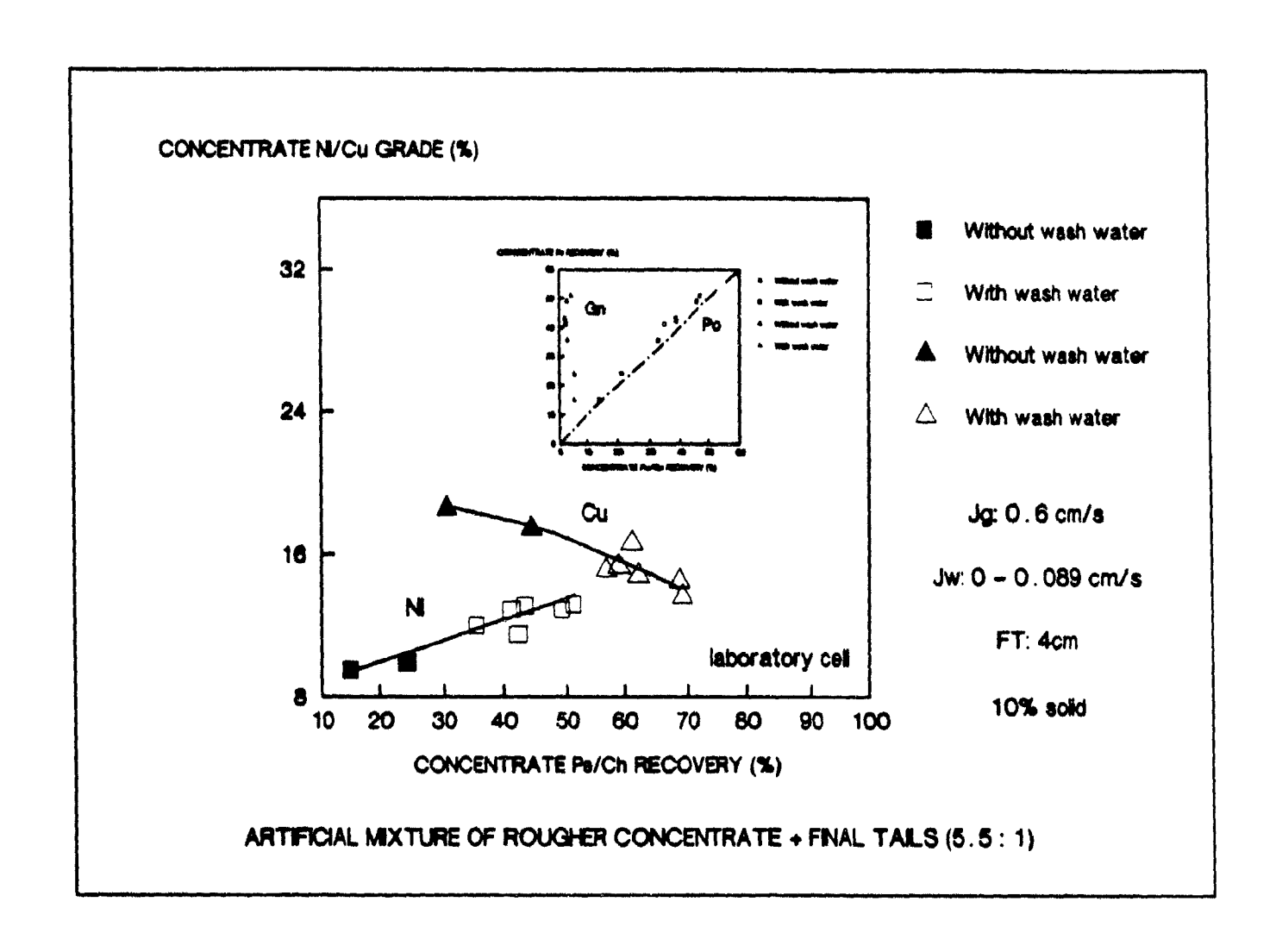
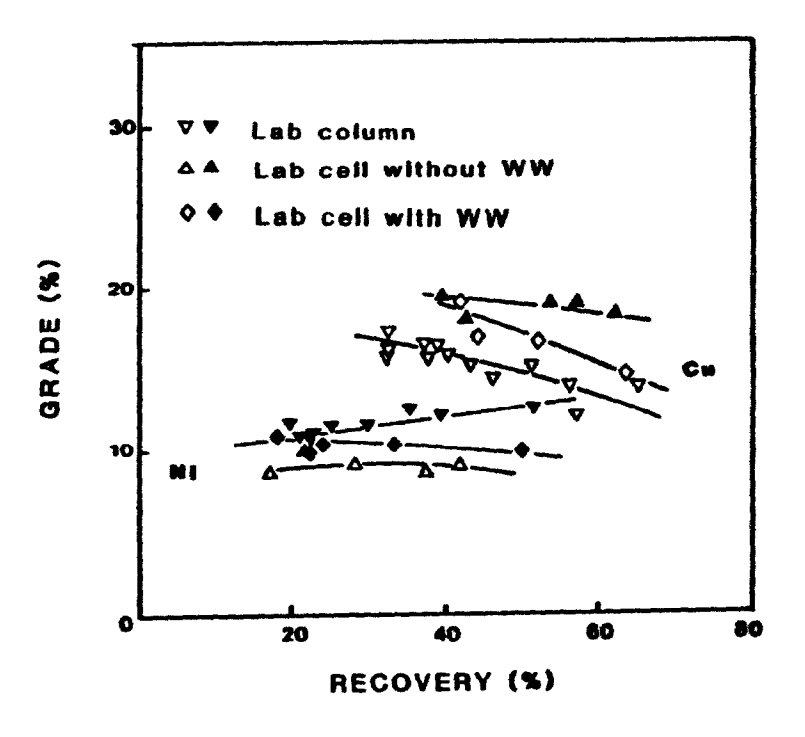


Figure 8.3: Grade-recovery and recovery-recovery curves for Ni, Cu, Po and Gn using the artificial mixture.



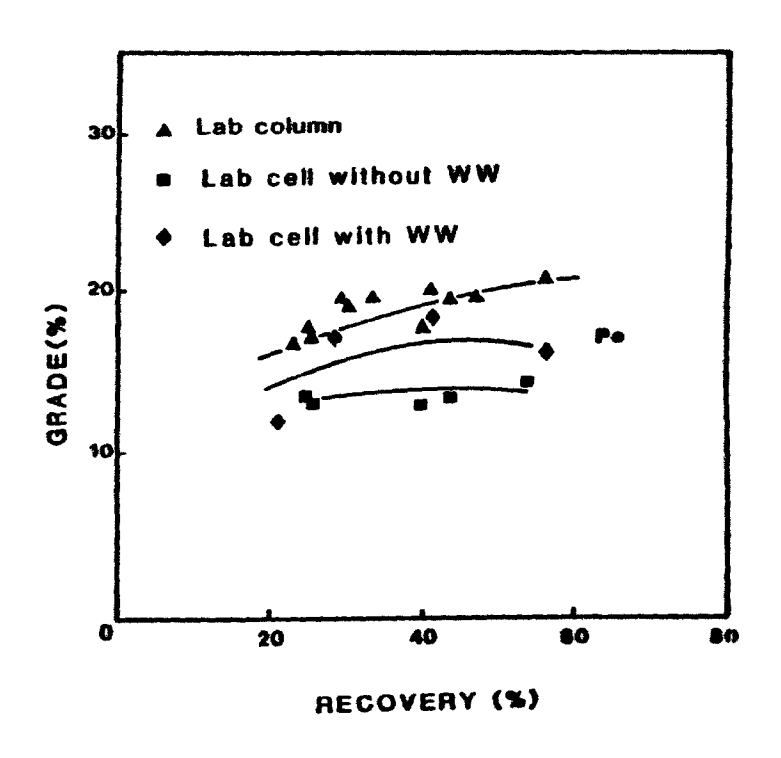


Figure 8.4: Grade-recovery curves for Cu, Ni, and Po for the laboratory cell with and without wash water addition and for a laboratory flotation column.

laboratory cell in the absence of wash water addition. With wash water, performance was slightly poorer because wash water floats Pe-Po and lowers Cu grade. Column flotation yielded the worst performance for Cu in these particular tests. However, a better grade-recovery curve was obtained with the column for Ni. The laboratory cell without wash water gave the worst grade-recovery curve for Ni. Addition of wash water improved Ni grade recovery at the expense of the Cu grade. It is quite possible that differences in hydrodynamics cause the column to be less selective: better froth recovery or lower detachment from bubbles for weakly hydrophobic particles (i.e. pyrrhotite). result is that the column yields much faster flotation rates, but with decreased selectivity. The performance of the cell with washed froth is intermediate between that of the cell without wash water and the column. This suggests that the main differences are in the froth, rather than the slurry phase.

In flotation, grade and recovery are significantly dependent on residence time in the cell. Residence times were varied from 3.9 to 9.1 min without wash water, from 2.8 to 10.2 min with wash water, and 1.3 to 2.8 min for column flotation (higher residence times could not be achieved due to the column height). Figures 8.5a, b, c, and d show the effect of pulp residence time in the cell and column on mineral recoveries. All data points were plotted and straight lines were drawn using linear regression. Cu, Ni, and Po do not behave much differently in the three systems; gangue does.

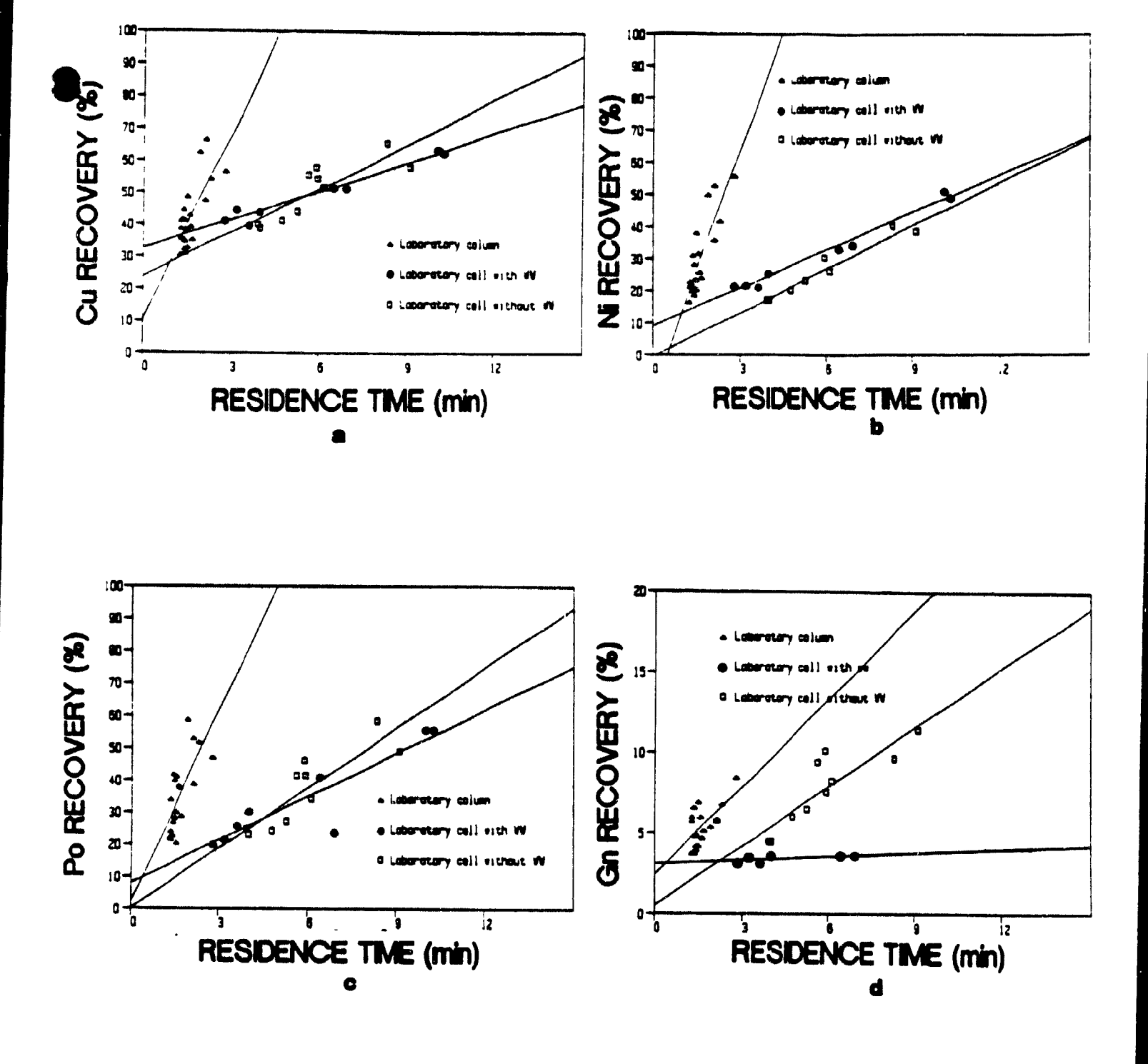


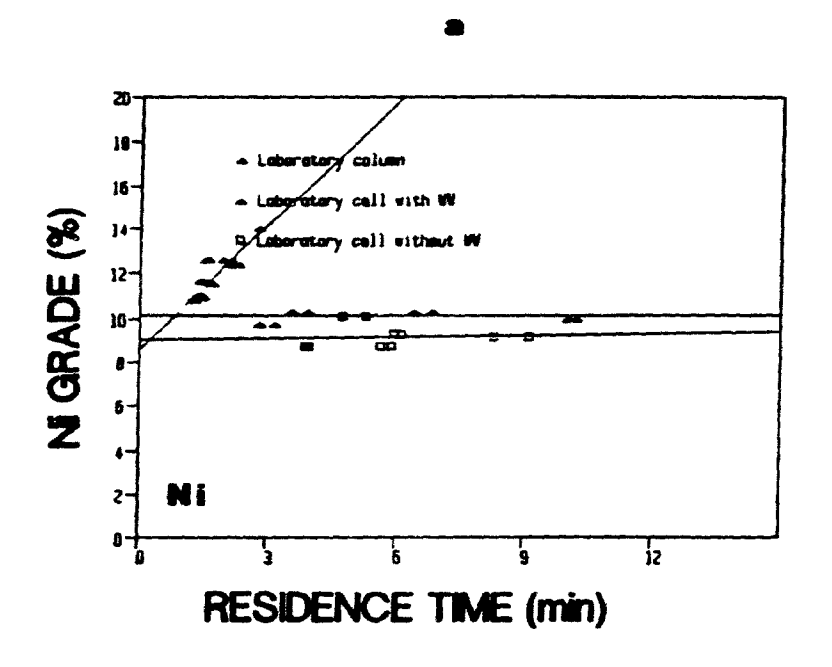
Figure 8.5: Recovery versus residence time for Cu, Ni, Po, and Gn using artificial mixture sample for laboratory cell and column.

Flotation column recoveries for Cu, Ni, and Po sharply increase with increasing residence time. In the mechanical cell, increases in recovery are more gradual, because of slower flotation kinetics.

Figure 8.5d clearly shows that cleaning (i.e. gangue rejection) is more effective in the cell with wash water than in the column. This result is surprising, as the column would be expected to outperform the mechanical cell, even with wash water. This suggests that either gangue has some residual hydrophobicity, or that the quiescent environment of the column does not achieve full dispersion.

The effect of residence time on Ni and Cu grades is given in Figures 8.6a and b. It is most important in the flotation column: Ni grade increases and copper grade decreases sharply with increasing residence time. In the cell, residence time has little effect on nickel grades. Higher Ni grades were obtained with wash water. Copper grades decrease with increasing residence time, but to a lesser extent than in the column. This is largely due to an increase in Po recovery.

Figure 8.7a shows the Cu recovery versus Ni recovery for the laboratory cell and column. The laboratory cell performs a better Cu-Ni separation than the laboratory column. The best Cu-Ni separation (i.e. selectivity) occurred without water addition in the laboratory cell.



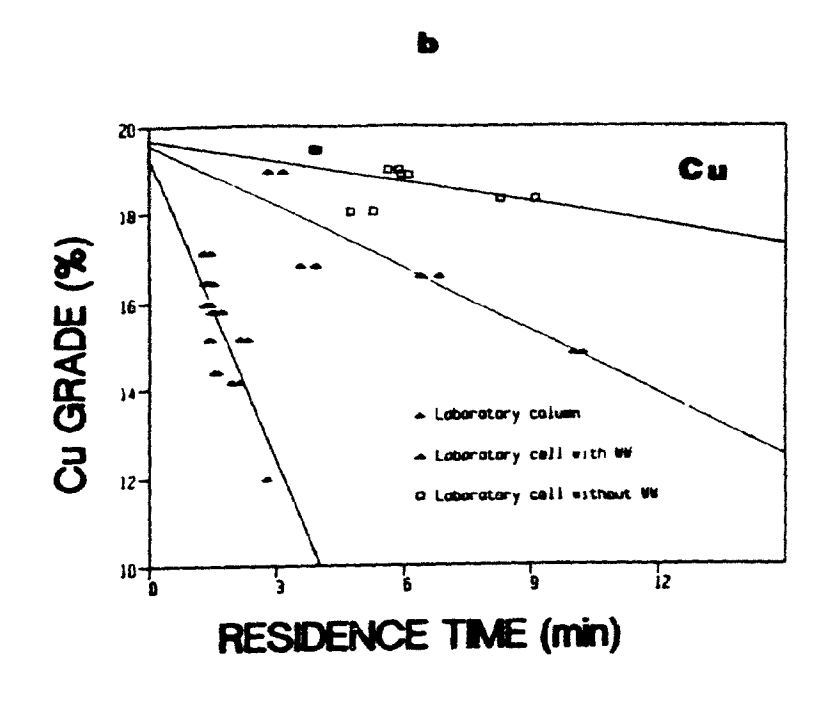


Figure 8.6: Grade versus residence time for Ni and Cu with laboratory cell and column using artificial mixture.

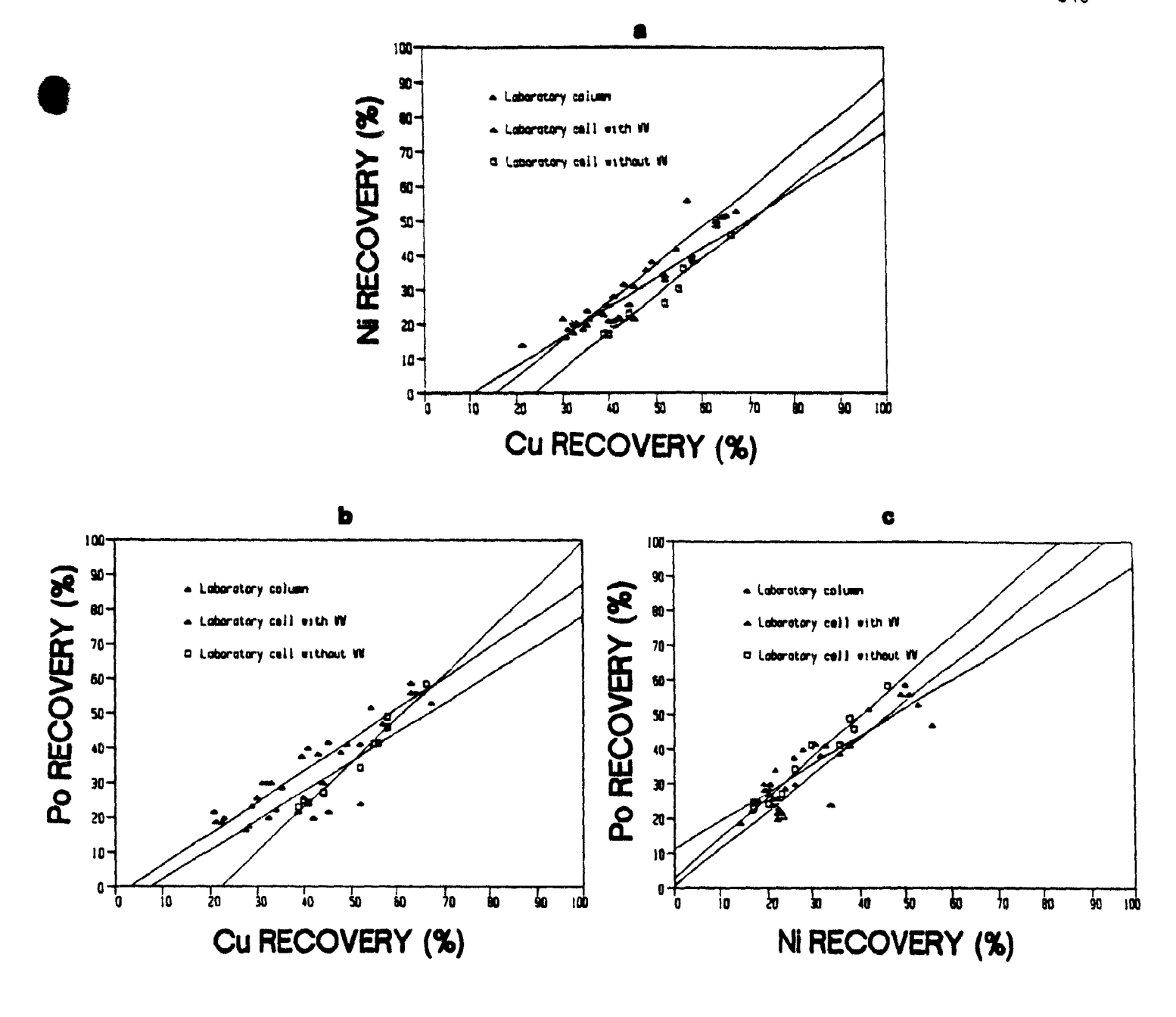


Figure 8.7: Separation curves for laboratory cell and column.

A plot of Cu recovery vs. Po recovery is given in Figure 8.7b. At lower recoveries (< 50%), the worst Cu-Po separation was obtained with the flotation column and the best with the laboratory cell in the absence of wash water. Figure 8.7c shows there is almost no Ni-Po separation. The performance of the three units appears nearly indistinguishable.

Effect of Wash Water on Final Ni Concentrate Flotation: Table 8.9 shows Ni grade and recovery increase with increasing J from 0 to 0.076 cm/s (Test 4). The Cu content of Ni concentrate is lower with wash water than without it. Ch, Po, and Gn concentrate contamination increases with increasing Ni grade and recovery. Here the dominant effect of wash water is to stabilize froth and increase recovery of all species. In these test series, gangue recovery is very high, presumably due to Pe-Gn locking. Final Ni concentrate should not contain much free gangue. Rejection of locked gangue seems to be difficult. Ch recovery is lower than that of other species, possibly because it is partially deactivated.

TABLE 8.9: Effect of wash water addition rate on Final Ni concentrate flotation (Test 4).

	GRADE conc.		R	E C O V E concentrat		
J	Ni	Cu	Pe	Ch	Po	Gn
(cm/s)	(%)	(%)	(%)	(%)	(%)	(%)
FEED	6.69	1.22				
0 0.050 0.061 0.076	7.01 7.72 8.03 8.05	1.01 0.85 0.89 0.94	35.2 46.7 50.0 52.7	25.4 23.6 27.2 31.5	32.3 36.7 40.4 47.8	36.5 45.1 49.3 58.6

Figure 8.8 compares the grade-recovery curves with and without wash water using the final Ni concentrate (Test 5). It is possible to achieve a better grade-recovery curve with wash water. Cu contamination of the Ni concentrate is lower with wash water. As can be seen from the bottom graph, Gn and Po behave like Pe, suggesting that it is not fully liberated. However, the behaviour of Ch is different maybe largely due to a good liberation and pH effect.

8.3.2 Pilot-Plant Scale Tests

The effect of J_{w} on gangue recovery was determined at four different J_{w} using silica flour (Test 9). Figure 8.9 shows that gangue recovery is minimum at an intermediate J_{w} ; it is higher without water or high J_{w} . The optimum wash water addition rate is around 0.07 cm/s, similar to the optimum J_{w} found for laboratory scale flotation cell.

Effect of Wash Water Addition Rate on the Primary Rougher Concentrate Flotation: The primary roughers produce a bulk Cu-Ni concentrate. This product was floated with and without wash water addition to characterize the Cu Rougher circuit where the main objective is Cu and Ni separation. Ni and Po are depressed with NaCN at a pH of 12 while Cu is selectively floated. Since the Cu rougher tails is sent directly to the smelter as a Cu-Ni concentrate, Pe recovery must be minimized in the bulk concentrate. The Cu rougher concentrate is cleaned in the Cu cleaner circuit to produce a final Cu concentrate at 29% Cu, less

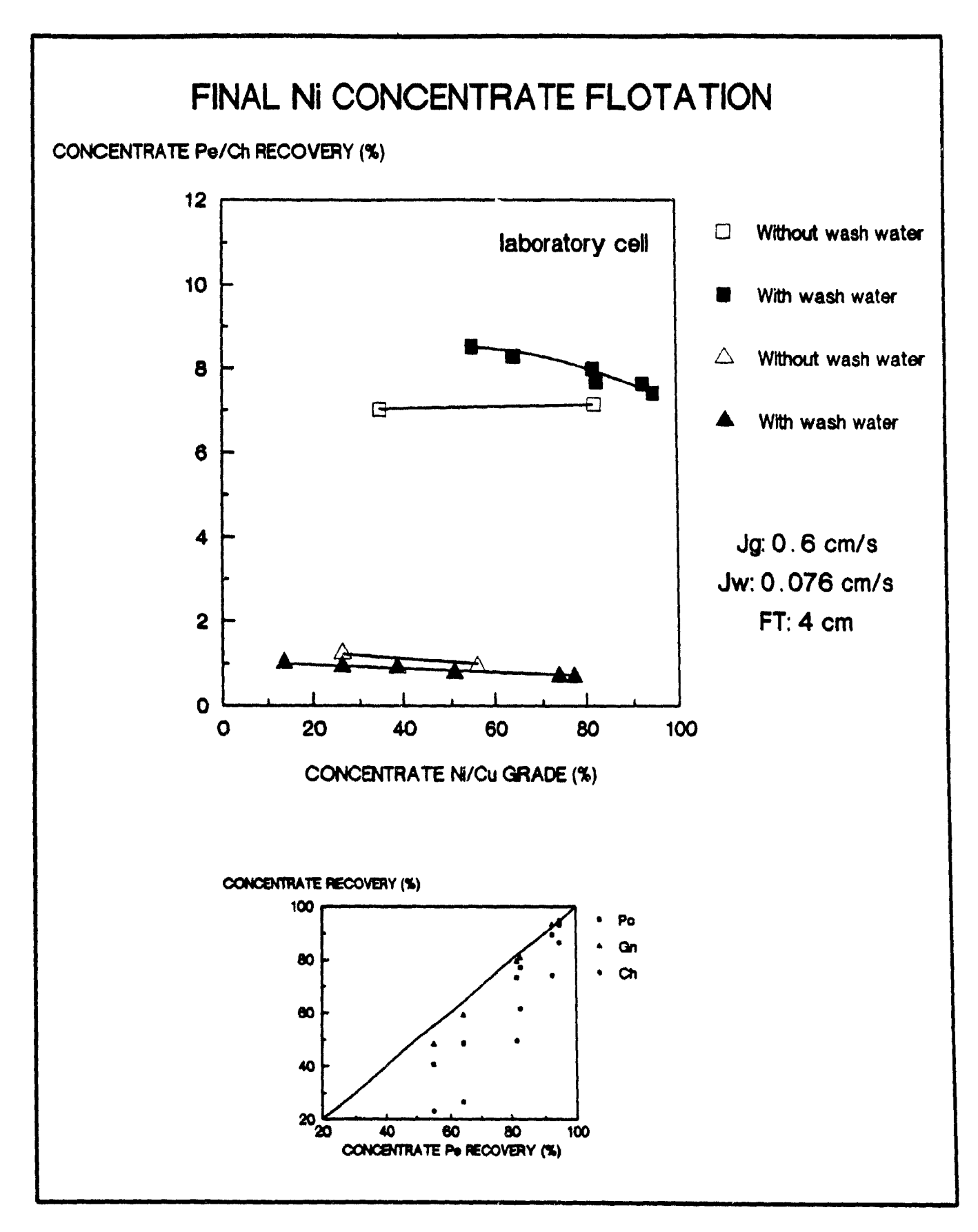


Figure 8.8 Grade-recovery and recovery-recovery curves curves of final Ni concentrate flotation with and without wash water addition in laboratory cell.

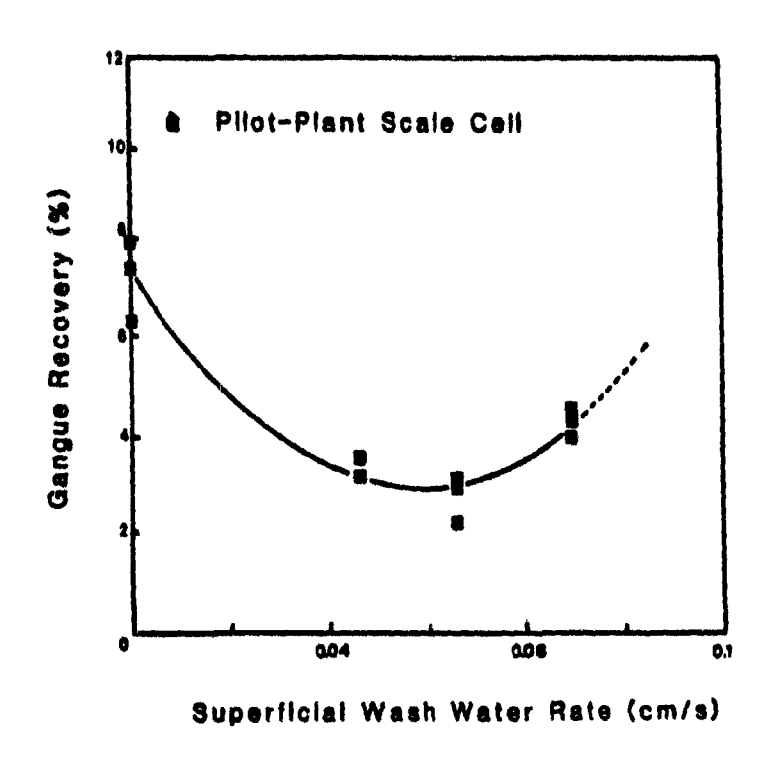


Figure 8.9. Effect of superficial wash water rate on gangue (silica) entrainment.

than 0.6% Ni and virtually no Po. Therefore, Cu recovery is not crucial.

Figure 8.10 compares of metallurgical performance with and without wash water. Feed grades were 12.7% Ni and 14% Cu. Average pulp residence times are 3.5 and 4.9 minutes with and without wash water, respectively. Average water recovery is 24.9% without water addition, and 27.2% with wash water. The following conclusions can be drawn:

- wash water significantly decreases pentlandite recovery (from 14.3% to 5.6%)
- the concentrate Cu grade is 2.7% higher at a reduced chalcopyrite recovery with wash water addition.
- wash water significantly rejects Po and Gn to the tailings. Non-sulfide gangue rejection by wash water is more significant than Po rejection.
- gangue recovery is high.

Effect of Wash Water Addition on the Cu Rougher Concentrate Flotation: The Cu rougher concentrate is cleaned in the Cu cleaner cells to produce a Cu final concentrate at low Ni, Po, and Gn content. A high Ch recovery is not crucial. The tails are returned back to the Cu rougher circuit for Cu-Ni separation. Feed grades were 3.0% Ni and 22.6% Cu.

Figure 8.11a shows the effect of wash water addition on Cu grade-recovery. Higher Cu grades can be achieved at lower Ch recovery in the presence of wash water addition. Wash water improves the grade-recovery curve by about 3% at low Cu recovery.

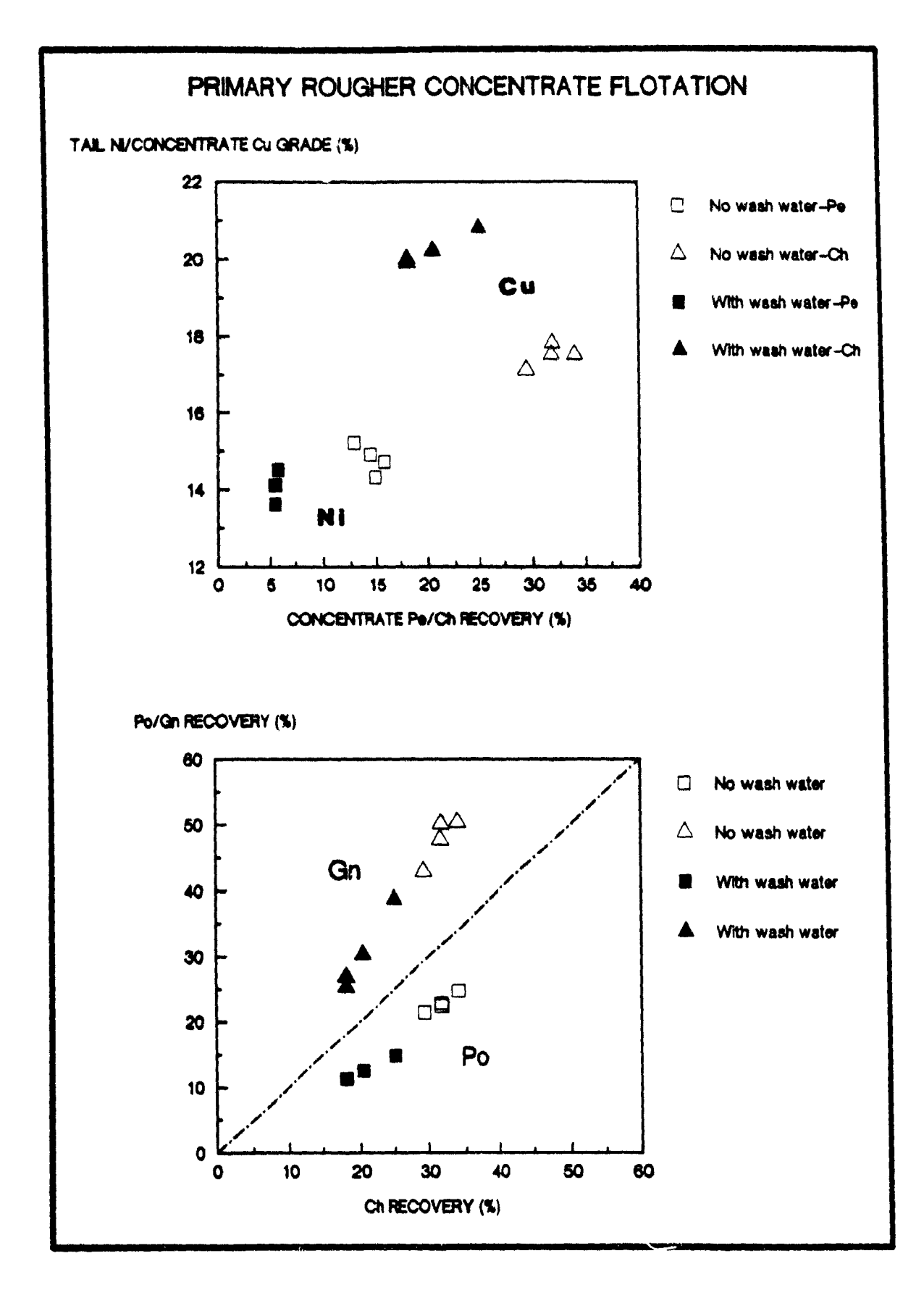


Figure 8.10: Grade-recovery curves for Cu rougher concentrate in pilot cell.

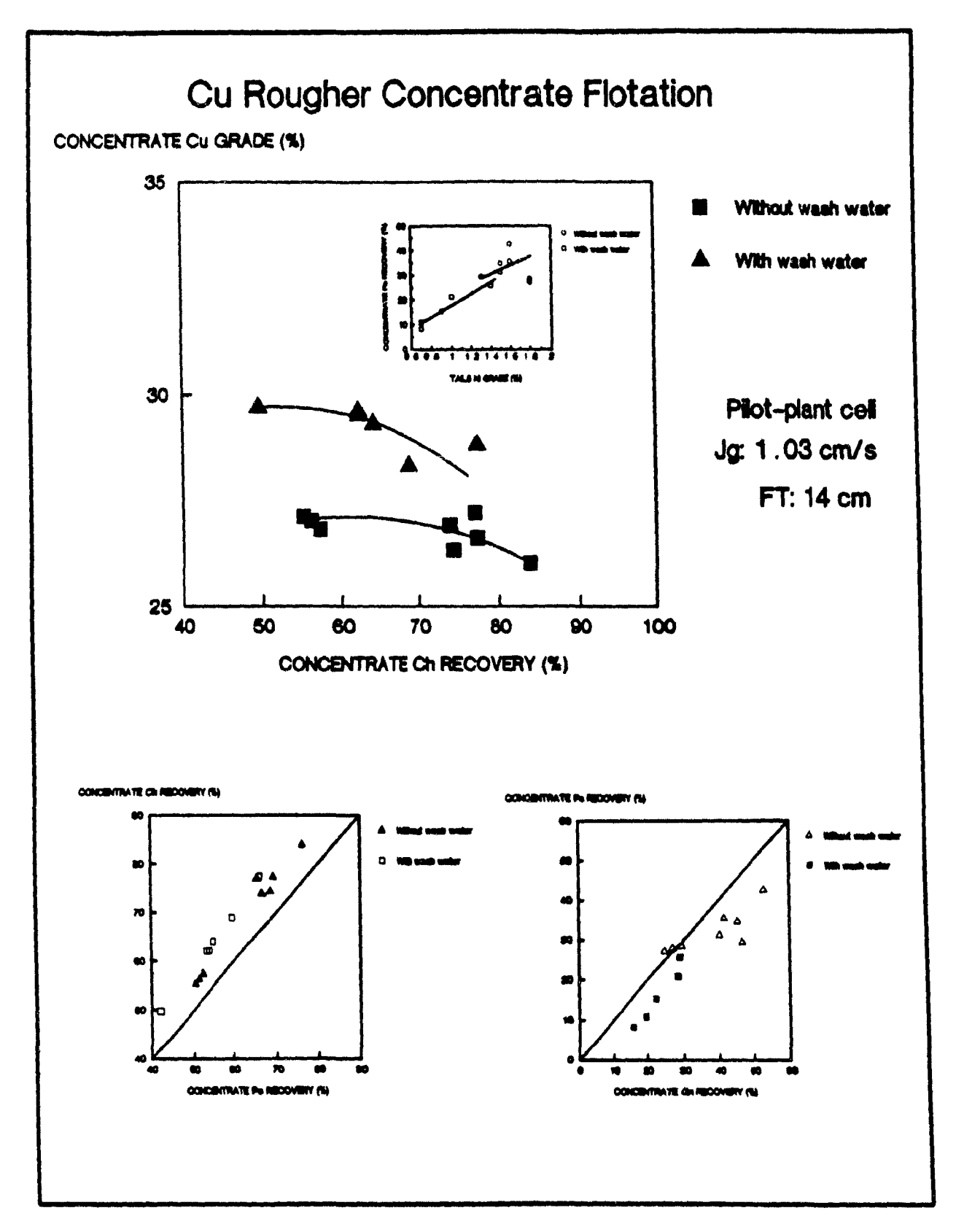


Figure 8.11: Grade-recovery and recovery-recovery curves for Cu rougher concentrate flotation with and without wash water in the pilot cell.

and 2% at high recovery. Pe rejection to the tails can be seen from the inserted graph. Cu concentrate Ni contamination is lower in the presence of wash water. Recovery-recovery curves for Ch-Po and Pe-Gn show that wash water rejects Gn and Pe quite significantly, but little Po. This suggests a natural Po/Ch and Gn/Pe associations.

Effect of Wash Water on Final Ni Concentrate Flotation

The metallurgical objective for this stream is to reduce its Po content as much as possible. The final Ni concentrate is the combination of four different streams: the secondary rougher concentrate (SRC) the copper rougher tails (CRT), the mags flotation concentrate (MFC), and the non-mags flotation concentrate (NMFC). Table 8.10 shows their contribution to final Ni concentrate (provided by mill staff). Po content was not available, but must be different for all streams.

TABLE 8.10: Contribution of different streams to the final nickel concentrate.

Stream	Wt%	% Ni	% Cu
SRC	46	5. 5	1.9
CRT	30	13.4	3.0
MFC	10	3.0	1.8
NMFC	14	4.7	4.4

Froth formation was difficult; therefore, the usual frother dosage was doubled to achieve good froth recovery over the cell lip. Flotation operation was difficult, due to poor froth

stability; thus, only two samples in the presence and absence of wash water were taken. Feed grades were 6.5% Ni and 0.8% Cu. Average residence times were 3.0 and 4.2 min with and without wash water, respectively.

Concentrate Ni grade is 9.5% without and 12.2% with wash water. Pe recovery decreases from 22.7% to 17.2% with wash water (Table 8.11). Po and gangue recoveries decrease even more, from about 13% to about 6%. Wash water achieves significant Ni upgrading at the expense of some Pe recovery.

TABLE 8.11: Effect of wash water addition on final Ni concentrate flotation.

	ADE		RECOVERY			
conc.	tails	_	conc	_		
NI (*)	Cu	Pe	Ch	Po	Gn (*()	
(%) 	(%)	(%)	(%)	(%)	(%)	
6.5	0.8	FEED				
	w	ITHOUT WASH WA	TER ADDI	TION		
9.7	0.8	20.2	20.6	12.6	13.4	
9.3	0.6	25.3	30.3	13.9	13.2	
9.5	0.7	22.7	25.4	13.2	13.3	
	W	ITH WASH WATER	ADDITIO	N		
12. 1	0.7	16.7	15.9	5.9	6.1	
12.2	0.6	17.7	17.0	6.0	6.0	
12.2	0.6	17.2	16.5	6.0	6.1	

8.4 Summary

8.4.1 Laboratory Scale Tests

Primary Rougher Flotation:

- Ni, Cu, and Po recovery significantly increases with increasing wash water rate. There is a higher gangue rejection with wash water. The effect of wash water is clearly to stabilize froth. Thus, wash water can be utilized in the primary rougher circuit to increase bulk Cu-Ni flotation.
- In the concentrate, Ni and Po grades increase with increasing wash water flowrate; however, Cu grade decreases, because recovery increases are more substantial for Ni and Po than for Cu.
- The effects of wash water flowrate and temperature are small.
- Better Cu-Ni separation is obtained with the laboratory cell without wash water addition.

Final Ni Concentrate Flotation:

- Wash water can be used to increase concentrate Ni grade at a lower Ch, Po, and gangue content. The higher the Ni grade, the lower the Ni recovery. Here, gangue and Po are not free and could be locked with Pe.

8.4.2 Pilot-Plant Scale Tests

Primary Rougher Flotation:

- Wash water significantly increases the rejection of Pe, Po, and gangue to the tails at a higher Cu grade, but a lower Ch recovery.

· * #0

Cu Rougher Flotation:

- Wash water rejects Pe, Po, and gangue to the tails and increases Cu grade by 2-3%, at a reduced recovery.

Final Nickel Flotation:

- Ni can be upgraded at a reduced recovery with wash water. Both Po and gangue are then significantly rejected.

In most cases, wash water significantly decreases gangue entrainment and increases concentrate grade. In some cases, wash water can also stabilize the froth and increase recovery. Free gangue can easily be rejected by wash water, but locked and/or hydrophobic gangue rejection is difficult. This study showed that the effect of wash water should be evaluated size-by-size. For the Strathcona Cu-Ni ore, a liberation study and mineralogical examination of the concentrate and tail products with and without wash water are strongly recommended.

CHAPTER 9

PLANT-SCALE WASH WATER AMENABILITY TESTS AT THE STRATHCONA MILL OF FALCONBRIDGE

Introduction

Wash water amenability tests carried out at the Strathcona mill involved plant-scale bank tests in the Non-magnetic circuit.

Cumulative grade-recovery and recovery-recovery curves were generated and compared with and without wash water.

Eleven tests were performed to determine the effect of wash water rate and distributor design on metallurgical performance.

Grade profiles of nickel (Ni), copper (Cu), pyhrrotite (Po), and insoluble gangue (Gn) were determined.

9.1. Previous Investigations on the Non-magnetic Circuit:

Flint and Dobby (1986) performed laboratory-scale column tests using the Non-mag circuit feed to compare the circuit and column performance. The multiple pass method was used to increase residence time and generate grade-recovery curves. The Non-mag circuit performance was determined by a sampling campaign.

They concluded that the column operated under present circuit conditions did not offer any advantage over the conventional cells used in the Non-mag circuit. They claimed that the gangue was naturally floatable (i.e. hydrophobic) due to presence of talc in the ore. Incomplete gangue/sulphide liberation (locking), slime coating, and CuSO₄ activation, which is added in the scavengers, were the other reasons suggested. Their column tests showed about 30% gangue recovery.

Recently, del Villar (1988) conducted column flotation tests, using a 5 cm diameter and 10 m high column, to determine the amenability of flotation columns for the Non-mag circuit. Column and mechanical cell (5L) grade-recovery curves were compared. He concluded that laboratory cells outperformed the column both in upgrading and Po rejection.

Figure 9.1 shows one of the most recent mill sampling campaign results performed by the Falconbridge personel (Dec. 1987). Ni, Cu, Po, and Gn grades are 1.2%, 0.5%, 72.1%, and 23.6%, respectively. Ni is upgraded to 3.6% and Po and Gn grades decreased to 44.9% and 40.2%, respectively, at the primary stage.

There are two identical rows (i.e. N-J and P-L) and two stages in the Non-mag circuit. The first stage includes ten 2.8 $\rm m^3$ (100 $\rm ft^3$) cells in series (N19-28 or P19-28) and the second stage has eighteen 1.4 $\rm m^3$ (50 $\rm ft^3$) cells in series. All cells are separated from each other by dividers (i.e. cell-to-cell type).

Since the Non-mag circuit has a high gangue content, it may be a good candidate for testing the effect of froth washing. For this test work, row N (cells number 19 to 24) was used. Feed is pumped from thickener #3 underflow into the feed box adjacent to the first cell. In the Non-mag circuit, slurry level is maintained by the height of the overflow pipe (i.e. ring riser system) in the tailing box.

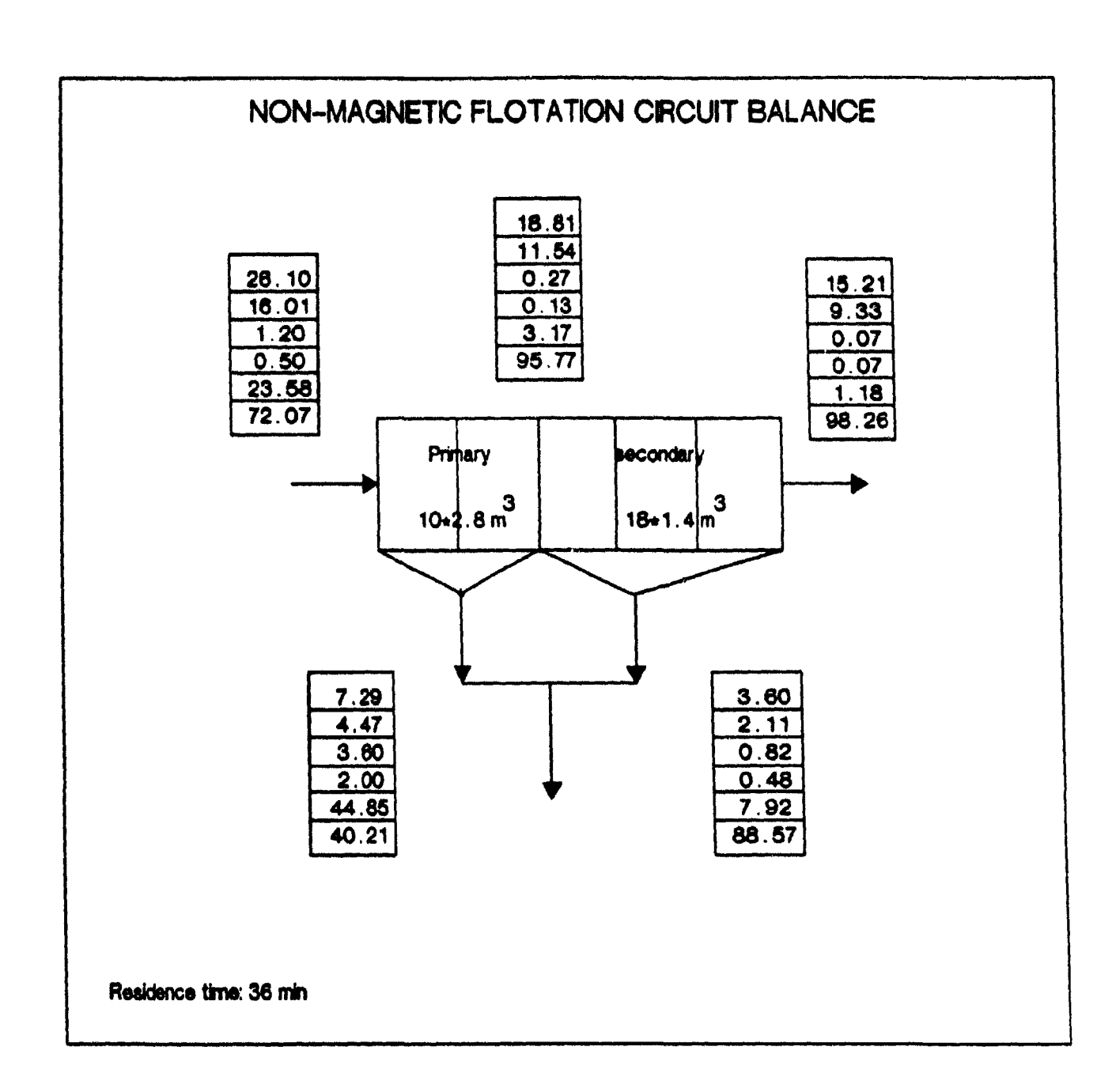


Figure 9.1: Non-magnetic flotation circuit balance.

(tpd solid, % mass with respect to feed, % Ni, % Cu. % Po, and % Gn).

9.2. Wash Water Distributor Design Considerations

The following criteria were used to design plant scale wash water distributor:

- uniform and gentle water distribution throughout the froth surface. Poor distribution will lead to local excess of wash water (causing channelling) and will leave some sections of the froth poorly cleaned.
- the distributor should be maintenance free. Blinding of holes due to use of recycled water or precipitation of dissolved salts should be prevented.
- the wash water distributor should not prevent normal maintenance such as impeller replacement, cell cleaning etc., and should easily be cleaned.
- the distributor material should be durable, inexpensive, light, easily machined (for threading and drilling holes), and resistant to circuit reagents.

To obtain uniform water distribution, proper consideration must be given to the flow behavior in the distributor. The criterion used for uniform distribution was to achieve 60% of pressure loss at the hole, even for holes furthest away from the water source.

A BASIC computer program was written to evaluate the effect of the main operating parameters on the total pressure head loss in the wash water distributor designed for a bank. The program calculates the necessary pressure head at the beginning of the main pipe to maintain equal water flowrate. The computer program takes into account pressure losses across all holes (nozzles) and frictional losses in the pipe between nozzles. It neglects pressure losses due to fittings and valves.

The program requires the input of the superficial wash water rate, washed cell cross-sectional area, perforated and main pipe diameters, hole diameter and interval, number of perforated pipes in each cell and distance between perforated pipes, number of cells in each bank and distance between cells (i.e. cell length). The program is capable of calculating water velocities in the pipes, pressure drops, and determine the necessary head to maintain a target wash water rate for the bank.

Table 9.1 shows the effect of the main operating variables on the pressure drop and wash water flow rates. Wash Water flowrate can only be reduced by decreasing superficial wash water rate. The pressure head required to maintain homogeneous water distribution strongly depends on hole diameter and the number of holes on each perforated pipe (i.e. hole interval). The bigger the holes and the higher the number, the lower the pressure head required to maintain homogeneous water distribution. Increasing perforated pipe diameter and main pipe diameter leads to a reduced pressure head requirement, but the effect is smaller.

Table 9.1: Effect of operating variables on pressure drop and wash water flowrate for a bank.

Operating variable	PRESSURE		FLO	FLOWRATE	
	(kg/cm	PSI)	(L/min	(USGPM	
Superficial wash water re	ate (cm/s)				
0.050	6	85	204	54	
0.075 0.100	13 23	191 340	302 404	80 107	
Perforated pipe diameter	(m)				
0.0127	28	403	404	107	
0.0191 0.0254	24 23	347 339	404 404	107 107	
Hole diameter (m)					
0.001	120	1700	404	107	
0.0015	23	339	404	107	
0.002 0.003	8 2	110 26	404 404	107 107	
Number of perforated pip	es in each ce	. 11			
3	31	448	404	107	
4	23	339	404	107	
Number of holes on each	perforated pi	pe			
280	12	172	404	107	
140	23	339	404	107	
70	45	637	404	107	
Main pipe diameter (m)					
0.0254	38	542	404	107	
0.0381	24	342	404	107	
0.0508	23	339	404	10	

Table 9.2 shows operating variables chosen for the plant distributor design.

Table 9.2: Operating variables chosen for the plant wash water distributor.

main pipe diameter : 3.81 cm (1 1/2 inches) perforated-branch pipes : 1.905 cm (3/4 inch)

diameter

: 0.3 cm hole diameter hole interval : 1 cm superficial wash water rate* : 0.075 cm/s
number of perforated pipes : 4

number of perforated pipes

in each cell

number of cells in each bank : 6 : 150 cm cell length distributor height from froth : 30 cm

surface

For a 6-cell Denver D30 (100 ft³) bank, the total wash water flowrate is 302 L/min (80 USGPM) and the total pressure required to maintain homogeneous water distribution is 1.5 kg/cm² (21 PSI). Under these conditions more than 60% of the pressure is lost at the nozzles rather than in the pipes.

For a given distributor, there exists a minimum superficial water velocity at which ali holes become active. However, in a start-up situation it is necessary to exceed the minimum velocity in order to initiate complete operation of all holes. At low J s, water droplets detach from the holes when the gravity forces overcome the interfacial forces. At high J.s., a jet is formed, which breaks up into drops. Jet height depends on distributor height, orifice spacing, etc.

^{*}optimum for laboratory and pilot-plant scale tests

The height of the distributor network from the froth surface also has a very significant effect on the impact energy upon hitting the top of the froth. Water droplets discharged from the perforations fall with a constant acceleration. The distance (S) travelled is given by:

$$S(t) = \frac{1}{2} g \cdot t^2 + v_0 \cdot t$$
 9.1

where t: time in seconds

g: gravity acceleration (980 cm/sec²)

v: initial water discharge velocity from the perforated pipe hole (cm/s)

S: the distance between the distributor network and the froth surface (cm)

The collision (impact) velocity of water droplet with the froth surface (v_s) is given by:

$$v_c = g.t + v_0$$
 9.2

Table 9.3 shows the calculated impact velocities for varying $J_{\rm w}$ and distances between the distributor and the froth surface. Both increase impact velocity, but height has clearly the most important effect.

The collision velocity can be reduced by 42% by lowering the distributor from 30 cm to 10 cm above the froth surface. Since excessive impact velocities can reduce froth stability, the height should be as small as possible.

Table 9.3: Effect of distributor height and superficial wash water rate on water droplet discharge and collision rates.

s	J w	v _o	t	g.t	v _c	N P
(cm)	(cm/s)	(cm/s)	(sec)	(cm/s)	(cm/s)	
30	0.016	1.52	0.2459	241	242.5	4
30	0.033	3. 13	0.2443	239	242.1	4
30	0.043	4.08	0.2433	238	242.1	4
30	0.051	4.83	0.2426	238	242.8	4
30	0.037	3.51	0. 2439	239	242.5	2
30	0.055	5.21	0.2422	237	242.2	2
30	0.070	6.63	0.2408	236	242.6	2
30	0.085	8.06	0.2393	235	243.1	2
10	0.016	1.52	0.1413	138	139.5	4
10	0.033	3.13	0.1397	137	140.1	4
10	0.043	4.08	0.1388	136	140.1	4
10	0.051	4.83	0.1380	135	139.8	4
10	0.037	3.51	0.1393	137	140.5	2
10	0.055	5.21	0.1376	135	140.2	2
10	0.070	6.63	0.1363	134	140.6	2
10	0.085	8.06	0.1349	132	140.1	2

9.3 Experimental Procedure

Bank tests were performed using a plastic and portable wash water distributor network. The following tests were carried out to determine the amenability of wash water for the Non-mag circuit:

- determine the effect of wash water on metallurgical performance at different wash water rates.
- determine the effect of wash water distributor geometry on metallurgical performance (i.e. number of perforated pipes in each cell).
- sample the froth by a suction type device (Figure 9.2). Two samples in the froth, one sample at the interface, and another one in the slurry phase were taken to evaluate grade profiles. The effect of wash water on selectivity was determined.
- measure size-by-size metallurgical performance in the presence and absence of wash water.

9.3.1 Test Program: Eleven successful tests were performed on the primary Non-mag bank with and without wash water to evaluate the effect of wash water on metallurgical performance: three tests without wash water and four tests with wash water using four and two of the perforated pipes in each cell. For the two pipe tests, the intermediate valves were turned off and therefore only the two front pipes were in operation.

Froth samples were sucked using a 1.2 cm in diameter pipe connected to a peristaltic Masterflex pump by a flexible tubing. The samples were collected in Erlenmayer flasks. The sampling probes were located in the centre of the cell and 40 cm apart from the cell lip (Figure 9.2).

The effect of particle size on grade and recovery was determined for two test series; one with wash water and the other without. Feed, concentrate, and tailing samples were dry and wet screened for 10 and 15 minutes, respectively, using 147, 74, and 37 µm screens. The Ni, Cu, and S content of each size fraction was determined.

9.3.2 Installation of the Wash Water Distributor Network: The PVC portable wash water distributor was made at McGill and transported to the mill. Threaded pipes and fittings were combined together near the flotation bank and the network was then fixed on the existing metallic supports, which are 30 cm above the froth surface. Installation and dismantling of the distributor network were easy and did not cause circuit disturbance. The first cell

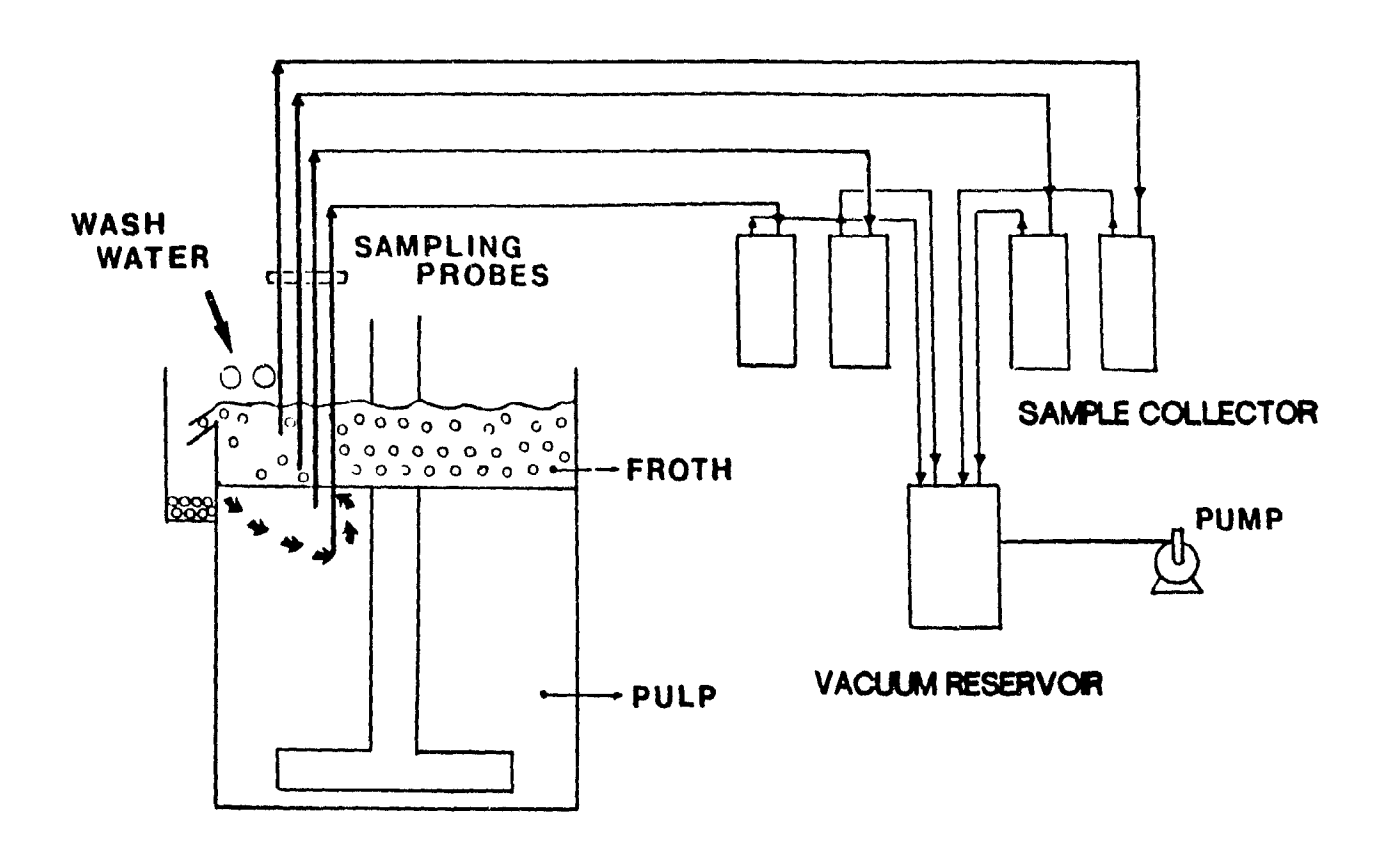


Figure 9.2: Froth sampling equipment for froth profile determination.

had only three perforated pipes, due to space limitation, and the remainder four (A, B, C, and D).

A water outlet near the bank was used as a wash water source. This water is recycled and normally used to wash froths in launders. Figures 9.3a and 3b show the overall view of the assembled distributor on the supports.

9.3.3 Wash Water Flowrate Calibration: At the beginning of the tests, wash water from each perforated pipe was separately collected at known time intervals to determine flowrates and check distribution homogeneity. Figures 9.4a and 9.4b show the wash water flowrate from each perforated pipe for each cell number. Wash water flowrate in cell one is slightly higher because it has three perforated pipe. Pipe B in cell number four was poorly punctured and has less wash water. However, as a whole, the distributor network worked as designed for a large range of Js. Figures 9.5a and 9.5b show that water distribution is homogeneous and droplets, rather than jets, are formed. Jw was calculated on the basis of the froth surface sprayed: 1.5 m * 1 m with four pipes and 1.5 m * 0.5 m with two pipes.

9.3.4 Sampling Procedure: Three types of samples were collected. Feed samples were taken from the pipe flowing in the feed box using a diversion pipe. Timed concentrate samples were collected from the cell lips using lip samplers. Cell lips were cleaned before sample collection. A bank tailing sample was also taken using a plunger type bottle sampler (Figure 9.6). The

of Canada

National Library Bibliothèque nationale du Canada

Canadian Theses Service Service des thèses canadiennes

NOTICE

AVIS

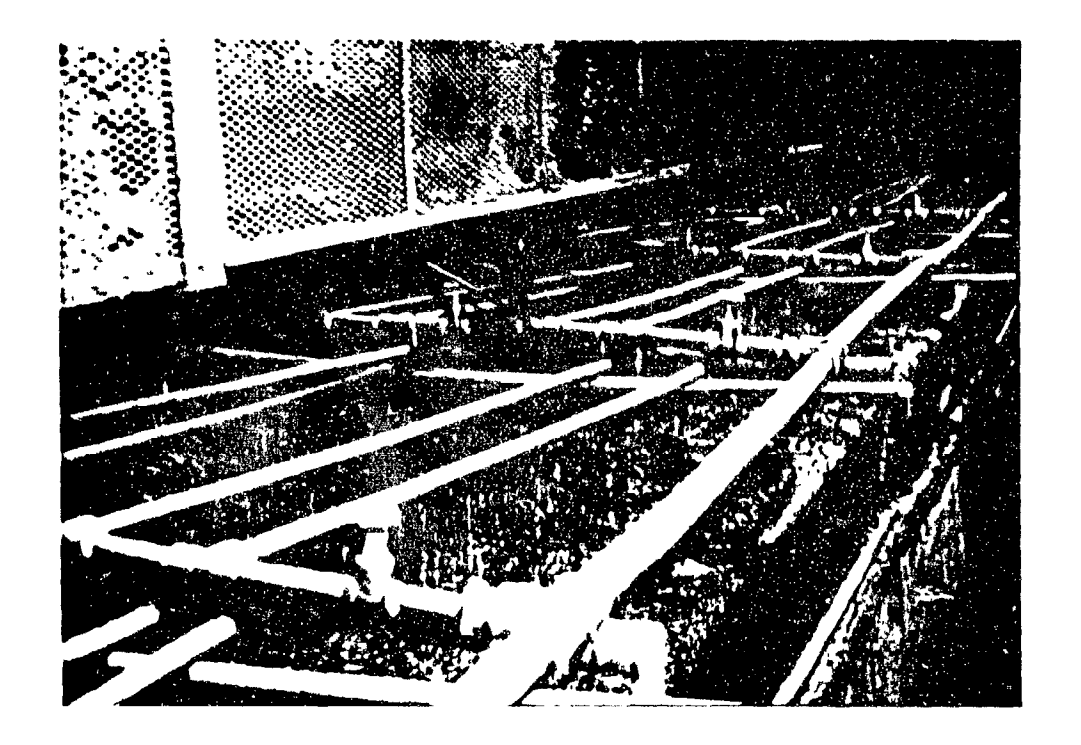
FOR MICROFILMING.

UNFORTUNATELY THE COLOURED OF GREY.

THE QUALITY OF THIS MICROFICHE
IS HEAVILY DEPENDENT UPON THE
QUALITY OF THE THESIS SUBMITTED

LA QUALITE DE CETTE MICROFICHE
DEPEND GRANDEMENT DE LA QUALITE DE LA
THESE SOUMISE AU MACROFILMAGE.

MALHEUREUSEMENT, LES DIFFERENTES ILLUSTRATIONS OF THIS THESIS ILLUSTRATIONS EN CONLEURS DE CETTE CAN ONLY YIELD DIFFERENT TONES THESE NE PEUVENT DONNER QUE DES TEINTES DE GRIS.



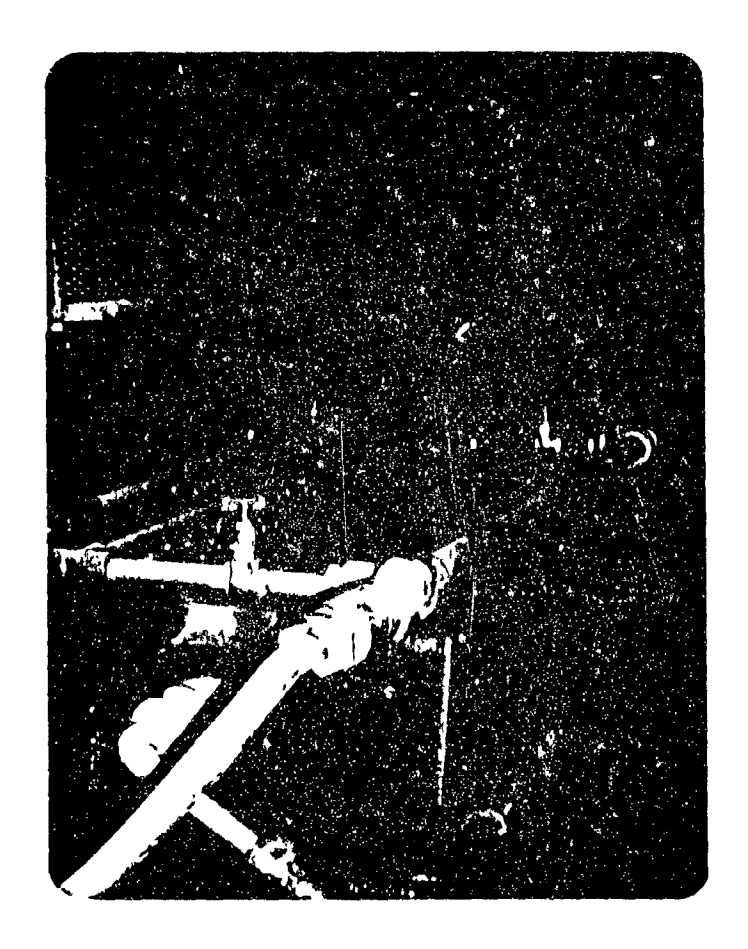


Figure 9.3: Overall view of the plant wash water distributor network at the non-magnetic bank.

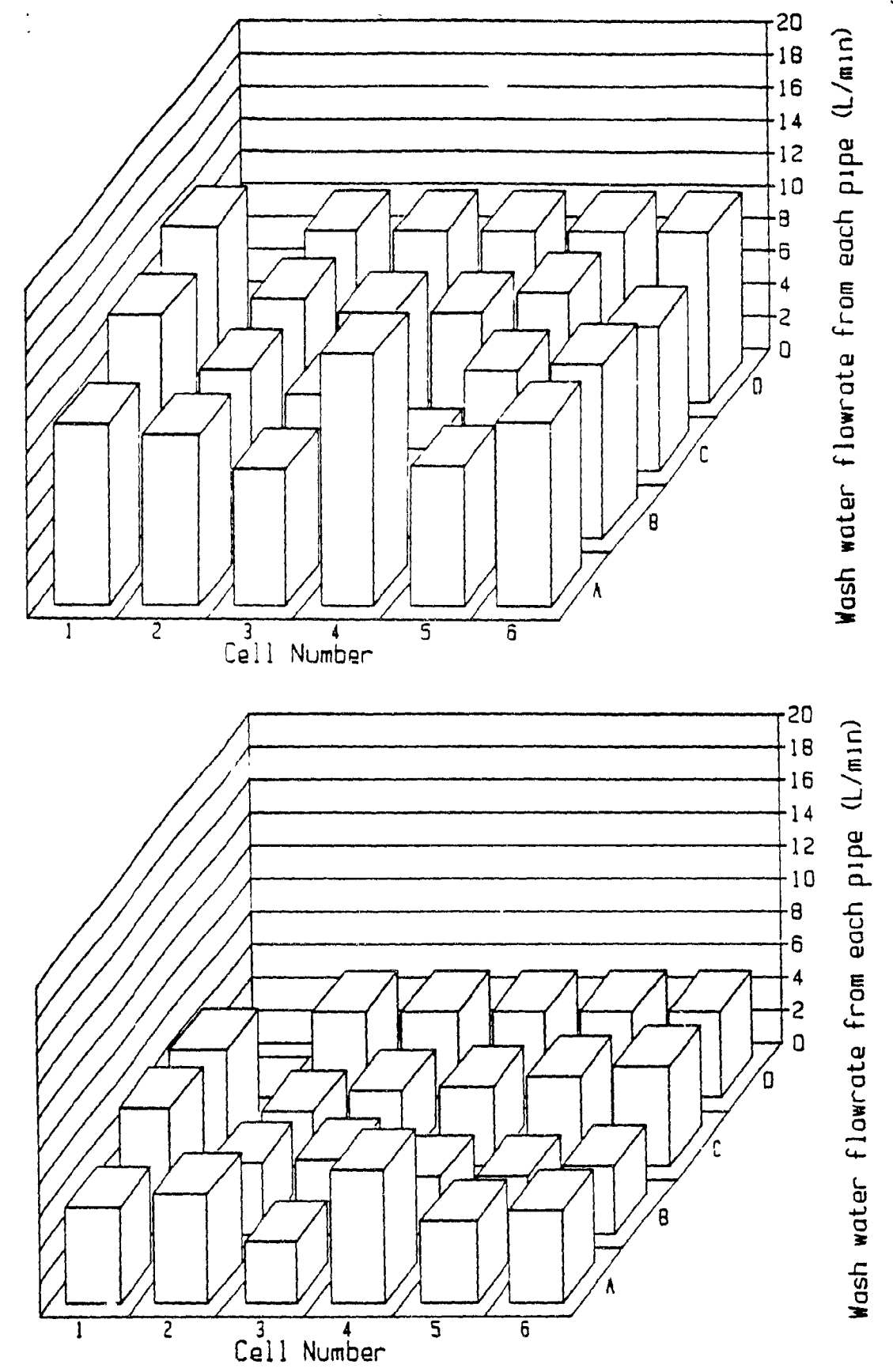


Figure 9.4: Wash water flowrates from each perforated pipe at a low (a) and high (b) flowrates.



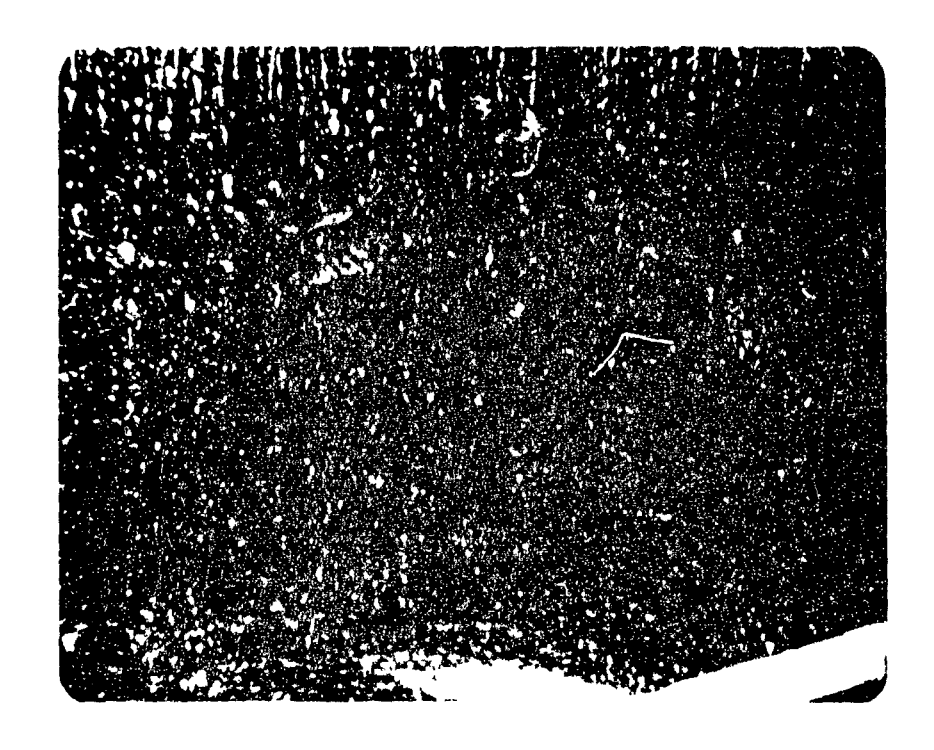


Figure 9.5: Water addition homogenity and droplet generation.

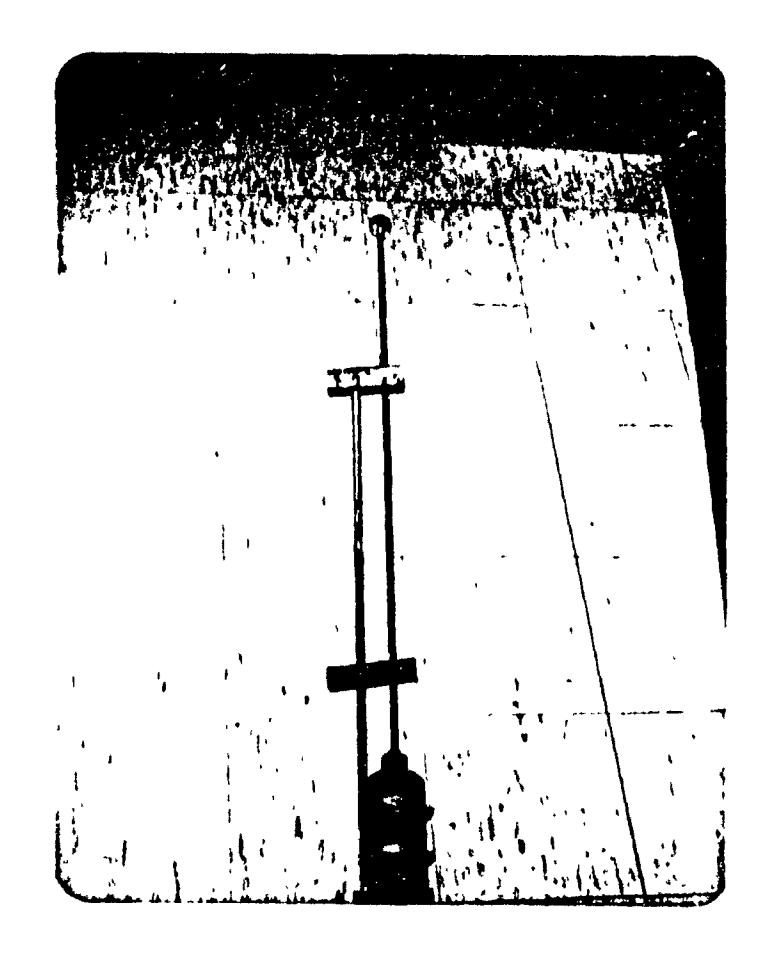


Figure 9.6: Plunger type of slurry sampler used for tailing sampling.

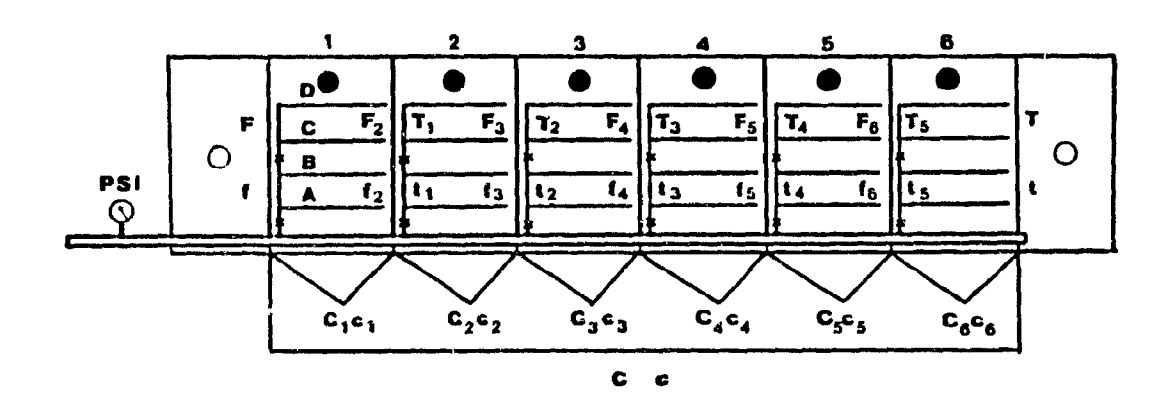


Figure 9.7: Schematic top view of the distributor network.

sampler in a closed position was immersed in the tailing pipe; the bottle lid was opened from the handle to fill it with slurry sample, and then closed when full.

After each change, the circuit was allowed 30-40 minutes to stabilize. Before sampling, stability was checked from the control room. The sampling campaign was started by taking feed and tailing samples and then concentrate samples from cell lips were collected starting from cell number 1 to 6 Since the first cell length is slightly shorter than the rest of the cells, a smaller lip sampler was used for it. Another sampler was used for the other cells. The lip sampler was cleaned with one litre of water after each cell sampling. Three cuts were taken from each stream over a 40 minute period.

- 9.3.5 Sample Preparation: Wet samples were first weighed, vacuum filtered, and dried on a low heat hot plate. Dried samples were weighed, screened with a 595 µm (30 mesh) screen and splitted using a riffle. 40 to 50 gram samples were taken for Ni, Cu, and S assays. Feed and tailing samples were pulverized for 20 seconds. Some rejects were also kept for size analyses. Samples were analyzed at the Metallurgical Technology Center of Falconbridge.
- 9.3.6 Calculation Procedure: A schematic top view of the distributor network is shown in Figure 9.7 along with the variables used in calculations performed with LOTUS 123. Cumulative (bank) and stage (individual cell) recoveries were calculated using the following equations.

$$C = C_1 + C_2 + C_3 + C_4 + C_8 + C_8$$
 9.3

$$c = \frac{c_1 C_1 + c_2 C_2 + \dots + c_6 C_6}{C_1 + C_2 + C_3 + C_4 + C_5 + C_6}$$
9.4

Overall bank recovery:

$$R_{b} = \frac{c(f - t)}{f(c - t)}$$
9.5

Bank feed and tailing flowrates:

$$F = \frac{c.C}{R_{b.}f} \quad \text{and} \quad T = F - C \quad 9.6$$

Cumulative recovery depends on the bank feed:

$$R = \frac{c_1 C_1}{f.F}$$
9.7

$$R_2 = \frac{c_1 C_1 + c_2 C_2}{f_1 F_2}$$
9.8

$$R_3 = \frac{c_1 C_1 + c_2 C_2 + c_3 C_3}{f.F}$$
9.9

$$R_{6} = \frac{c_{1}C_{1} + c_{2}C_{2} + c_{3}C_{3} + \dots + c_{6}C_{6}}{f.F}$$
9.10

Stage recovery depends on the individual cell feeds:

$$T_1 = F_2 = F - C_1$$
 9.11
 $T_2 = F_3 = F_2 - C_2$ and so on 9.12

Stage recovery for each cell:

$$R_{1} = \frac{c_{1}C_{1}}{fF}$$
9.13

$$R_{2} = \frac{c_{2}C_{2}}{f_{2}F_{2}}$$
9.14

$$R_{3} = \frac{c_{3}C_{3}}{f_{3}F_{3}}$$
9.15

$$R_{g} = \frac{c_{g}C_{g}}{f_{g}F_{g}}$$
9.16

Mass balanc ng the total feed concentrate and tail data was also completed to verify that the above procedure did not introduce significant ϵ rrors.

9.4 Results and Discussion

9.4.1 Washing the Entire Froth Surface with Four Perforated Pipes in Each Cell

Figures 9.8a, b, c, and d show the cumulative concentrate grade and recovery curves at different superficial wash water rates for Ni, Cu, Po, and insoluble Gn. The same figures also show the results of laboratory column flotation and mechanical cell tests performed by del Villar (1988) at the Strathcona mill using the non-magnetic feed. Cumulative concentrate grade decreases with increasing recovery. In the absence of wash water addition, Ni and Cu grade-recovery curves are lower (Figures 9.8a and 9.8b). Wash water addition at a superficial rate of 0.033 cm/s improves the concentrate Ni grade slightly, others do not. Cu grades are higher with wash water addition. It appears that conventional flotation even without wash water addition outperforms column flotation for the non-magnetic circuit. Tests with a laboratory

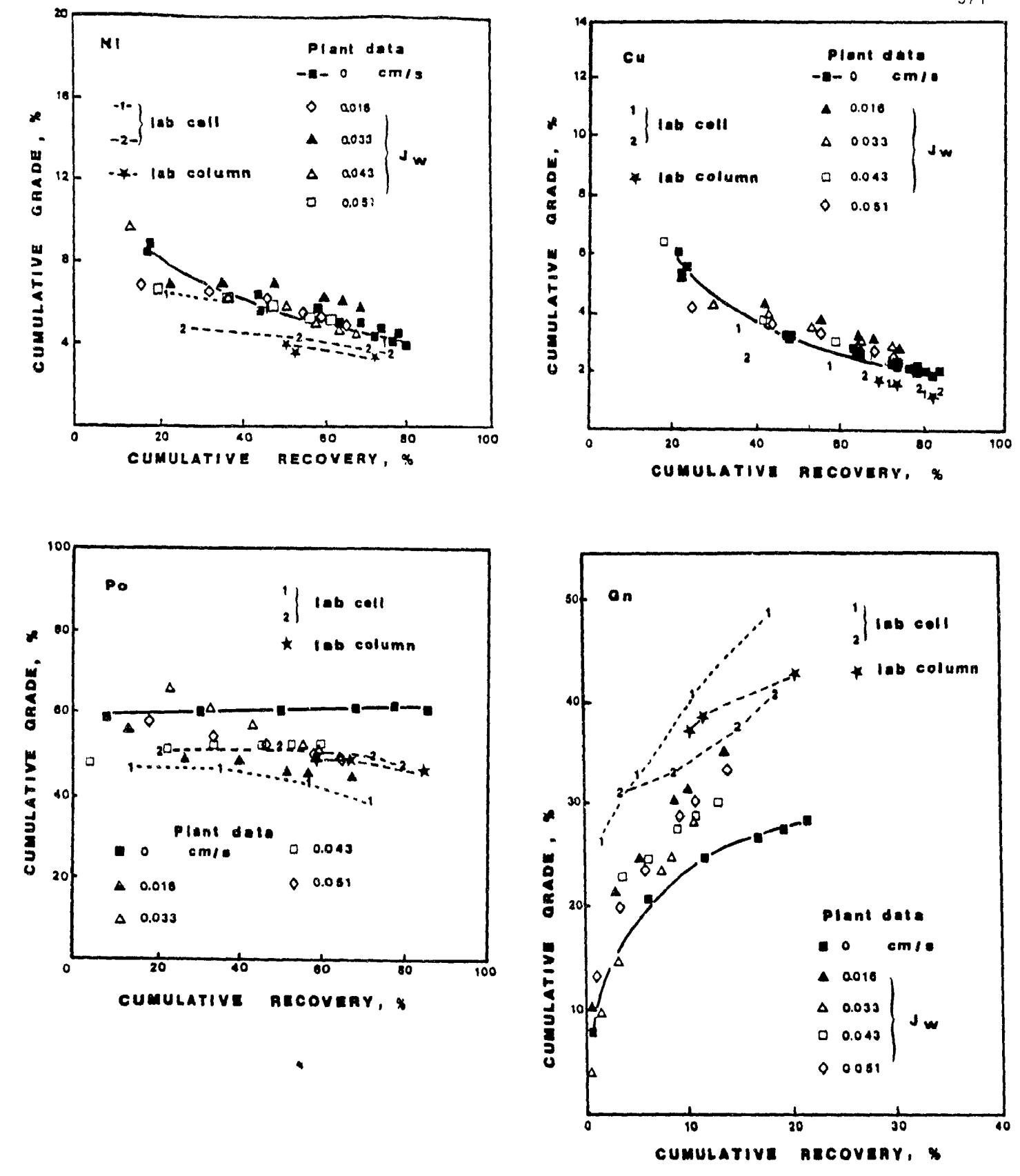


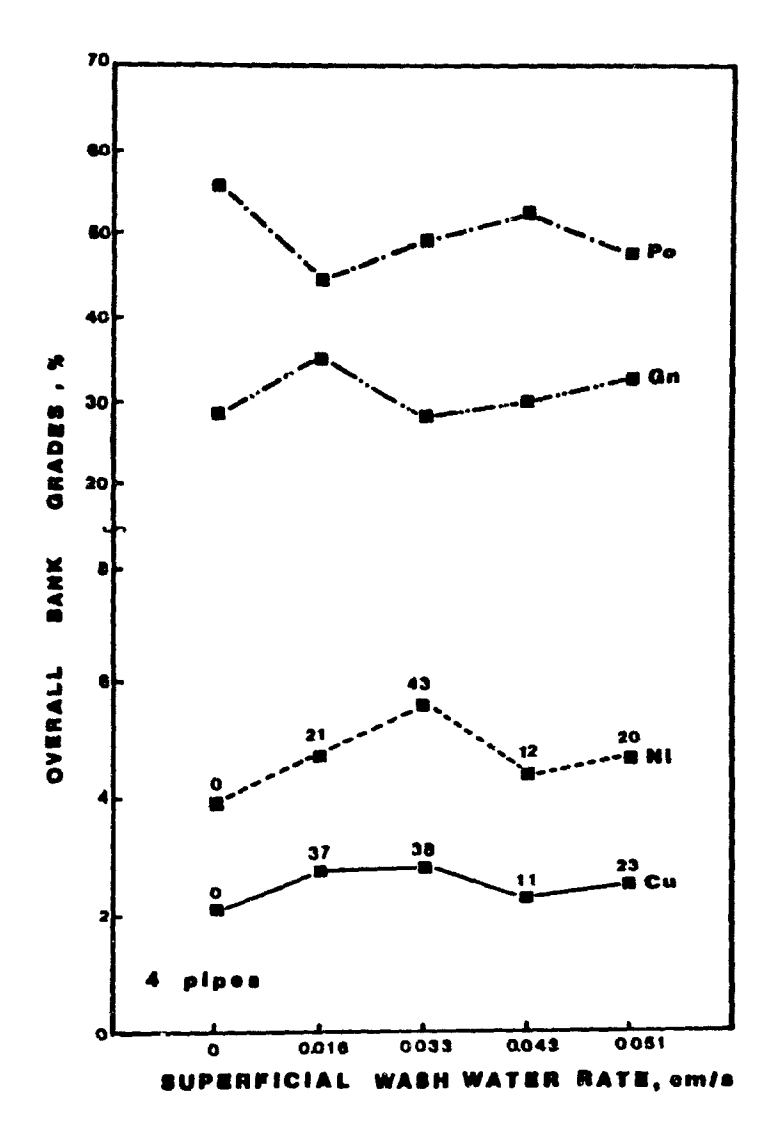
Figure 9.8: Cumulative grade-recovery curves for Ni (a), Cu (b), Po (c), and Gn (d) for the non-magnetic circuit using four pipes.

cell at 16% and 28% solids seem to underestimate the real circuit performance.

As can be seen from Figure 9.8c, the Po grade remains almost constant in the absence of wash water addition. Wash water significantly decreases both Po grade and recovery. The decrease in Po recovery is important because the concentrate of this bank directly goes to the smelter.

Cumulative gangue grade-recovery curves are shown in Figure 9.8d at different wash water addition rates. Gangue recovery is around 21% without wash water, and is reduced down to 11% with wash water ($J_{\rm w} = 0.033 \, {\rm cm/s}$), which corresponds to a 48% reduction in entrainment. Gangue recovery in column flotation appears similar to circuit performance in the absence of wash water addition.

Overall bank concentrate grades are shown in Figure 9.9 as a function of superficial wash water rate for Ni, Cu, Po, and Gn. There is an increase in Ni and Cu bank grades with wash water. The numbers on the data points represent percent increases in grade with respect to no wash water. The maximum increase in Ni and Cu grades were obtained at a $J_{\rm w}$ of 0.033 cm/s. The change in Po and Gn grades are not very important as they constitute most of the concentrate.



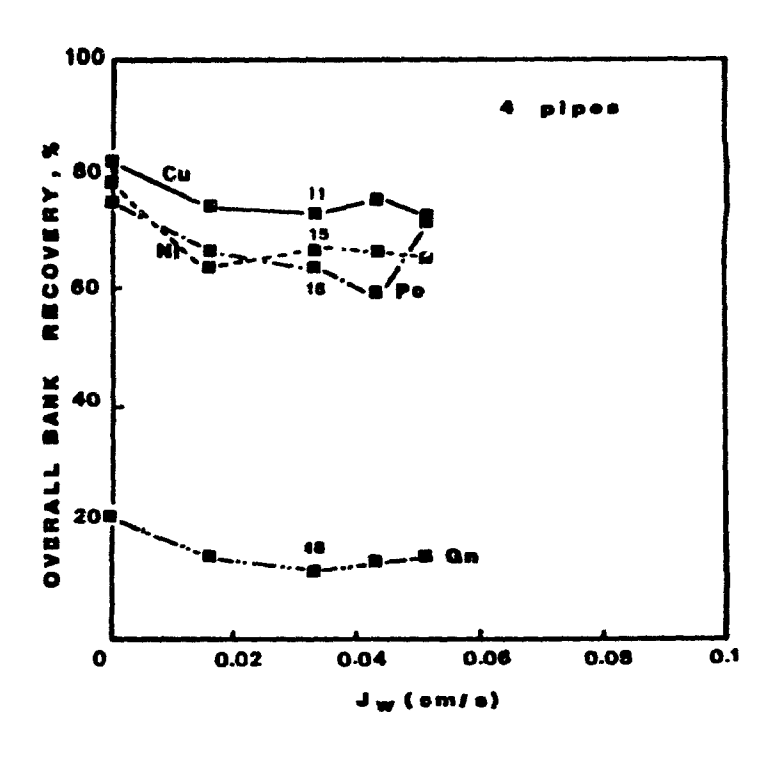


Figure 9.9: Overall bank grades versus superficial wash water rate using four pipes.

Figure 9.10: Overall bank recoveries versus superficial wash water using four pipes.

Overail bank (combined) concentrate recoveries as a function of superficial wash water rate is given in Figure 9.10. Numbers represent decreases in recovery. A 48% gangue and 15% Po recovery decrease was achieved at reduced Cu and ' recoveries. The optimum J was determined at the maximum grade increase for Ni and maximum Po and Gn rejection.

Figure 9.11 shows the stage (individual cell) gangue recovery as a function of cell number in the bank at different superficial wash water addition rates. Gangue recovery is higher in each cell in the absence of wash water addition. Wash water significantly decreases gangue recovery in each cell. Maximum gangue stage recovery was obtained in cell number 4 due to the one perforated pipe with uneven distribution.

9.4.2 Washing the Front Part of the Froth Surface with Two Perforated Pipes in Each Cell

Figures 9.12a, b, c, and d show the cumulative grade-recovery curves for Ni, Cu, Po, and Gn at J_w of 0.037 (99 L/min), 0.055 (148 L/min), 0.070 (190 L/min), and 0.085 (265 L/min) cm/s along with laboratory column flotation results. Again column flotation offers no advantage over the circuit even without wash water. A significant increase in concentrate Ni grade was achieved with wash water at lower recoveries (Figure 9.12a). Two pipes addition is much better than four pipes. The best wash water superficial rate is 0.055 cm/s. The results at superficial wash water rate 0.070 cm/s seem to be suspicious, especially for the last cell. Superficial rate of 0.085 cm/s is above the optimum, presumably because of froth mixing and froth bed destruction.

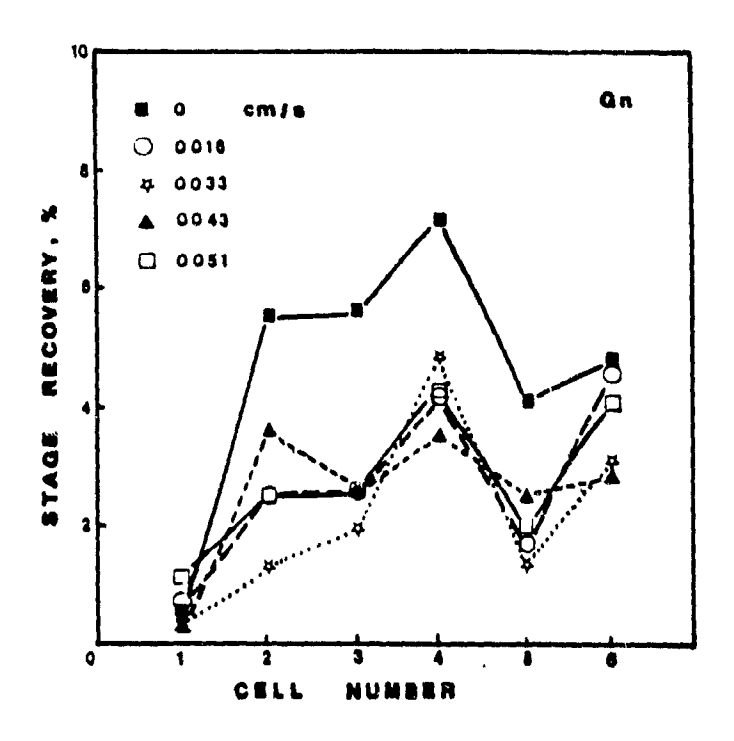


Figure 9.11: Stage gangue recovery from each cell using four pipes.

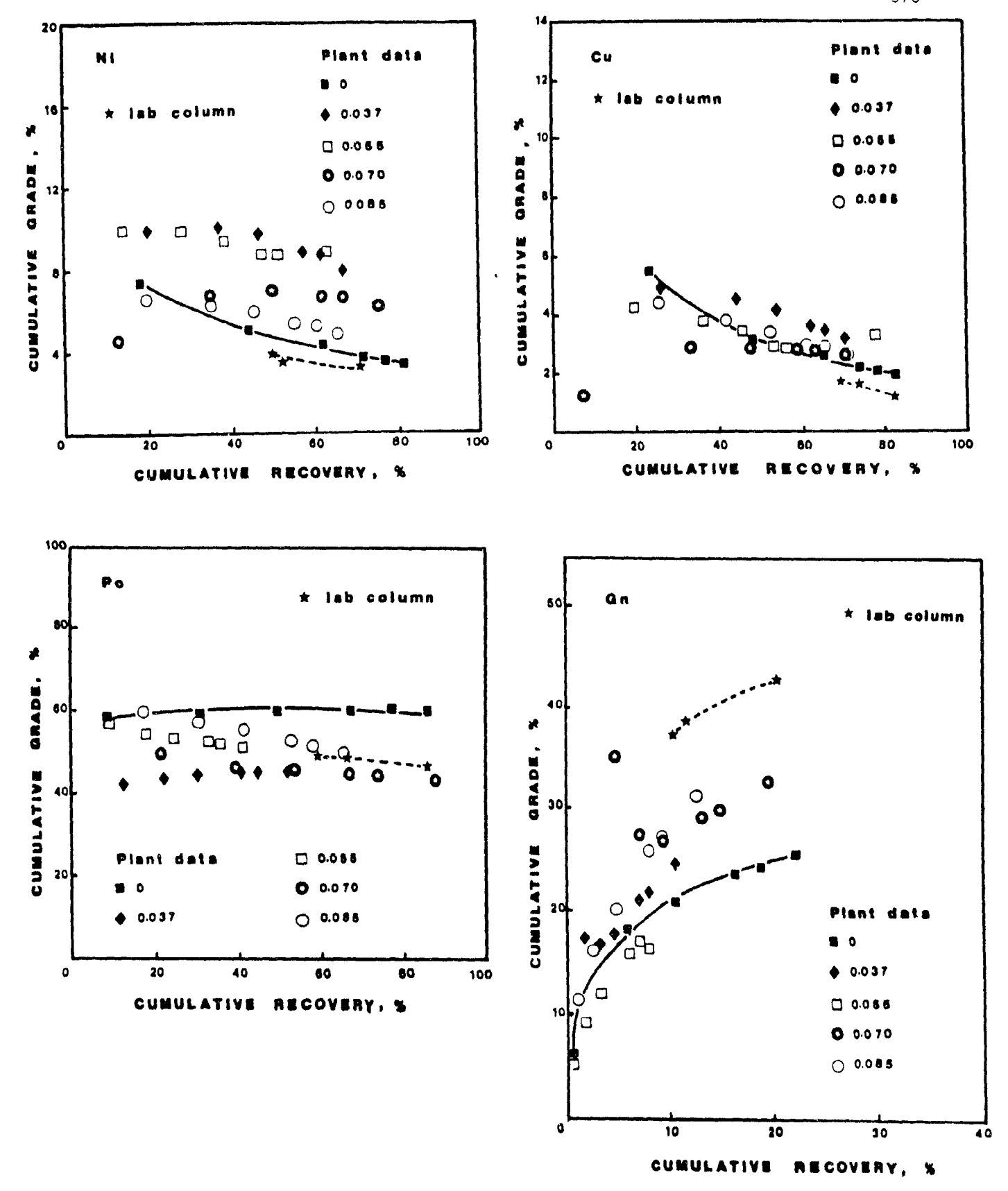


Figure 9.12: Cumulative grade-recovery curves for Ni (a), Cu (b), Po (c), and Gn (d) at the non-magnetic circuit using two pipes.

There is a slight increase in Cu grade at superficial wash water rates of 0.037 and 0.055 cm/s (Figure 9.12b). Po grade again remains almost constant in the absence of wash water (Figure 9.12c). Significant decreases in both grade and recovery were achieved at Jw=0.037 and 0.055 cm/s. Figure 9.12d shows the cumulative gangue grade-recovery curves. In the absence of wash water gangue recovery is maximum. Significant reductions in entrainment were obtained with wash water addition. Again results at superficial wash water rate of 0.070 cm/s are suspicious.

Figure 9.13 shows cumulative Ni grades for each cell along with feed grades at different wash water rates. Grade ratios (feed grade/overall bank grade) are 1.78, 2.44, 2.43, 2.33 at superficial rates of Ο, 0.037, 0.055, and 0.085 respectively. The grade ratios are much higher with wash water. Figure 9.13 also shows Ni grades with the lab column and cell (batch operation without wash water) obtained by del Villar (1988) using the non-magnetic feed. Head grades are lower for lab column and cell tests, but their grade ratios are 2.24 and 2.42, respectively. For the non-magnetic circuit mechanical cells outperform flotation columns for Ni upgrading even without wash water.

Due to variations in bank feed assays, the use of graderecovery curves may be misleading, therefore recovery-recovery curves will be used for better comparison. Figures 9.14a and b show the overall bank recoveries at different wash water rates.

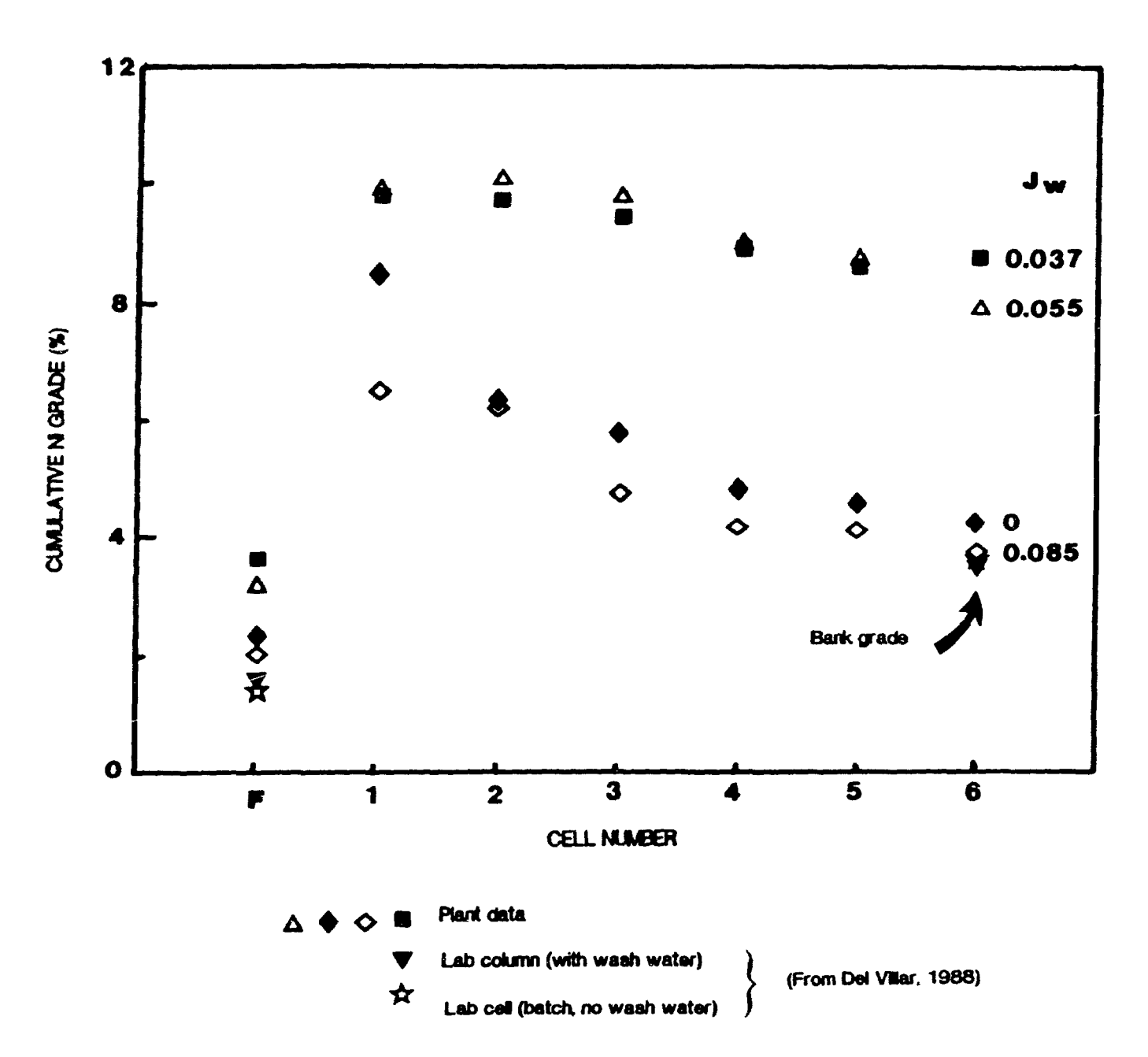


Figure 9.13: Cell-by-cell cumulative Ni grades along with feed grades with two pipes.

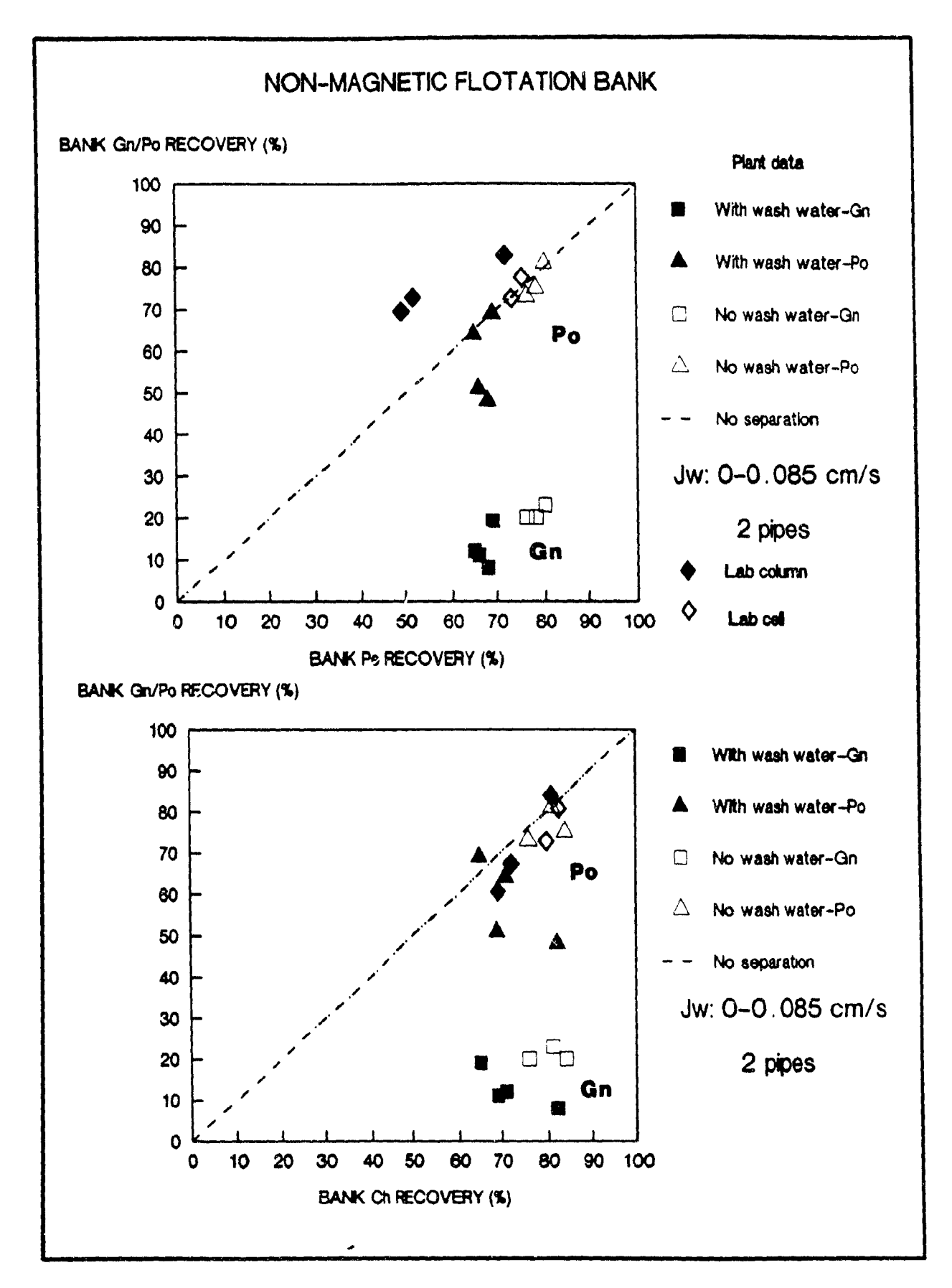


Figure 9.14: Overall recovery-recovery curves for Pe and Gn/Po and Ch and Gn/Po at different wash water rates with two pipes.

Clearly, the effect of wash water is to decrease the recovery of all species. The decrease in recovery for Po and Gn is more substantial than that of Ch and Pe. At the optimum J (0.055 cm/s), Po recovery decreased from 77% to 41%, Gn recovery from 20% to 7.7%, and Pe recovery from 77% to 63%. The flotation column performance is worse than mechanical cells both in Ni upgrading and Po rejection. The performance of batch lab tests is close to the non-magnetic circuit performance without wash water.

To better compare operation with and without wash water, the cumulative recoveries of Pe, Po, and Gn were compared (individual sampling of the cell concentrates makes this possible). The recovery-recovery curve without wash water was obtained from three separate tests; although not all points were identical, all sat on the same curve. Figure 9.15 shows that cumulative Po and Gn recoveries are lower with wash water (for 0.055 and 0.085 cm/s). Overall bank Po and Gn recoveries, identified with arrows, are lower with wash water.

The flotation feed is relatively coarse (60% -74 μ m), which minimizes entrainment effects and may cause liberation problems. Another masking effect is the natural hydrophobicity of Po, which is evident from lab and pilot results. Examining size-by-size behaviour, especially in the fine range, will minimize liberation considerations and maximize the effect of entrainment.

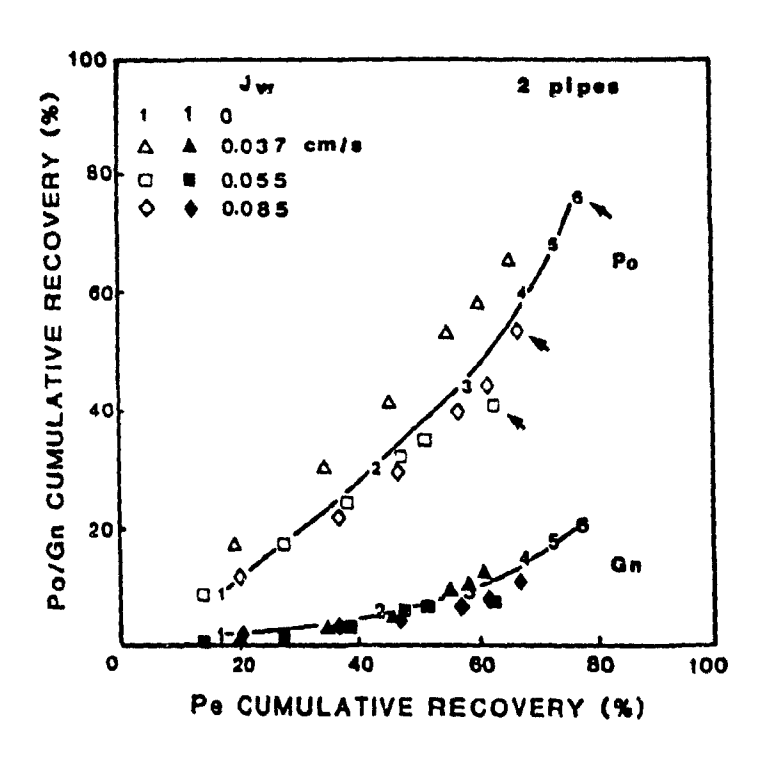


Figure 9.15: Cumulative non-magnetic bank recovery-recovery curves for Pe and Po/Gn with two pipes.

Figure 9.16 shows the size-by-size cumulative recoveries at the $J_{\rm w}$ of 0 and 0.055 cm/s. At constant Pe recovery, wash water decreases fine gangue recovery by half, and fine Po recovery by about 25%. In the coarse range, gangue rejection is also significant. Po recovery appears higher in the first cell, but lower in subsequent cells; after the sixth cell, overall performance with wash water sits on the same recovery-recovery curve as no wash water. More plant tests are necessary to clarify these results.

Figure 9.17 shows size-by-size metallurgical performance with and without wash water addition ($J_{\rm w}=0.055$ cm/s). Bank Ni grades from all size classes are higher with wash water. Ni recovery from +147, +74, and -37 μ m are lower and from +37 μ m are higher with wash water. Cu grades from each size class are higher while Cu recoveries are lower with wash water. Po and Gn recoveries are significantly lower with wash water.

Cell-by-cell Ni grades along with feed, tailing, and combined concentrate grades are given in Figure 9.18. Without wash water, only the first three cell in the non-magnetic circuit achieves Ni upgrading, while the rest fails. There is a steady decrease in the cell grade along the bank. With wash water, all of the cells achieve Ni upgrading. Ni grade is more uniform throughout the bank. Combined concentrate grades from each size classes are much higher with wash water. This may be caused by the decreased mean residence time.

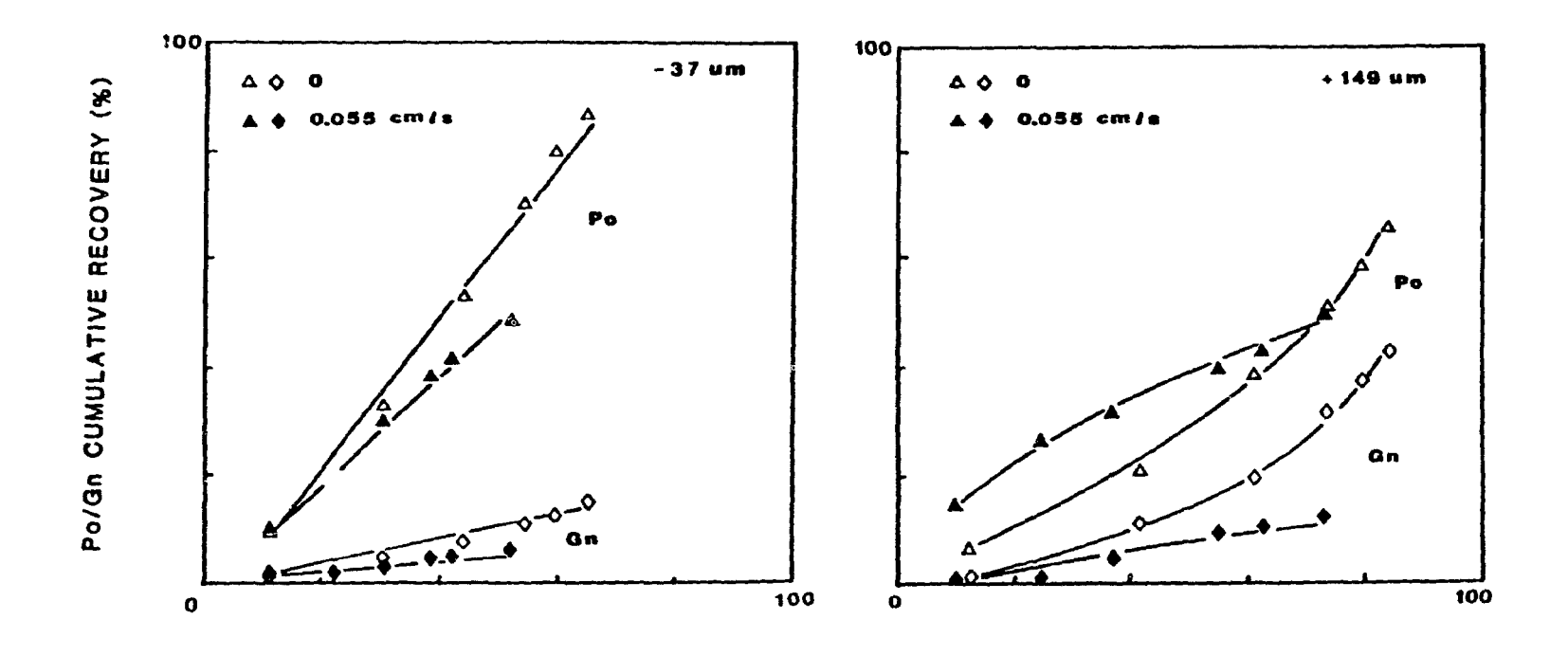


Figure 9.16: Size-by-size cumulative Pe and Po/Gn recovery-recovery curves with and without wash water.

Pe CUMULATIVE RECOVERY (%)

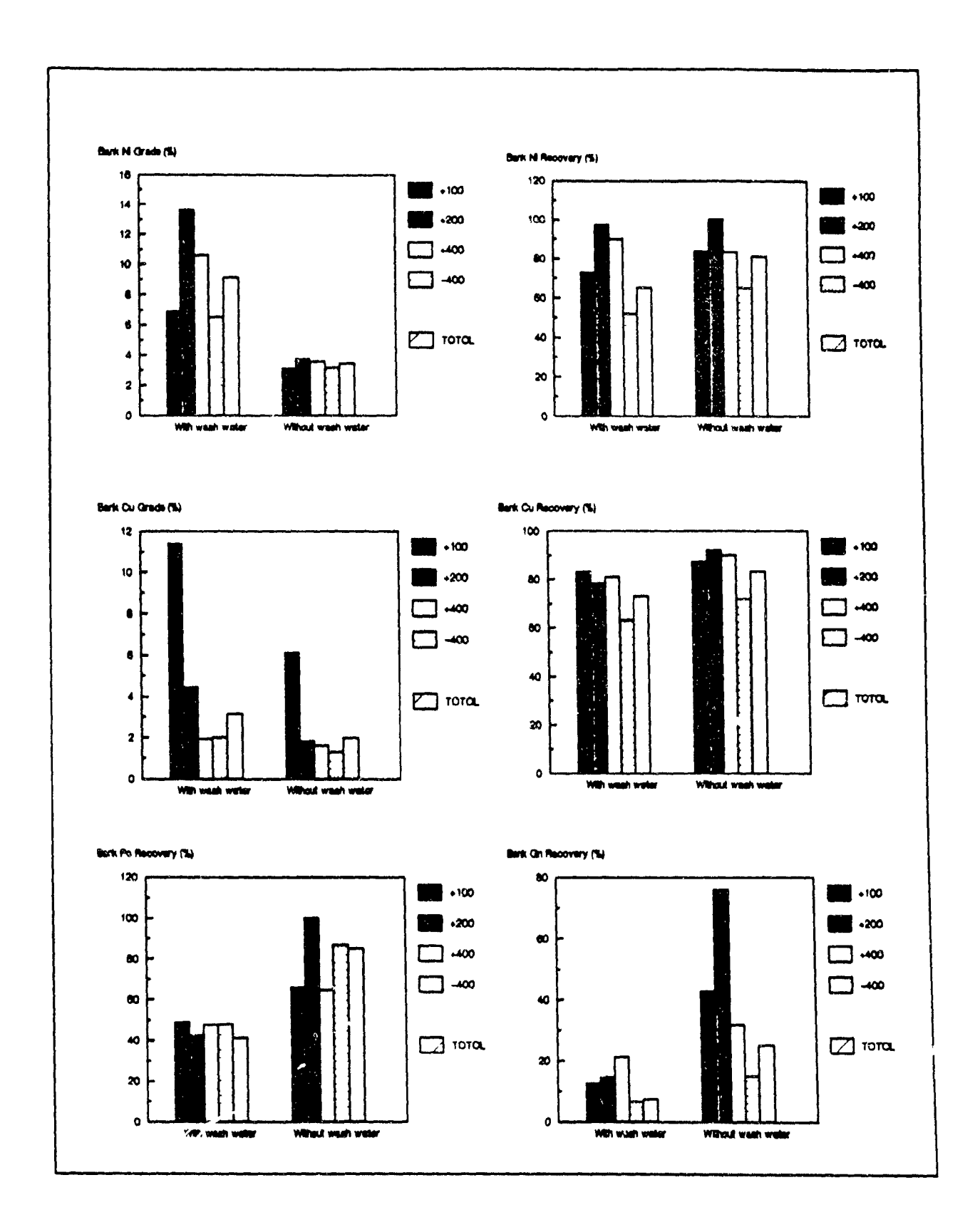


Figure 9.17: Effect of wash water on size-by-size metallurgical performance at the non-magnetic circuit using two pipes.

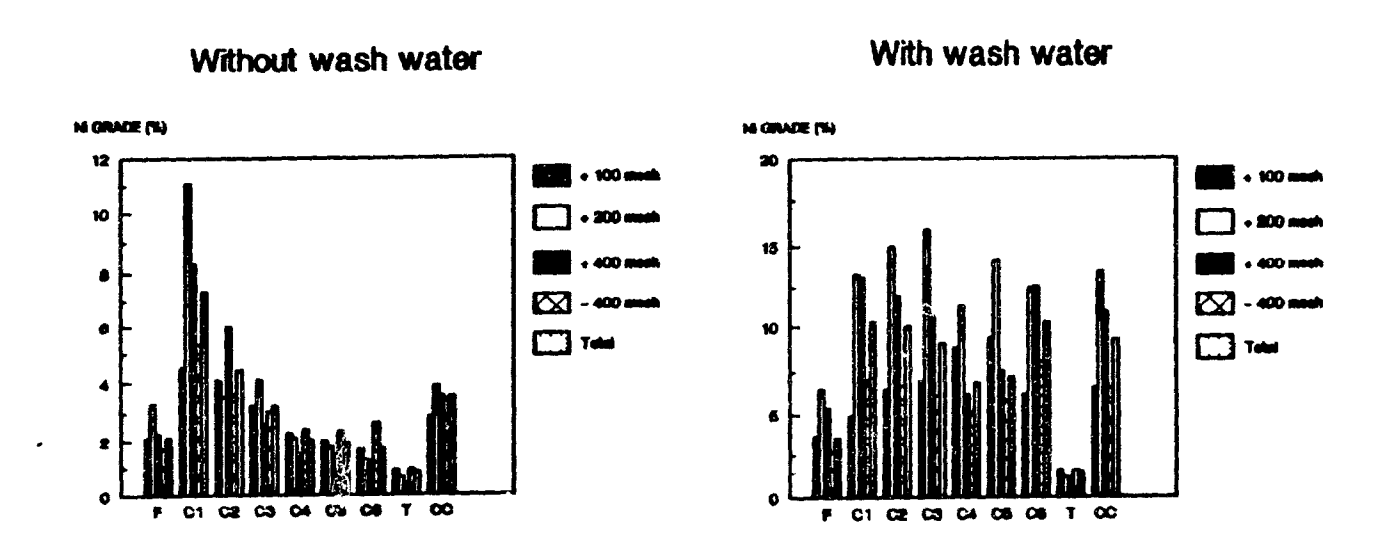


Figure 9.18: Cell-by-cell Ni grade from different size classes with and without wash water (Jw: 0.055 cm/s and two pipes).

The effect of superficial wash water rate on cumulative (bank) gangue and water recoveries is shown in Figure 9.19. There are minimums for both water and gangue at the same Jw; both curves are similar. However, gangue recovery is greater than water's presumably because it is not fully liberated or weakly hydrophobic. The presence of talc in the ore would suggest the latter. Figure 9.20 shows the effect of J on Po and water recoveries for the 2 and 4 pipe additions in each cell. Po does not exactly behave like water (i.e. it may be locked with pentlandite and/or chalcopyrite or be hydrophobic).

9.4.3 Effect of Wash Water on % Solid

In the primary non-magnetic bank, feed grade, feed size distribution and % solid vary significantly. Due to sampling problems, it was found that % solids were not very reliable. Figure 9.21 shows the % solid changes in the bank at three different Jws. There is a significant decrease in % solid in the bank as the pulp progresses from the first cell to the last.

9.4.4 Effect of Wash Water on the Grade Profiles in The Froth Phase

Figures 9.22 shows Ni, Cu, Po, and Gn grade profiles as a function of the distance from the froth surface in the absence and presence of wash water for cell numbers 2, 4, and 6. Ni, Cu, and Po grades increase towards the froth surface while Gn grade significantly decreases. Clearly Po behaves as a hydrophobic species. Ni and Cu grades always are higher in the presence of

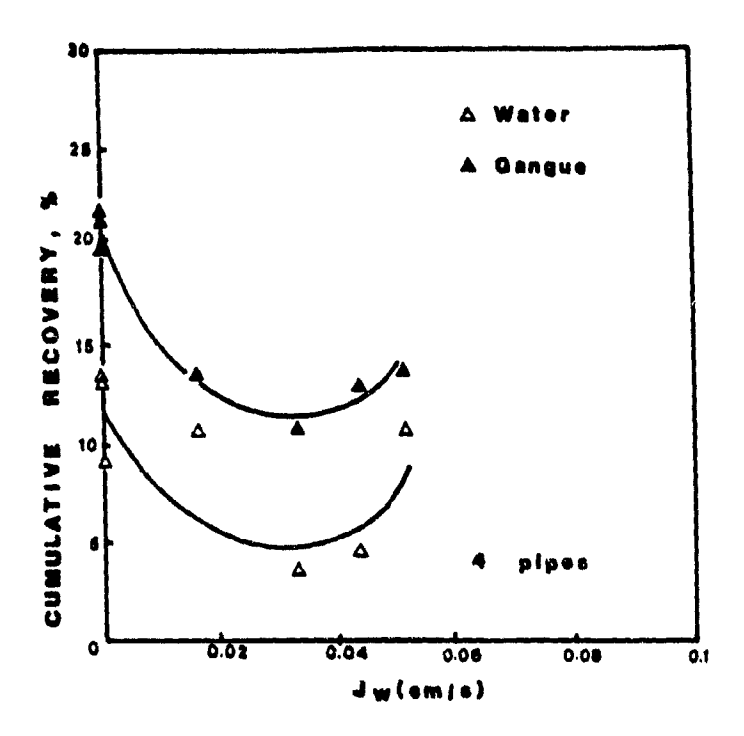


Figure 9.19: Cumulative gangue and water recoveries versus superficial wash water rate with four pipes.

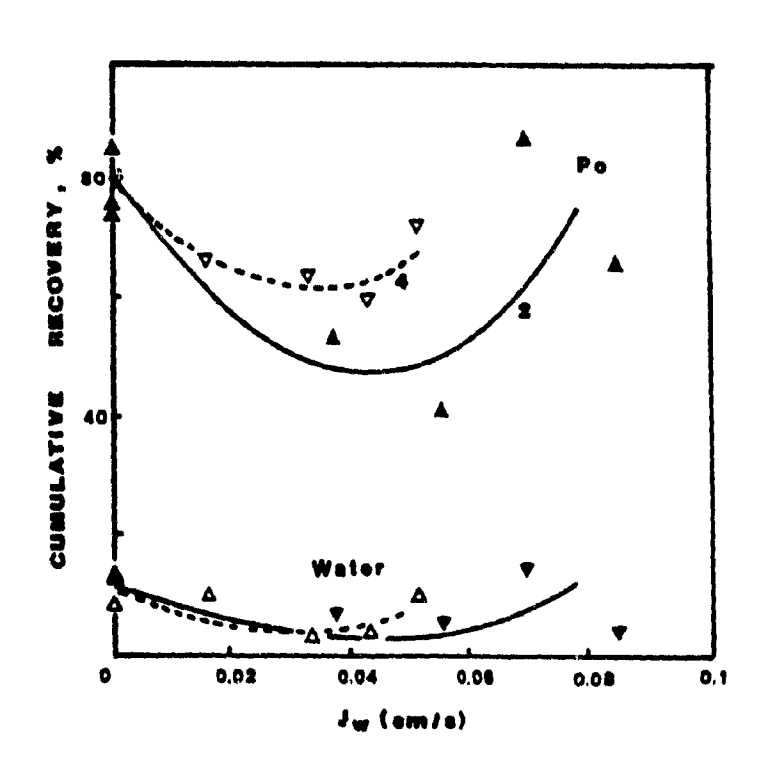


Figure 9.20: Cumulative Po and water recoveries versus superficial wash water rate with two pipes.

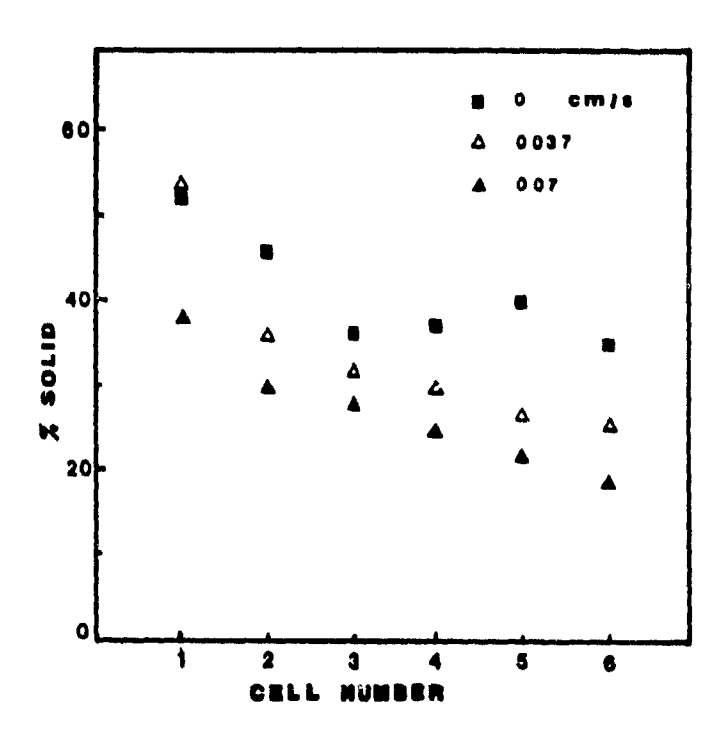


Figure 9.21: Cell-by-cell concentrate %solids at different wash water rates.

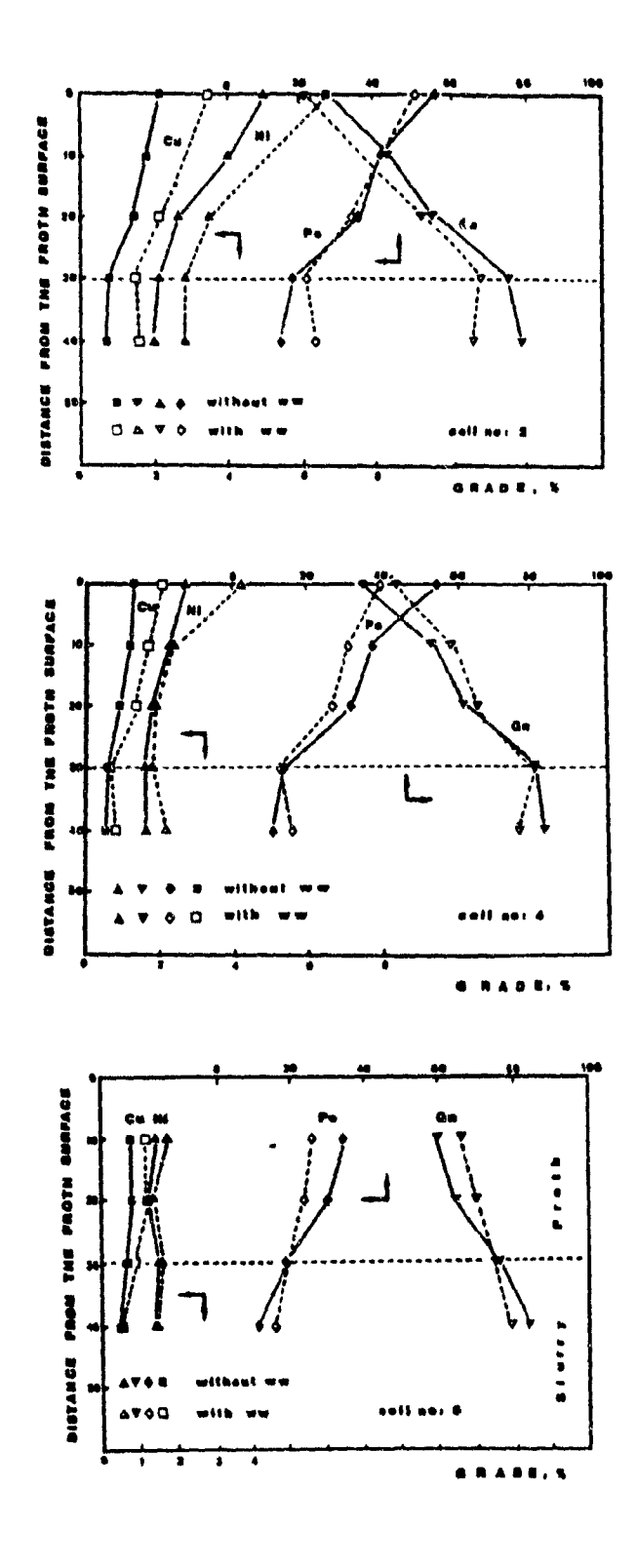


Figure 9.22: Froth Ni, Cu, Po, and Gn grade profiles with and without wash water.

wash water. Po grade is always lower with wash water. Po rejection is very substantial in cell 4 and 6. Gangue rejection in cell 2 is significant, while in cell 4 and 6, gangue grade is higher with wash water.

9.5 Conclusions

- 1. With four pipes, cumulative Ni and Cu grade increases 43% and 38%, respectively with wash water (Jw: 0.033 cm/s) at lower recoveries. Gn and Po recoveries were reduced by 48% and 15% with wash water. In the systems examined in this chapter, mechanical flotation always outperforms column flotation in Ni upgrawing and Po rejection.
- 2. With two pipes, the cumulative Ni and Cu grades are significantly higher, and Gn and Po grades are substantially lower at a J of 0.055 cm/s. At the same Pe recovery, wash water decreased fine gangue recovery by half, and Po recovery by about 25%. Variations in both bank feed assays and feed fineness make the direct comparison difficult. Washing the frontal froth surface with two pipes appears to be metallurgically better than a large surface with four pipes.
- 3. In the non-magnetic bank, gangue particles follow water, which indicates that they are mostly free, while Po does not, which indicates a possible locking or naturally hydrophobicity.
- 4. Upgrading of Ni and Cu, and rejection of Po and Gn in the froth was verified with froth grade profiles with wash water.

- 5. Ni recovery may be increased by decreasing the distance between wash water distributor and the froth surface, which decreases the collision rates between bubbles and water droplets.
- 6. Size-by-size metallurgical performance is a very useful tool to evaluate the effect of wash water for the non-magnetic circuit, which may contain coarse and locked particles.

CHAPTER 10

PLANT-SCALE WASH WATER TESTS

AT

EASTMAQUE GOLD MINES LTD.

10.1 Background About Eastmaque

Eastmaque Gold Mines Ltd. has the first commercial project recovering gold from mine tailings deposited in the Kirkland Lake area. The company has 9 Mi of tailings that were dumped in the lake during the early years of gold mining in the area by five gold producers from 1918 to 1934 (Wetjen and Irvine, 1988). The tailings, which have an average grade around 1.4 g/t, are recovered from a maximum depth of 14 m by a dredge using a submersible pump.

The material, which contains pyrite with gold and silica gangue, is pumped 600 m to the mill where extraneous debris is removed. The tailings are then ground to about 80% -45 µm (325 mesh), activated with Aero 350 and 3477, and fed to two cylindrical Maxwell cells, which recover most of the fast floating gold-bearing pyrite at a high grade. Maxwell tails are floated in twelve 14 m³ (500 ft³) Denver cells, which have free flow to launders on both sides. These cells are arranged in rougher and scavenger stages. Rougher and scavenger concentrates are cleaned twice to produce a concentrate assaying 56.7 to 70.88 g/t Au (2 to 2.5 oz/t) (see Figure 10 3). The cleaner cells are 2.8 m³ (100 ft³) Denver with overflow paddles. The flotation cell slurry level is maintained constant by the discharge weir height. Froth thickness in the secondary cleaner cells is around 25 cm. MIBC is used as a frother.

The final concentrate is thickened and pressure filtered before being trucked to the Noranda Horne smelter. The Eastmaque mill treats around 650000 t/y. The annual gold production is 24000 oz at a direct operating cost of \$US 182/oz.

10.2 Experimental

10.2.1 Distributor Set-up

Four cells in the 2nd cleaner bank were used to test the effect of wash water on gangue rejection. A plastic wash water distributor network with two branches in each cell was fixed behind the froth paddles (see Figure 10.1). The distributor was 30 cm above the froth surface. Figure 10.2 shows the distributor producing gentle water droplets. Wash water was introduced counter-current to the bank slurry flow. (i.e. highest wash water flow was applied to the last cell where the gangue grade in the concentrate is highest. Superficial wash water rate was 0.05 cm/s, which was the optimum determined at the Falconbridge Strathcona mill.

10.2.2 Test Work Program

Six tests were performed in one week. Table 10.1 shows the summary of test work. The first two tests lasted one day each, while the others took only two hours each. During wash water tests, flotation cells were operated as usual by the operators who increased or decreased the air flowrate to the banks as deemed

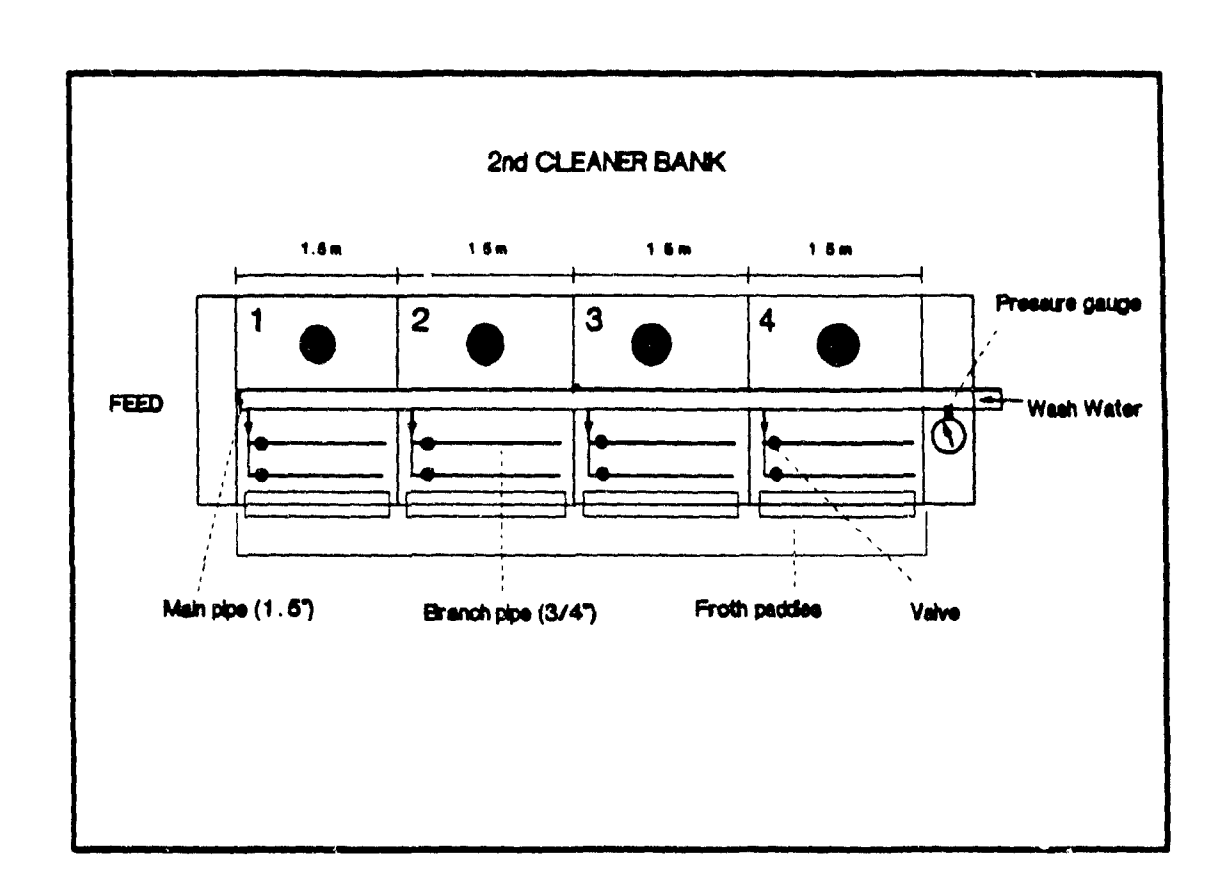


Figure 10.1: Wash water distributor network.

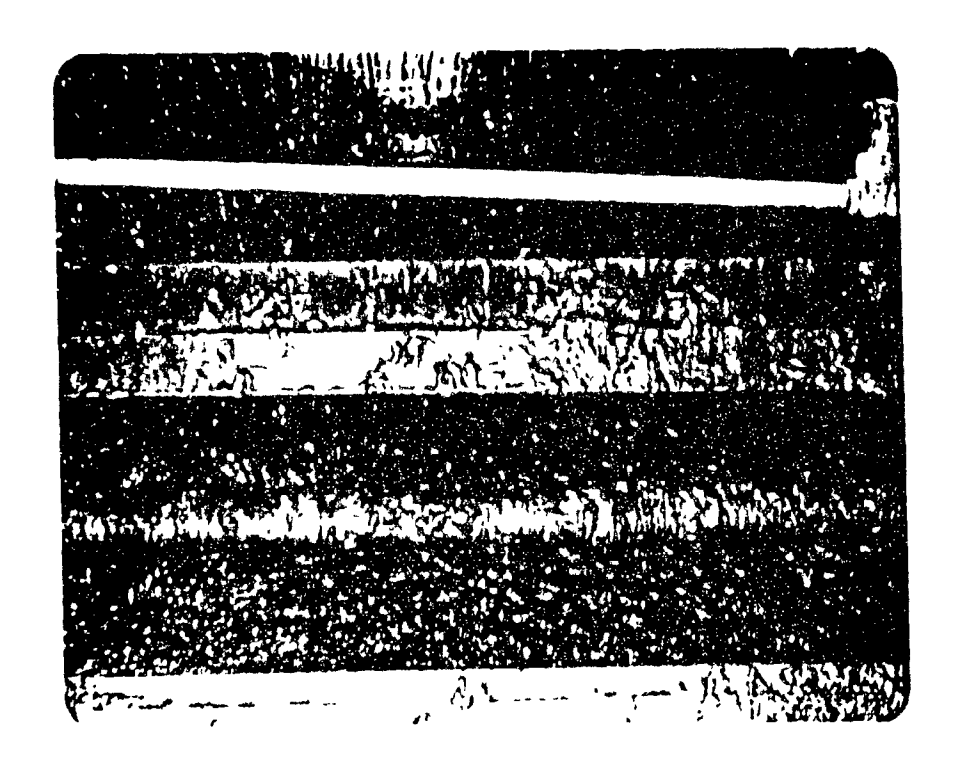


Figure 10.2: Wash water distributor is in operation.

necessary. According to flotation operators, the secondary cleaner bank operation was smoother and froth overflow to the launders was better with wash water.

The objective of tests 1 and 2 is to compare overall flotation circuit performance without and with wash water, respectively. Eight cuts from 13 streams were taken by appropriate samplers (i.e. cutters, plastic bottles, and metallic containers) over an 8 hour period (see Figure 10.3).

For test 2, wash water was added to the 2nd cleaner bank overnight before sampling to achieve steady-state condition. A salt tracer test using 250 g LiCl was also carried out in test 2. The dissolved salt tracer was added to the first cell of the bank and samples from the bank feed, tailing, and concentrate were collected to determine the feed water suppression with wash water.

Tests 3 and 4 were carried out using the front branch pipe in each cell at the same J_{w} . In these tests only the 2nd cleaner bank's performance was evaluated by taking 4 samples (i.e. Maxwell, 1st cleaner, and 2nd cleaner concentrates and 2nd cleaner tails) with and without wash water, respectively.

Table 10.1: Summary of plant test work at the Eastmaque mill.

No	Test Date	Test Objective		.st. /pe	Temp. °C	Trac. LIC1	Size Anal.
1	Sept.5	circuit performance without wash water cell no 1 to 4	All flot circuit 13 samples		T _P =17	no	yes
2	Sept.7	circuit performance with wash water cell no: 1 to 4	All flot. circuit 13 samples	2	T _p =17	yes	yes
3	Sept.7	bank performance with wash water cell no: 1 to 4	2nd cleaner bank 4 samples	1	T _p =17	no	no
4	Sept.7	bank performance without wash water cell no 1 to 4	2nd cleaner bank 4 samples		T _p =17	no	no
5	Sept.8	cell performance without wash water cell no: 4	2nd cleaner cell 3 samples		T _p =17	no	no
6	Sept.8	cell performance with warm wash water cell no: 4	2nd cleaner cell 4 samples	2	T = 17 T = 45 T _f = 23	no	yes

(dist: distributor, trac: tracer, anal: analysis, p. pulp,

ww: wash water, and f: final pulp)

The effect of warm wash water with two branch pipes in each cell was determined using only 4th cell of the 2nd cleaner bank in test 5 and 6. The use of whole bank was not possible due to lack of warm water. For these tests, the pulp temperature without wash water was 17°C, wash water temperature 45°C, and final pulp temperature with warm wash water was 23°C.

10.2.3 Sample Preparation

Each sample was weighed, filtered, dried, weighed, rolled, and screened at the end of each test. Samples were assayed for gold at the Swastika Laboratories Ltd. Products from tests 1, 2, and 6 were sized. First, samples were screened at 147 μm to break the lumps and then wet screened at 37 μm for 10 minutes. The +37 μm fraction was dry screened with 105, 74, 53, 44, and 37 μm screen sets for 15 minutes. Some of the -37 μm fractions were cyclosized for 10 minutes. All products were classified into six size classes for Au assaying. For test 2, liquid tracer samples were filtered and analyzed for Li by an atomic absorption.

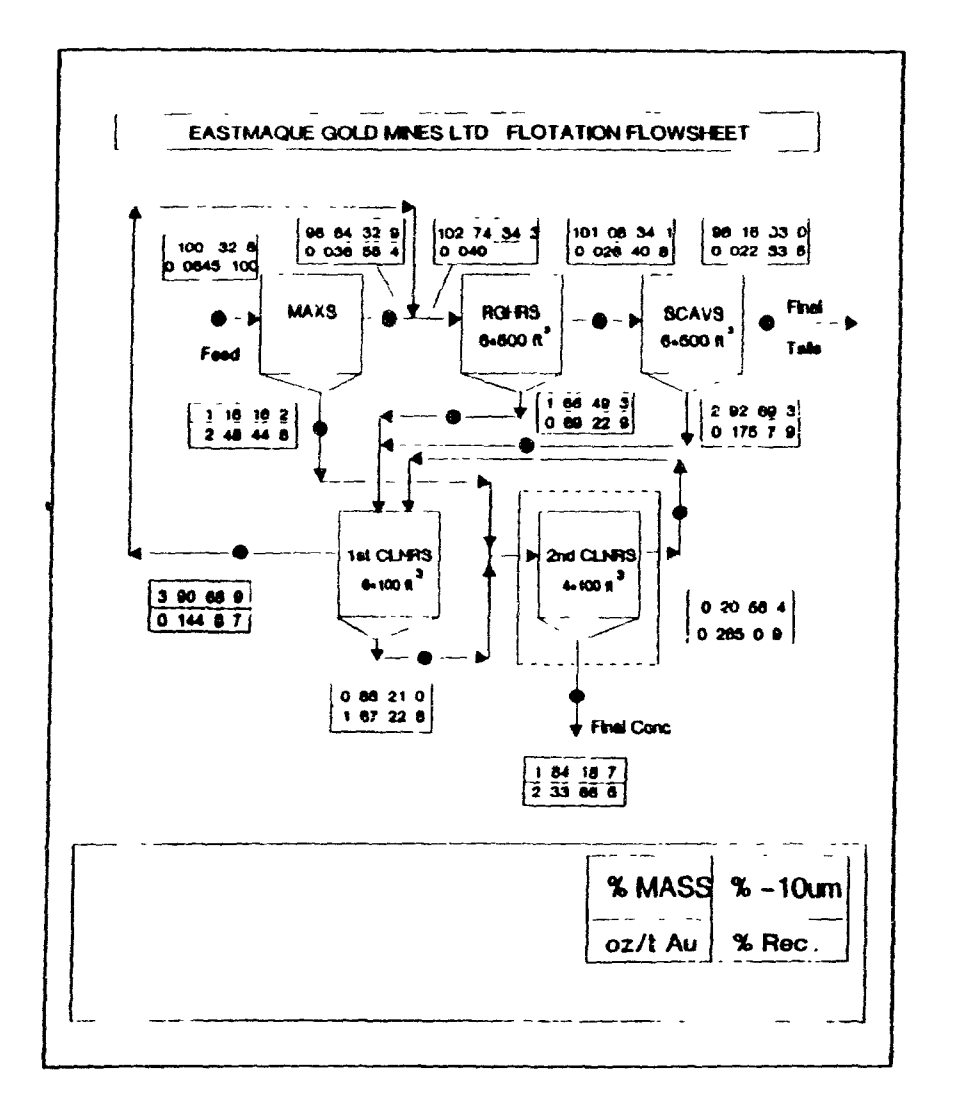
10.2.4 Data Processing

Raw data were mass balanced using a standard algorithm (Smith and Ichiyen, 1974) method and calculations were made using the LOTUS 123 program. % solids was not mass balanced, because of water addition to the launders.

10.3. Results and Discussion

10.3.1 Effect of Wash Water on Overall Flotation Circuit Performance

Figure 10.3 shows the flotation circuit performance without and with wash water as a function of % mass, % -10 µm, gold grade and recovery. Feed grade without wash water is slightly lower. Final concentrate grades are 2.66 and 2.33 oz/t with and without wash water, respectively. A 14% increase in final gold grade at a



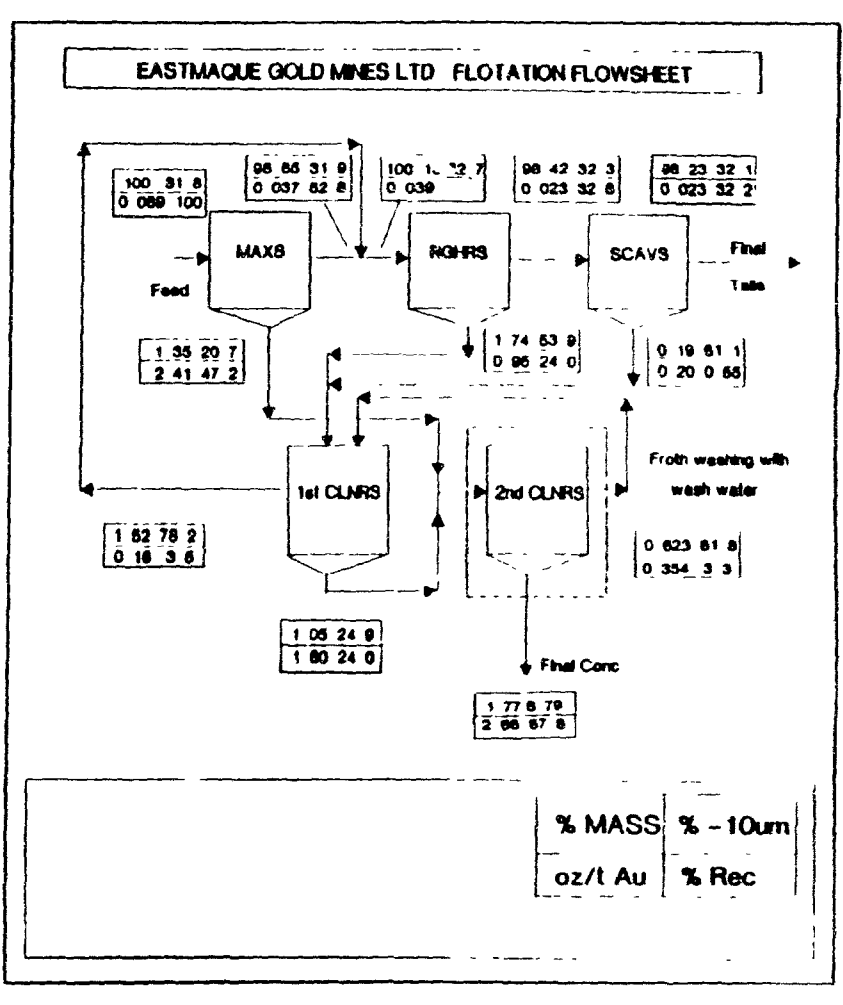
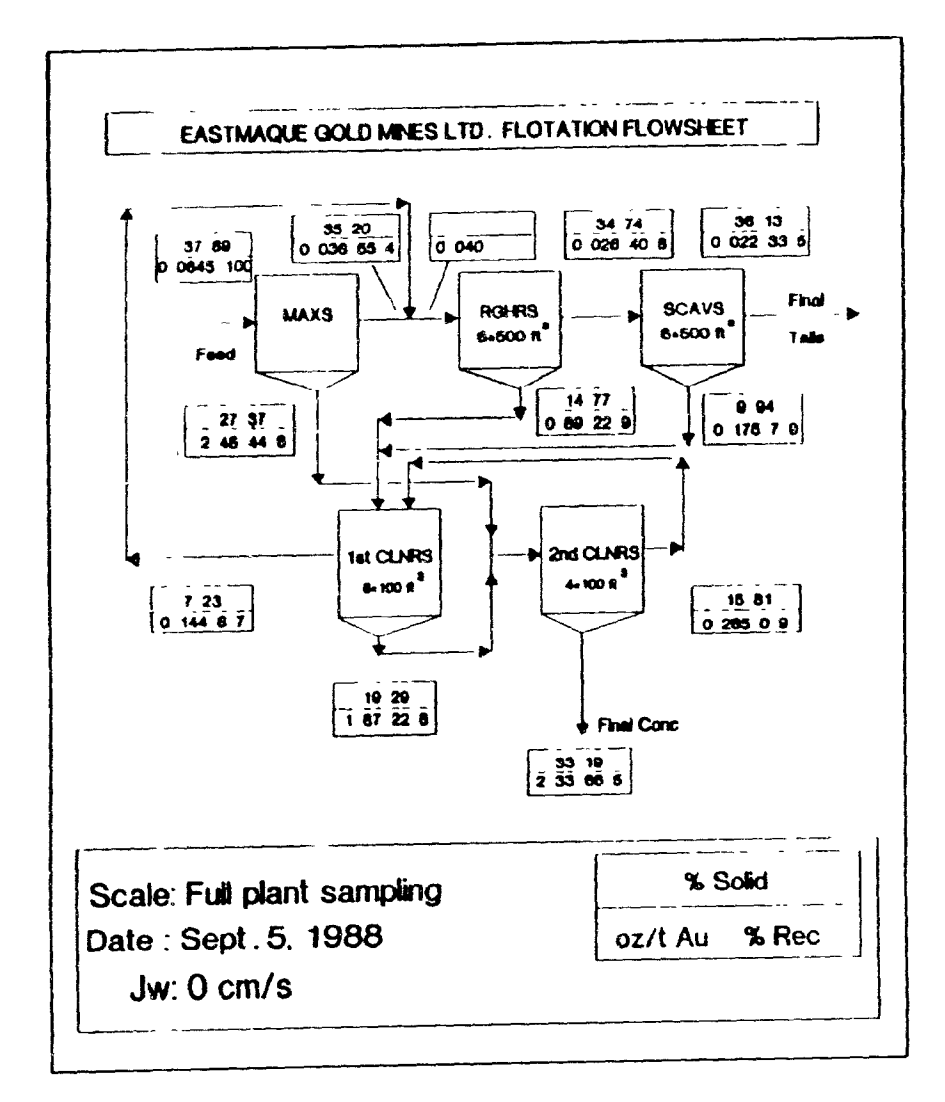


Figure 10.3: Effect of wash water on overall flotation circuit performance with and without wash water (Circles shows the sampling points) (Test 1 and 2).

slightly higher recovery reduces final concentrate tonnage for shipping to the smelter and increases quality. With wash water, the percentage of -10 μm is significantly lower. Fines are returned to the first cleaner and then to the roughers and scavengers.

Figure 10.4 shows the % solids in the flotation circuit in the absence and presence of wash water. The secondary cleaner concentrate and tails are significantly diluted with wash water due to a low feed flowrate to the bank. Final tailing is also more dilute (which may be advantageous to reduce pumping and plugging problems in the long tailing discharge line), but this is not primaraly due to wash water, whose flowrate could not possibly have a significant effect on final tail density. During wash water tests, the thickener and filter easily handled the additional water. Since the wash water is added in the last stage of cleaning, there was no flotation capacity reduction.

Size-by-size gold grades with and without wash water are given in Figure 10.5. Feed size for both cases are very close to each other. The final concentrate with wash water contains significantly less fines. Concentrate gold grades with wash water are higher for all size classes. Gold loss in the final tails is significant for the coarsest size class, which may indicate that gold bearing pyrite is not well liberated and requires further



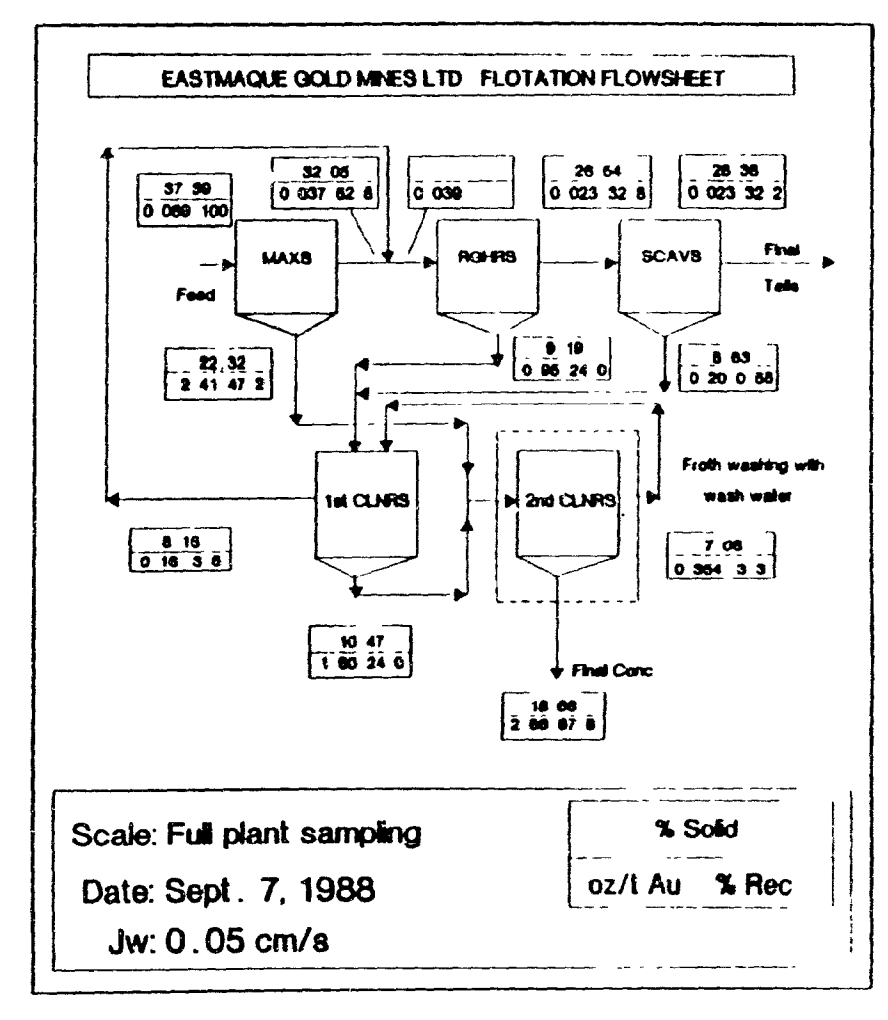


Figure 10.4: % solids in the flotation circuit with and without wash water (Test 1 and 2).

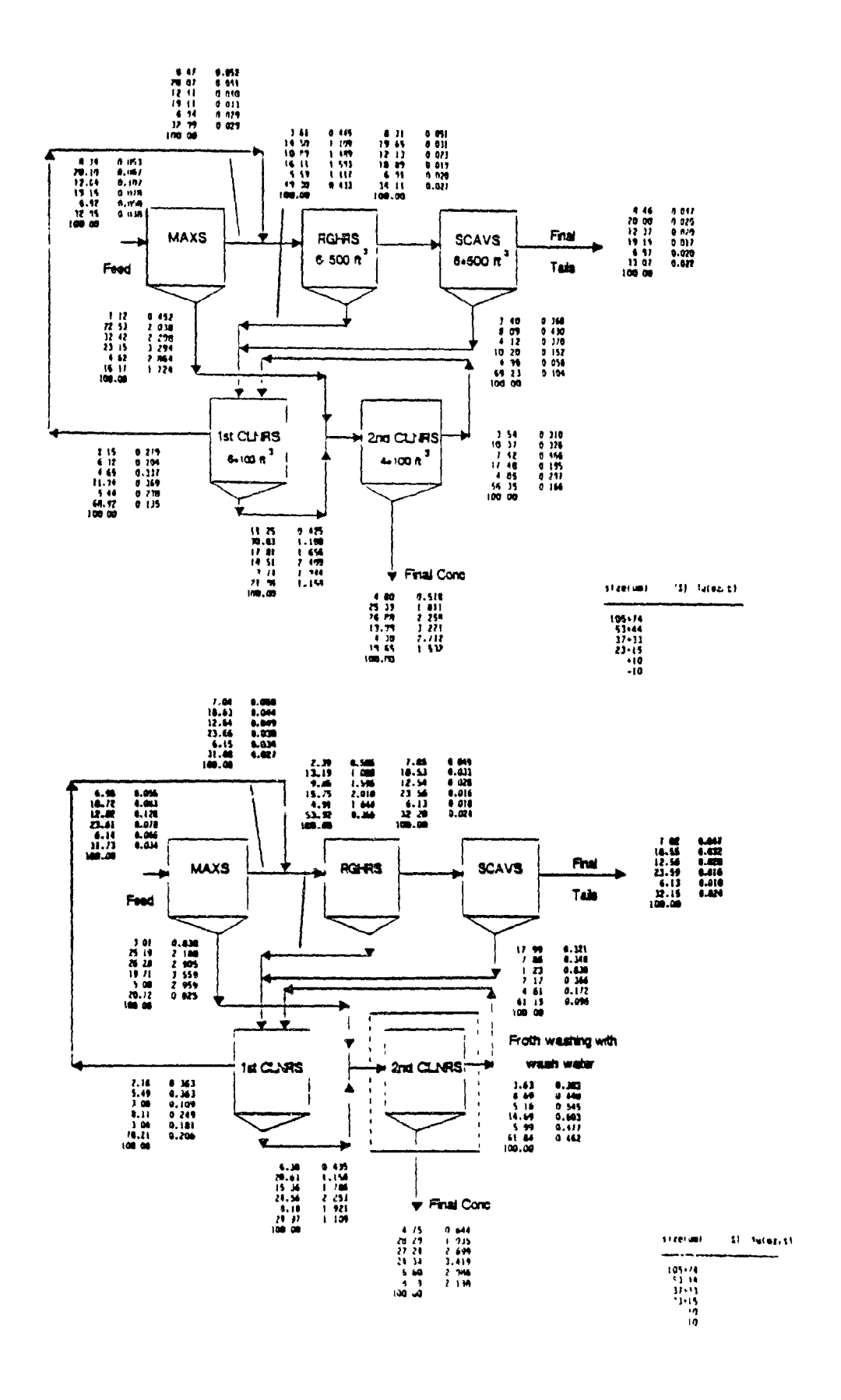


Figure 10.5: Size-by-size gold grades in the flotation circuit with and without wash water (Test 1 and 2).

grinding. Concentrate gold content of the intermediate size classes is higher than the coarsest and finest size classes. This further suggests the hypothesis of poor pyrite liberation and also suggests that hydrophilic entrainment can be further curbed down.

Size-by-size gangue and gold recoveries with respect to feed are shown in Figure 10.6. Cangue content is determined by assuming that pure pyrite assays 3.56 oz/t Au, which was the maximum gold grade achieved. Gangue recovery to the final concentrate is significantly lower for the finest size class with wash water. The maximum gold losses to the final tails are from the coarsest and finest size classes. Coarsest losses, e.g. 86% in the +74 μ m (200 mesh), are likely due to poor liberation; finest losses, e.g. 70% in the -10 μ m, could be due either to oxidized pyrite or poor flotation kinetics.

It is likely that gold in the -10 μ m is associated with iron oxides; this could be verified with cyanidation tests. If this is the case, its recovery by flotation is virtually impossible. The -10 μ m constitutes about a third of the feed mass; fortunately, its gold content is the lowest of all size classes, 0.04 oz/t.

10.3.2 Effect of Wash Water on Bank Performance

Figure 10.7 compares the 2nd cleaner bank performance with and without wash water, which is added by a single pipe in each cell. Final concentrate gold grade is 2 82 oz/t with wash water,

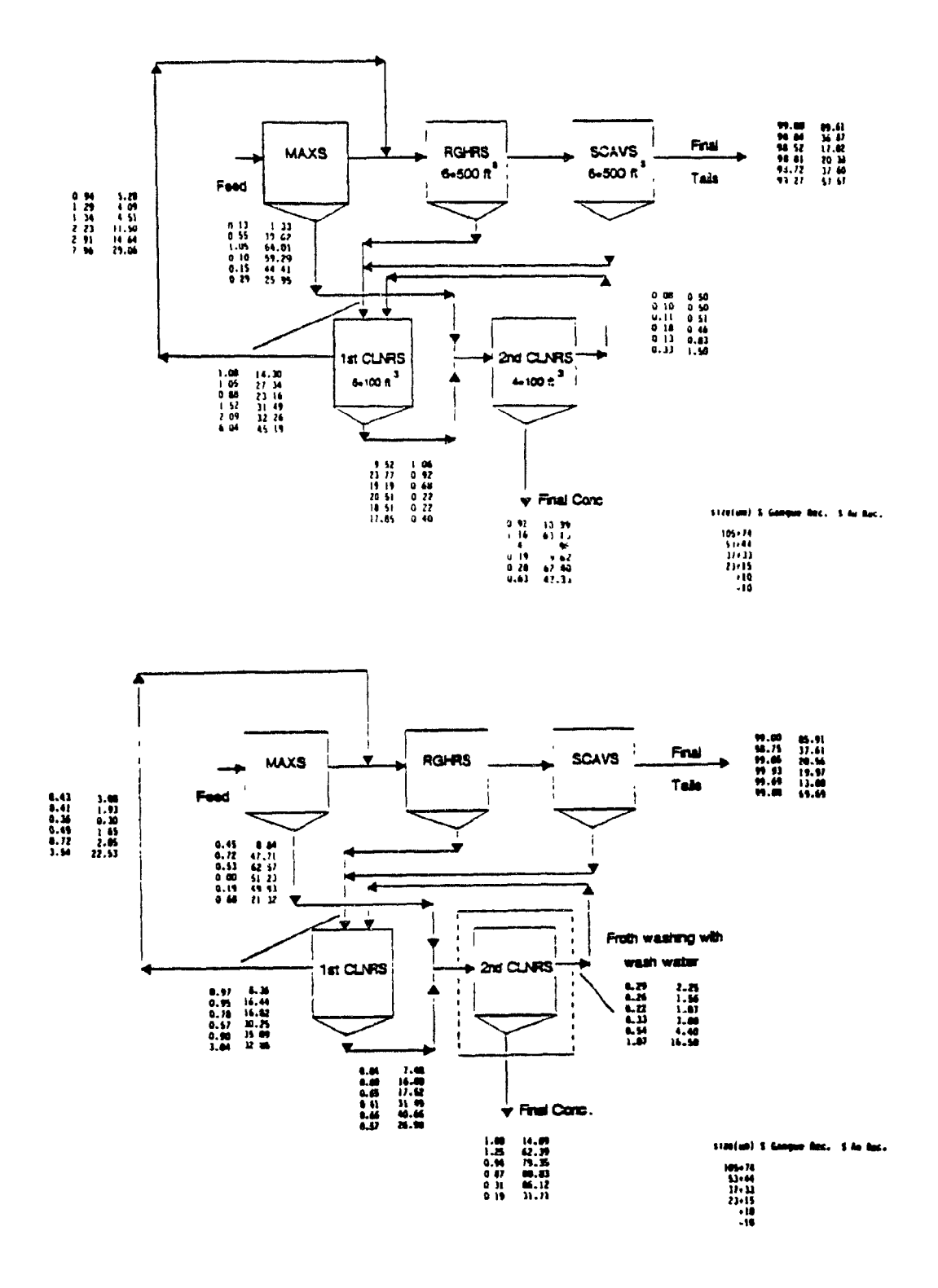


Figure 10.6:.Size-by-size gangue and gold recoveries with and without wash water (Test 1 and 2).

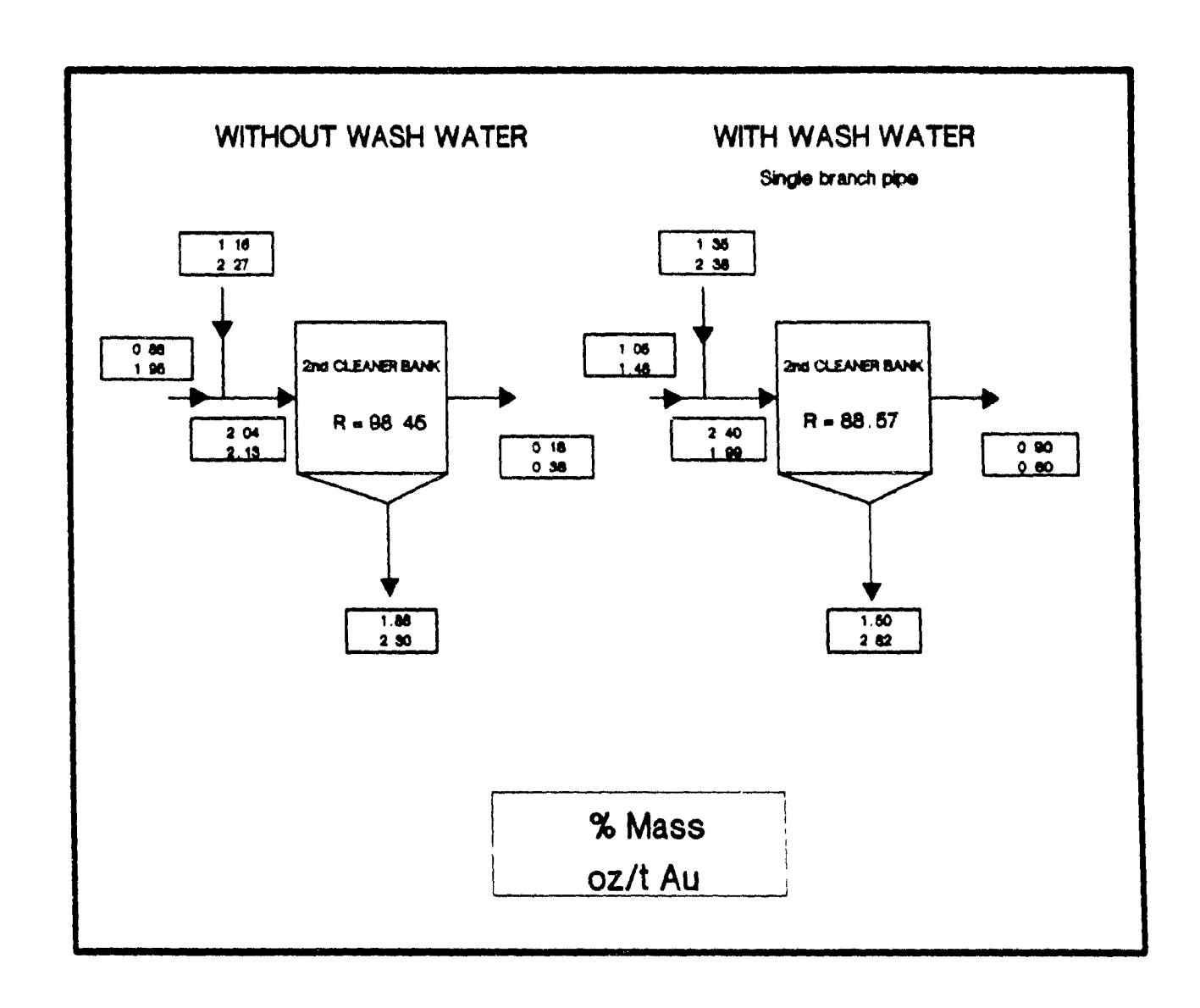


Figure 10.7: Effect of wash water on the 2nd cleaner bank performance (Test 3 and 4).

which is 23% higher than without wash water. However, the concentrate recovery decreased from 98% down to 89% with wash water, probably due to the strong water discharge rate from the distributor. The use of two pipes per cell appears to be more attractive than a single pipe.

The first two tests showed that although bank gold recovery decreased from 98.7% to 95.4% because of wash water, overall recovery was not affected. If this would be the case here, clearly the use of a single strand would be extremely advantageous. This would need to be demonstrated over a long time period before the decision is made to use a simple washing strand per cell.

10.3.3 Temperature Effect

Table 10.2 summarizes test 6 results with warm wash water in the 4th cell of the 2nd cleaner bank (no wash water to the first three cell). With wash water the 4th cell concentrate contains the minimum amount of -37µm fraction: 95% of the -37µm fraction, which contains less gold, is rejected to the tails. Generally, Au grade goes down significantly along the bank. The 4th cell concentrate grade is higher than the 3rd cell showing that warm wash water helps the increase gold grade. Thus, wash water eliminates the decrease in concentrate grade from cell 3 to 4, and yields a slight increase. More test work is needed to confirm the results.

Table 10 2 Test 6 results with warm wash water on the 4th cell.

	+37µm	-37µm	Calc.	Overall	Average
	WITH	WARM WASH WA	TER		
4th cell tail					
Mass (%)	5	95			
Au(oz/t)	0.211	0 112	0.117	0.20	0.159
4th cell conc.					
Mass (%)	60	40			
Au(oz/t)	1.550	0.550	1. 150	1.10	1.125
3rd cell tail					
Mass (%)	18	82			
Au(oz/t)	0. 183	0.126	0.136	0.25	0.193
3rd cell conc.					
Mass (%)	43	57			
Au(oz/t)	0.610	1.450	1.090	1.10	1.095

10.3.4 Tracer Test Results

Figure 10.8 shows Li concentration versus time curves for tailing, concentrate, and feed. Li content is highest in tailing. The concentrate Li content is significantly lower than that of tailing's due to dilution of feed water with wash water. There is a small amount of tracer recycle in flotation circuit. All of the tracer exits the bank within three hours. The average residence time in the 2nd cleaner bank is 51 minutes.

Feed water recovery, $\mathbf{R}_{\underline{\mbox{\scriptsize J}}},$ was calculated from:

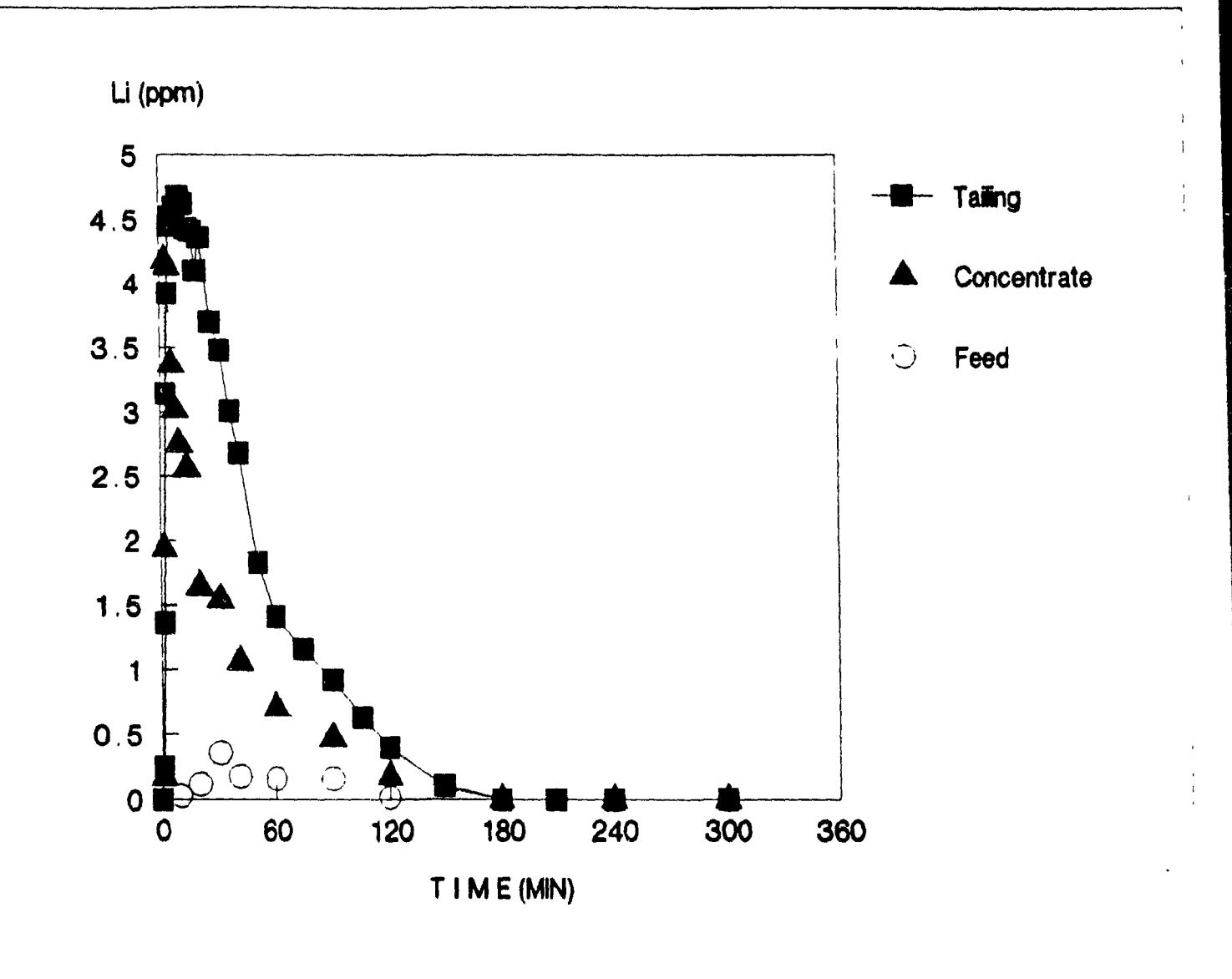


Figure 10.8: Li concentration versus time for the tracer test (Test 2).

$$R_{w} = \frac{\int_{c}^{c} C_{c}(t) \cdot Q_{cw} dt}{\int_{c}^{c} C_{c}(t) \cdot Q_{cw} \cdot dt} + \int_{c}^{c} C_{c}(t) \cdot Q_{cw} \cdot dt}$$
10.1

C: concentrate tracer concentration

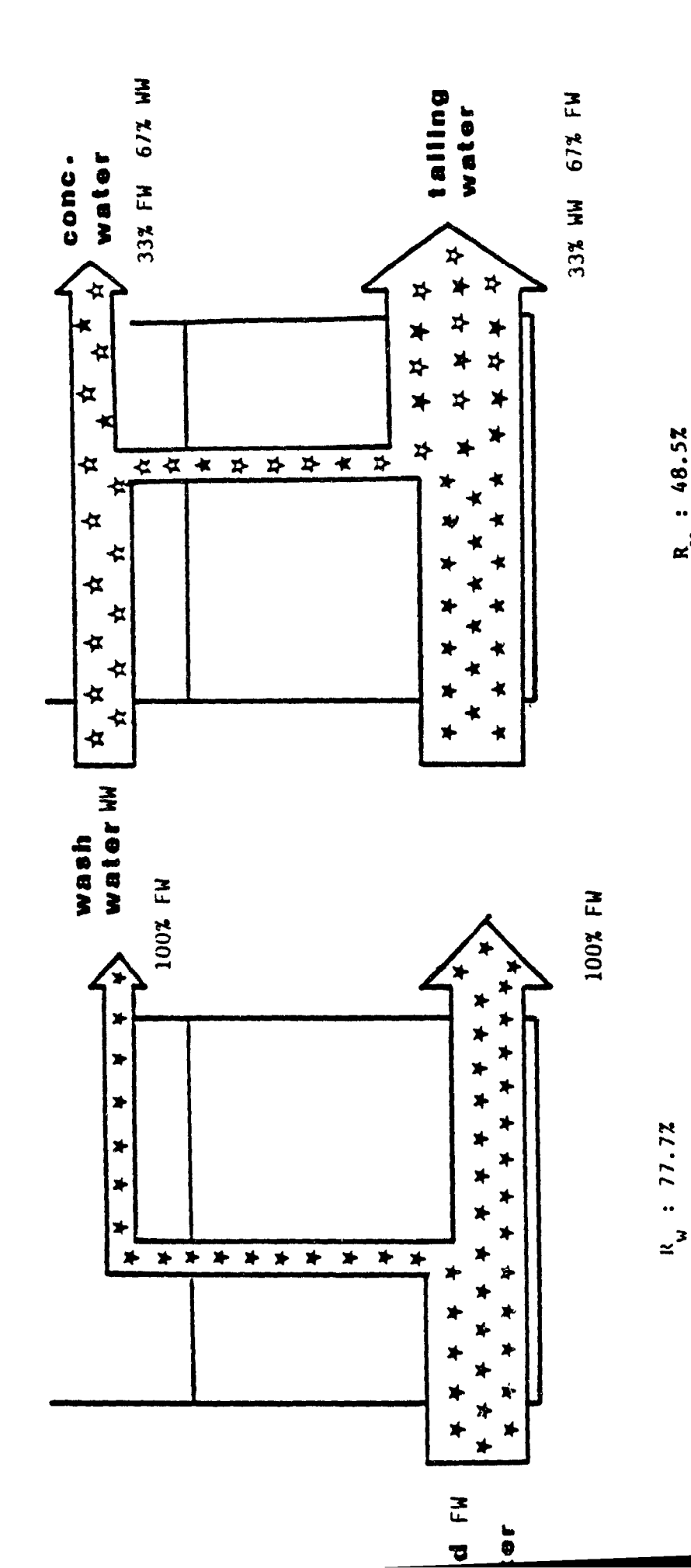
C. : tailing tracer concentration

 Q_{cw} : concentrate water flowrate

 Q_{tw} : tailing water flowrate

Total water recoveries are 48.5% and 77.7% with and without wash water. Feed water recovery with wash water is 33% as compared to 77.7% without wash water, which corresponds to a 58% reduction in the feed water recovery. Figure 10.9 illustrates the composition of concentrate water in the presence and absence of wash water. Replacement of feed water containing gangue particles with wash water is the main reason for increased concentrate grade in these tests.

Gangue recoveries and classification coefficients (i.e. gangue recovery/water recovery) in the 2nd cleaner bank is given in Table 10.3. The lower the classification coefficient (Z^{\bullet}), the better the gangue rejection Gangue recovery (R_g) for each size class is drastically lower with wash water in the 2nd cleaner bank. The classification coefficients are significantly lower with wash water than without it



With Wash Water

Without Wash Water

Figure 10.9: Feed and wash water splits.

R.: 48.5%

Table 10.3: Classification coefficients and gangue recoveries in the 2nd cleaner cell (Test 1 and 2).

	With was	With wash water		Without wash water	
Size (μm)	R _g (%)	Z	R _g (%)	2	
	18	0.38	51	0.66	
15+10	37	0.76	68	0.87	
-10	15	0.31	65	0.83	

10.3.5 Economic Impact of the Wash Water on Flotation Performance

As can be seen from the results of test 1 and 2, final concentrate grade can be increased by about 14%. Although gold recovery is higher with wash water, this increase will not be taken into account in the economic evaluation to be on the conservative side. There is a very good possibility that the recovery increase is real, and due to the decreased retention time, which limits pyrite surface oxidation. More experimental data over a long time period is necessary to support this claim. Table 10.4 shows the summary of results

10.4 Summary

It is clearly shown that wash water can increase final concentrate grade about 14% possibly at a slightly higher gold recovery. Wash water does not have any detrimental effect to Eastmaque current mill operation, it can generate an extra yearly revenue of about a quarter of a million dollars at almost no cost (i.e distributor for the 2nd cleaner bank costs less than 500 \$).

The use of froth washing at the Eastmaque mill is strongly recommended to reduce the concentrate tonnage and possibly to increase gold content. Warming wash water may provide further savings, but this should be economically and metallurgically tested in a bank scale before reaching a firm conclusion. Further grinding of mill feed may reduce coarse gold loss to the final tails.

Table 10.4: Economic impact of wash water.

	Without wash water	With wash water
Feed (t/d)	2500	2500
Grade (oz/t)	0.069	0.069
Gold content (oz/d)	172.50	172.50
Final Concentrate		
Recovery (%)	66.50	66.50
Grade (oz/t)	2.33	2.66
Gold content (oz/d)	114.71	114.71
Concentrate (t/d)	49.23	43.13

Yearly additional economic benefits

(assuming 330 d/y, transportation and smelting costs: 135 \$/t)

SAVINGS - **\$272.000**

CHAPTER 11 GENERAL CONCLUSIONS

CONCLUSIONS

11.1 General Summary

Gas holdup in the slurry phase is one of the most important factors charterizing the hydrodynamics of a mechanical flotation cell. Overall gas holdup in the slurry phase can be predicted using Calderbank's model. Local and point gas holdup measurements showed that the gas phase was not homogeneously distributed. Superficial gas rate significantly increases gas holdup in the slurry phase leading to higher gangue entrainment into the froth phase. As the size of the flotation cell increases, the superficial gas rate has to be increased, to maintain a constant air flow number, an important scale-up criterion (Harris, 1976). Thus, entrainment into the froth phase is expected to be more important in plant-scale.

Two different zones in a washed froth were recognized: an expanded bubble bed, 1-2 cm thick, near the interface and a packed bubble bed above. This structure is similar to that described by Yianatos (1987) for column flotation froths. The expanded bubble bed is made of small bubbles (2-3 mm) generally homogeneous in size, and is relatively wet ($\varepsilon_1 > 26\%$). The packed bubble bed is drier, $5\%<\varepsilon_1<15\%$; but unlike Yianatos's (1987) model, retains highly spherical bubbles. The higher bubble content is achieved by coalescence, which yields a wider bubble size distribution (2-10 mm). The gas holdup profile in the froth phase strongly depends

on the superficial gas and wash water rates, frother dosage, and impeller speed.

A predictive water recovery model depending on the well and momentum conservation equations was established. Cell discharge coefficients were determined as 0.009 and 0.013 for laboratory and pilot cells, respectively.

The effect of some operating variables on mean residence time and feed water recovery was determined at laboratory scale. It was found that wash water decreases the bubble residence time both in the slurry and froth phases, which is one of the deleterious effect of wash water addition. An increase in gas rate on froth thickness increases gas residence time in the froth phase.

The effect of superficial gas and wash water rate on gangue profile in the slurry phase is small. Gangue content in the froth decreases with increasing wash water rate or decreasing gas rate. Most of the gangue is rejected near the slurry-froth interface.

A criterion was developed to calculate the classification coefficient for hydrophilic particle rejection. It was found that particle settling velocity is negligible for fine particles (-10 μm).

The cleaning action taking place in the froth was visually verified. The perforated pipe type of distributor was best for homogeneous and gentle water addition in laboratory scale cells. Wash water addition location has a significant effect on gangue rejection. Additions above the froth phase have more advantages However, distributor geometry has little effect on gangue entrainment. There is an optimum wash water addition rate between 0.03 and 0.07 cm/s. Excess wash water is not attractive due to increased water requirements and excessive pulp dilution. It also increases gangue recovery due to froth mixing, short-circuits material from the pulp to the concentrate and causes severe bubble breakage and froth bed collapse.

Wash water can reduce entrainment more than 50%. Mechanical or ultrasonic vibration and temperature gradient between pulp and wash water can be used to further reduce gangue entrainment (around 10-20%).

A classification coefficient and water recovery were correlated to predict gangue recovery. This classification coefficient was originally derived to quantify the effect of particle size on entrainment. It was adopted here to predict overall free gangue recovery for full size distributions with a reasonable success. Results from different scales (2L to plant) strongly suggest that Z decreases with increasing cell size, from

0.7 (2L) to 0.3 (plant). The Z versus gangue size relationship is virtually non-existent at lab scale. This partly explains why Z can be used irrespective of gangue size. At plant scale, where horizontal and vertical travel distances are longer, the effect of particle size on Z is much sharper, and the simplified entrainment model should be used with caution

The dynamic response to wash water and gas rate was determined in the pilot cell using tracer and conductivity techniques. Two types of electrode system (HEA and VEA) were developed to compare wash water distributor performance and monitor froth washing efficiency. Tracer tests confirmed that there was a minimum feed water penetration at an intermediate wash water rate. Higher gas rates have deleterious effects on froth washing capability.

Laboratory and pilot-scale flotation tests with the Strathcona Cu-Ni ore provided from different streams showed that in most cases, wash water significantly decreases gangue entrainment and increases concentrate grade; in some cases, wash water stabilizes the froth and increase recovery. Rejection of free gangue particles is readily achieved, but locked and/or partially hydrophobic particle rejection may be achieved, depending on the nature of solids (i.e. particle size, hydrophobicity, population density etc.), froth stability, froth wetness and wash pattern.

Plant-scale wash water amenability tests at the non-magnetic circuit of Falconbridge showed that Ni upgrading and non-sulphide gangue rejection with wash water are higher at a decreased Ni recovery. Due to the relatively coarse nature of the feed, the effect of wash water was much more clearly observed in the -37 μ m fraction.

Full plant scale wash water tests performed at the 2nd cleaner bank of Eastmaque showed that final Au grade can be increased by 14% at a slightly higher Au recovery. For this plant, a high water recovery without wash water was identified. Dilution of pulp with wash water reduced residence time, and possibly pyrite oxidation problems. Wash water reduced feed water recovery from 78% down to 33% and fine gangue recovery (-10µm) from 65% down to 15%.

11.2 Scale-Up

The effect of wash water scales-up remarkably well from 6.5L to 2800L. At plant-scale, water consumption can be minimized by washing the froth surface adjacent to the overflow weir. This section corresponds to the most severe entrainment (Moys, 1978). Thus, it becomes difficult to estimate superficial wash water rate, as the sprayed surface is clearly not the total surface. In this study, the sprayed surface was estimated at the total surface when washing with four pipes (1.5m*im) and half that when using

only two pipes per cell (15m*0.5m). The resulting superficial wash water rate then varies between 0 03 and 0 1 cm/s for the flowrates used. There is some evidence that 0 1 cm/s is above the optimum addition rate, whereas 0 02 cm/s is below. Between 0 03 and 0 07 cm/s, there is little evidence of much effect for wash water rate, as laboratory and pilot results suggests.

11.3 Limitations of Wash Water

The limitations of wash water are two-fold. First, gangue rejection is only partial. The Eastmaque case could be an extreme as water recovery without wash water was unusually high, above 70%. With wash water, the dramatic increase in tails flowrate and replacement of feed water by wash water in the concentrate both contributed significantly to a reduction of entrainment, by a factor of three. More realistic expectations may be to reduce entrainment by half, as observed in most laboratory and pilot-tests.

A second limitation is the decrease in residence time due to dilution (a similar problem is observed with flotation columns). This is particularly apparent with the Strathcona data, which show decreased recoveries with wash water. At Eastmaque, the flotation circuit has extra capacity, and gold recovery dropped in the 2nd cleaner with wash water. However, the lost gold was later recovered in the first cleaners. Thus, no visible loss of

recovery was observed; rather, overall gold recovery actually went up with the use of wash water.

11.4 Practical Implications of Wash Water for Plant Applications

In flotation cells, a substantial amount of waste is carried into the froth by inter-bubble water, which degrades separation. Fine gangue particles (>20µm), which are weakly attached or held in the inter-bubble water, have a negligible settling velocity and virtually behave like water. One of the most effective ways to reject them is to provide a downward water flow (i.e. positive bias) with wash water added above the froth surface. Wash water forces feed water, which contains gangue particles, down to the slurry phase, and stabilizes froth by compensating water loss and reducing coalescence. With wash water, bubbles remain spherical and are further apart from each other. There is less surface shrinkage and competition for sites on bubble surface. Wash water can also prevent overloading, which inhibits drainage, by lightening the froth and allows the concentrate to be pulled harder.

In general, wash water is most beneficial for single stage flotation (e.g. coal), thin froth flotation (e.g. potash or phosphate), fine feed (e.g. reground feeds) or low grade material. (e.g. tail reclamation).

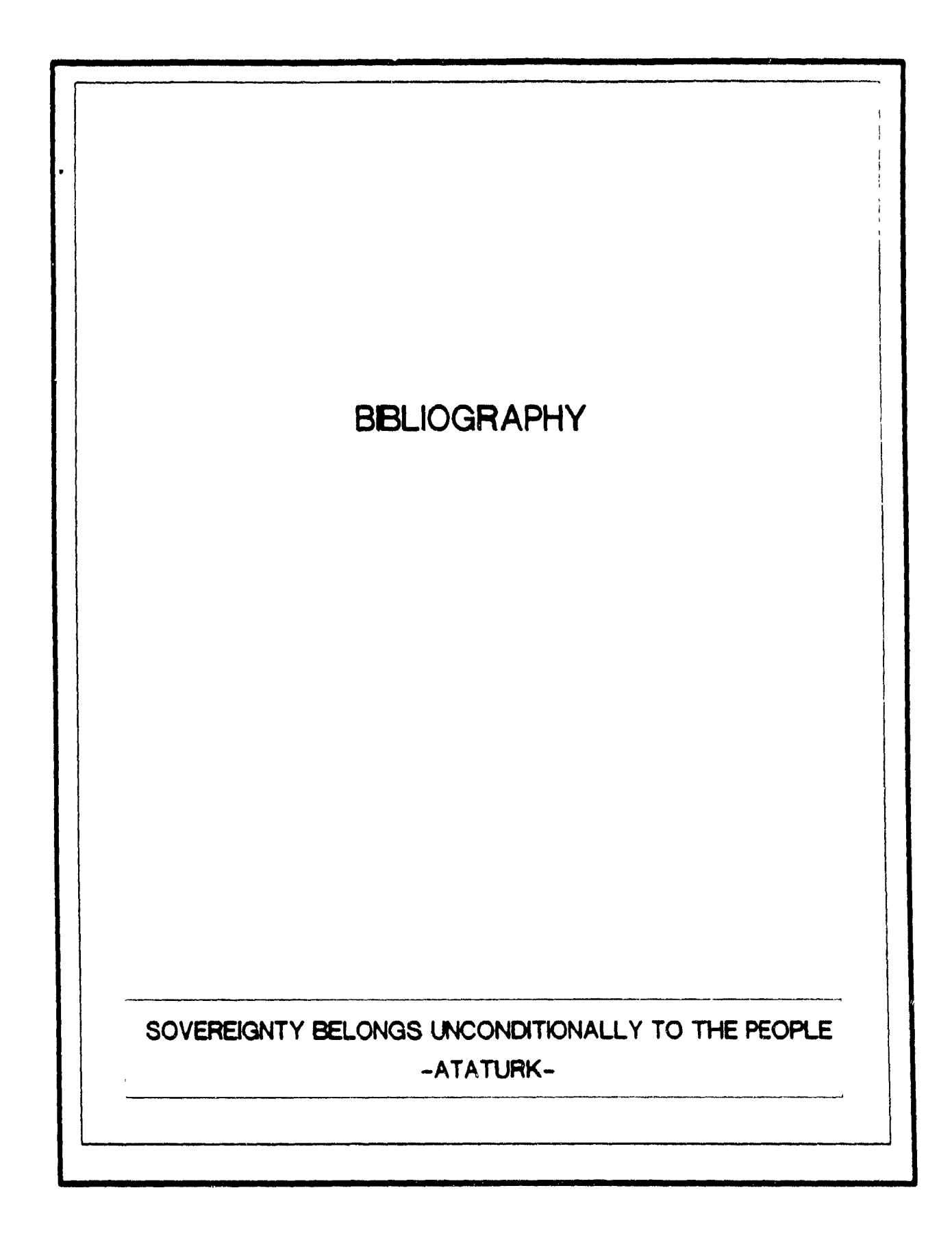
Generally, it is necessary to wash the entire froth surface in laboratory and pilot cells due to the short horizontal and vertical travel distances in the froth, while washing the front froth surface with one or two pipes is sufficient in plant However, froth stabilization is then lost, and the recovery of hydrophobic species is lowered

Although economies in water usage and cost may be realized by limiting its use to the latter stages of separation, one recent experience shows that in some cases, entire circuits (e.g. Zinc Corporation of America, New York) can be retrofitted advantageously (R. Kemp, private communication, 1989).

The use of wash water in flotation plants can be economically and metallurgically attractive, simple and, most importantly inexpensive to test and implement. Before making significant and expensive changes in existing flotation circuit flowsheets (e.g implementing flotation columns), froth washing, which may achieve comparable results, should be fully tested.

11.5 Suggestions for the Future Work

- 1. The combined effect of wash water and gas rate should be quantified at plant scale. The deleterious effect of high gas rates may be overcome by washing the entire froth surface at higher superficial wash water rates.
- 2. Scaling-up of the classification coefficent should be investigated. Existing data do not include results from various scales with the same feed.
- 3. The decrease in the recovery of hydrophobic species with wash water is potentially harmful. Various means of restoring recovery should be investigated, such as increased froth thickness, gas rate, distributor height etc.
- 4. The effect of depressant and frother addition in the wash water should be tested in plant scale where longer retention times may make them more successful than at laboratory scale.
- 5. The use of flow modifier to locally increase froth residence time in froth or a screen mesh at the interface to decelerate the bubbles before entering the froth phase along with wash water should be further tested both in mechanical and column cells.
- 6. Conductivity techniques to monitor froth washing efficiency or to select best operating conditions should be applied to three phase pulps.



BIBLIOGRAPHY

Agranat B.A., Khavskii N.N., Khan G.A., Pantteleva N.F. and El'bert A.V., Flotation in Water Subjected to Ultrasonics, The Use of Ultrasonics in Extractive Metallurgy Symposium, Moscow Inst. of Steel and Alloys, Technicopy Ltd., England, 1973, pp. 55-65

Albertson M.I., Barton J.R. and Simons D.B., Fluid Mechanics For Engineers, Prentice Hall, 1960.

Arbiter N., Harris C.C., and Yap R.F., Hydrodynamics of Flotation Cells, SME-AIME Trans, Vol. 244, March 1969, pp. 134-148.

Arbiter N. and Harris C.C., Impeller Speed and Air Rate in the Optimization and Scale up of Flotation Machinery, SME-AIME Trans., March 1969, pp. 115-117

Azbel D.S. and Chermisinoff N.P., Fluid Mechanics, Ann Arbor Sci. Pub., 1983, Chap. 11.

Barbery G., Engineering Aspects of Flotation in the Mineral Industry: Flotation Machines, Circuits and Their Simulation, Scientific Basis of Flotation, NATO-ASI Series, Ed. By K.J. Ives, 1984, pp. 289-348.

Bascur O.A. and Herbst J.A., Dynamic Modelling of a Flotation Cell with a View Towards Automatic Control, XIV Inter. Min. Proc. Cong., Toronto, 1982.

Bascur O.A. Modelling and Computer Control of a Flotation Cell, Ph.D. Thesis, The Uni. of Utah, 1982.

Bergmann L., Del Ultraschall und Seine Anwendung in Wissenschaft und Technik VI Aufl., Hirzel-Verlag, Stuttgart, 1954.

Bisshop J.P. and White M.E., Study of Particle Entrainment in Flotation Froths, IMM London, 1985, pp. C191-194.

Calderbank P.H., The Interfacial Area in Gas-Liquid Contacting With Mechanical Agitation, Trans. Instn. Chem. Engnrs, Vol. 36, 1958, pp. 443-463.

Calderbank P.H., Mass Transfer, In Mixing Ed. By V.W.Uhl and J.B. Gray, Academic Press, 1967, Ch.6.

Cutting G.W., Barber S.P. and Watson D., Prediction of Flotation Plant Performance from batch Tests Using Process Models: Effect of Froth Structure, XIV Inter. Miner. Proc. Congress (CIM), Toronto, Paper IV-14, 1982.

Degner V.R. and Sapey J.B., Wemco/Leeds Flotation Column Development, In Column Flotation'88, Ed. by K.V.S. Sastry, SME, 1988, pp. 267-281.

Del Villar R., Column Flotation Amenability and Scale-up Tests, report to Falconbridge, 1988

Dobby G., Ph.D. Thesis, McGill Uni., Montreal, Canada, 1984.

Dobby G. and Finch J A., Mixing Characteristics of Industrial Flotation Columns, Proceedings of 17th CMP Conference, 1985.

Dowling E.C., Klimpel R R. and Alpan F F., Use of Kinetic Models to Analyze Industrial Flotation Circuits, Presented at The Reinhardt Schuhmann Inter Sym., SME, Warrendale, PA, 1986.

Engelbrecht J.A. and Woodburn E.T., The Effect of Froth Height, Aeration Rate and Gas Precipitation on Flotation, Jour. of South Afr. Inst of Mining and Metall., Oct 1975, pp. 125-133.

Feron C., Privite communication, 1987.

Flint I.M. and Dobby G., Nonmagnetics and Copper Circuit Column Test Reports, Internal Report, Falconbridge Ltd, Sudbury, Oct. 1986, 26 pages.

Flint L.R., Factors Influencing the Design of Flotation Equipment, Miner. Sci. Engrn., Vol. 5, No. 3, July 1973.

Frew J.A. and Trahar W.J., Roughing and Cleaning Flotation Behaviour and the Realistic Simulation of Complete Plant Performance, Inter. Jour of Miner. Proc., 9, 1982, pp. 101-120.

Glembotskii V.A., Klassen V.I., and Piaksin I.N., Flotation, Primary Sources, New York, 1972.

Greaves M. and Kobbacy K.A.H., Power Consumption and Impeller Dispersion Efficiency in Gas-Liquid Mixing, Inter. Chem. Eng. Sypm. Series, No. 64, 1981, L1.

Harris C.C. and Mensah Biney, Aeration Characteristics of Laboratory Flotation Machine Impellers, Inter. Min. Proc. Journal, 4, 1977, pp. 51-67.

Harris C.C. Schock E.M., Khandrika S.M., and Pinzo W.L., Concentration Profiles in a Laboratory Flotation machine: Development of a Simple Technique, Powder Tech., 35, 1983, pp. 211-221.

Hemmings C.E., An Alternative Viewpoint of Flotation Behaviour Ultrafine Particles, IMM London, 1980, pp. C113-120.

Herbst J.A. and Bascur O.A., Alternative Control Strategies for Coal Flotation, Minerals and Metall. Processing, Feb. 1985, pp. 1-8.

Hukki R.T., Hot Flotation Improves Selectivity and Raises Mineral Recoveries, World Mining, 1970, pp. 74-76.

Jameson G.J., Physical Factors Affecting Recovery Rates in Flotation, Minerals Sci. Engng. Vol 9, No. 3, July 1977, pp. 103-118.

Jowett A and Safvi S M.M., Refinements in Methods of Determining Flotation Rates, Trans SME-AIME, Vol. 217, 1960, pp. 351-357

Jowett A. and Ghosh S.K. Flotation Kinetics Investigations to Process Optimization, New York Gordon and Breach Sci. Pub. 4, 1965, pp. 175-184.

Jowett A, A Gangue Mineral Contamination of Froth, Brit. Chem Engng, Vol. 11, 1966, pp. 330-333.

Jowett A., Investigation of Residence Time of Fluid in Flotation Cells, Brit. Chem. Engrg. Apr. 1961, pp. 254-258.

Kawatra S.K. and Seitz R.A., Effect of Froth Structure on Coal Flotation and Its Use in Process Control Strategy Development, APCOM 84, IMM London, 1984, pp. 139-147.

Kaya M., The Effect of Air Flowrate and Froth Thickness on Batch and Continuous Flotation Kinetics, Master of Eng. Thesis, McGill Uni., Canada, 1985.

Kaya M. and Laplante A.R., Investigation of Batch and Continuous Flotation Kinetics in a Modified Denver Laboratory Flotation Cell, Can. Metall. Quaterly, Vol. 25, March 1986, pp. 1-8.

Kaya M. and Laplante A.R., Factors Influencing Design, Hydrodynamics, Mixing, Residence Time Distribution, Scale-up, Selection and Sizing of Flotation Machines, Presented at Mineral Separation Systems Seminar, McGill Uni., May 1986a.

Kaya M. and Laplante A.R., Laboratory and Pilot-Plant Scale Flotation Tests with the Strathcona Cu-Ni Ore to Assess the Fotential of Wash Water Addition in Mechanical Flotation Cells, Progress Report V, submitted to Falconbridge Ltd, 1988.

Kaya M. and Laplante A.R., Plant Scale Wash Water Amenability Tests at the Strathcona Mill of Falconbridge, Progress Report VI, submitted to Falconbridge Ltd., Aug. 1988.

Kaya M. and Laplante A.R., Evaluation of the Potential of Wash Water addition and Froth Vibration in Mechanical Flotation Cells, in the 2nd International Mineral Processing Symposium, Ed. by Y. Aytekin, Izmir, Turkey, Oct. 1988, pp. 175-184.

Kaya M. and Laplante A.R., Plant Scale Wash Water Tests at Eastmaque Gold Mines Ltd., report submitted to Eastmaque Gold Mines Ltd., Dec. 1988, 16p.

Kaya M. and Laplante A.R., Froth Washing in Mechanical Flotation Machines, paper presented at the 21st Annual Meeting of Canadian Mineral Processors (CMP), Jan. 1989.

Kelsall D F., Applicability of Probability in the Assessment of Flotation Systems, Bul. IMM, 70, 1961, pp. 191-204.

Kemp R , Private communication, 1988.

Kerr A.N. and Kipkie W.B., Recent Process Developments at Inco's Copper Cliff Miling Complex, In Complex Sulfides-Processing of Ores, Concentrates and By-Products, Ed. by A.D. Zunkel, AIME, 1985, pp. 525-548.

Klassen V I. and Pikkat-Ordynsky G.A., Improving the Flotation of Coal by Spraying the Froth, Coke and Chem., Moskow, No.1, 1957, pp. 15-19.

Klassen V. I. and Mokrousov V. A., An Introduction to the Theory of Flotation, Butterworths, 1963, Ch. 22.

Koh P.T.L. and Warren L.J., Flotation of Ultrafine Scheelite Ore and the Effect of Shear-Flocculation, 13th Inter. Miner. Proc. Cong., Warsow, 1979, Ed. by J. Laskowski.

Konigsmann K.V., Hendriks D.W. and D'Aoust C., Computer Control of Fiotation at Matagami Lake Mines, Vol. 69, No. 767, March 1976, pp. 117-121.

Laplante A.R., Effect of Air Flowrate on the Kinetics of Flotation, Ph.D. Thesis, Uni. of Toronto, 1980.

Lee J.C. and Meyrick P.L., Gas Liquid Interfacial Areas in Salt Solutions in an Agitated Tank., Trans. Instn. Chem. Engnrs., Vol. 48, 1970, pp. T37-45.

Levenspiel O., Chemical Reaction Engineering, Wiley, 2nd Ed., 1972.

Luttrel G.H., Adel G.T. and Yoon R.H., Modeling of Column Flotation, Presented at SME Meeting, Denver, Feb. 1987.

Luong H.T. and Volesky B., Mechanical Power Requirements of Gas-Liquid Agitated Systems, AIChE Journal, Vol.25, No. 5, Sept. 1979, pp. 893-895.

Lynch A.J., Johnson N.W., McKee D.J. and Thorne C.G., The Behaviour of Minerals in Sulphide Flotation Process with Reference to Simulation and Control, Jour. of South Afr. Inst. of Mining and Metall. Apr. 1974, pp. 349-365.

Lynch A.J., Johnson N.W., Maniapig E.V., and Thorne C.G., In Mineral and Coal Flotation Circuits, Elsevier Sci. Pub. Comp., 1981, Ch.8.

Malinovskii V.I., Froth Separation, The Soviet Jour. of Non-Ferrous Metals, Vol. 11, No.8, 1970, pp. 81-84.

Mann R., Gas-Liquid Stirred Vessel Mixers: Towards a Unified Theory Based on Networks-of-Zones, Chem. Eng. Res. Des , Vol. 64, Jan. 1986, pp 23-25.

Marrucci G and Nicodemo L., Coalescence of Gas Bubbles in Aqueous Solutions of Inorganic Electrodes, Chem. Eng. Sci., 1967, Vol. 22, pp. 1257-1265.

Masliyah J. H., Hindered Settling in a Multi-Species Particle System, Chem. Eng. Sci., Vol. 34, pp. 1166-1168.

Maxwell J.C., A Treatise on Electricity and Magnetism, Vol. 1, Ch. IX, Clarendon Press, Oxford, 1873, pp. T37-45.

McKee D.J., Fewings J.H., Manlapig E.V. and Lynch A.J., Computer Control of Chalcopyrite Flotation at MIM Ltd., A.M. Gaudin Memorial Volume, In Flotation, SME, 1976, Ch. 34.

Micheal B. J. and Miller S. A., Gas-Liquid Agitated Systems, AIChE Journal, Vol. 8, No. 2, May 1962, pp. 262-271.

Mika T.S. and Fuerstenau, A Microscopic Model of the Flotation Process (in Russian), VIII Inter. Miner. Proc. Cong., Leningrad, Vol.2, 1969, pp. 246-269.

Miller F.G., Reduction of Sulfur in Minus 28 Mesh Bituminous Coal, Trans. SME-AIME, March 1964, pp. 7-15.

Miller F G., The Effect of Froth Sprinkling on Coal Flotation Efficiency, Trans. AIME, Jun. 1969, pp. 159-165.

Miller D.N., Scale-up of Agitated Vessels Gas-Liquid Mass Transfer, AIChE Jour., Vol. 20, No. 3, May 1974, pp. 445-453.

Moys M.H., Study of Plug Flow Model for Flotation Froth Behaviour, Inter. Jour. Miner. Proc., 1978, pp. 21-28.

Moys M.H., Study of Processes Occurring in Flotation Froths, Ph.D. Thesis, South Africa, 1979.

Moys M.H., Residence Time Distributions and Mass Transport in the Flotation Froths, Inter. Jour. of Miner. Proc., 13, 1984, pp. 117-142.

Murphy D., Strathcona Mill Sampling Campaigns on Nov. 1987, Falconbridge Interoffice Memorandum.

Mururka R. N., Privite communication, 1988.

Nagata S., Mixing Principles and Applications, J. Wileys&Sons, 1975, Ch. 8.

Nesset J.E., The Aplication of Residence Time Distributions to Flotation Circuits, Presented at CIMM Tech. Session, Bathurst, N.B., 1896.

Nicol S.K., Malcolm D.E., and Chyeteh K., Fine Particle Flotation in an Acoustic Field, Inter J of Miner Proc., 17, 1986, pp 143-150

Niemi A., Dynamics of Flotation, Acta Polytech. Scand. Chem. Metall. Ser. No. 48, 1966, pp. 17-52.

Nienow A.W., The Dispersion of Solids in Liquids, In Mixing of Liquids by Mechanical Agitation, Ed. by J.J. Ulbrecht and G.K. Patterson, Gordon Breach Sci. Pub., 1985, Chap. 8.

Nienow A.W., Konno M., and Bujalski W., Studies on Three Phase Mixing: A Review and Recent Results, Chem. Eng. Res. Des., Vol.64, Jan. 1986, pp. 35-43

O'Connor C.T., Dunne R.C., and Botelho DeSousa A.M.R., The Effect of Temperature on the Flotation of Pyrite, Jour. of S. Afr. Inst. Min. Metall., Vol. 84, No. 12, pp. 389-394.

O'Connor C.T., Dunne R.C. and Bothelho DeSousa A.M.R., The Effect of Temperature on Pyrite From Two Different Ores, XV Inter. Min. Proc. Cong., Cannes, 1985, pp. 211-221.

Pebbles K.N. and Garber H J., Chem. Eng. Prog., 49, 1953, p.58.

Perry R.H. and Green D., Perry's Chemical Engineers Handbook, Sixth Ed., McGraw Hill, 1984, pp. 5-21, 5-23.

Plouf T.M., Design and Development Considerations for the Denver 36 m³ DR Flotation Machine, In 13th Inter. Miner. Proc. Cong. Proceedings, Ed. by J. Laskowski, Vol. 2, Warsaw, 1979.

Retnivtzev V.I. and Dmitriev Yu G., Ultrasonic Cleaning of Minerals, Proc. 7th IMM London, 1963-64.

Rey M. and Raffinot P., Flotation of Ores in Sea Water, High Frothing; Soluble Xanthate Collecting, World Mining, June 1966, pp. 18-22.

Rushton J.H. et al., Ind. Eng. Chem., 36, 517, 1944.

Rushton J.H., Power Characteristics of Mixing Impellers, Part II, Chem. Eng. Proc., Vol. 46, No. 9, 1950, pp. 467-476.

Silva L.B., Modelo Fisico de Una Celda de Flotacion (in Spanish), Thesis, Universidad Technica Federica Santa Maria, 1983.

Slaczka St. A., Effects of Ultrasonic Field on the Flotation Selectivity of Barite from a Barite-Fluorite-Quartz Ore, Inter. Jour. of Miner. Proc., 20, 1987, pp. 193-210.

Steiner L., Hunkeler R. and Hartland S., Behaviour of Dynamic Cellular Foams, Trans. Instn. Chem. Engrs., 55, 1977, pp. 153-163.

Stoev S M., Influence of Ultrasonic Vibrations on Secondary Concentration of Minerals in a Froth, Trans. IMM, 76, 1967, pp. C284-286.

Sun S.C., Destruction of Flotation Froths with High Frequency Sound, SME-AIME, Trans., Oct, 1951, pp. 865-867.

Sun S.C. and Mitchell D.R., Ultrasonic Desliming and Upgrading of Ores, SME-AIME Trans., June 1956, pp. 639-644.

Trahar J A., A Rational Interpretation of the Role of Particle Size in Flotation, Inter. Jour. Miner. Proc., 8, 1981, pp. 289-327.

Van Dierendonck L.L., Fortuin J.M.H., and Venderbos D., The Specific Contact Area in Gas-Liquid Reactors, Chem. Reac. Eng. Proceedings of the 4th Europian Symp., Brussels, Sept 1968, pp. 205-215.

Westerterp K.R., Van Dierendonck L.L., and De Kraa J.A., Interfacial Area in Agitated Gas-Liquid Contractors, Chem. Eng. Sci., Vol. 18, 1963, pp. 495-502

Woodburn E.T. and Loveday B.K., The Effect of Variable Residence Time on the Performance of a Flotation System, Jour. of S. Afr. Inst. Min. Metall., Vol. 65, pp. 612-618.

Wrobel S.A, Flotation Froths, Their Action, Composition and Structure, In Recent Developments in Mineral Processing, Inst. Min. and Metall, London, 1953, pp. 431-454.

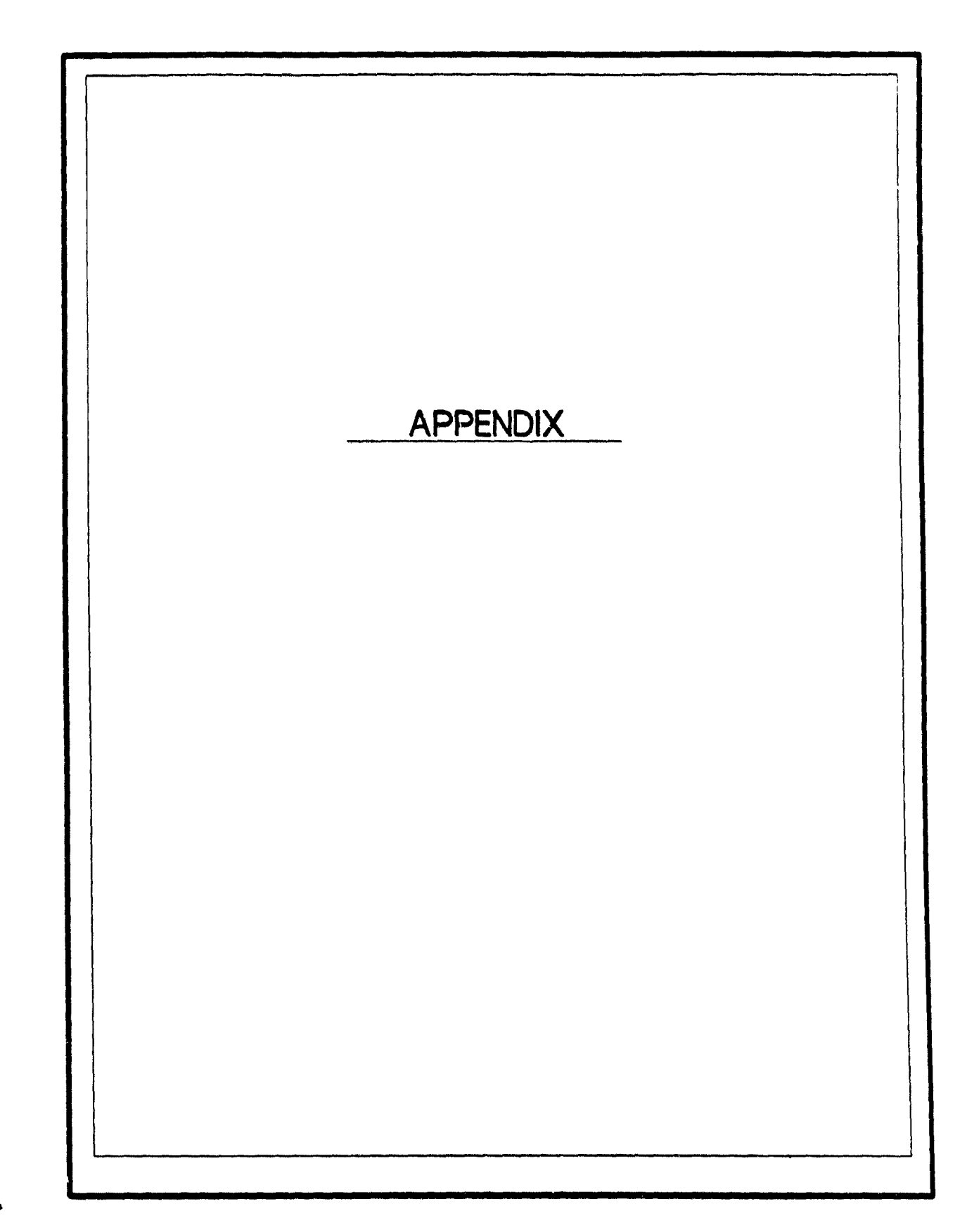
Yianatos J.B., Laplante A.R., and Finch J.A., Estimation of Local Gas Holdup in the Bubbling and Froth Zones of a Gas-Liquid Column, Chem. Eng. Sci., Vol. 40, No. 10, 1985, pp. 1965-1968.

Yianatos J.B., Finch J.A. and Laplante A.R., Holdup Profile and Bubble Size Distribution of Flotation Column Froths, can. Metall. Quaterly, Vol. 25, March 1986, pp. 23-29.

Yianatos J.B., Column Flotation Froths, Ph.D. Thesis, McGill University, Montreal, Canada, 1987.

Youn R.H., Flotation of Coal Using Microbubbles and inorganic Salts, Mining Congress Journal, 68(12), 1982, pp.76-80.

Yung C.N., Wung C.W., and Chang C.L., Gas Holdup and Aerated Power Consumption in Mechanically Stirred Tanks, The Can. Jour. of Chem Eng., Vol. 57, Dec. 1979, pp. 672-676.



```
204
         NEXT I
       DATA
 205
                    0.5,0.5,0.5,0.5,0.5,0.5,0.5
        FOR 1 = 1 TO 3
         READ GH(1)
 207
        NEXT 1
        DATA 0.32, J.86, J.89, D.93, J.94, J.95, J.96, J.975
 209
 210 FOR [ = 1 TO 8
 211 LH([) = 1 - GH([) - ES([)
211 LH(1) * 1 - SH(1) - ES(1)

215 T(1) = GH(1) * H(1) / JG

220 RS(1) = RL * LH(1) + RP * ES(1)

225 DEF FN YY(U) = INT (1000 * 1) + .5) / 1000

230 PRINT "LH(1) = ',LH:1) PRINT 'T(1) = *,T(1)

232 PRINT "RS(1) = ",RS(1)

300 REM CALCULATION OF J(0)

300 REM CALCULATION OF J(0)
NEM LARGULATION OF J(0)
305 REM VOLUME FLOWRATE CM3/S
310 JO = 6 * JG * AC * TH / OB
312 PRINT "JO =", JO
315 REM SLURRY FLOWRATE 3/SEC
320 EO = JO * GS
325 PRINT "EO* ', EO
 350 REM CALCULATION OF DROPBACK CONSTANT, K
 350 K = ( - LOG (EH / ED)) * JG / (EG * =T)

365 PRINT "K= ", K

370 JPS(I) = 5 * (DP ~ 2) * (LH(I) ~ 2.7) * (RP - RS(I)) / (18 * MU)

375 US(I) = JPS(I)
 380 MP(I) = 3P * JS(I) * RL * LH(I) / MU

385 VS(I) = JPS(I) / I + 3.5 * 'MP(I) ^ 0.6871)

387 IF ABS (JS(I) - VS(I)) ^ 0.001 THEM GOTO 390

388 JS(I' * VS(I)

399 GOTO 380
 390 UL [] * UW + JC) / LH([)
400 PRINT 'VS(')= "./S(!)
410 PRINT 'UL !)= './L(!)
460 EI !) = E0 * EXP -
470 RI ! = EI !) - E4
475 PRINT 'EI ! = E1 ! ?
                                         - K + T(7)))
                                          - PPINT 'RI'()= ",RI ;
 700 REM CALCULATION OF DM(H)

702 DM(I) = [EI(I) * DH(I) / JG] + (RI(I) / (VS(I) + JL(I)))) * H(I)

704 ES(I+1) = DM(I) / ,RP * AC * H(I))
 705 YEXT [
 725 SS = 3
730 FOR : = 1 TO 8
 310 SS = SS + DM(1)
 330 NEXT I
 900 REM CALCULATION OF BANGUE PROFILE
905 FOR I * 1 TO 8
 22 \ (1)MC = (1)4D CIE
 315 YEXT [
 950 DEF FN YY('3) - INT '1000 - 3 + .5) / 1000
 960 PRINT PRINT 1000 REM TABLEN YY(EI(I)), TAB( 5), FN YY(RI(I)), TAB9 FN YY(DM(I)), TABLE FN YY(GP(I))
 1100 PRINT TAB: FN YY(DM(I)), TAB( 5); FN YY(GP(I))
 2001
          PRINT PRINT
 2005 PRINT ES(I)
 2010 NEXT I
```

APPENDIX 2.1 SLURRY ZONE TORTUOSITY

Take a cross-section of dispersion in between the electrodes, (D*1), in which there is a large number of bubbles (Figure a). Consider a simplified cross-section (Figure b) where n is the number of circles of diameter D equivalent to the cross-sectional area occupied by gas. The gas holdup equals the fraction of the cross-sectional area occupied by gas, i.e

$$\varepsilon = \frac{n.\pi.(D^2/4)}{(D.1)} = \frac{n.\pi.D}{4}$$
 2a

To estimate tortuosity ($L_{\mathcal{E}}/L$) consider the length of the path in the cross-section containing these n circles (Figure c). Assuming the path lines follow parallel contours the mean length (dashed line) is

$$L_s = L + n(1 8465D - 1.4142D) = L + 0.4322nD$$
 2b

Substituting Eqs (2a) and (2b) yields

$$L_{\varepsilon}/L = 1 + 0.55\varepsilon$$
 2c

APPENDIX 3.1

FROTH ZONE TORTUOSITY

In this zone tortuosity is associated with polyhedral bubble shape. Consider a cross-section, (D*1), as described in Figure a. The equivalent cross-section is shown in Figure b, with D now being the diameter of a sphere with the same volume as regular dodecahedron, a shape commonly assumed. The gas holdup will again be related by Eq. 2a, provided the circles can be overlapped

In order to estimate tortuosity, consider the length of the path for a dodecahedral bubble of edge length "a". Figure c Assuming that ion migration takes place only along the borders, for a single bubble two routes are possible: R-W-T-P-S (length 4a) and R-V-Q-T-P-S (length 5a). Taking the average equivalent to two parallel resistances, the mean length is

$$\frac{L_{\varepsilon}}{n} = \frac{2}{((1/4a)+(1/5a))} = 4.444a$$
 3a

From the properties of the pentagonal dodecahedron D=2.444a, so that

$$L_{e} = 1.818nD$$
 3b

Substituting Eqs (3a) and (3b) yields

$$L\varepsilon/L = 2.315\varepsilon$$
 3c